

RECENT CHANGES IN SPECIFICATION AND CODE REQUIREMENTS FOR CONNECTION DESIGN IN THE UNITED STATES

Charles J. Carter, S.E., P.E.
Director of Engineering and Continuing Education
American Institute of Steel Construction, Chicago, IL, USA

Nestor R. Iwankiw, P.E.
Vice President of Engineering and Research
American Institute of Steel Construction, Chicago, IL, USA

ABSTRACT

Many new specifications and codes have been introduced in the United States in the past few years. This paper provides a summary of recent changes in the current specifications and codes that are applicable in steel building design and construction.

INTRODUCTION

Many new specifications and codes have been introduced in the United States in the past few years. Following is a summary of the current specifications and codes that are applicable in steel building design and construction:

- 1999 AISC *Load and Resistance Factor Design Specification for Structural Steel Buildings* (1)
- 1997 AISC *Seismic Provisions for Structural Steel Buildings* (2) with 2000 AISC *Seismic Provisions Supplement No. 2* (3) (note: this supplement replaced 1999 AISC *Seismic Provisions Supplement No. 1* (4) in its entirety)
- 1997 AISC *Specification for the Design of Steel Hollow Structural Sections* (5)
- 1993 AISC *Specification for Load and Resistance Factor Design of Single-Angle Members* (6)
- 2000 AWS D1.1 *Structural Welding Code – Steel* (7)
- 2000 RCSC *Specification for Structural Joints Using ASTM A325 or A490 Bolts* (8)

Changes have been made in most of these specifications and codes that affect the design and/or construction of connections. Following is a summary of the changes that have been made in each of these specifications and a more detailed look at a few of the more important ones in the 2000 RCSC Specification.

The connection requirements for seismic design are still being developed as a part of the 1997 AISC Seismic Provisions and 2000 Supplement No. 2. Additionally, at the time of writing this paper, the SAC Joint Venture is finalizing the Guidelines documents that will be published by the Federal Emergency management Agency (FEMA). The reader is referred to those sources

for information on changes in connection design and construction requirements for seismic design.

It has been assumed in the writing of this paper that the reader will have a copy of the above specifications and codes for reference.

GENERAL SUMMARY OF CHANGES

The following major changes have been made in requirements for the design and construction of welded joints:

- Limitations on effective length of fillet welds have been clarified and revised. The new provisions focus the applicability of the limitation to end-loaded fillet welds and provide a straightforward means to calculate the effective length as a function of the actual length and the weld size.
- The requirements for fillet weld terminations in Section J2.2b of the 1999 AISC LRFD Specification have been revised and clarified.
- Notch-toughness requirements have been added in Section J2.6 of the 1999 AISC LRFD Specification. Filler metal with a specified minimum Charpy V-notch (CVN) toughness of 20 ft-lbs at 40 degrees F is required for:
 - Complete-joint-penetration groove welded T- and corner joints subject to tension normal to the effective area when backing bars are to be left in place (exception: a lesser CVN rating is permitted if the joint is treated as a partial-joint-penetration groove weld)
 - Complete-joint-penetration groove welded splices subject to tension normal to the effective area in Group 4 and 5 shapes and built-up shapes with plates more than 2 in. thick.
- A more detailed listing of other major changes in the 2000 edition of AWS D1.1 can be found in the Foreword to that document. Additionally, a system of underlining and/or vertical line marking in the margin has been used throughout the 2000 edition of AWS D1.1 to indicate specific changes that have been made.

The following major changes have been made in requirements for the design and construction of bolted joints:

- New provisions have been added in the 1999 AISC LRFD Specification and 2000 RCSC Specification allowing the use of snug-tightened ASTM A325 bolts in applications involving static tensile loading.
- Provisions covering the design of bolts in combined shear and tension in Section J3.7 and Appendix J3.7 in the 1999 AISC LRFD Specification and Section 5.2 in the 2000 RCSC Specification have been revised.
- Slip-critical joint design provisions have been swapped in Section J3.8/J3.9 and Appendix J3.8/J3.9 in the 1999 AISC LRFD Specification.
- Bearing strength calculations in Section J3.10 of the 1999 AISC LRFD Specification and Section 5.3 of the 2000 RCSC Specification have been modified to a clear-distance basis.
- As has been the case before, it is occasionally indicated in the 2000 RCSC Specification that information is required to be shown on the design drawings or in other contract documents. Similarly, it is indicated in the 2000 RCSC Specification when the approval of the Engineer of Record is required for some aspect of a bolted joint. As a convenience to the user, a summary of the drawing information and approvals required from the Engineer of

Record has been added in Section 1.4 in the 2000 RCSC Specification. This subject is discussed in greater detail later in this article.

- Explicit coverage of the material and geometric requirements for washer-type indicating devices, twist-off-type tension-control bolt assemblies and alternative design fasteners has been added in Sections 2.6, 2.7 and 2.8, respectively, in the 2000 RCSC Specification.
- Explicit coverage of ASTM F1852 twist-off-type tension-control bolt assemblies has been included throughout the 2000 RCSC Specification. These fastener assemblies were previously covered in general under the alternative-design fastener provisions.
- Provisions allowing the thermal cutting of bolt holes with the approval of the Engineer of Record have been added in Section 3.3 in the 2000 RCSC Specification. Previously silent on this subject, the new RCSC Specification allows the use of flame cutting, plasma cutting and other thermal cutting processes if approved by the Engineer of Record.
- New information has been added in Section 4 of the 2000 RCSC Specification to address the applicability and suitability of the various joint types: snug-tightened joints, pretensioned joints and slip-critical joints. The requirements in this Section also serve to identify the applicable design, installation and inspection requirements for each of the joint types. This item is discussed in greater detail later in this paper.
- In Section 5.5 in the 2000 RCSC Specification, the limitation on prying force for applications that involve tensile fatigue has been reduced from 60 percent of the total applied load to 30 percent. This change was made based upon review of the available research and engineering judgment.
- Provisions for pre-installation verification of fastener assemblies have been clarified in Section 7 in the 2000 RCSC Specification. These provisions apply as they are invoked in Section 8.2 for pretensioned joints and slip-critical joints.
- The intent and applicability of the installation requirements and inspection requirements have been simplified, clarified and expanded significantly in Sections 8 and 9, respectively, in the 2000 RCSC Specification. These topics are discussed in greater detail later in this article.
- Arbitration provisions to be used in the case of a dispute for pretensioned joints and slip-critical joints have been clarified in Section 10 in the 2000 RCSC Specification.

The following major changes have been made in requirements for the design and construction of connecting elements:

- *Revised Provisions for Block Shear Rupture* – The provisions in 1999 AISC LRFD Specification Section J4.3 have been modified to account for the possibility in block shear rupture that the block can tear out in a rupture/rupture mode. That is, block shear rupture strength is now checked for three possible modes of failure:
 - Shear rupture in combination with tension yielding when the rupture strength of the shear plane(s) exceeds the rupture strength of the tension plane(s)
 - Tension rupture in combination with shear yielding when the rupture strength of the tension plane(s) exceeds the rupture strength of the shear planes(s)
 - Shear rupture in combination with tension rupture when this total strength is less than the controlling combination in the forgoing two options
- *Revised Provisions for Fatigue* – A significant revision has been made to the fatigue provisions in 1999 AISC LRFD Specification Appendix K3. In lieu of the step-function approach taken in previous editions of this specification, fatigue design in this new edition is based upon calculation of design stress range based upon the number of cycles anticipated in design and the type of detail used. Additionally, the number of fatigue cases covered has been significantly expanded.

NEW DRAWING INFORMATION REQUIREMENTS IN THE 2000 RCSC SPECIFICATION

As a convenience to the user, Section 1.4 in the 2000 RCSC Specification contains a summary of the information that is needed from the Engineer of Record. The section name "Drawing Information" implies that this information should be shown in the design drawings. However, the letter of the requirements in that section indicates that the information can be included in any of the contract documents, at the discretion of the Engineer of Record.

The required information has also been simplified significantly. The ASTM designation and type of bolt to be used and the joint type (see the next section in this article) must be indicated. If a slip-critical joint is specified, two additional requirements may apply. First, the required class of slip resistance (i.e., Class A, Class B or Class C) must be indicated. Second, if the connections are to be selected and/or completed by someone other than the engineer of record for subsequent review and approval by the engineer of record, it must be indicated whether slip resistance is to be checked at the factored-load level or the service-load level.

The Commentary on this section also provides a summary of the several cases where the approval of the Engineer of Record would be required to do something. Such approval is required for:

- The reuse of non-galvanized ASTM A325 bolts;
- The use of washer-type indicating devices other than those covered by ASTM F959;
- The use of fastener assemblies other than those with bolts covered by ASTM A325, A490 or F1852;
- The use of faying-surface coatings in slip-critical joints with a slip coefficient that is intermediate between 0.33 (Class A) and 0.5 (Class B);
- The use of thermal cutting in the production of bolt holes;
- The use of oversized, short-slotted or long-slotted holes in lieu of standard holes; and,
- The use of a value of D_u (pretension multiplier in LRFD) or D (slip probability factor in ASD) other than the default value of 1.13 or 0.80, respectively, in calculations of slip resistance.

PROPER SPECIFICATION OF JOINT TYPE FOR BOLTED JOINTS

Section 4 in the 2000 RCSC Specification provides a clear basis for the proper specification of joint type by the Engineer of Record, based upon the type of load that the fasteners in the joint transmit. For joints with fasteners that are loaded in shear or combined shear and tension, the joint type can be specified as snug-tightened, pretensioned or slip-critical. For joints with fasteners that are loaded in tension only, the joint can be specified as snug-tightened or pretensioned. Table 4.1 in the 2000 RCSC Specification provides a more detailed summary of the appropriate joint types given the type of load transmitted. Once the joint type is specified, the remaining requirements for design, as well as installation and inspection (see the next section in this paper), are also defined.

Snug-Tightened Joints

Snug-tightened joints are permitted except when pretensioned joints or slip-critical joints are required. Essentially, that means that most joints can be specified as snug tightened, except when pretensioned is required in the fasteners (with or without faying surfaces that are prepared to achieve slip resistance).

Bolts in snug-tightened joints must be designed to provide the required resistance in shear, tension or combined shear and tension on the fasteners and bearing on the connected material. Installation and inspection requirements are as described in the next section of this paper.

It is also worthy of note that, with the 2000 RCSC Specification and based upon the historic usage of ASTM A307 bolts and recent research on high-strength fasteners, snug-tightened joints are also permitted for statically loaded applications involving ASTM A325 bolts and ASTM F1852 twist-off-type tension-control bolt assemblies in direct tension. However, snug-tightened installation is not permitted for these fasteners in applications involving non-static tensile loading, nor for tensile applications involving ASTM A490 bolts.

Pretensioned Joints

Pretensioned Joints are only required in the following applications:

- Joints in which fastener pretension is required in the specification or code that invokes the 2000 RCSC Specification (1999 AISC LRFD Specification Section J1.11 and 1997 AISC Seismic Provisions Section I-7.2a, for example);
- Joints that are subject to significant load reversal (near-full or full load in one direction followed by near-full or full load in the other direction, like is characteristic of seismic loads, but not wind loads);
- Joints that are subject to fatigue load with no reversal of the loading direction (i.e., cycled loading that does not involve a change in the sign of the load);
- Joints with ASTM A325 or F1852 bolts that are subject to tensile fatigue; and,
- Joints with ASTM A490 bolts that are subject to tension or combined shear and tension, with or without fatigue.

Bolts in pretensioned joints must be designed to provide the required resistance in shear, tension or combined shear and tension on the fasteners, bearing on the connected material and tensile fatigue, if applicable. Installation and inspection requirements are as described in the next section of this paper.

Slip-Critical Joints

Slip-Critical Joints are only required in the following applications involving shear or combined shear and tension (i.e., not applicable for applications involving tension only):

- Joints that are subject to fatigue load with reversal of the loading direction (i.e., cycled load that does involve a change in the sign of the load);
- Joints that utilize oversized holes;
- Joints that utilize slotted holes, except those with applied load approximately normal (within 80 to 100 degrees) to the direction of the long dimension of the slot; and,
- Joints in which slip at the faying surfaces would be detrimental to the performance of the structure.

Bolts in slip-critical joints must be designed to provide the required slip resistance and the required resistance to shear or combined shear and tension on the fasteners, bearing on the connected material and tensile fatigue, if applicable. Installation and inspection requirements are as described in the next section of this paper.

INSTALLATION AND INSPECTION REQUIREMENTS FOR BOLTED JOINTS

The requirements in the 2000 RCSC Specification for installation and inspection are invoked by the joint type specification. In all cases, proper storage of the fastener components is required.

Snug-Tightened Joints

For proper installation of fastener assemblies in snug-tightened connections, all bolt holes must be aligned so that the bolts are not damaged during insertion. Once bolts are placed with washers as required, and nuts, the assembly is used to compact the joint progressing systematically from the most rigid part of the joint, bringing the connected plies into firm contact.

For proper inspection of snug-tightened bolted joints, it must be ensured that the proper fastener components were used, the connected elements were fabricated properly, and the bolted joint was drawn into firm contact. Because pretension is not required for the proper performance of a snug-tightened joint, the installed bolts should not be inspected to determine the actual installed pretension. Likewise, arbitration (described in 2000 RCSC Specification Section 10) is not appropriate.

Pretensioned Joints

There are four approved methods for proper installation of fastener assemblies: turn-of-nut pretensioning, calibrated wrench pretensioning, twist-off-type tension-control bolt pretensioning and direct-tension-indicator pretensioning. Although there are differences in how extensively the requirements apply, in each of these methods, the pre-installation verification requirements in 2000 RCSC Specification Section 7 must be met for pretensioned installation. Also, in each case, the snug-tightened condition is the starting point.

When Joints are designated as pretensioned, they are not subject to the same faying-surface-treatment inspection requirements as is specified for slip-critical joints.

Turn-of-Nut Pretensioning: For installation, after snug-tightening the joint, the nut (or bolt head) rotation specified in the RCSC Specification must be applied to all fastener assemblies in the joint, progressing systematically from the most rigid part of the Joint in a manner that will minimize relaxation of previously pretensioned bolts.

For inspection, in addition to meeting the inspection requirements for snug-tightened joints, the inspector should observe the pre-installation verification testing required. Subsequently, the inspector can either ensure by routine observation that the proper rotation is applied to the turned element or visually inspect match-marks after pretensioning

Calibrated Wrench Pretensioning: For installation, after snug-tightening the joint, the calibrated installation torque (not a tabulated or assumed value) must be applied to all fastener assemblies in the joint, progressing systematically from the most rigid part of the joint in a manner that will minimize relaxation of previously pretensioned bolts.

For inspection, in addition to meeting the inspection requirements for snug-tightened joints, the Inspector should observe the pre-installation verification testing required. Subsequently, the inspector should ensure by routine observation that the proper calibrated installation torque is applied to the turned element.

Twist-Off-Type Tension-Control Bolt Pretensioning: For installation, after snug-tightening the joint without severing the splined end, the installation wrench must be applied to all fastener

assemblies in the joint, progressing systematically from the most rigid part of the joint in a manner that will minimize relaxation of previously pretensioned bolts.

For inspection, in addition to meeting the inspection requirements for snug-tightened joints, the Inspector should observe the pre-installation verification testing required. Subsequently, the inspector should ensure by routine observation that the splined ends are properly severed during installation.

Direct-Tension-Indicator Pretensioning: For installation, after snug-tightening the joint, the direct-tension-indicator gaps should be compressed, progressing systematically from the most rigid part of the joint in a manner that will minimize relaxation of previously pretensioned bolts.

For inspection, in addition to meeting the inspection requirements for snug-tightened joints, the Inspector should observe the pre-installation verification testing required and that the appropriate feeler gage is accepted in at least half of the spaces between the protrusions of the direct tension indicator prior to pretensioning and that the protrusions are properly oriented away from the work. Subsequently, the inspector should ensure by routine observation that the appropriate feeler gage is refused entry into at least half of the spaces between the protrusions.

In each of these methods, no further evidence of conformity is required. Furthermore, a pretension that is greater than the specified minimum pretension is not cause for rejection.

Slip-Critical Joints

Installation in slip-critical joints is identical to that for pretensioned joints. Inspection is also identical, except that the inspector should also verify that the faying surfaces of slip-critical joints meet the appropriate requirements.

CONCLUSIONS

Many new specifications and codes have been introduced in the United States in the past few years. This paper provided a summary of the changes that have been made in each of these specifications and a more detailed look at a few of the more important ones in the 2000 RCSC Specification.

REFERENCES:

- (1) American Institute of Steel Construction, 1999, *Load and Resistance Factor Design Specification for Structural Steel Buildings*, AISC, Chicago, IL.
- (2) American Institute of Steel Construction, 1997, *Seismic Provisions for Structural Steel Buildings*, AISC, Chicago, IL.
- (3) American Institute of Steel Construction, 2000, *Seismic Provisions Supplement No. 2*, AISC, Chicago, IL.
- (4) American Institute of Steel Construction, 1999, *Seismic Provisions Supplement No. 1*, AISC, Chicago, IL.
- (5) American Institute of Steel Construction, 1997, *Specification for the Design of Steel Hollow Structural Sections*, AISC, Chicago, IL.

- (6) American Institute of Steel Construction, 1993, *Specification for Load and Resistance Factor Design of Single-Angle Members*, AISC, Chicago, IL.
- (7) American Welding Society, 2000, *AWS D1.1 Structural Welding Code – Steel*, AWS, Miami, FL.
- (8) Research Council on Structural Connections, 2000, *Specification for Structural Joints Using ASTM A325 or A490 Bolts*, AISC, Chicago, IL.

Update on ECCS TC10 and Eurocode 3 Efforts

ir. C.M. Steenhuis
Eindhoven, University of Technology, the Netherlands
Dipl. Ing. J. Kouhi
VTT Building Technology, Finland

ABSTRACT

In this paper, a short overview is presented on the activity of Technical Committee 10 of the European Convention for Constructional Steelwork (ECCS TC10). This committee deals with Structural Steelwork Connections. Furthermore the status of the conversion process of Eurocode 3 from European pre-standard (ENV) to European standard (EN) is reported. The focus is on Eurocode 3 part 1.8, which deals with connections.

1. ACTIVITY REPORT OF ECCS TECHNICAL COMMITTEE 10

The Technical Committee of the European Convention for Constructional Steelwork (ECCS TC10) deals with structural steelwork connections. The committee forms a European Network for practitioners and researchers from ECCS member countries. In total, the committee has 30 full members and 17 corresponding members. A number of corresponding members maintain relationship with other Technical Committees of the ECCS. The committee meets twice a year, with normally about 20 to 25 participants.

The objectives of the committee are as follows:

- steel promotion by simple and safe rules for economical connections;
- preparation of background material for Eurocode 3 and 4, especially concerning connections;
- contribution to CEN-TC 135. This committee works on ENV 1090 (execution);
- forming an international platform for discussion;
- harmonising and co-ordinating research in the field of steel connections;
- defining gaps in knowledge;
- preparation of publications.

Figure 1 shows the organisation scheme of the committee. The committee has three working groups:

- Working group 1: connection practice. This group is chaired by practitioners;
- Working group 2: joints;
- Working group 3: connectors.

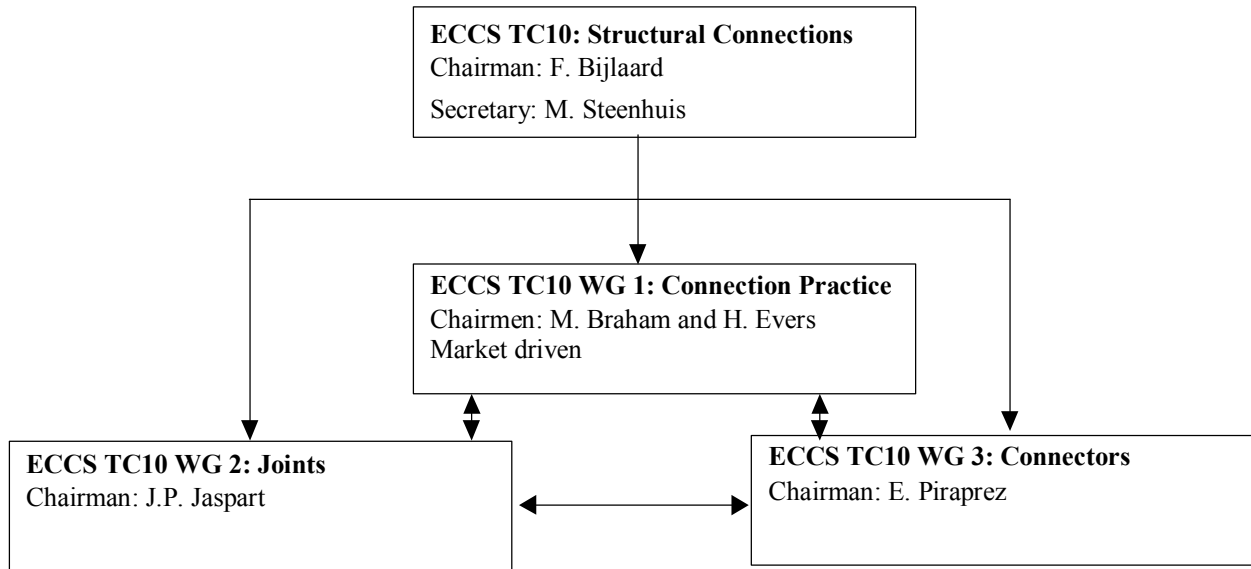


Figure 1: Organisation of ECCS TC10

Working Group 1 is market driven, whereas Working Groups 2 and 3 are technology pushed. The relation between Working Group 1 and the two other working groups is important. The Working Group 1 encounters questions from practice, which are brought to the attention of the other working groups.

The topics of Working Group 1 (Connection Practice) are: economy, valorisation, dissemination, education, innovation, benchmarking, etc. Recent and current activities are: collection of questions from practice, preparation of a guide for fasteners, preparation of benchmark examples, development of a design guide for base plate joints and special connections.

The topic of Working Group 2 (Joints) is: joint representation for structural analysis. This involves characterisation, idealisation, modelling classification of joint properties in structural analysis. Recent and current activities are: design rules for moment-normal force (M-N) behaviour of beam to column connections, technical assistance to Working Group 1, support to CEN TC135 (ENV 1090), support to CEN TC135 (conversion of ENV 1993, Eurocode 3 to EN, see further on in this paper).

The topics of Working Group 3 (Connectors) are: bolts, rivets, welds, studs, play and finish connections, clamps, etc. Recent and current activities are: support to CEN TC135 (ENV 1090), support to CEN TC135 (conversion of ENV 1993, Eurocode 3 to EN), technical assistance to Working Group 1, publication about use of bolts and test reports on requirements for preloaded bolts, tightening, fitness for purpose etc.

2. CONVERSION PROCESS OF EUROCODE 3 FROM ENV TO EN

As intended in the European Commission's original objectives, the primary intention of the Eurocodes was to establish a set of common rules for the design of Buildings and Civil engineering works. It will serve as reference documents to be recognised by authorities of the Member states. In essence, two main ideas are substantiating the Eurocodes program: "harmonisation" and "competitiveness" of the European construction sector as a whole.

In the next years, all Eurocodes will be converted from European Prestandard (ENV) to European Standard (EN). This process concerns the following Eurocodes, see Table 1.

Table 1: Eurocodes to be converted to EN.

EN 1990		Basis of design
EN 1991	Eurocode 1:	Actions on structures
EN 1992	Eurocode 2:	Design of concrete structures
EN 1993	Eurocode 3:	Design of steel structures
EN 1994	Eurocode 4:	Design of composite steel and concrete structures
EN 1995	Eurocode 5:	Design of timber structures
EN 1996	Eurocode 6:	Design of masonry structures
EN 1997	Eurocode 7:	Geotechnical design
EN 1998	Eurocode 8:	Design of structures for earthquake resistance
EN 1999	Eurocode 9:	Design of aluminium structures

At this moment, the Eurocodes may be used in the different European CEN-Member countries together with a Nation Application Document (NAD). This situation will change after completion of the conversion process. The converted Eurocode may then be used together with a National Annex.

In the course of this paper, it will be focussed on Eurocode 3 - Design of steel structures. The proposed structure of Eurocode 3 in EN version contains different subsets:

The internal subset

The "internal" subset which contains essentially the EC3 documents, is itself subdivided into:

- "slave documents" which comprises the generic design parts ("general rules" and particular generic rules). The generic or basic design parts cover self sufficient and independent sets of design rules (for example: Fatigue, Plates and Shells buckling, ...).
- "master documents" which gathers together all design application parts relevant to specific fields of construction (Buildings, Bridges, Towers and Masts,...).

The external subset

The "external" subset to EC3 is essentially composed of the Parts making up the whole of "Basis of design" and "Actions on Structures" (Eurocode 1).

The idea behind this sub-division is that from "master documents", for instance EN 1993-3 (Buildings), reference is made towards the relevant clauses in the "slave documents", for instance EN 1993-1-8 (Design of joints). Between "master documents" references are not allowed and

from "slave documents" it is not referred back to master documents. With help of these principles a clear structure will be achieved and no information will be repeated, as is the case in the ENV version of Eurocode 3.

The "slave documents" will be contained in EN 1993-1. The preliminary titles of the different parts of EN 1993-1 are:

- EN 1993-1-1, Design of steel structures - General rules
- EN 1993-1-2, Design of steel structures - Fire
- EN 1993-1-3, Design of steel structures - Cold-formed structures
- EN 1993-1-4, Design of steel structures - Stainless steel
- EN 1993-1-5, Design of steel structures - Plates structures
- EN 1993-1-6, Design of steel structures - Shell structures
- EN 1993-1-7, Design of steel structures - Plated structures transversely loaded
- EN 1993-1-8, Design of steel structures - Design of joints
- EN 1993-1-9, Design of steel structures - Fatigue strength of steel structures
- EN 1993-1-10, Design of steel structures - Selection of material for fracture toughness and through-thickness properties

The following "master documents" are foreseen:

- EN 1993-2, Design of steel structures - Bridges
- EN 1993-3, Design of steel structures - Buildings
- EN 1993-4, Design of steel structures - Silos, tanks and pipelines
- EN 1993-5, Design of steel structures - Piling
- EN 1993-6, Design of steel structures - Cranes
- EN 1993-7, Design of steel structures - Towers, masts and chimneys

The work on Eurocode 3, Design of steel structures is dealt with in CEN Technical Committee 250 Sub Committee 3 (CEN TC250/SC3). An overview of the organisation scheme is given in Figure 2. Figure 2 shows how a project team, in this case PT 1.1 is supported in the conversion work by the ECCS Validation Group and the National Technical Contact. The latter are people appointed by the National Standards Organisations. The ECCS Validation Group consists of the chairman of the respective ECCS Technical Committees. In case of ECCS TC10, an ad-hoc working group gives support to the Project team on rules for joints.

At this moment, work is in progress on EN 1993 Parts 1.1, 1.8, 1.9, 1.10 and Part 3. The time schedule is for these standards is:

- first draft to the Secretariat before 31 December 1999;
- final draft to the Secretariat before 31 October 2001;
- formal vote launched, 2002.

Most rules on joints are foreseen to be placed in EN 1993-1-8 (Design of joints). However, EN 1993-1-1 (General Rules) contains (for the moment) some basic rules on connectors as welds and bolts. The proposed table of contents of EN 1993-1-8 (Design of joints) is:

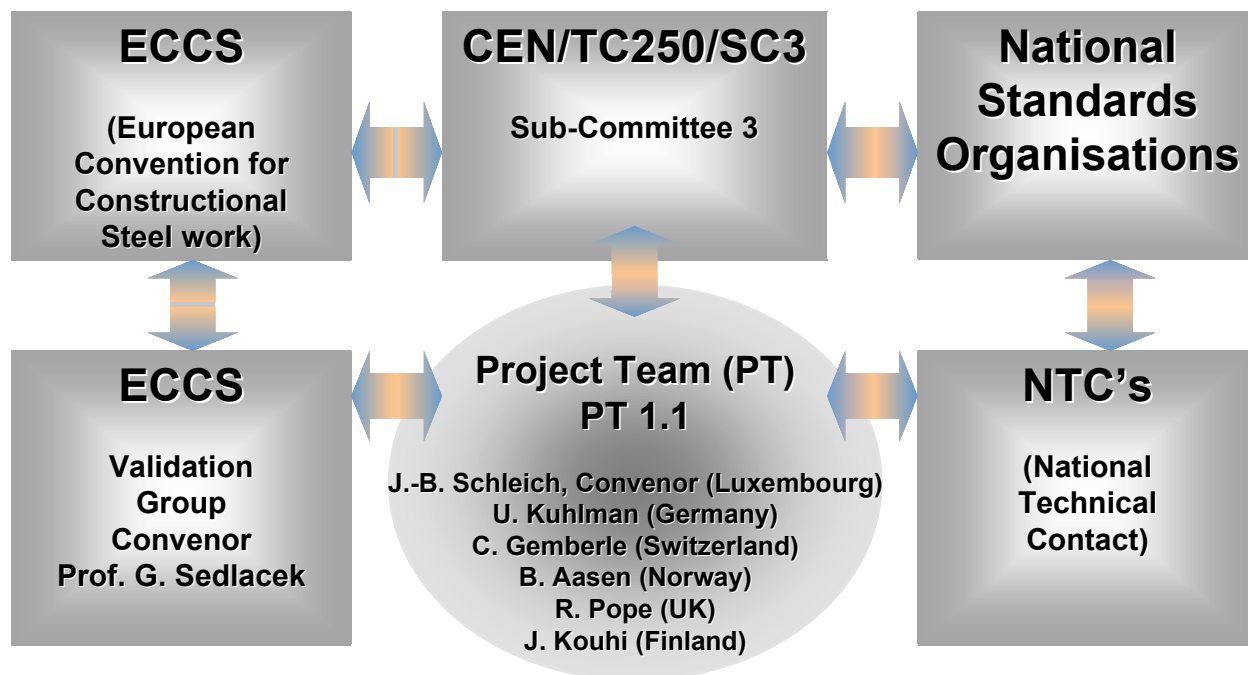


Figure 2: Organisation of Conversion of ENV 1993 to EN 1993

- 1 Basis
- 2 Basis of Design
- 3 Connections made with bolts, rivets or pins
- 4 Welded connections
- 5 Analysis, modelling and classification
- 6 Structural joints connecting H or I sections
- 7 Hollow section lattice girder joints

Project Teams for Part 1.3, Part 1.4, Part 1.5 and Part 2 have started their work in 2000. It is expected, that the formal voting for these parts will be in 2002-2003.

APPENDIX: LIST OF EUROCODE CONVERSION ABBRIVIATIONS

EU	European Union
CEN	European Committee for Standardisation
ENV	European prestandard
EN	European standard
ECCS	European Convention for Constructional Steelwork
SC	Sub-committee
PT	Project Team
NAD	National Application Document
NA	National Annex
NTC	National Technical Contact
VG	Validation Group

COST BASED ENGINEERING AND PRODUCTION OF STEEL CONSTRUCTIONS

H.G.A. EVERS, ICCS bv The Netherlands
IR. F. MAATJE, ICCS bv The Netherlands

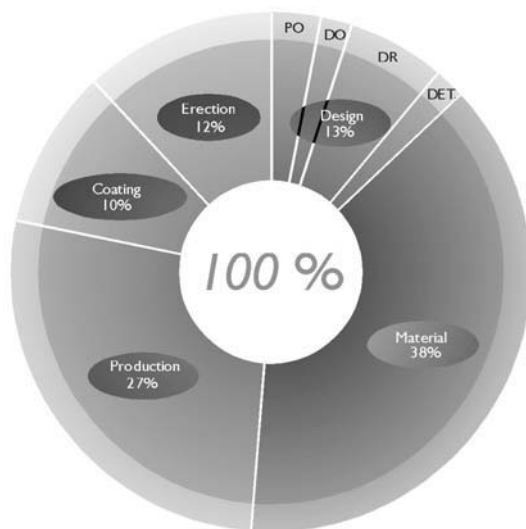
ABSTRACT

In the last years Steel construction companies in Northern Europe have mainly invested in production machines in the factory: Sawing and drilling machines, punching and shearing machines and Robot flame-cutting. Investments, which reduce the production costs of the Steel structure, looking at the complete development of a building quite at the end of the whole process. We as ICCS bv state that there are more savings possible if investments are done in the engineering and design, at the start of a project. This will be the subject of our lecture. To know what the possible savings are, the engineer needs to have good knowledge about costs of Steel constructions and software that helps him to make costs clear. In our lecture we will present the state of art of software tools available for the steel construction industry.

WHERE ARE COSTS IN STEEL CONSTRUCTION

In order to be able to reduce costs, it is necessary to know how the costs of creating a steel structure are build up. In regard to this we would like to make the following statement: Approximately 50% of the total costs in a steel structure can be redirected to the connections in the structure.

Roughly, the following cost items in a steel structure can be identified:



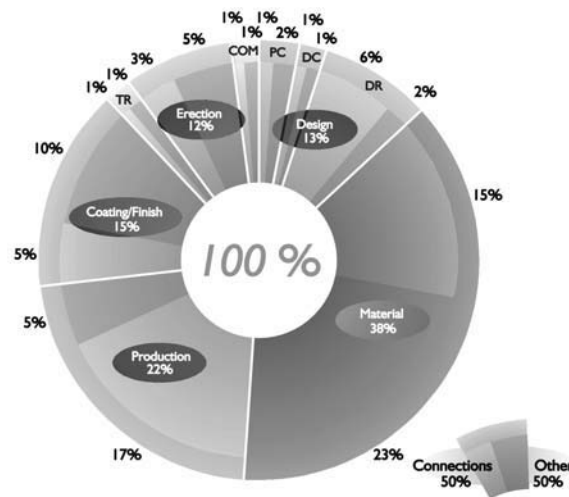
- 1) Design 13%
- 2) Material 38%
- 3) Production 27%
- 4) Coating 10%
- 5) Erection 12%

Looking at a standard Steel structure with a price of € 1.14/kg the percentages of the costs are shown in the figure below.

	Total in €	%	% related to connections		
Total		13%	8.6%		
1) Design costs	€ 0.15	$\left\{ \begin{array}{l} 2\% \times 33\% = 0.7 \\ 3\% \times 55\% = 1.7 \\ 8\% \times 77\% = 6.2 \end{array} \right.$			
2) Material costs	€ 0.43		38%	40%	15.2%
3) Production costs	€ 0.31		27%	63%	17.0%
4) Coating costs	€ 0.11	10%	35%	3.5%	
5) Erection costs	€ 0.14	12%	45%	5.4%	
		100%		49.7%	
			↓ % Connections		

COSTS RELATED TO THE CONNECTIONS

The costs in the connections are made visible in the next figure. Each part is divided into a light and a dark area: the light area is the part that is attributed to the connections, the darker area is attributed the other costs.



Design costs: These can be divided in:

- 1) Pre-design
- 2) Detailed design
- 3) Detailing and work preparation

1) Pre-design: 33% of costs related to connections:

In the pre-design most of the time is spent on main frame design and the stability of the structure. In the pre-design the engineer only has to consider connections that influence the global behaviour of the structure: The so called rigid or semi-rigid connections. Simple calculation rules are available (SG-TCA10a).

2) Detailed design: 55% of costs related to connections:

In this phase the engineer has to detail all the connections that influence the behaviour of the structure in detail. When semi-rigid connections are used the behaviour of the steel frame is influenced by these connections.

3) Detailing and work preparation: 77% of costs related to connections:

The draftsman spends nearly all his time on detailing connections in the steel structure. Using StruCad, the draftsman spends 10% of the time to set up the steel frame. The rest of the time is spent on detailing the connections and printing and plotting the drawings.

Material costs: 40% of costs related to connections:

In normal Steel structure plates contributed approximately 5% of the total weight. Using rigid connections, the field moment will be reduced. The amount of used material can be less. So there is a strong relationship between the type of connection and the amount of material in the structure.

Production costs: 63% of costs related to connections:

Nearly all the work in the shop is related to the connections of the steel structure: Prefabricating plates and cleats, the tack welding of the plates to the beams and columns and welding.

Coating costs: 38% of costs related to the connections:

The coating of the small parts like plates and cleats of the steel construction takes more time than coating the main beams and columns relatively.

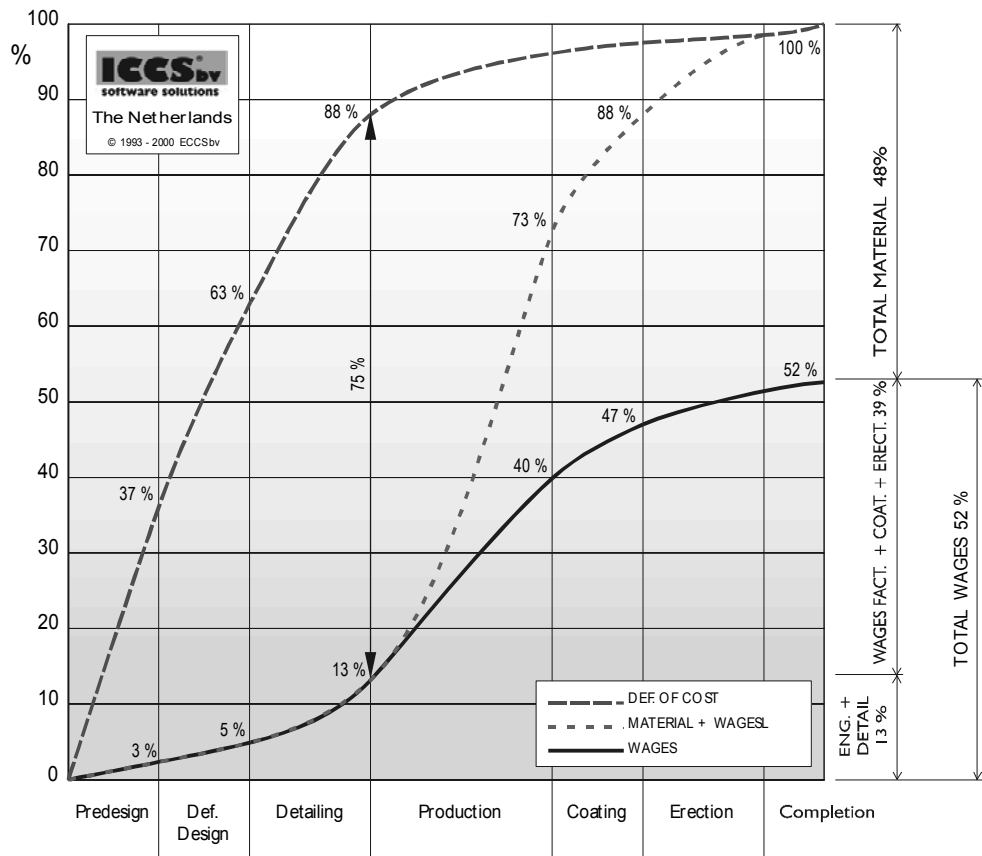
Erection costs: 45% of costs related to the connections:

It is clear that on the erection site the connections are fitted together. Easy connections will be less time consuming than difficult connections

This means that approximately 50% of the costs are directly related to the connections in a steel structure. In order to reduce costs in the total process it is of great importance to look at the connections at an early stage. In Dutch practice there are a lot of examples of projects that ended in court due to severe problems with the connections. In frame analysis packages it is very easy to analyze a structure in which all frame elements are rigidly connected. However, in practice, it is (almost) impossible to connect frame elements fully rigid. If it possible, then the costs of that particular connection will be very high.

As many costs are related to the connections, it is fair to say that at the end of the detailing the final price of the structure is determined for approximately 88%. The connections determine the material and hence the production in the shop and on site.

The next figure illustrates this.



How are the costs built up?

On the horizontal axis the progress in the project is shown. The percentages of costs are given along the vertical axis.

The continuous line represents the costs of the wages made during the project. The middle dashed line represents the total costs made during the project. The left dashed line shows the amount of costs that is fixed.

As in the design and detailing phase many costs are fixed. It is very important for an engineer to have a tool with which he can estimate what the financial consequences of his decisions during the design will be.

ICCS bv developed this tool: a software package called ICCS-TVC. The software package is able to estimate the cost of steel structure based on the specific infrastructure and production facilities of a specific steel fabricator.

ICCS-TVC TECHNICAL ESTIMATING

This software package has been developed in co-operation with several steelwork companies. Hence, ICCS-TVC is a package for the daily practice of steelwork companies.

The first version of ICCS-TVC was launched in 1988, being a DOS application based upon an Oracle database. At the end of 1997 a whole new version of TVC was brought to completion. This version is full Windows based and includes links with MS Excel and MS Word. ICCS-TVC uses a graphical input.

The ICCS-TVC contains four modules:

- 1) Simple “manual” estimating
- 2) 3D graphical input of steel construction (GET)
- 3) Connection generator
- 4) Production cost engine

These modules will be explained in more detail:

1) Simple “manual” estimating

Appropriating and inserting of material, possibly with hours or h/ton.

2) 3D graphical input of Steel construction

Using 3D for detailing Steel structures has become the standard. The benefits of this system are clear and are used widely in the Steel industry. In the past 10 years software for the 3D systems has become mature and hardware has become cheap and fast. At this moment these systems are mainly used for the detailing and not for estimating. But for an estimator the system can also be very powerful if the system is adjusted to his working method. The following advantages are present:

- 1) The contractor gets a clear overview of what is estimated (What You See Is What You GET) (Graphical Estimating Tool)
- 2) 2D and 3D hidden line drawing can be generated for the customer, possibly in AutoCAD size (clarity for the customer).
- 3) Changes can easily be done

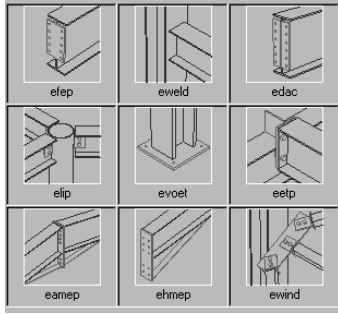
Important note: For the estimator isn't it necessary to put the beams and columns on the exact position, for example TOS.

In practice graphical estimating is as fast as manual input

3) Connection generator

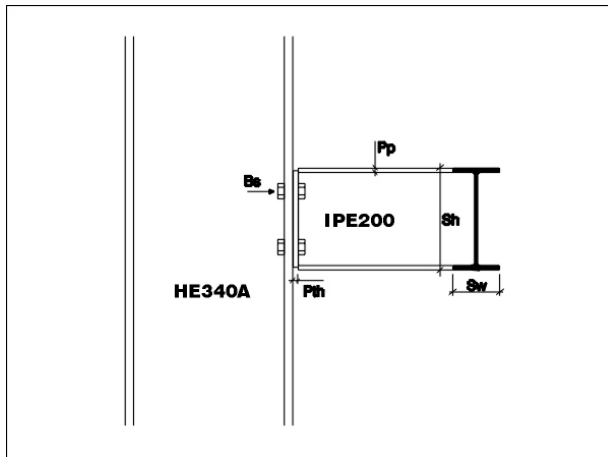
In the beginning of this manuscript it was made clear that 50% of the costs are related to the connections. This means that for an estimator it is very important to know what kind of connections are used and what roughly the dimensions of the connections are. At this stage not many connections are already detailed, but in order to make an accurate estimate more information is required. For this, ICCS bv developed “estimate connections” which can be assigned to the members in the 3D model.

The aim of the estimate is not to detail all the connections but to get a rough idea of the number of plates, bolts and welds are required to build the steel construction.



Within the estimation-program there are nine types of connections. Each type of connection generates the required connection parts (plates, welds, bolts, notches etc.), taking the connections into account.

The dimensions of the connection parts are determined by user definable formulas that describe the relationship between the sizes of the sections that are connected, and the dimensions of the connection. See figure.



End plate thickness $P_{th} = [range] \text{ or } P_f$
 End plate width $P_w = S_w$
 End plate length $P_l = S_h$

Weld size $a = 0,5 \bullet P_{th} = 0,5 \times P_f$
 Weld length $l = 4 \bullet S_w + 2 \bullet S_l$

S_w = section width
 S_h = section size

Number of bolts depends on S_h
 Number of sizes depends on S_h

Sizes endplate connection

Just by selecting the end types all the needed information about the connections will be generated automatically.

When the sizes of the connections have been determined, production costs can be estimated.

4) Production cost engine

The production costs are determined in two steps: First, for every part the program determines which labour-places need to be visited to produce the part. Secondly, the program calculates the exact time on the all the labour-places the part will visit.

The following basic labour-types are considered:

- 1) Shortening
- 2) Generating holes
- 3) Tack-welding
- 4) Welding
- 5) Other (notching, curving, blasting etc.)

Both shortening and generating holes can be executed in several ways:

Shortening: Sawing, shearing, burning or purchasing on length
Generating holes: Drilling, punching and burning

Basic labour-types are being chosen judging several criteria.

The normal logistic order of the production process is also very important in order to estimate production time. Within ICCS-TVC, the logistic order of the production process can be described in detail.

The estimation is being generated based upon the standard logistics within ***the Company's parameters*** .

The following issues are known:

- 1) Dimensions of the connection parts
- 2) Necessary labour methods

Using specific formulas that describe the relation between the parts of the connection parts, the section and ***the company-dependant parameters***, the production times are estimated fully automatically. These production times can be into part-production-times. For each labour method a specific formula has been programmed.

The summarized time for each labour method is in fact a summation of the following six part-production-times:

- Net production time
- Machine logistics
- Geographical logistics
- Information
- Measurement
- Non productive time

*Entering
labour place data*

The screenshot shows a software window titled "Labourplaces" with a close button (X) in the top right corner. At the top, there are two dropdown menus: "Labourplace" (set to "cutting") and "Combined with" (empty). Below these are two tabs: "Main sections" (selected) and "Graphics". The main area contains a grid of input fields for various parameters:

X-coordinate [m]	20	Transit speed [mm/sec]	65
Y-coordinate [m]	20	Informationtime straight [min]	2,5
NP factor	0,3	Informationtime beveled [min]	6
Transportspeed [m/sec]	0,38	Measurement [min]	1
Cranecapacity [ton]	3	Stock searching [min]	5
Picking up time [min]	5	Start-stop time [sec]	8
Machinecosts [£/h]	40	Labourspeed [mm ² /min]	3800
Personnelcosts [£/h]	50	Max. sawingheight [mm]	900

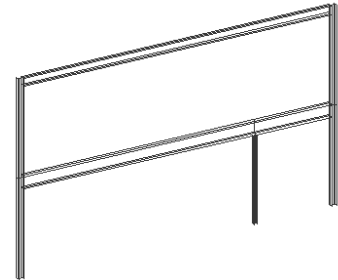
At the bottom of the window, there are three buttons: a file icon, a "STOP" button, and a question mark icon.

EXAMPLE OF COST BASED ENGINEERING AND PRODUCTION OF STEEL STRUCTURES

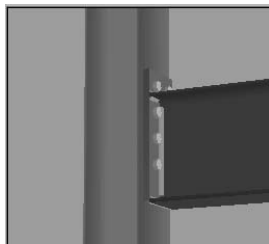
In the worked out example it is illustrated how an engineer can design a cost efficient portal frame with the following software tools:

StruCad Engineer: Graphical input
 STAAD/Pro: Frame design according to EC3
 CoP: Connection design according to EC3 annex J
 ICCS-TVC: Estimate

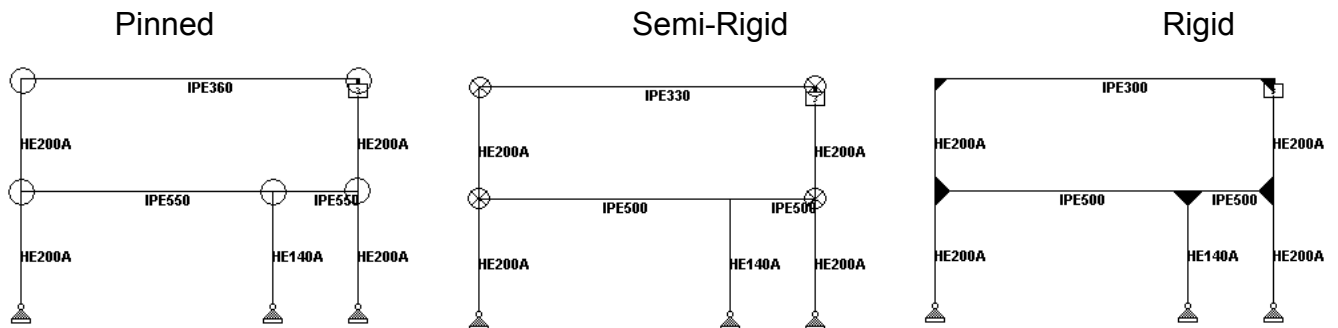
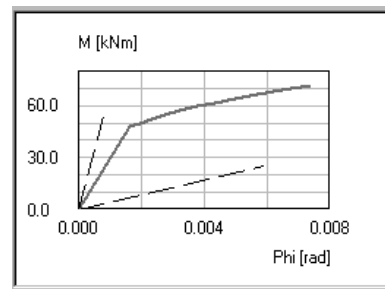
Braced portal frame: three types: Pinned connections
 Semi rigid connections
 Rigid connections



The frame is setup in StruCad Engineer, and imported frame into STAAD/Pro. With CoP the stiffness of the semi-rigid connections and the rigid connections are calculated. Then these are implemented in the frame analysis.



Resistance
 $M_{j,Rd} = 62.1 \text{ kNm}$
 $V_{j,Rd} = 483.8 \text{ kN}$
 Stiffness
 $S_{j,ini} = 21308 \text{ kNm/rad}$



Results of ICCS-TVC with the parameters of an average steel fabricator from the Netherlands, the following table can be extracted:

Weight [kg]	2818.0		2445.0		2572.0	
Costs Item in €	Pinned		Semi-Rigid		Rigid	
Material	38.3%	934.8	34.6%	785.0	33.4%	829.1
Details	3.6%	87.6	3.6%	82.6	3.6%	87.6
Production	26.0%	634.8	29.3%	658.4	32.5%	805.5
Coating	11.2%	274.5	11.3%	257.3	10.8%	267.7
Erection/Transport	20.9%	510.5	21.4%	484.2	19.8%	492.4
Total €	100.0%	2442.2	100.0%	2267.5	100.0%	2482.2
€ / kg		0.867		0.923		0.967
% of the total price	107.7%		100.0%		109.5%	

(All units are € unless noted otherwise)

In this case the construction with semi-rigid connections gives the most cost effective construction. The Simple Endplate connection already gives a high stiffness

CONCLUSION:

Using the latest technology in steel design makes the steel fabricator more competitive. Using benefits of the latest technology an integrated design is necessary: 3D-Modelling, 3D-Analysis, Connection Design and Estimating in the design.

FUTURE DEVELOPMENTS IN SEISMIC DESIGN PROVISIONS: LIFE AFTER SAC

James O. Malley
Senior Principal, Degenkolb Engineers
225 Bush Street, Suite 1000
San Francisco, CA 94104-4207 USA

ABSTRACT

The 1994 Northridge, California earthquake caused significant damage to steel moment resisting frame structures. Since Northridge, there has been a major focus in the United States on improving the design provisions of this class of building. With the culmination of the FEMA/SAC project in the year 2000, the focus of future efforts is likely to shift. This paper will discuss possible areas of focus and development and highlight potential research needed to more fully implement these concepts into future codes and design practice.

INTRODUCTION

The January 17, 1994 Northridge earthquake caused significant damage to steel moment resisting frame structures. Prior to this event, many engineers felt that this class of building was among the most seismically resistant structural systems. The unexpected damage caused by this event has led to extensive research and investigation into this system. One major effort in this regard was the FEMA funded SAC Steel project. This six year, \$10 million program addressed a large number of issues related to the performance of base and weld filler materials, inspection practices, connection performance and system performance. Substantial component and connection testing was performed on a number of connection configurations. Data was also collected from past earthquakes in the United States and Japan. A reliability based approach was developed to generate numerical procedures for estimating the performance of this class of buildings. These investigations and research have led to the development of a series of guidelines documents that will assist engineers in the seismic design of new steel buildings, the evaluation and rehabilitation of vulnerable existing buildings, and the repair of damaged buildings. An accompanying document addressing quality assurance and control issues has been developed to ensure that projects implementing these guidelines are completed as intended. It is expected that these guidelines will be implemented into building codes and design practice in a timely manner after their publication.

With the culmination of the FEMA/SAC project in the year 2000, the focus of future efforts related to the seismic performance of steel structures will likely shift. Potential areas for future development that will lead to improved seismic design provisions include the following:

- continued development of quantitative approaches to performance based engineering for moment frames and other systems,
- continued development of pre-qualification of various moment frame connections, including design manuals,
- increased attention on the design of partially restrained moment connections,
- development of provisions for the design of steel plate shear wall systems,
- development of provisions for the design of buckling restrained braced frame systems,
- application of advanced analysis techniques in design,
- increased development of composite systems, including more explicit design provisions,
- use of base materials with special properties, such as low yield point,
- development of provisions for explicit application of damping in steel frame structures.

This paper will discuss the present status of these areas and highlight potential research needed to more fully implement these concepts into future codes and design practice.

DEVELOPMENT OF SEISMIC CODES AND STANDARDS BEFORE THE NORTHRIDGE EARTHQUAKE

Prior to the 1994 Northridge earthquake, the development of seismic codes and standards generally was performed through the implementation of research and engineering judgement by a committee. Research provided to these committees was generated from the work of individual professors from grants provided by the National Science Foundation or industry. Until the early 1990's, the majority of the committee implementation work was accomplished by the Seismology Committee of the Structural Engineers Association of California (SEAOC). For many years, the outstanding work of this committee became the basis for the seismic provisions of the Uniform Building Code (UBC) (7).

The process of development of seismic code provisions for the original structural systems (moment resisting frames and concentrically braced frames, e.g.) followed a somewhat circuitous and disjointed path. As new research was performed on these systems, modifications to the existing provisions would be made to attempt to incorporate the new information. Long delays in incorporating the research work were common. In addition, not all research was considered by the code developers, in many cases due to poor communication channels. In some instances, industry practices were incorporated into code provisions without adequate research and analysis.

In the 1980's, a change in approach occurred, that has been very beneficial to the timely and proper implementation of research results into seismic design provisions. This change in approach was centered around the research performed on a new

structural system, the eccentrically braced frame, by Professor Egor Popov and his students at Berkeley. The ten year plus program of physical testing, analytical research and development of this system was carried out with the ultimate goal of complete understanding of the expected performance of the system in severe earthquakes. Each of the studies generated results that became useful in the development of code provisions. Shortly after the completion of this research, the 1988 UBC included this system as part of the building code. This systematic approach to the development of new (or improved) structural systems for incorporation into building codes was subsequently followed by Professor Subhash Goel and his students at the University of Michigan in the development of the Special Concentrically Braced Frame and Special Truss Moment Frame systems.

In approximately 1990, the American Institute of Steel Construction (AISC) began to be much more active in the design of seismic code provisions for steel buildings. In 1992, the first edition of the AISC Seismic Provisions was published (1). This document was the first set of seismic provisions in the United States that was based on the Load and Resistance Factor Design (LRFD) approach. The provisions were developed to be as consistent as possible with the Allowable Stress Design (ASD) provisions developed by SEAOC for the UBC. This was also a major step forward, since strength based provisions are clearly a more rational approach for seismic design where inelastic behavior is expected during severe earthquake shaking.

THE NORTHRIDGE EARTHQUAKE AND ITS AFTERMATH

The damage suffered by steel moment frames again demonstrated that each earthquake teaches engineers lessons requiring improvements in design and construction. One of the most glaring lessons from the Northridge earthquake related to the performance of the welded flange, bolted web moment connection that was widely used, and became “pre-qualified” in the 1988 Uniform Building Code. The connections built with this detail did not behave in the ductile manner expected by engineers, causing a complete examination of the design approach for these structures.

The SAC Steel Program, initiated late in 1994 with FEMA funding, was a major component in this examination. The SAC program, along with the efforts of private engineers, the steel industry and other government agencies (most conspicuously the National Institute of Standards and Technology), unleashed an unprecedented level of study and research on this system. The research program attempted to systematically examine the moment frame system from virtually every design and construction aspect.

The Northridge damage shook engineers’ confidence in existing design approaches to the extent that full scale connection testing became required for the use of moment frame construction. Materials testing of both the base metals used in modern steel wide flange construction and the weld filler metals was also undertaken. System analyses to better understand the demands that moment frame systems and their connections could be subjected to in a major event were performed. Detailed local connection analyses using the finite element method were combined with connection testing programs to

develop connection design approaches. All of this work culminated with the publication of a set of FEMA guidelines documents (FEMA 350 through 353) in the late summer of 2000 (2-5).

The FEMA guidelines on new construction are included in FEMA 350 “*Recommended Seismic Design Criteria for New Steel Moment Frame Buildings*” (2). This document provides detailed guidance on all aspects of the design of steel moment frames. It includes a new performance based approach to the design of these structures, a major advancement that will set the stage for parallel developments on other systems in the future. One of the most important developments included in the design is the return to a situation where connection specific testing results need not be provided for each new building. It became clear that the continuation of the requirement to provide such test results for all new designs would jeopardize the continued viability of this system for use in seismic applications. The FEMA guidelines therefore, have developed a set of “pre-qualified” connection details that engineers may use within prescribed limitations.

But, this is not to say that the publication of the FEMA guidelines signals a return to the procedures prior to the Northridge earthquake. One of the enduring lessons from the earthquake is the need to avoid extrapolating design provisions far beyond the available laboratory testing and research results. The pre-qualifications in FEMA 350 were carefully developed with the intent that they would place enough restrictions that the connections to be designed within these limits would ensure the anticipated ductile performance. Only very limited extrapolation beyond available test results was allowed.

WHAT’S IN STORE IN THE FUTURE?

The publication of the FEMA/SAC Guidelines signals the completion of an intense and exciting era in the improvement of the seismic design and construction of steel frame buildings. It is anticipated a number of enduring legacies will result from this program. The first will be that the research and code development communities will be much more aware of the need to develop design guidance based on as complete a level of understanding as possible. Engineers will better appreciate the need to stay abreast of new developments in their field, and how to properly extend existing procedures and approaches to their designs. Finally, those involved in the fabrication, erection and inspection of steel frame buildings will be more keenly aware of the need to properly implement quality assurance and quality control requirements in the building codes and project specifications.

The new era that follows the completion of the SAC project will also cause a shift in the focus of future efforts related to improving the seismic performance of steel structures. Other steel systems will likely be subjected to additional study and development. The performance based engineering approach developed for steel moment resisting frames by SAC will be extended to other systems. New materials will be developed and new applications and combinations of existing materials will be employed. These developments will continue to improve the ability of steel structures to resist the damaging effects of future earthquakes. The following paragraphs will briefly describe a number of areas of potential future research and development.

Continued Development of Performance Based Engineering

The development of explicit analytical techniques for performance based seismic engineering in the SAC project was a major advancement that has laid the groundwork for the implementation of these approaches into future engineering practice. It is clear from the SAC program that tremendous amounts of data (from both physical testing and analysis) are needed in order to estimate performance. The fundamental approach developed by SAC is applicable to all structural systems. The research community has embraced this approach and is attempting to extend it to other systems. Most specifically, the Pacific Earthquake Engineering Research (PEER) Center has adopted this approach in their program to better understand the performance on reinforced concrete structures. The steel industry is likely to extend this approach to other steel frame systems such as concentrically and eccentrically braced frames. The system can be used to establish confidence levels for performance based on the available information. How much and how reliable the information is directly impacts the level of confidence in a structural system or design. As a result, this procedure could be used to systematically identify where the most crucial gaps in the available data (element and material testing, e.g.) exist. Focusing future efforts on these identified gaps would make effective use of the available funds.

Extension and Expansion of SAC Connection Pre-qualifications

The SAC Guidelines recommend that, within certain limitations, a series of moment connection types (a total of nine different approaches) can be used in buildings without the need for project specific testing. This will provide engineers with a wide range of choice for their moment frame connection designs. As noted above, though, the pre-qualifications are limited in their scope to ensure that the intended performance can be achieved. It is likely that engineers will be interested in expanding the pre-qualification limits for various conditions. Areas where the pre-qualifications may be expanded could include the following:

- Increasing the beam depth. For some of the connections (bolted flange plates, extended end plates, etc) the pre-qualifications are limited to beam depths that were tested in the SAC program. Additional connection testing on deeper beams with designs based on the SAC guidelines design approach presented would be required to extend the existing limitations.
- Increasing the beam size. All the connections have a limitation on beam weight. It is not unreasonable to assume that large projects may be designed with sizes that exceed the present limitations. With additional test data, the beam size limitation could be increased.
- Increasing the column depth. Presently, the SAC guidelines only pre-qualify connections for application in Special Moment Frames (SMF's) when W14 column sections (or shallower) are used. This is because of the limited, and somewhat less successful performance of connections tested with deeper columns. The need for resistance to torsion deformations of the columns needs to be better understood through additional testing and analysis. This is perhaps the most pressing need

identified at the end of the SAC project, since the use of deep columns is a cost effective moment frame design approach in many instances.

- Inclusion of pre-qualifications to the connection to the weak axis of columns. Like the deep column issue noted above, connections to the weak axis of wide flange columns are not pre-qualified by SAC for use in SMF's. While not as widely applied as deep columns, there are instances when engineers desire to use weak axis connections (additional redundancy, e.g.). Tests in the SAC program, while encouraging, were not comprehensive enough to warrant pre-qualification. Additional testing and analysis on this topic could allow such pre-qualification.
- Inclusion of pre-qualification to box columns. The concerns are virtually identical to those discussed above for connections to the column weak axis. Extensive testing of connections with box columns has been performed in Japan, with generally successful results. Corroborative testing and analyses in the United States could allow the extension of connection pre-qualification to box columns. Engineers could also consider incorporating internal continuity plates and stiffeners with the box columns to more closely simulate wide flange columns.

In addition to the expansion of the pre-qualifications of connections that are in the SAC Guidelines, it is also likely that new connection concepts will be developed, tested and analyzed in the future. It is also possible that in the future, engineers will be able to use nonlinear finite element analysis techniques as a more fundamental part of the pre-qualification process. This will require increased confidence in the ability of analysis procedures to predict performance, especially regarding the eventual failure mode of the various details.

Increased Development and Application of Partially Restrained Moment Connections

The SAC Guidelines include a fully bolted partially restrained moment connection as one of the pre-qualified connections. It is likely that engineers will be intrigued with the use of this detail for a number of reasons. First, this detail avoids the use of welding, which could simplify and speed up the fabrication and erection. Extensive system analyses of buildings designed with partially restrained frames have demonstrated their viability for use in seismic regions. Taking major portions of the deformations into connection elements provides a means of inelastic behavior that could allow easier repair after a major earthquake than many of the fully restrained details. Partially restrained connections are also more conducive to redundant systems that are desirable to some engineers.

The design of structures with partially restrained connections is somewhat more calculation intensive than for designs with most fully restrained details. Both the system analyses and the detailed connection design procedures are more complex. The widespread application of partially restrained frames in seismic regions will require the development of analytical tools that can easily and explicitly capture the deformation of connections into the design process.

Development of Provisions for the Design of Steel Plate Shear Wall Systems

Steel plate shear wall systems have been sporadically employed in the United States since the early 1970's. Early applications were for hospital structures where severe design requirements were placed on the structures. These buildings were designed based on the yielding of the steel plate elements. More recently, research in Canada has demonstrated that tension field theory typically applied to plate girder design could be used in the design of steel plate shear walls, and that good seismic performance was possible. Canadian seismic design provisions now include this system.

Testing in the United States to date on large scale specimens has been limited, but promising. Extension of the system beyond the parameters used in existing testing (walls with openings, e.g.) will likely be desired by engineers applying the existing information to their designs. This system appears to be promising because of its' high initial stiffness and potentially high ductility. Addition research and development effort will be needed for this system to find wide application.

Development of Provisions for the Design of Buckling Restrained Braced Frame Systems

The performance of concentrically braced frame systems has always been limited by the ability of the brace elements to behave in a ductile manner. During the 1980's and early 1990's, Professor Subhash Goel and his students at the University of Michigan performed extensive testing and analytical research that resulted in significant improvements in the ductility of these elements and this system. This culminated in the incorporation of Special Concentrically Braced Frames (SCBF's) into seismic design provisions.

Even with these improvements, though, the ductility of this system is somewhat limited, since it relies on the inelastic buckling of the brace elements, a means of inelastic deformation that is not as desirable as the material yielding modes of other systems. The good system performance is the result of properly controlling the design of the overall system. Over the last ten years, another approach to brace design has been developed in Japan. In this approach, the braces are restrained from overall buckling. The brace therefore yields in both tension and compression. These braces exhibit full stable hysteretic behavior, without the pinched loops that are characteristic of more traditional braces.

Nippon Steel has developed an approach for a buckling restrained brace that is subject to a U.S. patent. This brace has been widely tested and appears to provide excellent ductility. Other systems for restraining the brace element from buckling could also be developed. At present, there are no design provisions for the application of this system, though a joint effort to do so by the Structural Engineers Association of California (SEAOC) and the American Institute of Steel Construction (AISC) is underway. The desirable ductile behavior of these braces makes it likely that this system will receive widespread application in the future.

Application of Advanced Analysis Techniques in Design

Structural design has traditionally relied on first order elastic analysis. Second order effects due to P-Delta displacements have now become commonplace parts of widely used structural analysis tools in design work. Recently, the application of nonlinear analysis that explicitly accounts for material nonlinearity has found use in the seismic evaluation of existing structures, in documents such as FEMA 273. At the present time, this takes the form of nonlinear static analysis (so called “pushover” analysis) in most cases, with fairly simple, piecewise linear models for the material behavior. It is not unreasonable to expect that future developments will include the ability to perform nonlinear time history analysis as part of the design process for new buildings, with the ability to accurately model element and connection hysteretic behavior based on definition of the local configuration. Developing the element libraries and data retrieval processes will be challenging. But, it is likely that the most challenging part of employing nonlinear analyses into the design process will be preparing rational rules for the application of these approaches in building codes.

Nonlinear Finite Element Method (FEM) analyses will also become a more commonly used tool for local connection and element behavior in the future. Local connection behavior demands, including large deformation effects due to local buckling, can be accurately modeled by programs such as ABAQUS and Nike-3D. As engineers become more adept and familiar with these techniques, they will be applied to develop new approaches to connection design. This procedure could also become useful in limiting the need for full scale connection testing to demonstrate performance, but will need to be done with caution so that the analysis can properly portray the local demands.

Increased Development of Composite Systems

The 1997 AISC Seismic Provisions included an entire section that deals with structures that include composite steel and reinforced concrete elements (1). These provisions attempt to allow the engineer to take advantage of the various strengths of these two structural materials in rational combinations that will provide good seismic performance. The design provisions for these systems and elements are based on limited testing and the use of the requirements for the structural steel and reinforced concrete provisions. The provisions are generally less prescriptive than those for structural systems that are composed of one structural material. The interfaces between the various elements in these systems are generally prescribed to be stronger than the connecting elements, to force the inelastic behavior into the various members.

The application of these provisions into design practice has not been widespread to date. One of the deterrents to the use of composite systems is the need to coordinate the structural steel and reinforced concrete trades, two subcontractors that have traditionally not needed to interact on any substantive basis. There are perceived schedule implications involved with such coordination that will lead directly to increased structural costs. Future work through additional testing and code provision development may help to ease this concern, through making the design approach more transparent.

Use of Base Materials with Special Properties, Such as Low Yield Point

The general trend in the production of structural steel over the entire one hundred year plus existence of the industry has been to strive for increased yield strength. Increasing yield strength allows for the reduction in steel tonnage, thereby reducing structural costs. This impetus has led to the development of 50 ksi materials for structural steels as the present standard production.

This approach makes perfect sense for standard design applications where the structural demands are always within the elastic range of response. In seismic design, though, it is expected that substantial yielding will occur during the design basis earthquake. The basic design philosophy, therefore, is to control the locations of yielding and inelastic deformation to areas that are predictable and reliable. When relying solely on the use of a single grade of structural steel, this can often result in a structural strength that is well above the minimum required by the code. For these systems, the use of *lower strength, high ductility* materials could be advantageous. In these cases, by using low strength materials, the remainder of the system could be designed to remain elastic more economically, but with the expectation of similar structural performance. For example, link beams in eccentrically braced frames could incorporate such steels, allowing the designer to better “tune” the design of the remainder of the system, including the foundation. In addition, the design of some structural systems, such as moment frames, has been controlled by code drift, rather than strength, requirements. Economically produced lower strength steel would be viable for these systems as well.

In Japan, at least one producer markets a plate material with an extremely low yield point (less than 20 ksi at initial yield) for special seismic applications. A more realistic level for structural applications in the United States may be in the range of 30 ksi. The biggest question will be the size of the market for such materials, since the cost of producing such a steel will not make sense unless a threshold level is achieved.

Development of Provisions for the Explicit Application of Damping in Steel Structures

Over the past decade, a number of systems have been developed to increase the level of damping in building structures as a means of reducing earthquake induced lateral displacements. Friction, viscous, visco-elastic, and hysteretic dampers have all been developed and implemented into building structures. The damping levels inherent in modern steel structures is lower than that of reinforced concrete or other materials, so it is likely that additional damping will be more effective. For most of these dampers, the ease of making the connection between the dampers and the members makes structural steel systems the most straightforward means of incorporating these elements.

Code provisions for the incorporation of damping into building structures are presently only in the development stages. The 2000 edition of the Building Seismic Safety Council's *Recommended Provisions for Seismic Regulations for New Buildings and Other Structures*, will include a new appendix on structures with damping systems. These provisions will be tested and applied on a trial basis, which will improve the procedures, and eventually lead to incorporation into model building codes. Increased design of systems with damping will undoubtedly result.

CONCLUSION

Triggered by the Northridge earthquake, the last six years has led to major developments in the seismic design of steel structures in the United States. The primary focus has been on improving the recommendations and code provisions for the design of moment resisting frame buildings. This focus has also resulted in improvements to all structural steel systems, through improved code provisions, and better design, fabrication, erection and quality control. With the conclusion of the FEMA/SAC project in 2000, the focus will shift to other issues, such as performance based design, application of advanced analysis techniques, the development of new systems, and the incorporation of damping elements directly into building structures. If the momentum and level interest generated on the moment frame issue can be channeled into these areas, it is likely that major advances can continue to be made in the seismic design of steel structures. These advances will be faster and more effective with cooperation and coordinated effort of researchers and code development bodies in the United States and other countries subject to earthquakes.

REFERENCES

1. American Institute of Steel Construction, *Seismic Provisions for Structural Steel Buildings*, 1997, with 1999 Supplement, Chicago, Illinois, 1997.
2. Federal Emergency Management Agency, FEMA 350 -*Recommended Seismic Design Criteria for New Steel Moment Frame Buildings*, prepared for FEMA by the SAC Joint Venture, Washington, D.C., July, 2000.
3. Federal Emergency Management Agency, FEMA 351 -*Recommended Seismic Evaluation and Upgrade Criteria for Existing Welded Steel Moment Frame Buildings*, prepared for FEMA by the SAC Joint Venture, Washington, D.C., July, 2000.
4. Federal Emergency Management Agency, FEMA 352 -*Recommended Postearthquake Evaluation and Repair Criteria for Welded Steel Moment Frame Buildings*, prepared for FEMA by the SAC Joint Venture, Washington, D.C., July, 2000.
5. Federal Emergency Management Agency, FEMA 353 -*Recommended Specifications and Quality Assurance Guidelines for Steel Moment Frame Construction*, prepared for FEMA by the SAC Joint Venture, Washington, D.C., July, 2000.
6. Building Seismic Safety Council, *2000 NEHRP Recommended Provisions for Seismic Regulations for New Buildings and Other Structures, Part 1- Provisions and Part 2- Commentary*, Washington, D.C., 2000.
7. International Conference of Building Officials, *Uniform Building Code*, Whittier, California.

MORE WORK IS REQUIRED

J Colin Taylor, Steel Construction Institute, UK.

In code drafting, “open questions” on connections issues include block shear, effects of hole spacing on bearing resistance, high strength steels, interaction of shear and tension in “friction grip” connections, long joints, design criteria for pins, resistance of fillet welds, deformation limits, end distance in backing plates, end distance for web “doubler” plates, circular yield lines, staggered holes and effects of packing on fully-threaded bolts.

The paper draws attention to potential research topics of practical use.

BLOCK SHEAR

Originally seen as an issue for bolted shear connections at beam ends, block shear is now also recognised as a potential failure mode at the ends of axially loaded bars. Two distinct types of block shear can occur, see Figure 1. At beam ends there is one failure plane in shear and one in eccentric tension, whereas in gusset plates there are two failure planes in shear, with one in pure tension.

Although AISC codes currently apply the same formula to both, other design codes such as Eurocode 3 use a formula only for the first type and cover the second type by rules for hole spacing combined with limits on bearing resistance.

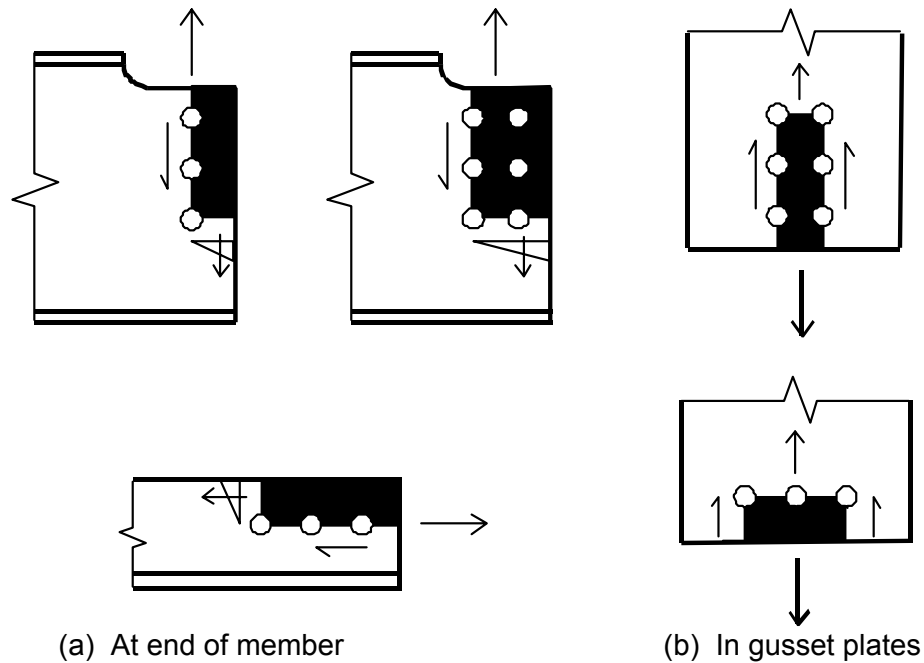


Figure 1: Block shear

As papers on gusset plates and block shear are scheduled for Session 6, further detail is not given here, except to make two clarifications. The calibration done for Eurocode 3 indicated that for beam ends the eccentricity of the tension component cannot be neglected. It also showed that for the net tension area the deduction for a single row of bolt holes is 0.5 times the hole size, but the comparable deduction for cases with two rows of bolts should be 2.5 times the hole size. This was determined by analysing the test results, but appears to be due to the outer bolt row being located nearer the peak tensile stress at the outer edge.

However the main point to note is that only 15 test results are available for block shear at beam ends. A total of 19 tests were performed, but 4 failed in other modes.

Another point is that block shear can occur at the end of an angle bar in tension, but in this case the effect is complicated by being combined with eccentricity of connection, shear lag of the unconnected leg and partial fixity of the end connection.

Finally, Figure 2 indicates a possible block shear failure mode for a welded end connection, but no test data appear to be available for this.

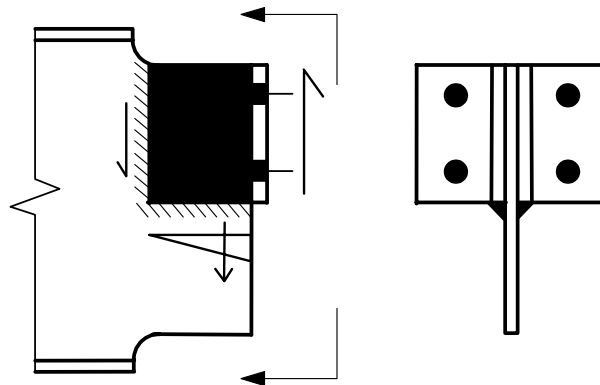


Figure 2: Block shear – welded cleats

BEARING

Amongst the criteria for bearing resistance of bolts is avoidance of block shear. The spacing and pitch of bolts, combined with code values for bearing stresses, are intended to cover this. However resistance to this form of block shear is a complex matter to predict. Failure is initiated when ultimate strain is surpassed at the critical point, but the total resistance is due to a combination of shear and tension, with shear lag and non-linear response. Thus the length and aspect ratio of the line of failure affect the resistance. It is probable that the shape of the stress-strain curve is also relevant, thus additional test results would be helpful in validating FE predictions and any improved design rules developed.

HIGH STRENGTH STEELS

Inevitably the majority of the design rules in codes were originally developed for mild steels with “classical” stress-strain curves, exhibiting a distinct yield point and an extensive yield plateau. Modern “concast” steels (with alloy content due to re-use of scrap) are different, especially the high strength and super strength grades. A number of design rules have been valid for such steels, but others have not. A first step would be a thorough survey of what further checks are needed. Pitch and spacing of bolts, edge and end distances, plus the effects of holes on various resistances, all seem to be candidates. Some traditional rules seem to be related to the

use of rivets or the avoidance of corrosion when exposed to rain, assuming outmoded protective coatings.

TENSION AND SLIP-RESISTANT CONNECTIONS

The distribution of the clamping force in a preloaded connection through the thickness of the connected plies is believed to be barrel-shaped, as indicated in Figure 3. The distribution at the outer surfaces is related to the contact areas under the head and nut of the bolt, strain compatibility modifying this elsewhere. The effect is commonly simplified in the form of an equivalent cylinder of the same axial compressibility.

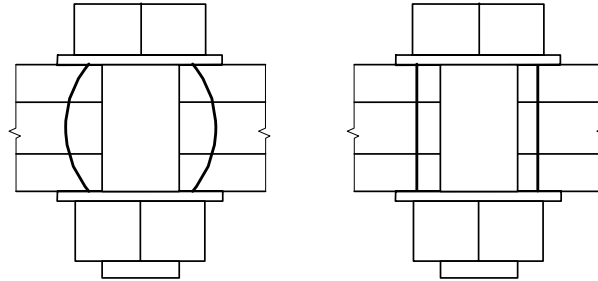


Figure 3: Pre-loaded bolts

The cross-sectional area of this cylinder affects the net clamping force available at interfaces in the presence of applied external tension. If the compressive strain in the connected material is neglected, the clamping force is reduced to zero when the applied tension is equal to the pre-load. The formula in Eurocode 3 indicating a residual clamping force in this case equal to 20% of the initial pre-load is based on a cylinder of compression with an area equal to 4 times that of the bolt.

The effective area of the bolt will be between the shank area and the tensile stress area, the value depending on the grip and the threaded length. The theory also assumes linear elastic behaviour at 1.2 times the pre-load, but the greatest uncertainty would appear to be the basis for the area ratio of 4. From Figure 3 this seems likely to vary with the thickness of the connected plies. The matter has been debated for many years but experimental evidence, for or against, seems to be lacking.

LONG JOINTS

The concept of a “long joint” is well established. A long joint can be either a bolted or a fillet-welded lap joint with force transfer in shear. Differential strain in the connected components leads to a non-uniform distribution of force. The end bolts fail before sufficient re-distribution is achieved to equalise the forces in each bolt. Similarly, in a welded joint the fillet welds fail at the ends before those near the centre can contribute to the transfer of force.

The problem in each case is that two quite different formulations have been developed, but the database of test results is quite inadequate to enable a clear decision to be made about the better alternative.

For bolts, a distinction needs to be made between cases where the shear resistance of the bolt, or the bearing resistance of the connected plates, governs. Where the bearing stress is high, the local deformation of the plates improves ability of the connection to re-distribute forces uniformly between bolts. This had been a source of confusion, but has now been established by additional tests, complemented by numerical analysis.

What remains at issue is the limiting length of a bolted joint in which a uniform distribution of forces can be assumed, when the shear resistance of the bolts governs. Some experts

maintain that non-dimensionality means that the limiting length must be proportional to the bolt diameter, as in Eurocode 3. The alternative analysis is that the differential strain to be overcome, and thus the limiting joint length, is related solely to the absolute length. Indeed as the ability of a bolt to deform in shear is related to the stress developed in it, not its diameter, substituting smaller diameter bolts of greater strength should increase the deformation capacity, not reduce it. This is of limited relevance, as it would also reduce the bearing resistance, which might well change the failure mode, thus avoiding the problem.

A number of tests are available and these form the basis of the AISC limiting length, which is expressed as an absolute value. However these were mainly done with 7/8th inch (22 mm) bolts and the small number of tests with other sizes is insufficient to be conclusive, given the scatter of results due to the influence of other parameters.

A comparable, but more complex, situation exists for fillet welds. In both cases more tests are needed, though there is also scope for complementary numerical analysis.

DESIGN OF PINS

Wide variations are evident between the design resistances for pins given in different codes. This appears to be related to different (often unstated) assumptions about the type of pinned connection envisaged. Where the reason for using a pin is to facilitate repeated de-mounting and re-assembly, there is a need to avoid irreversible deformation. Where the purpose is to provide the means for rotation, even elastic deformation must be severely limited. However pins are also increasingly used in situations where neither of these considerations applies, so the design criteria can be closer to those for bolts, always bearing in mind the absence of the benefits derived from the clamping effect of bolt tightening.

In particular many codes quote bearing resistances that are apparently based on strength criteria, but are in fact based on limiting deformations under service loads. What is needed is to identify more clearly the intended purpose of each limit. There is also a need to clarify the deformation limits needed for free rotation and for ease of de-mounting and re-assembly.

RESISTANCE OF FILLET WELDS

In the case of fillet welds, the work needed is not so much to acquire further test data as to devise an agreed systematic representation of what is already available, in the form of clear design rules. One problem area is the relation between electrode strength, strength of parent metal and resistance of fillet welds. Another is the consistent formulation of the resistance of a fillet weld to longitudinal and transverse forces at any angle to the throat.

Eurocode 3 relates fillet weld resistance to the tensile strength of the steel to be welded, subject to an over-riding requirement to use appropriate electrodes. However the dominant parameter is actually the tensile strength of the electrode, with only a secondary role for that of the steel.

This is compounded by the specification of electrodes by their yield strength and a policy of leaving electrode selection to welding engineers, instead of making it part of the structural design process. The inevitable result is to inhibit the use of high strength steels by keeping their design and specification beyond the scope of ordinary designers.

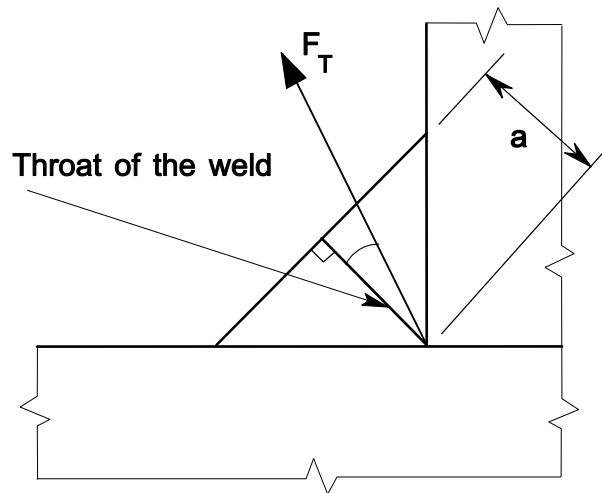


Figure 4: Fillet weld, transversely loaded at an angle to the throat

Eurocode 3 also relates the effects of the forces applied to a fillet weld to stresses calculated on the throat and combined using an IIV formula comparable to a Von Mises yield criterion. This ignores the fact that the failure criterion is rupture, not yield. The model ignores the offset between the throat and the fusion faces, which seems to be traded off against the effects of assuming that the fusion faces are pinned joints that do not develop moments.

As a result, the ratio of the resistance to a transverse force producing pure shear on the throat to that for one producing pure tension is 0.58 compared to the ratio of 0.75 based on tests. To avoid non-conservative results for pure shear, all transverse resistances are kept low, thus penalising the common case of force transfer parallel and perpendicular to the fusion faces.

Progress cannot be made without abandoning the IIV formula, in favour of one related to the actual resistance of fillet welds.

SLOTTED HOLES

With an increased use of slotted holes, both straight and “kidney-shaped”, has come a requirement for clarification whether bearing resistances need to be modified to suit them. Tests in the UK have led to two such reports and similar work on straight slots has been carried out in Belgium, the Czech Republic and the USA.

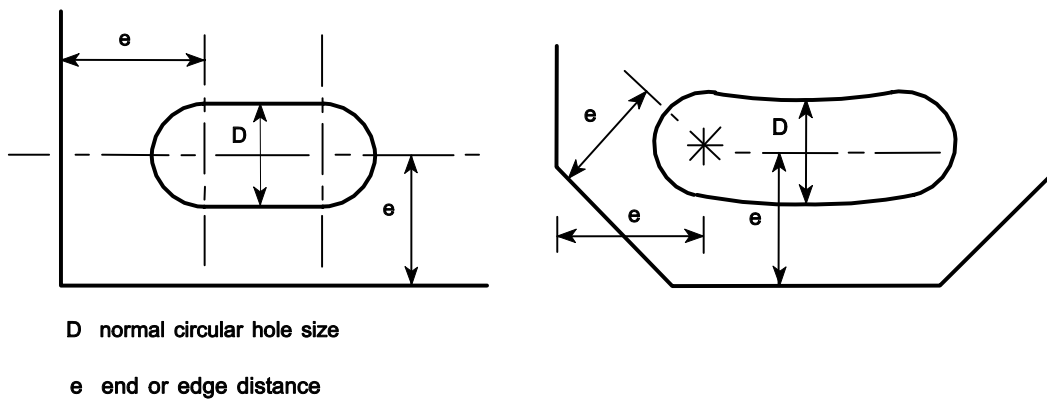


Figure 5: Slotted and kidney-shaped holes

Code rules for bearing resistance generally seek to cover numerous potential failure modes, of which the most critical is usually permanent deformation under service loads, provided that there is sufficient edge and end distance.

A surprising feature in the UK tests was that, compared to the bearing resistance for normal circular holes, a larger reduction appeared to be needed for slots 2.5 times longer than the normal hole size D than for those $3.5D$ in length.

It was also found that the reference tests for normal circular holes gave deformations different from those reported in earlier test programs. It would appear that other parameters such as spacing, pitch and edge distance, possibly in combination, may have a greater influence than previously thought. Other possibilities are material properties or the methods used to form the holes, but unless one of these is the cause, there seems to be scope for a more detailed study of the behaviour of plate material within multiple-bolted joints.

BACKING PLATES

Sufficient general test data is available to establish the behaviour of backing plates in augmenting the resistance of outstand flanges in T-stub type tension connections and to validate a design procedure. There is one glaring exception, the minimum value of the distance e needed from the end bolt to the end of the backing plate.

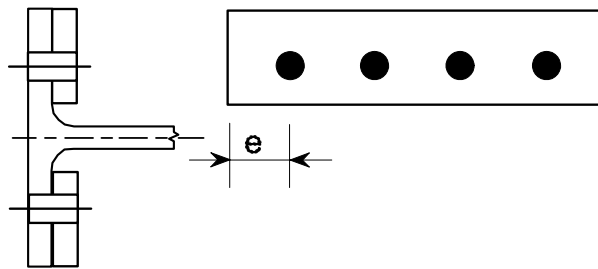


Figure 6: Backing plates

Existing tests have simply ensured that ample length was available to produce the normal pattern of yield lines assumed in design and where design rules give guidance it is no more than an assumption. In practice it may be important to reduce e as much as possible, so authoritative data would be valuable in enabling more reliable information to be given.

DOUBLER PLATES

A similar situation exists for column web doubler plates in joints without web stiffeners. The web doubler plate needs to continue above and below the beam flanges, but how far? There does not seem to be any test evidence for the required value of the dimension e .

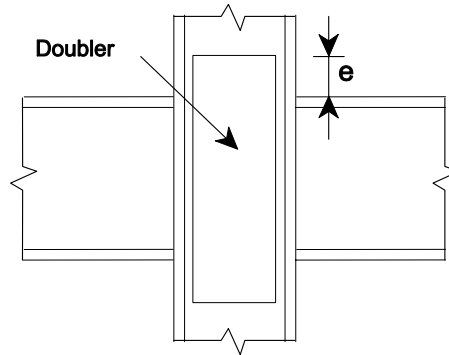


Figure 7: Web doubler plate in joint without web stiffeners.

CIRCULAR YIELD LINES

In a tension connection, if a plate is sufficiently thin, and the bolts are spaced sufficiently far apart and sufficiently far from the edge, the usually expected patterns of yield lines do not form. Instead circular yield lines develop in the form of a ring around each bolt.

If the load is increased, the plate around a bolt has been observed to deform in the form of a bell, but the design resistance is normally based on the point at which the circular yield line is fully formed, before gross deformation commences.

The design procedures in Eurocode 3 have so far been adapted to include circular yield lines as a further alternative to be considered when determining the length of equivalent T-stub. However forming circular yield lines also modifies prying action. It has been suggested that a better procedure might be to treat this as a limit on the resistance that can be developed by each bolt, as is done in the case of the “punching-shear” resistance of a bolt head or nut

Only a limited number of tests have produced circular yield lines, so additional test evidence would be useful in resolving this point.

STAGGERED HOLES

The same formula is given in numerous (but not all) codes for determining the deduction to be made for staggered bolt holes in calculating the net area. This seems to be based on tests many years ago when riveting was common. Extensive use of staggered holes used to be made in the flange angles and flange plates of riveted plate girders.

It seems likely that the rule was developed at a time when mild steel was the only strength grade of structural steel was in use in most countries. It is not clear to what extent the effects of strain hardening and the value of the ratio of yield strength to tensile strength may have been already covered in the formula, if as appears it is empirical. As modern test procedures include provisions that utilise these effects, there is a possible danger of “double counting”.

However there are few, if any, test results available to check this.

EFFECTS OF PACKING

The rules that appears in AISC codes, British Standards and Eurocodes have three different formats, but they are all based on one and the same test program. This found that introducing packing in bolted joints did not affect the shear or bearing resistance, but it did noticeably increase the deformation. Additional uniform deformation might not necessarily matter, increased deformation in one flange of a column, but not the other, could have more serious

consequences. Accordingly, the various code rules given are all aimed at limiting the additional deformation.

The joint tested used standard bolts. However for reasons widely documented elsewhere, use is now made of “fully threaded” bolts and it seems likely that joints through packing might deform more when made using fully threaded bolts. Indeed some designers have mentioned it as a reason for not using fully threaded bolts.

As a minimum, a test should be performed for fully threaded bolts, similar to that already carried out for normal bolts.

Moment-Frame Connection Qualification Criteria for Seismic Applications

Ronald O. Hamburger, SE
Chief Structural Engineer
EQE International, Inc.

ABSTRACT

Beam-column connections are critical to the performance of moment-resisting steel frames. Adverse connection performance can pose both local and global hazards. Loss of connection stiffness and strength can lead to the premature development of large interstory drifts and P-delta instabilities, while complete connection failure can result in local impairment of gravity load carrying capability. Despite the importance of connection behavior to frame performance, it is only in recent years that either the structural steel or reinforced concrete design specifications have adopted standardized connection qualification protocols. While these protocols represent a vast improvement over the qualitative procedures employed in the past, significant improvements can be made in these procedures. Connection qualification protocols should be based on total energy and displacement inputs that are representative of anticipated design loading, and should provide sufficient data to be useful in the performance-based design procedures currently being developed.

INTRODUCTION

Beam-column connections are essential to the behavior of moment-resisting frame structures, in their response to earthquake ground shaking. There are two basic functions these connections must perform. The most basic of these functions is to provide transfer of gravity loads from the beam to the column so that the beam remains attached to the structure. The second, and perhaps more critical function, is to provide rigidity against lateral sidesway and to provide for transfer of sidesway related flexural stresses between the beams and columns. The beam-column connection must retain the ability to perform both of these functions for the credible levels of loading likely to be induced by the combined effects of gravity and earthquake-induced loading.

Three primary properties have long been recognized as essential to the successful performance of beam-column connections. These are strength, stiffness and deformation capacity, or ductility. Prior to the 1994 Northridge earthquake, there were no consensus standards as to what constituted adequate strength, stiffness and deformation capacity for moment-resisting connections. In general, there was informal agreement among researchers and engineers, that connections capable of developing the nominal strength of the weakest of the connected members, through a cyclically applied plastic deformation of perhaps 0.02 radians should provide adequate service. However, the widespread connection damage experienced by steel

frames in the 1994 Northridge earthquake, recognition by the building codes that probable drift demands on structures can be significantly larger than 0.02 radians, and the move by the concrete industry to develop precast concrete moment-resisting frame systems, lead to the recent adoption of a series of standard criteria, or protocols, for the qualification of moment-resisting connections, as adequate for service.

Current American Institute of Steel Construction design specifications (1) categorize connections either as fully restrained (FR) or partially restrained (PR). For fully restrained connections it is required to be demonstrated by test of at least two prototypical connections that the connection assembly is able to maintain the angle between interconnecting members, while developing at least 80% of the plastic moment capacity of the weakest of the connected members, through a prescribed pattern of ramped, static, cyclic deformation that includes at least one full cycle of deformation at a plastic deformation of 0.03 radians. Partially restrained connections also may be utilized, provided that they at least have the strength to resist code-specified seismic loads in combination with other loads, can accommodate the same rotations specified for type FR connections, and provided that it can be shown by rational analysis that the additional deformation due to connection flexibility can be accommodated by the building considering potential instability due to P-delta effects.

The American Concrete Institute has also recently published criteria for connection qualification (2), for use with construction of precast concrete moment-resisting frames, intended for seismic applications. This document has similar requirements to the protocol specified for qualification of connections by AISC, except that only one prototype connection assembly need be tested and the maximum deformation of the prototype test is somewhat smaller than that specified for similar steel systems.

There is room for improvement of both of these somewhat similar, albeit different connection prequalification protocols. An ideal protocol should be equally applicable to systems of either material, as well as to composite systems, and should be appropriate to the performance-based design methodologies currently being developed. As part of a large, multi-year, federally funded program to address the connection damage that occurred in the Northridge earthquake, the SAC joint venture recently published recommended criteria for connection qualification (3) that can serve as a model for such improved connection prequalification protocols. This paper provides an overview of these criteria.

PERFORMANCE-BASED DESIGN METHODOLOGIES

Building codes in the United States are rapidly moving towards the adoption of performance-based design procedures for earthquake resistance, as well as for other hazards buildings are designed to resist, such as fire. Figure 1 below presents a generalized flow chart for performance-based design procedures. The process starts with the identification of a series of performance objectives, which the design should be capable of meeting. In the case of earthquake-resistant design, these performance objectives consist of specifications of the permissible amount of structural damage, given earthquake hazard levels. Next a conceptual and preliminary design for the structure is developed. It is then necessary to verify that this design will be capable of meeting the intended performance objectives, and if it is incapable of doing this, to revise the design until successful verification can be performed. There are three basic methods available for demonstrating that a design can meet the desired performance goals. It is

possible to perform calculations, using rational principles of engineering mechanics; it is possible to build one or more prototypes of the design and test them to demonstrate adequate performance capability, or the design can be proportioned and detailed to conform to prescriptive, deemed-to-comply standards.

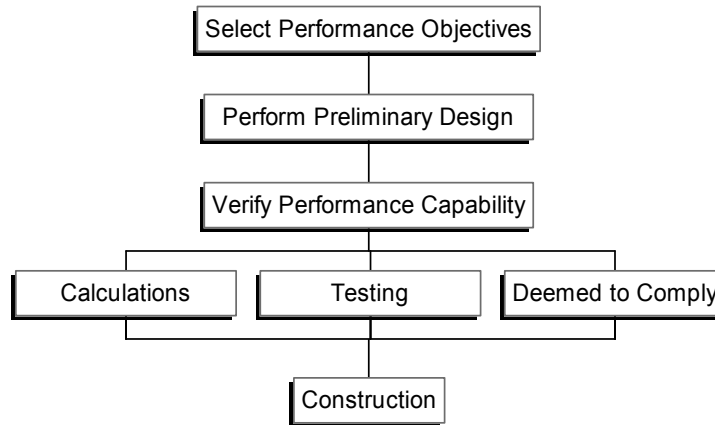


Figure 1 – Generalized Flow Chart for Performance-based Design

Most building codes in effect in the United States today adopt a series of seismic performance objectives based on the recommendations of SEAOC (4). These objectives are typically expressed in a matrix format that ties permissible damage to buildings in various occupancy categories to the severity of earthquake hazards. The version of this matrix adopted into the commentary to the *1997 NEHRP Provisions* (5), which form the basis for seismic provisions contained in the new International Building Code 2000 (6) is presented in Figure 2.

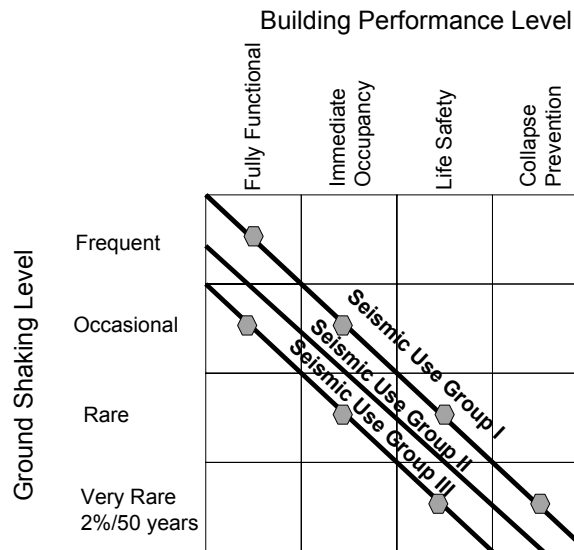


Figure 2 – Building Performance Matrix in 1997 NEHRP Provisions

In this matrix, performance is expressed as conforming to the “Fully Functional,” “Immediate Occupancy,” “Life Safety” and “Collapse Prevention” levels. The Fully Functional and Immediate Occupancy levels are similar with regard to structural performance and represent a state in which no significant impairment of structural stability, strength or stiffness has occurred.

The Collapse Prevention level represents a state of near complete structural degradation and impending collapse. The Life Safety level is an intermediate state, in which substantial structural damage is permitted, but in which margin remains, relative to the onset of collapse. Earthquake hazards are expressed in terms of the probability of exceedance of ground shaking intensity. For most buildings, classed as Seismic Use Group I, the basic performance objective is to provide Collapse Prevention, or better, performance for hazards with a 2% probability of exceedance in 50 years. For buildings with large occupancies (Seismic Use Group II) and buildings housing critical emergency response facilities (Seismic Use Group III), better performance is targeted. For all of these Seismic Use Groups, it is anticipated that in the event of more probable and less severe ground shaking, progressively better performance would be obtained.

Until the 1994 Northridge earthquake, nearly all design, and in fact, most design performed today, relied on the use of prescriptive, deemed-to-comply standards to demonstrate adequate performance capability. However, when it was discovered that the prescriptive, deemed-to-comply, moment-resisting connection contained in the building codes at that time was subject to premature failure, this option for design of steel moment-resisting connections was removed from the building code. In its place, the *Uniform Building Code (UBC)* (7) and the AISC Seismic Provisions (1) substituted a requirement that connections be qualified by a combination of testing and calculation. The *UBC* provided little guidance on how to perform such testing and calculations, however, *Interim Guidelines* (8) developed by the SAC Joint Venture, recommended the use of a minimum of 2 prototype specimens, tested using the ATC-24 (9) protocols, and demonstrated capable of sustaining 0.03 radians of plastic rotation without significant strength degradation. This recommendation was quite arbitrarily selected, and represented the best judgement of the participants in the SAC project, rather than a criterion that had been rigorously demonstrated to be capable of providing adequate performance. Despite the arbitrary nature of this qualification protocol, the AISC Seismic Provisions adopted these recommendations, in modified form into Appendix S and they remain the basis of connection qualification for steel structures in the building code today.

CONNECTION PERFORMANCE PARAMETERS

Figure 3 presents, a simplified, but representative hysteretic plot for a typical cyclic test of a ductile, fully restrained moment-resisting connection. Several important regimes of behavior can be observed in this figure. First there is the region of elastic behavior, characterized by repeatable linear response at low levels of deformation input. As deformation level is increased, nonlinear behavior initiates, and is characterized both by increased strength, as plasticity spreads through the section and strain hardening initiates. At the deformation level labeled θ_{SD} in the figure, peak assembly strength will be attained and beyond this point connection strength will degrade. This behavior may be controlled by buckling of the connection plates or beam flanges, or by initiation of fracture in one of the connecting elements. If fracture does not occur at the point of peak strength in the assembly, it will eventually occur at some larger deformation level. Finally, at very large deformation levels, if the test is continued, the connection will experience a complete failure and will no longer be able to fasten the beam to the column for transfer of gravity shear forces. Partially restrained connections will experience similar behavior modes, though the shape of the hysteretic curves will typically be somewhat more pinched than those shown for this fully restrained connection.

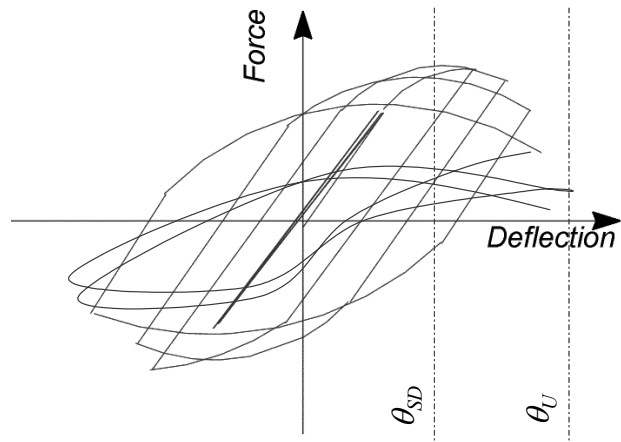


Figure 3 – Representative Force-Deformation Hysteretic Curve for Connection

Beyond considerations of the ability of the connection to provide transfer of beam shears resulting from gravity loading, the characteristics of connections that are important to assessment of the structure's overall behavior are those that affect how much lateral drift will be induced in the structure, when subjected to ground shaking. The global capacity of a moment-resisting frame is typically controlled by large drifts which result in the onset of p-delta instabilities. The onset of these p-delta instabilities relate primarily to the secondary stresses induced by geometric nonlinearity but can be significantly augmented by the onset of instantaneous negative stiffness in the connection assembly, such as is exhibited in Figure 3, above, at deformations larger than θ_{SD} . Nonlinear analyses conducted under the SAC program of investigations (10) have shown that the important properties of moment-resisting framing, and the connection assemblies that comprise this framing are elastic strength, elastic stiffness, the deformation at which strength degradation initiates, and the ultimate deformation capacity of the assembly, indicated as θ_U in the figure.

SAC RELIABILITY FRAMEWORK

The SAC program of investigations include thousands of nonlinear response history analyses of building frames and nearly two hundred connection assembly tests, resulting in a large database of statistics on the seismic behavior of frames. In order to implement this data into a series of rational performance-based design criteria, the SAC program used a statistical, structural reliability formulation that is similar in concept and approach to the load and resistance factor design approaches contained in the AISC specifications (11). In this approach, interstory drift angle, rather than force, is used as the primary design parameter. As implemented in *FEMA-350* (3) frame design is evaluated for adequacy by analyzing the frame for design earthquake loading, determining the maximum interstory drift induced into the frame by the design earthquake shaking, factoring this interstory drift with demand factors that account for the uncertainty and variability inherent in demand calculation as well as bias inherent in the analytical method employed, and comparison with interstory drift capacities, that have been factored by resistance factors to account for uncertainty and variability inherent in capacity estimation. The basic design equation is in the form:

$$\lambda = \frac{\gamma_a D}{\phi C}$$

The demand and resistance factors are determined as products of integration of the probability that demand will exceed capacity, over the hazard curve for the site, which is an expression of the probability that ground shaking demands of given intensity will occur. The formulation for calculation of these products of integration are as follows:

$$\gamma = e^{\frac{k}{2b}\beta_{RD}^2}, \gamma_a = C_B e^{\frac{k}{2b}\beta_{UD}^2}, \phi = e^{\frac{k}{2b}(\beta_{UC}^2 + \beta_{RC}^2)}$$

When drift demand is evaluated for ground shaking hazards with a specific probability of exceedance, for example 2% in 50 years, and the factored demand-capacity ratio λ has a computed value of unity, this indicates mean confidence that drift demands will not exceed drift capacity, at this probability of exceedance. Computed values of λ less than unity indicate greater than mean confidence and values greater than unity indicate less than mean confidence. Confidence is specifically computed based on the number of total logarithmic standard deviations in uncertainty, β_{UT} , that λ lies above or below unity. The values of the various measures of uncertainty and variability have been established based on the results of the SAC investigations.

The *FEMA-350* design criteria are intended to provide approximately a 90% level of confidence that buildings will have less than a 2% probability of experiencing earthquake induced interstory drift that could result in development of global instability in a 50 year period. They are also intended to provide approximately a 50% confidence level that there is less than a 2% chance in a 50 year period that earthquake induced drift in a building will exceed the ultimate capacity of connections, θ_U . This performance capability may be demonstrated by calculation, using the factored demand-capacity ratio as described above, or alternatively, a deemed-to-comply approach may be used. Included in *FEMA-350* are a series of prequalified connections that when detailed as indicated in the document, and used in frames that conform to the strength, stiffness and other criteria contained in the document, are deemed to be capable of providing this performance capability.

The process of connection prequalification is based on a developmental program that includes an analytical model that predicts the behavior of the connection, and that can be used to explore the important connection design parameters including the relative strength of beams and columns, the panel zone strength, and the size and weight range of the structural shapes, as well as laboratory testing of sufficient full scale specimens to confirm that important behavioral modes are predictable throughout the range of design parameters for which the prequalification is to apply. As a minimum, five prototype assemblies must be subjected to prototype testing.

Under the SAC program, assemblies were subjected to two basic types of loading protocols. One of these is a slightly modified version of the ATC-24 (9) loading history. This loading history was modified to more closely represent the typical energy input to moment-connections in frames subjected to ground shaking demands with a 2% probability of exceedance in 50 years. The modified ATC-24 protocol is representative of the demands placed on connections that are subjected to moderately long duration shaking, but which are not located in the near field of the fault rupture. The second loading history was developed to represent the typical demands on a moment-resisting connection anticipated when a frame is subjected to ground shaking dominated

by strong velocity pulses, such as is typical of the fault normal component of ground shaking, within a range of few kilometers of the fault rupture.

The two loading histories can affect connections in very different ways. Under the modified ATC-24 protocol the connection is subjected to a large total energy input, however, at large levels of cumulative input energy, the strength of the connection has typically degraded, due to buckling of connection elements, and as a result, the amount of force imposed on individual connection elements may be limited. In the second, near-field protocol, a large displacement cycle, to 0.06 radians total displacement, is imposed at the onset of testing, and is then followed by repeated cycles of lower level excitation. The peak strength of the connection assembly is typically larger under this protocol, as during the first large pulse loading, buckling has not yet accumulated and strength degradation has not occurred. The result is that force-sensitive portions of the connection that are protected by cyclic degradation of other parts of the assembly, when loaded using the ATC-24 approach, may see larger demand and fail, under the near-field protocol. It should be noted that the SAC project only applied this near-field protocol to a few connections and in each case it was found to result in acceptable connection behavior, that is, failure did not occur. However, all of these tests were on welded fully restrained connections. It is possible that the near-field protocol could control on some types of connections.

For successful prequalification under the SAC criteria connections intended for use in Special Moment Frame (SMF) service are required to be capable of providing median total interstory drift angle capacities at strength degradation, θ_{SD} , of 0.04 radians and median ultimate interstory drift angle capacities, θ_U , of 0.05 radians. For Ordinary Moment Frame (OMF) service median strength degradation interstory drift angle capacity θ_{SD} , of 0.02 radians and ultimate capacity θ_U of 0.03 radian are required. In addition, the coefficient of variation for these capacities, as obtained from test data, are required to be less than 20%. If larger coefficients of variation are obtained from the testing, then the drift angle capacities indicated above are applied to the mean minus one standard deviation, rather than to the median value. These limiting drift angle capacities, used by the SAC project were selected based on the analyses of prototype buildings that were performed as part of the project investigations. Specifically, prototypical designs for 3 story, 12 story and 20 story buildings were developed and analyzed for response to design level ground shaking. The statistics from these analyses were used to develop the logarithmic standard deviations relating to uncertainty and variability used in determining the demand factors. In these analyses, it was assumed that connections had the characteristics represented in the acceptance criteria indicated above.

In the SAC program, in addition to being used to demonstrate that a connection can be prequalified for SMF or OMF service, that is capable of being used in a deemed-to-comply manner, laboratory testing is also used to provide data necessary to application of performance verification using the factored demand-capacity ratio. Specifically, the median value of θ_{SD} obtained from testing is taken as the local, or connection level, acceptance criteria for Immediate Occupancy performance. The median value of θ_U is taken as the local, or connection level, acceptance criteria for Collapse Prevention performance. The standard deviation of the log of the θ_{SD} and θ_U values obtained from testing are respectively used to calculate the resistance factors, as previously described.

The SAC studies focused primarily on frames incorporating full strength, fully restrained connections. However, the framework is equally applicable to connection details that are not

capable of fully restrained behavior and also to connection details that are not capable of developing the full strength of the connected members. To properly extend the SAC approach to frames incorporating such connections, it would be necessary to develop designs of prototype buildings that incorporate such connections, and to perform sufficient nonlinear analyses of these prototype buildings to obtain the statistical quantities necessary to derive the various demand and resistance factors.

In order to simplify the classification of connection prequalifications, the current system of connection designation, either as fully restrained or partially restrained, should be revised. An improved system could include classification of connections as full strength – full stiffness, full strength – partial stiffness, partial strength – full stiffness, and partial strength – partial stiffness. The behavior and response of framing systems incorporating connections having each of these characteristics should then be independently determined, using prototype designs, in order to determine the necessary strength and stiffness limits needed to reliably meet the design performance objectives previously described.

SUMMARY

Current AISC and ACI criteria for the qualification of connections for suitability for service in deemed-to-comply designs of frames intended for seismic applications currently consider only the plastic rotation capacity of the connection, relative to a single behavior condition, strength degradation. However, the deformation at which strength degradation occurs should not be the only parameter considered when demonstrating the suitability of a connection for seismic service. As seen in the case of many steel buildings damaged by the Northridge earthquake, strength degradation of individual connections, even through such undesirable behaviors as the onset of brittle fracture, is not by itself, either a life threatening or limiting behavior for the moment-resisting frame. Frames can tolerate extensive damage to individual connections without experiencing either partial or total collapse.

Connection qualification criteria should consider the ultimate global behavior of the frame of which the connection is a part, as well as the local behavior of the individual connection. Further, the criteria should be rationally tied to the performance levels and exceedance probabilities of interest in modern, performance-based design approaches.

The reliability framework adopted by the SAC project in the development of recommended criteria for the design of moment-resisting steel frames is a rational approach that considers the important behaviors of structural framing systems, and allows direct incorporation of component test data including consideration of uncertainty and variability in demand and capacity prediction. In the FEMA-350 publication, this framework has been used to present a consistent series of criteria for the qualification and prequalification of connection designs for service in SMF and OMF systems. This approach can be modified to apply to other types of construction and can be used to develop appropriate connection qualification criteria for these other systems.

ACKNOWLEDGEMENT

The information presented in this paper is largely based on research performed by a number of investigators under the FEMA/SAC program for reduction of seismic hazards in moment-resisting steel frames. The author wishes to acknowledge the support of the Federal Emergency

Management Agency, and specifically, FEMA's project officer, Mr. Mike Mahoney and FEMA's technical advisor, Mr. Bob Hanson, without whose assistance, this work would not have been possible. The author also wishes to acknowledge the contribution of the numerous researchers and engineers whose work contributed to the development of this material. In particular, the author wishes to acknowledge the contributions of Messrs. C. Allin Cornell, Douglas Foutch, Helmut Krawinkler, Stephen A. Mahin and James O. Malley for their invaluable assistance and contributions.

NOTATION

b	coefficient relating the change in drift demand to the change in ground shaking severity
k	slope of the hazard curve in logarithmic coordinates, evaluated at the design probability of exceedance
C	interstory drift capacity
D	computed interstory drift demand
β_{RC}	standard deviation of the natural logarithm of the variability in capacity as a function of hazard
β_{RD}	standard deviation of the natural logarithm of the variability in demand as a function of hazard
β_{UC}	standard deviation of the natural logarithm of the uncertainty in capacity as a function of hazard
β_{UD}	standard deviation of the natural logarithm of the uncertainty in demand as a function of hazard
β_{UT}	total logarithmic standard deviation in uncertainty calculated from the logarithmic standard deviation relating to uncertainty in demand and capacity, considering any cross correlation between demand and capacity
ϕ	resistance factor that accounts for uncertainty and variability inherent in drift capacity estimation as a function of earthquake hazard level
γ	demand variability factor that accounts for the variation in maximum demand, as a function of earthquake hazard level
γ_a	demand uncertainty factor that accounts for uncertainty and bias inherent in calculation of drift demand
λ	factored demand to capacity ratio
θ_{SD}	interstory drift angle at which peak connection assembly strength is attained
θ_U	interstory drift angle at which connection loses the ability to transfer gravity shears from the beam to the column

REFERENCES

1. American Institute of Steel Construction, *Seismic Provisions for Structural Steel Buildings*, April 15, 1997, AISC, Chicago, IL
2. American Concrete Institute, *Connection Qualification Program for Precast Concrete Joints*, Report No. ITG-1, 1999, ACI, Northbrook, IL
3. SAC Joint Venture, *Recommended Seismic Design Criteria for New Steel Moment-Frame Buildings*, Report No. FEMA-350, June, 2000. Federal Emergency Management Agency, Washington, D.C.

4. Structural Engineers Association of California, *Vision 2000, A Framework for Performance-Based Earthquake Engineering*, 1996, SEAOC, Sacramento, CA
5. Building Seismic Safety Council. *NEHRP Recommended Provisions for Seismic Regulation of New Buildings and Other Structures, and Commentary, Reports No. FEMA-303 and 304*, 1998, Federal Emergency Management Agency, Washington, D.C.
6. International Code Council, *International Building Code-2000*, February, 2000, ICC
7. International Conference of Building Officials, *Uniform Building Code, 1997 Edition*, 1997, ICBO, Whittier, CA.
8. SAC Joint Venture, *Interim Guidelines for Evaluation, Inspection, Repair, Upgrade and Design of Welded Steel Moment Frame Structures, Report No. FEMA 267*, August, 1995, Federal Emergency Management Agency, Washington, D.C.
9. Applied Technology Council, *Guidelines for Seismic Testing of Components of Steel Structures, Report No. ATC-24*, 1992, ATC, Redwood City, CA
10. Krawinkler, H., *State of the Art Report on Systems Performance, Report No. FEMA-355C*, September, 2000, Federal Emergency Management Agency, Washington, D.C.
11. AISC, *Load and Resistance Factor Design Specifications*, 1993, AISC, Chicago, IL

Seismic Behavior of Steel Braced Frame Connections to Composite Columns

Charles W. Roeder, Gregory MacRae and Christopher Waters
University of Washington

ABSTRACT

Concrete filled tubes (CFT) offer large axial stiffness and load capacity and are suitable for columns in braced frames. However, brace-to-beam-to-column connections are a concern. Past designs vary widely, and their seismic behavior is uncertain. Past applications of CFT columns in braced frames are summarized. The difficulties in connection design are discussed, and nonlinear computer analyses to evaluate the seismic performance of these connections are reviewed. An experimental investigation of the connection performance will be performed.

INTRODUCTION

Concrete filled tubes (CFT) columns have been used for seismic resistant construction, because they offer significant advantages over either steel or reinforced concrete. The concrete provides compressive strength and stiffness to the steel tube and restrains local buckling. The steel tube provides formwork to the concrete, minimizes the cost of the concrete placement, reinforces the concrete for axial tension, bending and shear, and enhances the ductility of the column. CFT columns are particularly well suited for braced frames, because large axial strength and stiffness are needed. This combination is particularly desirable for seismic design, because braced frames are very efficient for seismic design, and lateral loads place great demands on the columns. Further, seismic design requires a combination of strength, stiffness and ductility from the structural system.

While CFT columns are desirable for braced frames, there is little guidance regarding the design and construction of connections between the braced frame and the CFT columns. Variations of brace-to-beam-to-column connections (BBC connections) have been used, but there has been no research regarding the seismic performance of these connections. As a consequence, the seismic behaviors of the alternative BBC connections are not understood, and the relative economy of the various alternatives is uncertain.

PAST APPLICATIONS

A number of buildings have been constructed with braced frames and CFT columns. This usage appears to have initiated in the United States. CFT columns have been widely used in Japan and other countries well before they were commonly used in the US, but the usage in these other countries has primarily been with moment resisting frames. The first U.S. high-rise project (Hooper et al. 1) with CFT columns was the 100 First Street Plaza in San Francisco, California. This building is illustrated in Fig. 1. It is 27 stories tall, and it employs a braced frame with moment connections and CFT columns at the four corners of the braced core. Since that period, other braced frame buildings with CFT columns have been constructed. Building heights have been up to 60 stories. A building with more than 100 stories has been designed but not constructed. Other structures, such as the University of Washington football stadium, also used variations of this structural system.



Figure 1. First Street Plaza Building Constructed with Braced Frames and CFT Columns

While different buildings have used braced steel frames with CFT columns, a wide range of BBC connections have also been employed. Figure 2 schematically shows several of these connection alternatives. The alternatives illustrated in Figs 2a and 2b employ large gusset plates that penetrate into the CFT column. In Fig. 2a, the gusset plate has a number of shear connectors to help distribute the brace and beam forces and moments between the steel and concrete in the CFT column, while Fig. 2b has a plain gusset plate with no shear connectors. Figure 3 illustrates another detail that has been used occasionally. Shear connectors are attached to the inside of the tube to help distribute moments and forces between the steel and

the concrete, but the brace and the beam are attached to the steel tube with a typical steel-to-steel connection. Braced frames with CFT columns have been frequently used in the US, but seldom used in Japan. However, at least one recent braced frame building in Japan has employed CFT columns, and the BBC connections for this building are schematically shown in Fig. 2d. Japanese engineers commonly use CFT columns with moment resisting frames, and they use an internal diaphragm connection. Figure 2d is a variation of the internal diaphragm connection. The diaphragms penetrate into the tube and interlock with the concrete fill. This interlock should help distribute brace and beam loads to the steel and concrete of the CFT column. This later connection requires four complete joint penetration welds around the perimeter of the tube at each beam-column intersection.

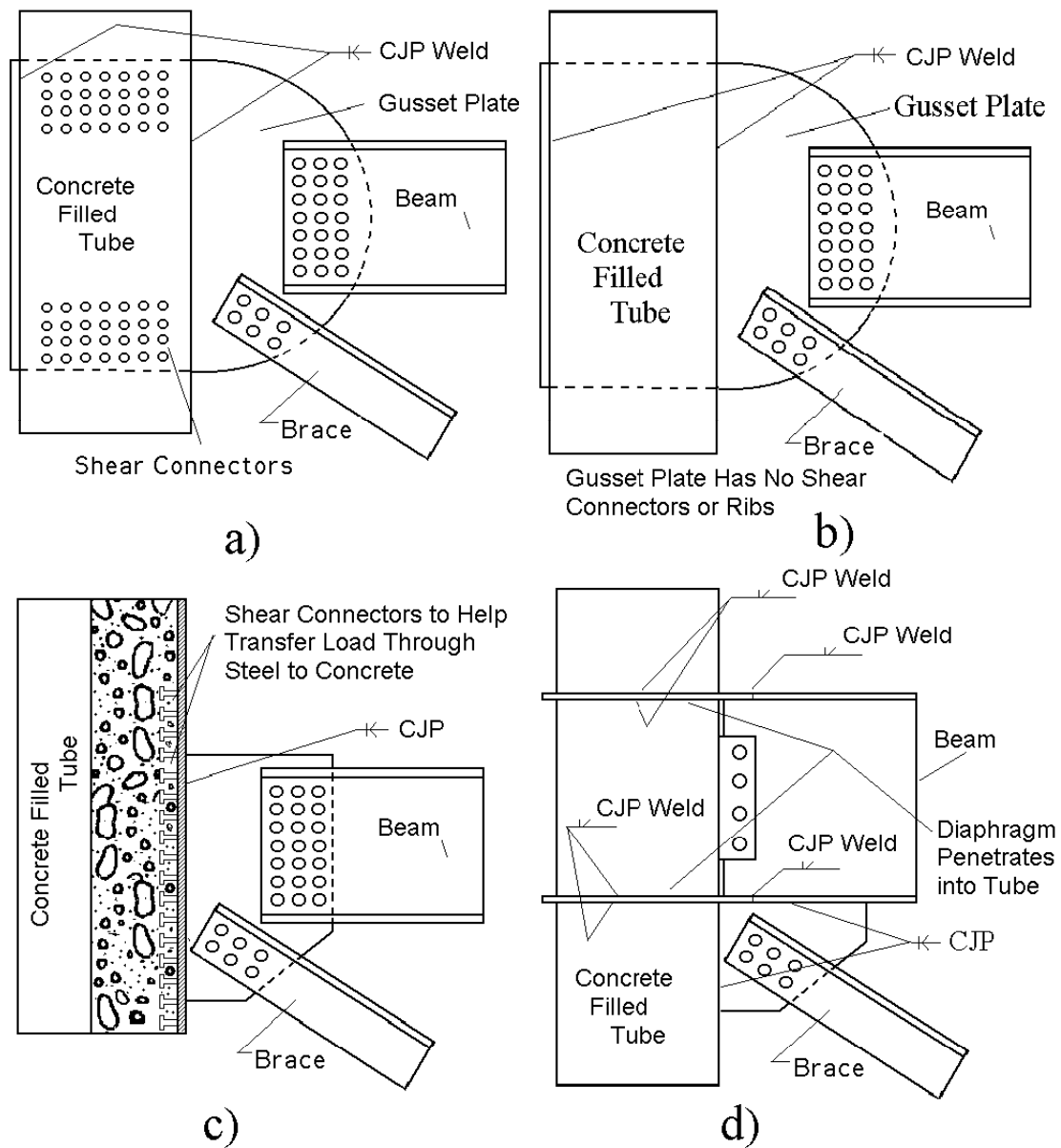


Figure 2. Typical Brace-Beam- Column Connections for Braced Frames with CFT Columns

SEISMIC DEMANDS

Seismic design is performed so that the building remains elastic and completely serviceable during and immediately after small frequent earthquakes. Significant inelastic deformation is permitted during large earthquakes that have a small probability of occurrence. The inelastic deformation changes the stiffness of structure and dissipates energy, and these combine to provide moderate building response during major earthquakes at significantly reduced initial cost of the structure. The consequence of this inelastic deformation is permanent yielding and deformation of the structure. Therefore, the engineer must assure that the structure retains its basic integrity during these severe earthquakes without building collapse or loss of life. This multi-level performance design procedure requires that the engineer consider the strength, stiffness, ductility and inelastic performance of the system. The inelastic performance of braced frames is dominated by yielding and buckling of the braces. Columns assist in resisting the lateral loads, but they also support gravity loads and prevent collapse of the structure. Connections transfer moments and forces from member to member. Premature failure or fracture of the columns or connections results in poor performance which defeats the goals of the seismic design approach. As a consequence, seismic design requirements (AISC 2) for braced frames require that the brace be the weak link. The connections and the columns are designed to be strong enough to sustain the full compressive buckling load and the full tensile yield load of the brace. Inelastic deformation of the braces is tolerable, since it

- retains the economy of the design,
- limits forces delivered to columns, connections and other elements, and
- benefits the inelastic response of the structure.

However, the inelastic buckling and deformation of the brace places additional demands on the connection. All of these requirements must be satisfied with full consideration of the inelastic structural deformation and the uncertainty in material properties and performance of the as-built structure.

As a consequence of this design method, one key issue in the seismic design of braced frames with the CFT columns is the determination of whether the BBC connections are able to achieve these objectives. These connections must develop and retain the resistance necessary to transfer brace and beam forces and moments, while the structure and the bracing members sustain large inelastic deformations. The BBC connection must also distribute these forces and moments between the steel tube and the concrete fill if the CFT column is to perform as required. Multiple requirements must be achieved if this performance goal is to be met. First, the steel tube serves as tensile reinforcing to the CFT column, and so the tensile force must be distributed to the steel tube. Second, the concrete fill stiffens and strengthens the steel for compressive load, and so the compressive force must be distributed between the concrete and the steel. Third, the steel tube serves as sole flexural reinforcement to the concrete, and therefore the steel tube must either carry the full bending capacity of the column or it must at least resist all tensile stress due to bending moments. Finally, the steel acts as shear reinforcement to the concrete, and so shear forces must be distributed between the steel and concrete in some appropriate manner. This complex distribution of force is not magically achieved. It requires that there either be reliable shear stress transfer between the steel tube and the concrete fill as illustrated in Fig. 3, or as an alternative, the BBC connections must aid in the force distribution and transfer.

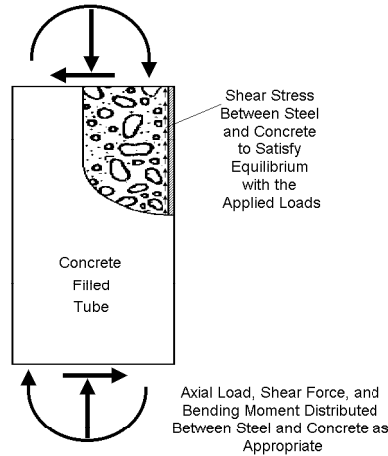


Figure 3. Stress Transfer Between Steel and Concrete

POTENTIAL PROBLEMS IN DESIGN OF THESE CONNECTIONS

The ability to achieve the shear stress transfer required by equilibrium and illustrated in Fig. 3 is an issue of some concern. Past research evaluated this shear transfer (Roeder et al. 3, and Roeder 4), and the shear transfer demands are found to be large and very localized as illustrated in Fig. 4. This figure shows that the force or moment that is applied to either the steel tube or the concrete fill must be appropriately shared with the other material in a very short distance (usually much less than one tube diameter). Braced frames place large demands at every BBC connection. If the shear stress transfer capacity between the steel tube and concrete does not exceed the demand, slip occurs and causes permanent changes to the steel concrete interface.

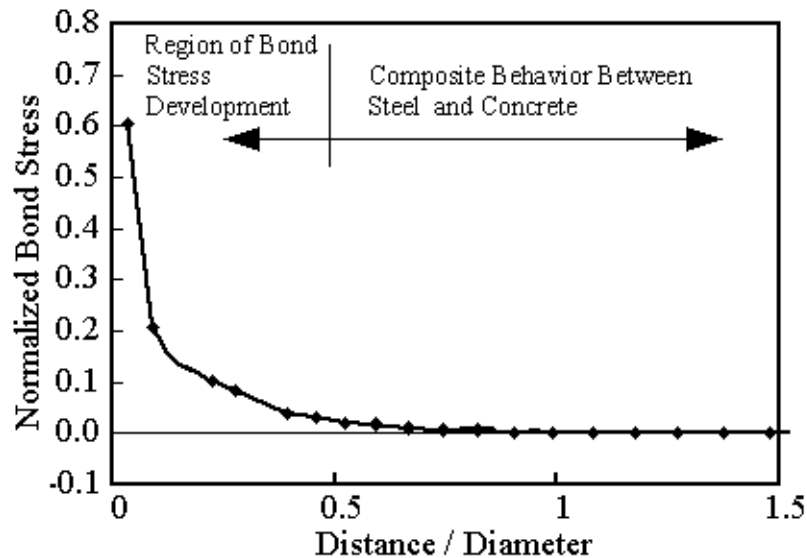


Figure 4. Distribution of Stress Transfer Demands

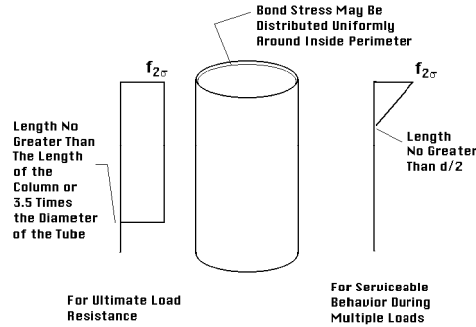


Figure 5. Proposed Bond Stress Evaluation Model for CFT

The shear stress transfer capacity was evaluated (Roeder et al. 3, and Roeder 4) for CFT elements, and the important engineering criteria for safety, serviceability and economy are -

- shear connectors are not needed when the natural shear transfer capacity exceeds the demand, but
- mechanical shear transfer must be employed for the full transfer requirement whenever demand exceeds capacity.

At the ultimate load performance level, shear transfer demand can be uniformly distributed over the perimeter of the tube and a length equal to the smaller of the column length or 3.5 times the tube diameter as illustrated in Fig. 5. At the serviceability limit state, the triangular shear stress demand distribution can be used over a length equal to one half the diameter of the tube. The shear transfer capacity was shown to be a function of the tube diameter, d , and diameter to thickness ratio, d/t . The shear stress capacity that is two standard deviations below the mean capacity, $f_{2\sigma}$, is

$$f_{2\sigma} = 1.24 - 0.0702 (d/t) + 0.0029 d \quad (\text{in MPa and } d \text{ is in mm}) \quad (1)$$

The transfer capacity is effectively zero for tubes with large diameter and large d/t ratio, because of separation that may occur between the steel and concrete and the limited confinement provided by thin tubes. Most CFT columns used in the US are large diameter tubes with large d/t ratios, and so the natural shear stress transfer is clearly inadequate for seismic design of most BBC connections.

INELASTIC COMPUTER ANALYSIS

The shear transfer demands needed to make the CFT column a functional part of the braced frame as illustrated in Fig. 3 exceed the shear transfer capacity available within most CFT columns. Therefore, the BBC connection must aid in this transfer, or mechanical transfer devices must be employed within the critical area (see Figs. 4 and 5) of the CFT columns. A series of non-linear analyses with the ABAQUS computer program were completed to evaluate these options. Most BBC connections used for seismic design of buildings employed penetrating gusset plate connections as illustrated in Figs. 2a or 2b. The penetration of this gusset plate should help to distribute moments and forces between the steel tube and the concrete fill, and so variations of these connections provide the basis of the nonlinear analysis. The BBC connection employed in the U. of Washington stadium and illustrated in the photo of

Fig. 6 is the prototype for this analysis. This prototype was selected because it is of intermediate scale to BBC connections used in existing structures. The connection is quite large with an outside diameter of approximately 710 mm, but it is much smaller than connections used on a number of the large buildings noted earlier.



Figure 6. Photograph of Prototype Connection

A detailed finite element grid illustrated in Fig. 7 modeled the connection. The elements were 3 dimensional 8-node brick elements, and the steel was modeled as a bi-linear plastic material with a yield stress of 345 MPa, a Poisson's ratio of 0.3, an ultimate tensile stress of 380 MPa, and a strain hardening ratio of 4% of the elastic modulus. The tube thickness was 12.5 mm (for a d/t of approximately 57) in the basic model, but this thickness (and the resulting d/t) was varied throughout the study. There was considerable difficulty in modeling the concrete. Initially the ABAQUS unreinforced concrete element was employed, but this model consistently failed to converge in regions where moderately large stress and strain developed. The ABAQUS concrete model is not designed to handle situations in which the concrete is well confined, and therefore the tension softening curve was artificially extended to provide some apparent ductility (although at extremely low tensile stress) to the behavior. The tensile strength of the concrete was limited to less than 8% of the compressive strength, but the compressive strength of the concrete was a variable parameter in the study. The interface between the steel and concrete surfaces were also parameters of interest. Because of the limited stress transfer capability noted earlier, no adhesion or rigid attachment between the steel and concrete were permitted. The interaction between steel and concrete elements was modeled using contact pairs consisting of master (steel) and slave (concrete) surfaces. Hard contact was specified, requiring that the clearance between the surfaces be zero before the surfaces may interact. When in contact, the surfaces are permitted to transfer normal stress and shear stress through friction. The coefficient of friction was initially chosen to be 0.3, but this coefficient of friction was also a parameter considered in the study. Before any loads are placed on the model, the clearance between all steel and concrete surfaces is zero.

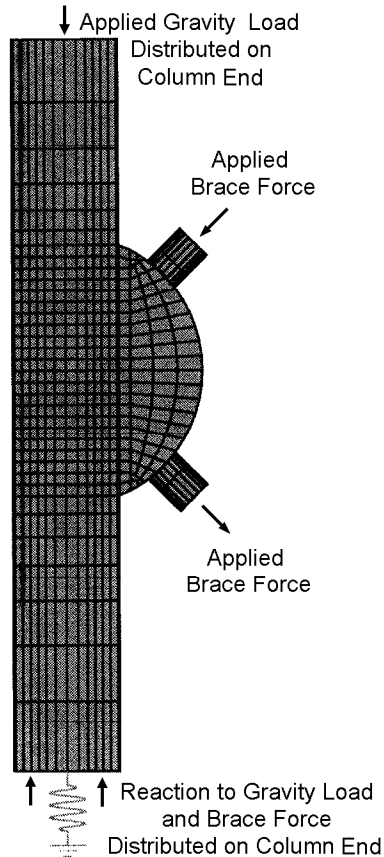


Figure 7. Schematic of Analytical Model

The loads illustrated in Fig. 7 were monotonically applied to the specimen. The gravity loads in the CFT column were applied first, and the brace loads were later simultaneously applied in increments to observe the nonlinear behavior of the connection. The maximum brace loads were computed based upon the tensile yield and compressive buckling capacity of the diagonal brace pair. The compressive load on the CFT column was a parameter of interest in the analysis, and this load was varied between 10% and 30% of the compressive load capacity of the column. The model utilized symmetry, and the model was split through the center of the CFT column and gusset plate as shown in Fig. 7. Out-of-plane movements and in-plane rotations were restrained on this plane of symmetry, but all other deflections and rotations were permitted. The loads were applied so that the specimen was always in equilibrium, and so supports of the assemblage were theoretically not required. However, accidental imbalance occurs because of roundoff and other errors. As a result, a single node located at the centroid of the column was pinned or restrained with a spring at each of the top and bottom cross-sectional surfaces. These restraints prevented rigid body translation in the plane of symmetry and rigid body rotation (vector directions defined by right hand rule) perpendicular to the plane of symmetry. The plane of symmetry constrained the other components of rigid body translation and rotation. A spring element with a stiffness of 350.4 kN/mm was applied at the bottom of the column. The resulting model had 5100 elements and 8863 nodes. Computer analyses required periods from as little as a few hours to more than a day for completion on Sun Sparc Workstation.

PARAMETERS AFFECTING CONNECTION PERFORMANCE

Initial analyses evaluated convergence and mesh refinement of the model but are not discussed here. Later analyses show that the connection relies primarily on the bearing capacity of the concrete, as the primary load path from the braces to the concrete. This is illustrated in the contours of compressive stress in the concrete below the gusset plate in Fig. 8. The maximum bearing is delivered through the edge of the gusset plate into the concrete. The large bearing stresses occur in the concrete immediately below the gusset plate at the corner intersection of the plate and tube. In Fig. 8, the average compressive stress in the concrete is slightly approximately 10.2 MPa, but the actual bearing stress is 58.9 MPa under the loaded edge of the gusset plate and 29.2 MPa at the opposing corner. The concrete is well confined in this area. The highly stressed area is in hydrostatic compression, and the material can probably tolerate stresses larger stress than the uniaxial compressive capacity of the concrete, but the limitations of the finite element model result in convergence problems at these highly stressed locations. Stress concentrations are noted in the steel tube and the gusset plate at these junctures, but the stresses in the steel are larger and the consequences of the high stress are less severe in the analytical solution. Yielding is noted at several locations in the gusset plate and the steel tube, but it is quite local. The juncture of the gusset plate and the steel tube, and the attachment of the brace to the gusset plate are such locations.

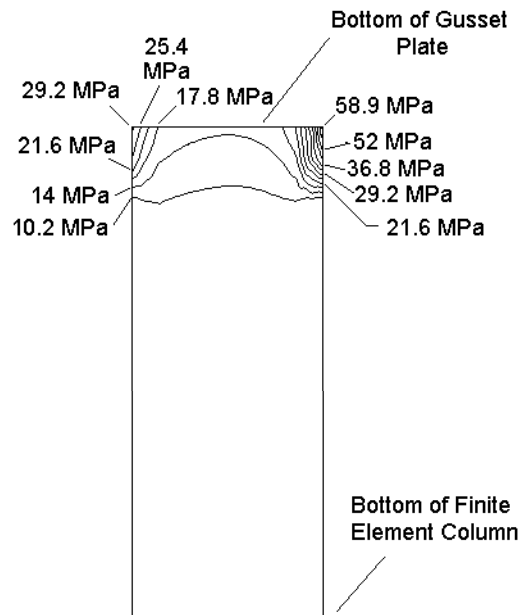


Figure 8. Stress Contours in Concrete Below the Gusset Plate

While bearing of the gusset plate on the concrete is the critical transfer mechanism, some load transfer occurs because of friction between the steel and concrete. There was no attachment between the steel and concrete. As a result, friction provides the only stress transfer between the steel tube and the concrete fill or between the side of the gusset plate and concrete. This friction transfer was smaller than the bearing stress transfer noted above, but it was not insignificant. In the models using a high coefficient of friction (0.4), the force transferred by frictional shear transfers approximately 32% of the total vertical component of brace forces. As the coefficient of friction increases and larger portions of the brace force are distributed to the concrete through friction, the maximum bearing stress beneath the plate

decreases as shown in Fig. 9. The reduction in stress is not huge, but the demand is pulled below the ultimate capacity of the concrete and reduces the local strain demand and potential for crushing. Friction depends on the surface condition of the steel and concrete and shrinkage effects, and these factors are not easily controlled. As a result, the extent to which this friction transfer can be used is unclear.

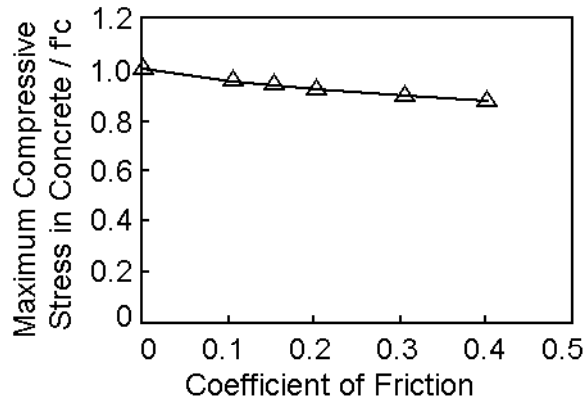


Figure 9. Effect of Increased Friction on the Maximum Concrete Bearing Stress

There was significant slip between the steel and concrete. Figure 10 shows the pattern of slip between the gusset plate and the concrete of a typical specimen. The slip occurs because the strain in the steel and concrete are not compatible, and the shear stress transfer does not distribute the stress between the steel and concrete rapidly enough to achieve strain compatibility. The slip is largest near the mid height of the gusset plate near the loaded edge. At this location, the steel gusset plate is highly stressed, while the concrete is only lightly stressed, and the slip occurs in the region with relatively large strain differential. Slip is a concern because it represents a potential source of deterioration within the CFT column and connection and it decreases as the coefficient of friction increases. Slip was also noted between the concrete and the steel tube, but this slip was more uniform for a given length.

Other parameters were evaluated. The effect of the strength of the concrete on the BBC connection behavior was considered. Concrete with increased strength tolerates the large bearing stress such as illustrated in Fig. 9 better, but it doesn't reduce the slip and deformation with the connection or otherwise improve the load transfer between steel and concrete. Increased wall thickness of the steel tube significantly reduced the maximum bearing stress in the concrete. A larger portion of the transfer appeared to occur between the concrete and the steel tube, since the greater stiffness of the walls of the tube provided better confinement and resulted in larger contact stresses and friction along that interface. Increased thickness of the gusset plate directly lowered the maximum bearing stresses on the concrete.

The potential use of shear studs on the gusset plate as illustrated in Fig. 2a and on the inside of the tube as illustrated in Fig. 2c was also investigated. Shear studs do not appear to be an effective way of improving the shear transfer between the steel and concrete. Shear studs are relatively flexible, and they develop their full shear resistance only after sustaining (Taylor 5) a relative deformation. The slip occurring within these BBC connections provides a small relative deformation, but it is not large enough to effectively develop shear studs. Other mechanical transfer devices with greater stiffness may benefit the connection performance. The capacity of the connection to transfer and distribute load between the steel and concrete is dependent on the concrete strength and the thickness of the plate and tube. The stress

concentration at the junction between the tube and the bottom edge of the plate is a critical point within the connection.

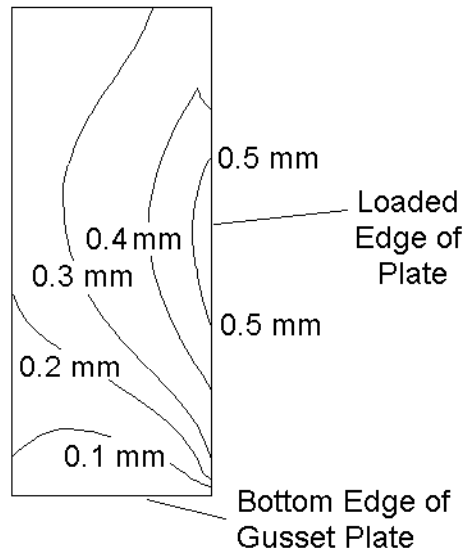


Figure 10. Slip Between the Gusset Plate and Concrete Fill

CONCLUSIONS

In order for CFT braced frames to behave well, transfer of force from the braces in the column infill concrete is necessary. Due to the large diameter, d/t ratios and force demands expected in typical US frames, friction between the concrete and steel was shown to be unreliable for design. Also, the use of shear connections is unsatisfactory since excessively large deformations are required to develop there shear transfer. Direct bearing of steel against the concrete was shown to be a promising method for force transfer. Testing and further analysis are presently underway and final conclusions should be available in approximately 18 months.

ACKNOWLEDGEMENTS

This work is funded by the National Science Foundation under Grant CMS-9905797. "Concrete Filled Tube Braced Frame Testing". Dr. S. C. Liu and Dr. V. Gopu are the Program Managers for this study. Their support is greatly appreciated. Mr. John Hooper and Prof. C. B. Brown are technical advisors on the project. They are providing practical insight into the use of CFT columns in actual braced frame construction and assisting with analysis and evaluation of the research results.

REFERENCES

1. Hooper, J.D., Roeder, C.W., Kelmencic, R., and Nordquist, K., Concrete-Filled Tubes for High-Rise Construction, Civil Engineering, ASCE, Washington, D.C., February 1999.
2. AISC, Seismic Provisions for Structural Steel Buildings, AISC, Chicago, IL 1997.
3. Roeder, C.W., Cameron, B. and Brown, C.B., (1998) "Composite Action in Concrete Filled Tubes," *Structural Engineering*, ASCE, Vol 125, No 5, May 1999.

4. Roeder, C.W., "Composite Behavior Between Steel and Concrete Systems for Lateral Loads," ASCE Special Publication, Proceedings, Engineering Foundation Conference on Composite Construction IV, Banff, Canada, June 2000.
5. Taylor, A.W., "A Study of the Behavior of Simply Supported Composite Beams," A thesis submitted in partial fulfillment of the requirements for the degree of Master of Science in Civil Engineering, University of Washington, Seattle, WA, 1985.

Design requirements for plug and play type joints in mixed and steel-concrete composite construction

Jan W.P.M. Brekelmans BSc,
TNO Building and Construction Research, Rijswijk ZH, The Netherlands
Prof. Frans S.K. Bijlaard MSc,
Delft University of Technology, faculty of Civil Engineering and Geosciences, Delft, The Netherlands

ABSTRACT

In the paper new types of joints are discussed in view of reduction of costs of steel frame structures by using so-called plug and play joints for easy and safe on-site construction. Examples are given for these types of beam-to-column joints in mixed structures that are characterised by simplicity and fast erection methods. These joints could also be used in traditional steel-concrete composite flooring systems. The influence of the loading on the structure with respect to the forces and moments in the joint is analysed. For plug and play joints no specific design rules are available in Eurocode 3, Part 1.8: 'Steel joints' or chapter 9 of Eurocode 4, Part 1.1: 'Composite joints'. The paper describes the basis of design for these types of joints.

INTRODUCTION

Cost optimisation is one of the most important items in steel construction in order to be competitive in the market of buildings. The joints determine almost 50% of the total costs of a steel structure. As a consequence of the modernisation of the fabrication process, the fabrication costs have decreased spectacularly. On the other hand the on-site labour costs have increased rapidly nowadays due to lack of construction workers and more strict safety measures that have to be taken. Fast and safe construction methods with joints that can be applied easily are required for the near future.

New types of joints are used in so called Slim Floor construction. In this type of flooring, the steel beams are integrated into a prefabricated concrete hollow core slabs or in a deep deck composite slabs.

The so-called plug and play beam-to-column joints in these mixed structures are characterised by simplicity and fast erection methods. These joints can also be used in traditional steel-concrete composite flooring systems. These so-called plug and play joints should lead to faster construction onsite and reduce the need for construction workers to work in dangerous situations high above ground level.

The costs of fabrication of these plug and play joints should be the same or preferably even lower than the costs of traditional joints with bolts and welds. The costs of fabrication may even slightly be higher than the costs of traditional joints provided that the total costs of fabrication in the workshop and onsite construction work of the steel structure decrease significantly.

INVENTORY OF POSSIBILITIES FOR ALTERNATIVE JOINTS IN 'SLIM FLOOR' CONSTRUCTION

To describe possibilities of alternative joints in 'Slim Floor' construction first an analogy with a traditional steel-concrete composite floor construction is made.

In a traditional steel-concrete composite floor construction, in the construction stage the beam is often designed as a simply supported single span beam. In these cases the beam-to-column joints most often have a welded end plate or web-cleats as connecting parts. In the final stage, after installing the composite slab, the beam-to-column joint can behave either as a hinge or as a partially moment resistant joint dependent on the detailing of the joint. In case a tensile force in the reinforcement can be transferred via horizontal shear devices of the beam to the compression zone in the bottom flange of the beam, a semi-rigid and partial-strength joint between the beam and column will occur. Filler plates between the column and the bottom flange of the beam will result in such a compression zone. A partial depth end plate welded to the web and the top flange of the beam only and no compression zone present, will result in a hinged joint in the construction stage as well as in the final stage. As a third option the joint can behave as a moment resistant joint in both stages. The later case is not often used in steel-concrete composite construction. Generally, the beams are designed as simply supported single span beams with minimum crack reinforcement at the supports. In that case the composite action is most effective at mid span. The moments at the supports remain relatively low because of the presence of minimum crack reinforcement. This design philosophy is summarised in table 1.

It can be concluded that, dependent on the detailing of the connecting parts of the joint, various load distributions can occur. In case of an end plate welded to the flanges and the web of the beam and connected with 4 bolts to the column, the joint will be resistant against torsion (see fig. 1). This is important because during the construction stage eccentric loading takes place, which might not have been taken into account. Furthermore the joint has sufficient robustness to resist unforeseen accidental loading situations.

Nowadays, in Europe, there is a growing market for so called 'Slim Floor' construction. To reduce storey height and to increase flexibility in partitioning, steel beams are integrated in the depth of the floor. The I-shaped beam sections have a wider bottom flange. On this flange deep deck composite slabs or prefabricated concrete hollow core slabs are installed. Because of the decrease of construction height the composite action is less effective. The beams are less stiff and hence the span lengths are smaller. As a result more columns and beam-to-column joints need to be installed. For that reason new types of beam-to-column joints are developed. From an assembly point of view the joint should be a plug and play type of joint. Self-positioning plug and play joints that can resist each possible loading situation would be most ideal. In table 2

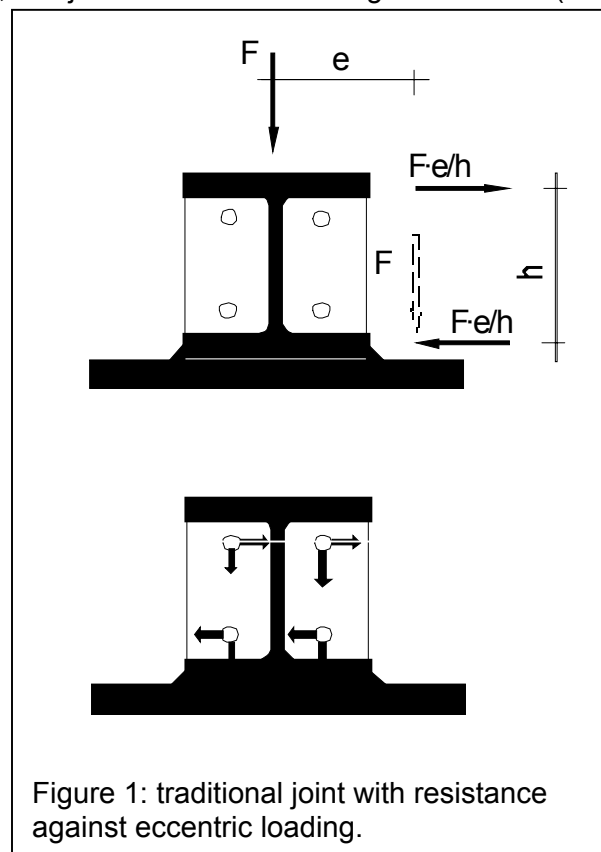


Figure 1: traditional joint with resistance against eccentric loading.

an overview is given of various types of plug and play joints. The application and the mechanical behaviour are described shortly.

Table 1: Examples of primary beam to secondary beam connection

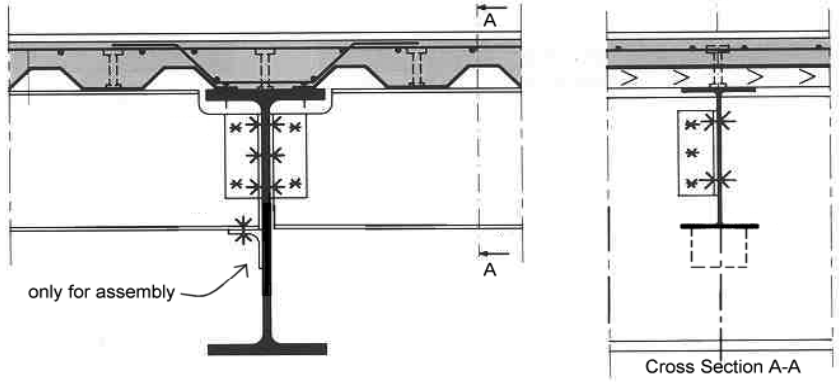
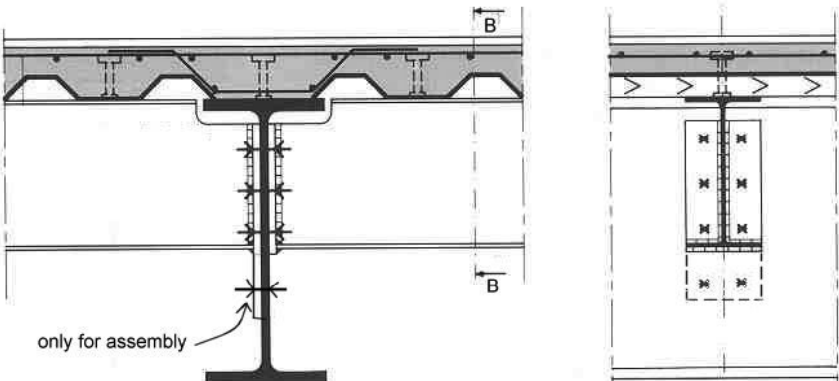
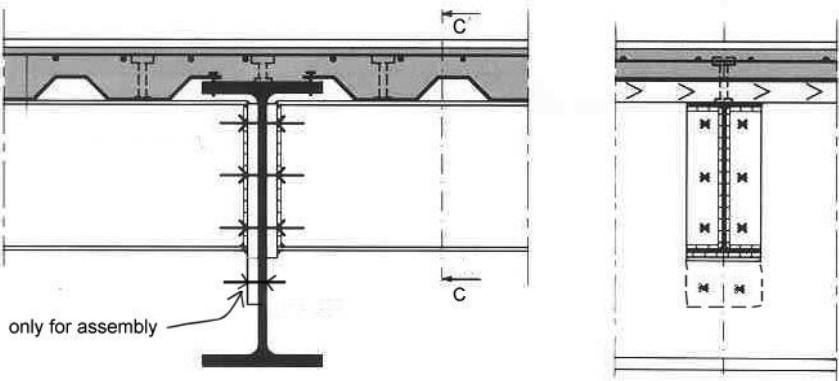
Con- struction stage	Final stage	Examples of primary beam to secondary beam connection
Hinge	Hinge	
Hinge	Moment resistant	
Moment resistant	Moment resistant	

Table 2: Types of plug and play joints


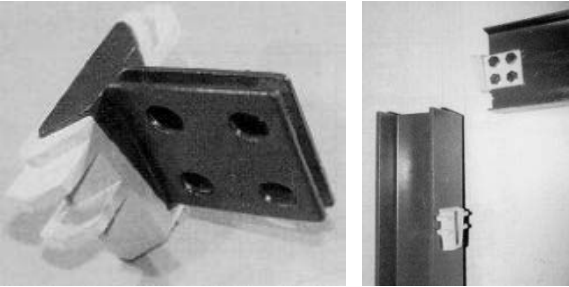
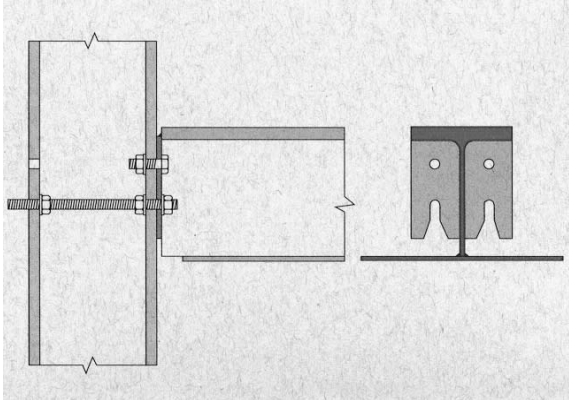
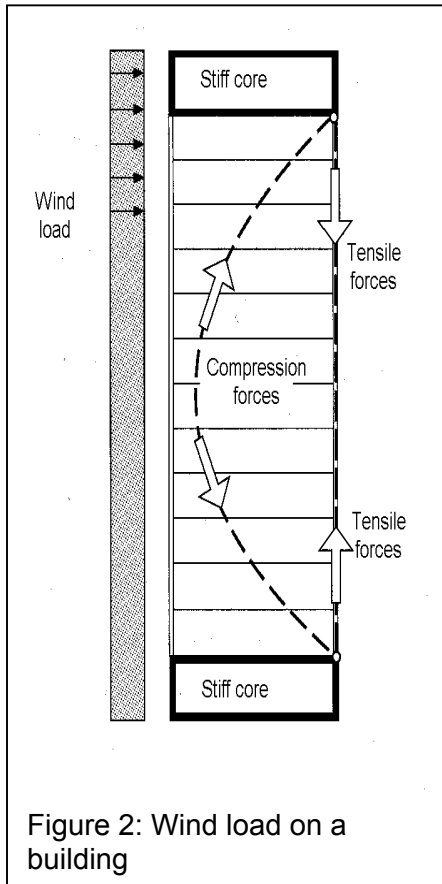
Type of joint	Application	Mechanical behaviour
	<p>Type of plug and play joint used in storage racks. Imperfections are very small</p>	<p>Joint can resist to some extent M - V - N (moment, vertical shear, axial load) and torsion</p>
	<p>Type of plug and play joint developed in USA. Connecting part is bolted to the beam before assembly. Imperfections are very small.</p>	<p>As illustrated some resistance against torsion. Hinged support due to web joint. Joint can resist to some extent V – N. In plane rotation capacity comes from bolted connection in web of beam.</p>
	<p>Semi plug and play joint. Positioning is possible. Additional bolts have to be installed afterwards. Imperfections are moderate.</p>	<p>Joint can resist to some extent V – N and torsion.</p>

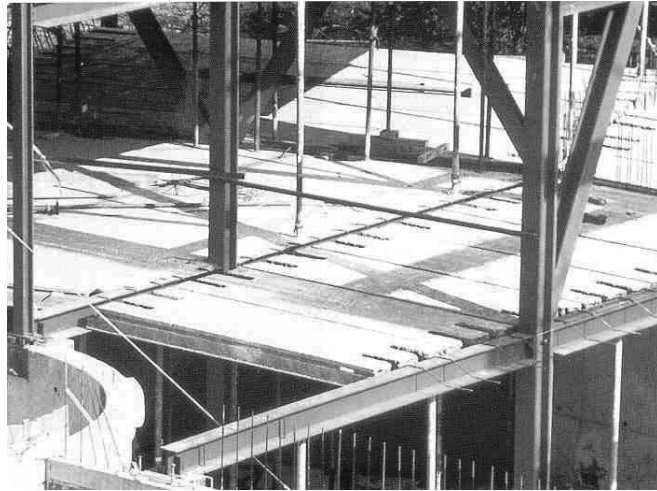
Table 2: Types of plug and play joints (continue)

	<p>End plate with hole to be installed over console.</p>	<p>Resistance against torsion and tension depends on clearances between console and beam and the shear resistance of the console plate.</p>
	<p>Hole in upper flange of beam to be installed over console with pin.</p>	<p>Joint can resist V. Resistance against torsion and tension depends on clearances between console and beam and the shear resistance of the pin.</p>

CONSEQUENCES OF LOADING ON THE STRUCTURE FOR THE FORCES IN JOINTS



Most steel frame structures with traditional joints with connecting parts as bolts and welds are designed on the basis of forces resulting from plane frame analyses. The spatial behaviour of structure due to the loading is most times neglected because the resistance of the traditional joints against these resulting forces is normally sufficient. The wind loading on a building can produce tensile forces in the joints (see fig. 2), while eccentric loading on the floor



can produce torsion moments in joints (see fig. 3). Traditional joints have by themselves sufficient resistance against these tensile forces and torsion moments. Because bolts in holes, designed primarily for shear and or bending moments, are almost always capable of carrying these "secondary" forces and moments. In fact these forces are not "secondary" but primary forces and moments due to the spatial behaviour of the structures under the loading actions.

In designing new concepts for plug and play joints the designer needs to be explicitly aware of these forces and moments, which can implicitly be neglected in designing traditional joints.

Actions that produce these "secondary" forces and moments are wind loading, accidental loading such as earthquake, fire and explosion.

During an earthquake structures undergo severe ground movements, which the structure must follow without total collapse. Local plasticity, especially in the connecting parts of the joints, can cause damage, but provided that the design is done adequately, it dissipates energy and prevents the structure from brittle fracture.

A local fire causes expansion and deflection of beams and columns. Therefore it is essential that joints have sufficient deformation and rotation capacity to avoid premature and progressive collapse.

Under an explosion it is inevitable that damage will occur, but the remaining structure should be able to resist the present loading without progressive collapse.

Also loading that can appear in the onsite construction phase produces most times tensile and torsion in the beams and joints.

The main task of the designer is to design plug and play joints that demonstrate explicitly robustness in order to prevent premature and progressive collapse.

CONSEQUENCES OF DETAILING OF JOINTS FOR DISTRIBUTION OF FORCES AND MOMENTS IN JOINTS AND REQUIREMENTS WITH RESPECT TO STIFFNESS, STRENGTH AND ROTATION CAPACITY FOR JOINTS

The distribution of forces and moments in the structure due to the loading is a result of the strength and stiffness distribution in the structure. So the structural properties of the joints such as stiffness, strength and rotation capacity, together with those of the structural components like beams and columns, produce these forces in the joints. This means that the choices made by the designer in designing the joints including the connecting parts are of direct influence on the level of forces and moments in these joints.

In fact, construction is joining components such as columns and beams together while designing is making choices for components taking the structural properties such as strength and stiffness into account.

Traditional design

In traditional design it is assumed that the joints are stiff and strong and that the forces and moments in the structure are determined using the linear-elastic theory. Because it was assumed that the joints were stiff, it needs to be checked whether the joints are really stiff. In many cases in practice this is neglected. The strength of the joints is adjusted to the level needed. As a result most joints have low deformation or rotation capacity. Last but not least, the fabrication costs are very high.

Modern Design

In modern design the joints are considered as structural components such as columns and beams with properties as stiffness, strength and deformation capacity. These structural properties of the joints are incorporated into the design on the same level as those of columns and beams. The joint layout should only be influenced by fabrication considerations and considerations for easy and safe construction on-site. The structural safety verification of all components including that of the joints is dependent on the design method used to determine the distribution of forces and moment in the structure.

- a. In case that the elastic theory is used, the beams need to be checked for strength and for lateral torsional buckling, the columns need to be checked for strength and for beam-column stability (incl. lateral torsional buckling) and the connecting parts of the joints need to be checked to have sufficient strength to transfer bending moments, shear forces and tensile forces.
- b. In case that the plastic theory is used, the beams need to be checked for lateral torsional buckling only, the columns need to be checked for beam-column stability (incl. lateral torsional buckling) only and the joints need to be checked to have sufficient deformation (in fact rotation) capacity.

- c. In case that the elastic-plastic-non linear theory is used, the beams and columns need to be checked for lateral torsional buckling only and the joints need to be checked to have sufficient deformation (in fact rotation) capacity.

The Eurocode 3 "Common unified rules for steel structures" contains performance based requirements to carry out these checks. The extend to which plug and play joints can be checked using Eurocode 3 depends on the creativity of the designer to recognise components in the connecting parts of these joints that are similar to the components given in the chapters for joints in that design code. If necessary experiments have to be carried out and the results have to be evaluated statistically, in order to obtain reliable values for the stiffness, strength and rotation capacity of these plug and play joints.

CONCLUSIONS

In order to keep a competitive position in the market, the costs of steel structures, in particular steel frames, need to be reduced as much as possible. As the costs of steel frame structures are determined for about 50% by its joints, the need to design modern plug and play joints is of increasing economic importance. In this way the costs of on-site construction work together with safety measures can be reduced significantly. Although design codes like Eurocode 3 "Common unified rules for steel structures" are still based on traditional joints with bolts and welds, in many cases the design rules can be used for the design and verification of so-called plug and play joints in which traditional components can be recognised. This is because the design rules for joints are related to the components in which almost all joints can be sub-divided and because the requirements for stiffness, strength and rotation capacity of joints are given in so-called performance based requirements and are irrespective of the type of the joint. However, where non-traditional components like clamps and hooks are used, experiments have to be carried out and the results have to be evaluated statistically, in order to obtain reliable values for the stiffness, strength and rotation capacity of these plug and play joints.

Safety Concepts for Ductility of Joints

ir. C.M. Steenhuis
Prof. ir. F. van Herwijnen
Prof. ir. H.H. Snijder
Eindhoven, University of Technology, the Netherlands

ABSTRACT

Nowadays, in design standards, ductility requirements for joints are formulated in terms of deemed-to-satisfy rules, i.e. provided that certain design requirements are met, the joint may be assumed to behave sufficiently ductile to ensure a safe structural behaviour. Higher strength steels in general possess a lower ductility compared to normal steels. Consequently, in structures made of higher strength steels, the ductility of the joints connecting the members becomes a design issue. In this paper, preliminary results are presented of a research carried out in Eindhoven on the relation between the ductility of joints in steel structures and the frame reliability. Different safety concepts are treated for the ductility problem of joints. A procedure is given for a rational treatment of the ductility problem in relation to the reliability of the frame. The paper ends with conclusions and recommendations for further research.

INTRODUCTION

Users of buildings expect that the structures of these buildings are safe. This safety can be quantified in terms of reliability, i.e. a quantifiable probability that a structure will perform its intended function for a specific period of time under defined conditions. The complement of reliability is defined as the probability of failure.

The Joint Committee of Structural Safety (1) distinguishes different methods to determine the failure probabilities of structures:

- Level 1 methods: design methods with partial safety factors which are calibrated probabilistically based on an accepted failure probability;
- Level 2 methods: probabilistic with approximations, such as first and second order reliability methods;
- Level 3 methods: fully probabilistic methods, such as analytical and numerical integration and Monte Carlo Simulations to calculate the failure probability.

Besides, Level 0 methods are distinguished, like the allowable stress method. Level 0 methods have a basis in design tradition and have a non-probabilistic, deterministic nature.

Modern design standards, like the Eurocodes (2, 3) or the Dutch national codes (4, 5) have adopted Level 1 methods, because of their applicability and their probabilistic basis. Also parts of these standards are still based on Level 0 methods.

Level 1 and Level 0 methods are also applied in standards for design of steel joints.

An example of a Level 1 method is the resistance check of a failure mode of a joint, which has the general form:

$$\gamma_S S_{\text{char}} \leq \frac{R_{\text{char}}}{\gamma_R} \quad (1)$$

where S_{char} , R_{char} are the characteristic values of the loading (solicitation, S) respectively the resistance (R) of the joint. The factors γ_S , γ_R are the partial safety factors to be applied.

An example of Level 0 methods is the check of the deformation capacity of a bolted connection loaded in shear. For instance, in the Dutch Standard (5) it is written that if such a connection fails due to bearing of the plate, it may be assumed that there is sufficient deformation capacity for plastic design. This requirement is based on a large number of test results (6), from which it was concluded that the bearing type of failure leads to large plastification of the joints without brittle failure. Another example of such a Level 0 rule is that a beam-to-column joint may be assumed to have sufficient deformation (rotation) capacity for plastic design, provided the joint fails by shear of the web panel.

It has to be noted that the rules for checking the deformation capacity given above are in a so-called deemed-to-satisfy format. Not all rules are in this format. Eurocode 3 (3) states as design principle that the required deformation capacity of a joint should be smaller than the available deformation capacity. In that case, design guidance should be given on how to calculate the required and the available deformation capacity. More generally, in modern design standards, design rules for the resistance of joints are mostly based on Level 1 methods. In contrast, the rules for deformation capacity (the other mechanical property of joints, which has an influence on the reliability of a structure) are mostly based on Level 0 methods. The third mechanical property of a joint, the stiffness has mainly an effect on the serviceability. In Figure 1 the mechanical properties of a beam-to-column joint are given as represented in a bi-linear diagram: M_j for moment resistance, S_j for rotational stiffness and ϕ_j for rotation (i.e. deformation) capacity. These definitions are in accordance with Eurocode 3.

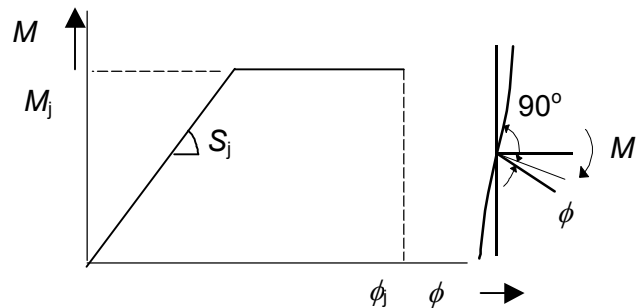


Figure 1: Bi-linear moment rotation diagram of a beam-to-column joint

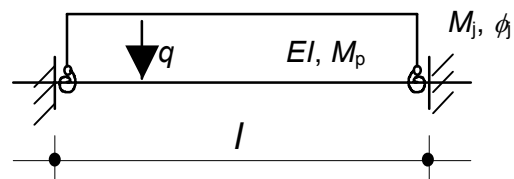


Figure 2: Mechanical system

This paper focuses on deformation capacity. With the use of higher strength steels, the strength ratio between the connected steel parts and the possibly brittle connectors as bolts and welds changes. In that case, failure of these brittle connectors may become governing. This yields a decrease in deformation capacity.

As the knowledge reflected in modern design standards on deformation capacity of joints is rather limited, there is a need for better understanding of deformation capacity as a design issue. A number of questions arise. Firstly, what is the required deformation capacity of a joint? Secondly, what is the available deformation capacity of a joint? Lastly, how can the check of deformation capacity be embedded in a safety concept. This paper deals with the last question.

This paper presents a procedure to assess the impact of the deformation capacity of a joint on the reliability of a structure. This procedure is illustrated by a simple example. At the end of this paper, the presented procedure will be commented and recommendations will be given for future research.

The work presented here is part of a research on the relation between deformation capacity and structural reliability carried out at the University of Technology in Eindhoven, the Netherlands.

A LEVEL 1 APPROACH FOR DEFORMATION CAPACITY

The availability of sufficient deformation capacity of a joint or a plastic hinge location in a structure can be checked by comparison of the required deformation capacity with the available capacity. The required deformation capacity follows from the frame analysis. The available deformation capacity is a characteristic of a joint or a plastic hinge location in a member. Eurocode 3 (3) on steel joints, ECCS publication 109 on composite joints (7), Kuhlmann (8) and Kemp and Dekker (10) use this general principle for verification of deformation capacity. Kemp and Dekker for instance formalized this check as:

$$\phi_r \leq \frac{\phi_a}{\gamma_{mr}} \quad (2)$$

where: ϕ_r is the required inelastic deformation capacity for ultimate limit state conditions, ϕ_a is the available inelastic deformation capacity based on tests or a model and γ_{mr} is a partial safety factor to allow for many uncertainties in modelling etc.. It should be noted that ϕ_a and ϕ_r do not include the elastic deformations, in contrast to Eurocode 3 and ECCS publication 109. For composite beams, Kemp and Dekker proposed a value for γ_{mr} of about 2 for ductile failure modes and a value for γ_{mr} of about 3 for non-ductile failure modes. The value of γ_{mr} is thus related to the failure mode occurring in the plastic hinge location.

Formula (2) is almost in a format applicable for a Level 1 approach to the check of deformation capacity (compare for instance with Formula (1), representing a typical Level 1 resistance check). Only, the statistical basis of Formula (2) needs to be clarified: ϕ_r should include partial safety factors on the solicitation side and should relate to characteristic or mean values for the required rotation capacity, ϕ_a is based on characteristic or mean values for the available rotation

capacity and γ_{mr} should be assessed on a reliability basis. The determination of the value of the partial safety factor γ for deformation capacity is further elaborated in this paper.

PARTIAL SAFETY FACTORS FOR DEFORMATION CAPACITY

This paragraph describes a procedure to quantify values for partial safety factors for deformation capacity. The procedure refers to the model level of a structure (8). At the model level, the actual curves are converted to a force-deformation diagram containing a resistance, a stiffness and a plastic deformation. Figure 1 shows an example of such a curve at the model level.

The proposed procedure for quantification of partial safety factors γ for deformation capacity consists of the following steps:

1. A variety of structures to be investigated are selected. These structures are designed according to existing design standards, for instance the Eurocodes, adopting the proposed values for partial safety factors from these standards. These proposed values result from intensive calibration processes and lead to safe and economical structures in practice.
2. Then, the failure probability $P_{f,excl}$ of the structure is determined by taking into consideration the loading, the mechanical properties of members and joints and the failure modes. The mechanical properties are considered as stochastic variables, with a mean value, a standard deviation and a certain distribution type. Failure due to lack of deformation capacity is excluded. This system is called the reference system.
3. The following step is that the failure probability $P_{f,incl}$ of the structure is determined including failure due to lack of deformation capacity. A certain value is assumed for the partial safety factor γ for deformation capacity.
4. The increase of failure probability when comparing the system where deformation capacity is taken into consideration and the reference system can be calculated as $\Delta P_{f,rel} = (P_{f,incl} - P_{f,excl}) / P_{f,excl} * 100\%$.
5. By repeating the calculations of step 3 and 4 for different values for the partial safety factor γ for deformation capacity, the relationship can be determined between the partial safety factor γ and the increase of failure probability.

In the following paragraph, this procedure is illustrated.

EXAMPLE

Step 1: Selection and Design of the Structural System

The mechanical model of the structural system to be studied in this example is given in Figure 2. It is a beam connected to a core by means of joints. The beam is loaded by a uniformly distributed load.

It is assumed that in the mid span of the beam a plastic hinge may form. For simplification of this example, the rotation capacity of this hinge is assumed to be sufficient.

The beam is connected to the column by means of two rotational springs with a strength M_j and a rotational capacity of ϕ_j , see Figure 1 in accordance with Eurocode 3 (3). Although the stiffness S_j is also a characteristic of the joint, in this case, it is not of interest.

Numerical values for the partial safety factors adopted in this example should be based on design standards (2, 3, 4, 5). In this example, the following values for the partial safety factors are adopted: $\gamma_q = 1,5$, $\gamma_{M_p} = 1,0$, $\gamma_{M_j} = 1,25$. This is a simplification of data given in the design standards.

The Level 1 design criterion for this simple structure for the failure mode loss of equilibrium is:

$$\frac{1}{8} q_{\text{char}} \gamma_q l^2 \leq \frac{M_{p,\text{char}}}{\gamma_{M_p}} + \frac{M_{j,\text{char}}}{\gamma_{M_j}} \quad (3)$$

where $M_{p,\text{char}}$, $M_{j,\text{char}}$, q_{char} are the characteristic values of the beam resistance M_p , joint resistance M_j and uniformly distributed load q and γ_{M_p} , γ_{M_j} , γ_q are the corresponding partial safety factors.

It is assumed that the length of the beam l and the bending stiffness of the beam EI are deterministic variables. Furthermore, the uniformly distributed load q , the strength of the beam M_p , the strength of the joint M_j and the rotational capacity ϕ_j are assumed to be stochastic variables.

In literature (9, 11), data are given for the distribution types of loading and strength functions. The distribution types may be non-normal distributed. Although not realistic, for sake of simplicity in this example all stochastic variables are assumed to be uncorrelated normal distributed variables with average μ_q , μ_{M_p} , μ_{M_j} and μ_{ϕ} , standard deviation σ_q , σ_{M_p} , σ_{M_j} and σ_{ϕ} and coefficient of variation v_q , v_{M_p} , v_{M_j} and v_{ϕ} . In this example it is sufficient to know only the coefficients of variation a-priori. The assumed values are: $v_q = 0,3$, $v_{M_p} = 0,1$, $v_{M_j} = 0,2$, $v_{\phi} = 0,2$.

Step 2: Determination of the Failure Probability Excluding Lack of Deformation Capacity

In the structure of Figure 2, if lack of deformation (rotation) capacity is not considered, basically one failure mechanism can occur. This is loss of equilibrium. The failure probability is indicated as $P_{f,\text{eq}}$. The system fails due to loss of equilibrium if the safety margin Z_{eq} is negative:

$$Z_{\text{eq}} = -\frac{1}{8} q l^2 + M_p + M_j < 0 \quad (4)$$

Since q , M_p , and M_j are stochastic variables, the reliability index $\beta_{Z,\text{eq}}$ is:

$$\beta_{Z,\text{eq}} = \frac{\mu_{Z,\text{eq}}}{\sigma_{Z,\text{eq}}} = \frac{-\frac{1}{8} \mu_q l^2 + \mu_{M_p} + \mu_{M_j}}{\sqrt{(-\frac{1}{8} \sigma_q l^2)^2 + \sigma_{M_p}^2 + \sigma_{M_j}^2}} \quad (5)$$

With help of this $\beta_{Z,\text{eq}}$ and available tables the failure probability $P_{f,\text{eq}}$ can be determined.

The coordinates of the design point are as follows:

$$q^* = \mu_q - \alpha_{q,\text{eq}} \beta_{Z,\text{eq}} \sigma_q \quad (6)$$

$$M_p^* = \mu_{M_p} - \alpha_{M_p,\text{eq}} \beta_{Z,\text{eq}} \sigma_{M_p} \quad (7)$$

$$M_j^* = \mu_{M_j} - \alpha_{M_j,eq} \beta_{Z,eq} \sigma_{M_j} \quad (8)$$

where $\alpha_{q,eq}$, $\alpha_{M_p,eq}$, $\alpha_{M_j,eq}$ are weighing factors which show with which weight the corresponding variables q , M_p and M_j participate in the value of the probability of failure:

$$\alpha_{q,eq} = \frac{\frac{1}{8} \sigma_q l^2}{\sqrt{\left(-\frac{1}{8} \sigma_q l^2\right)^2 + \sigma_{M_p}^2 + \sigma_{M_j}^2}} \quad (9)$$

$$\alpha_{M_p,eq} = \frac{\sigma_{M_p}}{\sqrt{\left(-\frac{1}{8} \sigma_q l^2\right)^2 + \sigma_{M_p}^2 + \sigma_{M_j}^2}} \quad (10)$$

$$\alpha_{M_j,eq} = \frac{\sigma_{M_j}}{\sqrt{\left(-\frac{1}{8} \sigma_q l^2\right)^2 + \sigma_{M_p}^2 + \sigma_{M_j}^2}} \quad (11)$$

The relation between the characteristic value of the stochastic variables, the design point and the partial safety factors is as follows:

Solicitation side:

$$\gamma_q = \frac{q^*}{q_{char}} = \frac{\mu_q - \alpha_{q,eq} \beta_{Z,eq} \sigma_q}{\mu_q + 1,96 \sigma_q} = \frac{\mu_q - \alpha_{q,eq} \beta_{Z,eq} V_q \mu_q}{\mu_q + 1,96 V_q \mu_q} = \frac{1 - \alpha_{q,eq} \beta_{Z,eq} V_q}{1 + 1,96 V_q} \quad (12)$$

Resistance side:

$$\gamma_{M_p} = \frac{M_{p,char}}{M_p^*} = \frac{\mu_{M_p} - 1,96 \sigma_{M_p}}{\mu_{M_p} - \alpha_{M_p,eq} \beta_{Z,eq} \sigma_{M_p}} = \frac{1 - 1,96 V_{M_p}}{1 - \alpha_{M_p,eq} \beta_{Z,eq} V_{M_p}} \quad (13)$$

$$\gamma_{M_j} = \frac{M_{j,char}}{M_j^*} = \frac{1 - 1,96 V_{M_j}}{1 - \alpha_{M_j,eq} \beta_{Z,eq} V_{M_j}} \quad (14)$$

By rewriting the equations and filling in the numerical values for the partial safety factors and the coefficients of variation, the failure probability due to loss of equilibrium can be determined: the reliability index $\beta_{Z,eq} = 5,68$ and thus $P_{f,excl} = P_{f,eq} = 6,75 \cdot 10^{-9}$.

Step 3: Determination of the Failure Probability including Lack of Deformation Capacity

In this step, the failure mechanism loss of equilibrium has to be examined again. This follows simply step 2. However, the other failure mechanism that can occur is lack of rotation capacity of the joint.

The check of this mechanism can be presented as given in Figure 3. In this figure, the moment rotation characteristic of the joint connecting the beam to the core is plotted. Furthermore, the so-called beam-line is plotted, giving the relationship between the moment in the joint M and the rotation of the joint ϕ . In the extreme cases, when moment $M = 0$, the rotation $\phi = \frac{q l^3}{24 EI}$, i.e. a simple supported beam, and when the rotation $\phi = 0$, the moment $M = \frac{q l^2}{12}$, i.e. a beam with clamped supports. If the joint characteristics, designated by M_j and ϕ_j , lie above the beam-line, there is sufficient deformation capacity in the joint. The actual moment and rotation occurring in

the joint can be read from the point where the beam-line and the joint moment-rotation curve intersect. In other words, this mechanism can be described by the equation:

$$Z_{\text{rot}} = -\frac{1}{12} q l^2 + M_j + \phi_j \frac{2 E I}{l} < 0 \quad (15)$$

If $Z_{\text{rot}} < 0$, the system fails.

In this example, the partial safety factor for deformation capacity is in first instance taken equal to $\gamma_{\phi_j} = 1,0$. This value is just taken as a sample value. In step 5 of this example, for other values of γ_{ϕ_j} a reliability assessment is carried out.

The procedure of determining the reliability of the system for rotation capacity is similar to the procedure for determining the reliability of the system for equilibrium. The failure probability due to lack of rotation capacity is then: $P_{\text{f.rot}} = 6,75 \cdot 10^{-9}$.

The mechanical system as given in Figure 2 has now two different failure mechanisms:

- loss of equilibrium;
- lack of rotation (deformation) capacity.

The failure probability for loss of equilibrium will be indicated by $P_{\text{f.eq}}$, the failure probability for insufficient rotation capacity is $P_{\text{f.rot}}$. For the total system, the failure probability can be indicated as $P_{\text{f.incl}}$. This $P_{\text{f.incl}}$ is dependent on both mechanisms.

When one of the failure modes occurs, the whole system will fail. Therefore, the system may be considered as a serial system. It is, however an issue that in some (or many) cases, the system may fail due to both mechanisms at the same time. Of course, this simultaneous collapse is just a mathematical occurrence. This means that if one of the two failure modes is not considered; the system will fail due to the other failure mode. In reality the system will fail due to either loss of equilibrium or lack of rotation capacity.

The failure probability space of the system is shown in Figure 4, where a Venn diagram is shown. The overlapping area of $\{Z_{\text{eq}} < 0\}$ and $\{Z_{\text{rot}} < 0\}$ is the area where both failure mechanisms occur simultaneously. The failure probability of the system can be determined as follows:

$$\max (P_{\text{f.eq}}, P_{\text{f.rot}}) < P_{\text{f.incl}} < P_{\text{f.eq}} + P_{\text{f.rot}} \quad (16)$$

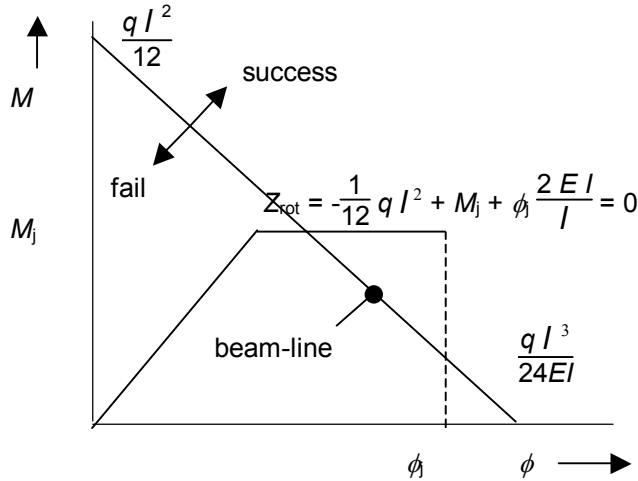


Figure 3: Beam-line

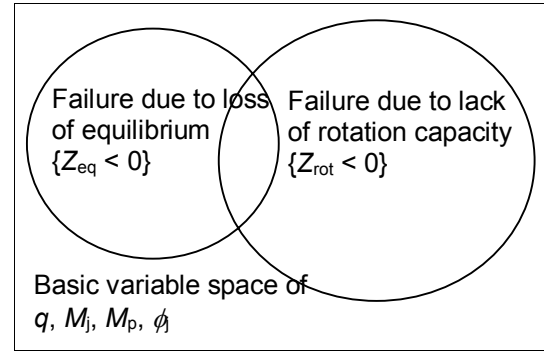


Figure 4: Venn diagram of system failure

A procedure is given by Ditlevsen (13) to determine a better value for $P_{f.incl}$ than with formula (16). This procedure is adopted in this example.

By calculating the Ditlevsen bounds for this system, an upper and lower bound for the system failure probability can be calculated: $P_{f.incl.up} = 13,05 \cdot 10^{-9}$ and $P_{f.incl.low} = 12,60 \cdot 10^{-9}$. The sum of failure probabilities $P_{f.eq} + P_{f.rot}$ is equal to $13,5 \cdot 10^{-9}$, which is close to the upper Ditlevsen bound.

Step 4: Increase in Failure Probability

Based on the previous results the increase in system failure probability can be determined as follows:

$$(12,60 - 6,75) / 6,75 \cdot 100\% < \Delta P_{f.rel} < (13,05 - 6,75) / 6,75 \cdot 100\% \quad (17)$$

$$86\% < \Delta P_{f.rel} < 93\% \quad (18)$$

In other words, the failure probability of the system with $\gamma_{\phi} = 1,0$ where rotation capacity is taken into account increases with 86 to 93% compared to the situation where only loss of equilibrium is considered.

As an upper bound of the increase of the failure probability, also $P_{f.eq} + P_{f.rot}$ of equation may be considered. In that case, the increase of failure probability can be determined as:

$$\Delta P_{f.rel} = (13,50 - 6,75) / 6,75 \cdot 100\% = 100\% \quad (19)$$

Step 5: Relation between the Partial Safety Factor and the Increase in Failure Probability

The procedure given in this section has been carried out for a variety of values for γ_{ϕ} between 1 and 2. For each value of γ_{ϕ} , the increase in failure probability is plotted in Figure 5.

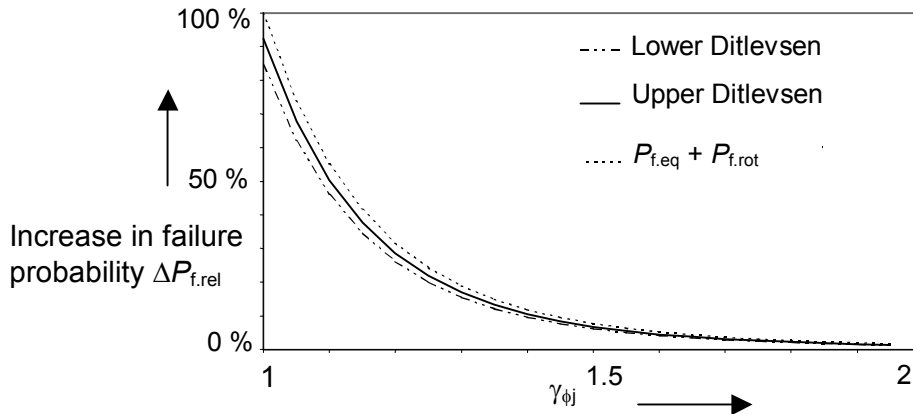


Figure 5: Effect of partial safety factor on increase of failure probability

In Figure 5 three lines are plotted. Two lines, the upper Ditlevsen bound and the lower Ditlevsen bound represent two boundaries. The real increase of failure probability will occur between those lines. The third line is the upper bound approximation $P_{f,eq} + P_{f,rot}$ of the increase of failure probability. Figure 5 can be used to make a political choice about acceptance of a lower reliability of the structure dependent on the choice of a partial safety factor γ_{ϕ_j} , e.g, for $\gamma_{\phi_j} = 1,5$, the failure probability increases by about 10%.

DISCUSSION

The feasibility of the procedure as described in previous paragraphs was illustrated with an example. This example was rather typical in the sense that the Z functions were linear and that the stochastic variables were normally distributed. Furthermore, the mechanical behaviour of the system was strongly simplified, for instance, simplified frame modelling, simplified non-linear effects and the choice of some deterministic variables.

The procedure given in this paper needs to be further elaborated. The foreseen future developments to be carried out at the Eindhoven University of Technology focus on different subjects:

- The studied structure in this example is rather simple. More complicated structures should be investigated.
- The procedure is given for the model level of a structure (by using simplified force-deformation curves). The relation between the test level (by using non-linear curves based on tests) and the model level should be further investigated in terms of reliability. Especially attention should be paid to the definitions used for design resistance, stiffness and deformation capacity and their impact on the safety of a structure (15).
- The results of the investigations are dependent on the possible failure modes considered. It may well be possible that some failure modes, which may occur in a real structure, are not taken into account (for instance lateral-torsional buckling of the beam was not considered in the example of this paper). The effect of such an omission on the relation between the partial safety factor for deformation capacity and the increase in failure probability should be investigated.
- Realistic distribution types of stochastic variables and correlations should be considered.

- The effect of the choice of deterministic variables should be investigated.

With the help of parametric studies, the effect of variables on the partial safety factor for deformation capacity should be investigated.

CONCLUSIONS AND RECOMMENDATIONS

In this paper, a procedure has been described to determine partial safety factors for deformation capacity for joints in steel and composite building structures. The idea is that a system failure probability is determined for a reference system without taking deformation capacity into consideration. Then, the system reliability is determined for the case where deformation capacity is taken into consideration. This is done for a given value of the partial safety factor for deformation capacity. The effect of different values of this partial safety factors on the failure probability can be studied with repeated calculations.

The feasibility of the procedure has been demonstrated based on a simple example. The example shows clearly the relation between the choice of the partial safety factor for deformation capacity and the reliability. Future work consists of a more realistic modelling of the problem.

With the help of this procedure, a parameter study can be carried out to find the sensitivity of the partial safety factors for deformation capacity with respect to different variables in a structural system. This is a step forward to gathering knowledge on influencing factors for deformation capacity in structural design problems.

REFERENCES

- (1) JCSS, Common unified rules for different types of construction and material, CEB bulletin No. 116E, 1976.
- (2) Eurocode 1 ENV 1991-1-1, Basis of design, CEN, Brussels, 1992.
- (3) Eurocode 3 ENV 1993-1-1, Design of steel structures Part 1.1. General rules for buildings, CEN, Brussels 1992.
- (4) NEN 6702:1991, TGB 1990, Belastingen en vervormingen, Nederlands Normalisatie Instituut, Delft, 1997.
- (5) NEN 6770:1997, TGB 1990, Staalconstructies - Basiseisen en basisrekenregels voor overwegend statisch belaste constructies, Nederlands Normalisatie Instituut, Delft, 1997.
- (6) Stark, J., Bijlaard, F., Sedlacek, G. Bolted and welded connections in steel structures. In: Bjorhovde R. et. al. (ed.): Connections in steel structures - Behaviour, strength and design, , Elsevier, London New York, pp.8-17, 1988.
- (7) ECCS Publication 107. Composite steel-concrete joints in frames for buildings: Design provisions, ECCS, Brussels, August 1999
- (8) Kuhlmann, U., in J.P. Jaspart. Recent Advances in the Field of Structural Steel Joints and their Representation in the Building Frame Analyses and Design Process, COST C1 Brussels, 1999
- (9) ECCS Publication 94. Background documentation - Eurocode 1 (ENV 1991): part 1, Basis of design, ECCS Brussels, March 1996.
- (10) Kemp, A.R., Dekker, N.W. Available Rotation Capacity in Steel and Composite Beams, The Structural Engineer, 65:5, London, pp. 96-101, 1991

- (11) Vrouwenvelder A.C.W.M. and Siemes A.J., Probabilistic calibration procedure for the derivation of partial safety factors for The Netherlands building codes. Heron No. 32(4) pp.9-29, Delft, 1987.
- (12) Schneider J., Introduction to the Safety and Reliability of Structures, Structural Engineering Document 5, IABSE, Zurich, 1997.
- (13) Ditlevsen O., Narrow Reliability Bounds for Structural Systems. Journal of Structural Mechanics. Vol VII, No. 4, pp. 453-472, 1979.
- (14) Bijlaard F.S.K., Requirements for Welded and Bolted Beam-to-Column Connections in Non-Sway Frames, Joints in Structural Steelwork, ed. by J.H. Howlet, W.M. Jenkins and R. Stainsby, Pentech Press, London, United Kingdom, 1981
- (15) Steenhuis, C.M., Snijder, H.H. Van Herwijnen F., Review of Deformation Capacity of Joints Related to Structural Reliability. To be published in the Proceedings of the NATO ARW Ouranopoulis, Greece, May 2000 "The paramount Role of Joints into the Reliable Response of Structures", ed. by C.C. Baniotopoulos and F. Wald, Kluwer, Dordrecht, The Netherlands, 2000.

END-PLATE MOMENT CONNECTIONS: TEST RESULTS AND FINITE ELEMENT METHOD VALIDATION

Emmett A. Sumner, Timothy W. Mays, and Thomas M. Murray
Department of Civil and Environmental Engineering
Virginia Polytechnic Institute
Blacksburg, Virginia 24061, USA

ABSTRACT

A series of tests on the four bolt extended unstiffened and the eight bolt extended stiffened moment end-plate connections and a validation study utilizing the finite element method were conducted as a part of the SAC Steel Project. The connections were “heavy” beam-to-column connections between large hot-rolled members that included W24, W30, and W36 beams attached to W14 columns. It was determined that the extended moment end-plate connections can be designed to provide a great deal of ductility in seismic force resisting moment frames and that the finite element method can be used to predict the behavior of end-plate connections.

INTRODUCTION

A great deal of research on the behavior and design of steel seismic load resisting moment frames has been conducted over the past several years. The primary areas of research have been on welded connections and on finding alternative connections that provide adequate ductility. The extended moment end-plate connection is one alternative that has been investigated. As a part of the SAC Steel Project, a series of full-scale beam-to-column extended moment end-plate connection tests and a validation study utilizing the finite element method have been conducted at Virginia Polytechnic Institute and State University. The primary objective of the research program was to determine the suitability of the extended moment end-plate connections for use in seismic force resisting moment frames.

Moment end-plate connections consist of a plate that is shop-welded to the end of a beam that is then field bolted to the connecting member. The connections are primarily used to connect a beam to a column or to splice two beams together. The four bolt extended unstiffened and the eight bolt extended stiffened moment end-plate configurations are the subjects of this paper. The four bolt extended unstiffened end-plate connection consists of two rows of two bolts for each flange. One row is outside the flange on the extended part of the end-plate and the other is inside the flange. The eight bolt extended stiffened end-plate connection consists of four rows of two bolts for each flange. Two rows are outside the flange on the extended part of the end-plate and the other two are inside the flange. The extended part of the end-plate is stiffened by a triangular stiffener centered over the web of the beam. Typical configurations for both connections are shown in Figure 1.

The four bolt extended unstiffened and eight bolt extended stiffened end-plate assemblies were tested under cyclic loading in accordance with the *Protocol for Fabrication, Inspection, Testing, and Documentation of Beam-column Connection Tests and Other Experimental Specimens*, SAC (1). The connections were "heavy" connections between large hot-rolled shapes. Four beam and column combinations were used: W24x68 beam and W14x120 column, W24x68 beam and W14x257 column, W30x99 beam and W14x193 column, and W36x150 beam and W14x257 column. The beam and column members were ASTM A572 Grade 50 steel and the end-plates were ASTM A36 steel. All connections were made with 1 1/4 in. diameter ASTM A325 or ASTM A490 bolts. For each beam and column combination, two end plate configurations were tested. One test was with the connection designed to develop 110 percent of the nominal plastic moment strength of the beam (strong plate connection). The other connection test was designed to develop 80 percent of the nominal plastic moment strength of the beam (weak plate connection). To investigate the effects of a composite slab on the behavior of the connection, one test was conducted using the four bolt extended unstiffened strong plate connection with a 5 in. composite slab cast onto the top flange of the beam. The test matrix for this series of tests is shown in Table 1.

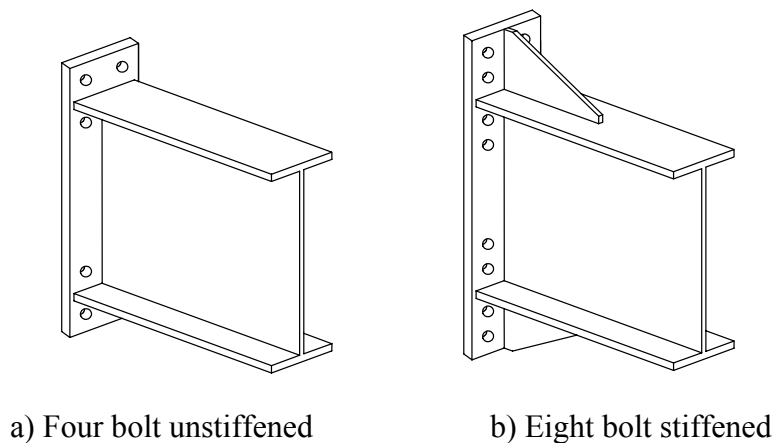


Figure 1: Extended end-plate connection configurations

DESIGN OF SPECIMENS

The design of the test specimens was done utilizing existing design methods for connections subject to monotonic static loading. The design procedure for the four bolt extended unstiffened connections uses a combination of yield line analysis for determination of the end-plate thickness and the modified Kennedy method, Murray (2); Kennedy et. al. (3) for the calculation of bolt forces. The Kennedy method is based on the "split-tee" analogy, which predicts the forces on the bolts including the effects of prying action. The design of the eight bolt extended stiffened connections was done using the detailed design procedure provided in the AISC Design Guide *Extended End-Plate Moment Connections*, Murray (4). The design guide procedure provides equations for the required plate thickness, based on strength and stiffness, and the determination of bolt forces including the effects of prying action. The equations were developed from regression analyses of data generated by the finite element method. The expected failure mode of the strong plate specimens was local flange and web buckling of the beam and the expected

failure mode of the weak plate specimens was end-plate yielding followed by bolt rupture. The column side of the connections was designed in accordance with the *AISC LRFD Manual of Steel Construction*, AISC (5) and the *AISC Seismic Provisions for Structural Steel Buildings*, AISC (6). The columns usually had continuity plates in line with both connecting beam flanges and a web doubler plate attached to one side of the web. The thickness of the continuity plates was approximately equal to the thickness of the connecting beam flanges.

Table 1: Test matrix

Specimen Identification*	Beam	No. of Connection Bolts** (Material)	End-Plate Thickness (in)
	Column		
4E-1 1/4 -1 1/2-24	W24x68	8 (A490)	1 1/2
	W14x120		
4E-1 1/4-1 1/8-24	W24x68	8 (A325)	1 1/8
	W14x120		
4E-1 1/4-1 3/8-24 with 5 in. composite slab	(2) W24x68	8 (A490)	1 3/8
	W14x257		
8ES-1 1/4-1 3/4-30	W30x99	16 (A490)	1 3/4
	W14x193		
8ES-1 1/4-1-30	W30x99	16 (A325)	1
	W14x193		
8ES-1 1/4-2 1/2-36	W36x150	16 (A490)	2 1/2
	W14x257		
8ES-1 1/4-1 1/4-36	W36x150	16 (A325)	1 1/4
	W14x257		

* 4E designates a four bolt extended unstiffened connection

8ES designates an eight bolt extended stiffened connection

** 1 1/4 in. diameter

FABRICATION OF SPECIMENS

The test specimens were fabricated by a combination of university laboratory personnel and commercial fabricators. The end-plate to beam connection was made using complete joint penetration groove welds for the flanges and fillet welds for the web. All welds were made in accordance with the *AWS Structural Welding Code*, AWS (7) using the Flux Cored Arc Welding (FCAW) process and E71T-1 welding electrodes. The flange welds were similar to AWS TC-U4b-GF utilizing a full depth 45-degree bevel and a minimal root opening, backed by a 3/8 in. fillet on the inside of the flanges. The root of the flange groove welds was backgouged after installation of the 3/8 in. fillet to remove any contaminants present from the fillet weld. As

recommended by Meng and Murray (8), weld access holes were not used. The beam web to end-plate connection consisted of 5/16 in. fillet welds on both sides of the web. Noteworthy is that the welding procedure used in the fabrication of the test specimens results in an area of non-inspected flange groove weld above the web of the beam. For the eight bolt extended stiffened connections, the stiffener to end-plate and stiffener to beam flange welds were complete joint penetration groove welds. All welds were inspected in accordance with AWS specifications, AWS (7).

TESTING

The primary test setup used in the evaluation of the connections consisted of an exterior beam-column subassembly with a single cantilever beam attached to the flange of a column. The tests were conducted in a horizontal position to allow use of the available reaction floor supports and for safety of testing. The typical test setup is shown in Figure 2. Lateral supports were provided for the beam at a spacing close enough to prevent lateral torsional buckling of the beam prior to development of its nominal plastic moment strength. A roller was used to support the beam tip and to eliminate any bending moments caused by gravity forces perpendicular to the plane of loading. The load was applied to the free end of the beam using a double acting hydraulic ram. No axial load was applied to the column.

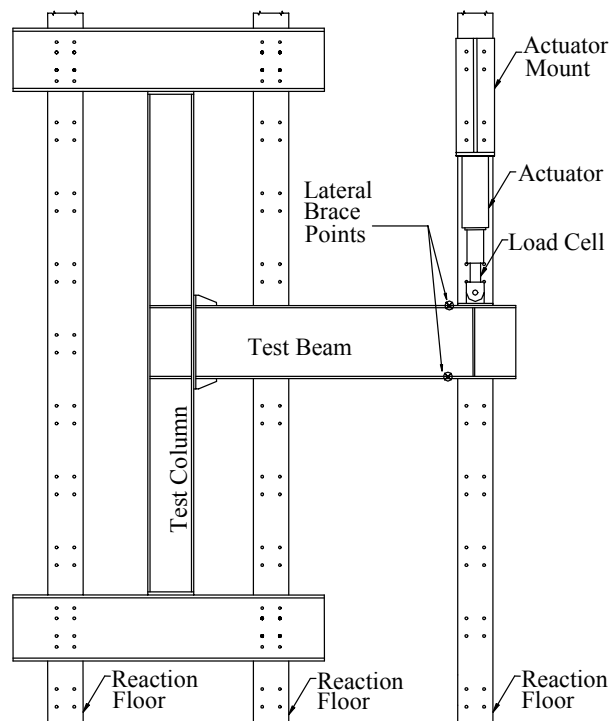


Figure 2: Plan view of test setup

Instrumentation of the test setup included a 200 kip tension-compression load cell, displacement transducers to measure the beam displacement at the point of loading, displacement transducers aligned with the column continuity plates to measure the rotation of the column at the

connection, displacement transducers to measure the panel zone rotation, instrumented calipers to measure end-plate separation from the column flange, strain gages to measure the beam and column flange strains, and strain gage rosettes to measure the panel zone strains. Additional displacement transducers were used to measure any rigid body movements of the column ends due to shifting of the test frame. All of the connection bolts were instrumented with strain gages that were installed inside the unthreaded portion of the bolt. The bolts were calibrated prior to testing to establish the load-strain relationship for each bolt. This allowed for accurate tightening of the bolts during assembly of the connection and monitoring of the bolt strains during testing.

The four bolt extended unstiffened connection test with a composite slab was an interior beam-column subassembly with two cantilever beams attached to opposite flanges of a single column. The test was conducted in a vertical position and utilized W24x68 beams and a W14x257 column. The test setup is shown in Figure 3. The base of the column was supported by a clevis pin assembly attached to support frame beams. The ends of the beams were supported by pinned-end rigid links consisting of a hydraulic ram and a tension-compression load cell attached to support frame beams. The load was applied to the free end of the column using a double acting hydraulic ram. No axial load was applied to the column. Lateral supports were provided at the ends of the beams beyond the support points and at the top of the column at the loading point. Instrumentation of the test setup was similar to the previously described tests.

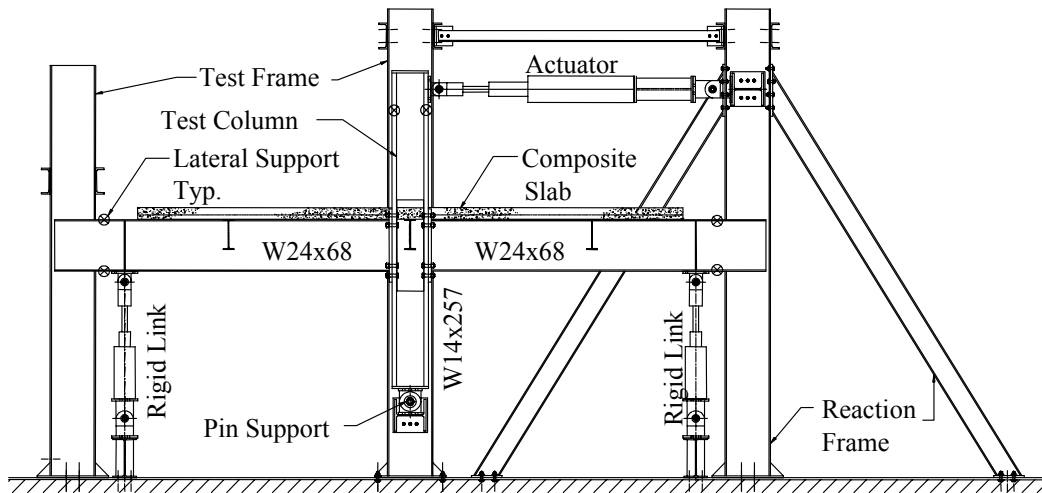


Figure 3: Elevation of slab test setup

Prior to testing, the connection bolts were tightened to the minimum pretension specified in the *AISC LRFD Specification*, AISC (5). The specimen was then whitewashed to aid in the observation of yielding within the connection region. The instrumentation was then reset and the loading was applied. The specimen was loaded in a quasi-static or "slow cyclic" manner in accordance with the *SAC Loading Protocol*, SAC (1). The loading protocol is based on the total interstory drift angle of the beam-column assembly. The interstory drift angles can be achieved by displacing either the beam tip or the column tip. In the horizontal connection tests, a hydraulic ram was used to displace the beam tip until the rotation angles specified by the loading protocol were achieved. In the vertical composite slab test, the column tip was displaced. Any rigid body rotation of the subassembly due to shifting of the test frame was monitored and subtracted

from the total rotation to ensure that the proper rotation angle was achieved. Data points were recorded at regular intervals throughout the duration of the test using a PC-based data acquisition system.

EXPERIMENTAL RESULTS

The six bare steel extended end-plate connection specimens behaved as expected. The strong plate connections (110% of the beam strength) resulted in failure of the beam, local flange and web buckling, with little or no distress observed within the connection region. The weak plate connections (80% of the beam strength) resulted in failure of the connection with one exception, the W30x99 weak plate eight bolt extended stiffened connection (8ES-1.25-1-30) resulted in failure of the beam. The four bolt extended unstiffened connection test with the composite slab did not behave as expected. The beam connections were strong plate connections, which initially resulted in local flange buckling of the beam bottom flanges, but ultimately resulted in tension rupture of the bottom flange bolts.

With the exception of the composite slab test, the strong plate specimens exhibited a great deal of ductility and energy dissipation capacity. Beam flange local buckling, the primary failure mode, is a predictable limit state that provides a ductile failure mechanism. There was no yielding or other distress of the connection region observed during the tests, which indicates that the strong plate connections remained elastic throughout the duration of the test. The total interstory drift rotations that were sustained for at least one complete loading cycle for the strong plate tests ranged from 0.050 to 0.060 radians. The maximum inelastic rotations that were sustained for at least on loading cycle ranged from 0.028 to 0.038 radians. Typical moment vs. total rotation and moment vs. inelastic rotation plots for the strong plate tests are shown in Figure 4.

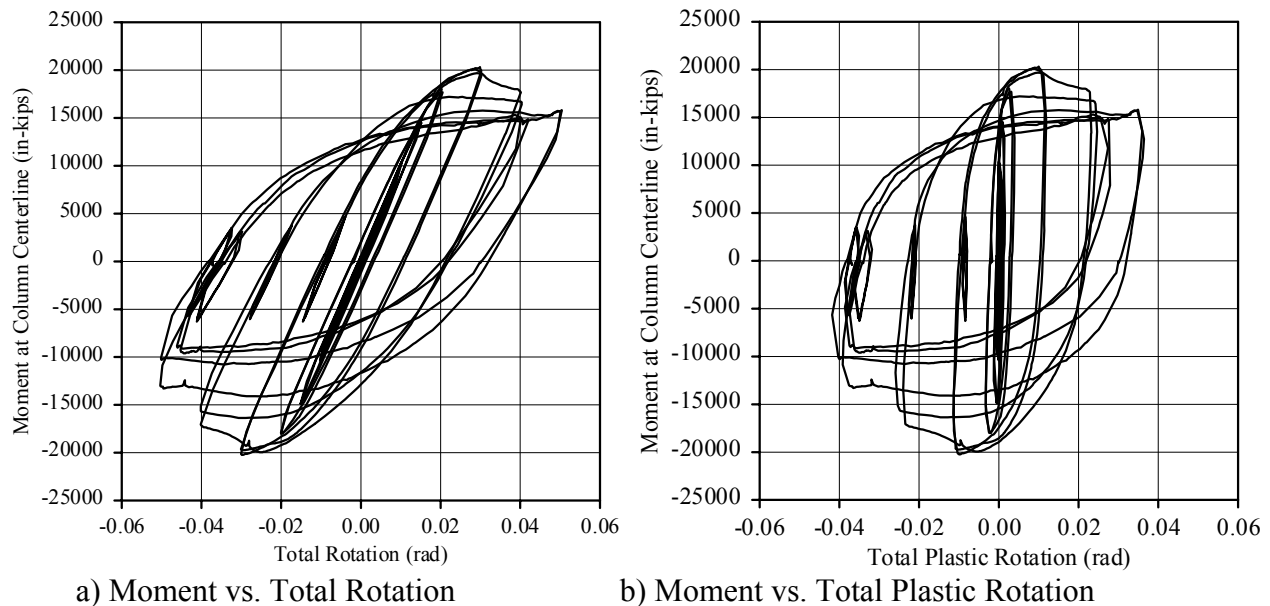


Figure 4: Typical plots of the specimen response (8ES-1.25-1.75-30)

The four bolt extended unstiffened connection test with the composite slab exhibited a moderate amount of ductility prior to its brittle failure. The bottom flanges of both beams buckled and then the bottom flange connection bolts ruptured in subsequent cycles. The total interstory drift rotations of the assembly were $+0.075 / -0.051$ radians which corresponds to inelastic rotations of $+0.053 / -0.030$ radians.

As expected, the weak plate tests did not exhibit as much ductility as the strong plate tests. The behavior of the weak plate connections was controlled by yielding of the end-plates followed by bolt rupture. In some cases, yielding of the connection region was observed as early as the third load step (0.0075 radians). These controlling limit states are more variable than the beam failure and ultimately result in brittle failure mechanisms. The total sustained interstory drift rotations for the weak plate tests ranged from 0.030 to 0.056 radians with sustained inelastic rotations greater than 0.011 radians.

The behavior of the bolts was of particular interest during the testing. The bolts in the strong plate tests gradually lost the majority of their pretension force as the load cycles increased in magnitude. The maximum observed bolt strains for these connections were only slightly higher than the initial pretension strains. A typical bolt strain vs. moment plot for a strong plate connection is shown in Figure 5a. The weak plate connection bolts were observed to have strains rising sharply above the initial pretension strains as the load steps increased in magnitude. At the higher load steps, the bolts would yield as indicated by permanent set of the bolt strains. As the bolts approached failure, the bolt strains increased very sharply exceeding the range of the strain gages. A typical bolt strain vs. moment plot for a weak plate connection is shown in Figure 5b. Noteworthy is that there were no observed differences in ductility or behavior of the A325 and A490 bolts.

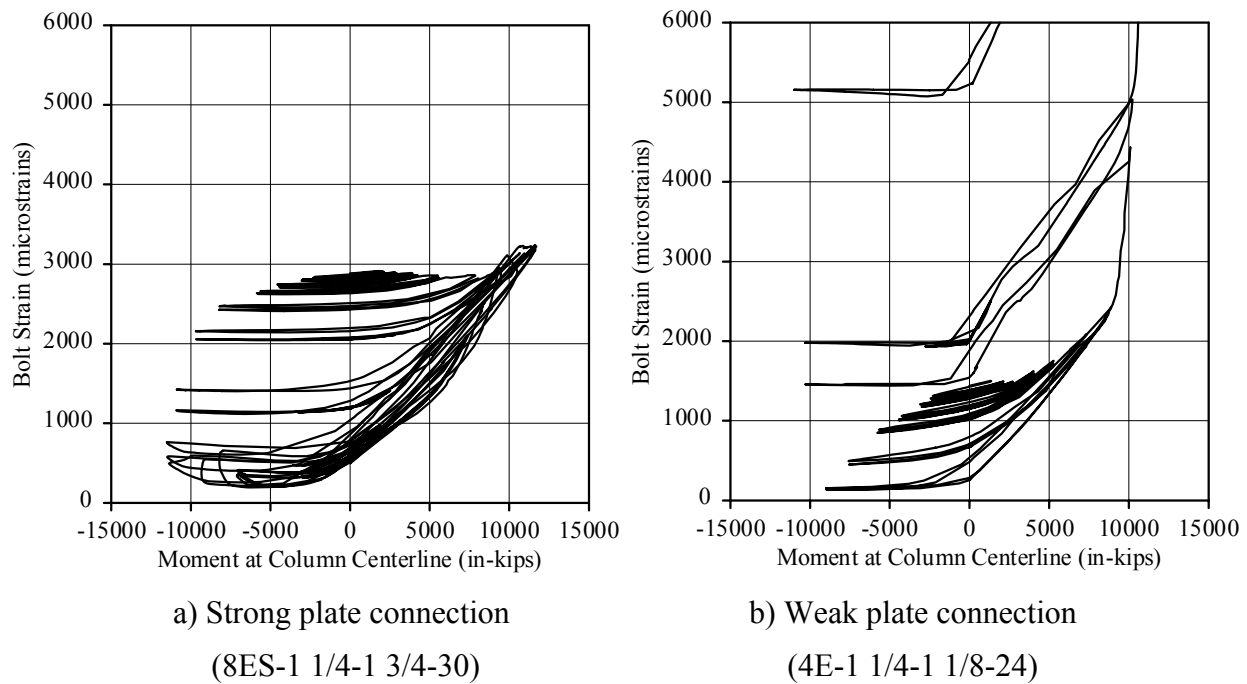


Figure 5: Typical bolt strain vs. applied moment plots

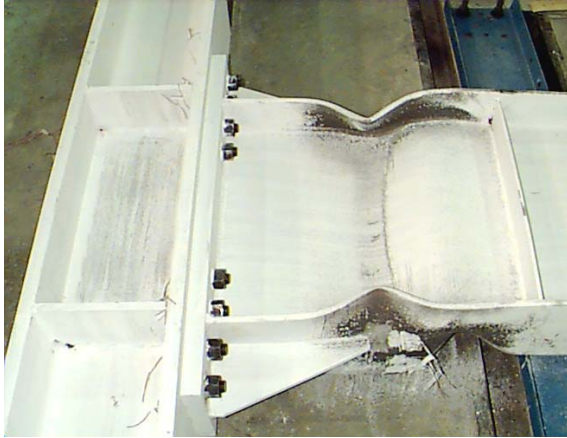
A summary of the test performance is shown Table 2. A photograph of a typical beam failure is shown in Figure 6a. The local flange buckling and severe yielding of both flanges and the web is visible. A typical connection failure is shown in Figure 6b. The severe yielding of the end-plate around the bolts and flange is clearly shown.

Table 2: Summary of test performance

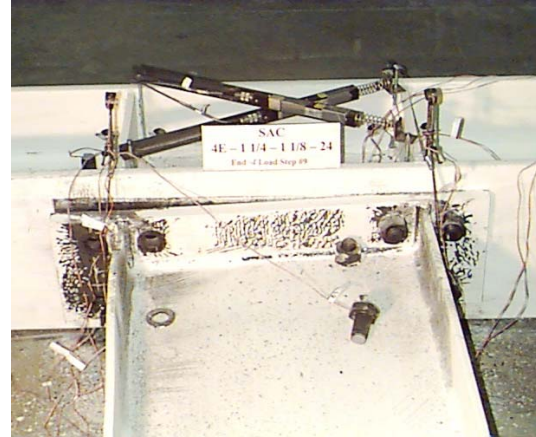
Test Identification	$M_{\max} / M_{n \text{ BEAM}}^*$	$\theta_{\text{Total Sustained}}$ (rad)	$\theta_{\text{P Max Sustained}}$ (rad)
4E-1 1/4-1 1/2-24 (Strong Plate)	1.00	0.052	0.038
4E-1 1/4-1 1/8-24 (Weak Plate)	0.95	0.040	0.021
4E-1 1/4-1 3/8-24 with composite slab (Strong Plate) 5"	North Beam	1.28	0.050
	South Beam	1.27	0.060
8ES-1 1/4-1 3/4-30 (Strong Plate)	1.00	0.050	0.036
8ES-1 1/4-1-30 (Weak Plate)	1.06	0.056	0.039
8ES-1 1/4-2 1/2-36 (Strong Plate)	1.06	0.050	0.028
8ES-1 1/4-1 1/4-36 (Weak Plate)	0.89	0.030	0.011

* M_{\max} = Maximum applied moment at the face of column

$$M_{n \text{ BEAM}} = R_y [(F_y + F_u)/2] Z_x = 1.1[(50+65)/2] Z_x$$



a) Strong plate connection
(8ES-1 1/4-1 3/4-30)



b) Weak plate connection
(4E-1 1/4-1 1/8-24)

Figure 6: Photographs of typical failures

FINITE ELEMENT MODELING

Current design practice in the United States requires that steel connections that are part of seismic lateral force resisting systems be tested prior to use. However, proper use of the finite element method may provide a basis for justifying a connection configuration for seismic design use. To examine this possibility, finite element models were developed and the results compared to results from several of the tests. The 4E-1 1/4-1 1/8-24 specimen results are reported here. Additional analyses and more detailed results are found in Mays (9).

The ANSYS finite element program was used to model the connection. Solid eight-node brick elements that include plasticity effects were used to model the beam section and column flange. Solid twenty-node elements were used to model the bolts and end-plate. Symmetry about the beam web centerline was used. Contact elements were included between the end-plate and the rigid column flange to model movement of the end-plate away from the column flange. The loading at the end of the beam cantilever matched the “backbone” curve of the experimental results. Prying forces and plastic behavior in the bolts were tracked until divergence occurred due to numerical instability.

Figure 7 shows a portion of the finite element model and the Von Mises stress distribution at the tension flange region. The Von Mises stresses shown are for an applied moment of 10,080 in-kips, which closely corresponds to the maximum applied moment of 10,600 in-kips from the experimental test. For this model the beam material yield stress was taken an assumed value of 55 ksi and the end-plate material at the measured value of 37.9 ksi. The beam flange stresses in Figure 7a indicate that yielding has not occurred; however the end-plate material yield stress is exceeded as shown in Figure 7b.

a) Beam-to-column flange connection

b) Isolated end plate

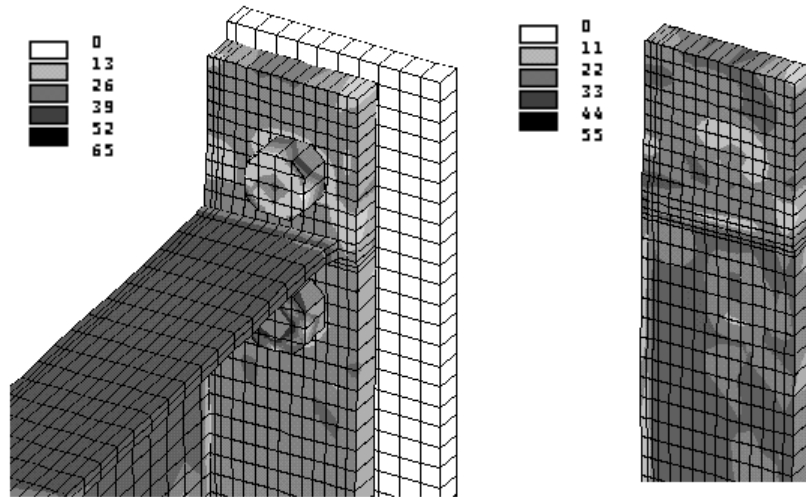


Figure 7: Von Mises stress (ksi) distribution for 4E-1 1/4-1 1/8-24

Figure 8 shows nearly identical relationships for the measured and finite element method predicted applied moment versus end-plate separation curves. Figure 9 compares experimental and finite element method predicted bolt forces as a function of applied moment. As expected, the monitored exterior bolt yielded before the monitored interior bolt. The exterior portion of the end-plate is less stiff than the interior portion and therefore exterior bolt forces tend to be greater because of larger prying forces. These results indicate that, indeed, the finite element method may possibly be used to qualify other end-plate connection configurations for use in seismic lateral force resisting frames.

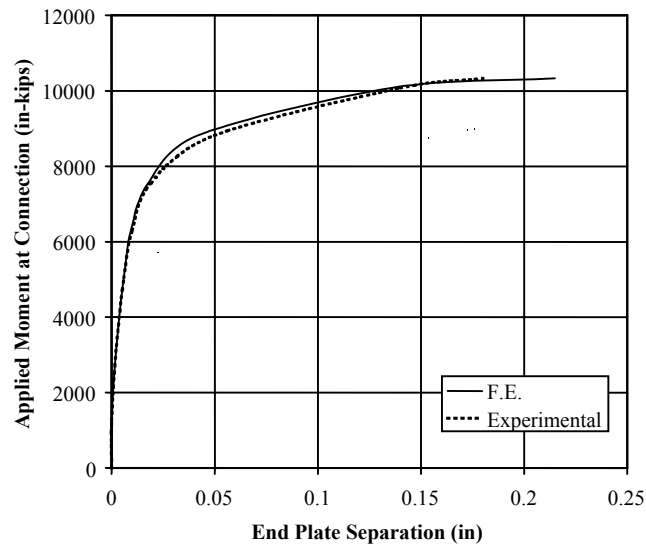


Figure 8: Applied moment vs. end plate separation for 4E-1 1/4-1 1/8-24

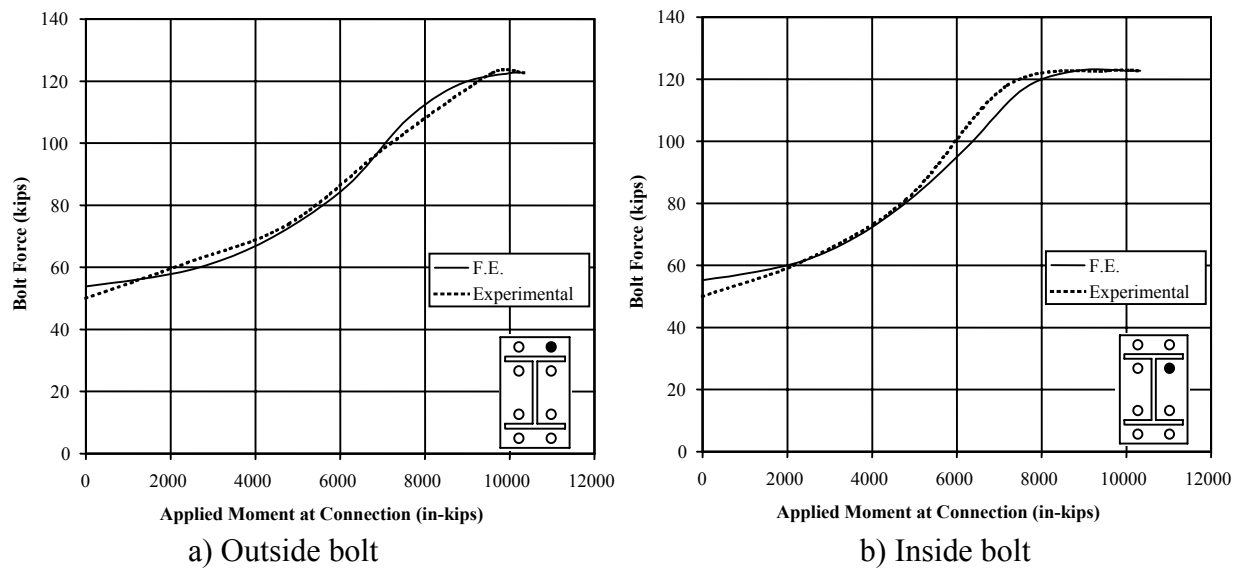


Figure 9: Bolt force vs. applied moment for 4E-1 1/4-1 1/8-24

SUMMARY

The results of the six extended moment end-plate connection test indicated that the four bolt unstiffened and eight bolt stiffened extended moment end-plate connections can be designed to withstand cyclic loading and are suitable for use in seismic force resisting moment frames. The strong plate connections exhibited the most ductility while the weak plate connection typically failed in a brittle manner. Results from the test conducted with a composite slab, indicates that the effects of the slab should be considered in the design of the connections. The results from the finite element modeling indicate that the finite element method can be used to predict the behavior of end-plate connections. Additional details and discussion of the extended moment end-plate connection testing completed as a part of the SAC Steel Project can be found in Sumner *et al* (10).

ACKNOWLEDGMENTS

Funding for this research was provided by the Federal Emergency Management Agency through the SAC Joint Venture. SAC is a partnership of the Structural Engineers Association of California, the Applied Technology Council, and California Universities for Research in Earthquake Engineering. Appreciation is extended to FEI Limited and Cives Steel Company for their donation of labor for the fabrication of the test specimens and to PSI, Inc for the donation of welding inspection services. Appreciation is also extended to Nucor-Yamato Steel Company and The Lincoln Electric Company for the donation of test materials.

NOTATION

F_u	=	specified minimum tensile strength
F_y	=	specified minimum yield stress
in.	=	inch, inches
ksi	=	kips per square inch
rad	=	radians
vs.	=	versus
Z_x	=	plastic section modulus

REFERENCES

1. SAC (1997). *Protocol for Fabrication, Inspection, Testing and Documentation of Beam-Column Connection Tests and Other Experimental Specimens*, Report No. SAC/BD-97/02, SAC Joint Venture.
2. Murray, T. M., (1988). "Recent Developments for the Design of Moment End-Plate Connections," *Journal of Constructional Steel Research*, Vol. 10, pp. 133-162.
3. Kennedy, N. A., Vinnakota, S., Sherbourne, A. (1981). The split-tee analogy in bolted splices and beam-column connections, *Joints in Structural Steelwork*, John Wiley and Sons, New York, pp. 2.138-2.157.
4. Murray, T. M., (1990). *AISC Design Guide Extended End-Plate Moment Connections*, American Institute of Steel Construction, Chicago.
5. AISC (1994). *Load and Resistance Factor Design Manual of Steel Construction*, American Institute of Steel Construction, Chicago.
6. AISC (1997). *Seismic Provisions for Structural Steel Buildings*, American Institute of Steel Construction, Chicago.
7. AWS (1998). *Structural Welding Code - Steel AWS D1.1-98*, American Welding Society, Miami.
8. Meng, R. L. and Murray, T. M. (1997). "Seismic Performance of Bolted End-Plate Moment Connections," *Proceedings of the 1997 National Steel Construction Conference, Chicago, Illinois*, AISC, May 7-9, 1997, 30-1 – 30-14.
9. Mays, T. W., (2000). *Application of the Finite Element Method to the Seismic Design and Analysis of Large Moment End-Plate Connections*, Ph.D. Dissertation, Virginia Polytechnic Institute and State University, Blacksburg, Virginia.
10. Sumner, E. A., Mays, T. W. and Murray, T. M., (2000). "Cyclic Testing of Bolted Moment End-Plate Connections," Research Report SAC/BD-00/21, CE/VPI-ST 00/03, Department of Civil and Environmental Engineering, Virginia Polytechnic Institute and State University, Blacksburg, Virginia.

DESIGN AND BEHAVIOR OF A REAL PR BUILDING

Clinton O. Rex, Ph.D., P.E.
Arvind V. Goverdhan, Ph.D.
Stanley D. Lindsey and Associates Ltd.
2300 Windy Ridge Pkwy; Suite 200 South
Atlanta, Georgia 30339, U.S.A.

ABSTRACT

The use of PR-Connections in steel buildings can result in very economical designs. In addition, because the fabrication details are not complicated and most welding is eliminated, PR buildings are fast and simple to erect. The writer's firm has designed several constructed buildings that utilize PR-Connections. The purpose of this paper is to present an analytical study of one such building. This study considers the design and behavior of the PR connections, columns, beams, and resulting frames. The study also considers the effect of connection modeling and connection shakedown on the final design.

INTRODUCTION

The writer's firm has been associated with the design and construction of a variety of PR buildings. The fabricators and erectors that have worked on these buildings find that they are fast and simple to erect in comparison to more traditional rigid frame (FR) buildings that typically require a substantial amount of field welding. In addition, in certain circumstances, using PR connections has reduced the overall steel weight for the building.

Despite these obvious advantages, there are very few if any other firms in the United States designing PR buildings. There are most likely a variety of reasons for this; however, in the writer's opinion there are three major reasons. First, the current literature does not provide clear guidance as to when or if PR buildings are more economical than FR buildings. This type of literature has to come from an authoritative body such as The American Institute of Steel Construction (AISC) or from designers and builders of real projects. Second, there is currently not a single authoritative guide to designing PR buildings. The writer's firm has had to put together a design procedure that is based on a stack of journal papers, research reports, and design guides. In addition, after all the literature has been reviewed, there are still a variety of gaps and problems with the design guidance. Third, there is a lack of appropriate computer software tools commercially available to the designer which incorporate the design guidance in the literature. In the writer's opinion, hand methods for the design of PR buildings are not and will not be used by practicing engineers. Reliable and well-documented design software must be available.

This paper presents an analytical study of a real PR building. In this study, specifics regarding the design of the connections, beams, and columns are presented. In addition, two specific design considerations are examined. The first consideration is what impact the analytical representation of the moment-rotation curve has on the building design. The second consideration is how connection shakedown, resulting from transient loads, influences the ability to reduce beam sizes in PR moment frames compared to beam sizes determined by assuming simple supports.

STUDY BUILDING

The study building is a four-story office building in Louisville, Kentucky. The floor system is constructed of four-inches of normal weight concrete on 9/16-inch permanent form deck. The deck sits on steel bar joists that rest on wide-flange steel girders. The building cladding consists of pre-cast concrete panels. The lateral system consists of PR frames in the North-South direction and FR frames in the East-West direction. A schematic of the typical floor plan for the building is presented in Fig. 1.

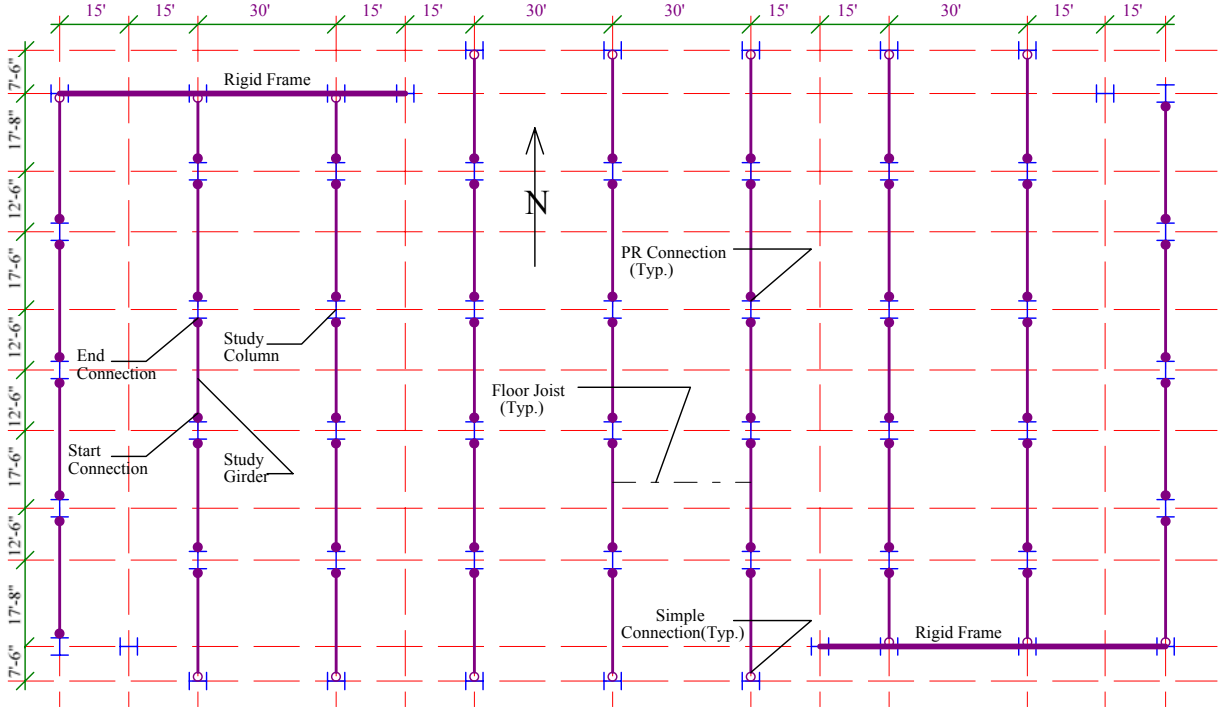


Figure 1 – Study Building Level 2 Floor Plan

BUILDING LOADS

Typical floor loads included a dead load (DL) of 56 psf, a superimposed dead load (SD) of 30 psf and a reducible live load (LL) of 80 psf. Floor loading within the core of the building included a dead load of 56 psf, a superimposed dead load of 10 psf and a non-reducible live load (NRL) of 125 psf. Typical roof loading included a dead load of 20 psf, a superimposed dead load of 10 psf, and a non-reducible live load of 20 psf. Within the mechanical penthouse

(located on the roof) a dead load of 113 psf, a superimposed dead load of 10 psf, and a non-reducible live load of 50 psf were used. A superimposed dead load of approximately 720 plf was assumed for the pre-cast panels.

The wind (WL) and earthquake (EQ) lateral loads are summarized in Table 1 below. A basic wind speed of 70 miles per hour (mph) and an A_v of 0.07 and an A_a of 0.05 were used to calculate the lateral loads. In the North-South (N-S) direction the wind forces exceed the EQ forces and control the design of the PR-frames. In the East-West (E-W) direction the EQ forces exceed the wind forces and control the design of the rigid-frames. This combination of wind forces controlling the design in one direction while EQ forces control the design in the opposite direction is typical for the design of many office buildings along the east coast of the USA.

Table 1 – Summary of Building Lateral Loads

Level	Wind E-W (Kips)	Wind N-S (Kips)	EQ E-W (Kips)	EQ N-S (Kips)
Roof	32	81	60	60
Floor 4	24	47	64	64
Floor 3	21	43	35	35
Floor 2	20	40	17	17
Base Shear	97	211	176	176

BUILDING ANALYSIS

A three-dimensional model of the entire building including all PR frames, FR frames, and leaner columns was used. Gravity loads were applied to frame beams with appropriate live load reductions. Wind loads were applied as point loads to master nodes at each floor. The master nodes were located at the center of wind force and a rigid diaphragm was assumed at each floor to distribute the wind load. All the analysis was conducting using an in-house program.

A Stage I analysis of the building was conducted first. This was a first-order (no P- Δ or P- δ) non-linear connection, path independent analysis of the building considering only gravity loads. Non-linear connection analysis simply means that the full non-linear connection moment-rotation behavior was considered in the analysis. This is done by using a secant stiffness that is based on the current moment and rotation at the connection which follows the moment-rotation behavior input for the connection. Path independent means that the connection is assumed to load and unload along the non-linear connection curve. Consequently, the sequence of loading does not influence the result. The purpose of this analysis is to determine the column loads that result from the applied beam loads. The resulting column loads are then corrected to reflect the fact that not all of the floor members that frame into the columns were present in the model and that there is a difference in live load reductions for beams and columns. This is done using a method similar to that described by Ziemian (1).

A Stage II analysis was then conducted. This analysis was a second-order (with P- Δ and P- δ), non-linear connection, path independent analysis. The second-order behavior is incorporated

into the analysis by use of a stability function stiffness matrix for the column elements, which is described in Chapter 8 of Beaufait et al. (2). In addition, load combinations are prescribed such that a single analysis is done for each load combination rather than superimposing the analysis results from the primary loads (DL, SD, LL, NRL, WL) that make up the load combination. This is the typical analysis conducted by the writer’s firm for most PR building designs.

A Stage III analysis was then conducted. This analysis is the same as the Stage II analysis with the exception that the connections are represented with a fixed linear stiffness rather than the full non-linear moment-rotation behavior. The connection stiffness assumed was the secant stiffness associated with 0.0025 radians as recommended in ASCE (3).

A Stage IV analysis was the last analysis conducted in the study. This analysis was a second-order (with P-Δ and P-δ), non-linear connection, path dependent analysis. The path dependence is incorporated into the analysis by assuming a connection behavior with more realistic loading and unloading assumptions. This behavior is shown graphically in Fig. 2 and is described in more detail later. In this analysis, a number of load cases are considered. Each load case is made up of a series of load steps. Each load step is one of the primary loads multiplied by a load factor. The load cases considered in this analysis are presented in Table 2 below. The 0.4 live load in combination with wind is based on Ellingwood (4). Because the PR frames are of interest in this study the WL in the load cases is the WL in the N-S direction. The Stage IV analysis is considered to be the most exact analysis; however, it should be noted that it is impractical to use on a daily design basis.

Table 2 – Load Cases For Stage IV Analysis

Analysis Step	Case S1	Case S2	Case S3	Case S4	Case S5	Case S6	Case S7
Step 1	+1.0 DL	+1.0 DL	+1.0 DL	+1.0 DL	+1.0 DL	+1.0 DL	+1.0 DL
Step 2		+1.0 SD	+1.0 SD	+1.0 SD	+1.0 SD	+1.0 SD	+1.0 SD
Step 3			+1.0 LL	+1.0 LL	+1.0 LL	+1.0 LL	+1.0 WL
Step 4			+1.0 NRL	+1.0 NRL	+1.0 NRL	+1.0 NRL	-2.0 WL
Step 5				-1.0 LL	-0.6 LL	-0.6 LL	+2.0 WL
Step 6				-1.0 NRL	-0.6 NRL	-0.6 NRL	-1.0 WL
Step 7					+1.0 WL	+1.0 WL	+1.0 LL
Step 8					-2.0 WL	-2.0 WL	+1.0 NRL
Step 9					+2.0 WL	+2.0 WL	
Step 10						-1.0 WL	
Step 11						+0.6 LL	
Step 12						+0.6 NRL	

CONNECTIONS

Steel PR connections were used. Composite connections could not be used because of the bar joist floor framing. The steel connections were top and bottom seat-angle with web angle connections. The typical connection detail used on the project is shown in Fig 2. It should be noted that only one connection type was used on the entire job. The connections angle sizes were not adjusted to try to “tune” the building as has been suggested in past literature. Such

variations in angle sizes throughout the job results in increased complexity and installation problems.

The moment-rotation behavior for the connection was determined using Eq 1 below and is shown graphically in Fig 2. M_{cu} is the ultimate moment capacity of the connection and θ_0 is a reference rotation take as M_{cu} / K_{ci} where K_{ci} is the initial stiffness of the connection. The parameter n is a shape parameter. A method for calculating values for each of these variables is given in Mayangarum (5). M_c and θ_c are the connection moment and rotation respectively.

$$\frac{M_c}{M_{cu}} = \frac{\frac{\theta_c}{\theta_0}}{\left[1 + \left(\frac{\theta_c}{\theta_0}\right)^n\right]^{\frac{1}{n}}} \quad (\text{Eq 1})$$

In the Stage I and II analysis, the connection is assumed to load and unload along the non-linear connection curve shown in Fig. 2. In the Stage III analysis the connection is assumed to load and unload along the secant stiffness shown in Fig. 2. In the Stage IV analysis the connection is assumed to initially load along the non-linear connection curve; however, subsequent unloading and reloading is assumed to occur along a line with a slope similar to the initial connection stiffness.

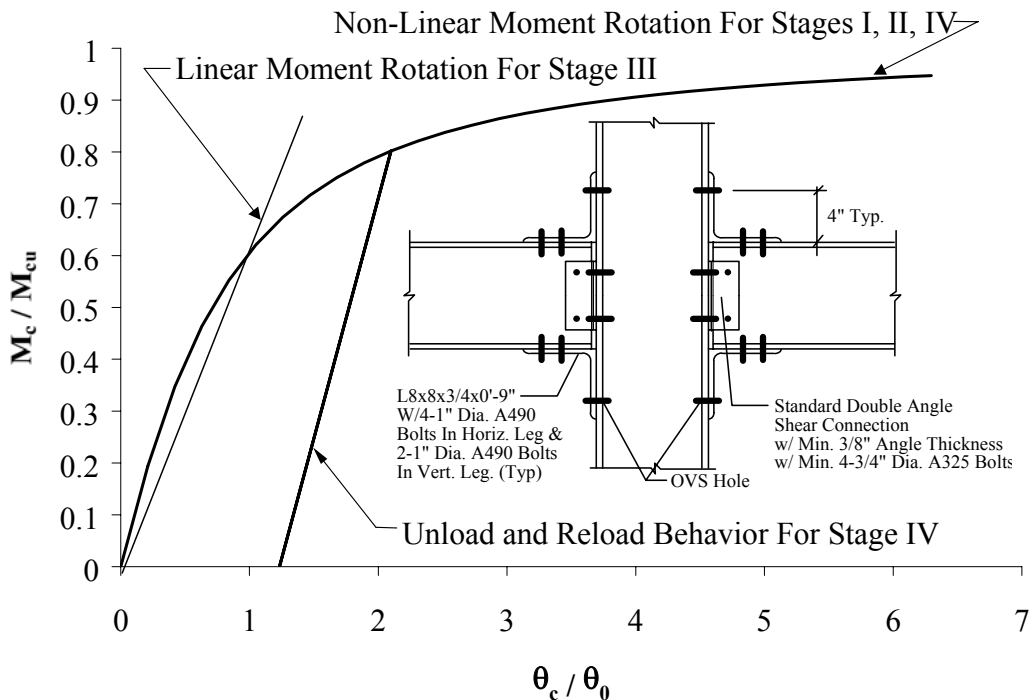


Figure 2 – Typical PR Connection

In the event of a moment reversal, the connection behavior was assumed to be anti-symmetric about the abscissa except that the origin of the non-linear behavior was shifted to coincide with the rotation at the point of moment reversal. This is essentially the hysteretic behavior recommended by Surochnikoff (6); however, the writers recognize that this is most likely not an appropriate hysteretic behavior for the top and bottom angle connections used. Despite this understanding, the hysteretic behavior was chosen because the study results showed that the connections did not go through a moment reversal. Consequently, the first quadrant of the hysteretic behavior was believed to be the most important and is believed to be valid for this connection type. However, it should be noted that future PR connection research should include cycles in the positive rotation quadrants to better define this behavior.

The typical beam sizes on the job were W21 and W24 beams. Values of the connection and beam parameters are shown in Table 3 below. The quantity M_{cu}/M_p is the ratio of connection strength over the plastic moment strength of the bare steel beam. This range of connection to beam strengths is typical for the PR buildings designed by the writer's firm. This ratio is notably less than the 0.75 ratio recommended by ASCE (3).

Table 3 – Summary of Connection and Typical Beam Properties

Beam	M_p (K-in)	M_{cu} (K-in)	M_{cu}/M_p	K_{ci} (K-in/rad)	n
W21x44	4296	2127	0.50	777,461	1.05
W21x68	7200	2127	0.30	777,461	1.05
W24x68	7968	2417	0.30	1,005,000	0.97

Summary plots of the connection moment-rotation behavior for the start and end connections on the study girder (shown in Fig. 1) are presented in Fig. 3 and 4. As can be seen in Fig. 3 and 4, the connections do not go through a moment reversal for Load Cases S4 and S6. In both of these load cases the beams are fully loaded and then some portion of the live load is removed. Subsequent gravity loading and lateral loading result in the connections simply following up and down the linear unloading curve. This occurs for two reasons. First, there is no moment reversal. Second, the connection moments generated by the wind loading are less than the live load removed and are less than the connection moment that remains when the live load is removed.

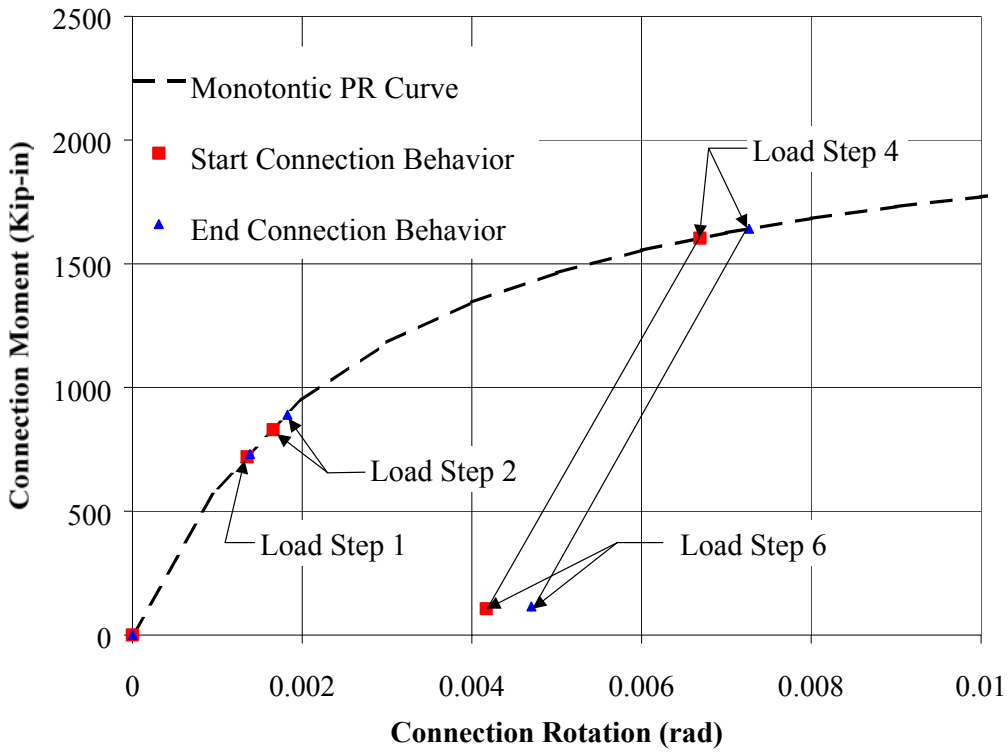


Figure 3 – PR Connection Behavior For Load Case S4

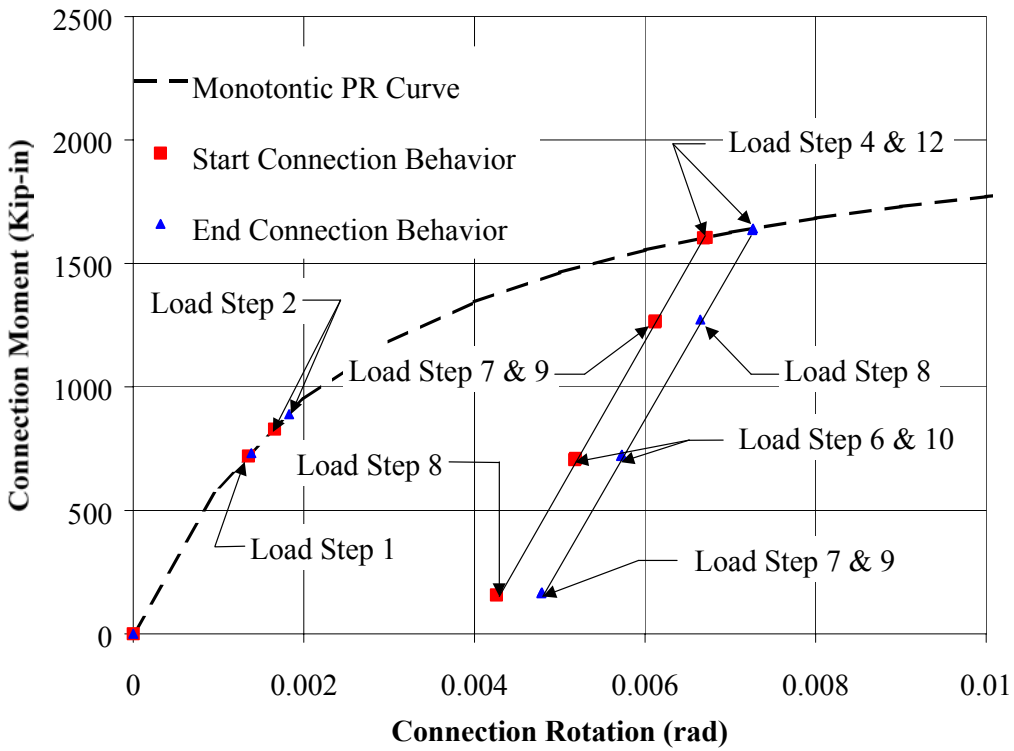


Figure 4 – PR Connection Behavior For Load Case S6

BUILDING BEHAVIOR

The period and story drifts are the primary building characteristics considered in design. A modal analysis was used to determine the frame period. Because this is an elastic analysis, a constant connection stiffness must be used (i.e. not the non-linear connection behavior). In design the frame period is typically used to determine seismic forces. The lower the period the higher the seismic forces. Consequently, the initial stiffness of the connection was used in the modal analysis. This results in the lowest frame period and conservative seismic forces. The building period in the N-S direction (PR frame direction) was calculated as 1.83 seconds. The building period in the E-W direction (FR frame direction) was calculated as 2.55 seconds.

As discussed above, the wind lateral forces in the direction of the PR frames were higher than the seismic lateral forces. Consequently, the drift resulting from wind loads is the only drift of interest in this design. The study frame drifts for the Stage II, III, and IV analysis are summarized in Table 4.

Table 4 – Summary of Frame Drift Resulting From Wind (in)

Level	Roof	4	3	2
Level Height (H) (Ft)	58.1	43.7	30.1	16.6
H/400 (in)	1.74	1.31	0.90	0.50
Stage II Analysis				
S5 +/- WL	2.29	1.94	1.33	0.63
Stage III Analysis				
S5 +/- WL	1.38	1.15	0.81	0.43
Stage IV Analysis				
S5 +WL	1.25	1.05	0.75	0.40
S5 -WL	-1.25	-1.05	-0.75	-0.40
S6 +WL	1.25	1.05	0.75	0.40
S6 -WL	-1.25	-1.05	-0.75	-0.40
S7 +WL	1.53/1.32	1.29/1.10	0.9/0.77	0.46/0.41
S7 -WL	-1.12	-0.93	-0.65	-0.37

Consider the results of the Stage IV Analysis first. For Load Case S5 and S6, the full live load was applied and then 0.6 of the live load was removed before wind loads were applied. As shown in Fig.4, this type of loading resulted in the connections behaving elastically for subsequent wind loading and unloading. Consequently, the building drifts are the same in each direction and for both of the load combinations. In Load Case 7 the connections were not unloaded prior to the wind loading occurring. Consequently, when wind load was applied in the positive direction (South), the start connection loaded along the non-linear connection curve while the end connection unloaded along the elastic unloading curve. This is shown in Fig. 5. In the subsequent negative loading (North), the start connection re-loaded along the elastic curve until it hit the original non-linear curve and then started loading along the non-linear curve. The end connection simply unloaded along the elastic unloading curve. After this point, the

connections follow the elastic loading and unloading curve during any further wind loading in either direction. The result of this loading sequence is that the building develops a permanent set in the direction of the first applied wind loading and that after one full load reversal the wind deflections in the direction of the first loading will reduce. This is shown for the S7+WL entry in Table 4. The first value is the building drift resulting from the first wind load. The second value is the building drift that results from any subsequent wind load after a full wind load reversal. Because the connections behave elastically after the first full wind loading in the negative direction, the story drift in the negative direction does not exhibit this reduction in drift. The permanent set in the building is one-half the difference between the final drift in the positive direction and the drift in the negative direction. For Load Case 7 the permanent set is one-half of 1.32 inches – 1.12 inches, or 0.1 inches.

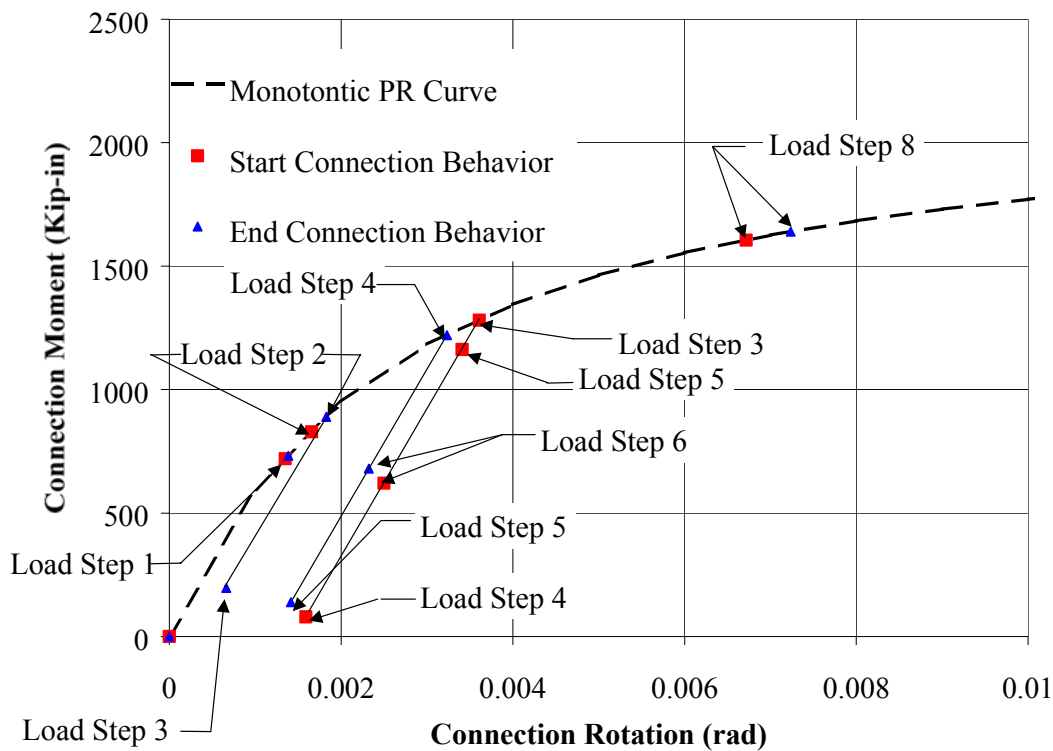


Figure 5 – PR Connection Behavior For Load Case S7

Next, consider the differences between the Stage II, III, and IV Analysis results. Because of the path independent nature of the Stage II and III Analysis, the lateral drift results are the same for Load Cases 5, 6 and 7. Consequently, the results for Load Case 5 are the only results presented. Review of Table 4 shows that the Stage II analysis provides a very conservative estimate of building drift compared to the Stage IV analysis. The Stage III analysis provides a much better estimate of the building drifts. The reason for the large discrepancy between the Stage II and Stage IV analysis can be attributed to the resulting elastic behavior the connections attain after an unloading cycle. The unloading can occur during removal of live load and / or wind load cycles. The resulting elastic behavior means that less connection rotation is required to develop the connection moments required to resist the wind forces. Less rotation results in less building drift.

COLUMN BEHAVIOR

The study column location is shown in Fig. 1. A gravity analysis for each column was done including live load reductions. The ultimate axial column load (P_u) was determined to be 651 Kips. A W12X72 was selected as a preliminary column size. This column has an axial load strength of 655 Kips assuming an effective length factor of 1.0. A Stage II building analysis was done using the standard ultimate strength load combinations prescribed by the building code. The combination of gravity plus lateral ended up controlling the design with design forces of $P_u = 524$ Kips and $M_u = 171$ Kip-ft. A W12X87 column size was required for these design forces. The effective length factor was calculated as 1.65 using the method outlined by Driscoll (7).

BEAM BEHAVIOR

The study beam location is shown in Fig.1. The loads on this beam were 1.686 Kips/ft DL, 0.301 Kips/ft SD, and 3.763 Kips/ft NRL. Beam depth within the floor plate was limited to 21-inches to minimize the floor-to-floor height. A preliminary design based on a beam with simple connections resulted in a W21x83 preliminary size. The preliminary design was controlled by the moment strength limit state where M_u was approximately 7956 Kip-inches. After the building was analyzed and some design iterations were completed, a final beam size of a W21X68 was chosen. This reduction in beam size resulted in roughly a 7% reduction in steel weight for the typical floor.

Table 5 – Summary of Study Beam Deflections and Moments

Load Case	Deflections (in)			Positive Moments (Kip-in)		
	Stage II	Stage III	Stage IV	Stage II	Stage III	Stage IV
S1	0.15	0.17	0.15	854	908	854
S2	0.18	0.19	0.18	1003	1031	1003
S3	0.75	0.61	0.75	3767	3212	3767
S4	0.18	0.19	0.37	1003	1031	1752
S5	0.43	0.36	0.53	2163	1904	2557
S6	0.75	0.61	0.75	3767	3212	3767
S7	0.75	0.61	0.75	3767	3212	3767

The deflections and moments from the Stage II, III and IV analysis are presented in Table 5 below. First consider the results of the Stage IV analysis. The S1 deflection is the DL deflection. The S2 deflection is the combined DL and SD deflection. Consequently, the incremental deflection associated with adding the SD is the S2 deflection minus the S1 deflection. Similarly, the incremental deflection associated with the live load deflection is the S3 deflection minus the S2 deflection. For the study beam the incremental live load deflection is 0.57 in. When the live load is removed, as in Load Case 4, the connection behaves elastically and the resulting deflection is larger than the S2 deflection because of the plastic deformation that has taken place in the connection. From the design standpoint, this simply means that a

Stage II Analysis will provide accurate live load deflection estimates assuming the connection does not degrade because of moment reversals.

Now compare beam deflections considering Stage II, III, and IV results. The Stage II and IV results are identical except for Load Case S4 (the reasoning for this was discussed above) and for Load Case S5. The deflection for Load Case S5 is larger in the Stage IV analysis than in the Stage II analysis for the same reasons it is larger in Load Case S4. The plastic connection deformation caused by the full gravity loading and then unloading of a portion of the live load resulted in larger connection rotations than in the Stage II analysis. Again, from a design standpoint this means that as long as the combined wind, dead, and reduced live load moments don't exceed the dead and full live load moments then the full live load deflection determined from a Stage II analysis will be correct and can be used for design.

The Stage III results show that as the load is increased the calculated deflections go from conservative to un-conservative estimates. This is an obvious observation any time a constant stiffness is assumed for the connection. The ability of a Stage III analysis to predict beam deflections is very sensitive to the assumed stiffness. Because of this, a Stage III analysis is not recommended for beam deflection estimates. Review of the beam moments presented in Table 5 show the same type of relationships seen for beam deflections.

CONCLUSIONS

This paper has presented the design and analytical study of a real PR building. The following conclusions were determined for the building considered in this study:

1. Connection behavior stayed in the positive moment and positive rotation region of the moment rotation curve. Consequently, connection shakedown had no real effect on the design. Future research on PR connections should include cyclic testing of the connections in the positive rotation region to better define the connection behavior in this region.
2. Initial beam and column sizes can be estimated by assuming simply supported beams and braced columns.
3. A Stage II analysis results in overly conservative building drift estimates; while, a Stage III analysis provided much better drift estimates.
4. If wind, dead, and reduced live load connection moment does not exceed the dead and full live load connection moment then a Stage II analysis can be used to accurately predict the full live load beam deflections.
5. A Stage III analysis should not be used to determine beam deflections because of how sensitive the deflections are to the stiffness assumed in the analysis.

These conclusions are based on the design and analysis of a single building. The validity of these conclusions when considering other buildings will depend on a variety of factors including but not limited to the building geometry, the gravity and lateral loads and the number of PR frames.

REFERENCES

- (1) Ziemian, R.D., and McGuire, W. (1992), "A Method for Incorporating Live Load Reduction Provisions in Frame Analysis," *Engineering Journal* 29(1):1-3, American Institute of Steel Construction
- (2) Beaufait, F. W., Rowan, W. H. Jr., Hoadley, P.G., Hackett, R. M (1975), *Computer Methods of Structural Analysis*, Third Edition, Prentice Hall.
- (3) ASCE Task Committee on Design Criteria for Composite Structures in Steel and Concrete (1998) "Design Guide For Partially Restrained Composite Connections" *Journal of Structural Engineering*, 124(10): 1099-1113, American Society of Civil Engineers
- (4) Ellingwood, B. (1989) "Serviceability Guidelines for Steel Structures," *Engineering Journal* 26(1):1-8, American Institute of Steel Construction
- (5) Mayangarum, A. (1996) "Design, Analysis, and Application of Bolted Semi-Rigid connections For Moment Resisting Frames," MS Thesis, Lehigh University, Bethlehem, PA.
- (6) Sourochnikoff, B. (1949) "Wind Stresses in Semi-Rigid Connections of Steel Framework," *Transactions, ASCE*, Paper No. 2402, p. 382
- (7) Driscoll, G.C. (1976), "Effective Lengths of Columns with Semi-Rigid Connections," *Engineering Journal* 13(4):109-115, American Institute of Steel Construction

Quick and Easy Design of Joints in Practice Using New Tools for Designers

**Dr. Klaus Weynand, Dr. Markus Feldmann
PSP – Prof. Sedlacek & Partner GmbH, Germany**

ABSTRACT

Modern standards for the design of steel structures give new and advanced options for the design of efficient and economic steel structures. As far as the design of joints is concerned, the exploitation of the advanced possibilities is rather time consuming for the designer if no appropriate tools for a quick and easy design are available. Different design tools now have been established: design sheets providing simple sets of formulae, design tables and software. The paper presents a complete set of such design tools. Aspects of economic design, optimisation of connection detailing as well as possibilities for learning and education on connection behaviour using these tools are discussed.

1 INTRODUCTION

Modern standards for the design of steel structures give new and advanced options for efficient and economic steel structures. The design of the connection plays a major role in that process. Thus the detailing of connections and the methods of considering the connection properties in the frame analysis will significantly influence the costs of a steel structure. This has been demonstrated by various investigations.

However, the exploitation of the advanced possibilities is rather time consuming for the designer if no appropriate tools for a quick and easy design are available. Currently different opinions are discussed in Europe concerning the further development of the Eurocodes. On one side it is expected that Eurocode 3 [1], [2] will provide design methods which will enable economic solutions in the design of steel structures. Of course this requires more sophisticated approaches for the design rules. On the other side some of the users of the Eurocodes are requesting simple codes for practice. But this is in conflict with the major request to make steel structures more economic. It would be unfortunate to make standards too simple as there is the loss of many possibilities to take profit of the new and advanced options mentioned above.

The message is quite clear: There is the need for sophisticated standards which form an accepted basis to design steel structures. Based on the methods given in these standards simple design

tools need to be developed and provided to practitioners. This is an optimal way to bring more economic solutions on the market with an acceptable effort needed by the designers.

In this light the paper presents different types of design tools which have been developed recently.

2 DESIGN TOOLS

Beside the need for background information the engineer requires simple design tools to be able to design joint in an efficient way. Three different types of design aids can be provided. The most appropriate type depends on various aspects.

Design tables are ready-to-use tables containing standardised joint layouts including dimension details and all relevant mechanical properties like resistance, stiffness and ductility. The use of tables is certainly the quickest way to design a joint. However, any change in the layout will require further calculations and tables are no more helpful. Here design sheets may be used.

Design sheets are set of simple design formulae. The aim is to allow a simple but quick hand calculation. Due to simplifications, the results could be more conservative or the range of validity is limited. Both design tables and design sheets can be published in handbooks.

Software The most flexible way is the use of software. Of course it takes a few minutes to enter all joint details, but there will be only few limitations in the range of validity and any re-calculation, for example due to a change in the layout, is a matter of a few seconds.

The following paragraphs present some of the design tools which have been recently developed for the design of joints according to the Eurocodes.

3 DESIGN BOOKS

3.1 ECSC manual “Frame Design Including Joint Behaviour”

In the frame of a European research project [3] funded by ECSC a design manual entitled “Frame Design including Joint Behaviour” has been prepared. The partners involved were the University of Liège in Belgium as co-ordinator, CTICM in France, CRIF in Belgium, TNO Delft in The Netherlands and RWTH Aachen in Germany. The ECSC user’s manual covers the following three main aspects:

- The design of commonly used beam-to-column joint configurations such as welded ones or bolted ones with end plates and flange cleats. Beam splices are also covered.
- Guidelines on how to incorporate joint behaviour in the structural analysis (both 1st order and 2nd order, elastic and plastic).

- Design checks for the ultimate limit states (frame and member resistance and stability, member and joint section checks, ...)

It is structured into three main parts which all deal with the three different aspects mentioned here above:

- Part 1 - Technical Background
A primary objective of the manual is to facilitate the use of Eurocode 3 and it has so been thought that this was requiring explanations about the general design philosophy to adopt in particular cases, the successive steps to follow, the assumptions to make and the formulae to use.
- Part 2 - Application Rules
In this section, practical guidelines are given in a straightforward manner. The designer should find there the recommendations he needs to perform frame analysis, joint design and structural verifications. All the formulae are expressed together with their limitations and their implications on further steps. For joints, all three types of design aids are included as described below.
- Part 3 - Worked Examples
Three different worked examples are included in the manual. They cover the whole frame and joint design procedure and not only some specific aspects as the joint characterisation or the frame analysis. They should help the designer in understanding the different steps of a semi-rigid frame design, and the sequence of these steps according to the practical situation to which he is faced: engineer or constructor responsible for both frame and joint design or share of the responsibilities between the engineer (frame design) and the constructor (joint design).

All the scientific aspects have been disregarded and the content of all the chapters has been limited to the minimum but sufficient information which appears to be strictly useful to practitioners.

An important step in the design process is the determination of the mechanical properties of the joints in terms of rotational stiffness, moment and shear resistances and rotation capacity. For what regards this characterisation, the three approaches are followed:

- Design sheets
These are short documents containing very simple rules allowing to calculate in an easy and quick way the stiffness and resistance properties of some well-defined types of joint configurations :
 - beam-to column joints with flush or extended endplates;
 - beam splices with flush endplates;
 - beam-to column joints with flange cleats.

These simplified procedures strongly reduce the amount of calculation in comparison with the application of EC3 Annex J but are anyway in agreement with the EC3 design philosophy.

- Design tables
These are tables covering standardised joints and providing the user with joint detailing and stiffness / resistance properties ; information allowing to classify the joints as pinned, semi-rigid or rigid, partial strength or full strength is also given.
- Software
A PC software called DESIMAN is able to characterise the mechanical properties of a wide range of traditional or non-traditional types of joints subjected to bending moments and shear forces. It includes graphical pre- and post-processors. The pre-processor allows a user's friendly introduction of the data. It is connected to bolt, plate, material and profile databases. It is also connected to another database in which all the calculations made can be stored, in order to be used further if needed. The post-processor of DESIMAN produces four main files:
 - A short one just giving the main results of the computation : design resistances in bending and shear, initial stiffness, collapse mode, ductility class for frame analysis (1/2 page).
 - The previous one to which the resistance and the stiffness of all the constitutive joint components are added. Such a file allows the designer to modify in an optimum way its joint when the design requirements are not fulfilled (1 page).
 - A calculation note (± 5 pages) presenting more detailed results of the calculations, for each component and for the joint. This note is useful when, for instance, the design has to be checked by a control office.
 - A full calculation note just like that which could be produced by hand, and in which the results of all the intermediate calculation steps are given.

3.2 DSTV catalogue “Standardised Joint in Steel Building Frames”

The German steel work association DSTV has been prepared a complete new revision of its well established handbook for standardised connections. This design book is seen as a very comprehensive design aid for designers which are not designing steel joints in its every day practice or those who are looking for a quick solution to connect standard profiles. The following paragraphs will give a brief survey on its contents and introduce the basic concept of this publications.

The so-called DSTV “Ringbuch” on “Standardised Joints in Building Frames“ [4] comprises two volumes. The first volume deals mainly with simple (nominally pinned) joints whereas the second volume contains moment resistant joints. A more detailed list showing the different types of connections is given in table 1.

All chapters listed in table 1 (each devoted to one specific type of connection) are presented within the same structure. Three main items provide the users with a complete set of information concerning the type of connection.

1. General information

In the first part a brief description of the design model is given including some background information. Furthermore the scope (range of validity) for the use of the design sheets and the design tables is listed.

2. Design sheets

This part provides formulae for hand calculations. Prior to the equations all data needed for the calculations are listed. The presentation of the following equations follows the so-called component method, i.e. the resistance of all individual components is calculated component by component and finally they are assembled to the design resistance of the joint. Both the rules acc. to Eurocode 3 and acc. to the German standard DIN 18800 are provided.

3. Design tables

The third part of each chapter consists of design tables. The tables contain all relevant dimensions for the standardised joint configurations. Again design values are given for calculations according to Eurocode 3 and DIN 18800. Beside the resistance of the joint the governing component is indicated. This is used to get further information regarding ductility or possible strengthening of the joint. An example is shown in figure 1.

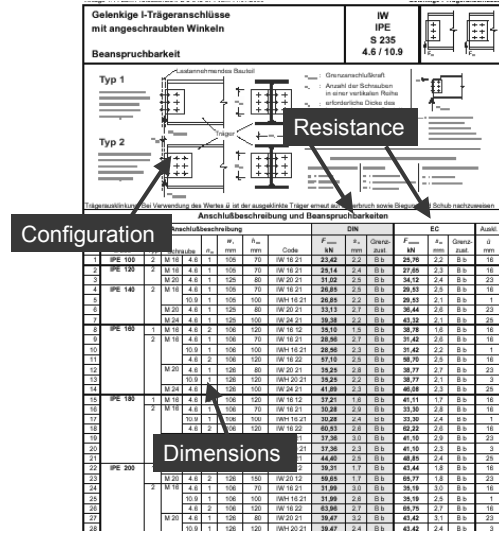


Figure 1: Design table prepared for Germany acc. to DIN and EC3

Handbooks have also been prepared in UK [5], [6] and in The Netherlands.

Table 1: Types of connections covered by DSTV Joint Design Book

Volume 1		Simple (nominally pinned) joints	
		Type IW Double web cleated connections	Type IS Header plate connections

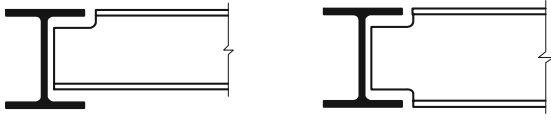
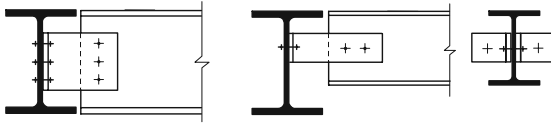
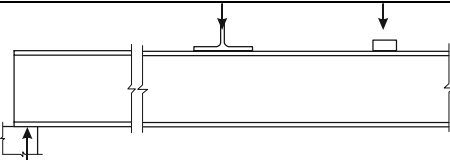
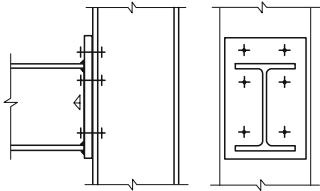
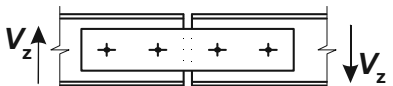
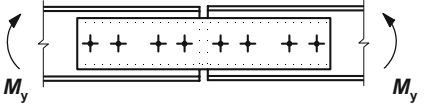
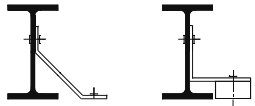
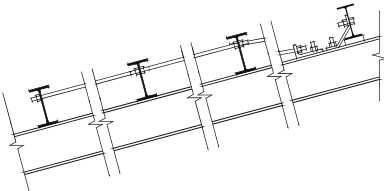
Volume 2	Type IK Notched beams	
	Type IG Double web cleated connections with long leg cleats (connecting I or H type uncoped beams)	
	Load introduction	
	Type IR Unstiffened beams at support or unstiffened beam-on-beam configurations	
	Moment resistant joints	
	Type IH Flush and extended end plate connections	
	Purlins	
	Type PG Nominally pinned purlin splices	
	Type PM Moment resistant purlin splices	
	Type PS Purlin supports	
Type PZ Tension members in roofs		

Table 1: Types of connections covered by DSTV Joint Design Book (cont.)

4 SOFTWARE

Beside the design book presented in the previous paragraphs a Windows based computer program called CoP (The **C**onnection **P**rogram) [7] has been developed. CoP is an innovative computer program for the calculation of joints, based on the new Annex J of Eurocode 3, which works according to the component method. This new calculation method not only leads to a

more economic structural design, but also gives better insight into the behaviour of the joint. The joint is central here, as it is an important factor in determining the cost of the structure. CoP has been developed at the universities of Aachen and Liège. The project leaders are co-authors of the new Annex J of Eurocode 3. With the aid of state-of-the-art software techniques a complete, extremely user-friendly Windows program emerged.

Some of the features which are of interest to be mentioned in this paper are discussed below:

- The input of joint data is quite easy for engineers because CoP is not a CAD software with a graphical input. The user simply enters the joint properties in simple dialog boxes (see figure 2). He gets immediately a graphical 2D or 3D representation of its data. Beside the drawing of the joints the so-called check data routines check the data for code limitation and geometrical restrictions.

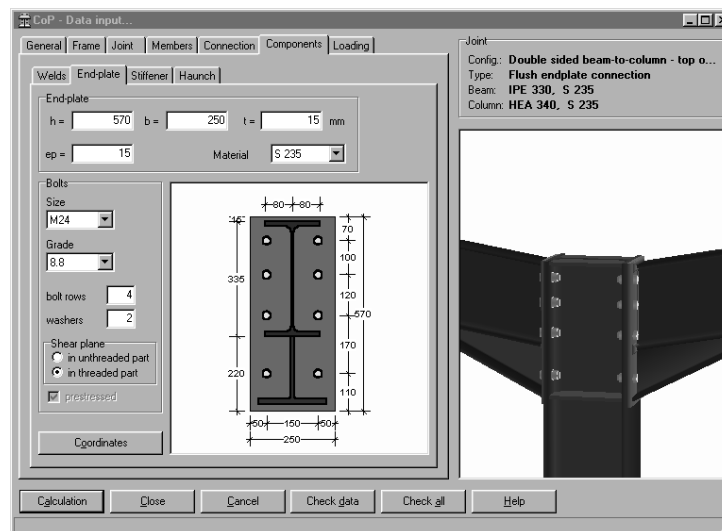


Figure 2: Simple data input in dialog boxes

- Calculation notes contain a complete step-by-step calculation including references to relevant clauses in the standard. Hence, there is no black box in the calculation procedure and a full check by building authorities is possible. A helpful feature is the possibility to select individual languages for user interface and the output (calculations notes) at the same time.
- In order to speed-up the data input databases are available containing the standardised joints of the DSTV catalogue. However the software allows for a design of a much more variety of joint detailing compared to the standardised joints. Beside the fact that further components are available such as column web stiffeners, backing plates, supplementary web plates or haunches and various joint configurations (see figure 3) the geometrical layout may vary within the limits given by the standard like number of bolt rows, position of bolt holes, etc.
- Optimisation routines will help to find economical solutions. So far a weld optimisation is now available which calculates appropriate weld sizes depending on the design situation selected.



Figure 3: Examples of typical joint configurations

CoP has been basically developed as a design tool for practitioners and as an education tool for students and engineers. However as for example individual material characteristics or safety factors may be used for the calculations, CoP can also be used as a research and development tools by scientists.

Finally an example is presented (see table 2) which shows how the software can be used to find a “good” joint detailing. Good joint detailing means a safe design and an appropriate performance of the joint on one side and an economic solutions on the other side. It should be stated that this is just one of many examples and the user can certainly see other design targets using CoP.

The aim here is to demonstrate the following principles: “Playing around the joint detailing, observing the joint response and searching for simple, inexpensive detailing by fulfilling the required behaviour of the joint.”

In the presented example it is assumed that an end plate connection should be used to connect a beam to a column in a single sided joint configuration. The preliminary detailing and the different steps made to find the final layout are presented in table 2.

Step	Comment	Response of CoP
Start	Configuration: Beam IPE 500 Column HEA 340 End plate connection Design assumption: Rigid joint Frame analysis: $M_{Sd} = 220 \text{ kNm}$	

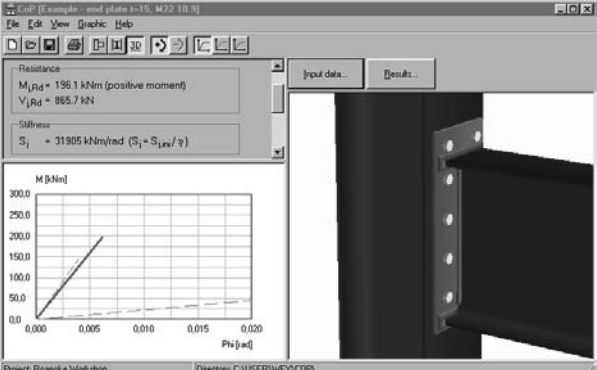
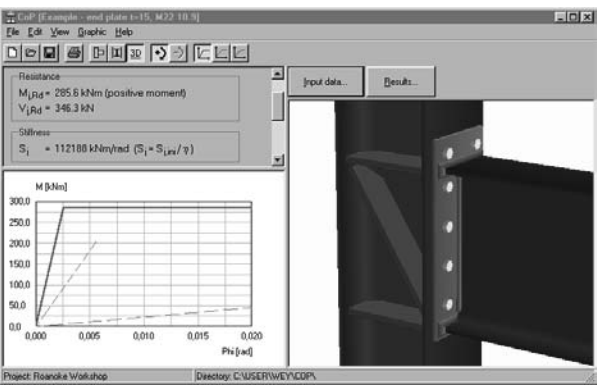
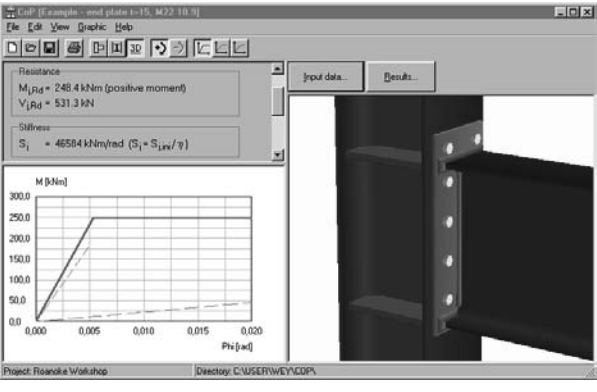
<p>Step 1</p>	<p>Design resistance: $M_{Rd} = 196 \text{ kNm} < 220 \text{ kNm}$ Classification: Semi-rigid Failure mode: Column web in compression</p> <p>As the failure is in the column web a complete stiffening is usually the “best” idea to avoid any further calculations or problems....</p>	
---------------	---	--

Table 2: Example for a possible optimisation of joint.

Step	Comment	Response of CoP
<p>Step2</p>	<p>Design resistance: $M_{Rd} = 286 \text{ kNm} > 220 \text{ kNm}$ Classification: Rigid Failure mode: End plate in bending</p> <p>Of course, the joint fulfils now all requirements. However fabrication cost can be reduced if less stiffeners are used.</p>	
<p>Step 3</p>	<p>Design resistance: $M_{Rd} = 248 \text{ kNm} > 220 \text{ kNm}$ Classification: Rigid Failure mode: Column web panel in shear</p> <p>The joint is still o.k. and ductile. The stiffeners would be cheaper, if they are not welded to both flanges.</p>	

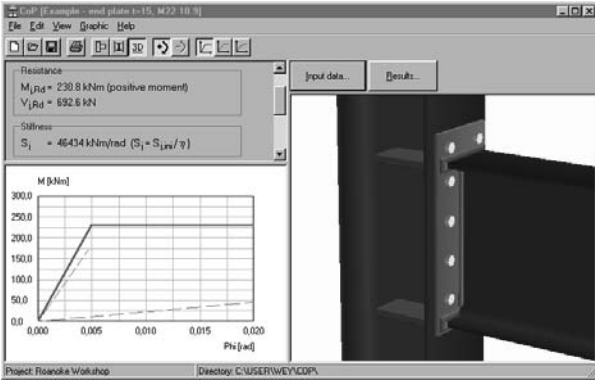
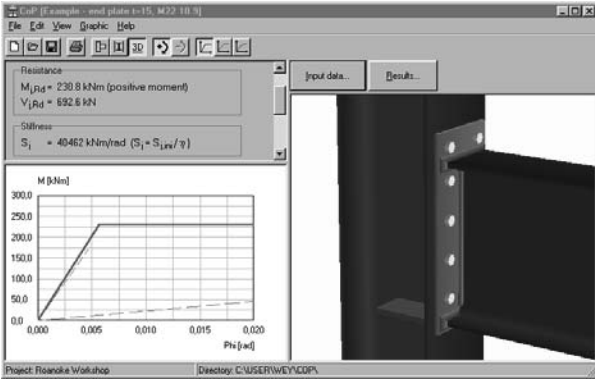
<p>Step 4</p>	<p>Design resistance: $M_{Rd} = 231 \text{ kNm} > 220 \text{ kNm}$ Classification: Rigid Failure mode: Column web panel in shear</p> <p>The resistance is reduced because the stiffeners do no more act as a frame. As the failure mode in the first calculation was column web in compression, it is finally checked, if the stiffener in the tension zone is really needed.</p>	
<p>Step 5</p>	<p>Final layout: All requirements are just fulfilled:</p> <p>Design resistance: $M_{Rd} = 231 \text{ kNm} > 220 \text{ kNm}$ Classification: Rigid Failure mode: Column web panel in shear</p>	

Table 2: Example for a possible optimisation of joint (cont.)

5 CONCLUSIONS

To achieve an economical design of the frames and of the constitutive joints - as it is now possible through the new concepts offered by Eurocode 3 - the designers require design tools adapted to their search of efficiency and profitability. The recent developments have performed a quite significant step in this direction by providing simple and clear guidelines for frame analysis and design and by proposing appropriate design tools for beam-to-column joints and beam splices. These design aids allow the designer to select the well-known “fully rigid” or “fully pinned” joints or to select “semi-rigid” joints which generally give a significant benefit by simplifying joints details, thereby reducing shop and erection costs.

For standardised connections, design sheets and design tables are published in Germany to provide the designer with a series of ready-to-use solutions for common types of connection such as simple connections with double web flanges or header plates, moment connection with flush or extended end plates and so on. For a more flexible and more powerful use the software tool CoP (The Connection Program) provides an easy and full access to items so far not covered by the design sheets or tables. Items like stiffeners, haunches, individual bolt positioning, inclined

beams, etc. can be easily considered. All tools are fully compatible with the European code Eurocode 3.

Concluding it can be stated that

- as Eurocode 3 is an accepted modern standard
 - and tools are available and will be further developed,
- joint design becomes
- economic due to advanced design methods,
 - easy and quick due to simple tools.

Next steps are the transfer of new techniques into practice and the education of designers to improve economy of steel structures using such new tools.

REFERENCES

- [1] CEN
Eurocode 3: Design of Steel Structures, Part 1 - 1; "General Rules and Rules for Buildings", ENV 1993-1-1, 1992.
- [2] CEN
New revised Annex J of Eurocode 3 "Joints in Building Frames", ENV 1993-1-1:1992/A2:1998
- [3] ECSC contract 7210-SA/212 and 7210-SA/320:
"Frame Design Including Joint behaviour", 1997
- [4] Deutscher Stahlbauverband DSTV:
"Typisierte Anschlüsse im Stahlhochbau" (*engl.*: Standardised Joints in Steel Building Frames), by G. Sedlacek, K. Weynand, S. Oerder, Stahlbau-Verlagsges. mbH Düsseldorf, 2000.
- [5] The Steel Construction Institute, The British Constructional Steelwork Association Ltd:
Joints in Simple Construction, Volume 1: Design methods (2nd. Edition), 1993, Volume 2: Practical application, 1992.
- [6] The Steel Construction Institute, The British Constructional Steelwork Association Ltd:
Joints in Steel Construction, Moment Connections, 1995.
- [7] Jaspart, J.P., K. Weynand, et al.:
CoP – The Connections Program, Software to design joints in Steel building frames, RWTH Aachen, MSM Liege, ECCS bv Hoofddorp, 1995-2000.

Critical Buckling Loads of Semi-Rigid Steel Frames

Lei Xu

Assistant Professor

Department of Civil Engineering, University of Waterloo
Waterloo, Ontario, Canada N2L 3G1

ABSTRACT

The problem of determining critical elastic buckling loads of steel frames under variable load patterns is discussed in this paper. In light of concepts of storey-based buckling and end-fixity factors to characterize the lateral sway buckling of frames and the semi-rigid behaviour of beam-to-column connections, respectively, the problem for determining the critical buckling loads is presented as a minimization and maximization problem with subject to stability constraints and is solved by a linear programming method.

INTRODUCTION

The assessment of column strength in framed structures are commonly carried out by evaluating the effective-length factor of columns in conjunction with the alignment charts in the current ASD or LRFD Specifications (AISC, [1](#), [2](#)). The concept of the effective length factor is considered to be an essential part of many analysis procedures and is valid for ideal structures. However, several assumptions on the buckling modelling of the frame were made in developing the alignment charts. When the assumptions are violated, the use of alignment charts results in erroneous effective-length factors.

The concept of storey-based buckling for unbraced frames is established based on the fact that an individual column cannot fail by lateral sway buckling without all of other columns in the same storey also buckling in the same sway mode (Yura, [3](#)). Therefore, lateral sway buckling of unbraced frames is a storey phenomenon. Various procedures of evaluating the stability of the frame based on this concept have been proposed (LeMessurier [4](#), Lui [5](#), Aritizabal-Ochoa, [6](#), Chong-Siat-Moy, [7](#)).

Beam-to-column connections play an important role in the resistance of structural frames to loads and maintain the stability of the structure. In the current practice of stability analysis of steel-framed building structures, the actual behaviour of connections is generally simplified to the two idealized extremes of either fully-rigid behaviour or ideally-pinned behaviour. Although the adoption of such idealized joint behaviour simplifies the stability analysis, it by no means

represents the actual behaviour of the structure. Therefore, the predicted response of the idealized structure may be quite unrealistic compared to that of the actual structure. This is because most connections used in current practice actually exhibit semi-rigid deformation behaviour that can contribute substantially to the stability of the structure as well as to the distribution of member force. Numerous experimental investigations on connection behaviour have clearly demonstrated that a pinned connection possesses a certain amount of rotational stiffness, while a rigid connection possesses some degree of flexibility. Neglecting realistic connection behaviour may lead to unrealistic predictions of the response and strength of structures, and therefore, to approximations in design. Therefore, beam-to-column connections should be treated as semi-rigid connections in the stability analysis of steel frames.

Over the years, considerable efforts have been made to incorporate the connection behaviour into the determination of stability strength of semi-rigid frames (Bjorhovde, 8; Chen and Lui, 9; Xu, 10; Kishi *et al*, 11; Christopher and Bjorhovde, 12). However, all of the foregoing studies that have been carried out so far are under the assumption that the frame is subjected to proportional loading. The variable loading case, which has taken into consideration the volatility of loads and is more closely related to actual situations in practice, is left unsolved due to the complexity of the problem. The main objective of this paper is to investigate the elastic in-plane buckling characteristics of semi-rigid unbraced frames under variable loading.

END-FIXITY FACTORS OF SEMI-RIGID MEMBER

To incorporate semi-rigid connection behaviour into frame stability analysis, the effects of connection flexibility are modelled by attaching rotational springs at the two ends of a beam-column member as shown in Figure 1. A so-called end-fixity factor r defines the stiffness of the connection to the attached beam-column member (Monforton and Wu, 13),

$$r_j = \frac{\alpha_j}{\phi_j} = \frac{1}{1 + \frac{3EI}{R_j L}}; \quad (j=1, 2) \quad (1)$$

where R_1 and R_2 are the rotational stiffnesses of the spring connections at ends 1 and 2; L and I are the length and cross-section moment of inertia of the beam-column member, respectively; and E is Young's modulus.

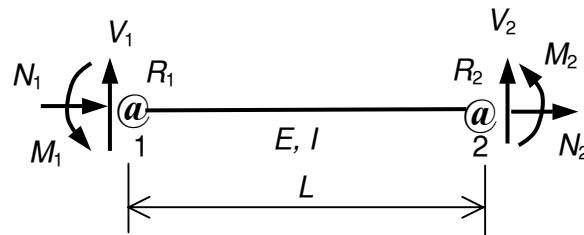


Fig. 1. Semi-rigid beam-column member

For pinned connections, the rotational stiffness of the connection is idealized as zero and thus the value of the end-fixity factor is zero ($r_j = 0$). For rigid connections, the end-fixity factor has a value of one ($r_j = 1$), because the connection rotational stiffness is taken to be infinite. A semi-rigid connection has an end-fixity factor between zero and one ($0 < r_j < 1$). By using the end-fixity factor, different member-end restraint conditions, such as rigid-pinned, rigid-semi-rigid, and pinned-semi-rigid, are readily modelled simply by setting the end-fixity factors at the two ends of the member to appropriate values. Therefore, the proposed analysis method is comprehensive

regardless of member end-rotational conditions and can be applied to the analysis of frames with any combination of pinned, rigid and semi-rigid connections.

The end-fixity factor also simplifies the analysis procedure for semi-rigid framed structures. The formulations of stiffness matrices for both first and second-order analysis, member end-reactions, span deflections, and effective-length factors of beam-columns can all be expressed in terms of the end-fixity factors (Xu, 14). The end-fixity factor has further value in design because it provides a physical interpretation of the extent of rigidity available in a connection. It also provides designers with a convenient way to compare the structural responses of a member with semi-rigid connections to those of one with rigid or pinned connections.

By Eq. (1), the relationship between the end-fixity factor and the connection stiffness is nonlinear, as shown in Figure 2. It is also clear that the relationship between the connection stiffness and the end-fixity factor is almost linear when the connection is relatively flexible with a value of the end-fixity factor between 0.0 and 0.5. However, as the end-fixity factor approaches 1.0, the required increase of connection stiffness becomes substantial. Therefore, designers should keep in mind that with a certain percentage increase in the end-fixity factor, the corresponding increment in connection stiffness may be quite different depending on whether the connection is relatively flexible or rigid. Gerstle (15) reports that the stiffness ratio, RL/EI for “rigid” connections, ranges from 10 to 50 in typical building design, which implies that the end-fixity factor ranges from 0.77 to 0.94.

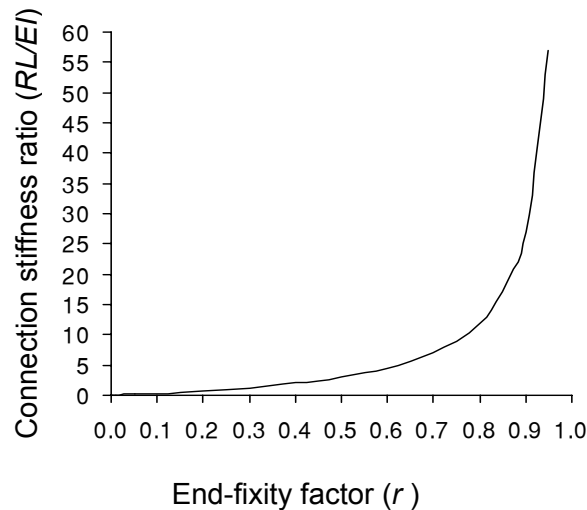


Fig. 2. Relationship between connection stiffness and end-fixity factor

The end-fixity factor is a better indicator of how connections affect the structural behaviour than the connection stiffness. The latter has little direct meaning in analysis. Figure 3 illustrates the variation of mid-span moments, end-reaction moments, and mid-span deflection of the beam with respect to the connection stiffness ratio, RL/EI , for a uniformly loaded semi-rigid beam with identical connection stiffnesses at both ends. Figure 4 shows the same information in terms of the end-fixity factor, r . Figure 3 shows that the relationships of the moments and the deflection to connection stiffness ratio of the beam are highly nonlinear when the ratio is between 0 and 20, and almost linear when the ratio is between 20 and 50. On the other hand, as shown in Figure 4, the relationships of the moments and the deflection to the end-fixity factor, for its full range of zero to one, are approximately linear. Thus, it is advantageous to characterize semi-rigid behaviour using the end-fixity factor rather than the connection stiffness.

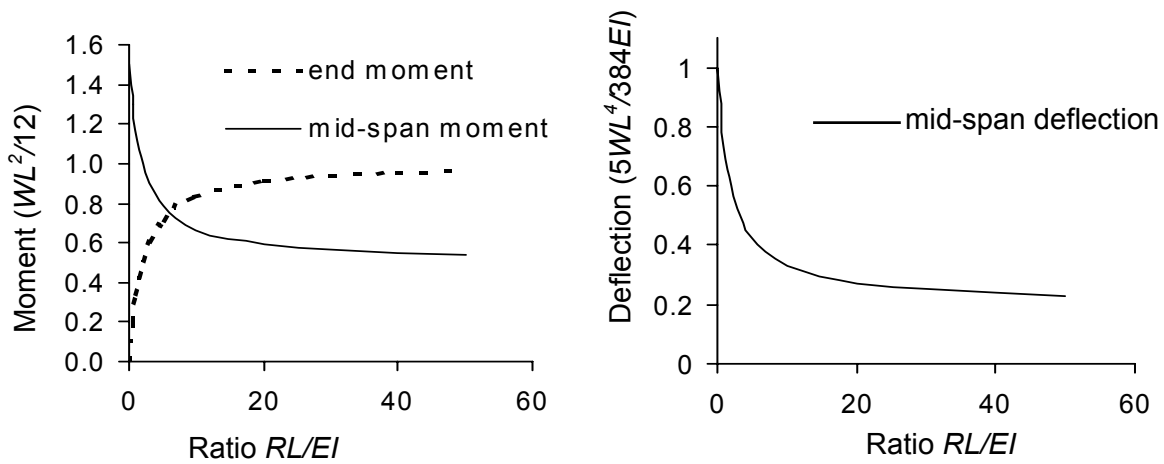


Fig. 3. Moment and deflection of a uniformly loaded beam vs. ratio RL/EI

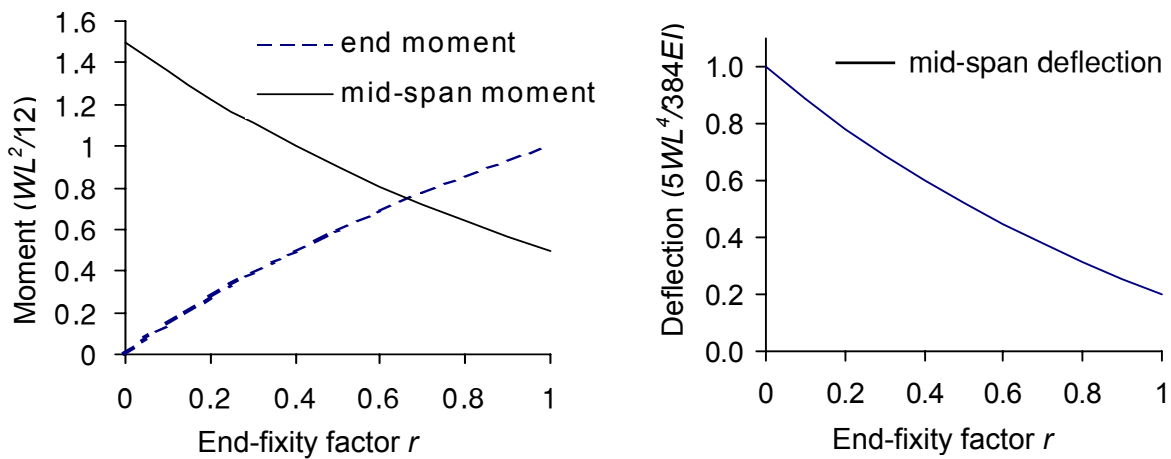


Fig. 4. Moments and Deflection of a uniformly loaded beam vs. end-fixity factor

It is observed from Figure 2 that when the connection stiffness is large, very significant changes in stiffness produce only very small changes in the end-fixity factor. Consequently, from Figure 4, such change has a negligible influence on both moments and deflection of the beam. Conversely, from Figure 2 with low values of connection stiffness, small increases in the stiffness result in appreciable increases in the end-fixity factor. Therefore, as Figure 4 shows there is a considerable effect on the bending moments and the deflection. Thus, in practice, when a real pinned connection has some stiffness, a considerable restraining moment may develop to the benefit of the structure. At the other extreme, attempting to achieve further increase in connection stiffness beyond that of a nearly rigid connection is inefficient and costly because it involves only a small change in the end-fixity factor. Consequently, it has little effect on the response of structure.

LATERAL STIFFNESS OF A SEMI-RIGID COLUMN

Shown in Figure 5 is an axially loaded semi-rigid column in an unbraced frame, in which EI_i/L_i is the flexural stiffness of the column and P_i is the column axial load. The end-fixity factors, r_l and r_u , define the rotational restraints provided by the connected beams at the lower and upper joints, respectively. Let

$$\phi_i = \sqrt{\frac{P_i L_i^2}{EI_i}} = \pi \sqrt{P_i / P_e} \quad (2)$$

The lateral stiffness of the column can be expressed as (Xu *et al*, 16)

$$S_i = \beta_i(\phi_i, r_l, r_u) \frac{12EI_i}{L_i^3} \quad (3)$$

where $\beta_i(\phi_i, r_l, r_u)$ is the modification factor of the lateral stiffness that accounts for the effects of axial force and column end rotational restraints.

$$\beta_i(\phi_i, r_l, r_u) = \frac{\phi_i^3}{12} \frac{a_1 \phi_i \cos \phi_i + a_2 \sin \phi_i}{18r_l r_u - a_3 \cos \phi_i + a_4 \phi_i \sin \phi_i} \quad (4)$$

where

$$a_1 = 3[r_l(1-r_u) + r_u(1-r_l)] \quad (5a)$$

$$a_2 = 9r_l r_u - (1-r_l)(1-r_u)\phi^2 \quad (5b)$$

$$a_3 = 18r_l r_u + [3r_l(1-r_u) + 3r_u(1-r_l)]\phi^2 \quad (5c)$$

$$a_4 = -9r_l r_u + 3r_l(1-r_u) + 3r_u(1-r_l) + (1-r_u)(1-r_l)\phi^2 \quad (5d)$$

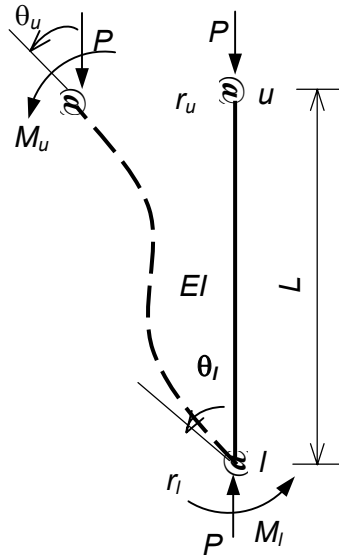


Figure 5. Lateral buckling of axially loaded semi-rigid column

It is difficult to evaluate the column critical buckling load due to the transcendental relationship between β_i and ϕ_i in Eq. (4), especially in a multicolumn-unbraced frame. Thus, a simpler approximation of Eq. (4) can be obtained by its first-order approximation of Taylor series expansion as

$$\beta_i(\phi_i, r_l, r_u) = \beta_{i0}(r_l, r_u) - \beta_{i1}(r_l, r_u)\phi_i^2 \quad (6)$$

where

$$\beta_{i0}(r_l, r_u) = \lim_{\phi \rightarrow 0} \beta_i(\phi_i, r_l, r_u) = \frac{(r_l + r_u + r_l r_u)}{4 - r_l r_u} \quad (7)$$

$$\beta_{i1}(r_l, r_u) = \frac{40 + 8(r_l^2 + r_u^2) + r_l r_u(r_l + r_u + 3r_l r_u - 34)}{30(4 - r_l r_u)^2} \quad (8)$$

The Taylor series expansion, Eq. (6), provides a satisfactory approximation of Eq. (4) in the evaluation of the critical buckling load of the column (Xu *et al*, 16).

STOREY-BASED BUCKLING OF UNBRACED SEMI-RIGID FRAMES

Unlike the alignment chart method, which ignores the fact that columns in a storey of the frame will restrain each other in resisting buckling, the interaction among the columns due to the fact that stronger columns brace the weaker columns in the sidesway buckling is taken into account in storey-based buckling. The condition for the multicolumn storey-based buckling in a lateral sway mode is that the total lateral stiffness of the storey vanishes. For the proportional loading case, the stability equation becomes

$$\sum_{i=1}^n S_i = 12 \sum_{i=1}^n \left(\frac{EI_i}{L_i^3} \beta_{0i} - \frac{P_i}{L_i} \beta_{1i} \lambda_{cr} \right) = 0 \quad (9)$$

where n is the number of columns in a storey, P_i is the axial force due to the specified load of column i , and λ is the critical load multiplier. Because the load pattern is predefined in the case of proportional loading; therefore, only one critical load multiplier, λ , is need to be determined as

$$\lambda = \frac{\sum_{i=1}^n \frac{EI_i}{L_i^3} \beta_{0i}}{\sum_{i=1}^n \frac{P_{si}}{L_i} \beta_{1i}} \quad (10)$$

In the case of variable loading, the conventional assumption of proportional loading is abandoned. Therefore, different load patterns cause the frame to buckle at different levels of critical loads. Because the magnitude of each individual load can vary independently in order to capture the worst load case in variable loading; therefore, there are n critical load multipliers, λ_i ($i = 1, 2, \dots, n$), which need to be determined. Thus, the stability equation for variable loading becomes

$$\sum_{i=1}^n \left(\frac{EI_i}{L_i^3} \beta_{0i} - \frac{P_i}{L_i} \beta_{1i} \lambda_i \right) = 0 \quad (11)$$

CRITICAL BUCKLING LOADS OF FRAMES UNDER VARIABLE LOADING

Eq. (11) involves n variables; therefore, there is no unique solution for critical loads. Among those critical loads, the one associated with the minimum and the maximum magnitudes of total loads define the lower and upper bounds of the critical loads, respectively. The load patterns associated with the minimum and maximum critical loads are the most critical and most favourable load patterns for the elastic buckling of the frame. The lower and upper bounds of the buckling loads and their associated load patterns have clearly characterized lateral buckling of the frame under extreme conditions, which is crucial to evaluate the buckling strength of the frame. The problem for determining the upper and lower bounds of critical buckling loads can be presented as a minimization and maximization problem,

$$\begin{array}{l} \text{Maximize} \\ \text{Minimize} \end{array} : \quad Z = \sum_{i=1}^n \lambda_i P_i \quad (12a)$$

$$\text{Subject to: } \sum_{i=1}^n \left(\frac{EI_i}{L_i^3} \beta_{0i} - \frac{P_i}{L_i} \beta_{1i} \lambda_i \right) = 0 \quad (12b)$$

$$P_{li} \leq \lambda_i P_i \leq P_{ui} = \frac{\pi^2 EI_i}{L_i^2}; \quad (i = 1, 2, \dots, n) \quad (12c)$$

where the objective function Z corresponds to either the upper or the lower elastic buckling load of the frame, and Eq. (12b) defines the storey-based lateral buckling condition of the frame. Eq. (12c) imposes a constraint on each individual load such that the magnitude of the load can not exceed its upper-bound, Euler buckling load, and should be greater than its lower-bound due to the specified dead load. The problem stated in Eqs. (12) is a linear programming problem and can be solved by the simplex method for determining either the maximum or the minimum critical buckling loads and associated load patterns.

EXAMPLE

Shown in Fig. 6 is a simple semi-rigid unbraced steel frame. The moments of inertia for columns 1 and 2 are $I_1 = 45.2 \times 10^6 \text{ mm}^4$ and $I_2 = 104 \times 10^6 \text{ mm}^4$, respectively. The moment of inertia of the beam is $I_3 = 617 \times 10^6 \text{ mm}^4$. The end-fixity factors for column bases are r_1 and r_2 while the end-fixity factors associated with the left- and right-ends of the beams are r_3 and r_4 , respectively. Young's Modulus of steel is taken as $E = 200,000 \text{ MPa}$.

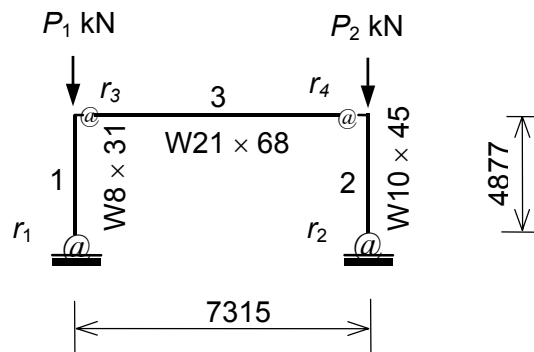


Figure 6. Semi-rigid unbraced steel frame

First, considering the cases that column bases are pinned with $r_1 = r_2 = 0$ and $r_1 = r_2 = 0.1$, respectively, let the end-fixity factors associated with the beam ($r_3 = r_4$) vary from zero to one. The corresponding upper and lower bounds of the critical buckling loads under variable loading, P_{max} and P_{min} , are evaluated from Eqs. (12) and illustrated in Figure 7. The buckling loads obtained from Eq. (10) under proportional loading with $P_1 = P_2$ are also plotted in Figure 7. The maximum differences between the upper and lower bounds of the critical buckling loads for the two cases are 4.55% and 4.29%, respectively. However, the corresponding maximum differences between the buckling load under proportional loading and the minimum critical buckling load under variable loading for the two cases are only 1.47% and 1.57%, respectively.

It is observed from Figure 7 that for flexible beam-to-column connections ($r \leq 0.3$), an increase in the end-fixity factor of the beam would result in considerable increase in the critical buckling loads of the frame. However, for nearly rigid connections ($r \geq 0.7$), further increase in the end-fixity factor has trivial effect on the critical buckling loads. Considering the relationship between the end-fixity factor and connection stiffness shown in Fig. 2, it is concluded that it is important and economical to consider the semi-rigid behaviour of connections in the design of unbraced steel frames with flexible beam-to-column connections.

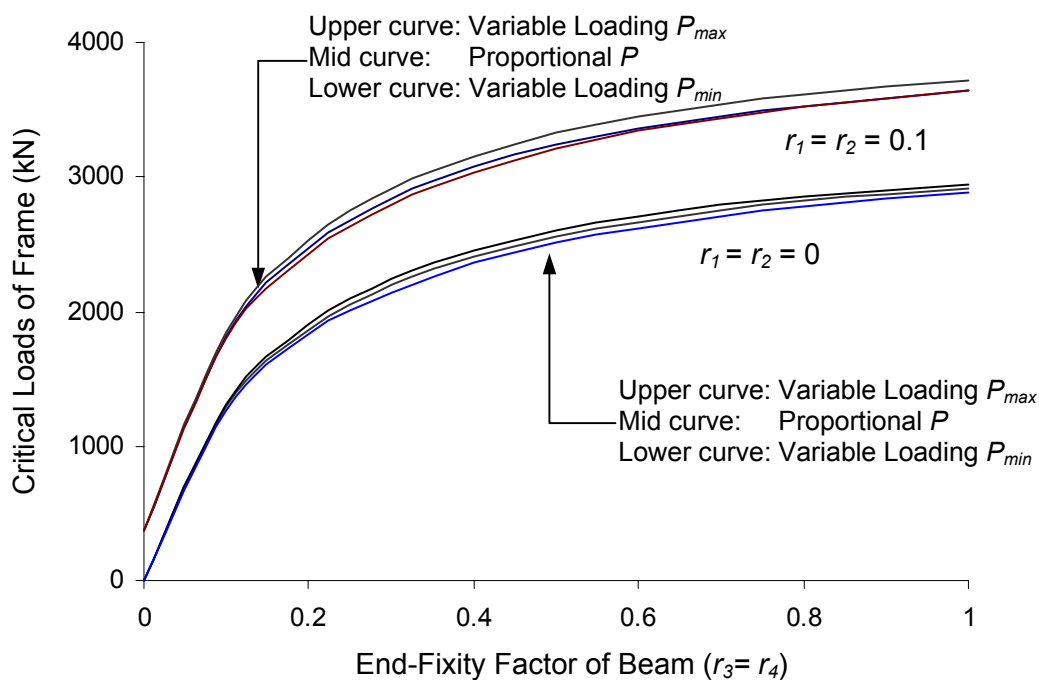


Figure 7. Critical loads of frame vs. end-fixity factor of beam

Second, considering that column 1 has rigid connections at both the lower and upper ends while column 2 is a lean-on column with pinned connections at its ends, the end-fixity associated with columns and the beam are $r_1 = 1.0$, $r_2 = 0$, $r_3 = 1.0$ and $r_4 = 0$. Based on Eqs. (12), the problem of solving the upper and lower bounds of critical loads under variable loading can be expressed as

$$\text{Maximize / Minimize: } P_1 + P_2$$

$$\text{Subject to: } 0.239P_1 + 0.205P_2 + 845.645 = 0$$

$$0 \leq P_1 \leq 3751 \text{ kN}$$

$$0 \leq P_2 \leq 8632 \text{ kN}$$

Because only two variables are involved in the above problem, graphical solutions are available as that shown in Figure 8. The magnitudes and the maximum differences of the upper and lower bounds of critical loads are listed in Table 1. The maximum difference between the bounds of critical loads is substantial with a value of 16.59%. However, considering the semi-rigid behaviour of connections, with $r = 0.8$ and 0.2 are adopted for rigid and pinned connections, respectively, the maximum difference of the critical loads is reduced to 5.5%.

Connection End-fixity Factor		Maximum Critical Buckling Load (kN)			Minimum Critical Buckling Load (kN)			$\left(\frac{\sum_{\max} P_i - \sum_{\min} P_i}{\sum_{\min} P_i} \right)$
Pinned	Rigid	P_1	P_2	$\sum_{\max} P_i$	P_1	P_2	$\sum_{\min} P_i$	(%)
$r = 0$	$r = 1.0$	0	4125	4125	3538	0	3538	16.59
$r = 0.2$	$r = 0.8$	0	5429	5429	3751	1395	5146	5.50

Table 1: Critical Loads of Simple Frame with Lean-on Column

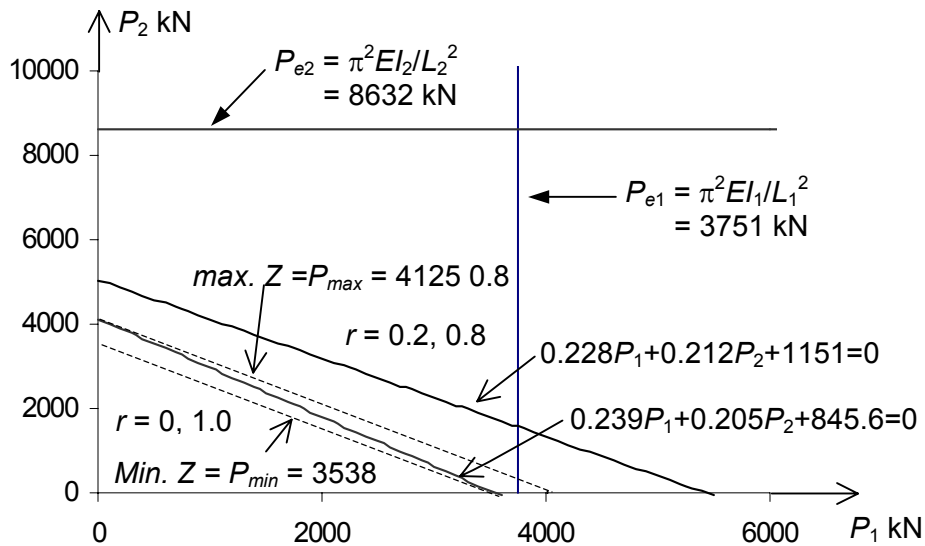


Figure 8. Graphical solutions of critical loads

CONCLUSION

Based on the concept of storey-based buckling, the stability of unbraced semi-rigid steel frames under variable loading is investigated. The maximum and minimum critical buckling loads under variable loading characterize the buckling strengths of the frame under extreme conditions; therefore, it is of importance for frame design. The benefit of considering semi-rigid behaviour of beam-to-column connections in the stability analysis of unbraced steel frames, particularly for those with flexible connections, is demonstrated. The fact that the maximum difference between the maximum and minimum critical buckling loads can be substantial for the frames with lean-on columns may suggest that traditional proportional loading approach may not be adequate to assess the load capacity for such frames. Therefore, the variable loading approach is recommended for the frames with lean-on columns.

ACKNOWLEDGMENT

This work was funded by a grant from the Natural Science and Engineering Research Council of Canada.

NOTATIONS

E	=	Young's modulus
I	=	moment of inertia of member
L	=	member length
M	=	flexural moment
P_i	=	axial force
P_e	=	Euler buckling load
r	=	end-fixity factor
r_l, r_u	=	end-fixity factor of lower and upper end of column
S_j	=	lateral stiffness of semi-rigid column
R_j	=	connection stiffness
Z	=	objective function
β	=	modification factor of column lateral stiffness
λ	=	critical load multiplier

REFERENCES

1. AISC, (1989). *Manual of Steel Construction-Allowable Stress Design*. American Institute of Steel Construction, 9th Ed., Chicago.
2. AISC, (1994). *Manual of Steel Construction-Load and Resistance Factor Design (LRFD)* (1994). American Institute of Steel Construction, 2st Ed., Chicago, Ill.
3. Yura, J.A. (1971). "The Effective Length of Column in Unbraced Frame." *Engineering Journal*, AISC, 2, 37-42.
4. LeMessurier, W.J. (1977). "A Practical Method of Second Order Analysis, Part 2-Rigid Frame." *Engineering Journal*, AISC, 2, 49-67.
5. Lui, E.M. (1992), "A Novel Approach for K Factor Determination", AISC, *Engineering Journal*, 4, 150-159.
6. Aristizabal-Ochoa, J.D. (1997). "Storey Stability of Braced, Partially Braced, and Unbraced Frames: Classical Approach." *Journal of Structural Engineering*, ASCE, 123(6), 799-806.
7. Cheong-Siat-Moy F. (1999). "An Improved K-Factor Formula." *Journal of Structural Engineering*, ASCE, 125(2), 169-174.
8. BJORHOVDE, R. (1984). "Effect of End Restraint on Column Strength-Practical Applications."

- Engineering Journal*, AISC, 1, 1-13.
9. Chen, W.F. and Lui, E.M. (1985). "Stability Design Criteria for steel members and frames in the United States." *Journal of Construction of Steel Research*, 5, 31-74.
 10. Xu, L. (1994). "Optimal Design of Steel Frameworks with Semi-Rigid Connections." Ph.D. Department of Civil Engineering, University of Waterloo, Canada.
 11. Kishi, N., Chen, W.F. and Goto, Y. (1997). "Effective Length Factor of Columns in Semi-Rigid and Unbraced Frames", *Journal of Structural Engineering*, ASCE, 123(3), 313-320.
 12. Christopher, J.E. and Bjorhovde, R. (1999). "Semi-Rigid Frame Design Methods for Practicing Engineers." *Engineering Journal*, AISC, 36(1), 12-28.
 13. Monforton, G. R. and Wu, T. S. (1963). "Matrix Analysis of Semi-Rigidly Connected Frames." *Journal of Structural Division*, ASCE, 89, ST6, 13-42
 14. Xu, L. (2000). "Second-Order Analysis for Semi-rigid Steel Frame Design", to be published in *Canadian Journal of Civil Engineering*.
 15. Gerstle, K.H. (1988). "Effect of Connection on Frames." *Journal of Construction Steel Research*, 10, 241-267.
 16. Xu, L., Liu, Y. and Chen, J. (2000). "Stability of Unbraced Frames under Non-Proportional Loading." Submitted for publication in *Structural Engineering and Mechanics*.

Site monitoring and Computational Analysis of Semi-Continuous Composite Steel Frame Structure

Robert Y. Xiao *

Department of Civil Engineering, University of Wales,
Swansea, UK SA2 8PP

C. D. Fisher

Department of Civil & Environmental Engineering,
University of Southampton, UK, SO17 1BJ

ABSTRACT

The paper discusses the site-monitoring which has been carried out on a real building that made full use of the semi-continuous design approach, the first ever in Europe to be designed and constructed. The finite element models have been set up to investigate the influence of using semi-rigid and partial-strength connections on steel frameworks. All these numerical results have been validated against the test data obtained on site testing. From these models it will be possible to establish new design methods for frame design utilising the strength and stiffness of composite floor and connections.

1 INTRODUCTION

Frames are traditionally designed as being perfectly pinned or perfectly rigid. These connections do not actually exist in real structures, with connection behaviour being between these two extremes. Assuming that the connection is pinned leads to an overly conservative design as no moment transfer can occur at the connection, meaning deeper steel sections required for the beams. Eurocodes give a classification for connections as pinned, rigid, or semi-rigid [1,2].

Connections are usually conservatively designed as pinned, due to the high fabrication costs of rigid connections. However, this allows a simpler frame design process. There has been research in recent years how to classify connection types [3,4], in which the connections have been classified by strength, stiffness and ductility. Other research has also shown the behaviour of column bases to be semi-rigid [5,6,7,8].

Site monitoring of the first building to make use of the semi-continuous design approach will be discussed for the present study. The monitoring was conducted at an academic complex in Southampton city-centre which has been discussed in ref.9, constructed for Southampton Institute. The structure is a five storey composite steel and concrete frame with L shape structural layout. The connections have been design as partial-strength and semi-rigid connections by the design methods proposed by Xiao *et al* [10,11] and Troup[12] and then referred to the relevant design codes. The plastic analysis then carried out for the whole frame [13]. The monitoring covered a primary and secondary beam during the construction and later loading of the structure. The results of the monitoring are discussed in the next section of the paper.

After the site monitoring the structure was modelled, using the ANSYS software package

for finite element analysis on the frame. The results for this were compared to those from the site monitoring. The computational model was used for further parametric analyses. In the next set of analyses the connection stiffness and column base stiffness could be changed, by making changes to the $M-\phi$ curve. It could then be seen how the joint stiffness affect the flexibility and strength of the frame, and by following on from the work of Xiao *et al* [14,15] new design principles could be established. The model was then expanded to model multi-storey construction Xiao *et al* [16].

2 SITE MONITORING

2.1 Structural section to be monitored

The monitoring was conducted for the structure at its construction stage. The fourth floor has been chosen for the site monitoring as this floor supports the greatest loads, particularly the plant room, and hence the floor slab is thicker than those of other floors. The plant room floor is in three stepped levels of thickness, 130mm, 175mm and 250mm, the latter two of these being constructed from normal weight concrete and the 130mm thickness from lightweight concrete.

Two of the supporting beams were monitored: a pre-cambered secondary beam, and a primary beam, which was propped during construction. These beams were chosen so that they were under the thickest of the floor areas and therefore subject to the highest loading cases. This will look at the construction method for the semi-continuous frame. Transducers were installed beneath both beams so that the deflections could be measured during the concrete pour, and then during later loading of the floor due to the lifting of the plant etc.

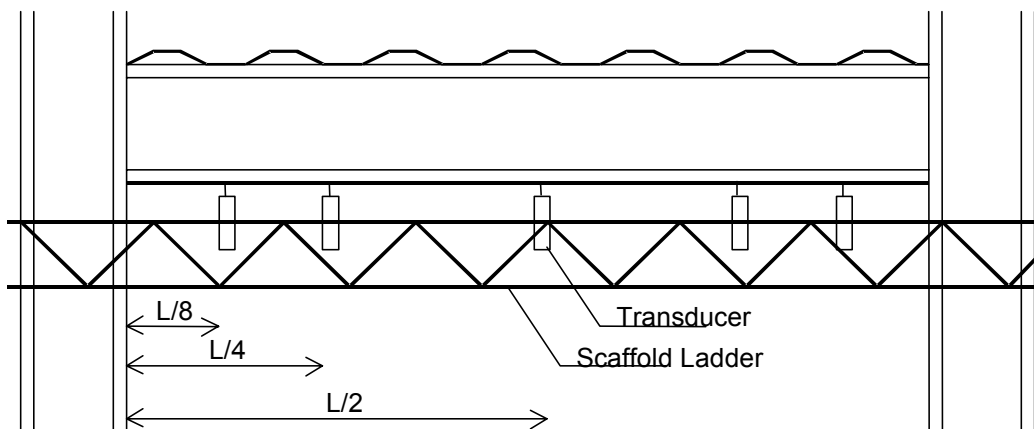


Figure 1.- Positioning of the transducers for the site monitoring

The transducers were mounted using scaffold ladder beams; these ladder beams were attached to the columns at each end of the beams being monitored. Six 50mm transducers were used on each of the two beams being studied. The spacing used for the transducers is shown in Figure 1. This spacing was chosen so that the transducers would be sited at the points of most interest, and could give a good indication of the deflected shape. Two transducers were placed at the mid-point of the span, as this is where the maximum deflection along the beam would occur. This point is of greatest interest, and therefore a reliable result is required.

A data-logger was programmed and the program was run manually and automatically through the experiment so that it was possible to control when the readings were taken. It was important to have as much data as possible at the times when the concrete was being poured directly over the beams being monitored (i.e. the times of greatest change in deflection). Fewer results are required when the concrete pour is taking place further away, as this would have a negligible effect on the deflections of the monitored beams. This arrangement proved to work well through the course of the experiment.

Construction of the floor was filmed during the pouring of the concrete, using a video camera, as it was important that the times of the concrete pour and the pour pattern could be accurately noted.

2.2 The Concrete Pour Experiment

Initial readings were taken before the start of the concrete pour. These readings were used as the offset readings for the transducers, and these values were input into the data-logger as part of the calibration stage, along with the calibration factors for the transducers that had been found from lab tests.

The first area of concrete to be poured was the area furthest from the monitored beams, so only a few readings were taken at this stage. Once the concrete pour was over the monitored beams, readings were taken at one or two minute intervals. The filming of the site also concentrated mainly on the area above the concrete pour. The experiment ran satisfactorily with no problems from any of the equipment used.

2.3 The Plant Lifting Experiment

The second stage of the experiment was to measure the deflections of the two monitored beams once the concrete had cured and the structure was acting as a composite structure. This was carried out in two stages. The first stage consisted of measuring the deflections whilst pallets of building blocks were situated directly over the mid-span of the monitored beams. The second stage was to measure the deflections once the plant, consisting of cooling units for the air-conditioning, was lifted. At the stage of the plant being lifted, the props had also been removed from beneath the primary beam.

Initial readings were taken before anything was moved, so that the results could be compared with those from the concrete pour experiment. It was shown that there was very little movement of the monitored beams over the time between the two stages of the experiment.

3 RESULTS OF SITE MONITORING

3.1 Construction

The final results after the concrete pour have been compared against two models. The frames were modelled using the QSE software package and the ANSYS finite element analysis software package. The wet concrete loads were used for the analysis, and these loads were distributed as rectangular loads.

As this chart shows, all the results for the secondary beam compare very well. For the stiffness method analysis the nodes were positioned where the transducers were attached in the experiment. However, for the finite element method more nodes were used, so that the

deflected shape could be shown in more detail. These results show that the beam-to-column connection for the secondary beam is acting like a simple connection with low rigidity.

The results for the secondary beam are shown in Figure 2 below.

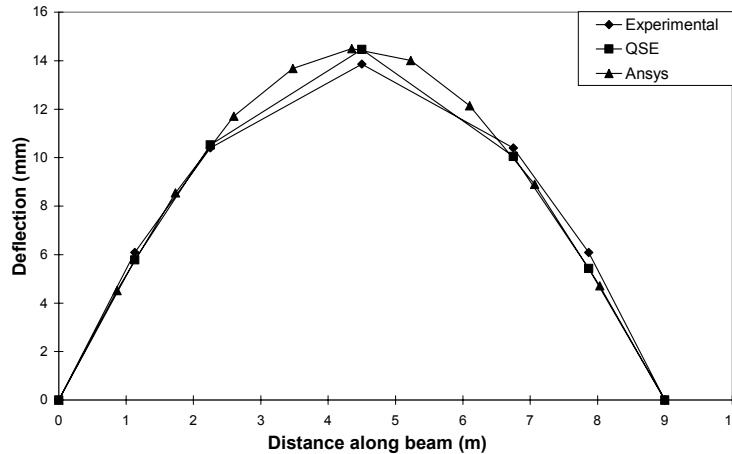


Figure 2. - Comparison of site monitoring and modelled results

The results for the main beam are shown in Figure 3.

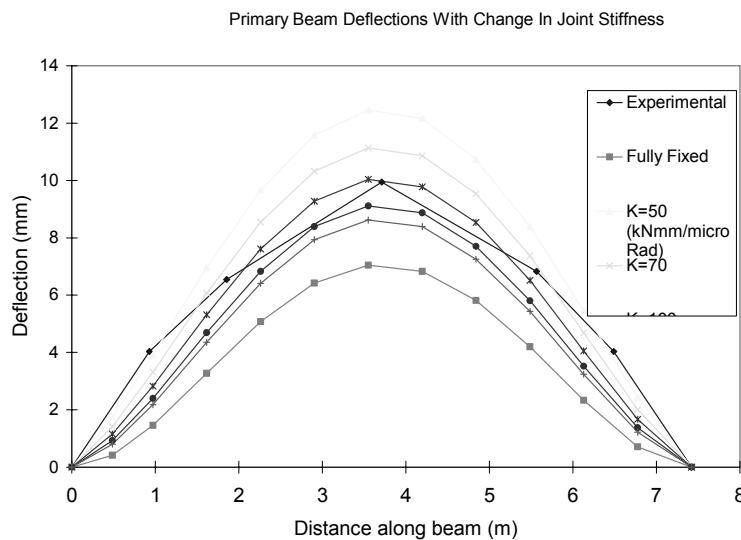


Figure 3. - Comparison of site monitoring of main beam

3.2 Completed Structure

This was carried out in two parts. The first part consisted of measuring the deflections of the beams whilst concrete blocks were situated directly over the mid-spans of the monitored beams. The second part was to measure the deflections of the beams once the plant, consisting of cooling units, had been lifted into place. For the first part the props were still in place under the

primary beam, but these had been removed by the time the measurements were taken for the lifting of the plant.

The pallets of lightweight blocks used to load the beams weighed approximately 1.5 tonnes. This load caused only very low deflections: 0.12mm for the primary beam, and 0.38mm for the secondary beam, were measured for the mid-span deflections when the blocks were placed at mid-span. As these results are so low, the percentage errors in the result could be quite high.

The lifting of the plant caused higher deflections. At this stage, the increases in deflection were measured at the mid-span as 1.32mm for the primary beam and 1.73mm for the secondary beam. The composite action between the metal decking and concrete floor creates a very stiff section, along with the extra stiffness from the steel connections.

4 FINITE ELEMENT MODELLING

The results from the model discussed above are for the secondary, pinned, beam. To model connection stiffness only ANSYS can be used, as QSE is fairly restrictive, and the connection stiffnesses cannot be modelled. The ANSYS model was constructed using beam elements, either BEAM3, a two dimensional elastic beam, or BEAM23, a two dimensional plastic beam. The connections were modelled using either COMBIN14, a linear elastic spring, or COMBIN39, a non-linear spring. The behaviour of the spring elements is shown in Figure 4 below.

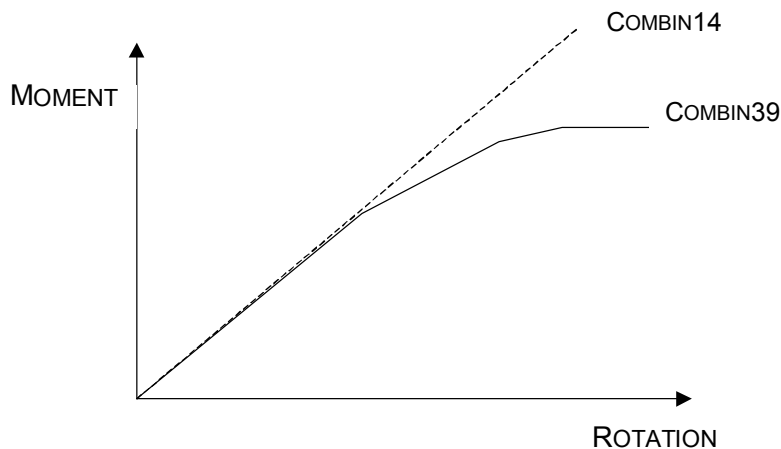


Figure 4. - M- θ curves for spring elements

The model was then modified with differing connection stiffness to find how these influenced the behaviour of the frame. This was carried out for both non-sway and sway frames. The connection stiffness were varied between perfectly pinned to perfectly rigid.

The model used for the finite element analysis is shown in Figure 5 below.

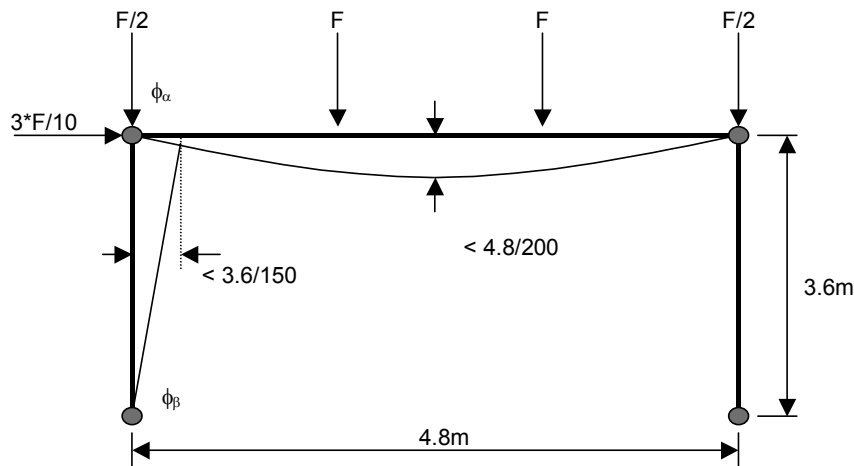


Figure 5. - Finite element model

4.1 Non-Sway Elastic Model

The elastic models are used mainly to find deflections at set loads for different beam-to-column connection stiffnesses, and different column base connection stiffnesses. The plastic models discussed later are used to find the ultimate loads of the frames.

The non-sway frame is used to find how the connection stiffnesses affect the beam's mid-span deflection. The mid-span deflection results are shown in Figure 6 below.

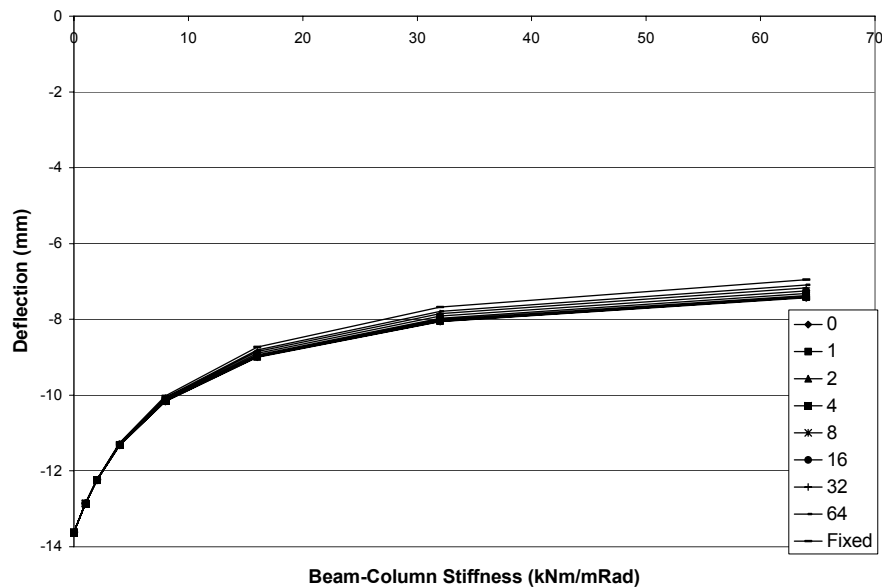


Figure 6. - Mid-Span, Non-Sway, deflections

The x-axis of the chart shows increasing beam-to-column stiffnesses. The chart demonstrates that the beam-to-column connections have a large influence over the mid-span deflection of the

beam, especially with increases at the lower end of the scale of stiffness. The influence becomes less with larger stiffnesses. Each of the lines represents a different column base stiffness. As each of the lines is very similar, it shows that the column base stiffness has very little influence over the mid-span deflection of a non-sway frame. These analyses show that the beam-to-column connection stiffness has a very large effect on the beam deflections, and hence the importance of the connection stiffness in efficient design.

4.2 Sway Elastic Model

The same set of models was used for the sway analyses, the only difference being that the non-sway model had a sway constraint at the column tip. It was expected that for these analyses there would be a far greater influence on deflection from the column base stiffness. Figures 7 and 8 show the sway deflection results.

Figure 7 shows how the beam-to-column stiffness affects the column sway. Each of the lines on the chart represents a column base stiffness in kNm/mRad. Figure 8 shows how the column base rotational stiffness affects the column sway, and each line on the chart represents a beam-to-column stiffness in kNm/mRad. These charts show that whilst the vertical beam deflection is dependent mainly on the beam-to-column connection stiffness, the sway deflection is equally dependent on both the beam-to-column connection stiffness and the column base rotational stiffness. The charts also show that an increase in stiffness at the lower end of the scale of stiffnesses has the most dramatic effect on lowering the deflections; this is true for both sway and beam deflections. This demonstrates that there is no need in design to pursue the high stiffness value for connection. This will result in significant stiffening in connections. This once proves that rigid design has its shortadvantage in overall frame consideration.

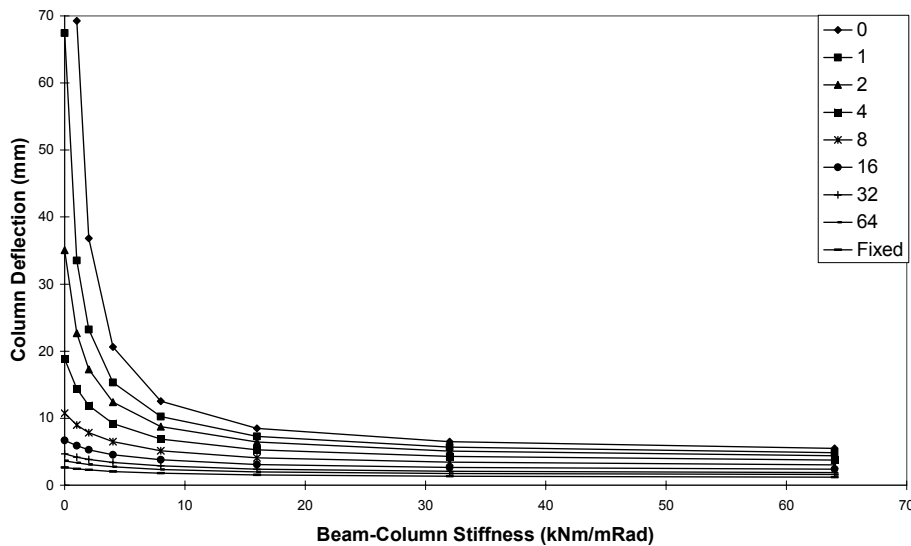


Figure 7. - Sway deflection with changing beam-to-column connection stiffness

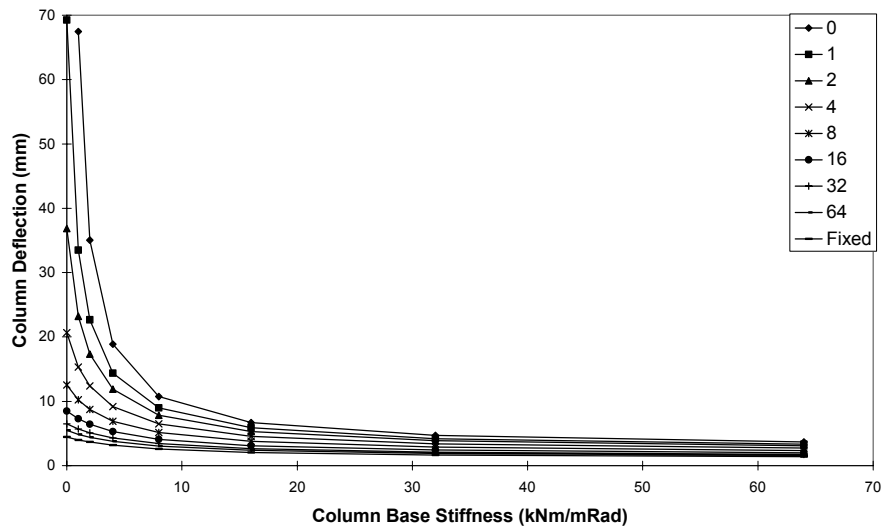


Figure 8. - Sway deflection with changing column base stiffness

4.3 Non-Sway Plastic Model

The same dimensions were used in the plastic model. The only change was in the elements used to describe the model: this time the plastic beam and the non-linear spring have been used. Using the non-linear spring also means that the spring properties have been defined differently. This will be simulated from the test programme. For the non-linear spring a maximum rotation has been used to define the spring, at a set moment. Previously the slope of the $M-\phi$ curve was used.

The analyses were run until a set deflection limit was reached. The deflection limit used was that defined by British Standards for serviceability. The load that was reached was then used and compared against the frame with fully fixed beam-to-column connections and column bases. Whether the frame had failed at the connections, or in one of the sections, depended upon the stiffness of the connections. The frames with weaker connections fail at the connection; the frames with the stiffer connections fail with a plastic hinge forming in the steel section.

Once the ratio of strength between the fully fixed frame, and a frame with semi-rigid connections, is found, then a set of equations can be set up which form the beginning of a design method. The design method is described by Xiao *et al* [14,15]. A joint stiffness factor has been proposed which includes the governing parameters for connection and frame. The results have been compared to those found in [14,15], and it was found that they agree very closely. The results were compared so that it would subsequently be possible to produce a multi-storey frame model. Figure 9 below shows how the ratio of strength, compared to the fully fixed frame, changes for different connection properties.

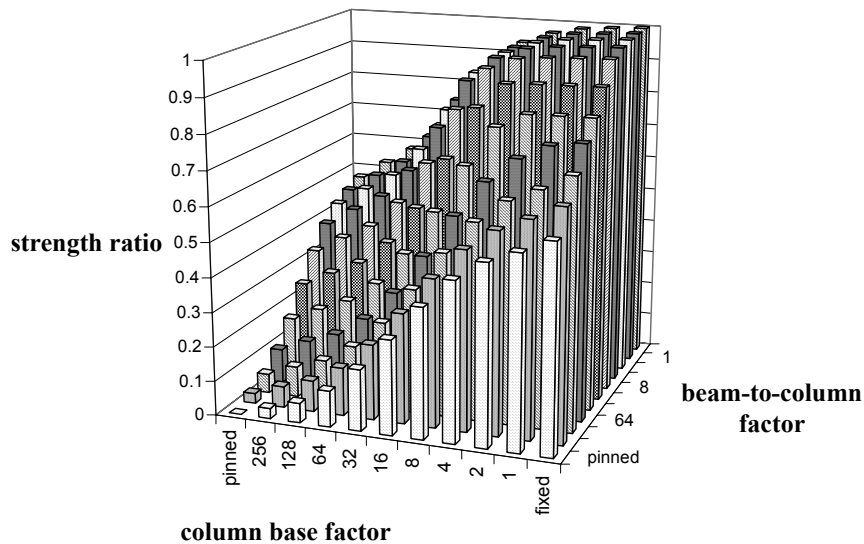


Figure 9. - Strength ratio, compared to fully fixed frame affected by connections

The results show, like those from the elastic analyses, that the strength of the sway frame is dependent both on the beam-to-column connection stiffness, and on the column base stiffness. The strength increase is most obvious at the lower end of the range of joint stiffness. Curve fitting analysis shows that these curves closely follow a third order logarithmic curve.

5 CONCLUSION

Site-monitoring has been carried out on a real semi-continuous designed building. The finite element models have been set up to investigate the influence of using semi-rigid connections on steel frameworks. From these models it will be possible to establish some new design methods for steel frames that utilise semi-continuous connections in terms of strength and deformation capacities. The design method is simple, not making additional demands on designers' time. By using semi-rigid design over simple pinned design steel costs can be saved, producing more efficient structures due to the reduced steel weight. The construction costs will not be as high as they would be for fully rigid connections, and the connections used are no different from those already used in construction.

6. Acknowledgement

The research reported here has been supported by EPSRC, Corus (formerly British Steel), Amey Construction Ltd and Gifford & Partners, Consulting Engineers. The authors acknowledge these supports to have the sit-work completed.

7. References

1. Commission of the European Communities, Eurocode 3: Design of Steel Structures 1992
2. Commission of the European Communities, Eurocode 4, Design of Composite Steel and Concrete Structures, 1994
3. Bjorhovde R., Colson A., Brozzetti J., Classification System for Beam-to-column connections. Journal of Structural Engineering, 1990, Vol. 116, No. 11, pp. 3059-3076.
4. Wong C. W., Mak H., Ko J. M., System and parametric identification of flexible connections in steel framed structures. Engineering Structures, 1995, Vol. 17, No. 8, pp. 581-595.
5. Koch E., Mang F., Schleich J.B., Seiler J., Stiglat K., (1993): Steel Columns Embedded In Concrete Foundation, Fourth International Conference On Structural Failure, Durability And Retrofitting, Singapore 14-15 July 1993.
6. Balogh J., Iványi M., (1995): Parametric Study of Column-Base Connections, Preliminary Report of the International Colloquium, European Session, Stability of Steel Structures, ed. Iványi M., Veröci B., Vol. 2, Budapest, pp. 11-16.
7. Pertold, J., Xiao, R. Y. and Wald, F, *Embedded Steel Column Base. Part I. Experiments and Numerical Simulation*, Journal of Constructional Steel Research, 2000 (in press)
8. Pertold, J., Xiao, R. Y. and Wald, F, *Embedded Steel Column Base. Part II. Design models*, Journal of Constructional Steel Research, 2000 (in press)
9. Nethercot, D.A. and Xiao, R. Y., *Connection Performance*, The Structural Stability Research Council, Atlanta, USA, (key-note paper), September 1998
10. Xiao, R. Y., Nethercot, D. A. and Choo B. S., *Composite Connections in Steel and Concrete (ii) Prediction of Moment Resistance of Composite Flush Endplate Connection*, Journal of Constructional Steel Research, Vol.1.37, No.1, 1996. pp63-90
11. Xiao, R. Y., *Experimental Behaviour and Design of Composite Connections*, Proc. of International Seminar on Large Scale Testing on Buildings. London, UK, July 1996, pp491-498
12. Troup, S. D., Numerical analysis and investigation of composite semi-rigid connections, PhD thesis, Department of Civil Engineering, University of Southampton, 1998
13. Xiao, R.Y., Dibb-Fuller, D and Wood G., *Opening in Composite Floor-Design implications*, Journal of Constructional Steel Research, Vol.46, Nos1-3, 1998, pp230
14. Xiao. R. Y., Pertold. J., Frame Analysis with Semi-Rigid Connections Rigidity Factor Method Part I Non-sway Mode. Under Review.
15. Xiao. R. Y., Pertold. J., Frame Analysis with Semi-Rigid Connections Rigidity Factor Method Part II Sway Mode. Under Review.
16. Xiao, R. Y. and Fisher, C. D., Computational Analysis and Design of Semi-Continuous Steel Frame Structures, The Fifth International Conference on Computational Structures Technology, Leuven, Belgium, September 2000

SEMI-CONTINUOUS BEAM-TO-COLUMN JOINTS AT THE MILLENNIUM TOWER IN VIENNA, AUSTRIA

Gerald Huber¹

Abstract

The Millennium Tower is situated to the north of the center of Vienna. With a height of 202 m it is the highest building in Austria. Realization was improved by new methods. The tower is a typical example of mixed building technology, combining composite frames with a concrete core. Special attention has been paid to the moment connections between the slim floors and the column tubes resulting in a drastically reduced construction time and thin slabs. The semi-continuity has been considered in the design at ultimate and serviceability limit states.

1. INTRODUCTION

1.1 The Project “Millennium City”

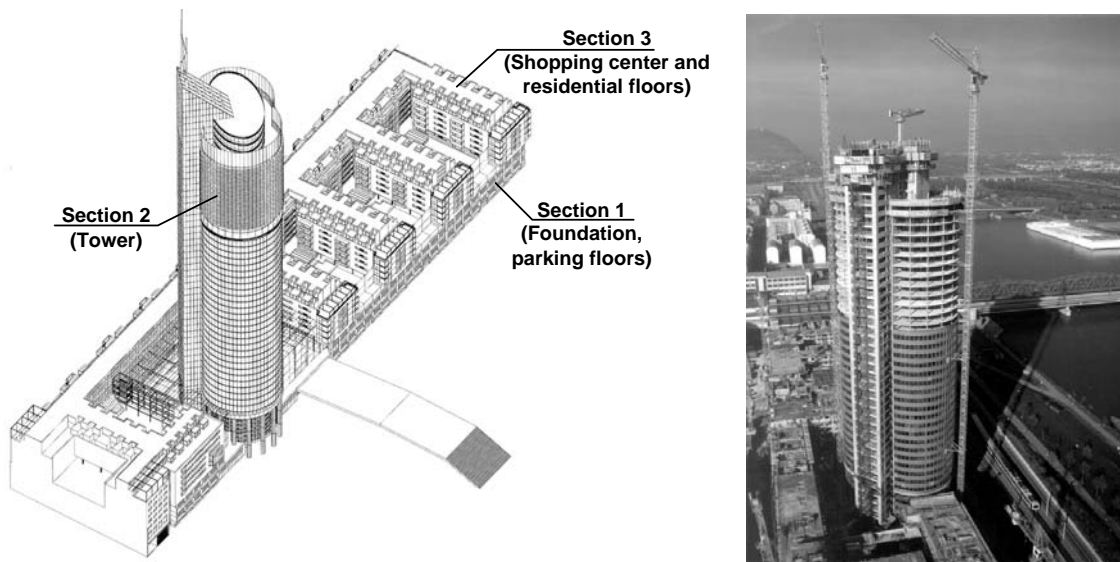


Fig. 1 Millennium City, Vienna

In 1996 the Vienna municipal council agreed to the “Millennium City” project of “Stumpf Immobilien- und Wohnungseigentum GmbH” (Vienna) with residential blocks (37.000 m²), a commercial area (25.000 m²) and an office tower (38.000 m²) planned by the team of architects Peichl-Podrecca-Weber (Vienna). The construction of this “City in the city” (*Fig. 1*) started in 1997 on a ground area of 15.500 m² - conveniently placed what regards transport facilities - with a capital expenditure of about 145 Million Euro (1).

¹ Univ.-Ass. Dipl.-Ing. Dr.techn. Gerald HUBER, Vice head of the Institute, e-mail: gerald.huber@uibk.ac.at
IStHM, Institute of Steel, Timber and Mixed Building Technology
University of Innsbruck, Technikerstrasse 13, A-6020 Innsbruck, Austria, <http://stahlbau.uibk.ac.at>

The overall project is separated into three sections: Section 1 includes four basements with a parking area for 1.500 cars and the tower foundation plate on 151 bored piles with a length of 25 m. Section 2 is the tower itself with 50 upper floors and an antenna of 30 m. Section 3 contains two shopping floors and six residential floors and has been erected simultaneously to the tower.

1.2 Millennium Tower

With a total height of 202 m it is the highest building in Austria. Work started in May 1998. By realizing 2½ up to even 3 floors per week the building shell was already completed in January 1999 after only 8 months of construction. The final handing over to the owner happened in April 1999. The plan of the tower with 1.080 m² consists of two overlapping circles for offices and a concrete core which contains the elevators and stairways, the foyer, archives and additional office area in the so-called tower back (Fig. 2). The core has been realized in conventional concrete building technology to transfer vertical forces and all horizontal forces due to wind and earthquake. At the other hand the tower circles are formed by concentric composite frames, which are only designed for vertical forces. The combination of concrete and composite building technology finally results in an overall “mixed building”.

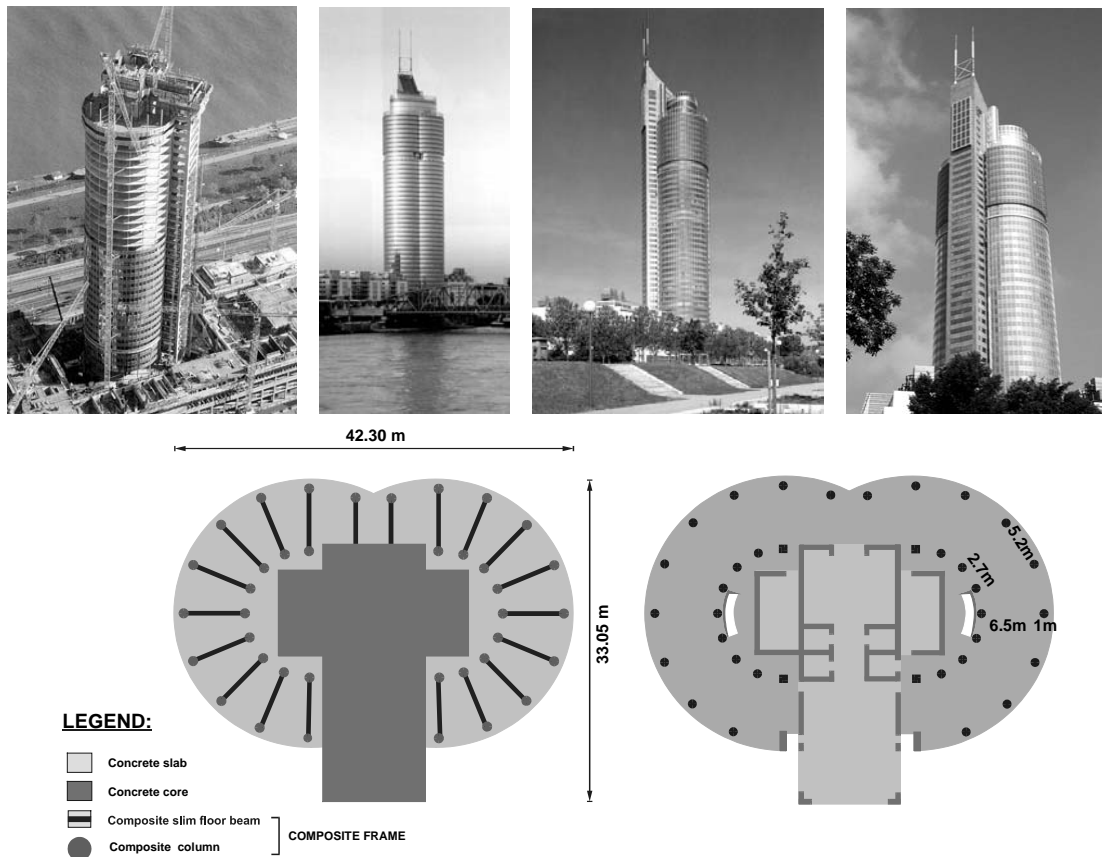


Fig. 2 Millennium Tower

The demands for an extremely fast and weather independent erection, very thin slabs (reduced dead load and lower facade costs) with a plane ceiling (easier installation) and very slender columns called for an ingenious solution, which included the following building innovations: Composite slim floor beams fully integrated into the thin slabs, moment-resisting (semi-continuous) joints enabling a frame action between the beams and columns and a new type of

shot-fired shear connector within the composite columns. The capital expenditure for the tower shell amounted to 12,5 Million Euro based on 1.500 tons of constructional steel, 2.500 tons of reinforcing steel and 15.000 m³ of concrete.

2. COMPOSITE FRAMES

2.1 General

The vertical forces of the two overlapping tower circles are carried by 20 external and 18 internal columns in a concentric distance of 6,5 m (Fig. 2). The external columns are located 1 m inside of the facade with a transverse distance of 5,2 m. The space between the internal columns is 2,7 m. The interplay between an external column, the external joint, the slim floor beam, the internal joint and the internal column forms a frame system (Fig. 3) with the effect of a considerable reduction of sagging moments, deflections and vibration of the slab. The frame capacity of transferring horizontal forces additionally to the concrete core has not been taken into account. The big number of analogous joints obviously justifies a very detailed planning to optimize the advantage of moment connection with regard to the erection time and costs.

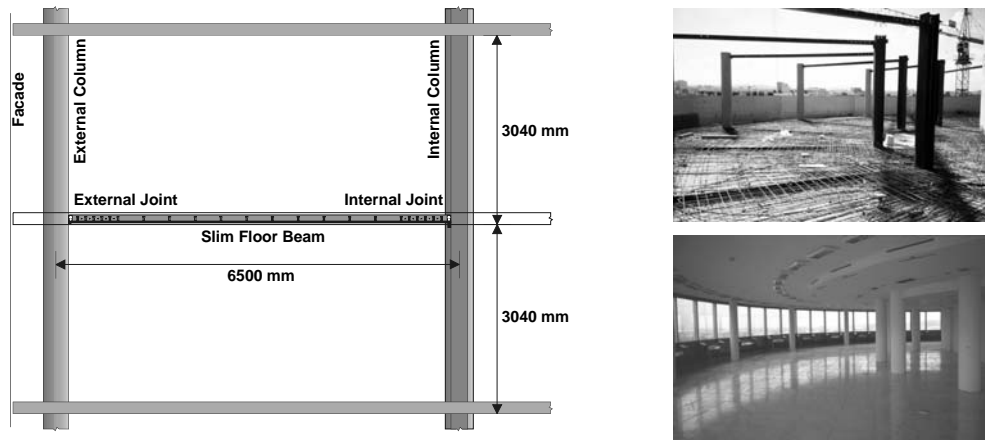


Fig. 3 Composite frames with semi-continuous joints

2.2 Beam cross section

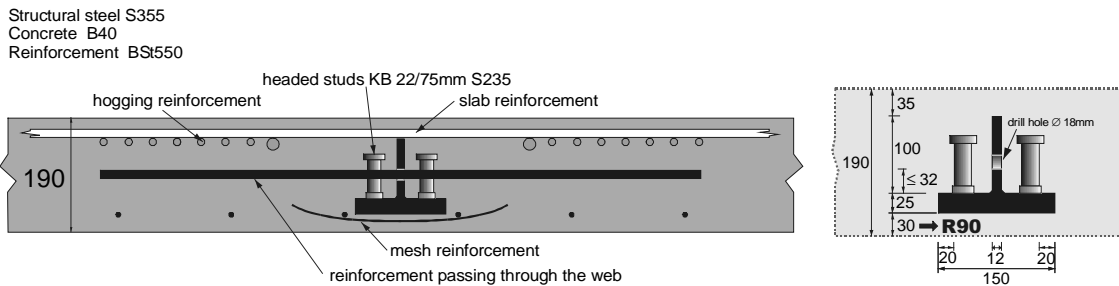


Fig. 4 Composite slim floor beam

The composite slim floor beams (Fig. 4) are built of welded T-shaped steel sections and a concrete slab with minimum sagging reinforcement and a considerable amount of reinforcement in the hogging region within the effective width. The shear connection is provided by headed studs. The non-linear characterization of the sagging cross section considering partial shear connection and that of the hogging cross section including the effect of tension stiffening has been performed with the software developed in (2) basing on Eurocode 4.

2.3 Column cross section

The demand for very slender columns led to composite sections with steel tubes and additional steel cores, both S355. The diameter of the tube, the size of the core and the concrete grade have been adjusted to the actual stresses depending on the floor number. As shown in Fig. 5 the diameter of the external columns varied from 324 up to 406 mm. To ensure optimal filling of the remaining space between tube and core self-compacting concrete of grades B40 to B60 has been used. To defuse the severe problem of different creep and shrinkage between the composite columns and the concrete core due to a different steel-to-concrete ratio the internal columns – closer to the concrete core – have been realized as concrete-encased rolled I-sections with a higher concrete percentage. Their diameter is 450 to 500 mm (Fig. 5). The normal stresses in the columns have been determined with influence areas basing on plastic redistribution. Except for the top columns the normal force is clearly dominating in comparison to the bending moments resulting from the frame action due to the semi-continuous joints. Design calculations under normal conditions and in case of fire (R90) have been based on Eurocode 4.

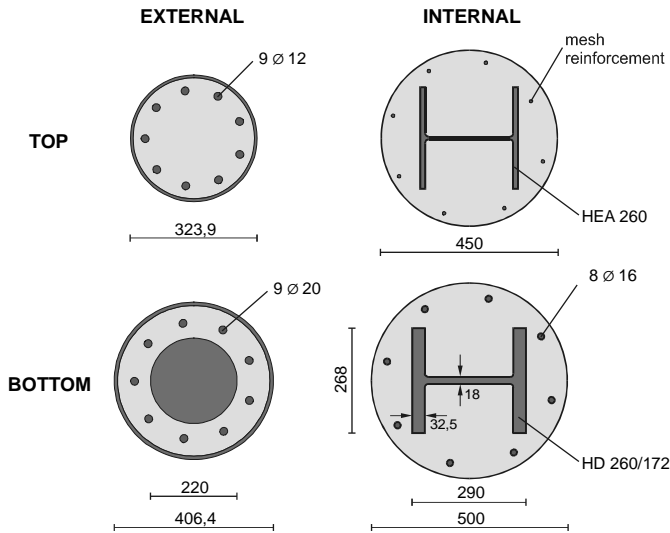


Fig. 5 Column cross sections

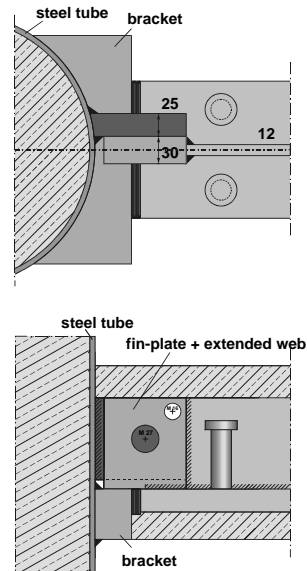


Fig. 6 Support of beam at external column

The vertical support forces of the beams are handed over to the column steel tube via a welded bracket (in cold stage) and a fin-plate (in case of fire) (Fig. 6). Parts of these concentrated forces then have to be passed to the chamber concrete and further to the steel core. Instead of conventional welded studs - as a novelty - shot-fired nails and bolts (Fig. 7) have been applied (3)(4).

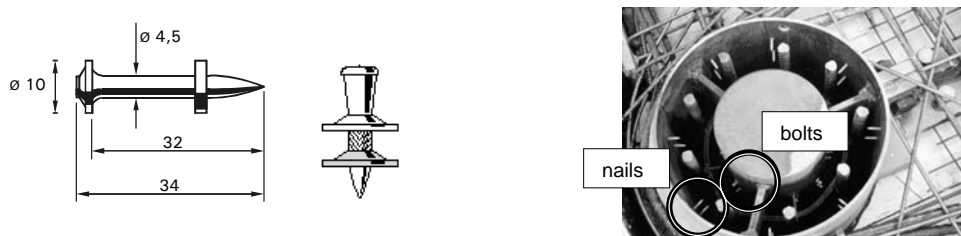


Fig. 7 Shot-fired nails and bolts for shear connection

3. SEMI-CONTINUOUS JOINTS

3.1 General

The use of composite slim floor beams in combination with composite columns solves two problems simultaneously which would appear in conventional concrete joints: punching and a low moment resistance combined with a brittle failure due to the limited load introduction of concrete in compression (Fig. 8).

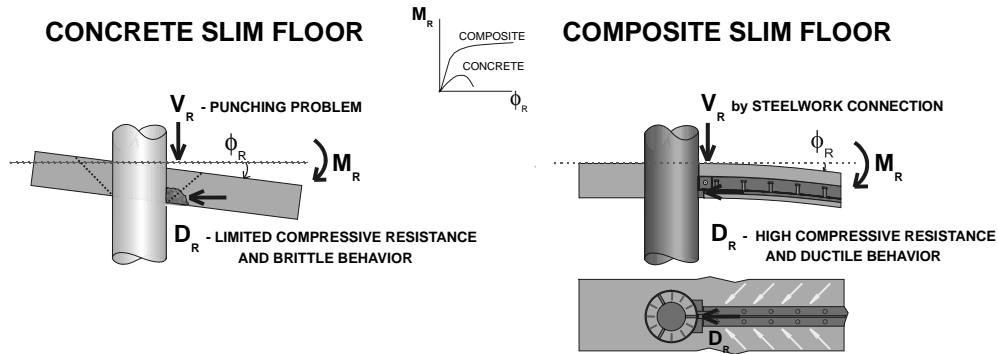


Fig. 8 Comparison between concrete and innovative composite slim floors

3.2 Joint configuration

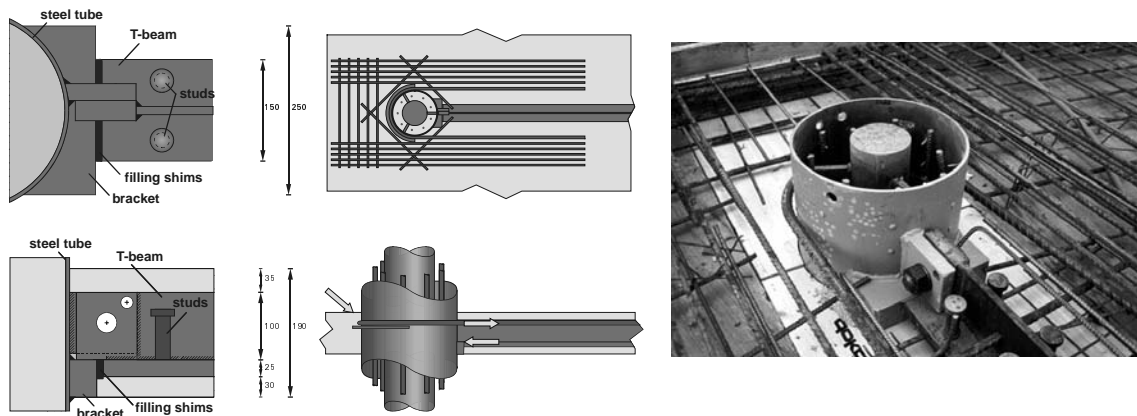


Fig. 9 Regular external joint configuration

Fig. 9 shows the actual configuration of a joint between an external column and a regular slim floor at the Millennium Tower. The compressive force is transferred from the beam flange via clearance filling shims into a bracket which is welded to the column tube. From there it spreads vertically and horizontally into the hollow steel section, the chamber concrete and the steel core. The tensile force of same size goes through the beam's shear connection into the hogging reinforcement. A reinforcement U-bar of 20 mm diameter goes around the column in direct contact. A saddle already welded in the shop ensures the exact location of this bar and therefore the joint's lever arm. The remaining restraint reinforcement (7 bars of 12 mm at both sides of the column) extends into the cantilevering part of the slab. Together with the transverse reinforcement and concrete struts a truss is built handing over the tension force into the column via bearing pressure. Especially in the case of such slim floor joints with a small lever arm, its constructive observation is crucial as a deviation of some centimeters already would cause a significant loss of stiffness and moment resistance.

Such a combination of a U-bar and a reinforcement truss can only be realized in the case of a cantilevering slab. As for the lower five floors the facade should be located directly behind the column an alternative to the regular joint had to be developed with additional U-bars resulting in a necessary slab outstand of only 6 cm (*Fig. 10*). To avoid splitting due to the arrangement of three U-bars an additional top saddle has been provided. By optimizing the reinforcement layout the overall response of these different external joint configurations is nearly similar in view of stiffness and resistance.

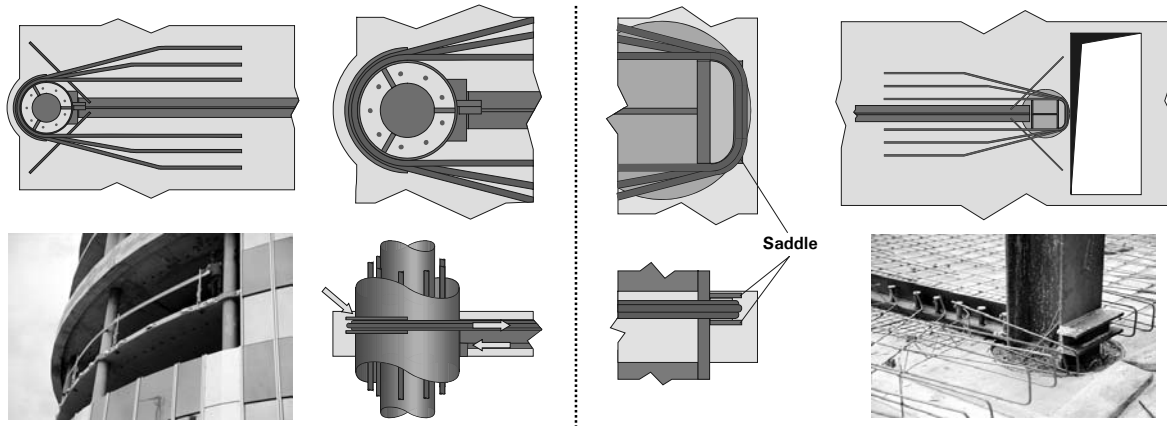


Fig. 10 External and internal joint configuration without cantilevering slab

3.3 Joint characterization

For the regular external joint configuration (*Fig. 9*) the following components can be identified contributing to the overall joint behavior. Component C1 is the redirection truss within the cantilevering slab set together by the longitudinal and transverse reinforcement in tension and diagonal concrete struts bearing to the column. The reinforcing U-bar, component C2, acts in the same way as C1 anchoring the tension forces into the column. So C1 and C2 are sharing the overall tension force as two parallel components. The bolt of the fin-plate (*Fig. 6*) is only used for vertical shear transfer in case of fire. An interaction in tension due to the moment-connection is prevented by hole clearance. Component 3 represents the slip between the T-shaped steel beam and the concrete slab due to incomplete shear interaction. The compression region is formed by the components C4, C5 and C6 reflecting the compression in the beam flange and the filling shims, the load introduction into the steel tube via the bracket and the stiffening effect of the chamber concrete within the tube. For such an edge joint the beam's hogging moment is not balanced by a similar connection on the other side and therefore the full restraint moment has to be transferred into the column. The concentrated load introduction in tension and in compression are then causing local shear (C7) and bending (C8) of the steel tube, reinforced by the chamber concrete (C9). *Fig. 11* gives an overview of the actual components and the key values of their individual behavior in view of initial stiffness (c or S) and design resistance (F_{Rd} or M_{Rd}) gained from analytical models according to the specified references. The detailed formulae can also be got from the example calculation in (5).

To get the overall moment-rotation response of the connection the influences of the individual components C1 to C6 have been assembled fulfilling equilibrium and compatibility according to the component model shown in *Fig. 12*. Simultaneously with a considerable degree of moment connection the Millennium Tower joints proved to be easy to handle both in view of erection and characterization. As there is only one row in tension the component curves could easily be added step by step parallel and serial without iterations (*Fig. 13*) using the computer program CoBeJo (2) which would even enable an iterative assembly for up to 7 rows in tension.


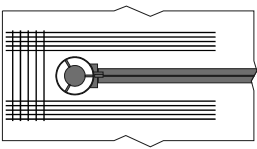

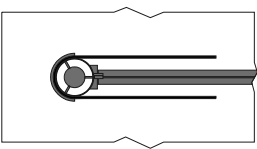
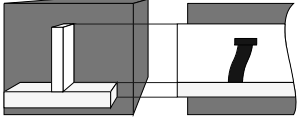

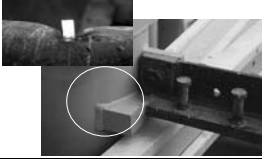
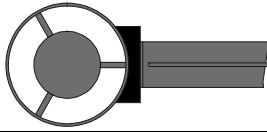

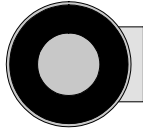

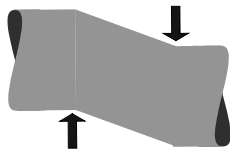
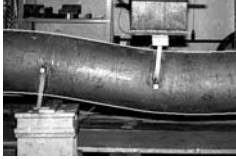
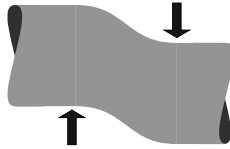
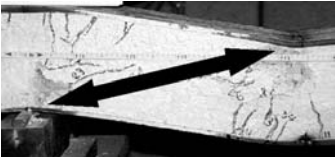
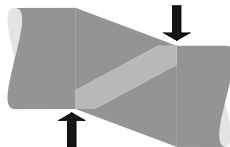
Components			Characterization
Connection (L)			
C1	redirection truss (longitudinal and transverse reinforcement plus concrete struts)	 	(6), (2), (7) $C_1 = 430 \text{ kN/mm}$ $F_{Rd,1} = 757 \text{ kN}$
C2	U-bar reinforcement	 	(6), (7) $C_2 = 352 \text{ kN/mm}$ $F_{Rd,2} = 300 \text{ kN}$
C3	slip due to incomplete shear interaction in the beam		(8) $C_3 = \infty \text{ kN/mm}$ $F_{Rd,3} = \infty \text{ kN}$
C4	compression in the beam flange and shims		(6) $C_4 = \infty \text{ kN/mm}$ $F_{Rd,4} = 1.331 \text{ kN}$
C5	load introduction into the steel tube via the bracket	 	(6), (9), (10) $C_5 = 53 \text{ kN/mm}$ $F_{Rd,5} = 147 \text{ kN}$
C6	stiffening in compression by the chamber concrete	 	(6), (9), (10) $C_6 = 2.917 \text{ kN/mm}$ $F_{Rd,6} = 1.100 \text{ kN}$
Shear panel (S)			
C7	shear deformation of the steel tube	 	(6), (9), (10) $S_7 = 24,3 \text{ MNm}$ $M_{Rd,7} = 56,2 \text{ kNm}$
C8	bending deformation of the steel tube	 	(6), (9), (10) $S_8 = 1.272 \text{ MNm}$ $M_{Rd,8} = 310 \text{ kNm}$
C9	stiffening in shear by the chamber concrete	 	(6), (9), (10) $S_9 = 6,4 \text{ MNm}$ $M_{Rd,9} = 41,6 \text{ kNm}$

Fig. 11 Joint components and their characterization

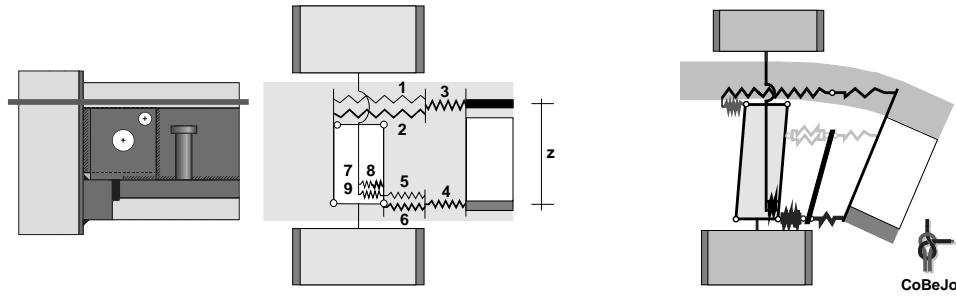


Fig. 12 Component model for assembly

Due to the very simple component interplay the key values of the connection's M-φ curve can even be estimated with the following formulae knowing that the lever arm z is 109 mm:

$$S_L = \left(\frac{1}{c_1 + c_2} + \frac{1}{c_3} + \frac{1}{c_4} + \frac{1}{c_5 + c_6} \right)^{-1} \cdot z^2 = 7.4 \text{ MNm} \quad M_{L,Rd} = z \cdot \min[(F_{Rd,1} + F_{Rd,2}); F_{Rd,3}; F_{Rd,4}; (F_{Rd,5} + F_{Rd,6})] = 115 \text{ kNm}$$

The overall M-φ curve of the shear panel has been set together by the individual influences C7 to C9 in an analogous way; at the one hand for the overall curve as shown in Fig. 14 and at the other hand estimating only the key values according to the following formulae:

$$S_S = \left(\frac{1}{1/S_7 + 1/S_8} + S_9 \right) = 30.2 \text{ MNm} \quad S_{S,Rd} = M_{Rd,9} + \min[M_{Rd,7}; M_{Rd,8}] = 98 \text{ kNm}$$

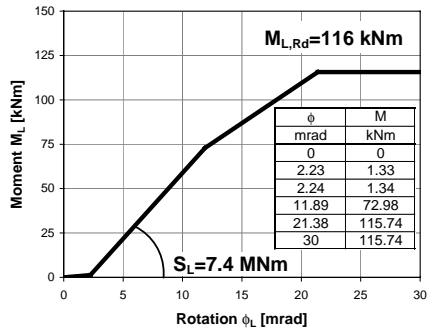


Fig. 13 M-φ curve of the connection (components C1 to C6)

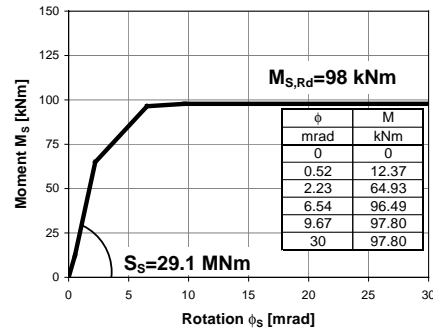


Fig. 14 M-φ curve of the shear panel (components C7 to C9)

3.4 Joint modeling

For a conventional joint configuration with double-sided connections the separate influences of the connections and the shear panel can be considered separately also in the global analysis. Neglecting the difference between the moment within the connection (M_L) and that of the shear panel (M_S) for the actual edge joint these two influences alternatively may be added in series resulting in a combined joint curve (Fig. 15) with the following key values:

$$S_j = \left(\frac{1}{S_L} + \frac{1}{S_S} \right)^{-1} = 5.9 \text{ MNm} \quad j_{Rd} = \min[M_{L,Rd}; M_{S,Rd}] = 98 \text{ kNm}$$

Fig. 16 shows the corresponding joint model with an infinitely rigid joint area and a rotational joint spring at the beam-to-column intersection point representing the overall joint deformability (11). The configuration of all joints at the Millennium Tower (external and internal, at the top and at the bottom) has been optimized in such a way that their response is nearly identical and therefore one single idealized bi-linear curve (Fig. 15) could be used for all joints of this building. A full-scale joint test impressively proved the analytical results.

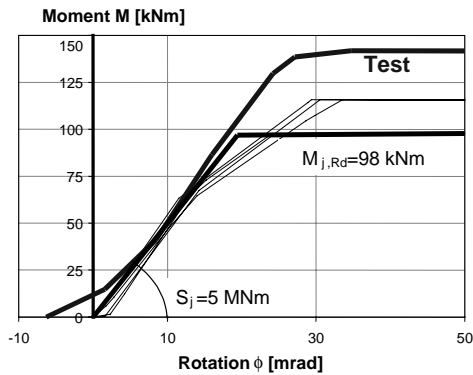


Fig. 15 Overall design joint curve

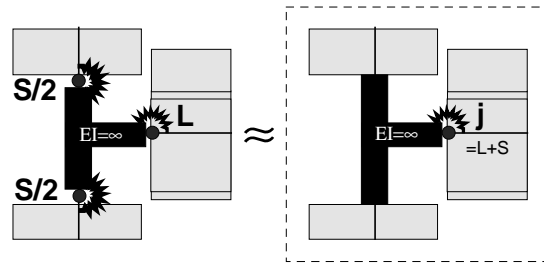


Fig. 16 Joint modeling

3.5 Global frame analysis

Knowing the response of the beams in sagging and in hogging, that of the columns and the joints out of the respective characterization the global frame analysis could be performed for ULS and SLS for all dead and imposed loads with the structural system shown in Fig. 17 (12). A comparative calculation with perfect hinges or fully rigid restraints shows that the actual semi-rigid joints lead to deflections and bending moments quite in the middle between these borderline cases as an optimum between design calculation and economic detailing.

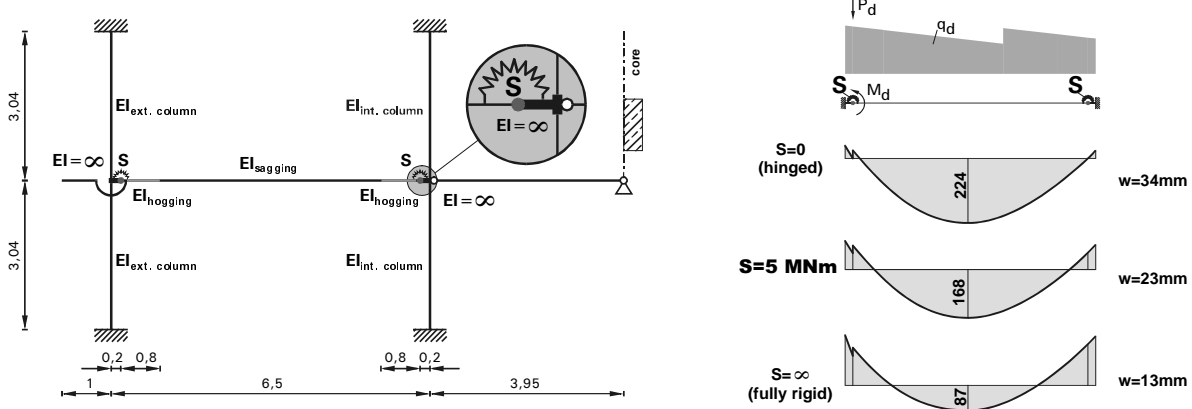


Fig. 17 Global frame analysis considering the joint behavior

CONCLUSIONS

It was shown that a simple support during erection can easily be transferred into a moment-resisting joint with considerable stiffness and resistance at final stage. Activating this frame action between beams and columns enables the realization of very slim floors under observance of ultimate and especially serviceability limit states. The analytical joint characterization was described in detail applying the component method. A full-scale joint test as well as measurements on site proved the calculated joint behavior. In addition the use of shot-fired nails and bolts as shear connectors within the hollow column sections helped speeding up the erection.

ACKNOWLEDGMENT

The enormous technical experience, the untiring research efforts and the friendly work climate of Univ.-Prof. Dipl.-Ing. Dr.techn. Ferdinand Tschemmerneegg, former head of IStHM, University of Innsbruck, who died in November 1999 in the age of 60, is gratefully acknowledged.

REFERENCES

- (1) TSCHEMMERNEGG F., "Innsbrucker Mischbautechnologie im Wiener Millennium Tower (Mixed building technology of Innsbruck at the Millennium Tower in Vienna)", *Stahlbau 68*, Ernst & Sohn, Berlin, p. 606-611, 1999.
- (2) HUBER G., "Non-linear calculations of composite sections and semi-continuous joints", *Doctoral thesis, Ernst & Sohn, Berlin*, ISBN 3-433-01250-4, 1999.
- (3) BECK H., "Nailed shear connection in composite tube columns", *Conference Report Eurosteel 99 in Praha*, ISBN 80-01-01963-2, 1999.
- (4) TAUS M., "Neue Entwicklungen im Stahlverbundbau am Beispiel Millennium Tower Wien und Citibank Duisburg (New developments in composite construction at the Millennium Tower in Vienna and the Citibank in Duisburg)", *Commemorative publication Prof. Dr. Ferdinand Tschammerneegg, IStHM, University of Innsbruck, Austria*, ISBN 3-9501069-0-1, 1999.
- (5) HUBER G., MICHL T., "Beispiele zur Bemessung von Riegel-Stützen-Verbindungen (Example calculation for a beam-to-column joint)", *Fachseminar und Workshop Verbundbau 3, Fachhochschule München/Munich, Germany*, 1999.
- (6) MÜLLER G., "Das Momentenrotationsverhalten von Verbundknoten mit Verbundstützen aus Rohrprofilen (The moment-rotation response of composite joints with composite tubular hollow columns)", *Doctoral thesis, IStHM, University of Innsbruck, Austria*, 1998.
- (7) HITTENBERGER R., "Zur Durchdringung von Stützen und Deckenplatten bei Verbundknoten (The interaction between columns and slabs for composite joints)", *Doctoral thesis, IStHM, University of Innsbruck, Austria*, 1992.
- (8) BADRAN M.Z., "Modelling of the connection zone of composite joints", *Doctoral thesis, IStHM, University of Innsbruck, Austria*, 1995.
- (9) HERZOG M., "Steifigkeitskalibrierung von Komponenten für Knoten in Mischbauweise mit Hohlprofilstützen für ENV1994-1-1, Annex J (Calibration of simplified stiffness formulae for steel and composite hollow column sections for ENV1994-1-1)", *Diploma work, IStHM, University of Innsbruck, Austria*, 1998.
- (10) TSCHEMMERNEGG F. (Coordinator), "Slim floor construction, Chapter 4: Calibration work for ENV1994-1-1", *INTAS Project 96-2154, Brussels*, 1999.
- (11) ANDERSON D. (Editor), "Design of Composite Joints for Buildings", *ECCS Publication No. 109*, ISBN 92-9147-000-52, Brussels, 1999.
- (12) HUBER G., RUBIN, D., "Verbundrahmen mit momententragfähigen Knoten beim Millennium Tower (Composite frames with semi-continuous joints at the Millennium Tower)", *Stahlbau 68*, Ernst & Sohn, Berlin, p. 612-622, 1999.

Cyclic Behavior and Seismic Design of Steel Shear Connections

Judy Liu, Ph.D.

Assistant Professor, School of Civil Engineering
Purdue University, West Lafayette, IN 47907-1284, USA

Abolhassan Astaneh-Asl, Ph.D., P.E.

Professor, Department of Civil and Environmental Engineering
University of California, Berkeley, CA 94720-1710, USA

ABSTRACT

An experimental and analytical program was undertaken to determine the contribution of typical shear, or simple, connections, including the floor slab, to the lateral resistance of steel structures. Through the experimental program, the cyclic behavior of typical shear connections was established. In the analytical program, this information was used for the development of models of moment-rotation response. These efforts have resulted in tools for establishing the role of simple connections in the seismic behavior of steel buildings.

INTRODUCTION

In an effort to establish the contribution of simple connections to the lateral resistance of steel structures, a combined experimental and analytical program was undertaken. Results from the experimental program suggested that simple connections, including the effects of the floor slab, behave as partially restrained connections. Information on their cyclic behavior was used for development of models of their moment-rotation response. Presented here is an overview of the test program, experimental results, and basic parameters from the moment-rotation models.

EXPERIMENTAL PROGRAM

The test program consisted of sixteen full-scale cyclic tests of simple connections. Specimens were designed as if from a building with W14x90 columns at 7.62 m (25'-0") spacing, with W18x35 beams framing into W24x55 girders. Connection details included typical 4-, 6- and 8-bolt shear tab connections, a supplemental seat angle, a stiffened seat, pre-80's shear tabs, and a top-and-bottom angle connection. Variations included the presence of the floor slab, the type of concrete used, the amount of reinforcement in the floor slab, and the presence of concrete within the column web cavity. Figure 1 shows a typical specimen with slab. The dimensions of the specimen were 7.62 m (25'-0") and 3.05 m (10'-0") pin-to-pin for the beams and columns, respectively. The slab was 2.44 m (8'-0") across. The floor was a 158 mm (6-1/4") concrete slab on 1 mm (20 gage) metal deck with 76.2 mm (3") ribs. The slab reinforcement included welded wire fabric for temperature and shrinkage, as well as nominal reinforcement across the girders for crack control. With nominal shear studs, the beams and girders were 20-30% composite. All bolts were ASTM-A325N. Table 1 gives details for test specimens. For more information on connection details, the reader is referred to Liu and Astaneh-Asl (1).

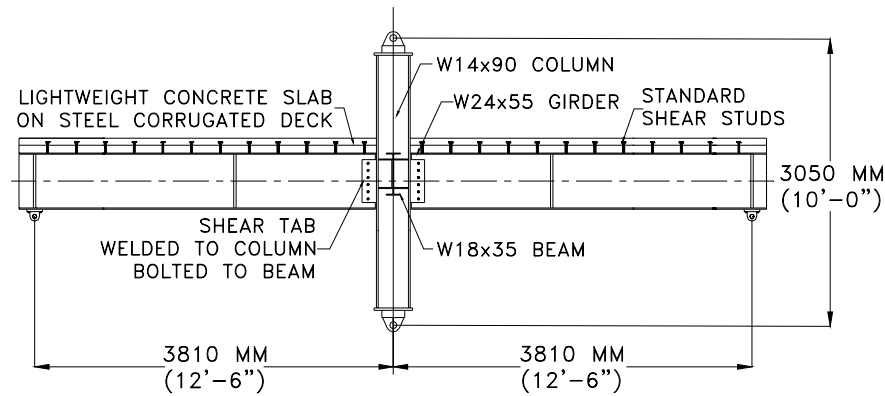


Figure 1. Typical specimen with floor slab

The test set-up was designed for the application of gravity loads and lateral drift (Figure 2). The column was pinned at the top and the bottom. Pin-ended struts at the ends of the girders provided vertical support while allowing for horizontal translation. Two actuators, one on each beam, were used to simulate the initial gravity loads on the system. The actuator at the top of the column applied increasing, cyclic, lateral displacements (SAC (2)). The drift angle was defined as the displacement at the top of the column divided by the column height, pin to pin.

Table 1. Test Specimens

#	Beam/ Girder	Bolts on Web	Seat / Flange Connection	Floor Slab		Concrete in Column
				Shear Studs	Slab Reinforcement	
1A	W18x35	4 - 22 mm	None	N.A.	N.A.	N.A.
2A	W24x55	6 - 22 mm	None	N.A.	N.A.	N.A.
3A	W18x35	4 - 22 mm	None	610 mm o.c.	Nominal	LW
4A	W18x35	4 - 22 mm	None	610 mm o.c.	D16 (No. 5)	LW
5A	W18x35	None	Stiffened	610 mm o.c.	Nominal	LW
6A	W24x55	6 - 22 mm	None	305 mm o.c.	Nominal	LW
7A	W24x55	6 - 22 mm	None	305 mm o.c.	Nominal	None
8A	W24x55	6 - 22 mm	203x102x19mm	305 mm o.c.	Nominal	LW
1B	W18x35	3 - 25 mm	None	N.A.	N.A.	N.A.
2B	W24x55	4 - 25 mm	None	N.A.	N.A.	N.A.
3B	W18x35	4 - 22 mm	None	610 mm o.c.	Nominal	NW
4B	W24x55	6 - 22 mm	None	610 mm o.c.	D13 (No. 4)	NW
5B	W24x55	4 - 25 mm	None	305 mm o.c.	Nominal	NW
6B	W24x55	6 - 22 mm	None	305 mm o.c.	Nominal	NW
7B	W33x118	8 - 22 mm	None	203 mm o.c.	Nominal	NW
8B	W24x55	None	203x102x19mm	305 mm o.c.	Nominal	NW

N.A.=Not Applicable; o.c.=on center; LW=lightweight concrete; NW=normal-weight concrete

CYCLIC BEHAVIOR OF TYPICAL SHEAR CONNECTIONS

In general, the tested connections showed significant moment capacity, ductile behavior and large drift rotations. Cyclic behavior tended to be characterized by bolt slip, yielding of steel, elongation of the bolt holes, and other ductile mechanisms.

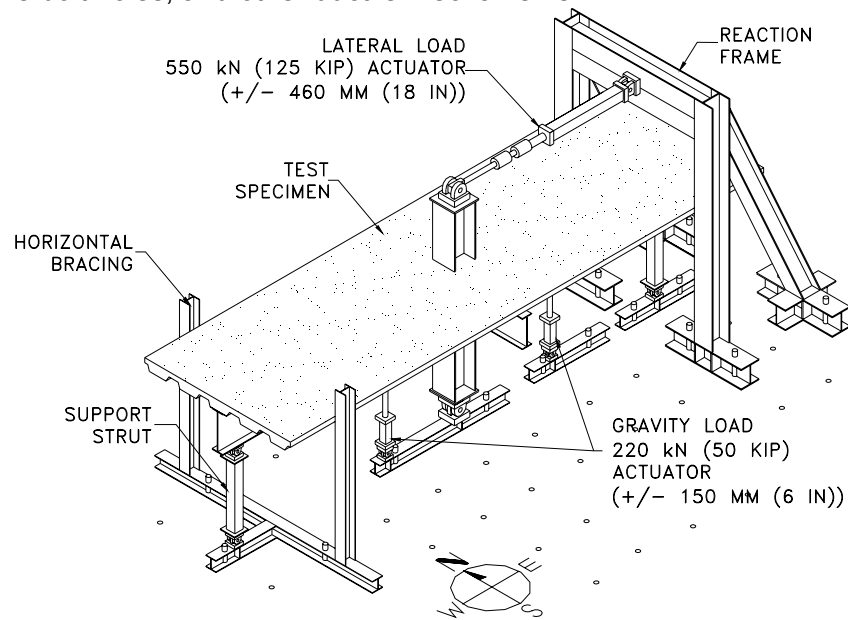


Figure 2. Test set-up

The shear tab connections with slabs (3A, 4A, 6A, 7A, 3B, 4B, 6B, 7B) acted as partially-restrained connections with maximum moment capacities on the order of 30 - 60% of the plastic moment capacities of the connected beams and girders. However, the slab contribution was typically lost after 0.04 radians due to the crushing of the concrete slab at the column. The connections then behaved similarly to bare steel shear tab connections (1A, 2A), with bolt slip, yielding in the shear tab and elongation of the bolt holes. Omitting the concrete in the column web cavity caused a 20% drop in maximum lateral load. The type of concrete and the addition of reinforcement around the column did not have such a significant effect on capacity. Binding of the beam flanges and column flanges at large rotations led to increases in stiffness and strength, as well as fractures in the shear tabs. Shear tab connections were able to reach large levels of drift while still carrying the applied gravity loads. For example, the 6-bolt shear tab connections with slab typically reached 0.11 radians of drift. Figure 3 shows the 4-bolt shear tab connection without slab (1A) at 0.14 radians of drift. Figure 4 shows a 6-bolt shear tab with slab at 0.03 radians and at the end of the test.

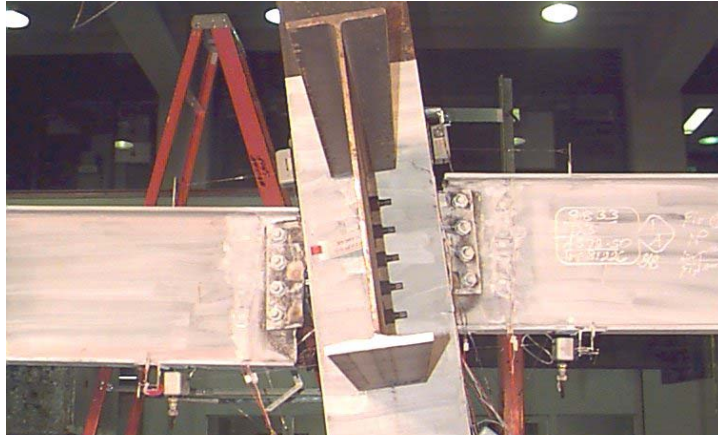


Figure 3. 4-bolt Shear Tab at 0.14 Radians of Drift



Figure 4. (Clockwise from Top Left) 6-bolt Shear Tab Connection with Slab (6B) at 0.03 Radians, Connection at 0.11 Radians (End of Test), Floor Slab at End of Test

The addition of a supplemental seat angle (8A) significantly increased the lateral resistance of the shear tab connection, with moment capacities on the order of 80% of the plastic moment

capacity of the girder. The initial stiffness was roughly twice that of the shear tab connection alone. The supplemental seat angle also demonstrated ductile behavior, marked by bolt slip, yielding in the tab and plastic hinging in the seat angle, and elongation of bolt holes in the shear tab, but also fracture along the bolt line of the shear tab, starting at 0.05 radians drift. The test was ended with fracture of one seat angle due to low cycle fatigue. Figure 5 shows the supplemental seat angle connection at the end of the test. Figure 6 shows a comparison of load versus drift for a 6-bolt shear tab specimen with slab (6A) and the same connection with the supplemental seat angle (8A).

Other connections generally demonstrated ductile behavior. For the shear tabs designed to pre-80's standards (1B, 2B, 5B), the deformation tended to be concentrated in the beam web rather than in the shear tab. On average, the bare-steel pre-80's connections demonstrated capacities of 10-20% of the plastic moment capacity of the beam. For the stiffened seat connection (5A), the yielding occurred primarily in the beam flanges. Fracture of the erection angle at the top of one beam occurred at 0.05 radians; this was followed by fracture of the two bolts connecting the bottom flange of the beam to the stiffened seat on the opposite side at 0.06 radians. The maximum moment capacity was roughly 50% of the plastic moment capacity of the beam. For the top-and-bottom angle connection (8B), the main mechanism was ductile plastic hinging of the angles. The ultimate failure mode at 0.06 radians was fracture of the bolts in shear. This connection had an initial stiffness comparable to the supplemental seat angle connection and moment capacity on the order of 80% of the plastic moment capacity of the girder. For more detailed summaries of the cyclic behavior of tested specimens, the reader is referred to Liu and Astaneh-Asl (3).

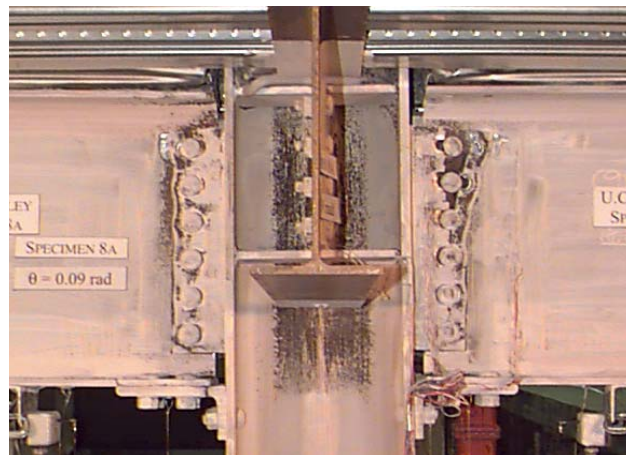


Figure 5. Supplemental Seat Angle Connection (8A) at End of Test

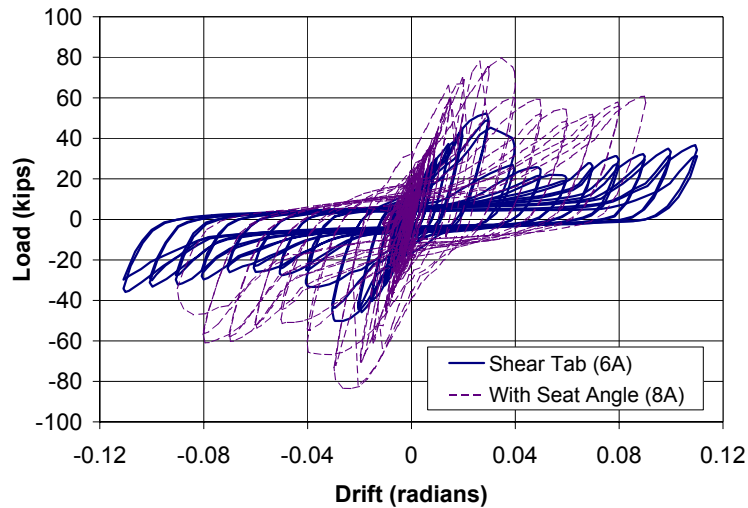


Figure 6. Load vs. Drift for Shear Tab and Supplemental Seat Angle Connections

DEVELOPMENT OF MODELS OF SHEAR TAB CONNECTIONS

Experimental results showed trends with regard to cyclic behavior of typical shear tab connections. For example, recorded moment-rotation responses for the shear tabs with slab invariably reach a peak and then, due to crushing of the concrete, drop in load at around 0.04 radians of drift. These observations and other data were used to develop guidelines for establishing simplified moment-rotation curves for shear tab connections with the slab. Among the parameters defined were ultimate rotation capacities, maximum positive bending moment capacity, maximum negative bending moment capacity, and initial stiffness.

Rotation Capacity of Shear Tab Connections

For shear tab connections, the limit state for rotation is defined as binding of the beam on the column, since this binding was consistently followed by shearing of bolts or fracture of plate. Binding is largely dependent on the position of the shear tab on the beam, the depth of the beam, and the distance that the beam flange has to travel before binding. Therefore, the equation for rotation capacity considers the gap between the beam flange and column flange, and the distance from the center of rotation of the connection to the farthest beam flange. Since, at the maximum rotation, the slab is typically damaged and ineffective, the center of rotation is considered to be about the center of the bolt group.

The equation for rotation capacity, θ_{total} , is:

$$\theta_{total} = g/d_f \quad \text{(Equation 1)}$$

where;

g = gap between the beam flange and the column

d_f = distance from the mid-height of the shear tab to the furthest beam flange, or the largest of d_1 and d_2 (Figure 7)

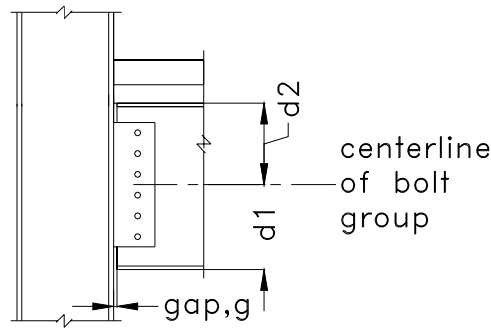


Figure 7. Parameters for Calculating Rotation Capacity

Calculation of Positive Moment Capacity of Shear Tab Connections with Slabs

For guidelines on estimating moment capacities of shear tab connections, the idea of a “bolt element” is introduced to simplify the distribution of forces throughout the shear tab (Figure 8). Experimental observations of failure modes and calculated capacities of bolt elements are combined in the procedures presented. An explanation of failure modes for shear tab connections is given in Liu and Astaneh-Asl (1).

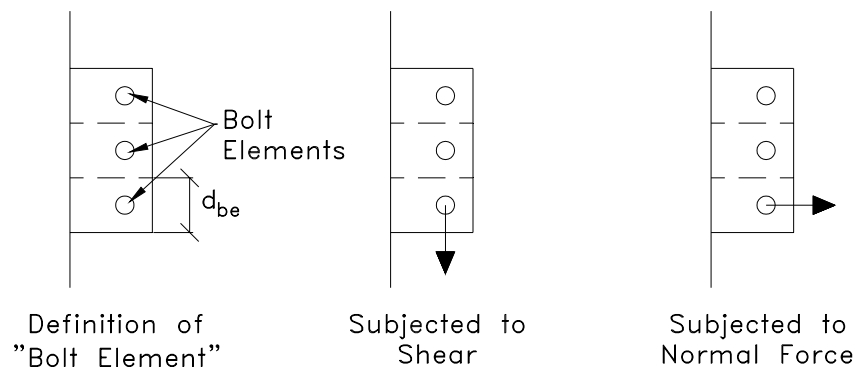


Figure 8. Bolt Elements for Calculating Moment Capacities

For the calculation of positive moment capacity, assumptions related to distribution of forces and effective depth of slab were made based upon experimental results. The assumption for the model is that the top bolt elements carry the shear load, and the bottom bolt elements are responsible for the bending moment. Assumptions on participation of the concrete slab were also determined from experimental results. The effective width of slab, b_{eff} , is assumed to be the width of the column face, flange or web, bearing on the concrete. The effective depth of the slab is also adjusted to account for the orientation of the metal deck and observed damage.

The following procedure was developed for evaluation of positive moment capacity:

1. Using the governing failure mode for a bolt element in shear, determine how many bolt elements are needed to carry the shear load. The top elements are assigned as shear elements.
2. Assume that the remaining bolt elements are used to resist the bending moment. Calculate T , the capacity of these elements in tension. For ductile failure modes, such as yielding and bearing and edge deformation, the force distribution is fully plastic, or rectangular. For brittle

failure modes such as net section or bolt fracture, the force distribution is linear, as shown in Figure 9.

3. Calculate C, the capacity of the concrete slab in compression. For this calculation,

$$C = 0.85(f'_c)(b_{\text{eff}})(a), \quad (\text{Equation 2})$$

where b_{eff} is the width of the column face (i.e., flange or web)

bearing against the concrete, f'_c is the strength of the concrete, and

$a = r$, for the deck parallel to the tab and beam (strong-axis)

$a = 0.6 r$, for the deck perpendicular to the tab and beam (weak-axis)

$r =$ depth of slab above the deck ribs

4. The smaller of C or T governs. By equilibrium, C equals T. Find either the new "a" of concrete or new number of bolt elements. Calculate the moment capacity.

The method shown provides conservative estimates of the moment capacity, with values in the range of 80 - 90% of the experimental values.

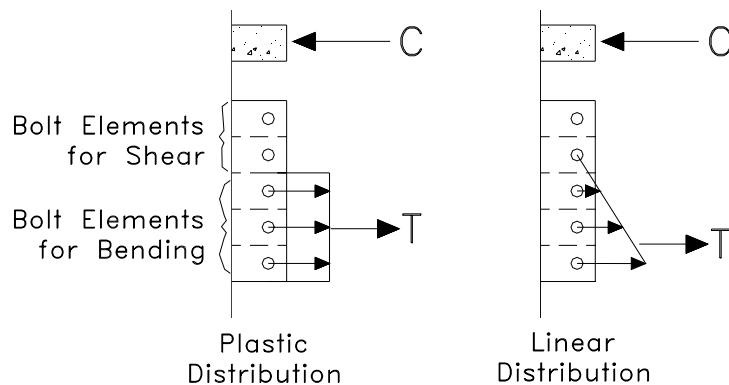


Figure 9. Force Distribution for Estimate of Positive Moment Capacity

Estimate of Negative Moment Capacity of Shear Tab Connections with Slabs

A similar approach was developed for calculating the negative moment capacity of a shear connection with slab. The contribution of the floor slab is conservatively assumed to be negligible. Moment capacity due to binding of the beam flange on the column is also ignored. With these considerations, one may use the following procedure for determining the negative moment capacities of shear tab connections with slabs:

1. Using the governing failure mode for a bolt element in shear, determine how many bolt elements should be allocated to carry the shear load. Assignment of these bolt elements as shear elements begins with the middle bolt(s) and is distributed evenly above and below the centroid of the bolt group.
2. Assume that the remaining bolt elements are used to resist the bending moment, and that the center of rotation of the connection is at the centroid of the bolt group. Use the appropriate force distribution to calculate C, the compression component, which is then equal to T, the tensile component.
3. Given the force distribution, calculate the moment arm and moment capacity.

The predicted capacities are approximately 95% of the observed experimental values for the bare-steel moment capacity.

Initial Stiffness of Shear Tab Connections with Slabs

Guidelines for estimating initial stiffness, $K_{initial}$, of typical shear tab connections with slabs were also established. Since slip was typically the first observed mechanism, the estimates are based upon a moment and rotation at which the connection is considered to have slipped, or M_{slip} and θ_{slip} . θ_{slip} is 0.0042 radians, based on slip rotations of all shear tab connections tested.

Calculations for M_{slip} are based upon the assumption of a plastic distribution of friction forces in the shear tab. For the calculation of friction forces, minimum bolt tension and the static friction coefficient as specified in AISC-LRFD Specifications (AISC (4)), are used. The shear tab is assumed to act entirely in tension through friction, and to be equilibrated by the slab in compression (Figure 10). Since, for typical shear tabs, the resulting effective depth of the slab is very small, the compression force is conservatively assumed to be acting at the very top of the concrete slab. The resulting values of M_{slip}^* tend to overestimate the experimental values for the specimens with slab. However, comparisons of the estimated values and the experimental values show that the application of a simple γ factor of 0.67 results in very reasonable estimates of M_{slip} . The equation for M_{slip} is :

$$M_{slip} = \gamma \times M_{slip}^* \quad \text{(Equation 3)}$$

The initial stiffness, $K_{initial}$, of the connection is implicit in the establishment of M_{slip} and θ_{slip} , and is simply M_{slip} divided by θ_{slip} .

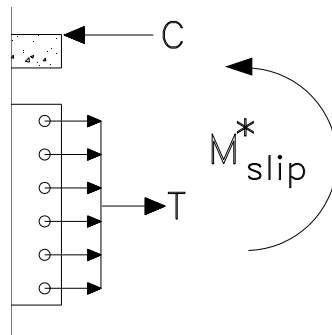


Figure 10. Force Distribution for Estimate of M_{slip}^*

Moment-Rotation Model of Shear Tab Connection with Slab

More parameters are required to complete the description of the moment-rotation behavior, as shown in Figure 11. These parameters are: θ_{max}^+ , θ_{max}^- , θ_{drop} and M_{drop} . The values provided for these rotation parameters were based on a compilation and averaging of backbone curves of moment-rotation for tested shear tab connections. Note that for θ_{ult}^+ and θ_{ult}^- , the equation for θ_{total} (Equation 1) may either be modified to account for positive and negative bending, respectively, or θ_{total} may be conservatively used for both. For more information on cyclic

behavior and modeling of shear tab connections, the reader is referred to Liu and Astaneh-Asl (1).

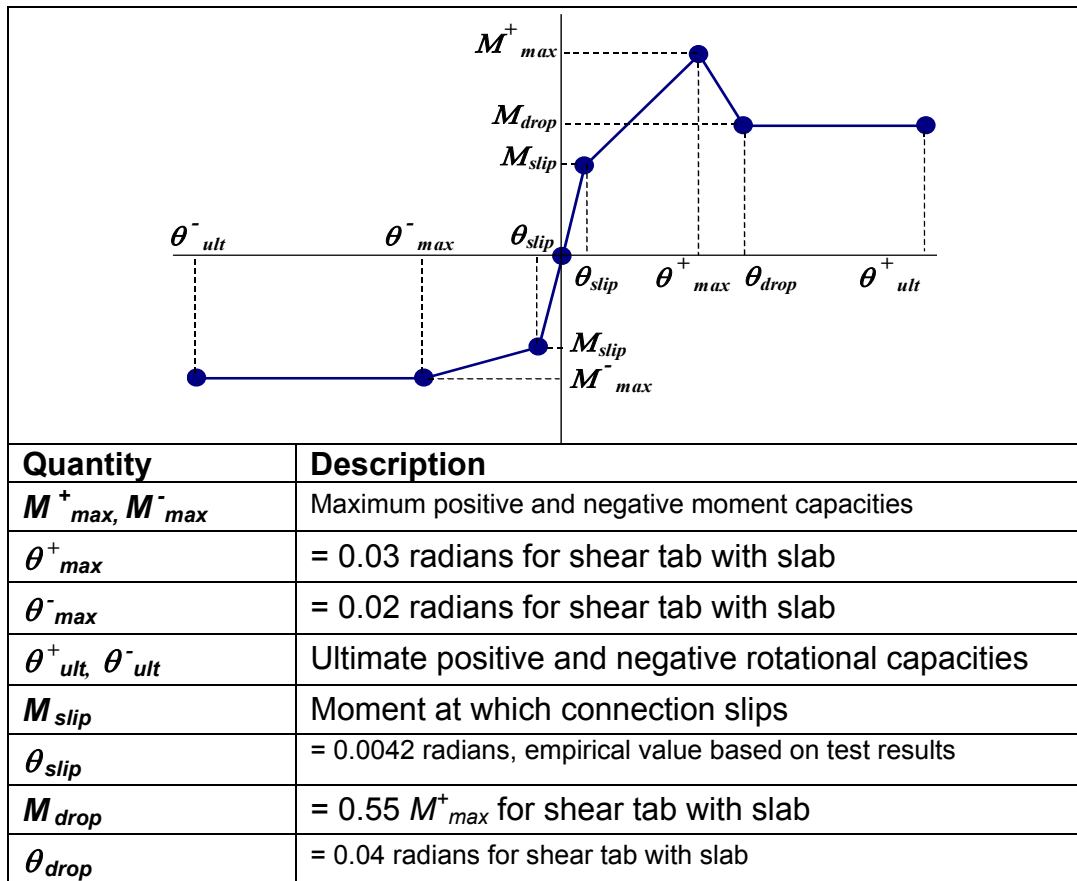


Figure 11. Moment-Rotation Model for Shear Tab Connection with Slab

CONCLUSIONS AND FUTURE WORK

Through an experimental investigation, simple connections with slabs were shown to behave as partially restrained connections. They were also shown to exhibit ductile behavior, reaching large drift rotations without loss of gravity loads. Trends in cyclic behavior formed the basis of models of moment-rotation response of typical shear tab connections with slabs. Continuing and future work includes use of these results and models to establish guidelines regarding the contribution of simple connections to the lateral resistance of steel structures.

ACKNOWLEDGEMENTS

The sponsor for this project was the Federal Emergency Management Agency (FEMA), through the SAC Joint Venture. Thanks are due to the SAC technical advisory panel on connections. In particular, the input by Professor Stephen A. Mahin, James O. Malley, Professor Charles W. Roeder, Dr. Peter Clark, C. Mark Saunders and Ronald O. Hamburger is sincerely appreciated. Thanks are also due to the American Institute of Steel Construction (AISC) and the Herrick Corporation. The steel was donated by Nucor-Yamato Steel. Verco Manufacturing donated the metal decking. Garcias Metal Specialties donated some labor for installation of the deck. John

Wolfe of Steven Tipping and Associates and Ted Winneberger of W & W Steel Company provided some typical details for shear tab and stiffened seat connections.

REFERENCES

- (1) Liu, J. and Astaneh-Asl, A., 2000, "Cyclic Testing of Simple Connections, Including Slab Effects; Final Report," *Report No. UCB/CEE-STEEL-00/01*, Dept. of Civil and Environmental Engineering, University of California, Berkeley.
- (2) SAC Joint Venture, 1997, "Protocol for Fabrication, Inspection, Testing and Documentation of Beam-Column Connection Tests and Other Experimental Specimens", *Report No. SAC/BD-97-02*, SAC Joint Venture, Sacramento, CA
- (3) Liu, J. and Astaneh-Asl, A., 2000, "Cyclic Behavior of Steel Shear Connections with Floor Slab," *Proceedings, 6th International Conference of the Association for International Cooperation and Research in Steel-Concrete Composite Structures*, Los Angeles, CA.
- (4) AISC, 1994, *Manual of Steel Construction, Load & Resistance Factor Design, Volume II*, American Institute of Steel Construction, Chicago, 1994, pp. 9-147 through 9-167.

CYCLIC BEHAVIOR OF STEEL AND COMPOSITE BEAM-TO-COLUMN JOINTS

L. Calado^a, L. Simões da Silva^b and R. Simões^b

^a Civil Engineering Department, Instituto Superior Técnico, Lisbon, Portugal

^b Civil Engineering Department, Universidade de Coimbra, Coimbra, Portugal

ABSTRACT

The paper presents the results obtained from experimental research on two types of European joint solutions, namely steel and composite beam-to-column connections. Steel joints were designed in order to investigate the influence of the connection detail (fully welded and top and seat with web angle) and the column size, while the composite ones were designed to analyze the influence of the slab, the internal and external localization of the joint and the type of the column, steel and composite.

INTRODUCTION

The use of steel and composite joints is inherent in every structural steel and composite building, whether it is of one story or one hundred stories. Therefore, the beam-to-column connection, due to its importance to all constructions, is significant both economically and structurally. Saving in connection costs as well as improved connection quality has an impact on buildings of all sizes. Because of the repetitive nature of connections, even minor material or labor savings in one connection are compounded and expanded throughout the entire building. It is important, then, for a design engineer to understand the behavior of the connection, not only from the point of view of the connection as a structural element, but also from the point of view of the connection as a part of the complete structural system.

The collaboration between the Instituto Superior Técnico and the University of Coimbra aims to contribute to find some answers on the cyclic behavior of steel and composite connections through experimental research on different typologies of these connections to ensure that steel and composite structures may behave in a safe way during the occurrence of an earthquake.

An experimental program on different types of steel and composite beam-to-column connections has been carried out on these two institutions. The experimental tests have been performed on specimens representative of frame structure beam-to-column joints close to the ones typical of European design practice. The test program was planned with the aim of assessing the influence of connection detail (fully welded and top and seat with web angle) and column size for steel connections and the influence of the localization of the joint (internal and external) and type of column (steel and composite) for composite connections. The main parameters influencing the cyclic response of these joints are briefly presented.

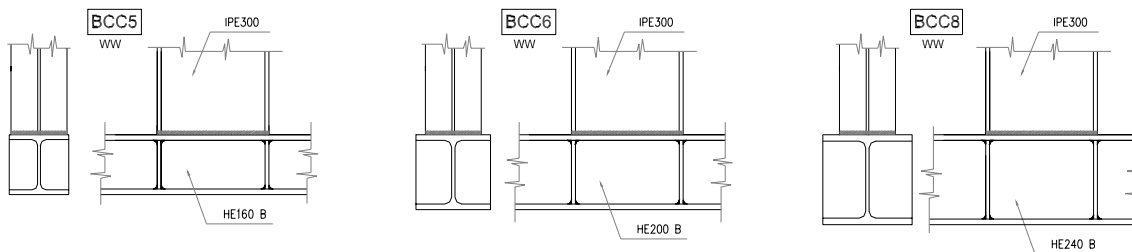
EXPERIMENTAL PROGRAM

Steel joints were tested at the Instituto Superior Técnico, Lisbon while composite ones were tested at the University of Coimbra.

Steel Joints

Two series of full-scale specimens have been designed and tested, Calado and Mele (1), Calado *et al* (2, 3, 4), namely a fully welded series (BCC5, BCC6 and BCC8) and a top and seat with web angle series (BCC9, BCC7 and BCC10). The specimens of the two series were T-shaped beam-column subassemblages, consisting of a 1000 mm long beam and an 1800 mm long column. The material used for the columns, beams, and angles was steel S235 JR. In each series the cross section of the beam was the same (IPE300), while the column cross section has been varied, being respectively HE160B for the BCC5 and BCC9 specimens, HE200B for the BCC6 and BCC7 specimens, and HE240B for the BCC8 and BCC10 specimens. In both series, the continuity of the connection through the column has been ensured by 10 mm thick plate stiffeners, fillet welded to the column web and flanges. In the fully welded specimens, Figure 1, the beam flanges have been connected to the column flange by means of complete joint penetration (CJP) groove welds, while fillet welds have been applied between both sides of the beam web and the column flange.

Figure 1 - Detail of the fully welded connections.



In the BCC9, BCC7 and BCC10 specimens, Figure 2, 120x120x10 angles have been adopted. Two rows of bolts were placed on each leg of the flange angles, while on the legs of the web angles there was only one row of three bolts. The bolts were M16 grade 8.8 preloaded according to the Eurocode 3 provisions (5), i.e. at $F_{P,CD} = 0.7 f_{ub} A_s = 87.9 \text{ kN}$.

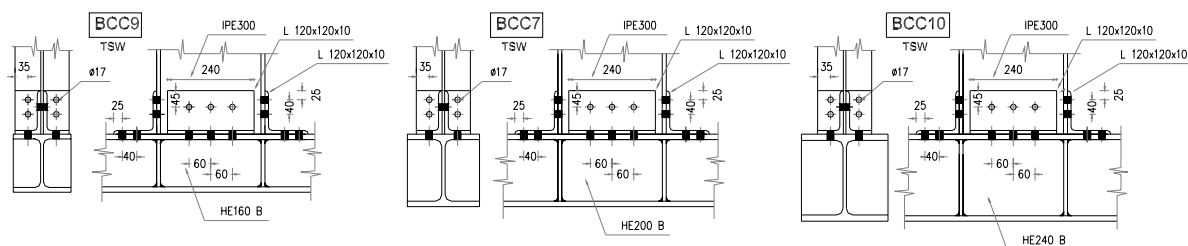


Figure 2 - Detail of the top and seat with web angle connections.

Composite Joints

The test program performed at the University of Coimbra on the cyclic behavior of composite joints included 4 prototypes, Simões (6) and Simões *et al* (7), being 2 in internal nodes and 2 in external ones. The prototypes were defined such that they could reproduce the connections in a common European framed structure, with spans of about 7m, 4m spacing between frames, live loads up to 4 kN/m² and a high energy dissipation capacity and a good fire resistance, Eurocode 3 (5) and Eurocode 4 (8). The steel connection is the same in all prototypes, corresponding to a beam connected to the column by one end plate, welded to the beam and bolted to the column.

In all cases, the beams consisted of an IPE 270, rigidly connected to a reinforced concrete slab (full interaction) by 8 shear block connectors. The slab, 900 mm wide and 120 mm thick, was reinforced with 10 ϕ 12 longitudinal bars and 10 ϕ 8 transversal bars per meter, with 20 mm cover. The steel connection consisted of a 12 mm thick end plate, welded to the beam and bolted to the column flange through 6 M20 bolts (class 8.8). The end plate was flushed at the top and extended at the bottom, in order to achieve similar behavior under positive and negative moments. The steel column was the same in all the tests (HEA 220), being encased by concrete (300 \times 300 mm) in tests E10 and E12, with longitudinal reinforcement of 4 ϕ 12, with one bar in each corner of the section and stirrups consisting of ϕ 6 bars 0.08 m apart. The following materials were chosen: S235 JR in the steel components, steel class 8.8 in the bolts, steel A400 NR in the reinforcing bars.

Two tests were also performed in internal nodes, test E11 corresponding to the prototype arrangement between composite beams and a steel column, and test E12 between composite beams and a composite column. General details of composite joints are presented in Figure 3.

Loading Histories

For the steel specimens the experimental program consisted of cyclic tests with constant and step-wise increasing amplitude displacement histories. This test type has been carried out according to the basic loading history recommended in ECCS (9). For internal and external composite specimens cyclic loading was applied only according to the methodology proposed by the ECCS.

Testing Apparatus

The test set-up available at the Instituto Superior Técnico, mainly consists of a foundation, a supporting girder, a reaction r.c. wall, a power jackscrew and a lateral frame, Figure 4. The power jackscrew (capacity 1000 kN, stroke \pm 200mm) is attached to a specific frame, pre-stressed against the reaction wall and designed to accommodate the screw backward movement. The specimen is connected to the supporting girder through two steel elements. The supporting girder is fastened to the reaction wall and to the foundation by means of pre-stressed bars.

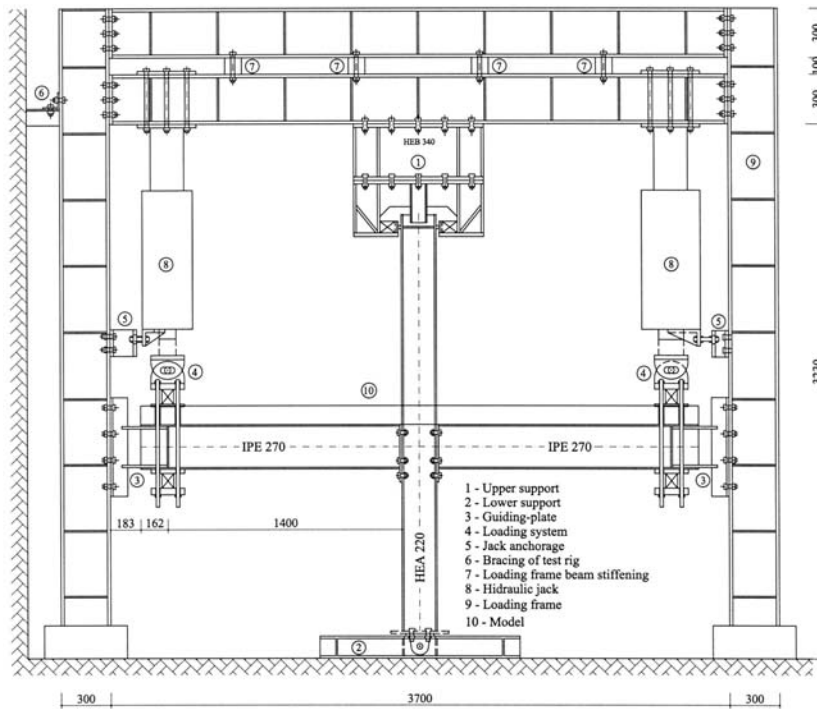


Figure 5 – Test set-up used for composite joints and available at University of Coimbra.

The tests on composite connections were performed at the University of Coimbra, and the test set-up used consists of a foundation, a supporting frame and two dynamic actuators with a capacity of 200 kN and 600 kN, and maximum displacement of 20 cm and 10 cm, which allow experimental tests on internal and external solutions, Figure 5. The composite specimens are connected to the supporting frame and fastened to the foundation.

Instrumentation

An automatic testing technique was developed in both laboratories to allow computerized control of the jackscrew and the dynamic actuators, of the displacement and of all the transducers used to monitor the specimens during the testing process. Specimens have been instrumented with electrical displacement transducers (LVDTs), which recorded the displacement histories at several points in order to obtain a careful documentation of the various phenomena occurring during the tests.

EXPERIMENTAL RESULTS

In the following only the moment rotation hysteresis loops obtained in the increasing amplitude tests are provided.

Steel Joints

A great regularity and stability of the hysteresis loops up to failure, with no deterioration of stiffness and strength properties characterize the cyclic behavior of welded joints, Figure 6. In the very last cycle specimens have collapsed with a sudden and sharp reduction of strength, due to fracture initiated in the beam flange and propagated also in the web.

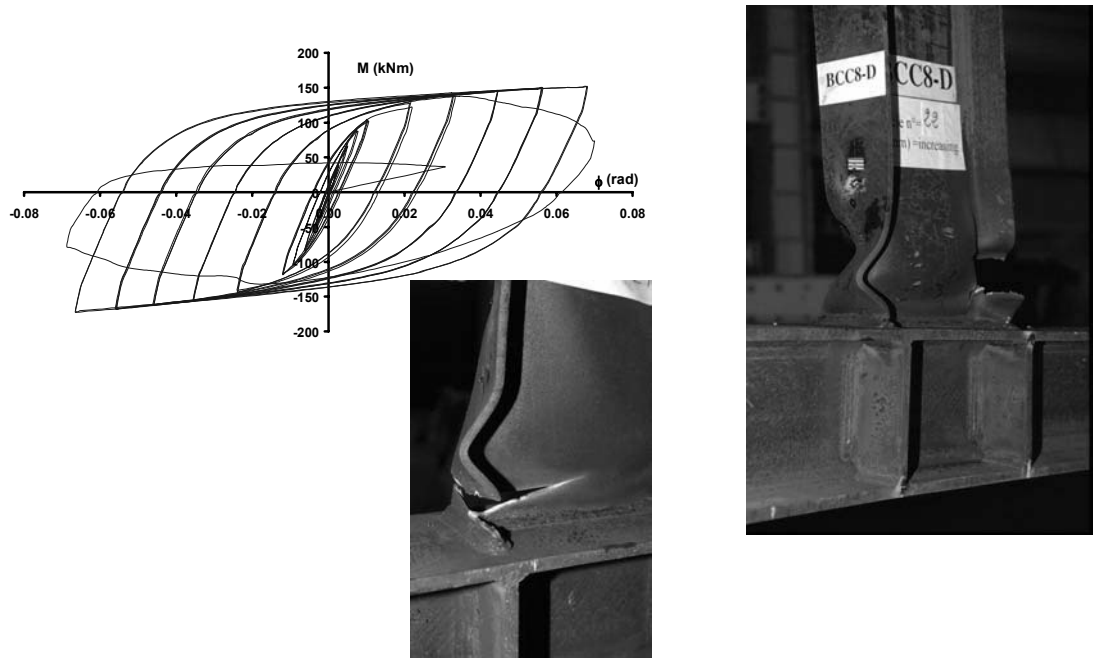


Figure 6 – Hysteresis loops and failure mode of a welded joint.

Significant distortion of the joint panel zone has been observed during the tests, though no remarkable plastic deformation occurred in the beam. The increasing of the size of the column specimens showed a gradual reduction of the peak moment starting from the second cycle, where the maximum value of the applied moment was usually registered. This deterioration of the flexural strength of the connection was related to occurrence and spreading of local buckling in the beam flanges and web. A well-defined plastic hinge in the beam has formed in all the tested specimens. In the specimens with large column size the panel zone deformation has not been remarkable, and the plastic deformation took place mainly in the beam.

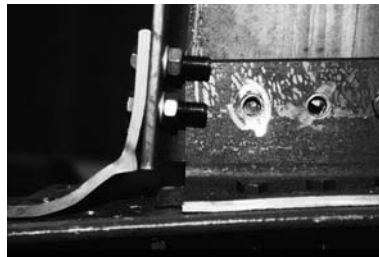
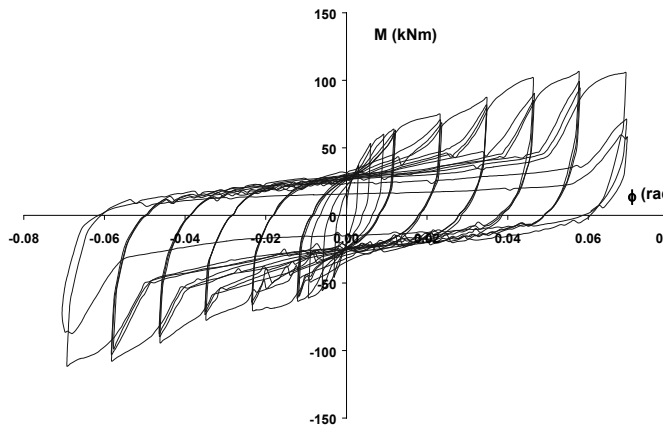


Figure 7 – Hysteresis loops and failure mode of a top and seat with web angle connections.

The cyclic behavior of the top and seat with web angle connections was characterized by bolt slippage and yielding and spreading of plastic deformation in the top and bottom angles, cyclically subjected to tension. Plastic ovalization of the bolt holes has also been observed mainly in the leg of the angle adjacent to column flange. The experimental curves, typical of this type of connection, showed pinching hysteresis loops, with a large slip plateau and subsequent sudden stiffening, Figure 7. At large applied displacements, which impose large rotations to the connection, the contact of the compression angle and the beam web to the column flange (gap closure) gave rise to sudden stiffening of the connection, which is evident in the experimental curves.

No significant rotation of the column and distortion of the panel zone have been observed throughout the experimental tests carried out on these specimens. In all tests carried out on these specimens, the collapse of the connection occurred due to fracture in the leg angle located on the beam flange, immediately after the fillet. Negligible scatters were observed in the moment capacity of the three connection series, as it was expected, since the inelastic behavior of the connection was governed by the angle.

Composite Joints

Two tests were performed in internal nodes, test E11 corresponding to a steel column, illustrated in Figure 8, and test E12 corresponding to a composite column and shown in Figure 9.

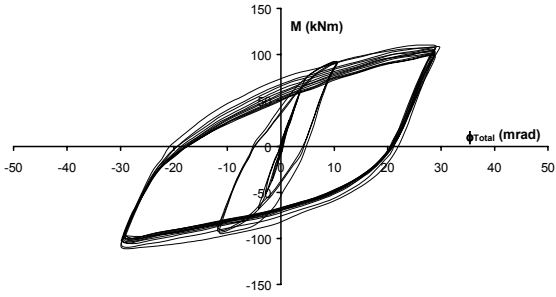


Figure 8 - Hysteresis loops and failure mode of an internal node with a steel column.

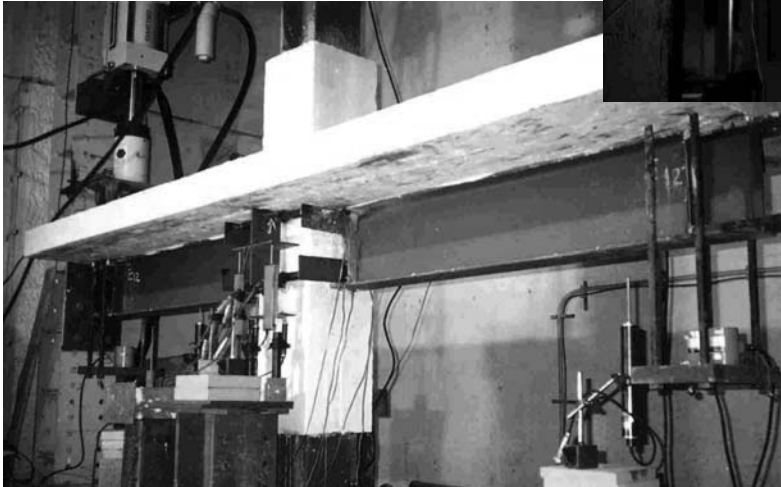
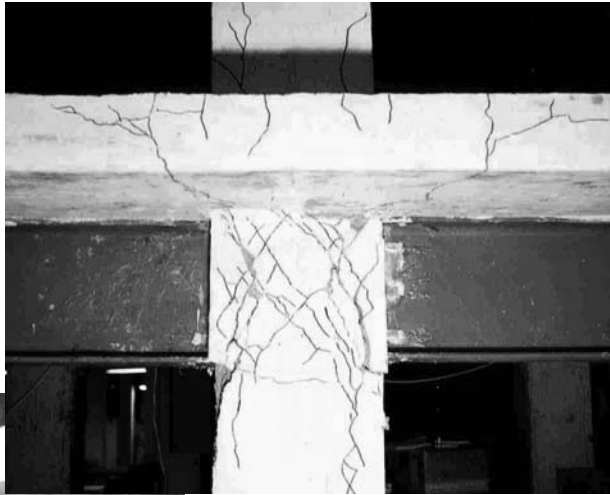
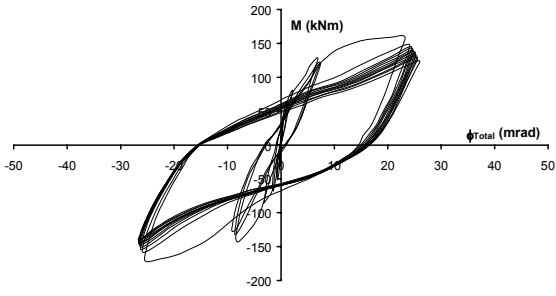


Figure 9 - Hysteresis loops and failure mode of an internal node with a composite column.

These joints presented high ductility with similar response for hogging and sagging moment. Because the maximum amplitude was not very high, the strength degradation was low. Based on the experimental results it was possible to conclude that after the cracking of the concrete in the web of the composite column the cyclic behavior of the specimen E12 (composite column) was similar to that of the E11 (steel column). This fact allows to say that the confinement of the concrete was not very efficient, although it was very competent in the monotonic tests performed in this type of joints.

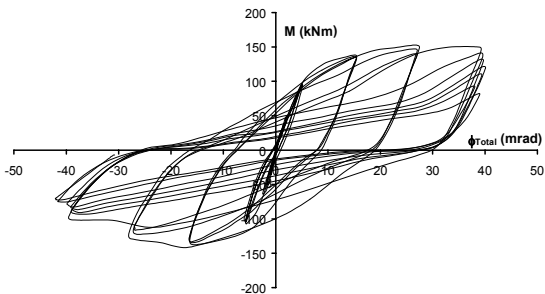


Figure 10 - Hysteresis loops and failure mode of an external node with a steel column.

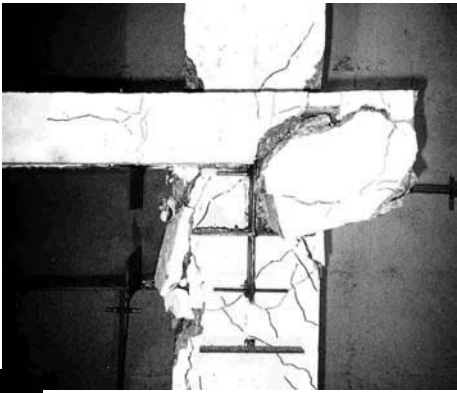
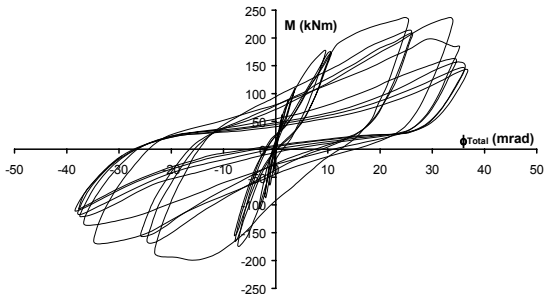


Figure 11 - Hysteresis loops and failure mode of an external node with a composite column.

Concerning external nodes, E9 with steel column (Figure 10), and E10 with composite column (Figure 11), the experimental curves exhibited some pinched hysteresis loops, with a slip plateau and subsequent strength degradation, which was unsymmetrical due to the unsymmetrical resistance of the connection. The strength degradation was mainly due to the deformation of the shear connectors and consequent slip between the slab and the steel beam.

As in external nodes, the ductility remained high except for test E10 under negative hogging moment, and the influence of the type of column, steel vs composite, occurred in the first cycles when the concrete was not cracked. After the cracking of the concrete the cyclic behavior of both connections, E9 and E10, was similar.

CONCLUSIONS

In this paper the major aspects governing the cyclic behavior of some European solutions for steel and composite joint have been evidenced against experimental results. It has been shown that for welded steel joints the behavior of the connection is strongly affected by the panel zone, which is directly related to the column size. On the contrary, for top and seat with web angle steel connections the panel zone does not affect the behavior of the joint, which instead is mainly, related to the tension angle geometry and strength properties. Concerning composite joints, the experimental tests performed have evidenced that the influence of the type of the column, steel or composite occurred in the first cycles when the concrete is not cracked. After that phase the behavior of the joints was similar. On the contrary, the localization of the joint, internal or external, has influence on the cyclic behavior of the connection. External joints have exhibited some pinched hysteresis loops while for internal nodes the cyclic behavior was more regular and stable.

ACKNOWLEDGMENT

Financial support from “Ministério da Ciência e Tecnologia” - PRAXIS XXI research project “Dynamic Behavior of Steel-Concrete Composite Structures” and the European research project INCO-COPERNICUS Joint Research Project “Reliability of Moment Resistant Connections of Steel Building Frames in Seismic Areas” (RECOs) is gratefully acknowledged.

REFERENCES

- (1) Calado, L. and Mele, E., 2000. "Experimental Behavior of Steel Beam-to-Column Joints: Fully Welded vs Bolted Connections". *Proc. 12th World Conference on Earthquake Engineering*, Auckland, New Zealand, January-February, paper No.2570/6/A
- (2) Calado, L., Bernuzzi, C. and Castiglioni, C. A., 1998, “Structural Steel Components under Low-Cycle Fatigue: Design Assisted by Testing”, *Structural Engineers World Congress*, SEWC, San Francisco.
- (3) Calado, L., De Matteis, G., Landolfo, R. and Mazzolani, F.M., 1999, “Cyclic Behavior of Steel Beam-to-Column Connections: Interpretation of Experimental Results”, *SDSS'99 Stability and Ductility of Steel Structures, Proc. 6th International Colloquium*, Timisoara (Romania), (ed. by D. Dubina and M. Ivanyi), Elsevier, 211-220.

- (4) Calado, L., Mele, E., and De Luca, A. 1999, "Experimental Investigation on the Cyclic Behavior of Welded Beam-to-Column Connections". *Proc. 2nd European Conference on Steel Structures, EUROSTEEL '99*, Praha, Czech Republic, Paper No.215.
- (5) Eurocode 3, ENV 1993-1-1, 1992, "Design of Steel Structures", CEN, European Committee for Standardization, Ref. No. ENV 1993-1-1: Brussels, Belgium.
- (6) Simões, R. A. D., 2000, "Behavior of Beam-to-Column Composite Joints under Static and Cyclic Loading", (in Portuguese), *Ph.D. Thesis*, Civil Engineering Department, University of Coimbra, Portugal.
- (7) Simões, R. A. D., Simões da Silva, L. A. P., and Cruz, P. J. S., 1999, "Experimental Models of End-Plate Beam-to-Column Composite Connections", *Proc. 2nd European Conference on Steel Structures, EUROSTEEL '99*, Praha, Czech Republic, 625-629.
- (8) Eurocode 4, ENV 1994-1-1, 1996, "Proposed Annex J for EN 1994-1-1, Composite Joints in Building Frames", CEN, European Committee for Standardization, Draft for meeting of CEN/TC 250/SC 4, Paper AN/57, Brussels, Belgium.
- (9) ECCS, 1986, "Seismic Design. Recommended Testing Procedure for Assessing the Behavior of Structural Steel Elements under Cyclic Loads", Tech. Comm. 1 - Structural Safety and Loadings, *TWG1.3 – Rep. No.45*.

CYCLIC TESTS ON BOLTED STEEL DOUBLE-SIDED BEAM-TO-COLUMN JOINTS

D. Dubina *, A. Ciutina **, A. Stratan **

* Prof. PhD, "Politehnica" University of Timisoara, Romania

** PhD student, "Politehnica" University of Timisoara, Romania

Abstract

The paper presents the main outcomes of experimental tests performed at the "Politehnica" University of Timisoara, on the purpose to evaluate performance of beam-to-column extended end plate connections. The experimental program consisted of monotonic and cyclic tests on double sided beam-to-column joints, loading being applied both symmetrically and anti-symmetrically. At the same time, detailed studies have been carried out on the fracture of beam to end plate welds.

Introduction

Steel moment-resisting frames (MRF) have been traditionally considered as a suitable structural system for low and moderate height buildings in seismic areas, due to their inherent local and global ductility, as well as due to large and clear spans they provide. The global performance of steel MRF in seismic areas is strongly influenced by properties of beam-to-column joints (resistance, rigidity and plastic rotation capacity). Traditionally, beam-to-column joints were required to be of rigid and full strength type. However, there can be noted a renewed interest in bolted connections for seismic applications, which are usually of semirigid and partial resistant type (1). At the same time, while the building industry in United States and Japan adopted site welded beam-to-column connections as the standard ones, bolted beam-to-column connections are preferred in Europe, due to higher quality of shop welds. Also, relatively weak panel zones allowed by modern seismic codes (2) will result in joints of the semirigid and partial resistant type.

The earthquakes of Northridge (1994) and Hyogoken-Nanbu (1995) revealed a series of undesirable brittle failure modes in welded beam-to-column connections, which undermined the high seismic performance of steel moment-resisting frames. This fact generated concern in the scientific community for the causes of the unexpected poor behaviour of welded beam-to-column moment connections. Extensive laboratory studies have been carried out in order to develop improved connection details and methodologies (3). It has been shown that new design of

earthquake resistant connections should incorporate both weld fracture mitigation measures (use of notch-tough weld metal, improvement in welding practices, use of weld access holes with improved fatigue resistance geometry, etc.) and flange overstress mitigation measures, that usually comprise changes in connection configuration (4).

Most of the new connection typologies are designed so as to shift the plastic hinge away from the column flange by reinforcing the connection with cover plates and vertical ribs, or by weakening the beam flange near the connection (the so called “dog-bone”). On the other hand, bolted connections are considered as an alternative to the welded connections not only for areas of low to moderate seismicity, but also for high seismic zones. Bolted connections have provided very good performance historically, and their distributed characteristics lead to redundant and tough structural systems, which are the key for a good seismic performance, Leon (1). Extended end plate connections are traditionally popular in Europe. Even if this type of connection does not eliminate completely the welding, as do tee-stub or angle cleat connections, it relies on higher quality of shop welding.

Experimental Program

The specimens considered in this study are part of two larger experimental programs (X and BX series) that comprised different connection typologies. Only bolted joints with extended end plate connections have been retained here. The structural members are standard hot rolled profiles in the case of X series (5), and built-up sections in the case of BX series (6). Both series of joints have been tested both under symmetrical loading (Figure 1a), and anti-symmetrical loading (Figure 1b).

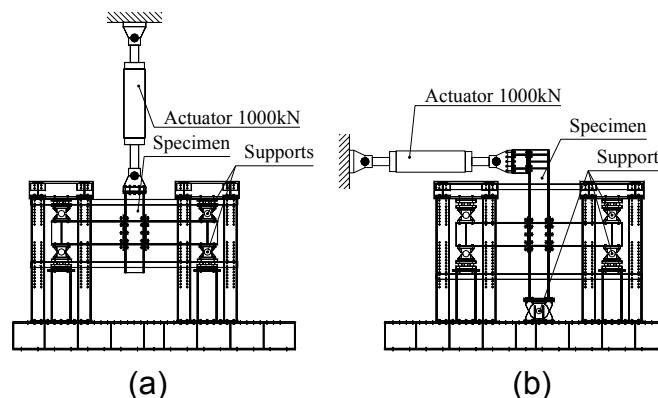


Figure 1. Testing set-up for symmetrical loading (a) and for anti-symmetrical loading (b).

X series. The joints of the X series are realised by means of an extended end plate (EP), representing a typical European connection. Connected members are standard hot-rolled profiles, connected about the strong axis (see Fig. 2a). The extended end plate connections have been designed as semirigid and partial resistant (according to EC3 - 7) for both symmetrical and anti-symmetrical joints, the weakest component being the end plate in bending.

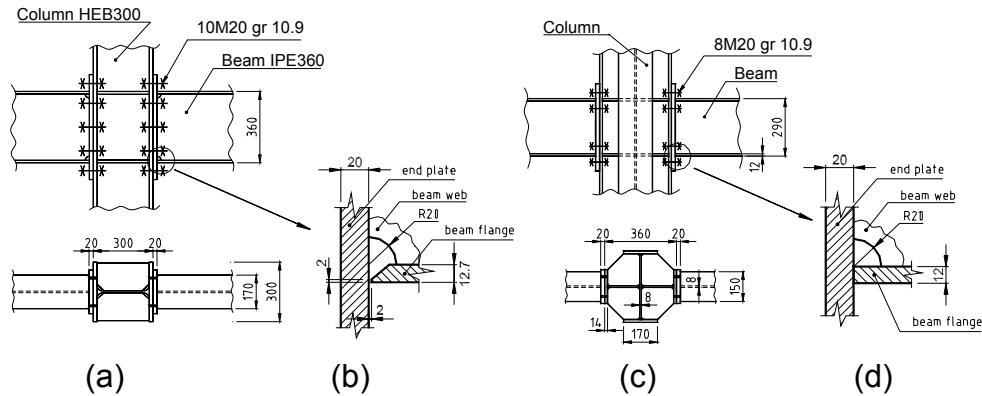


Figure 2. Connection configurations for X series (a, b) and BX series (c, d)

The welds of the beam flanges to the end plate are of full-penetration type (see Fig. 2b), while the beam web is welded with fillet welds. A total of four joints have been tested, two under symmetrical loading (XS-EP), and two under anti-symmetrical loading (XU-EP).

Two specimens of each joint type have been tested, following the simplified ECCS procedure (8) (no monotonically loaded specimen). Progressively increasing the load amplitude, the conventional yielding displacement e_y and the corresponding force F_y are determined, as the intersection between the initial stiffness line and the tangent to the F - e curve having a slope of 10% of the initial stiffness. Then, groups of three cycles at even multipliers of the yield displacement ($\pm 2e_y$, $\pm 4e_y$, $\pm 6e_y$, etc.) are applied, until the conventional failure criterion is attained. The failure of the specimen was considered when the force applied to the joint fell below 50% of the maximum load applied during the loading history. The load was applied quasi-statically, in displacement control.

BX series. The joints of the BX series are realised by means of extended end plate connection, the jointed members being of built-up sections. The beam is a usual “I” section, while the column is a “X” section (see Fig. 2c). Generally, this type of cross section is used for space moment resisting frames, due to similar stiffness on both directions and convenient three- and four- way moment connections. The use of X-shaped columns brings important changes in the behaviour of the beam-to-column joints. If transversal stiffeners are used, the effective shear area of the column web is increased due to column flanges parallel to the web. The increase of shear area introduces two effects in the joint behaviour subjected to seismic forces: an increase of connection stiffness, and an increase of the moment capacity. The testing program comprised six specimens: three joints under symmetrical loading (BX-SS), and three joints under anti-symmetrical loading (BX-SU). The bolts have been fully preloaded, except the last joint of each series that has been preloaded at half of the full preload value, in order to consider the influence of bolt preloading rate. Tests were performed in accordance with the ECCS Recommendations (8) complete procedure. The first specimen from each series was tested monotonically, and was used in order to determine the conventional yield displacement e_y . The monotonic test was the only difference between the two series of tests, while the rest of procedure was similar to the one described for the X series.

Materials. Steel characteristics of the main joint components according to mill certificates and conducted tensile tests are presented in **Table 1**. In the case of X series, the yield stress of the tested elements is higher than the specified one, the actual steel grade of beam and column being rather S275. At the same time a relatively low value of the yield stress of the end plate could be noted. For the BX series results of the coupon tests match fairly well to the mill certificates for beam flanges, column flanges and stiffeners, while the yield strength for the end plates, beam and column webs display important differences. Especially in the case of end plates, the steel is rather OL44 grade ($f_y = 270\text{N/mm}^2$, $f_u = 430\text{ N/mm}^2$), which was confirmed by studies on the chemical composition of the end plate material (10).

Table 1. Characteristics of main steel components.

Series	Design grade	Element		Yield stress, f_y [N/mm ²]		Tensile strength, f_u [N/mm ²]	
				Mill	Coupon	Mill	Coupon
X series	S235 $f_y - 235$ $f_u - 360$	Beam IPE360	flange	285.0	329.8	427.0	463.2
			web		348.4		464.0
		Column HEB300	flange	311.3	313.0	446.0	449.8
			web		341.8		464.4
		End plate		281.0	248.3	424.7	416.0
BX series	OL37 (S235) $f_y - 240$ $f_u - 360$	Beam	flange	303.0	310.1	391.0	470.6
			web	258.0	316.2	400.0	455.7
		Column	flange	258.0	295.2	400.0	444.2
			web	258.0	316.2	400.0	455.7
		End plate		235.0	295.5	421.0	484.3

Behaviour of specimens

The experimental results were monitored in terms of initial stiffness, maximum bending moments, ultimate rotations, the dissipated energy and the type of failure. **Table 2** gives the main results for both series of tested joints. The moment was computed at the column face.

X series

Symmetrically loaded specimens. The end plate was the weakest component, showing visible bending deformations at the level of beam flange in tension at cycles of $\pm 2e_y$. Cycles of $\pm 4e_y$ were characterised by cracking of the weld between beam bottom flange and end plate (initiated in the root of the weld) and local buckling of the upper beam flange. In the first cycle of $\pm 6e_y$ complete rupture of the bottom beam flange to end plate weld occurred, the crack propagating into the base metal (end plate on one side and beam flange on the other side). After the complete rupture of the beam bottom flange weld, beam web start cracking, near the weld to the column flange. In the case of XS-EP2 specimen one of the bolts from the second bolt row (at the bottom beam flange) failed in tension, leading to large deformations of the end plate at the bottom beam flange (see a). Due to loosening of bolts, a degradation of the joint stiffness occurred for the cycles of $\pm 4e_y - \pm 8e_y$.

Within the cycles of the same amplitude of $\pm 4e_y$ and $\pm 6e_y$ could be observed a degradation of the dissipated energy, especially for the $\pm 6e_y$ cycles.

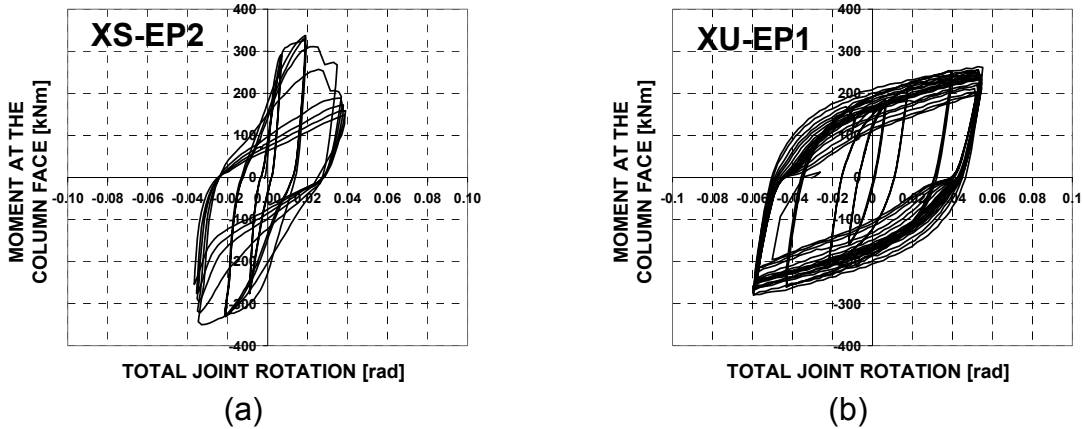


Figure 3. Moment-Rotation curves for X series specimens.

Anti-symmetrically loaded specimens. The first signs of inelastic deformations were observed in the panel zone, where paint started to blister at the $\pm e_y$ cycles. Plastic deformations in the panel zone increased progressively with the number of cycles. Deformations of end plate were observed starting with cycles of $\pm 2e_y$, a gap being formed between the end plate and column flange in the tension zone. First cracks in the welds between the beam bottom flange and end plate appeared at the $\pm 6e_y$, respectively $\pm 4e_y$ for the XU-EP1 and XU-EP2 specimens. Limited buckling of the beam flanges was also observed. Deformation of the end plate was also given by loosening of bolts, which decreased much the stiffness of the connection. Cracking of welds appeared at the top flange only at $\pm 8e_y$ displacement levels. After a number of plastic excursions at $\pm 8e_y$, complete rupture of the extended part of the end plate occurred. Starting from this point, the extended end plate transformed practically into a flush end plate (see Figure 4b).

Panel zone showed stable hysteresis loops over the entire loading history, with an important strain hardening. It was the main source of ductility and resistance up to the rupture of the end plate. The inelastic demand on the panel zone started to decrease at this point, leading to its “relaxation”. On the other hand, extended end plate connection showed a continuous degradation of both stiffness and moment over the loading history.

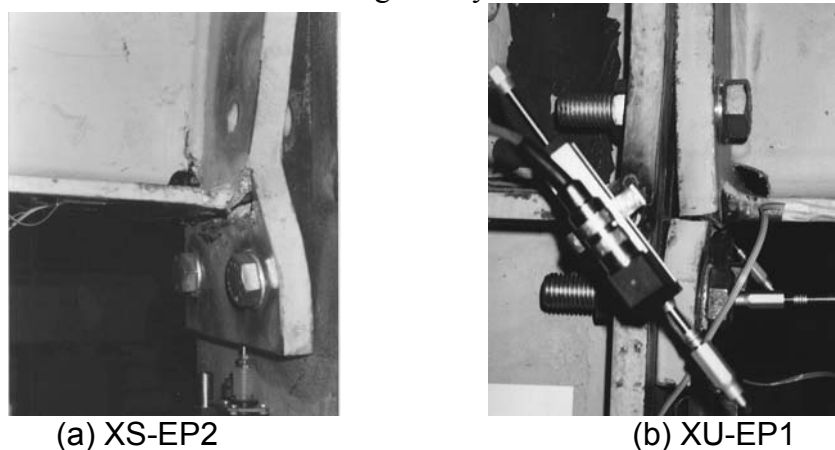


Figure 4. Cracking of the bottom flange and end plate (a), and rupture of the end plate (b).

In the case of XU-EP2 specimen, cracking of the beam flange in the Heat Affected Zone (HAZ), at the corner of the weld access hole occurred. Specimen failed by complete fracture of the beam web and top flange at the right connection and rupture of two bolts below the tensioned flange at left connection. An important drop in moment capacity accompanied it.

The dissipated energy is quite constant in the groups of three cycles up to $\pm 6e_y$, it begins to degrade when displacement levels of $\pm 8e_y$ are reached, mainly due to rupture of the extended end plate.

BX series

Symmetrically loaded specimens. The BX-SS-M specimen was loaded monotonically. Visible deformations of the end plate are noted starting with displacement levels of $3e_y$ in the tension zone of the beam. Significant bending of the column flanges is observed at $6-8e_y$. At approximately $9.5e_y$ (0.03 rad) a bolt from the first bolt row failed (see **Figure 5b**), leading to a sudden decrease of the moment. Loading was continued up to approx. $12e_y$ (0.043 rad), when a general loss of stability occurred due to insufficient lateral restraining.

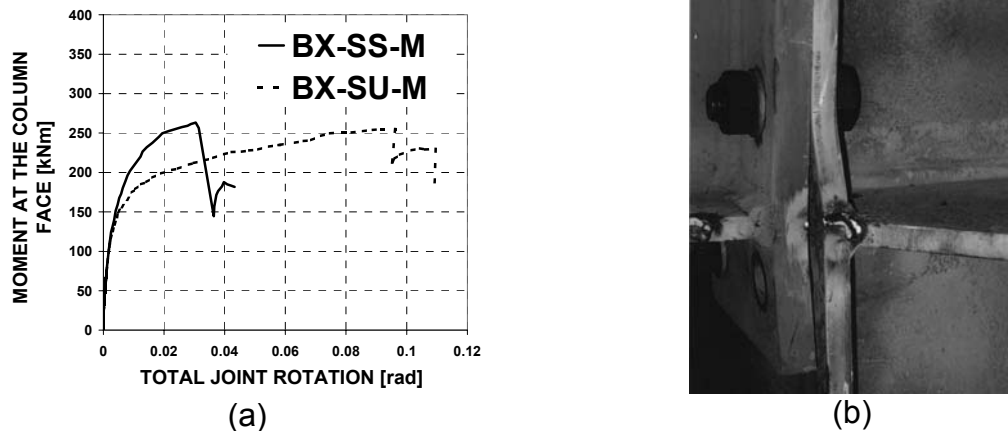


Figure 5. Moment - rotation relationships for the monotonic specimens of the BX series (a), and a bolt failure in the case of the BX-SS-M specimen (b)

In the case of cyclically tested joints, BX-SS-C1 and BX-SS-C2, the behaviour was initially similar to that of the BX-SS-M specimen, i.e. during the cycles of $4-6e_y$ plastic deformations of the end plate and column flange were observed. During the first positive cycle of $8e_y$ (BX-SS-C1 specimen) and 3rd cycle of $6e_y$ (BX-SS-C2 specimen, see **Figure 7a**) a sudden brittle failure of the lower left beam flange to end plate weld occurred, on the entire flange width. This was followed by cracking of the beam web to end plate weld, and by failure of the superior flange weld during the load reversal (BX-SS-C2 specimen). A rapid decrease in moment occurred, see **Figure 6a**, leading to the attainment of the failure criterion. Generally, the maximum rotations obtained for the cyclically loaded joints were dramatically reduced as compared to the monotonic test, due to premature weld failure (see **Table 2**).

Anti-symmetrically loaded specimens. Beginning with deformation levels of $1-2e_y$, shear of the panel zone was observed. At $4e_y$ bending of the end plate and column flanges become visible in the tensioned zone. In the compression zone, the beam flange buckled plastically at $5e_y$. These deformations continued to increase up to approx. $10.5e_y$ (0.096 rad), when a bolt from the extended part of the end plate failed, with a sudden decrease in the moment (see **Figure 5a**).

Shortly after, at approx. $11.5e_y$ (0.11 rad), the second bolt from the same row failed, leading to a further drop of moment.

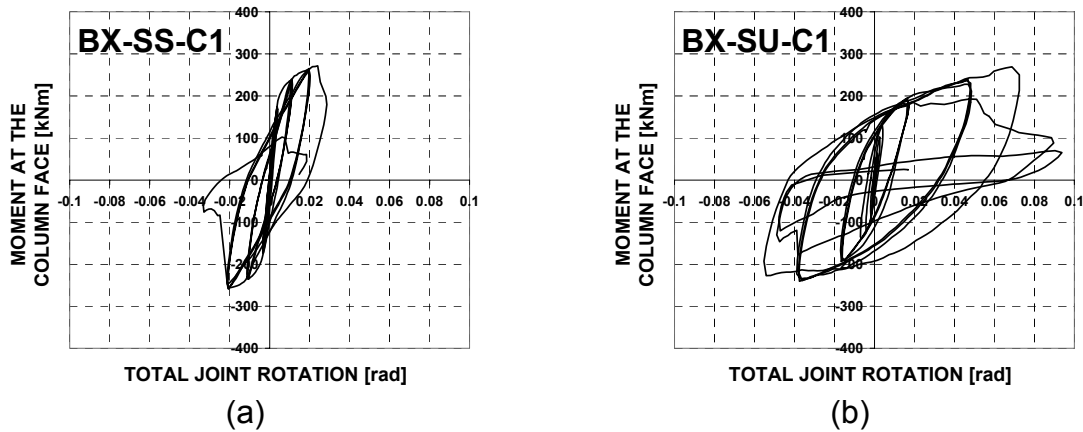


Figure 6. Moment - rotation relationships for the BX series

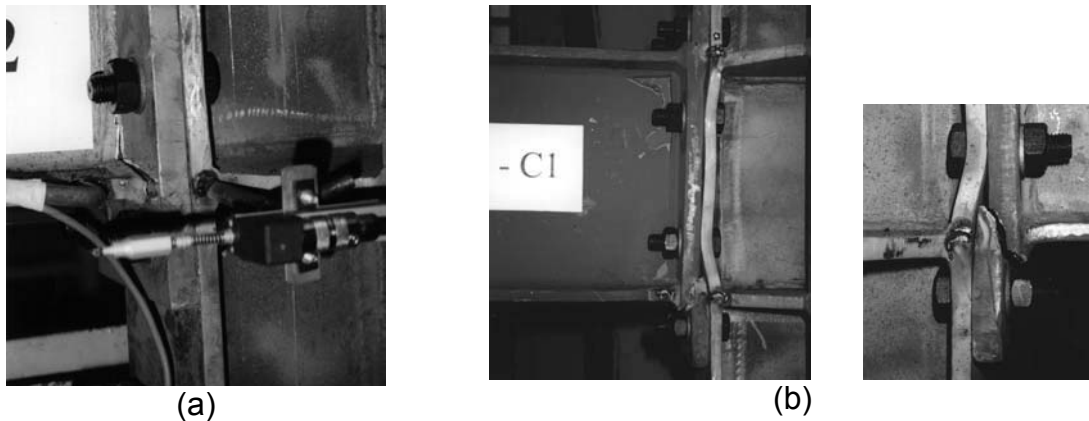


Figure 7. BX-SS-C2: Weld failure (a); BX-SU-C1: End plate failure (b)

Cyclically loaded anti-symmetrical specimens (BX-SU-C) started with plastic deformations of the end plate, column flanges, and shear of the panel zone, visible at $4e_y$ cycles. During the 1st cycle of $6e_y$, a crack in the lower left beam flange to end plate weld occurred, that propagated into the end plate (BX-SU-C1 specimen). In the next $6e_y$ cycle other two welds cracked, propagating into the end plate. Cracking of the end plate followed two patterns: lamellar tearing at the superior part and through-thickness cracking at the inferior part (see **Figure 7b**). A bolt failed in the 3rd $6e_y$ cycle, in the extended part of the end plate. In the case of the BX-SU-C2 specimen, first cracks initiated in the top right beam flange to end plate welds appeared already in the 3rd $4e_y$ cycle. In the first $6e_y$ cycle a crack formed at the lower weld, leading to lamellar tearing of the end plate. During the second cycle, 5 bolts from the left connection (undamaged) failed successively, 4 from the extended part of the end plate and one from an interior bolt row, leading to a rapid decrease in connection strength.

Influence of type of loading

Loading type (symmetrical or anti-symmetrical) affects significantly the response parameters of beam-to-column joints. The main component that introduces the difference is the panel zone in shear, recognised for its high ductility. The most important consequences on the cyclic behaviour

of beam-to-column joints are the reduced moment capacity and stiffness, and (in general) increased ductility with more stable hysteresis loops in the case of anti-symmetrical loading. For H column cross sections, the maximum resistant moment of anti-symmetrically loaded joints is considerably smaller than the one obtained under symmetrical loading (by 25%), while the joint rotation is much higher (by about 70%). This fact is only partially confirmed by the tests made on X-shaped column cross section joints. Actually, for the anti-symmetrical joints of the BX series the drop in moment capacity is very small (about 5%), while the increase in maximum joint rotation is quite important (more than 150%). Anti-symmetrical loading decreased the stiffness of the joint in average by 20% for X series and by 30% in the case of BX series.

Table 2. Experimental results for tested joints.

Specimen	φ_{\max}^+ [rad]	φ_{\max}^- [rad]	M_{\max}^+ [kNm]	M_{\max}^- [kNm]	$S_{j,ini}$ [kNm/rad]	E_{tot} [kNm rad]
XS-EP1	0.031	0.033	334.2	357.8	69539	76.70
XS-EP2	0.038	0.037	337.9	350.0	44205	120.2
XU-EP1	0.055	0.060	263.7	280.0	44081	661.5
XU-EP2	0.057	0.062	256.3	257.0	49004	924.6
BX-SS-M	0.043	-	263.3	-	48030	9.01
BX-SS-C1	0.028	0.021	271.6	259.1	57760	43.75
BX-SS-C2	0.017	0.018	261.8	259.8	67370	26.28
BX-SU-M	0.106	-	258.4	-	51500	21.02
BX-SU-C1	0.073	0.055	269.4	240.6	32080	145.54
BX-SU-C2	0.039	0.047	240.1	236.6	34180	88.37

The extent to which loading asymmetry influences joint response depends on the relative strength of the panel zone with respect to the connection strength. For X-shaped column cross-sections, if continuity plates are used, the column flanges parallel to the web act as a web stiffener. Still, they do not eliminate shear deformations completely, leading to a more ductile joint. Determination of joint characteristics in the case of X-shaped column cross-sections could be performed by the EC3 Annex J (7) methodology, slightly adjusting it to this joint typology (6).

Cyclic loading does not affect significantly the moment capacity of the joint, but it modifies the type of failure, decreasing the joint ductility. The main factor responsible for worse behaviour of beam-to-column joints under cyclic loading is the low-cycle fatigue phenomenon. In the case of BX series, the drop in ductility was about 50% for both symmetrical and anti-symmetrical loading, the moment capacity being practically unaffected.

Weld failure inspections

Two types of beam flange to end plate welds have been used in this study: full penetration welds for the X series (see **Figure 2b**), and fillet welds for the BX series (see **Figure 2d**). Though an exact assessment of influence of welding procedure is not possible since there are important differences between the two series themselves, significant differences could be noted in the behaviour of end plate connections with different welding procedures.

In the case of X series, an essentially different behaviour of the welded connection at the bottom and upper flanges could be noted, due to detailing of the welds. Both upper and bottom flanges of the beam have been welded in the downward position. In this way, the root of the full penetration weld is at the interior side of the upper flange, and at the exterior side of the bottom flange. Due to smaller stresses at the interior side of the beam flange and restraining caused by the beam web, upper beam flange is less prone to crack initiation at the root of the weld. This was confirmed by the experimental evidence, the bottom beam flange to end plate weld being usually the one to crack first. At the upper flange, detailing of the weld access hole is important, cracking of the beam flange at the toe of the weld access hole being observed in several cases. Fillet welds used in the case of BX series showed their inadequacy for cyclically loaded beam-to-column joints. Cyclic loading triggered the failure type of the BX series from bolt failure in the case of monotonic loading to weld cracking induced failure in the case of cyclic loading. Though most of the cracks were initiated in the beam flange to end plate welds or the HAZ, their evolution is quite different at symmetrically and anti-symmetrically loaded joints. This fact is especially evident at the BX series, where weld fracture at the end plate interface occurred under symmetrical loading, as compared to the end plate cracking (through-thickness or lamellar tearing) under anti-symmetrical loading, see and **Figure 7**. Shear deformations of the panel zone could be attributed to this behaviour. The so called local kinking (9) of the end plate and column flange due to shear deformations of the panel zone imposes higher strains at the corners of the joint than under symmetrical loading. These high alternating stresses imposed on the end plate at the exterior limits of the beam, combined with lower stresses on the welds due to smaller overall moment demand under anti-symmetrical loading shifted the formation of cracks from the welds to the end plate.

Due to the fact that generally the beam to end plate fillet welds at the BX series had an unsatisfactory behaviour under cyclic loading, detailed investigations have been performed on samples extracted from the BX-SU-C1 specimen end plate (10). Analysis of the chemical composition of the base material was performed (by spectrographic method), in order to determine the steel grade used in the fabrication of the end plates. It was established that from the point of view of chemical composition, the end plate material suites the OL44, qualities 2-4 steel grade, according to (11). Results of mechanical tests (tensile and Charpy tests) confirm that the steel grade was OL44 quality class 3. It is to be mentioned that the design steel was OL37 quality class 3 steel grade.

Microscopic investigation have shown that generally, there was a lack of fusion of the fillet welds into the base material, especially into the end plate, as shown in Figure 8a and b, this being an important factor in weld failure. Fracture initiated in the HAZ of the beam flange or end plate, propagating into the base material in the latter case (**Figure 8b**).

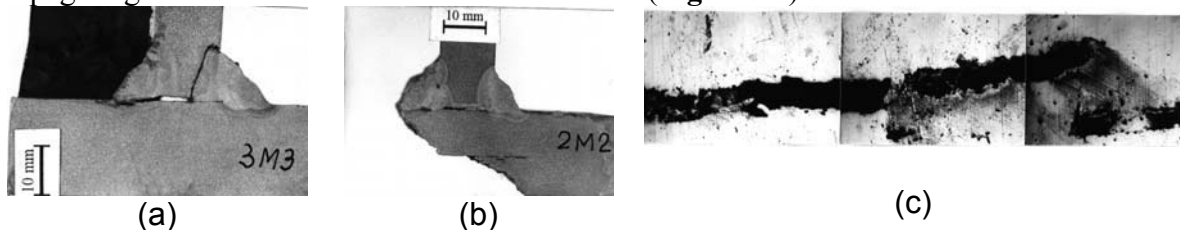


Figure 8. Cracking of the end plate and beam flange HAZ (a), cracking of end plate (b), and non-metallic inclusion in the left end plate of the BX-SU-C1 specimen (c)

The microscopic examination of the base metal showed a reduced degree of purity, due to non-metallic inclusions in the middle of the end plate cross section (**Figure 8c**). Presence of these inclusions diminishes plate characteristics in the through-thickness direction, due to lamellar tearing. Anyway, it seems that lamellar tearing itself was not of outstanding importance, since it evolved only due to weld-induced cracking. In order to improve the behaviour of beam-to-column connections under cyclic loading, it is crucial to realise good quality welds. Therefore, some recommendations have to be taken into account in design and manufacturing process: (a) full penetration welds should be used if load reversals are expected for the connected structural members, (b) notch-tough weld rods, (c) use of base material with guaranteed through-thickness quality, to reduce the tendency to lamellar tearing.

Conclusions

Extended end plate connections are sensible to most of the problems related to beam-to-column joints realised by direct welding of the beam to the column. However, due to shop welding, it is easier to mitigate these problems. Beam flange to end plate welds are of paramount importance for a good seismic behaviour of these joints. Full penetration welds with rewelded root shall be used between the beam flange and end plate. Fillet welds are inadequate at these locations, due to unsatisfactory behaviour under cyclic loading. Detailing of the weld access hole is important in order to avoid supplementary stress concentration at its corner. The preloading rate does not affect significantly the initial stiffness and moment capacity of the joint. However, higher values of ultimate rotations have been observed in the case of fully preloading specimens. Anyway, further research is necessary to confirm this observation.

Loading type (symmetrical or anti-symmetrical) affects significantly the response parameters of beam-to-column joints. The main component that introduces the difference is the panel zone in shear. The most important consequences on the cyclic behaviour of beam-to-column joints are the reduced moment capacity and stiffness and, (in general) increased ductility with more stable hysteresis loops in the case of anti-symmetrical loading. It comes necessary to use an appropriate model for interior (double-sided) beam-to-column joints that would make possible to reflect the different behaviour of this joints under gravitational and earthquake loading. It is important to use a model reflecting the real joint behaviour, as the joint will perform differently under the two loading conditions.

Use of X-shaped columns makes possible a convenient design of three- and four- way connections for space moment resisting frames. Also, it brings important advantages in the joint behaviour under anti-symmetrical loading over usual I or H shaped columns. Column flanges parallel to the considered web lead to a natural stiffening of the column panel zone. The increase in the panel zone shear area reduces significantly the drop in moment capacity for anti-symmetrically loaded joints with respect to symmetrical ones, but reduces in some extent the initial stiffness. Anyway, the stiffened panel zone participates to the plastic mechanism, assuring a significantly increased ductility of anti-symmetrically loaded joints.

Cyclic loading introduces differences between the type of failure. While for monotonic tests the failure was mainly by bolt failure and column flange/ end plate deformations, in the case of cyclic tests, it was by brittle failures induced in the beam flange to end plate welds. Therefore, fillet welds are not recommended in zones with load reversals.

Acknowledgements

Parts of the experimental programme presented herein were carried out at the “Politehnica” University of Timisoara within the European Programme COPERNICUS “RECOs” and the Romanian National Education Ministry / World Bank grant C/16. Support of the European Commission is gratefully acknowledged.

Notation

e_y – conventional yield displacement of a joint

F_y - conventional yield force of a joint

f_y - yield stress

f_u - tensile strength

ϕ_{\max}^+ - experimental maximum positive rotation of a joint

ϕ_{\max}^- - experimental maximum negative rotation of a joint

M_{\max}^+ - experimental positive moment capacity of a joint

M_{\max}^- - experimental negative moment capacity of a joint

$S_{j,\text{ini}}$ – initial stiffness of a joint

E_{tot} – total energy dissipated by a joint

References

1. Leon R. T. (1999). “Developments in the use of partial restraint frames in the United States”. *Control of semi-rigid behaviour of civil engineering structural connections*. COST C1. Liege, 17-19 September 1998, p 95-104.
2. AISC 97 (1997) *Seismic Provisions for Structural Steel Buildings*. American Institute of Steel Construction, Inc. Chicago, Illinois, USA
3. SAC (1997). Interim Guidelines Advisory No. 1. Supplement to FEMA-267 Interim Guidelines: Evaluation, Repair, Modification and Design of Welded Steel Moment Frame Structures. SAC Joint Venture, Report No. SAC-96-03, Sacramento, California, USA.
4. Stojadinovic B., Goel S. C., Lee K-H., Margarian A. G. and Choi J-H. (2000). Parametric Tests on Unreinforced Steel Moment Connections. *Journal of Structural Engrg.*, Vol. 126, No.1, January 2000.
5. Dubina, D. Ciutina, A., Stratan (2000). “Influence of loading asymmetry on the cyclic behaviour of beam-to-column joints”, Proceedings of the Third International Conference *Behaviour of Steel Structures in Seismic Areas*, STESSA’ 2000, 21-24 August 2000, Montreal, Canada.
6. D. Dubina, A. Stratan, A. Ciutina (2000). "Cyclic tests on bolted steel double-sided beam-to-column joints". NATO Advanced Research Workshop. *The Paramount Role of Joints into the Reliable Response of Structures. From the Rigid and Pinned Joints to the Notion of Semi-rigidity*. Ouranoupolis, Greece, 21-23 May 2000.
7. ENV 1993-1-1. (1997) *EUROCODE 3: Part 1.1. Revised Annex J: Joints in Building Frames*. Approved Draft: January 1997; Brussels: CEN, European Committee for Standardisation.
8. ECCS (1985). *Recommended Testing Procedures for Assessing the Behaviour of Structural Elements under Cyclic Loads*, European Convention for Constructional Steelwork, Technical Committee 1, TWG 1.3 – Seismic Design, No.45
9. Krawinkler H. (1995). “Systems Behaviour of Structural Steel Frames Subjected to Earthquake Ground Motion”, *Background Reports: Metallurgy, Fracture Mechanics, Welding, Moment Connections and Frame Systems Behaviour*. Report No. SAC-95-09. SAC Joint Venture, California, USA.
10. T. Moisa, R. Pascu, R. Romanu (2000). "Study on causes of weld fractures in extended end-plate connections under cyclic loads", Report No. 409/1999. Institute of Welding and Testing of Materials (ISIM).
11. STAS 500/2-80 (1980). Structural steels for general purpose. Grades. Ministry of metallurgical industry, Romania.

POST-TENSIONED MOMENT CONNECTIONS FOR SEISMIC RESISTANT STEEL FRAMES

James M. Ricles, Lehigh University, Bethlehem, Pa.
Richard Sause, Lehigh University, Bethlehem, Pa.
Maria M. Garlock, Lehigh University, Bethlehem, Pa.

ABSTRACT

A series of experimental tests were conducted to investigate the behavior of an innovative post-tensioned (PT) top-and-seat-angle wide flange (WF) beam-to-column moment connection for steel moment resisting frames subjected to seismic loading conditions. Nine large-scale specimens were tested. Each specimen represented an interior connection and consisted of two WF beams attached to a column. The parameters investigated in the study include the angle size, angle gage length, beam flange reinforcing plates, connection shim plates, and post-tensioning force. The results of the test program demonstrate that post-tensioned connections possess exceptional cyclic strength and ductility. Energy dissipation occurs in the angles while other structural members remain elastic. The initial elastic stiffness is comparable to that of a welded connection, and following severe inelastic cycles of drift the connection has little permanent deformation.

INTRODUCTION

Structural steel has been widely used in moment resisting frame (MRF) systems for buildings. The connections in steel MRFs are either welded or bolted, with welding becoming common during recent decades. A typical welded moment connection detail consists of a bolted shear tab with full penetration beam flange welds. During the 1994 Northridge earthquake, over 130 steel-framed buildings suffered unexpected connection fractures (1, 2). The cyclic strength and ductility of these connections were diminished as a result of the fractures. Several alternative moment connection details have been proposed since the Northridge earthquake in an attempt to develop ductile response under earthquake loading. These details are intended to avoid weld failure and force inelastic deformation to develop in the beams away from the welds. Consequently, after the design-level earthquake the beams with these connections will have permanent damage caused by yielding and local buckling. This damage can result in a significant residual drift of a MRF.

As an alternative to welded construction the authors developed a post-tensioned (PT) moment connection for use in seismic resistant steel MRFs. There are several advantages of a PT connection. These advantages include: (1) field welding is not required; (2) the connection is made with conventional materials and skills; (3) the connection has an initial stiffness similar to that of a typical welded connection; (4) the connection is self-centering without residual deformation, thus the MRF will not have residual drift after an earthquake if significant residual deformation does not occur at the base of the columns; (5) the beams and columns remain essentially elastic while inelastic deformation of the connection provides energy dissipation; and

(6) the angles are easily replaced. The connection utilizes high strength steel strands that are post-tensioned after bolted top and bottom seat angles are installed (Figure 1). The post-tensioning strands run through the column, and are anchored outside the connection region (Figure 2). Although the top-and-seat angles are easily replaced, experimental studies conducted by the authors show that the angles have a sufficient low-cycle fatigue life to perform well over several earthquake loading events.

This paper presents experimental studies of PT connection subassemblies subjected to cyclic inelastic loading. Nine large-scale specimens were tested. Each specimen represented an interior connection and consisted of two WF beams attached to a column. The parameters investigated in the study include the angle size, angle gage length, beam flange reinforcing plates, connection shim plates, and post-tensioning force. The angle parameters were shown to influence the connection's behavior, therefore, experimental investigations were also carried out on the angles alone to evaluate the effects of angle size and gage length on the PT connection.

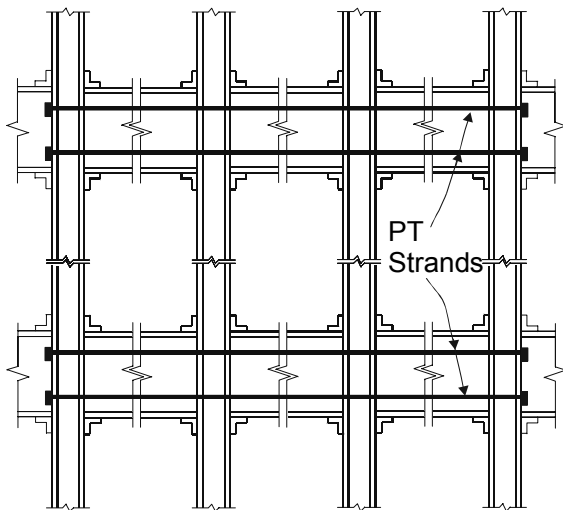


Figure 1. Elevation of a post-tensioned frame.

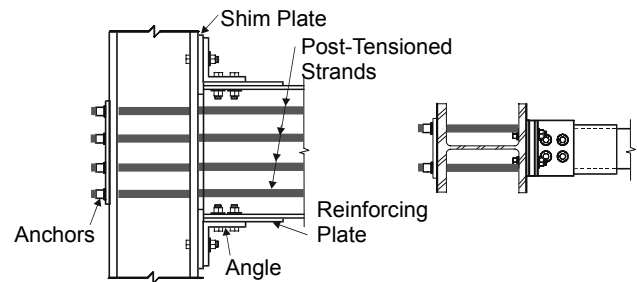


Figure 2. Post-tensioned connection detail at anchor point.

The development of the PT steel connection utilizes research from prior studies of PT precast concrete construction and partially restrained steel connections. For more details on this prior research see Garlock et al. (3) and Ricles et al. (4). The paper by Garlock et al. includes analytical studies performed on PT MRFs and compares the behavior of these PT frames to the behavior of the same frame with conventional welded moment connections. In these analytical studies the drift demand in MRFs with PT connections was found to be less than that in MRFs with fully restrained connections.

POST-TENSIONED CONNECTION

Connection Details

A PT steel MRF connection consists of bolted top and seat angles with post-tensioned high strength strands running parallel to the beam and anchored outside the connection (see Figure 1). The strands compress the beam flanges against the column flanges to resist moment, while the two angles and the friction at the beam and column interface resist shear. The proposed

details are shown in Figure 2 for a connection to an exterior column. The angles' primary purpose is to dissipate energy. However, they also provide redundancy to the force transfer mechanisms for transverse beam shear and moment. The beam flanges are reinforced with reinforcing plates to control beam yielding. Also, shim plates are placed between the column flange and the beam flanges so that only the beam flanges and reinforcing plates are in contact with the column.

Flexural Behavior

The idealized moment-rotation ($M-\theta_r$) behavior and the corresponding load-deflection ($H-\Delta$) behavior of a PT steel connection are shown in Figure 3, where θ_r is the relative rotation between the beam and column. The $M-\theta_r$ behavior of a PT connection is characterized by gap opening and closing at the beam-column interface under cyclic loading (Figure 3 insert). The moment to initiate this separation is called the decompression moment. The connection initially behaves as a welded connection, but following decompression it behaves as a partially restrained connection. The initial stiffness of the connection is the same as that of a welded moment connection when θ_r is equal to zero until the gap opens at decompression (event "a" in Figure 3). The stiffness of the connection after decompression is associated with the stiffness of the angles and the elastic axial stiffness of the post-tensioned strands. With continued loading, the tension angle of the connection yields (event "b"), with full plastic yielding of the tension angles occurring at event "c". The compression angles yield at event "d". Until the load reverses at event "e", the $M-\theta_r$ relationship has a nearly linear response where the connection stiffness is primarily due to the axial stiffness of the post-tensioned strands. Upon unloading, the angles will dissipate energy (between events "e" and "h") until the gap between the beam flange and the column face is closed at event "h" (i.e., when θ_r is equal to zero). A complete reversal in applied moment will result in a similar connection behavior occurring in the opposite direction of loading, as shown in Figure 3 where the $M-\theta_r$ and $H-\Delta$ relationships are symmetric.

As long as the strands remain elastic, and there is no significant beam yielding, the post-tensioning force is preserved and the connection will self-center upon unloading (i.e., θ_r returns to zero rotation upon removal of the connection moment and the structure returns to its pre-earthquake position). The level of the decompression moment, the flexural strength of the angles, and the elastic stiffness of the post-tensioning strands control the strength of the connection. The energy dissipation capacity of the connection is related to the angle flexural strength.

To ensure that the strands remain elastic, strands with lengths equal to one multiple of the beam clear span for each connection that the strands pass through are used. Thus, the deformation due to gap opening results in a small strain over a long strand length. The strands are post-tensioned to a stress level that is sufficiently below the yield stress.

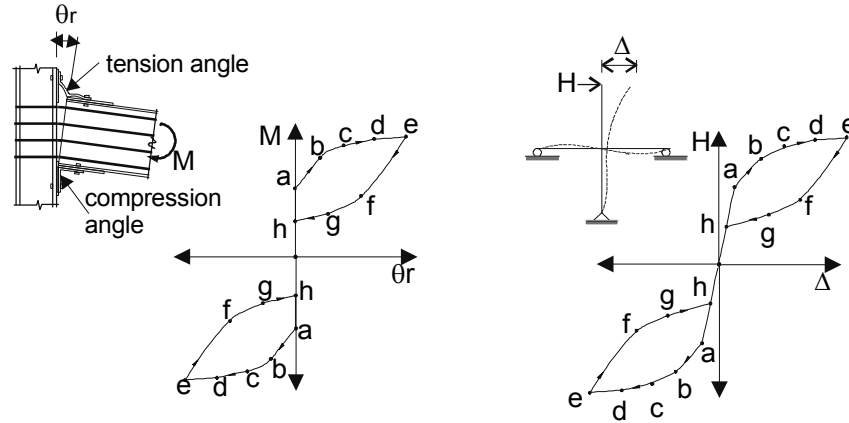


Figure 3. Moment-rotation and load-deflection behavior of a post-tensioned connection.

EXPERIMENTAL STUDIES

Subassembly Tests

Nine large-scale cruciform-shaped subassemblies with PT connections were tested. The test matrix is shown in Table 1. The main parameters of this study were angle size, angle gage, the presence of reinforcing plates, shim plates, and post-tensioning force. All specimens except PC1 had shim plates and reinforcing plates. The angle gage length, g , is the distance along the column leg of the angle from the fillet to the near edge of the washer plate. The gage length was expressed as a non-dimensional gage length-to-thickness (g/t) ratio. All angles were 254 mm long. More detailed information on these experimental studies can be found in Peng et. al (5).

Table 1. Specimen Test Matrix

Specimen	Angle Size	t (mm)	g/t
PC1	L152x152x7.9	7.9	9.0
PC2	L152x152x7.9	7.9	4.0
PC2-A	-	-	-
PC3	L203x203x15.9	15.9	7.2
PC4	L203x203x15.9	15.9	4.0
PC5	L203x203x25.4	25.4	4.0
PC6	L203x203x15.9	15.9	4.0
PC7	L203x203x15.9	15.9	4.0
PC8	L203x203x15.9	15.9	4.0

Each cruciform-shaped subassembly with PT connections simulated an interior joint of a MRF. The beam size for all the test specimens was W24x62 with 248 MPa nominal yield strength (F_y). The column size was W14x311 with 350 MPa F_y for Specimens PC1 through PC5. A concrete filled tube (CFT) consisting of a 406 x 406 x 13 mm steel tube with 74 MPa compression strength concrete was used for Specimens PC6 through PC8. Figure 4 shows the test setup. Each PT connection had a total of 8 strands, with 4 to each side of the beam web. Commercially available strands were utilized in the PT connection. Each strand had an area of 140 mm² and an ultimate strength of 1860 MPa. The spacing between strands was 127 mm. The strands

were initially stressed to approximately 35% of their ultimate strength (about 93 kN per strand). Each strand was anchored at the end of the beams in the cruciform subassembly just beyond where the roller reactions (rigid links) were located.

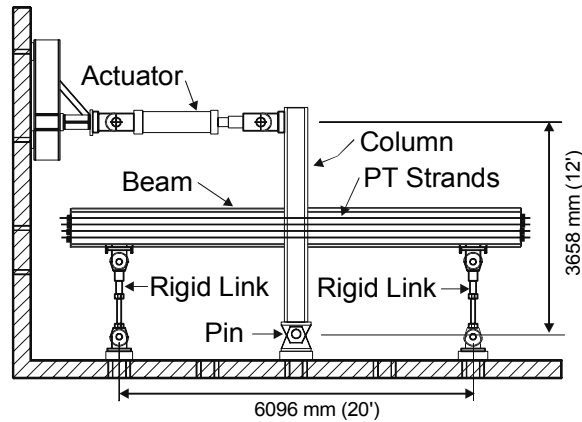


Figure 4. Subassembly test setup.

Shim plates were placed between the end of the beam and column face for construction fit-up and to avoid contact of the beam web with the column. The shim plates were 275 x 254 x 9.5 mm ($F_y=690$ MPa) for Specimens PC2 through PC5, and 275 x 254 x 19 mm ($F_y = 248$ MPa) for Specimens PC6 through PC8. Reinforcing plates were welded to the beam flanges. The reinforcing plates were 254 x 57 x 12.7 mm ($F_y = 690$ MPa) for Specimens PC2 through PC5, 610 x 203 x 12.7 mm ($F_y = 690$ MPa) for Specimens PC6 and PC8, and tapered 610 x (203 to 356) x 12.7 mm ($F_y = 690$ MPa) for Specimen PC7. Specimens PC2 through PC5 had two reinforcing plates on the inside of each flange, one on each side of the web. PC6 through PC8 had one reinforcing plate on the outside of each flange as shown in Figure 2. Specimen PC1 had neither shim plates nor reinforcing plates.

All connection bolts were 25 mm diameter. Two A325 bolts were used for column bolts (the bolts connecting the angle to the column) and beam bolts (the bolts connecting the angle to the beam) in the connection of Specimens PC1 and PC2. For Specimen PC5 two A490 column bolts and four A325 beam bolts were used. For the remaining specimens two A325 column bolts and four A325 beam bolts were used. The column bolts in each connection were snug tightened prior to applying the strand post-tensioning force. These bolts were then tightened to their required pretension following the application of the post-tensioning to the strands. This procedure avoided deforming the column leg of the top and seat angle. Strain gages were installed in the column bolts to verify the pretension as well as to monitor the bolt force during testing.

In each experiment the top of the column was subjected to a lateral displacement history consisting of a series of symmetric displacement cycles with increasing amplitude. The initial cycles involved elastic response below the decompression moment of the connection, with the latter cycles corresponding to a maximum story drift of 3% to 3.5%.

Subassembly Test Results

Figure 5 shows the load deformation ($H-\Delta$) and moment rotation ($M-\theta_r$) plot of Specimen PC4. The initial stiffness of this connection is nearly that of a fully restrained (FR) welded connection. Also, at zero load, the relative rotation and displacement are zero. This demonstrates the self-

centering capability of the connection. The decompression moment $M_{d,exp}$ was about 47% the plastic moment capacity of the beam, M_p . M_p was calculated as 576 kN-m using measured beam dimensions and tensile coupon values of the beam flange and beam web.

Figure 6 shows the effects of shim plates and reinforcing plates. Specimen PC1 did not have shim plates or reinforcing plates and therefore the region of the beam flanges in contact with the column yielded when the gap was open, but the beam web did not. When the gap closed, the flanges were no longer in good contact with the column. This caused a loss of stiffness and some self centering capability. The load displacement curves of all other specimens with shim and reinforcing plates look similar to the curve for PC4 shown in Figure 5.

Figure 7(a) and 7(b) show the effects of g/t ratio and angle size. Specimen PC4 had a smaller g/t ratio than PC3 and a larger thickness than PC2. The results show that connections with larger angle sizes and smaller g/t ratios dissipate more energy and achieve a greater moment for a given drift level.

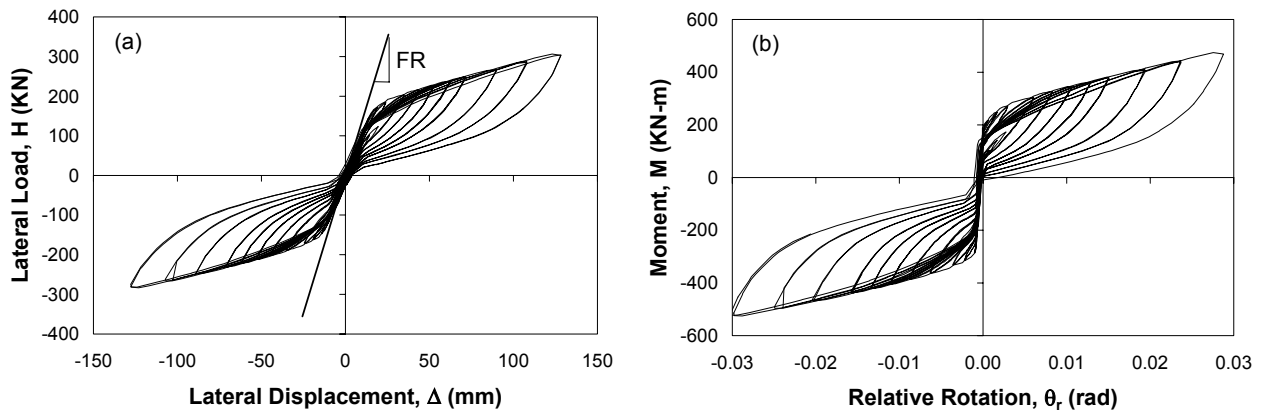


Figure 5. Specimen PC4 test results.

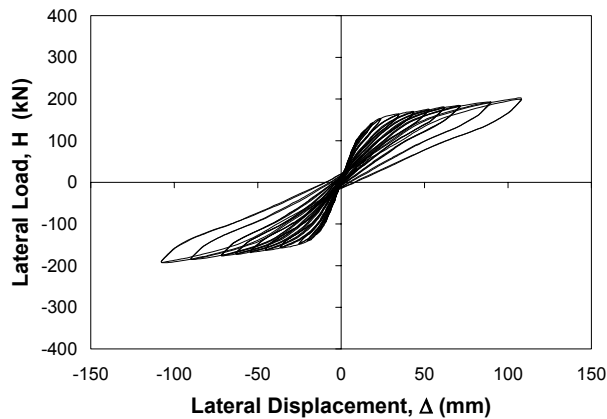


Figure 6. Specimen PC1 test results.

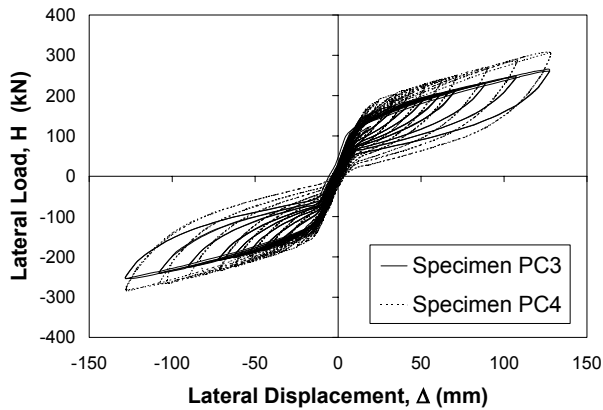


Figure 7(a). Effect of g/t ratio.

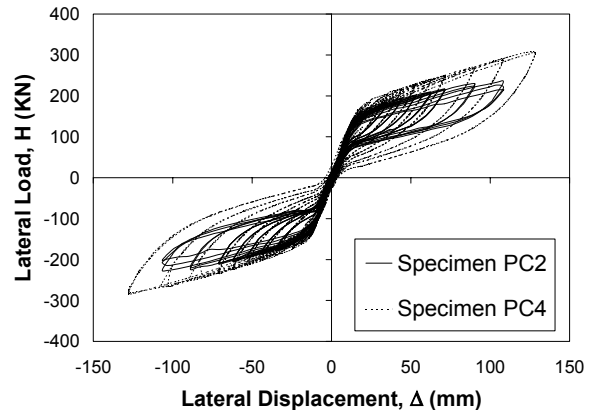


Figure 7(b). Effect of angle thickness.

By comparing the test results of Specimens PC6 and PC8, the beneficial effects of the post-tensioning strands are seen. Figure 8 shows that the post-tensioning strands (present in Specimen PC6 but not PC8) allow the connection to retain its self-centering capability. Also, PT strands increase the stiffness and moment capacity of the connection. Both specimens dissipate about an equal amount of energy.

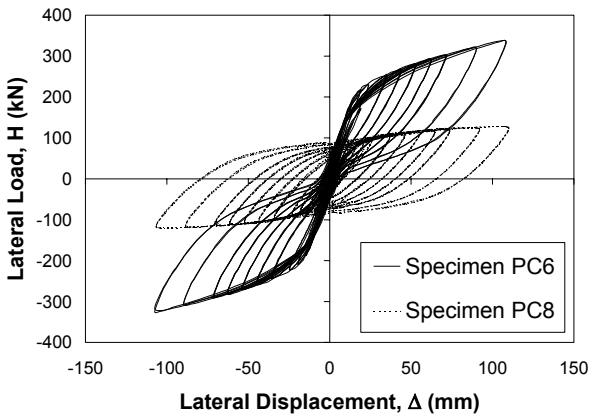


Figure 8. Effect of post-tensioning strands.

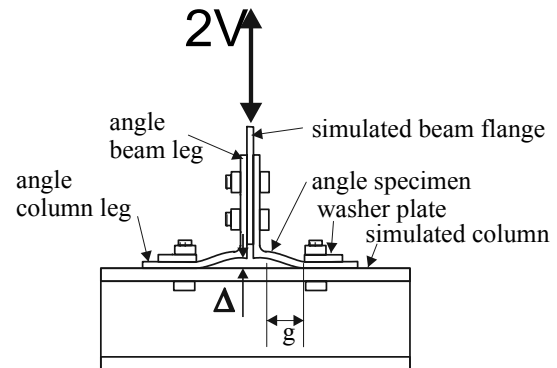


Figure 9. Isolated angle test setup.

A summary of the test results is shown in Table 2. A moment up to $0.95M_p$ was achieved in the connection (at the column face) at 3% drift ($M_{max,exp}$). The strand force at 3% drift, $T_{max,exp}$ never exceeded 54% of the ultimate strength of the strand, T_u , leaving a good margin of safety. A relative rotation, θ_r , of 0.021 to 0.030 radians at 3% drift indicates that the connections have excellent ductility since θ_r is analogous to the plastic rotation θ_p developed in a welded moment connection.

Test PC5 was terminated early because the bolts connecting the angles to the column developed large prying forces. Test PC2 was the only test in which the angles fractured. At the completion of this test, the angles were removed and the specimen was once again cyclically loaded as Specimen PC2-A. Without angles this connection developed $0.59M_p$. Since the angles provide most of the energy dissipation, Specimen PC2-A did not dissipate much energy (E_d).

Table 2. Response quantities of subassembly test specimens.

Specimen	$\frac{M_{d,exp}}{M_p}$	$\frac{M_{max,exp}}{M_p}$	$\frac{T_{max,exp}}{T_u}$	$\theta_{r, max}$ (rad)	E_d (Kn-m)
PC1	0.37	0.60	0.46	0.025	80
PC2	0.37	0.68	0.52	0.026	118
PC2-A	-	0.59	-**	0.030	2
PC3	0.40	0.72	0.53	0.021	105
PC4	0.47	0.89	0.51	0.025	157
PC5	0.47	0.59*	0.42*	0.014*	62*
PC6	0.45	0.93	0.54	0.026	273
PC7	0.45	0.95	0.54	0.025	278
PC8	n.a.	0.29	n.a.	0.031	263

*Specimen PC5 was stopped at 1.75% maximum drift.

**Post-tensioning force in Specimen PC2-A not monitored during testing.

Isolated Angle Tests

The angle parameters greatly influenced the connection behavior. Therefore, experimental studies were performed on isolated angles. For more details on these tests, see Garlock et. al (6).

In the test setup, two angles were placed back-to-back as shown in Figure 9. The test matrix is shown in Table 3. All angles were 178 mm long. The L203x203 and L152x152 angles had a nominal F_y of 345 MPa and 248 MPa, respectively. Specimens with 203 mm angles had four-32 mm A325 beam bolts. Specimens with 152 mm angles had only two of these bolts. The column bolts were 25 mm A325 bolts for all specimens except L8-34-4 and L8-34-6 which had 25 mm A490 bolts. All specimens except L8-58-4-NW had 178 x 57 x 12 mm plates as washers instead of standard bolt washers. The purpose of these washer plates was to force a plastic hinge to occur in the angle leg at the washer plate edge and to reduce the bolt prying force.

Table 3. Isolated angle test matrix.

Specimen	Angle Size (mm)	t (mm)	g / t
L6-516-4	L152x152x7.9	7.9	4.0
L6-516-9	L152x152x7.9	7.9	9.4
L8-58-4	L203x203x15.9	15.9	4.0
L8-58-4-NW	L203x203x15.9	15.9	4.0
L8-58-7	L203x203x15.9	15.9	7.2
L8-34-4	L203x203x19.0	19.0	4.0
L8-34-6	L203x203x19.0	19.0	5.8

*All specimens used washer plates except Specimen L8-58-4-NW which used a standard bolt washer.

The angles were cyclically loaded to specific levels of uplift, Δ , corresponding to SAC's testing protocol (7). The uplift values corresponded to estimated PT connection gap opening values at

given story drifts for a connection with a W36 beam. For example, a 25 mm uplift, Δ , (i.e. gap opening) corresponds to approximately 4% story drift for a connection with a W36 beam.

Figure 10 shows a plot of V vs. Δ for Specimen L8-58-4. V and Δ are the shear force in the angle (assumed to be half the actuator force) and the angle uplift, respectively, as shown in Figure 9. The hysteresis loops of this angle bear a resemblance to the hysteresis loops of PT connection PC4 shown in Figure 5. It was found that the angles can develop significant strength beyond the point at which a mechanism forms in the “column leg” (the leg of the angle that is connected to the simulated column). Figure 11 plots the data for peak V/V_p ratio value in each cycle against corresponding Δ for each specimen. V_p is the shear required to form a plastic mechanism, with the experimental value of V_p determined when a clear change in stiffness occurs in the $V - \Delta$ plot. A linear regression of V/V_p vs. Δ is also shown. Figure 11 shows that the post-yield strength appears to be independent of gage length and angle size, and is a nearly linear function of Δ . The value of V/V_p is equal to β , which is an angle overstrength factor that accounts for geometric hardening (due to large deformations) and material strain hardening. The β factor is used to predict the moment capacity of a PT connection as discussed later.

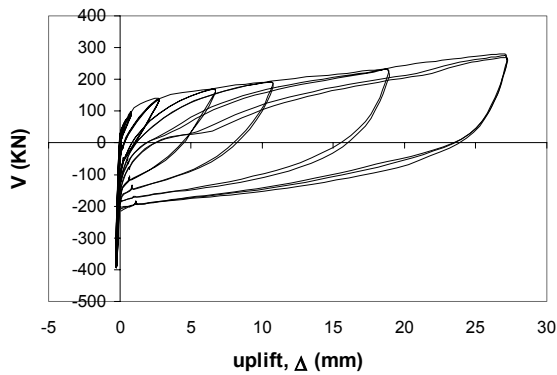


Figure 10. Isolated angle test results for Specimen L8-58-4.

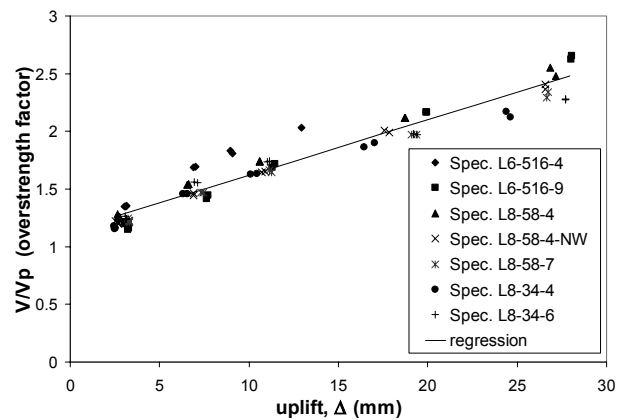


Figure 11. Angle overstrength factor.

The angle test results indicate that specimens with smaller g/t ratios dissipate greater energy, however, specimens with smaller g/t ratios have a shorter low cycle fatigue life. Therefore, an optimum gage length must be specified that will produce adequate energy dissipation and sufficient fatigue life. The results also show that the washer plate had a negligible influence on the angle behavior.

PREDICTING PT CONNECTION MOMENT CAPACITY

The level of post-tensioning force in the strands controls the decompression moment. Decompression occurs when the contact force resultant in the beam tension flange is zero. The theoretical decompression moment is equal to:

$$M_{d,th} = d_c \frac{T_o}{2} \quad (1)$$

T_0 and d_c are equal to the total initial post-tensioning force and the distance over the depth of the beam between the centroids of the contact areas between the beam flanges and column. This equation neglects the contribution of the bearing of the angle against the column face. To avoid excessive drift under gravity and wind load, $M_{d,th}$ should exceed the beam end moment due to gravity and wind load.

The moment capacity M_{max} of a PT connection is estimated considering the free body diagram shown in Figure 12. Assuming that the frame has undergone drift causing a relative rotation of θ_r between the end of the beam and column face, $M_{max,th}$ is determined as:

$$M_{max,th} = d_1 V_a + d_2 T + M_{aC} + M_{aT} \quad (2)$$

where d_1 , V_a , d_2 , T , M_{aC} , M_{aT} are equal to the depth from the center of rotation to the fillet of the tension angle column leg, the tension angle force resultant, the height from center of rotation to the resultant force of the post-tensioning strands, the resultant force of the post-tensioning strands, the moment developed in the compression angle beam leg, and moment developed in tension angle column leg, as shown in Figure 12.

The tension angle force resultant is equal to:

$$V_a = \beta \frac{2M_g}{g} \quad (3)$$

where β and M_g are the overstrength factor and angle moment developed at the end of the gage length g , respectively. The angle moment M_g is equal to the angle leg flexural capacity M_{pa} , whereby the angle shear V_p corresponds to $2M_{pa}/g$. β is based on test results of isolated angles [6] described earlier. The PT connection specimens had a gap opening of about 17 mm at 3% story drift. Examining Figure 11, this corresponds to a β value of about 2.

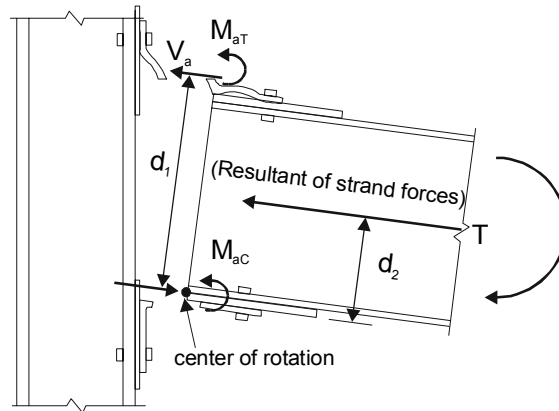


Figure 12. Free-body of PT connection.

Considering the effect of strand elongation and beam shortening following decompression of an interior connection, the total force of the post-tensioning stands can be shown to be equal to:

$$T = T_0 + \frac{AE}{L} d_2 \theta_r - \Delta T \quad (4)$$

where A, E, L, T_0 and ΔT are equal to cross-sectional area of the strands, modulus of elasticity of the strands, length of the strands, total initial post-tensioning force, and total decrease in post-tensioning force due to beam shortening after decompression of the PT connection occurs. The values of θ_r and ΔT vary with the story drift.

Figure 13(a) shows a plot of the average value of strand force versus the connection moment during the test of Specimen PC4. Notice that as the magnitude of the moment increases, the strand force increases. This is due to the elongation of the strands following decompression of the connection. Figure 13(b) compares the maximum value of the strand force in each cycle of the test of Specimen PC4 to the theoretical value based on Equation (4). This good correlation was also found for other specimens.

Table 4 shows that the correlation is good between $M_{\max,th}$, $M_{d,th}$ and $T_{\max,th}$, and the respective experimentally obtained values, where $T_{\max,th}$ is based on Equation (4). Both $M_{\max,th}$ and $T_{\max,th}$ are determined at the maximum story drift. For Specimen PC1 the difference between the maximum theoretical strand force, $T_{\max,th}$, and the maximum experimental strand force is larger than for the other specimens, due to the beam yielding leading to a shortening of the beam.

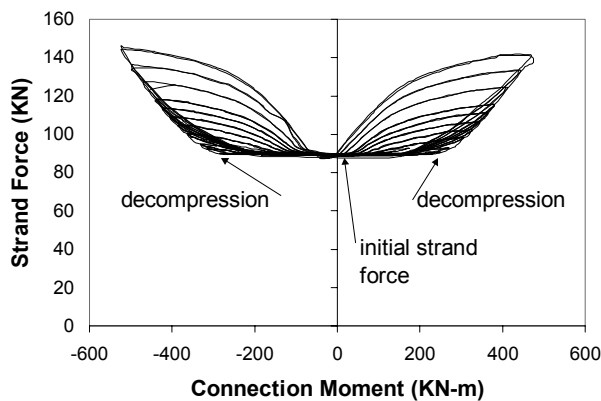


Figure 13(a). Average force per strand for Specimen PC4.

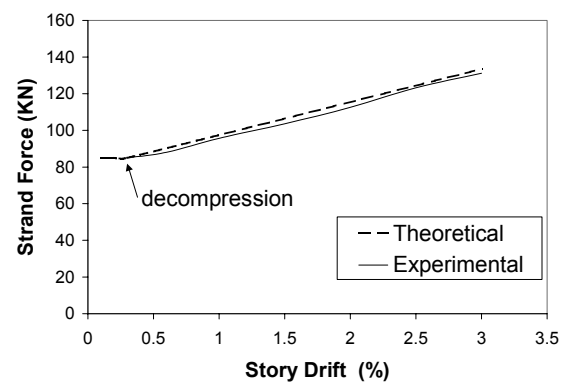


Figure 13 (b). Maximum experimental vs. theoretical strand force (Specimen PC4).

Table 4. Theoretical response compared to experimental response.

Specimen	$\frac{M_{d,exp}}{M_{d,th}}$	$\frac{M_{\max,exp}}{M_{\max,th}}$	$\frac{T_{\max,exp}}{T_{\max,th}}$
PC1	0.97	0.90	0.84
PC2	1.00	0.90	0.93
PC2-A	-	0.94	_***
PC3	1.14	0.92	0.98
PC4	1.38	1.00	0.98
PC5	1.38	0.70*	0.96*
PC6	1.15	0.95	0.97
PC7	1.18	0.99	0.99
PC8	n.a.	0.89	n.a.

*Specimen PC5 was stopped at 1.75% maximum drift.

**Post-tensioning force in Specimen PC2-A not monitored during testing.

SUMMARY AND CONCLUSIONS

The results of nine large-scale tests show that the PT steel connections can provide adequate strength and stiffness for a MRF system subjected to cyclic loading. Post-tensioning a top and seat angle connection results in a connection with an initial stiffness similar to that of a fully restrained welded connection and a strength that can develop the beam flexural capacity. The post-tensioning also provides a self-centering capacity, resulting in minimal story drift in a building after severe cyclic inelastic loading. Yielding occurred primarily in the top and seat angles. Since inelastic deformations are concentrated in the angles, it is easy to repair the building by replacing the angles.

It was found that connection shim plates and beam flange reinforcing plates are required in order to prevent the beam flanges from yielding under the large bearing forces developed at the zone of contact of the beam flanges and the column face. The size and gage length of the angles are shown to have an effect on the moment capacity and energy dissipation of the connection. Angles with either a larger thickness or smaller gage length produce a larger connection capacity and energy dissipation. The angle thickness and gage length, however, must be limited. An increase in angle thickness leads to larger bolt tension forces, and therefore requires more bolts. Shorter gage lengths result in larger accumulated plastic strain in the angles. This reduces the low cycle fatigue life of the angles. To maintain the self centering capability of the connection the post tensioning strands must be designed to remain elastic.

Expressions for predicting the connection moment capacity as a function of story drift were presented and found to agree well with the experimental results. These expressions are useful for design, where the required moment capacity must be provided while the self centering capability during an earthquake must be maintained.

Moment resisting frames with PT connections have been analyzed, and have been found to perform well. The drift in these frames was found to be less than that of MRFs with fully rigid connections. The results from these studies are reported elsewhere.

Acknowledgements

The research reported herein was supported by the National Science Foundation (NSF) and a Lehigh University Fellowship. Dr. Ken Chong and Dr. Ashland Brown are the cognizant NSF program officials. The research was also supported by a grant from the Department of Community and Economic Development of the Commonwealth of Pennsylvania through the Pennsylvania Infrastructure Technology Alliance (PITA). PITA is co-directed by Dr. Cristina Amon and Dr. Richard Sause. The opinions expressed in this paper are those of the authors and do not necessarily reflect the views of the sponsors.

REFERENCES

1. Youssef, N., Bonowitz, D., and Gross, J. (1995), "A Survey of Steel Moment Resisting Frame Buildings Affected by the 1994 Northridge Earthquake," NIST, *Report No. NISTIR 5625*, Gaithersburg, Md.
2. FEMA (1995), "Interim Guidelines: Evaluation, Repair, Modification and Design of Welded Steel Moment Frame Structures," Bulletin No. 267, FEMA, Washington, D.C.
3. Garlock, M, Ricles, J., Sause, R., Zhao, C., and Lu, L-W. (2000), "Seismic Behavior of Post-Tensioned Steel Frames," STESSA Proceedings, Montreal, Canada.

4. Ricles, J., Sause, R., Zhao, C., Garlock, M., and Lu, L. (1999), "Post-Tensioned Seismic Resistant Connections for Steel Frames," (submitted to Journal of Structural Engineering).
5. Peng, S.W., Ricles, J., Sause, R., Chen, T.W., and Lu, L-W. (2000), "Experimental Evaluation of a Post-Tensioned Seismic Resistant Connection", (submitted to Journal of Structural Engineering).
6. Garlock, M, Ricles, J., Sause, R., (1999), "Experimental Evaluation and Analytical Modeling of Bolted Angles Subject to Cyclic Loading", (in preparation for Journal of Structural Engineering).
7. SAC Joint Venture (1997) "Protocol For Fabrication, Inspection, Testing, and Documentation of Beam-Column Connection Tests and Other Experimental Specimens", Report No. SAC/BD-97/02, Version 1.1, October.

CYCLIC BEHAVIOR OF STEEL BEAM-TO-COLUMN JOINTS: GOVERNING PARAMETERS OF WELDED AND BOLTED CONNECTIONS

Luis CALADO¹, Elena MELE²

1 DECivil, Instituto Superior Tecnico, Lisbon, Portugal

2 DAPS, Università degli Studi di Napoli 'Federico II', Naples, Italy

Abstract

In this paper the results obtained from the experimental tests on two alternative connection solutions (fully welded and top-and-seat with web angles) designed for the same beam-to-column joint are presented. The test program was planned with the aim of assessing the comparative behaviour of bolted and welded connections, and for defining the effect of the column size and of the PZ design on the behaviour of the two types of connection, varying the applied loading history.

1. INTRODUCTION

One of the most important lessons derived from the Northridge and Hyogo Ken-Nanbu earthquakes has been the particular vulnerability of the beam-to-column connections in SMRF building structures. Starting from these observations, several research programs have been world-wide developed in order to enrich the experimental data base for assessing the major parameters influencing the cyclic behaviour of beam-to-column connections. In addition the need of accounting for the connection behaviour on the global structure performance has been underlined and theoretical models for reliably predicting stiffness, strength and deformation capacity of the connections have been developed.

Since recently bolted connections, in particular top and seat with web angles (TSW) connections, have not been considered appropriate in seismic applications, due to the partial strength and semirigidity characteristics. Therefore, TSW, though extensively investigated in the monotonic range, as reported in Kishi and Chen, (1), received less attention in the cyclic range.

Only recently it has been pointed out (Astaneh, (2); Elnashai *et Al.*, (3)) that the dynamic behaviour semirigid frames can be particularly favourable due to the period elongation, related to the connection flexibility and to the damping increase, related to highly dissipative friction mechanism deriving from a proper "slip capacity design". Both these effects act as a sort of self-isolation of the frame structure, thus leading to remarkable reduction of the seismic actions. It is worth to emphasise that also in the context of the SAC Steel Project, started immediately after the Northridge earthquake to address the specific problem of beam-to-column connections, a great interest in bolted configurations as alternative to the standard welded connections (Roeder, (4)), can be found.

In this research framework, a wide experimental program on different types (welded and bolted) of beam-to-column connections has been carried out at the Material and Structures Test Laboratory of the Instituto Superior Técnico of Lisbon. The experimental tests have been

performed on specimens representative of frame structure beam-to-column joints close to the ones typical of European design practice. Some preliminary experimental results on the welded connections have been presented in Mele *et Al.*, (5) and Calado *et Al.*, (6). In this paper a comparative assessment of the cyclic behaviour of welded and bolted beam-to-column connections is provided.

2. OBJECT AND AIMS OF THE PAPER

In this paper the results obtained from the experimental tests on two alternative connection solutions, namely top and seat with web angle (TSW) and fully welded connections (WW), designed for the same beam-to-column joints are presented. Six experimental tests have been executed on six (three welded and three bolted) different series of specimens, for a total of 36 tests. The test program was planned with the aim of assessing the comparative behaviour of bolted and welded connections, and for defining the effect of the column size and of the PZ design on the behaviour of the two types of connection, varying the applied loading history. In addition the accuracy of the "component method" of the Eurocode 3 Annex J (CEN, (7)) in predicting stiffness and strength of the connections is evaluated through the comparison with experimental monotonic results, and the possibility of extrapolating such theoretical prediction to the cyclic range is examined.

3. THE EXPERIMENTAL PROGRAM

3.1 The specimens

Two series of full scale specimens have been designed and tested, namely a WW specimen series (BCC5, BCC6 and BCC8) and a TSW specimen series (BCC9, BCC7 and BCC10). The specimens of the two series are T-shaped beam-column subassemblages, consisting of a 1000 mm long beam and a 1800 mm long column. The material used for the columns, beams, and angles is steel S235 JR, with nominal values of yield and ultimate stress respectively equal to $f_y=235$ MPa and $f_u=360$ MPa. In each series the cross section of the beam is the same (IPE300), while the column cross section has been varied, being respectively HE160B for the BCC5 (WW) and BCC9 (TSW) specimens, HE200B for the BCC6 (WW) and BCC7 (TSW) specimens, and HE240B for the BCC8 (WW) and BCC10 (TSW) specimens. In both the series, the continuity of the connection through the column has been ensured by horizontal 10 mm thick plate stiffeners, fillet welded to the column web and flanges.

3.1.1 WW specimens

In the WW specimens, the beam flanges have been connected to the column flange by means of complete joint penetration (CJP) groove welds, while fillet welds have been applied between both sides of the beam web and the column flange. The flexural strengths of the beam, column and panel zone, have been computed on the basis of the nominal yield stress and are reported in table 1.

	M_{pb}	M_{pc}	$M_{p,PZ}$
BCC5	147.6	83.2	91.1
BCC6	147.6	151.1	132.4
BCC8	147.6	247.5	182.9

Table 1: moment capacities (in kNm) of the WW specimens

From the simple comparison among the nominal plastic moments reported in table 1, it can be observed that in the three WW specimens the weakest component of the joint configuration is respectively: the column for the BCC5 specimen, the panel zone for the BCC6 specimen, the beam for the BCC8 specimen.

3.1.2 TSW specimens

In the BCC9, BCC7 and BCC10 (TSW) specimens, 120x120x10 angles have been adopted. Two rows of bolts are placed on each leg of the flange angles, while on the legs of the web angles there is only one row of two bolts. The bolts are M16 grade 8.8 (yield stress $f_{yb}=640$ MPa, ultimate stress $f_{ub}=800$ MPa, $A_s=157$ mm²), preloaded according to the EC3 provisions, i.e. at $F_{P,CD}=0.7 f_{ub} A_s = 87.9$ kN.

It is well known that two major phenomena characterise the behaviour of the TSW connection: the slippage of bolts and the yielding of the tension angle. For the TSW specimens herein described the bending moment corresponding to bolt slippage and angle yielding are reported in table 2, together with the beam and column moment capacities. From the comparison between the bending moments corresponding to bolt slippage and angle yielding, it derives that the specimens are "slip critical" connections, since slippage of top and seat angle bolts occurs at a load level higher than the one corresponding to yielding of the tension angle.

	M_{slip}	$M_{y,angle}$	M_{pb}	M_{pc}
BCC9	32 - 47.5	23.3	147.6	83.2
BCC7	32 - 47.5	23.3	147.6	151.1
BCC10	32 - 47.5	23.3	147.6	247.5

Table 2: threshold moment capacities (in kNm) of the TSW specimen

3.2 Loading histories

For each of the six specimen series, the experimental program consisted of six tests, one monotonic test and five cyclic tests, for a total of 36 tests. The cyclic tests have been carried out by applying both constant and step-wise increasing amplitude displacement histories. This latter test type has been carried out according to the basic loading history recommended in ECCS, (8). In this paper only the increasing rotation tests is reported.

3.3 Experimental set-up and specimen instrumentation

The test set-up, mainly consists in a foundation, a supporting girder, a reaction r.c. wall, a power jackscrew and a lateral frame. The power jackscrew (capacity 1000 kN, stroke ± 400 mm) is attached to a specific frame, pre-stressed against the reaction wall and designed to accommodate the screw backward movement. The specimen is connected to the supporting girder through two steel elements. The supporting girder is fastened to the reaction wall and to the foundation by means of pre-stressed bars. An automatic testing technique was developed to allow computerised control of the power jackscrew, of the displacement and of all the transducers used to monitor the specimens during the testing process. Specimens have been instrumented with electrical displacement transducers (LVDTs), which record the displacement histories at several points in order to obtain a careful documentation of the various phenomena occurring during the tests. The same arrangement of LVDTs has been adopted for the three WW and the three TSW specimen series.

4. CYCLIC TESTS

4.1 Premise

In the following the experimental results obtained in the test program are provided. In particular the cyclic behaviour and the failure modes observed for the six sets of specimens are described, and the moment rotation hysteresis loops obtained in the increasing amplitude tests are provided. In the moment rotation hysteresis loops hereafter presented, reference is made to three different values of rotation, namely: (1) the “unprocessed” total rotation given by the applied interstorey drift angle d/H ; (2) the beam rotation Φ_b and (3) the panel zone rotation Φ_{PZ} , both obtained through the measured LVTDs displacements of the specimens. Correspondingly, in the $M-d/H$ and $M-\Phi_{PZ}$ experimental curves the moment is evaluated at the column centreline, while in the $M_b-\Phi_b$ curves the moment is evaluated at the column face.

4.2 WW specimens

In figure 1 (a) the moment - total rotation ($M-d/H$) experimental curves resulting from the BCC5C, BCC6C and BCC8D tests (cyclic increasing stepwise amplitude) are plotted, while in figure 1 (b) both the corresponding moment – beam plastic rotation $\Phi_{b,pl}$ and the moment - panel zone rotation Φ_{PZ} curves are plotted. The beam plastic rotation has been obtained through the measured displacements at the beam instrumented section by subtracting the contributions of the beam and column elastic rotations as well as of the panel zone distortion.

4.2.1 BCC5

As can be derived from the curves reported in figure 1 (a) and (b), and as demonstrated also throughout the experimental program, the cyclic behaviour of the specimen BCC5 is characterised by a great regularity and stability of the hysteresis loops up to failure, with no deterioration of stiffness and strength properties. In the very last cycle the specimen has collapsed with a sudden and sharp reduction of strength, due to fracture initiated in the beam flange and propagated also in the web. During the tests, significant distortion of the joint panel zone has been observed, while not remarkable plastic deformation in the beam occurred.

4.2.2 BCC6

Throughout the test program, two different kinds of cyclic behaviour have been observed for the BCC6 specimens. In some cases the behaviour of the specimens is close to the behaviour observed for the BCC5 type, with almost no deterioration of the mechanical properties up to the last cycle, during which the collapse occurred. For the other tests a gradual reduction of the peak moment at increasing number of cycles is evident. In these cases, starting from the very first plastic cycles, local buckling of the beam flanges occurred, and a well defined plastic hinge has formed in the beam. The contribution of the panel zone deformation has not been as significant as in the BCC5 specimen type.

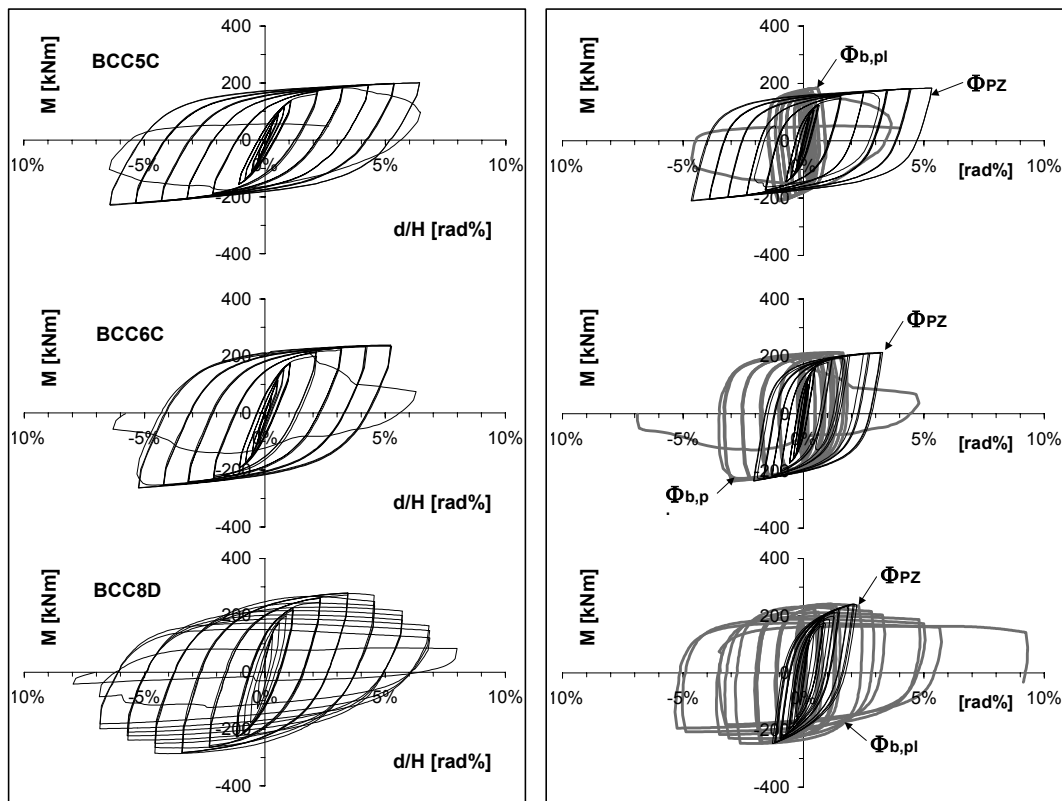


Figure 1: WW specimens: (a) moment-global rotation curves; (b) moment-beam plastic rotation and moment-panel rotation curves

4.2.3 BCC8

The hysteresis loops obtained from the tests on the BCC8 specimens show a gradual reduction of the peak moment starting from the second cycle, where the maximum value of the applied moment has been usually registered. This deterioration of the flexural strength of the connection is related to occurrence and spreading of local buckling in the beam flanges and web. A well defined plastic hinge in the beam has formed in all the tested specimens. In the specimens BCC8 the panel zone deformation has not been remarkable, and the plastic deformation mainly took place in the beam.

4.3 TSW specimens

In figure 2 (a) the moment - total rotation (M - d/H) experimental curves resulting from the BCC9D, BCC7C and BCC10C tests (cyclic increasing stepwise amplitude) are plotted, while in figure 2 (b) both the corresponding moment – beam rotation Φ_b and the moment - panel zone rotation Φ_{PZ} curves are plotted. As can be derived from the curves reported in figure 2, the shape of hysteresis loops of the three TSW specimens is very similar. The cyclic behaviour, the phenomena observed during the tests and the collapse modes are the same for the three specimen series, thus the following unique paragraph is devoted to describe the above issues for the three specimens.

4.3.1 BCC9 / BCC7 / BCC10

The cyclic behaviour of the TSW connections is characterised by bolt slippage and yielding and spreading of plastic deformation in the top and bottom angles, cyclically subjected to tension. Plastic ovalization of the bolt holes have also been observed mainly in the leg of the angle adjacent to column flange. The experimental curves, typical of this type of connection, shows pinched hysteresis loops, with a large slip plateau (very low slope of the experimental curve) and subsequent sudden stiffening. In fact when the specimen position is at $d = 0$, due to the concomitant effects of bolt slippage, hole ovalization and the plastic deformation of the angle legs adjacent to the column flange, the beam is completely separated from the column (gap open).

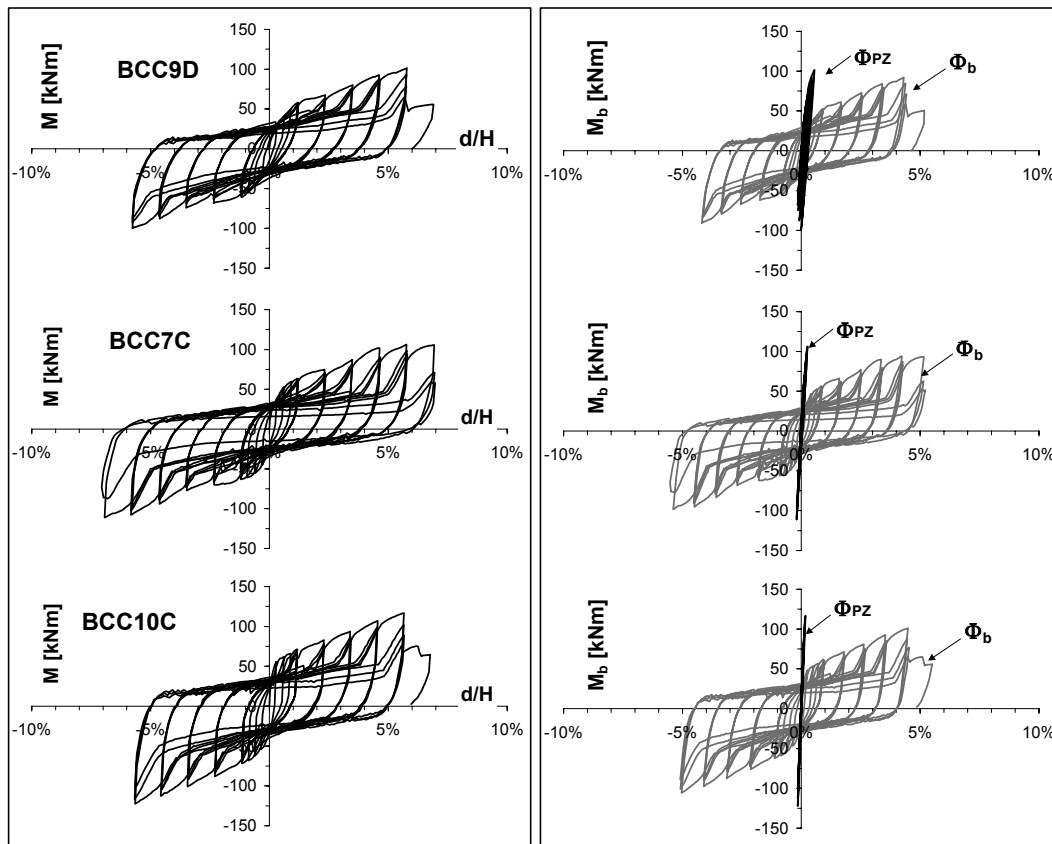


Figure 2 TSW specimens: (a) moment-global rotation curves, (b) moment-beam net rotation and moment - panel rotation curves

At large applied displacements, which impose large rotations to the connection, the contact of the compression angle and the beam web to the column flange (gap closure) give rise to sudden stiffening of the connection, which is evident in the experimental curves. No significant rotation of the column and distortion of the panel zone has been observed throughout the experimental tests carried out on the three specimens. At each step on the test, slight deterioration of the joint resistance in the three applied cycles can be observed in the experimental curves, mainly due to yielding and spreading of plastic deformation in the top and bottom angles, cyclically subjected to tension. In all the test carried out on the three specimen

series, the collapse of the connection occurred due to fracture in the leg angle located on the beam flange, immediately after the fillet. Negligible scatters can be observed in the moment capacity of the three connection series, as it is expected, since the inelastic behaviour of the connection is governed by the angle. Also the maximum values of global rotation experienced by the specimens is the same for the BCC9 and BCC10 series, and slightly larger for the BCC7 one.

5. MONOTONIC TESTS

The moment rotation curves obtained from the monotonic tests carried out on the six specimens are presented in figures 3 (a) and (b) which respectively report the results of the WW and TSW specimens. In these curves the moment is evaluated at column centreline and the rotation is given by the total interstory drift angle (d/H). In each figure also the moment panel zone rotation Φ_{PZ} are reported. From the experimental results on the two series of specimen the effect both of the connection typology (TSW and WW) and of the column cross section (HE160B, HE200B, HE240B) can be derived.

By comparing the two series of experimental curves it must be noticed that the three WW specimens show significant differences in the initial stiffness, maximum strength and deformation capacity, thus confirming the strong effect of the column cross section size already observed in the cyclic tests. On the contrary, the three TSW specimens present quite close experimental responses. This difference between the behaviour of WW and TSW specimens is mainly related to the design of the specimens, since in the TSW connections the weakest component is the same in the three specimens (the angle in tension), thus the beam, column and panel zone strength ratios does not affect the response of the specimens. Slight scatters can be observed in the initial stiffness, due to the different column and panel zone deformability, but the nonlinear portion of the curve and the maximum bending moment are very similar.

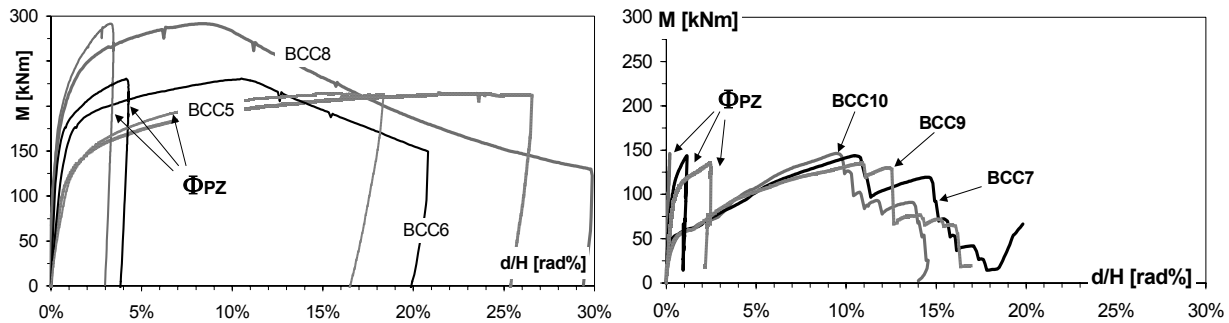


Figure 3 Monotonic experimental curves: (a) WW specimens; (b) TSW specimens

As already evidenced, the behaviour of the WW connections is affected by the column dimensions since the three combinations of beam and column framing in the joint give rise to panel zone strength values respectively: smaller than, approximately equal to and larger than the plastic moment of the beam, for the BCC5, BCC6 and BCC8 specimens. These observations are confirmed by analysing the main test data provided in table 3.

In particular it can be noticed that while in the WW specimens the panel zone distortion Φ_{PZ} significantly contributes to the specimen global rotation d/H (at the maximum value of the

bending moment registered in the relevant test), though at different extent in the three specimens, a completely different order of magnitude of this contribution is registered in the TSW connections. For the TSW specimens, instead, the rotations due to bolt slippage Φ_{slip} computed on the basis of the LVDTs measured displacements constitutes a major contribution to the total rotation d/H .

		M [kNm]	M_b [kNm]	d/H [%]	Φ_{PZ} [%]	$\Phi_{b,pl} - \Phi_{PZ}$ [%]
WW	BCC5	214	196	21.4	16.5	0.66
	BCC6	231	207	10.5	4.5	4.9
	BCC8	292	251	8.3	3.3	5.3
		M [kNm]	M_b [kNm]	d/H [%]	Φ_{PZ} [%]	Φ_{slip} [%]
TSW	BCC9	135	122.5	10.8	2.4	5.2
	BCC7	144	127	10.5	1.15	6.8
	BCC10	146	126	9.4	0.19	4.8

Table 3: main experimental data from the monotonic tests on the WW and TSW specimens

6. PREDICTION OF THE MONOTONIC BEHAVIOUR

Comparing the monotonic and the cyclic curves both for the BCC5 WW specimen, and for the BCC9 TSW specimen, it can be observed that the monotonic curve perfectly envelope the cyclic one. Thus it seems of primary importance assessing the prediction capacity of the monotonic behaviour offered by the available numerical models.

In figures 4 and 5 the monotonic curves, respectively of the BCC5 and BCC9 specimens, are compared to theoretical moment-rotation curves. In figure 4 (a) and (b) the reference experimental curves report the moment at the column centreline, M , vs the different rotation values, i.e.: the global rotation d/H , the beam and the PZ rotations, Φ_b and Φ_{PZ} , obtained from the LVDT measured displacements, and depurated of: rigid rotation of the specimen supports, elastic rotations of the beam and column. The theoretical curve is the one obtained through the application of the "component method" as outlined in the EC3 Annex J. In the figure 5 (a) and (b) the reference experimental curve reports the moment at the column centreline, M , vs the global rotation d/H . The theoretical curves obtained through: the application of the EC3 Annex J procedure, the model proposed by Kishi & Chen, (1) and the simplified approach proposed by De Luca *et Al.*, (9) are also shown in the figure. Both the figure 4 (b) and 5 (b) provide the detail of the curves up to 1% rotation.

6.1 WW BCC5 specimen

In the case of welded connections stiffened by means of continuity plates as the ones described in this paper, the Annex J procedure suggests to account for only one component in the evaluation of the rotational stiffness of the joint, i.e. the column web panel in shear, while the flexural strength of the joint is given by the resistance, multiplied by the lever arm, of the weakest among five basic components, namely the panel in shear, the column web in tension and in compression, the column flange in bending and the beam flange and web in compression. For the BCC5 specimen the panel shear resistance resulted the minimum one, thus confirming the governing role of the PZ in the deformation and failure modes of the BCC5

specimen observed in the tests. The moment rotation curve obtained through the Annex J procedure, improved as suggested in Faella *et Al.*, (10), shows a reasonable accuracy both in terms of strength (figure 4 (a)) and in terms of initial stiffness (figure 4 (b)). By observing that the monotonic curve of the BCC5 specimen envelopes the experimental curves obtained under cyclic loading, it seems that a reliable prediction of the joint monotonic behaviour is of major importance also for assessing the cyclic performance.

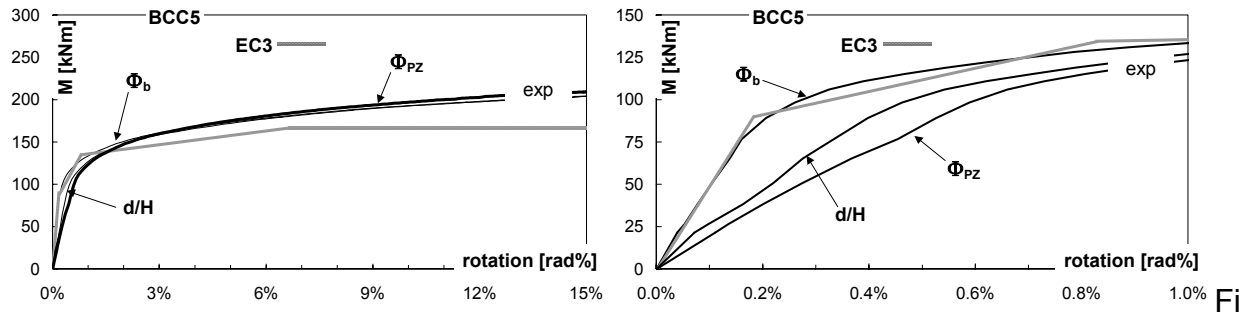


Figure 4 experimental vs theoretical curves: WW BCC5 specimen

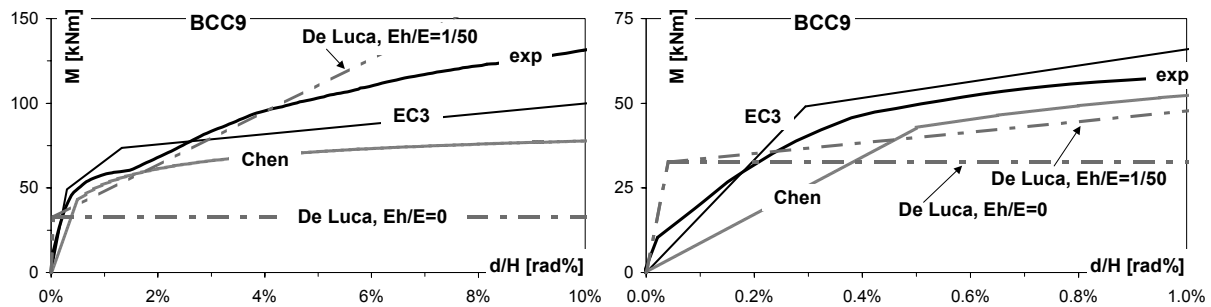


Figure 5 experimental vs theoretical curves: TSW BCC9 specimen

6.2 TSW BCC9 specimen

In the experimental curve of figure 5 (a) four major branches can be identified: an initial linear branch; a second, remarkably nonlinear branch, going approximately from 35 to 55 kNm, where the both the slip of bolts and yielding of the angle occur; a third sensibly linear branch which arrives at 85 kN, characterised by a reduced slope, where hardening of the angle occurs up to the failure of the first row of bolts; and a final, always approximately linear branch but with a reduced slope, where the angle, also due to geometry variation related to the loss of a bolt row, is further stretched and carry the load in simple tension. It is worth to notice that the ratio of the slope of the third to the first branch of the curve is close to the ratio E_h/E derived from the tension tests on the angle coupon, while the maximum bending moment registered in the test at the column face is close to the moment corresponding to the pure tensile bearing capacity of the angle. Similar considerations still hold by observing the other TSW experimental curves.

The prediction models do not represent all these phenomena, since the ultimate bearing capacity developed by the connection is due to a deformation state which is not compatible with the global stability of the structure. Therefore the purpose of the models is the prediction of the initial stiffness, the plastic threshold and the consequent nonlinear branch up to a given

deformation value, which should be compatible with the structure and checked against the deformation capacity of the connection. In this perspective, the EC3 model, applied with the improvements suggested by Faella *et Al.*, (11), matches quite closely the initial stiffness, slightly overestimates the plastic threshold given by $2/3$ of the resistance M_{jRd} , and provides a reasonable value of M_{jRd} . In addition, by considering a hardening slope equal to $1/55$ and accounting for a strength ratio $f_u/f_y=1.48$, as derived from the angle coupon tests, also a portion of the fourth branch can be match. The model of Kishi and Chen (1) also leads to a good estimation of strength, but does not match the initial stiffness, since it does not allow for bolt preloading. The simplified approach of De Luca *et Al.*, (9) provides a range which includes the experimental curve. A deeper assessment of the prediction capacity of the different models is not possible here due to space limitations.

7. SUMMARY AND CONCLUSIVE REMARKS

The experimental results obtained in this research allow to define the collapse modes, the rotation capacity and the ultimate bending strength of bolted and welded beam-to-column connections. In this paper the major aspects governing the cyclic and the monotonic behaviour of bolted (TSW) and welded (WW) connections have been evidenced against experimental results. It has been shown that the panel zone does not affect the behaviour of the TSW connections, which instead is mainly related to the tension angle geometry and strength properties. On the contrary the panel zone has demonstrated to affect at large extent all the response parameters (stiffness, strength and deformation capacity) of welded connections. Finally the application of the EC3 Annex J model (with some modifications suggested by other Authors) to two single examples of each connection typology, has shown to provide reasonable results.

ACKNOWLEDGMENTS

The financial support of MURST (Italy) and FCT (Portugal) is gratefully acknowledged.

NOTATION

Abbreviations

TSW = top and seat with web angles connection

WW = fully welded connection

PZ = panel zone

CJP = complete joint penetration

Symbols

f_y = yield stress

f_u = ultimate stress

f_{yb} = yield stress of bolts

f_{ub} = ultimate stress of bolts

$F_{P;CD}$ = bolt preloading force

M = bending moment at column centerline (experimental value)

M_b = bending moment at column face (experimental value)
 M_{slip} = bending moment corresponding to bolt slippage (theoretical value)
 $M_{y,angle}$ = bending moment corresponding to angle yielding (theoretical value)
 M_{pb} = plastic moment capacity of the beam section (theoretical value)
 M_{pc} = plastic moment capacity of the column section (theoretical value)
 M_{pPZ} = plastic moment capacity of the panel zone (theoretical value)
 d = applied displacement
 H = distance between the column centreline and the beam tip
 d/H = applied interstorey drift angle
 Φ_b = beam rotation
 $\Phi_{b,pl}$ = beam plastic rotation
 Φ_{PZ} = panel zone rotation
 Φ_{slip} = rotation due to bolt slippage
 E = Young modulus
 E / E_h = hardening ratio

REFERENCES

1. Kishi, N., Chen, W.F.(1990) Moment rotation relations of semirigid connections with angles. J. of Struct. Eng. ASCE, Vol..116.
2. Astaneh-Asl, A. (1995). "Seismic design of bolted steel moment-resisting frames." Steel Tips, Structural Steel Educational Council, Moraga, California, July.
3. Elnashai, A.S., Elghazouli, A.Y., Denesh-Ashtiani, F.A. (1998) Response of semirigid steel frames to cyclic and earthquake loads. J. of Struct. Eng. ASCE, Vol.124, No.8.
4. Roeder, C.W. (1998). Design models for moment resisting steel constructions. Proc. SEWC 1998. Paper T158-4
5. Mele, E., Calado, L., De Luca, A. (1999) Experimental behaviour of beam-to-column welded connections: effect of the panel zone design. Proc. XVII C.T.A., Napoli, Oct.
6. Calado, L., Mele, E., and De Luca, A. (1999). "Experimental investigation on the cyclic behaviour of welded beam-to-column connections". Proc. 2nd European Conf. on Steel Structures, PRAHA, Czech Republic, Paper No.215.
7. CEN TC250/SC3-PT9. (1997). Eurocode 3, Part 1.1. Rev. Annex J. "Joints in building frames". Ed. Approved Draft: Jan.
8. ECCS (1986). "Seismic Design. Recommended testing procedure for assessing the behaviour of structural steel elements under cyclic loads". Tech. Comm. 1 - Structural Safety and Loadings, TWG1.3 – Rep. No.45.
9. De Luca, A., De Martino, A., Pucinotti, R., Puma, R. (1995) (Semirigid ?) Top & Seat angle connections: Critical review of Eurocode 3 approach.. Proc. XV C.T.A., Riva del Garda, Oct.
10. Faella C., Piluso, V. and Rizzano, G. (1995). Modelling of the moment-rotation curve of welded connections: proposals to improve Eurocode 3 Annex J. Proc. XV C.T.A., Riva del Garda, Oct., 405-418.
11. Faella C., Piluso, V., Rizzano, G. (1996). Prediction of the flexural resistance of bolted connections with angles. Proc. IABSE Coll. on Semirigid Structural Connections, Istanbul, Sept.

BEHAVIOR OF WF BEAM-TO-SHS COLUMN CONNECTIONS USING SPECIAL SHAPED HIGH STRENGTH BOLTS

Atsuo TANAKA, Prof. Utsunomiya University
Hiroshi MASUDA, Assistant Prof, Utsunomiya University
Haruyoshi KADOYA, Director, Okabe Engineering Co.
Akiyoshi ITO, Director, Artes Design Corporation

ABSTRACT

Behavior of WF beam-to-SHS column connections using special shaped high strength bolts called Paddle Bolts was investigated by experimental study using full scale specimens. From the results of this test the static characteristics of this type beam-to-column connections becomes clear and this type of connections can be used practically both semi-rigid and rigid connections depending on the reinforcement at the column surfaces.

1. INTRODUCTION

In Japan special shaped high strength bolts (which are so called “Paddle Bolts” as shown in Fig.1) are used to connect WF beams to WF columns in some case from economical and quality viewpoints. Such connections are designed as fully moment resisting connections. In case Paddle Bolts are applied to connect WF beams to SHS columns as shown in Fig.2, many static problems must be solved. Those problems are prevention of local deformation due to large bolt holes and sectional shape of SHS column, fixing of the bolts at the joints of column and the secondary bending effects to the bolts due to shear force. In order to check the applicability of Paddle Bolts to the WF beam-to SHS column connections, experimental study was executed using 5 full scale specimens with various types of reinforcements. In this paper detail of the test, main test results and results of investigation are reported.



Fig.1 Paddle Bolt



Fig.2 View of WF Beam-to-SHS Column Connection

2. TEST SPECIMEN AND TEST SETUP

Full scale T-shaped specimens with beam-to-column connection were used. The figure of specimen and test setup is shown in Fig.3. The size of SHS column and WF beam are \square -300x300x16 and H-400x200x8x13. The beam was connected to the column by 4 M-36 Paddle Bolts. Two kinds of strength level of Paddle Bolts with same shape were used, that is 10T ($\sigma_u \geq 1000\text{N/mm}^2$, σ_u : tensile strength of material of bolt) and 11T ($\sigma_u \geq 1100\text{N/mm}^2$). Paddle Bolts were tightened in snug tight condition. The detail of Paddle Bolt and rectangular nut is shown in Fig.4. Three types of nuts are used depending on the detail of reinforcement at the connection, those are usual hexagon nut, enlarged hexagon nut with outer size for M42 and rectangular shaped nut shown in Fig.4. The detail of each beam-to-column connection is shown in Fig.5. The list of the specimens and its detail of connection is shown in Table 1. Specimen N-W has usual welded rigid connection and it is selected as standard. Each connection using Paddle Bolts was reinforced by 22mm thick plates(R.Plate), which were welded at the connected part of the column. Only specimen CCR-B had reinforcement also inside of the column. Depending on the fixing method of the bolt the shape of bolt holes and the shape of nuts varied in each specimen as shown in Fig.5 and Table 1. The notation C of the specimen means specimens with circular bolt holes and S means with rectangular holes. The notation -A means the specimen using 10T grade Paddle Bolts and -B means 11T grade Paddle Bolts. About specimens using 11T Paddle Bolts, free length of the bolts at the column connection e_c (see Fig.13) was set as short as possible. Mechanical properties of the material of the specimens are shown in Table 2.

Horizontal load was cyclically applied at the tip of the beam as shown in Fig. 3. The loading procedure is shown in Fig.6. Here δp is the calculated value of the displacement at the tip of the beam, which corresponds to the full plastic moment of the beam at the column face, using actual yield strength of the material of the beam.

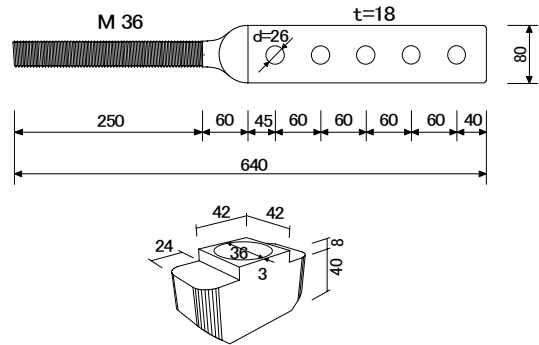


Fig.4 Detail of Paddle Bolt and Rectangular Nut

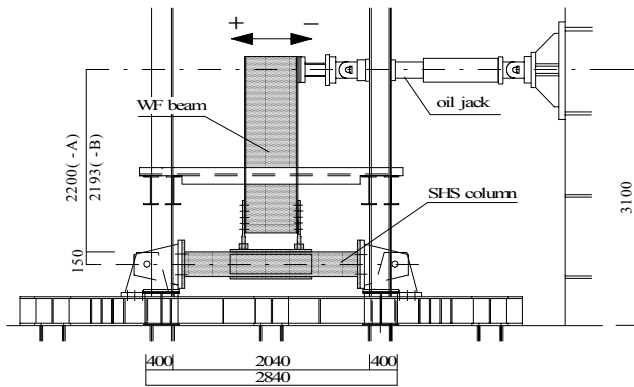


Fig.3 Test Setup

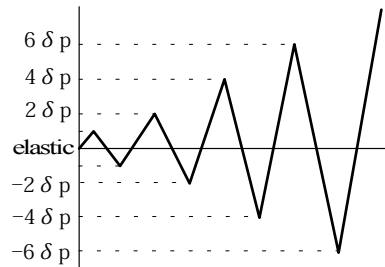


Fig.6 Loading Procedure

Table 1 List of Specimen

Specimen	Beam	Column	R.Plate		Size of Nut		Paddle Bolt	Shape of Bolt Hole			
			outside	inside	outside	inside		R.Plate	Column		
N-W	H-400 × 200 × 8 × 13 (SM490)	□-300 × 300 × 16 (BCR295)	-	-	-	-	-	-	-		
SS-A			-	-	-	-	M36(10T)	□	□		
CS-A			-	-	R-22	M42	rectangular nut	M36(10T)	○	□	
CS-B			-	-				M36(11T)	○	□	
CC-B			-	-				M42	M36(11T)	○	○
CCR-B			-	-				M36	M36(11T)	○	○

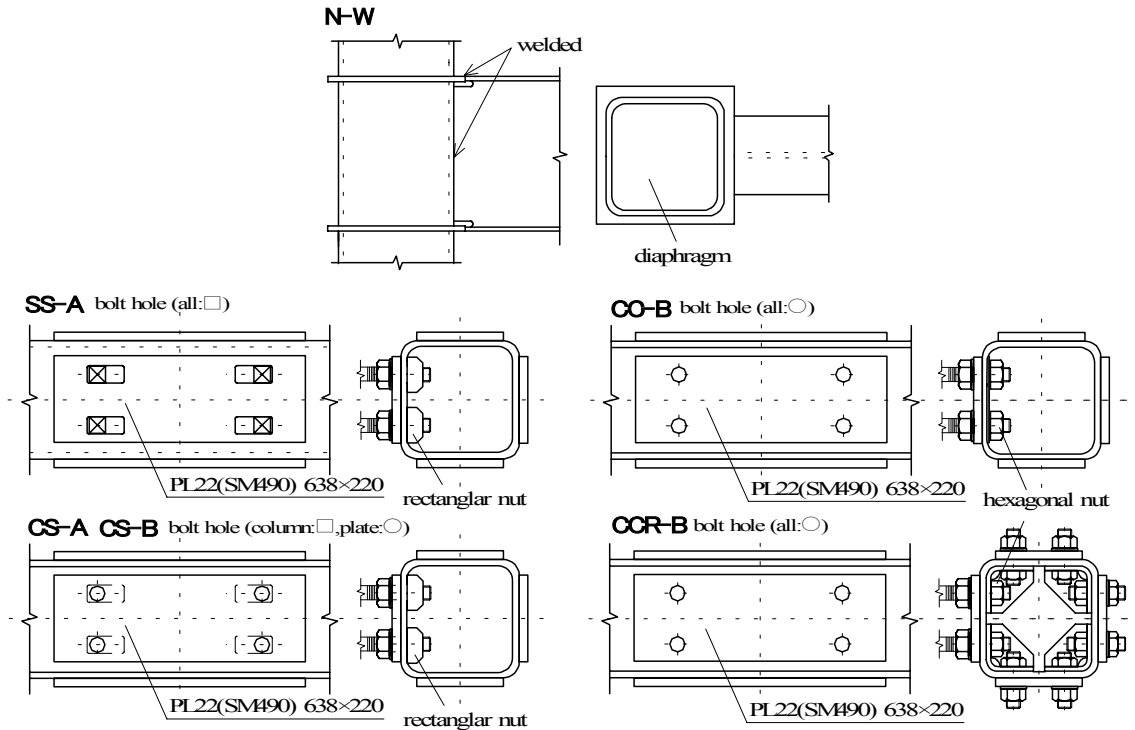


Fig.5 Detail of Connection of Each Specimen

Table 2 Mecanical Properties of Material

Test Piece	Steel Grade	YP (N/mm ²)	TS (N/mm ²)	Remarks	
PL8	a	SM490	407	564	web(expect CS-B)
	b		405	562	web(CS-B)
PL13	a	SM490	344	533	flange(expect CS-B)
	b		375	554	flange(CS-B)
PL16	a	BCR295	407	470	column(expect CS-B)
	b		419	484	column(CS-B)
PL19	a	SM490	334	504	diaphragm(N-W)
PL22	a	SM490	362	519	R.Plate(expect CS-B)
	b		321	525	R.Plate(CS-B)

YP: Yield Point
TS: Tensile Strength

Paddle Bolt	bTu(kN)	bσu(kN/mm ²)	Ae(mm ²)	Zp(mm ³)
M36(10T)	904	1106	817	556
M36(11T)	986	1207	817	556

bTu: Tensile Strength of Bolt
bσu: Tensile Strength of Material of Bolt
Ae: Net Sectional Area of Bolt
Zp: Plastic Section Modulus of Threaded Part

3. TEST RESULTS

Main test results are summarized in Table 3. P_{max} and P_y are the maximum strength and the yield strength of the specimen. α is the maximum strength factor calculated by P_{max}/cP_p , here cP_p is the calculated full plastic strength, which corresponds to full plastic moment of the beam at the critical location, where is assumed column surface for the specimen N-W and end bolt line of beam flange to Paddle Bolt joint for the specimen using Paddle Bolts., which is assumed column surface for the specimen N-W and end bolt line of beam flange to Paddle Bolt joint for the specimen using Paddle Bolts. δ_{max} is the displacement at the tip of the beam, which corresponds to the maximum strength. Applied load P versus displacement δ at the tip of the beam relationship of each specimen is shown in Fig.7.

About the specimen N-W brittle fracture of the beam flange close to the welded part occurred at the ultimate stage of loading. About each specimen using Paddle Bolts, fracture of tension side Paddle Bolt occurred at the ultimate stage of loading. At the specimen SS-A considerable large local deformation was observed at the bolted part of the column. At the another specimen such local deformation was not so evident. About the specimen CS-B,CC-B and CCR-B slight local buckling occurred at the compression side flange of the beam at the ultimate stage of loading. The states of fracture of Paddle Bolts are shown in Photo 1.

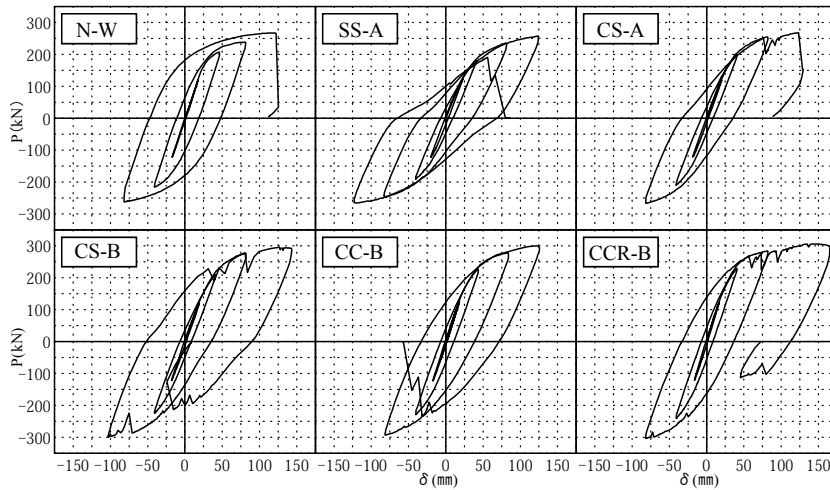


Fig.7 P- δ Relationship of Each Specimen



(SS-A)



(CS-B)

Photo 1 Fracture of Paddle Bolts

Table 3 Main Test Results

Specimen	Pmax(kN)	Py(kN)	δ max(mm)	α	Fracture Mode
N-W	268	186	126	1.22	* 1
SS-A	265	176	124	0.98	* 2
CS-A	268	206	130	0.99	* 2
CS-B	299	235	143	1.04	* 2
CC-B	301	242	126	1.11	* 2
CCR-B	306	253	165	1.13	* 2

* 1: brittle fracture of beam flange

* 2: break at the thread of tension side bolt

4. Investigation

4.1 Restoring force characteristics

Initial rigidity of each specimen and its ratio to that of specimen N-W is shown in Table 4. P- δ relationship of each specimen at the elastic range is shown in Fig.8. Judging from those Table and Figure specimen SS-A has initial rigidity of nearly 80% of that of the specimen N-W. About the specimen CS-A and CS-B the reduction of initial rigidity is less than 10% of that of specimen N-W. About the specimen CC-B and CCR-B initial rigidity is larger than that of the specimen N-W. It means that the reinforcement applied to the specimen CS-A and CS-B is almost effective and that of CC-B and CCR-B is effective enough.

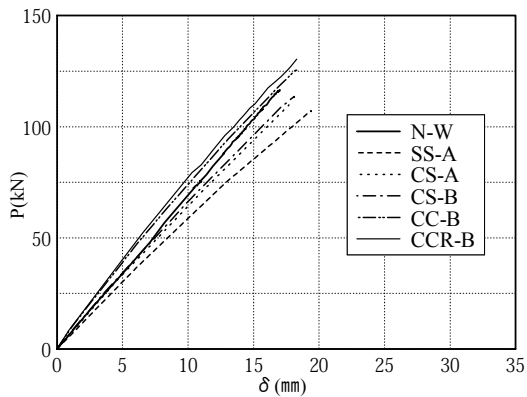


Fig.8 P- δ Relationship at Elastic Range

Table 4 Initial Rigidity of Each Specimen

Specimen	K(kN/mm)	K/ K_{N-W}
N-W	6.77	1.00
SS-A	5.65	0.83
CS-A	6.14	0.91
CS-B	6.24	0.92
CC-B	7.08	1.05
CCR-B	7.45	1.10

The skeleton curve obtained from P- δ relationship of each specimen about positive loading side is shown in Fig.9. From this Figure the difference between reinforcement at the connection and the difference between strength of Paddle Bolts become clear. The specimen N-W shows the largest deformation until failure. About the specimen SS-A initial rigidity, yield strength and plastic deformation until failure are clearly smaller than that of specimen N-W. About the specimen CS-A initial rigidity and yield strength are almost same to those of specimen N-W but plastic deformation until failure is almost half of that of specimen N-W. About the specimens using stronger Paddle Bolts, those are CS-B, CC-B and CCR-B, initial rigidity is almost same, yield strength and maximum strength are clearly large and plastic deformation until failure is nearly 2/3 in comparison with those of specimen N-W. Total absorbed energy of those specimens is

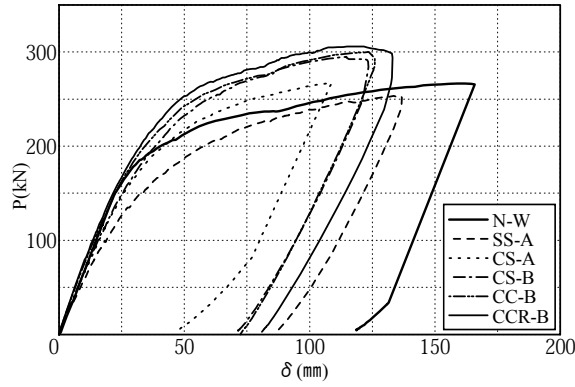


Fig. 9 Skeleton Curve of Each Specimen

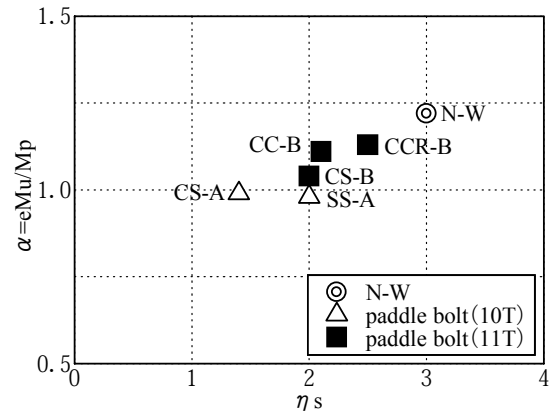


Fig.10 α - η_s Relationship

almost same to that of specimen N-W. It means that the synthetic static behavior of those specimens is almost same of that of specimen N-W. It means that the synthetic static behavior of those specimens is almost same of that of specimen N-W.

Fig.10 shows the relationship between maximum strength factor α and accumulated plastic deformation ratio η_s . η_s is calculated as $W_s/cP_p\delta_p$, where W_s is the total absorbed energy obtain from skeleton curve. From this Figure tendency of increasing α and η_s of specimen using stronger Paddle Bolts and better condition of the reinforcement at the bolted part of column is observed.

4.2 Local deformation at the bolted part

Fig.11 shows the strain distribution at the bolted part of reinforcing plate, which was attached to column surface. This Figure corresponds to the second loading cycle. The location of strain gage is shown in Fig.12. It is very clear that the strain at the line of bolts only shows very large value. It means that the local deformation at the connection is restricted only at the bolted part. The local deformation of this part is much different between each specimen, that means the efficiency of the reinforcement applied to each specimen is much different between each other.

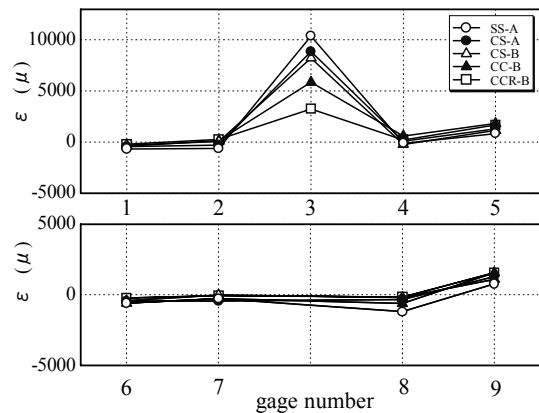


Fig.11 Strain Distribution at the Bolted Part

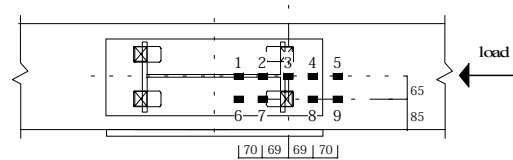


Fig.12 Location of Strain Gages

4.3 Estimation of maximum strength

From Table 3 it becomes clear that the maximum strength factor α of the specimens using Paddle Bolts are clearly smaller than that of the specimen N-W. At the original design of the

connections of specimens using Paddle Bolts it is assumed simply that bolts carry only the couple due to the applied bending moment. In such case the calculated maximum strength cP_{u1} of each specimen is large enough as shown in Table 5. The ratio of P_{max}/cP_{u1} is 0.74-0.79. That means more accurate estimation about the maximum strength of this type connection must be required. Observing from the detail of the beam end connection using Paddle Bolts, it is clear that the effect of secondary bending moment due to shear force, which is carried by the bolts, is considerably large, because the web of the beam did not connected to the column. In order to consider this effect the following assumptions are adopted.

- 1) The shear forces carried by tension side bolts P_1 and compression side bolts P_2 are decided in consideration of the deformation of those bolts due to shear forces (see Fig13).
- 2) The secondary bending moment occurred by the shear force is assumed to be same as the fixed end moment due to the compulsive vertical deformation of a both end fixed beam as shown in Fig.14. The span length of this beam is assumed to be the length between the end of nut and the loading point of the shear force.
- 3) The loading point of the shear force P_1 is the outside of the nuts, which connect the Paddle Bolts and flange of the beam. The loading point of the shear force P_2 is the end of the beam as shown in Fig 13.

Based on those assumptions the ratio of P_2 to P_1 is calculated $1.95(=(100/80)^3)$ about the specimens -A) or $2.24(=(85/65)^3)$ about the specimens -B).

Table 5 Calculated Maximum Strength cP_{u1}

Specimen	ℓ (mm)	h(mm)	P_{max} (kN)	cP_{u1} (kN)	P_{max}/cP_{u1}
SS-A	2132	418	264	355	0.74
CS-A	2132	418	268	355	0.75
CS-B	2117	418	298	385	0.77
CC-B	2117	418	300	385	0.78
CCR-B	2117	418	306	385	0.79

ℓ : Distance between loading point and end of Paddle Bolt (see Fig.13)

h : Distance between the center of both side Paddle Bolt (see Fig.13)

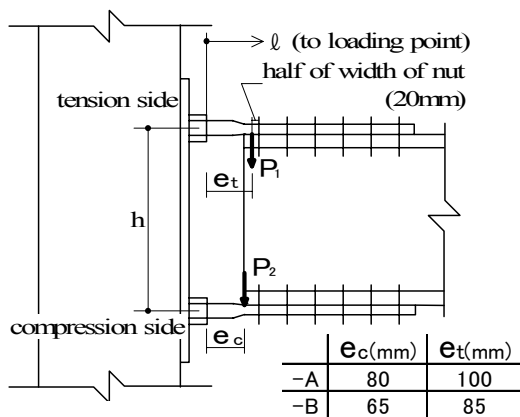


Fig.13 Assumption of Loading Point of Shear Force

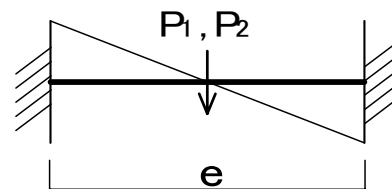


Fig.14 Assumption of Moment Distribution at P. Bolt

Table 6 Calculated Maximum Strength cP_{u2}

Carrying Ratio of Shear Load	cP_{u2} (kN)		P_{max}/cP_{u2}				
	-A	-B	SS-A	CS-A	CS-B	CC-B	CCR-B
$P_1=1/3, P_2=2/3$	239	276	1.10	1.12	1.08	1.09	1.11
$P_1=1/4, P_2=3/4$	260	298	1.01	1.03	1.00	1.01	1.03
$P_1=1/5, P_2=4/5$	275	312	0.96	0.97	0.96	0.96	0.98

In order to certify above mentioned thinking about the effect of secondary bending moment, maximum strength of each specimen cP_{u2} is calculated based on this thinking and is shown in Table 6. In this calculation the ratio of P_1 to P_2 is assumed simply 1:2, 1:3 and 1:4, considering small change of above mentioned condition. Judging from the results of this calculation the shear load carrying ratio of P_1 to P_2 is assumed to be 1:3 most appropriately and this results is considered to be almost proper.

4.4 Yield Strength of the Specimens

Yield strength of the specimen SS-A and CS-A was considered to be influenced by local deformation of the bolted part of the column. About another specimen yield strength was decided by yielding of the beam. About yield strength of those specimens the effect of secondary bending moment due to the shear force could not be observed, because yield ratio of Paddle Bolt is very high and such effect is covered by its elastic behavior at the loading stage of yielding of the beam.

5. Conclusions

In order to investigate the applicability of WF beam-to-SHS column connections using Paddle Bolts, experimental study was executed using full scale specimens. From this study following items become clear.

- 1) Main static characteristics such as initial rigidity, yield strength and plastic deformation ability of this type beam-to-column connections are clearly influenced by the detail of reinforcement at the bolted parts of column surface and the shape of bolt holes. In case the reinforcement is adequate the static characteristics of such connections are almost same as those of usual welded moment resisting beam-to-column connections.
- 2) The maximum strength of this type connection, which is decided by the fracture of the bolts, is greatly influenced by the effect of secondary bending moment due to the shear forces carried by the bolts. Such effect is estimated precisely and easily by simple assumptions.
- 3) The yield strength of this type connection is basically decided by the yielding of the beam in case reinforcement of the bolted part is appropriately. At this stage of loading the effect of secondary bending moment to the bolts due to shear force is not shown, because yield ratio of Paddle Bolt is very high.

PR COMPOSITE JOINTS UNDER CYCLIC AND DYNAMIC LOADING CONDITIONS: A COMPONENT MODELING APPROACH

G.A. Rassati and S. Noè
Department of Civil Engineering, University of Trieste
Trieste, Italy

Roberto T. Leon
School of Civil and Environmental Engineering, Georgia Tech
Atlanta, Georgia, USA

ABSTRACT

This paper presents a mechanical model suitable for the simulation of partially restrained (PR) connections subjected to monotonic and cyclic loads. The model is capable of simulating the behavior of a PR composite joint subjected to a generic load history, taking in account the influence of all the main components, including slip of the bolts, shear deformation of the panel zone and cracking in the slab. The model is also capable of determining the amount of energy dissipated by local plasticification in the various components, and thus allows an evaluation of their relative importance in the post-elastic behavior of the connection. For validation of the model, comparisons to the results of several experiments are discussed. These results show that the model is capable of tracking the main behavioral aspects observed in the tests, and provides very good quantitative fit to the experimental results.

INTRODUCTION

Steel-concrete composite PR frames can significantly enhance both the structural and the economical efficiency of office and commercial multi-story buildings, when compared to the more traditional steel or concrete solutions. Furthermore, it is possible to achieve an “engineering optimization” by incorporating the actual joint response into the analysis and design procedures (1, 2, 3), even in seismic zones. Partially restrained composite frames are in fact suitable for buildings in moderate seismic zones, and their use is explicitly mentioned in recent design codes (4, 5). Existing research (6, 7, 8, 9) demonstrates that PR, or semi-rigid, steel and/or composite frames can provide equal or better seismic performance when compared to their fully rigid counterparts. This is mainly due to the decrease of the natural frequency of the structure, which causes a corresponding decrease of the seismic forces. In addition, the PR connections, if correctly designed, can provide both ductility and a non-degrading hysteretic behavior under cyclic reversal loading. However, particular attention should be paid to the effects of the higher modes in the design of PR frames, which are usually neglected in the design of ‘conventional’ frames.

In order to make allowance for PR connection behavior, it is necessary to incorporate the actual joint response in the analysis and the design. This means that for the partially restrained frame design, a different modeling approach than that used for rigid frames is necessary. Three main categories of connection models can be identified: mathematical models based on curve-fitting to test results, 2D and 3D finite element models, and simplified mechanical models. Each of the different techniques of modeling the actual response of the connections has its advantages and drawbacks. Models based on curve-fitting are generally not recommended because they require extrapolation of numerous parameters and the database for any particular type of joint is rather small (10). The use of analytical models implies the acceptance of semi-empirical coefficients and formulations, in order to understand and explain such complex phenomena, thus losing in overall generality (11, 12, 13). Obviously, the more accurate way to model the actual behavior of a joint is by means of a thorough finite element idealization. This is very expensive in terms of time and effort, and is therefore not suitable for a design procedure (14, 15, 16). Moreover, a finite element analysis provides a large amount of local behavior data, from which it is difficult to identify trends in a global sense. Somewhere between the mathematical models and the finite elements methods lies the mechanical modeling approach. It inherits the characteristics of simplicity from the analytical methods, without directly depending on the experimental assessment of the connection characteristics. At the same time, the mechanical modeling approach works in an environment similar to the classic finite elements analyses, but provides a more focused set of results. The increase in calculation capacity in the modern personal computers has made this latter method the most applied in the recent years (3, 17, 18, 19).

This paper presents the development of a generic mechanical model suitable for the simulation of PR connections subjected to monotonic and cyclic loads. The model is capable of simulating the behavior of a partially restrained composite joint subjected to a generic load history, taking in account the influence of all the main components, including slip of the bolts, shear deformation of the panel zone and cracking in the slab. The model will be described first, and will be followed by a series of illustrative comparisons between its performance and published experimental data.

THE TRS1 MODEL

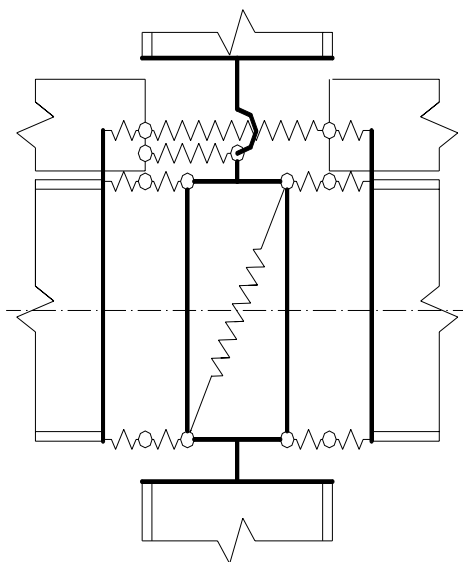


Figure 1 – The IBK model.

A robust mechanical model, shown in Figure 1, and known as the IBK model was developed by a team led by Tschemmerneegg (17, 20, 21, 22). This model has been validated by means of a thorough experimental program. This model is suitable for the simulation of cruciform joints under unbalanced negative (hogging) moments, but no provisions were made to allow for positive (sagging) or in general cyclically variable moments.

Based on the IBK model, and on the provisions of the Annexes J of both Eurocodes 3 and 4, a similar joint model that features full allowance for cyclic reversal loading has been implemented recently (19). The model, shown in Fig. 2, has been implemented

as a sort of super-element in a commercial finite element program, ABAQUS (23), by merging some user-defined elements. Overall, every cruciform beam-to-column joint consists of 25 nodes, 14 axial spring elements and 16 kinematic constraints.

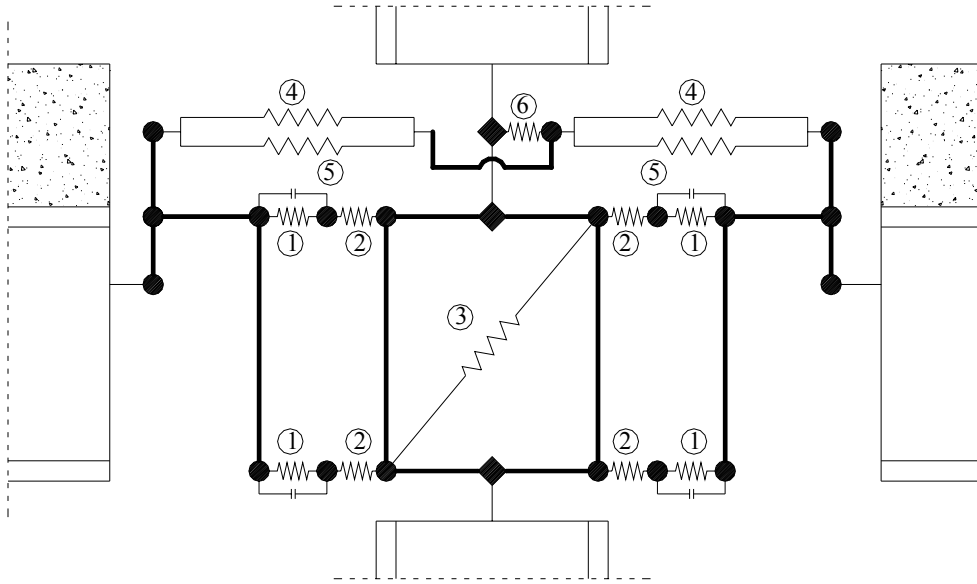


Figure 2 – The TRS1 model.

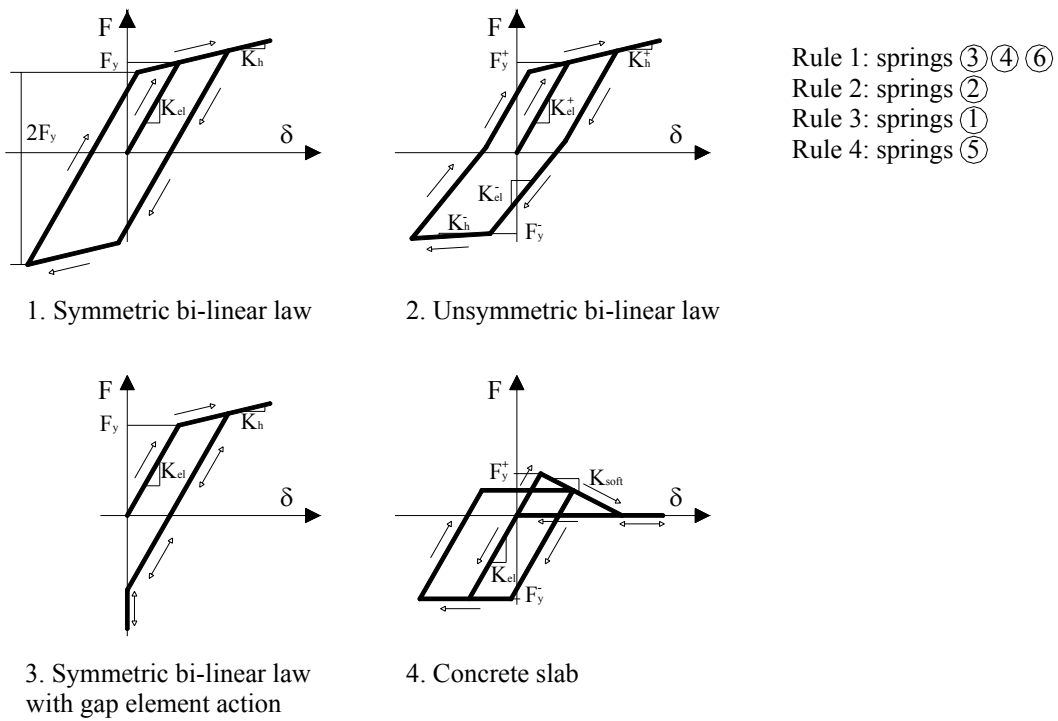


Figure 3 – Constitutive laws for the TRS1 model.

The constitutive laws for every spring have been derived basing on Eurocodes 3 and 4, as shown in Table 1. They are basically bi-linear elasto-plastic relationships with 5% hardening branches. Every rule has been derived and adapted to the cyclic case based on Tschemmernegg's monotonic rules, with two additions that were required to extend the model into the cyclic range: (a) the constitutive laws for the top and bottom steel connections do not allow a shortening with respect to the original length of the components; and (2) the deformation rules for the concrete slab that take into account the tension stiffening effect after the cracking has occurred in tension by means of a softening branch in the constitutive laws. The length of the spring to simulate slab effects has been chosen by taking into account the dimension of the portion of the composite beam in which the plane section hypothesis is not valid. A schematic representation of the constitutive laws for the elements is shown in Fig. 3. The most interesting component in the model is the so-called 'redirection' spring: this component accounts for the behavior of the concrete slab immediately outside and between the column flanges under unbalanced moments. In this case, the slab tends to bear on the outside of one flange and on the inside of the opposite one, while it tends to shift away from the column on the other side of the joint. This mechanism is quite complex, as the behavior of the redirection spring requires that account be taken of:

- the effective width of the slab directly interacting with the column;
- the behavior under compression of the column web
- the flexural behavior of the column flanges
- the variation of the bearing surface of the slab on the column flanges at the increase of the bending deformation of these.

Stiffness	EC3 – ANNEX JJ	EC4 –ANNEX J
Column web panel – compression	J.4.4 (1) (b)	J.4.4 (2)
Column web panel – shear	J.4.4 (1)	-
Column web panel – tension	J.4.4 (1)	
Steel connection - compression	J.4.4 (3)	
Steel connection - tension	J.4.4 (1)	
Slab rebars		J.4.4 (2)
Redirection		J.4.4 (2)

Strength	EC3 – ANNEX JJ	EC4 –ANNEX J
Column web panel – compression	J.3.5.3	J.3.5.3
Column web panel – shear	J.3.5.2	-
Column web panel – tension	J.3.5.6	
Steel connection - compression	J.3.5.4	
Steel connection - tension	J.3.5.5,7,8,9	
Slab rebars		J.3.5.5
Redirection		J.6.1, J.6.2

Table 1 – EC3 and EC4 clauses used for strength and stiffness evaluation.

For the evaluation of this component's characteristics, the proposed model has used the work referenced in the Eurocodes (2, 3), Tschemmernegg's work (22), and particularly the work of Bernuzzi and Menapace (24).

The only important mechanism that has been neglected in the implementation of this model is the slip between the concrete slab and the steel girder. It will be shown later that in the cases in

which that mechanism does not significantly affect the overall behavior of the joint, the model is capable to predict behavior with satisfactory accuracy. Work is underway to add this feature to the model, but as it stands, the model is unsuitable to simulate the behavior of joints and frames in which the shear slip is important (i.e., in presence of joints of columns to short girders). An interesting feature that has been added later in the numerical implementation of the model is the energy evaluation capability of every spring representing a deformation component of the connection. This helps identify which of the connection components needs more careful detailing, keeping in mind the energy dissipation requirements. In the next section, some validation simulations will be presented, as well as some of the analyses conducted in the past using the TRS1 model.

ANALYSES USING THE TRS1 MODEL

As a first step for the validation of the TRS1 model, simulations have been carried out in order to reproduce a series of experimental tests on cruciform specimens conducted at the University of Trieste (Benussi et al., 1995). The specimens were steel-concrete PR, isolated joints in a cruciform setup. For the sake of brevity, reference will be made only to the CT1C specimen (Fig. 4); simulations have been carried out for other specimens as well, with comparable results. Global results for specimen CT1C are shown in Figs. 5. The values of stiffness and strength for each component were derived according to the guidelines in Table 1 and following the constitutive laws shown in Fig. 3. The specimens were subjected to the ECCS 'short' procedure (ECCS, 1992), implying a symmetrical load history of beam end displacements. Note that due to the symmetry of the loading, the influence of the redirection spring and of the spring simulating the shear deformability of the column web panel is negligible. The comparisons between experimental and numerical moment-rotation show reasonably good agreement. From the moment-rotation diagram (Fig. 5), it is noticeable that the model overestimated both the positive and negative moments.

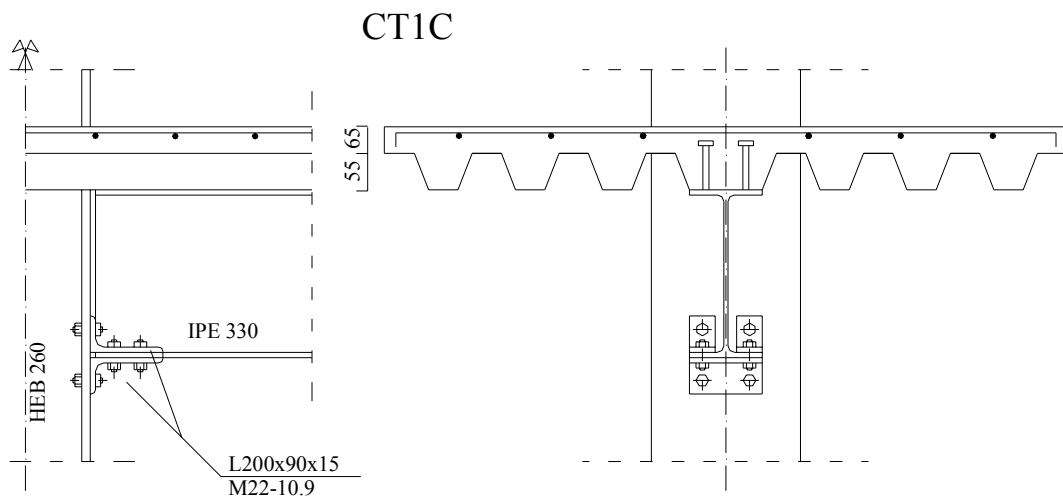


Figure 4 – The CT1C joint specimen.

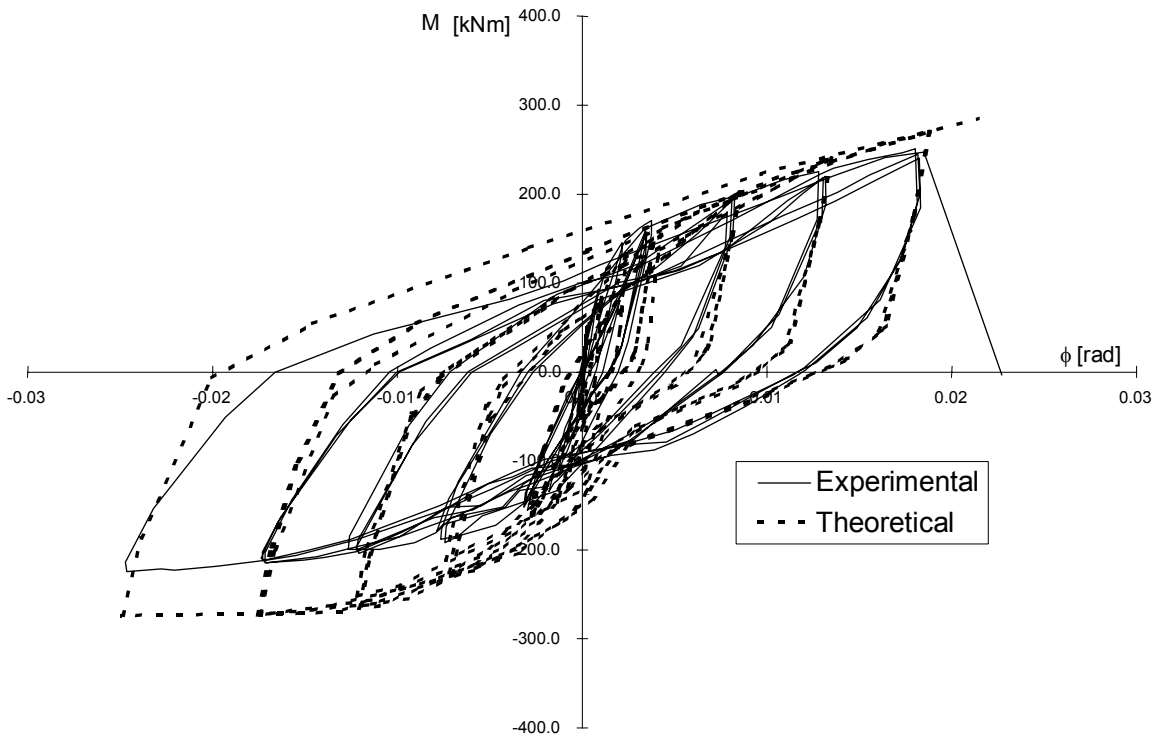


Figure 5 – Moment-rotation comparison for the left beam of CT1C.

In the positive moment region, the overestimation is slight, and the agreement between the experimental and calculated ultimate forces, and the elastic loading and unloading stiffness can be considered satisfactory. The simulation bounds well the pinching behavior, slightly overestimating what could be considered the yielding force. However, in the negative moment zone, the predicted ultimate load is definitely unsatisfactory. This is due primarily to the overestimation of the yield force and the underestimation of the hardening stiffness of some of the key components.

As seen from the initial comparisons to specimen CT1C, the model still needed some further calibration of the individual springs, but the model showed great potential to provide a closer look at the behavior of the single components of the joint during the cyclic loading. Further details about the CTx C simulations are given in (Rassati, 1997).

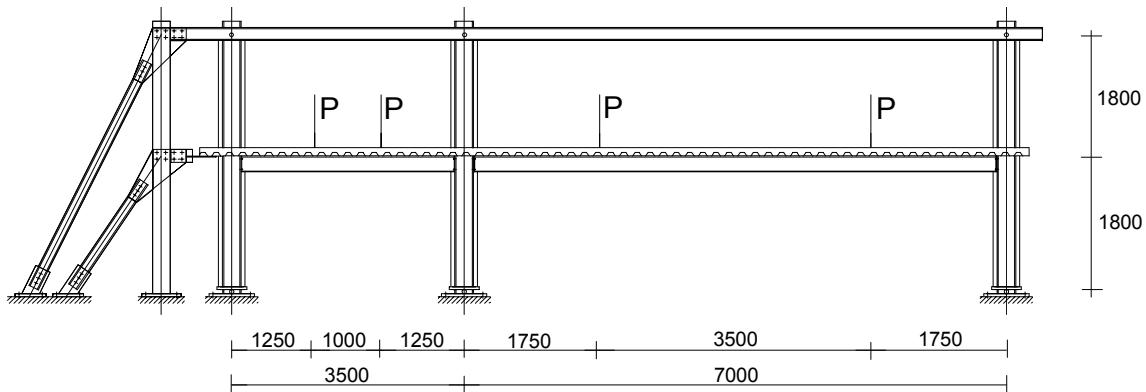


Figure 6 – Details of the UCS frame.

The next step in the model validation was the simulation of a cyclic, non-reversal loading test on two different sub-frames (Benussi et al., 1995; Noè, 1995). Both sub-frames were one-story, two-bays setups. One (specimen SCS) had a symmetric configuration (two equal span length of 5 m), while the other (specimen UCS) had a shorter left span (3.5 m) than the right one (7 m). Figs. 6 and 7 show details of the frames. The same materials and steel sections were used for both specimens. The load history was a monotonic ramp with two unloading cycles to check for the possible stiffness degradation.

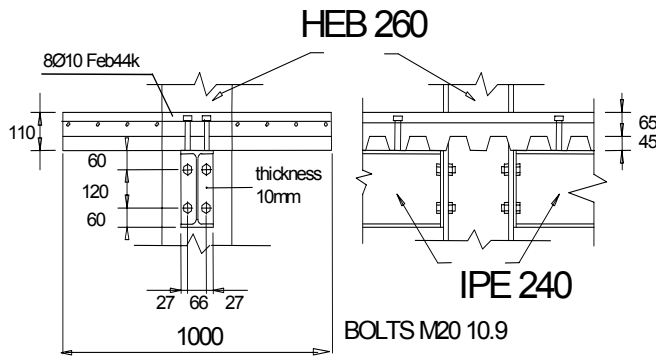
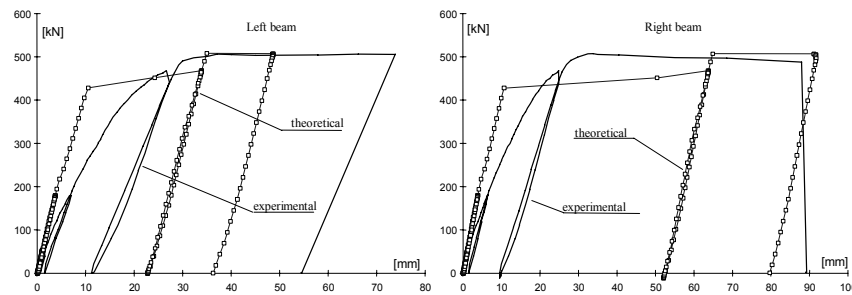
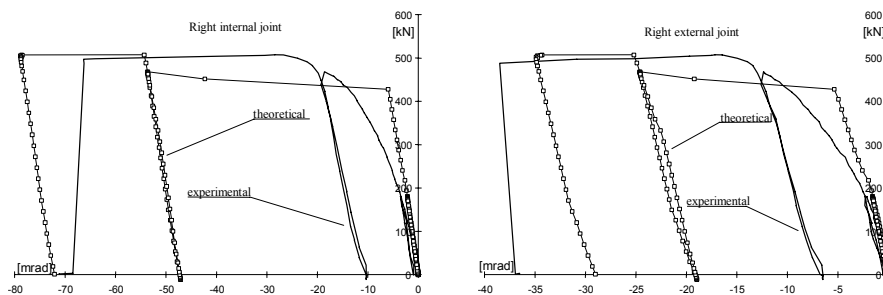


Figure 7 – Details of the UCS connection.

For the model, the TRS1 model was used, along with two-node cubic beam elements for the composite beams and columns. In addition, plastic hinge elements were inserted in correspondence to the load introduction sections on the beams. The latter was necessary to take into account that collapse mechanism, which was observed in the experiments. It is important to point out again the absence of a 'slip' spring in the TRS1 model. In cases like the UCS sub-frame, with its short span, the approximation could not be acceptable anymore.

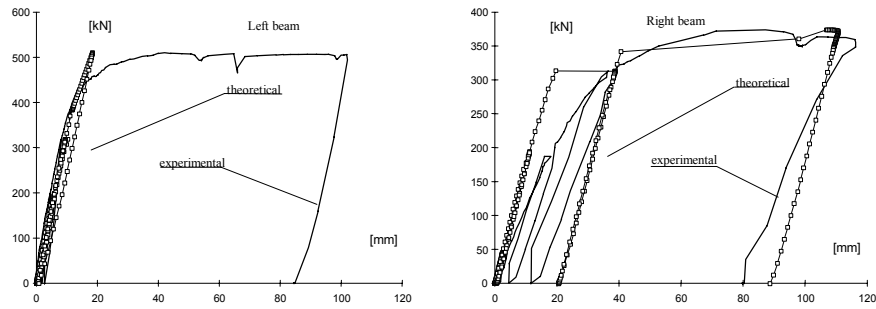


Figures 8a,b – SCS frame load-midspan displacements for left and right beams

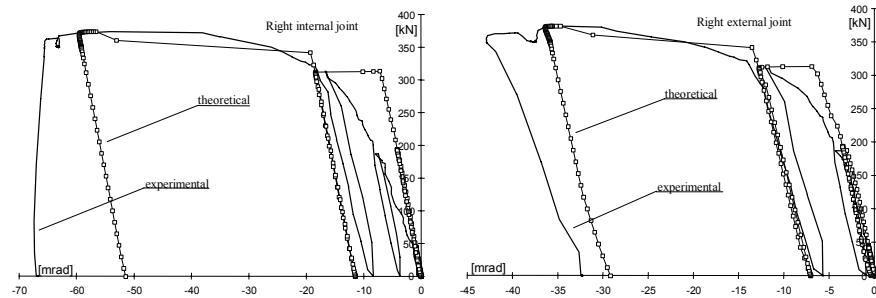


Figures 9a,b – SCS frame moment-rotation curves for internal and external joints

For the SCS frame, Figs. 8(a) and (b) show the load-midspan displacement for the left and right beam, respectively. It should be pointed out that some of the discrepancies shown in these figures between the predicted and measured values may be the result of how the loads are applied to the model. The comparisons of the ultimate rotations and deflections are particularly sensitive as to whether a load or displacement history is used. For these analyses, the loading



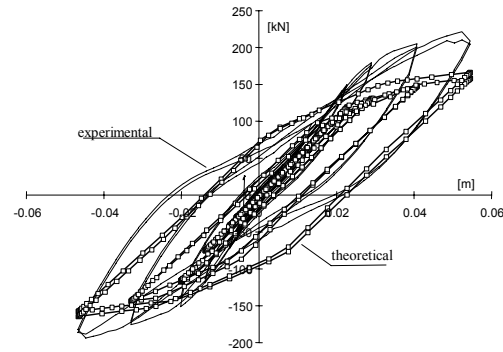
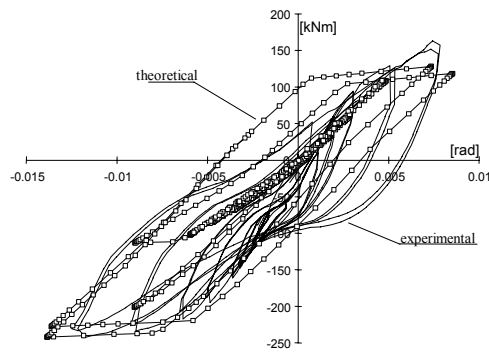
Figures 10a,b – UCS frame load-midspan displacements for left and right beams



Figures 11a,b – UCS frame moment-rotation curves for internal and external joints

measured on the real structure was applied on the model. When large inelastic effects occur and relative low hardening stiffness are used, a small discrepancy in the loading values may result in big differences in the rotations or displacements. Irrespective of this, the initial stiffness was predicted with good accuracy, as well as yielding and ultimate loads. For the SCS frame, the overall results of the simulation are fairly good also for the moment-rotation curves (Figs. 9(a) and (b), especially when looking at the extreme simplicity of the constitutive laws used. The results of the UCS frame, on the other hand, were not as good, as shown in Figs. 10 and 11. While the simulation of the behavior of the long (right) beam is as good as the for the SCS frame, the prediction of the behavior for the left (short) beam is unsatisfactory because the model neglects the shear slip between the beam and slab. Further details on these simulations are found in (19).

A further step in the validation of the TRS1 model was the modeling of a more complete specimen, subjected to cyclic loading. For this purpose the sub-frame tested by Leon et al. (1987), was modeled. The results are shown in Fig. 12 for a model with identical characteristics as that used for the simulations of specimen CT1C. Fig. 12(a) shows the moment-rotation diagram for the external left joint of the SRCF2C, and indicates that the calculated positive and negative ultimate moments are close to the experimental ones. In fact, the negative moment is predicted almost exactly, while the positive one is slightly underestimated. The elastic initial stiffness prediction is reasonably good, but not so the unloading stiffness. As for the rotations, the simulation results are fairly close to the experimental values. Even better results were obtained for the overall force-displacement diagram (Fig. 12(b)). Except for a slight underestimation of the positive force, probably due to an excessive flexibility of some steel component the calculated diagram appear to follow quite closely the experimental one. In comparison to the CT1C simulation discussed above, the SRCF2C frame simulation shows the influence of the 'redirection' and of the 'panel zone in shear' springs due to the asymmetry of the loading. This is an early evidence on how the slab behavior in the vicinity of the column can influence the overall behavior of the joint.



Figures 12a,b – SRCF2C frame moment-rotation and load-displacement sample curves

CONCLUSIONS

Even if the TRS1 model showed some drawbacks, some of them due to uncertainties in the springs characteristics (e.g. ‘redirection’ spring, concrete spring), some due to the neglecting of determinant behaviors in the connections, it demonstrated capable of simulating in a reasonably accurate fashion the behavior not only of the single connection but also of the whole structures involved. At this point, a new feature has been added to the model, i.e. the energy evaluation algorithms. In this way, the informations provided to the designer for each single component increase in detail, and it becomes possible to find out which component is the main source of energy dissipation in the connection, i.e. which one needs particular attention in detailing due to its importance in the overall behavior.

REFERENCES

1. ECCS (European Convention for Constructional Steelwork), 1992, *Recommended Testing procedure for assessing the behaviour of structural steel under cyclic loads*
2. CEN (European Committee for Standardization), 1994a, *ENV 1993-1-1 Eurocode 3: Design of Steel Structures – Part 1: General Rules and Rules for Buildings*
3. CEN (European Committee for Standardization), 1994b, *ENV 1994-1-1 Eurocode 4 - Design of Composite Steel and Concrete Structures: Part 1.1: General Rules and Rules for Buildings*
4. NEHRP (National Earthquake Hazard Reduction Program), 1998, *Recommended Provisions for Seismic Regulations for New Buildings and Other Structures*, FEMA 302, February
5. AISC (American Institute for Steel Construction), 1997, *LRFD Manuals*, Vol. 1 and 2
6. Mazzolani F.M., Piluso V., 1996, *Theory and Design of Seismic Resistant Steel Frames*, E.&F.N. SPON, Chapman & Hall
7. Leon R.T., Hoffman J.J., Staeger P.E., 1998, *Partially Restrained Composite Connections – A design guide*, Steel Design Guide Series, No. 8, AISC
8. ASCE (American Society of Civil Engineers), 1998, *Design Guide for Partially Restrained Composite Connections*, Journal of Structural Engineering, Vol. 124, No. 10, pp. 1099-1114
9. Chen W.F., Kishi N., 1987, *Moment-Rotation relation of Top and Seat Angle Connections*, Dept. Of Structural Engineering, Purdue University, Report CE-STR-87-4

10. Tschemmerneegg F., 1988, *On the nonlinear behaviour of joints in steel frames*, in *Connections in Steel Structures: Behaviour, Strength and Design* (ed. R. Bjorhovde et al.), Elsevier Applied Science Publishers, London, pp. 158-165
11. Noè S., Spanghero F., 1993, *Un modello del comportamento ciclico di giunti semi-rigidi composti* (in Italian), Giornate italiane della costruzione in acciaio, Viareggio (Italy)
12. White D.W., Chen W., 1995, Generalized models for semi-rigid connections, 3rd International Workshop on Connections in Steel Structures, Trento (Italy)
13. Amadio C., Puhali R., Zandonini R., 1989, *L'effetto della continuità parziale nei telai composti* (in Italian), Giornate italiane della costruzione in acciaio, Capri (Italy)
14. Aribert J.M., 1995, *Proposed clause J.4.5. in Annex J for EN1994-1-1*, COST meeting, Trento (Italy)
15. Rex C.O., Easterling W.S., 1995, *Finite element modeling of partially restrained beam-to-girder connections*, 3rd International Workshop on Connections in Steel Structures, Trento (Italy)
16. Tschemmerneegg F., Brugger R., Hittenberger R., Wiesholzer J., Huter M., Schaur B.C., Badran M.Z., 1994, *Zur Nachgiebigkeit der Verbundknoten* (in German), Stahlbau, Vol. 63, No. 12, pp. 380-387
17. Tschemmerneegg F., Queiroz G., 1995, *Mechanical modeling of semi-rigid joints for the analysis of framed steel and composite structures*, 3rd International Workshop on Connections in Steel Structures, Trento (Italy)
18. Benussi F., Noè S., Rassati G.A., 1997, *Components modeling of semi-rigid joints in composite frames under monotonic and cyclic loadings* (in Italian, English abstract), Giornate italiane della costruzione in acciaio, Abano Terme (Italy)
19. Tschemmerneegg F., Brugger R., Hittenberger R., Wiesholzer J., Huter M., Schaur B.C., Badran M.Z., 1995a, *Semi-rigid composite joints*, Technical paper T1, COST meeting, Trento (Italy)
20. Tschemmerneegg F., Frenkel V., Pavlov A.B., 1995b, *Comparison between test results and proposal for EC4-Annex J (panel zone of a composite joint)*, COST meeting, Trento (Italy)
21. Tschemmerneegg F., Huber G., 1995a, *Compression region in the panel zone of a composite joint*, Technical paper T2, COST meeting, Trento (Italy)
22. Tschemmerneegg F., Huber G., 1995b, *Shear region in the panel zone of a composite joint*, Technical paper T3, COST meeting, Trento (Italy)
23. Huber G., Tschemmerneegg F., 1998, *Modelling of beam-to-column joints*, Journal of Constructional Steel Research, Vol. 45, No. 2, pp. 199-216
24. Hibbitt, Karlsson & Sorensen, 1998, *ABAQUS 5.8 Standard User's Manual*, Vol. 1,2,3
25. Bernuzzi C., Menapace R., 1997, *Modellazione in campo ciclico di giunti trave-colonna per strutture composte in acciaio e calcestruzzo* (in Italian), Tesi di laurea, Università di Trento

EVALUATION OF DUCTILITY IN STEEL AND COMPOSITE BEAM-TO-COLUMN JOINTS: ANALYTICAL EVALUATION

Luís Simões da Silva^a, Luís Calado^b, Rui Simões^a, Ana Girão Coelho^c

^a Civil Engineering Department, Universidade de Coimbra, Coimbra, Portugal

^b Civil Engineering Department, Instituto Superior Técnico, Lisboa, Portugal

^c Civil Engineering Department, Instituto Superior de Engenharia de Coimbra, Coimbra, Portugal

Abstract

The current trend towards the use of partial strength, semi-rigid joints requires that enough ductility (rotation) is available, and thus the prediction of the full (non-linear) moment-rotation response of the joint. The component method currently provides independent procedures to evaluate the strength and initial stiffness of steel and composite joints. A unified, closed-form, analytical approach is presented in this paper that gives the full non-linear moment-rotation response of steel and composite joints, and, consequently, its strength, initial stiffness and maximum rotation.

1 INTRODUCTION

The current trend towards the use of partial strength, semi-rigid joints requires that enough ductility (rotation) is available, and thus the evaluation of the full (non-linear) moment-rotation response of the joint. The component method, currently widely accepted as the practical approach at predicting the behaviour of such joints (1), provides independent procedures to evaluate the strength and initial stiffness of steel and composite joints. These procedures, already incorporated in codes of practice (2, 3), were shown to reproduce satisfactorily these properties, while maintaining a relative ease of application.

The evaluation of ductility presents two added difficulties, when compared to strength and initial stiffness:

- (i) knowledge of the non-linear force-deformation response of each component;
- (ii) knowledge of the full (non-linear) moment-rotation response of the joint.

The first item still remains quite unexplored in the literature, most of the research effort being directed in the past towards the consistent evaluation of strength and initial stiffness of the various components (4); the second involves iterative numerical procedures, given that phenomena such as plasticity and instability are necessarily present.

Assuming that the non-linear behavior of the components is known, a unified, closed-form, analytical approach is presented in this paper that gives the full non-linear moment-rotation response of steel and composite joints, and, consequently, its strength, initial stiffness and maximum rotation. Also, the yielding sequence of the various components is identified.

2 EVALUATION OF DUCTILITY

2.1 Component characterisation

As stated above, a key aspect to the component method relates to the characterisation of the force-deformation curves for each individual extensional spring. In practical terms, the non-linear force-deformation curve may be approximated by several idealisations (5), as shown in Figure 1. Common to all is the identification of four sets of properties, namely elastic stiffness (k_e), post-limit stiffness (k_p), limit load ($F^C = P^B/2$) and limit displacement (Δ^f).

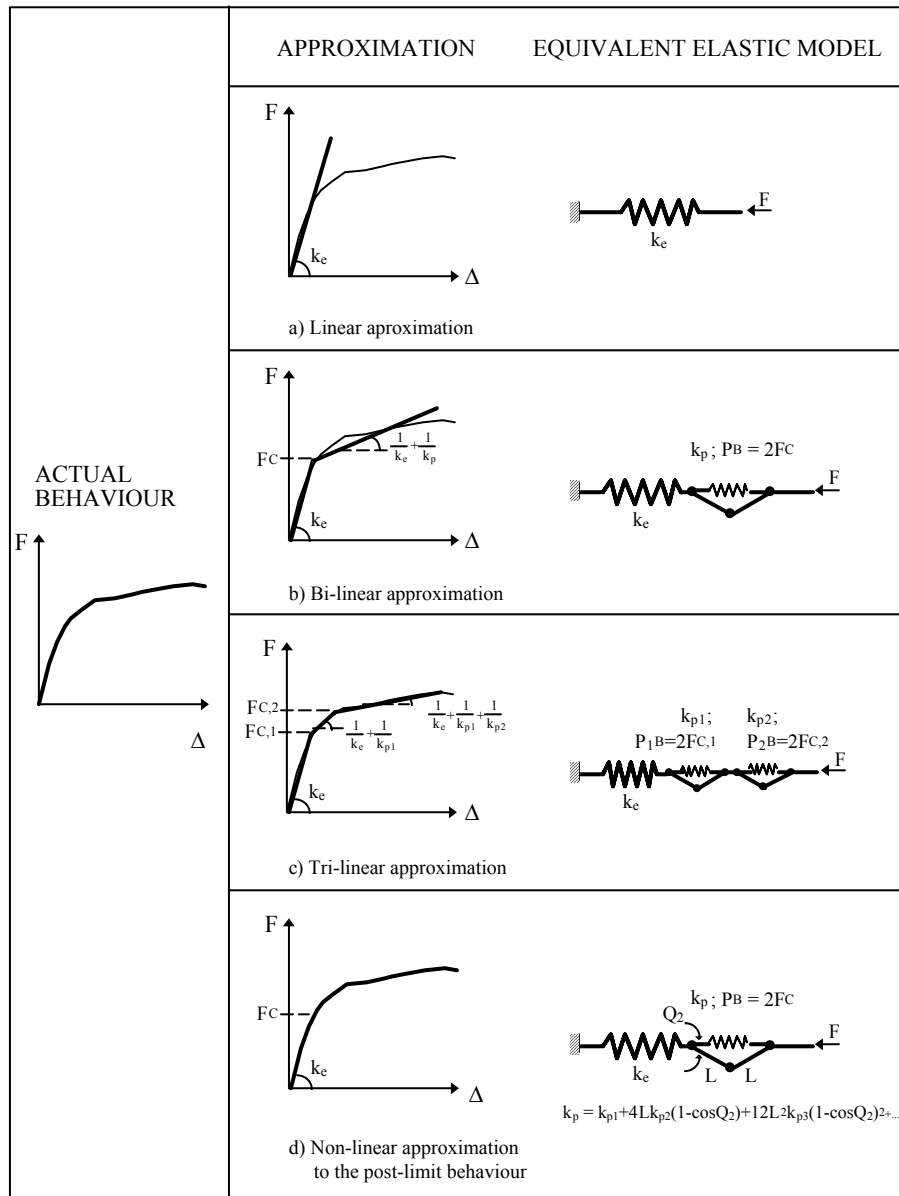


Fig. 1. Various idealisations of component force-deformation curves.

Following Kuhlmann *et al* (6), the various components may be classified according to ductility in three main groups: (a) components with high ductility, (b) components with limited ductility and

(c) components with brittle failure. Components with high ductility present a nearly unlimited deformation capacity, not imposing any bounds on the overall rotation ability of the joint, and include, for example: (i) column web panel in shear, (ii) end-plate in bending and (iii) column flange in bending. Components with limited ductility are characterised by a force-deformation curve exhibiting a limit point and a subsequent softening response, comprising: (iv) column web in tension and (v) column web in compression. Finally, components with brittle failure behave linearly until collapse, with very little deformation before failure, being adequately modelled with a linear approximation, typical examples being: (vi) bolts in tension, (vii) bolts in shear and (viii) welds.

2.2 Analytical models

To overcome the numerical complexity of the evaluation of the moment-rotation response of steel and composite joints, an equivalent elastic model was developed (7), able to yield closed-form analytical expressions. With reference to Figure 2, the proposed methodology (8) comprises the following steps, here illustrated for an extended end-plate steel joint:

- (i) for each bolt row in tension and shear and compression zones, association of all springs (components) in series into one single equivalent spring;
- (ii) association of all resulting tensile springs in parallel into an equivalent tensile spring
- (iii) application of the equivalent elastic model of Figure 2c, that yields identical results to the original elastic-plastic model of Figure 2b.

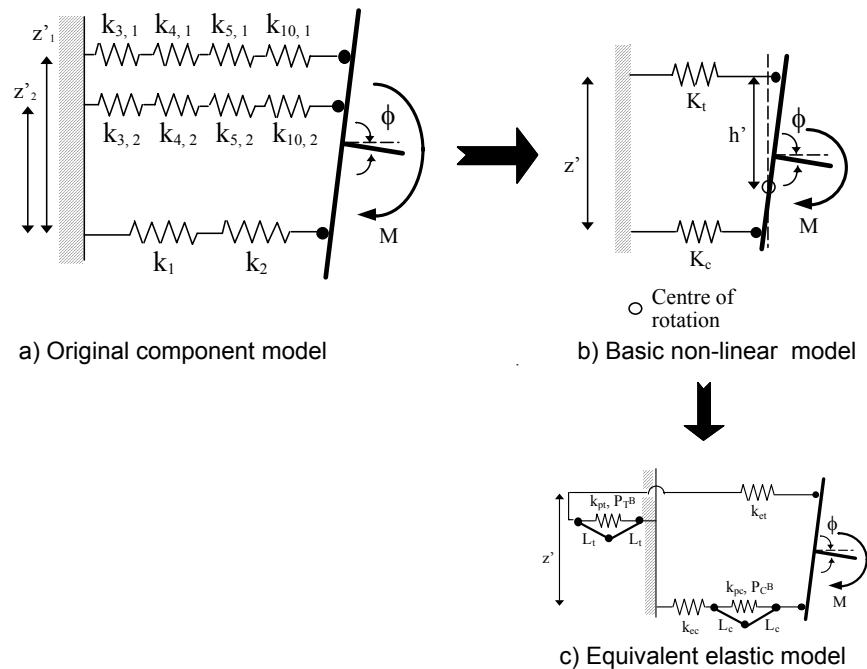


Fig. 2. General substitute model for steel joints.

As shown in Figure 1, both the spring transformations (series and parallel) and the equivalent elastic model require the choice of an adequate approximation for each resulting spring. Here, four possibilities are considered:

- (i) linear (L), the corresponding elastic model being simply an elastic spring with stiffness k_e ;
- (ii) bi-linear (BL), the post-limit stiffness being reproduced by an elastic spring with stiffness k_p and pre-compression $2F^C$;
- (iii) tri-linear (TL), with two post-limit branches characterised by stiffnesses k_{p1} and k_{p2} and corresponding pre-compressions $2F^{C1}$ and $2F^{C2}$;
- (iv) non-linear (NL), where the initial elastic part is followed by a polynomial non-linear branch given by:

$$k_p = k_{p1} + 4Lk_{p2}(1 - \cos q_2) + 12L^2k_{p3}(1 - \cos q_2)^2 \quad (1)$$

Next, the resulting equivalent elastic models are solved in the context of a post-buckling stability analysis using an energy formulation, further details of the mathematical derivation being found in (Z,8). With reference to Figure 3, two basic models are considered, for steel (Figure 3a) and composite (Figure 3b) joints, the latter case including a specific tensile row for the reinforcement (9).

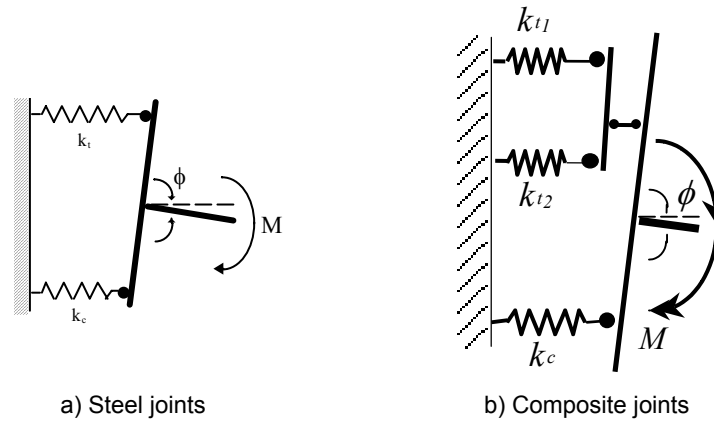


Fig. 3. Basic non-linear models.

For each case, several possibilities must be considered, corresponding to the various combinations of equivalent spring idealisations:

(a) Steel models

- (a.1) Model BL-BL: bi-linear idealisation of equivalent tensile and compressive/shear springs;
- (a.2) Model TL-BL: tri-linear idealisation of equivalent tensile spring and bi-linear idealisation of equivalent compressive/shear spring;
- (a.3) Model TL-NL: tri-linear idealisation of equivalent tensile spring and non-linear idealisation of equivalent compressive/shear spring;

(b) Composite models

- (b.1) Model BL-BL-BL: bi-linear idealisation of reinforcement, equivalent tensile and compressive/shear springs;
- (b.2) Model TL-BL-NL: tri-linear idealisation of reinforcement, bi-linear idealisation of equivalent tensile spring and non-linear idealisation of compressive/shear spring.

It is noted that all these combinations yield closed-form analytical solutions for the moment-rotation response of steel and composite joints that identify the yield rotation of all relevant levels of component deformation. Its application to typical examples of steel and composite joints is illustrated in the next section.

3 APPLICATION TO BEAM-TO-COLUMN JOINTS

3.1 Beam-to-Column Welded Steel Joint

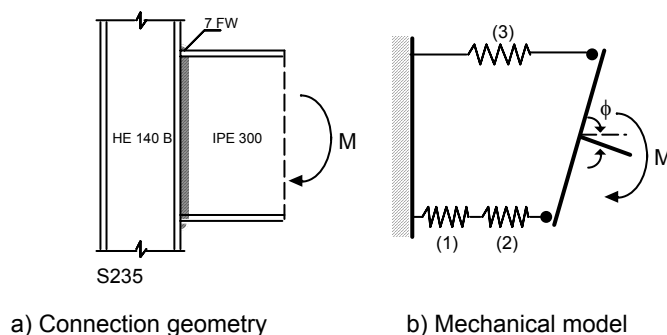


Fig. 4. Welded steel connection

In order to illustrate the application of the equivalent elastic models, one joint configuration was chosen from the database SERICON II (Klein 105.011) (10), corresponding to a welded beam-to-column steel joint, described in Figure 4, which was tested by Klein at the University of Innsbruck in 1985.

Component	F^C (kN)	k_e (kN/m)	k_p (kN/m)	\square^y (mm)
1	218.17	3.608×10^5	6.013×10^4	0.605
2	258.30	1.803×10^6	4.624×10^3	0.143
3	258.30	1.803×10^6	4.624×10^3	0.143

Table 1. Component characterisation

Figure 5 compares the experimental results with the analytical results, obtained using a bi-linear approximation for the components, the various stiffness and strength values being reproduced in Table 1.

Component	Component yielding sequence						Failure
	Absolute displacement \square_i (mm)			Relative displacement Δ_i / Δ_i^y			
1	-0.607	-1.372	-4.817	1.000	2.261	7.940	7.940
2	-0.121	-0.143	-38.640	0.847	1.000	269.798	269.798
3	0.121	0.143	38.640	0.847	1.000	269.798	269.798
	2.94	5.73	151.63	1.00	1.95	51.65	51.65
	Absolute joint rotation (mrad)			Joint ductility index			

Table 2. Ductility indexes for welded steel joint

The moment-rotation curve of Figure 5 shows yielding of the first component (column web panel in shear), followed by simultaneous yielding of the column web in compression and tension, at a joint rotation of about 0.006 radian. The ductile behavior of this joint is obvious, maximum rotation of 0.151 radians being reached without failure at the end of the test. Table 2 summarises the “yield” sequence of the various components and the corresponding levels of ductility.

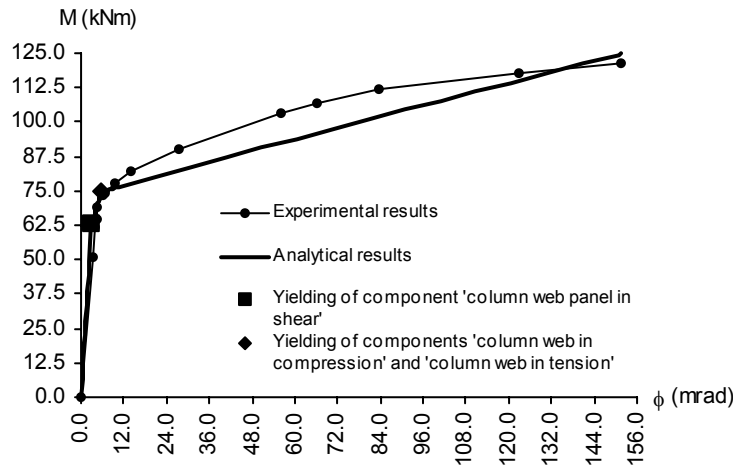


Fig. 5. Welded steel connection: moment-rotation curve (model BL-BL)

Figure 6 illustrates the application of two alternative models, TL-BL and TL-NL, using the same value of k_{p1} , highlighting the good adjustment of the non-linear model.

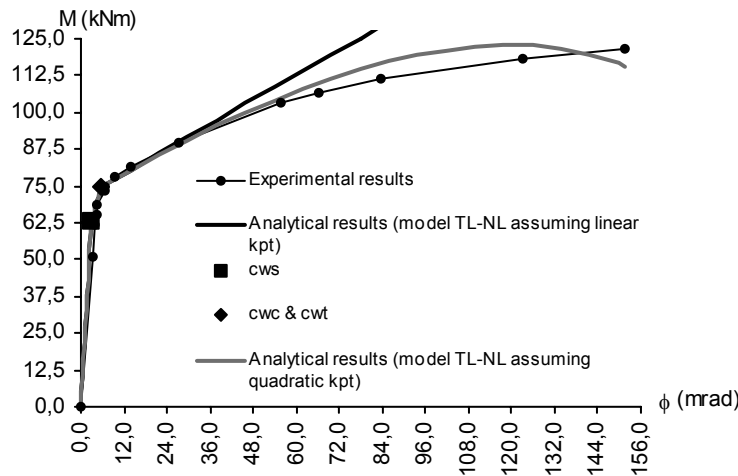


Fig. 6. Welded steel joint: moment-rotation curve (model TL-NL)

3.2 Extended End-Plate Bolted Beam-to-Column Steel Joint

The second example corresponds to an extended end-plate bolted steel joint tested by Humer at the University of Innsbruck (Humer 105.009), illustrated in Figure 7.

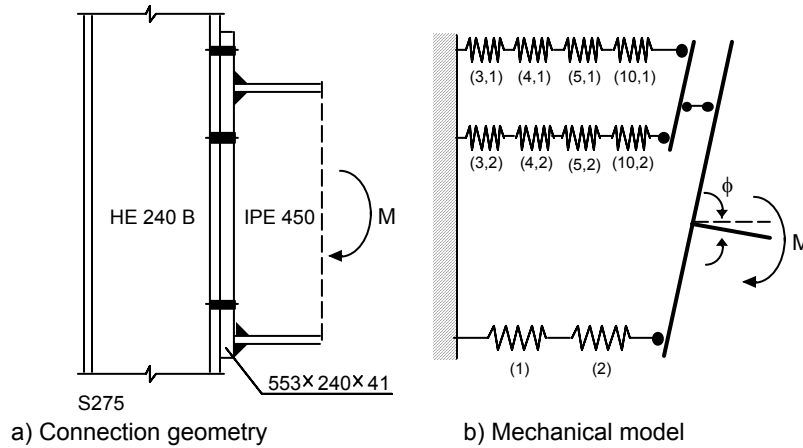


Fig. 7. Bolted extended end-plate steel joint

Table 3 indicates the chosen values for the various components. Using model BL-BL, Figure 8 compares the experimental results with the analytical results.

Component	F^C (kN)	k_e (kN/m)	k_p (kN/m)	\square^y (mm)
1	529.33	6.363×10^5	7.122×10^4	0.832
2	576.13	2.474×10^6	3.022×10^4	0.233
3.1	510.78	1.426×10^6	2.513×10^4	0.358
3.2	510.78	1.426×10^6	2.513×10^4	0.358
4.1	476.21	5.601×10^6	3.131×10^3	0.085
4.2	476.21	5.601×10^6	9.131×10^3	0.085
5.1	635.40	2.315×10^7	8.446×10^3	0.027
5.2	635.40	5.571×10^7	8.446×10^3	0.011
10.1	635.40	1.199×10^6		0.530
10.2	635.40	1.199×10^6		0.530

Table 3. Component characterization

Yielding starts at the compression zone (column web in shear (1) followed by the column web in compression (2)). Next, the first row of bolts of the joint becomes critical, as seen in Table 4, the following components yielding in succession: column flange in bending (4.1), column web in tension (3.1), the joint reaching 0.058 radians at the end of the test.

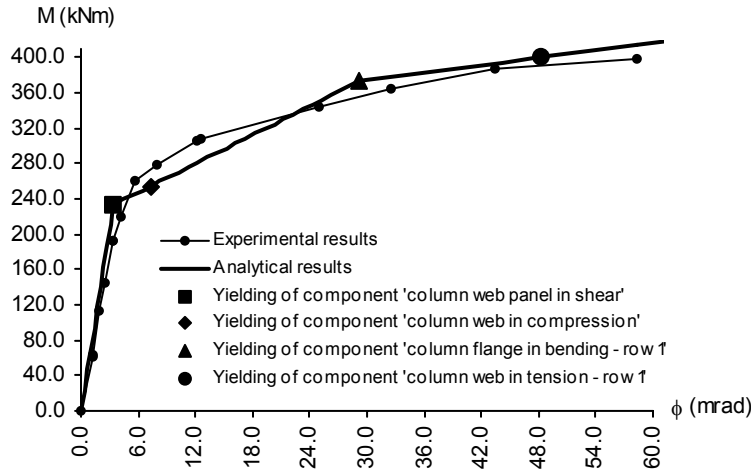


Fig. 6. Bolted extended end-plate steel connection: moment-rotation curve

Component	Component yielding sequence										Failure
	Absolute displacement Δ_i (mm)					Relative displacement Δ_i / Δ_i^Y					
1	-0.832	-1.562	-5.776	-6.724	-7.212	1.000	1.878	6.943	8.083	8.669	8.669
2	-0.214	-0.233	-9.271	-11.305	-12.352	0.919	1.000	39.808	48.543	53.038	53.038
3.1	0.209	0.227	0.334	0.358	1.083	0.583	0.635	0.932	1.000	3.022	3.022
3.2	0.162	0.177	0.259	0.278	0.287	0.453	0.493	0.724	0.775	0.801	0.801
4.1	0.053	0.058	0.085	11.134	16.851	0.625	0.681	1.000	130.946	198.187	198.187
4.2	0.041	0.045	0.066	0.071	0.073	0.486	0.529	0.777	0.831	0.860	0.860
5.1	0.013	0.014	0.021	0.022	0.023	0.469	0.510	0.749	0.804	0.832	0.832
5.2	0.004	0.005	0.007	0.007	0.007	0.364	0.397	0.582	0.623	0.644	0.644
10.1	0.248	0.270	0.397	0.426	0.441	0.469	0.510	0.749	0.804	0.832	0.832
10.2	0.193	0.210	0.308	0.330	0.341	0.364	0.397	0.582	0.623	0.644	0.644
	3.43	7.25	29.26	48.35	58.24	1.00	2.11	8.52	14.08	16.96	16.96
	Absolute joint rotation (mrad)					Joint ductility index					

Table 4. Ductility indexes for bolted extend end-plate steel connection

3.3 Flush End-Plate Bolted Beam-to-Column Composite Joint

In order to illustrate the application to composite joints, a double-sided bolted flush end-plate beam-to-column joint tested in bending by Simões at the University of Coimbra in 1998 (11) was selected, shown in Figure 7.

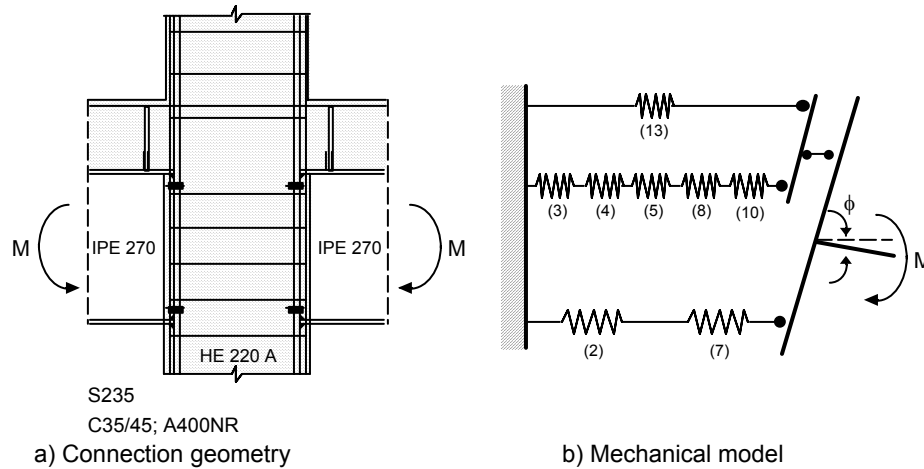


Fig. 7. Bolted flush end-plate composite joint

Table 5 reproduces the adopted component properties for model TL-BL-BL.

Component	F^C (kN)	k_e (kN/m)	k_p (kN/m)	\square^y (mm)
2	1550.20	3.244×10^6	1.000×10^1	0.478
3	504.00	9.404×10^5	1.000×10^1	0.536
4	346.20	2.982×10^6	1.000×10^4	0.116
5	293.70	2.322×10^6	1.000×10^4	0.126
7	578.50	∞	3.600×10^4	0.000
8	462.10	∞	∞	0.000
10	444.53	2.257×10^6	1.000×10^4	0.197
13	124.99	6.006×10^5	2.310×10^5	0.208
	477.28		1.200×10^3	

Table 5. Component characterization

Figure 8 compares the experimental and analytical results, The moment-rotation curve shows yielding of the first component (reinforcement), corresponding to the cracking of concrete in tension that occurs for relatively low values of bending moment and joint rotation (55 kNm and 0.8 mrad). It is noted that current Eurocode specifications for composite joints

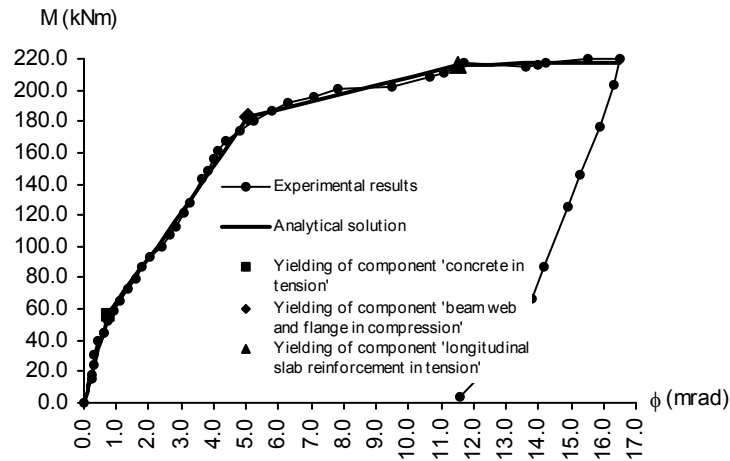


Fig. 8. Bolted flush end-plate composite joint: moment-rotation curve

(3) disregard the cracking moment of the joint. Next, at a rotation of 5.1 mrad, yielding of the beam web and flange in compression takes place, followed by yielding of the reinforcement. Table 6 summarises the “yield” sequence of the various components and the corresponding levels of ductility.

Component	Component yielding sequence								Failure
	Absolute displacement Δ_i (mm)				Relative displacement Δ_i / Δ_i^Y				
2	-0.055	-0.178	-0.212	-0.213	0.116	0.373	0.443	0.445	0.445
3	0.058	0.188	0.223	0.224	0.109	0.350	0.416	0.418	0.418
4	0.018	0.059	0.070	0.071	0.158	0.510	0.605	0.608	0.608
5	0.024	0.076	0.090	0.091	0.187	0.601	0.713	0.717	0.717
7	0.000	0.000	-3.007	-3.111	0.311	1.000	∞	∞	∞
8	0.000	0.000	0.000	0.091	0.119	0.382	0.453	0.456	0.456
10	0.024	0.078	0.093	0.000	0.123	0.397	0.471	0.474	0.474
13	0.208	2.053	2.554	4.729	1.000	9.866	12.274	22.724	22.724
	0.76	5.07	11.55	16.53	1.00	6.72	15.29	21.88	21.879
	Absolute joint rotation (mrad)				Joint ductility index				

Table 6. Ductility indexes for bolted flush end-plate composite joint

4 CONCLUDING REMARKS

A simple analytical procedure for the evaluation of the moment-rotation response of steel and composite joints was presented in this paper. It allows the consistent evaluation of strength, initial stiffness and ductility. Additionally, depending on the choice of component idealisation, this methodology is able to approximate, as closely as desired, the true moment-rotation response of the joint, further identifying all relevant changes in joint response.

Finally, it should be noted that proper application of the component method requires the adequate prediction of the post-limit stiffness of the various components, a task yet to be done.

5 ACKNOWLEDGEMENTS

Financial support from “Ministério da Ciência e Tecnologia” - PRAXIS XXI research project PRAXIS/P/ECM/13153/1998 is acknowledged.

6 REFERENCES

- 1 Weynand K, Jaspart J-P, Steenhuis M, The stiffness model of revised Annex J of Eurocode 3, in R. Bjorhovde, A. Colson and R. Zandonini (eds), *Connections in Steel Structures III*, Proceedings of the 3rd International Workshop on Connections in Steel Structures, Trento, Italy, pp. 441-452, 1995.
- 2 Eurocode 3, ENV - 1993-1-1:1992/A2, Annex J, Design of Steel Structures – Joints in Building Frames. CEN, *European Committee for Standardisation*, Document CEN/TC 250/SC 3, Brussels, 1998.
- 3 Eurocode 4, Draft prEN 1994-1-1, Design of composite steel and concrete structures – Part 1.1 (Draft n^o1): General rules and rules for buildings. CEN, European Committee for Standardization. Brussels, 1999.
- 4 Faella C, Piluso V, Rizzano G, *Structural steel semirigid connections: theory, design and software*. CRC Press LLC, 2000.
- 5 Simões da Silva L, Girão Coelho A, Mode interaction in non-linear models for steel and steel-concrete composite structural connections”, in *Proceedings of CIMS 2000 - 3rd International Conference on Coupled Instabilities in Metal Structures*, Lisboa, Portugal, 21-23 September, 2000 (in print).
- 6 Kuhlmann U, Davison JB, Kattner M, Structural systems and rotation capacity, COST Conference on Control of the semi-rigid behaviour of civil engineering structural connections, Liège, Belgium, pp. 167-176, 1998.
- 7 Simões da Silva L, Girão Coelho A, Neto E, Equivalent post-buckling models for the flexural behaviour of steel connections. *Comp. Struct.*, 2000 (in print).
- 8 Simões da Silva L, Girão Coelho A, A ductility model for steel connections, *Journal of Constructional Steel Research*, 2000 (in print).
- 9 Simões da Silva L, Calado L, Cruz P, Dynamic behaviour of composite structures with composite connections, in *Proceedings of STESSA 2000 - 3rd International Conference on Behaviour of Steel Structures in Seismic Areas*, Montreal, Canada, 21-24 August, 2000 (in print).
- 10 Cruz P, Simões da Silva L, Rodrigues D, Simões R, Database for the semi-rigid behaviour of beam-to-column connections in seismic regions. *Journal of Constructional Steel Research* 1998;46(120):1-3, 1998.
- 11 Simões da Silva L, Simões R, Cruz P, Behaviour of end-plate beam-to-column composite joints under monotonical loading, *Engineering Structures*, 2000 (submitted for publication).

Strength Determination of Heavy Clip-Angle Connection Components

James A Swanson, Ph.D. and Xiaojiang Gao
University of Cincinnati
Dept. of Civil & Environmental Engineering
PO Box 210071 - 741 Baldwin Hall
Cincinnati, OH 45221-0071

ABSTRACT

Most existing research data on clip-angle connections centers around connections that use light to medium weight angles ($t = 1/4''$ to $5/8''$) for connecting the beam flanges to the column flange. With the increased use of bolted connections in low to mid-rise structures, stronger and stiffer top-and-seat angle connections are needed to fill the gap between T-stub or end-plate connections and lighter angle connections. The results of ten cyclic tests of heavy angle components ($t = 1''$) are presented in this paper and are used to evaluate currently accepted design procedures.

INTRODUCTION

Two recent seismic events, the Northridge and Kobe earthquakes, exposed several weaknesses in fully welded beam-column connections. In the time since, several research projects have been conducted to identify and correct flaws in welded connection design procedures and to investigate alternative connection designs. One of those projects, SAC[†] subtask 7.03, was conducted at the Georgia Institute of Technology and focused on bolted T-stub and top-and-seat-angle connections as alternatives to fully welded connections for light to medium-weight beam sizes. The investigation consisted of tests of T-stub and angle components subjected to cyclic axial loads. The tests were designed to isolate flange components of bolted moment connections so that an economical parametric investigation could be conducted. A discussion of the experimental program was provided by Swanson (1) and Swanson and Leon (2).

[†] SAC is a joint venture made up of the Structural Engineers Association of California (SEAOC), the Applied Technology Council (ATC), and the California Universities for Research in Earthquake Engineering (CUREe). SAC is funded by the Federal Emergency Management Association (FEMA).

Although, the primary focus of the Georgia Tech project was the study of T-stub connections, a series of ten angle components were also tested. The data from this series of tests, however, was not thoroughly reduced and no design recommendations were made. This is unfortunate because the angle components that were tested were much heavier than those used in typical top-and-seat angle connections and represent an important addition to the existing base of data. The objectives of this paper is to present the angle test data collected at Georgia Tech, to evaluate two existing ultimate strength models for angle components, and to present an alternative ultimate strength model.

BACKGROUND

The determination of the ultimate strength of an angle component subjected to an axial load is a complex process. Of the possible failure modes, the most studied case is the development of a bending mechanism in the upstanding angle leg followed by failure of the tension bolts (i.e. the formation of a prying mechanism). In this paper, the prying models used by the AISC-LRFD (3) and Eurocode (4) specifications will be evaluated by comparing their strength predictions to the results of ten angle component tests that were conducted at the Georgia Institute of Technology (1, 2). A new strength model, based on a combination of the first two models, will then be presented and evaluated. All three of the models are based on the prying formulation developed by Kulak et al. (5) for T-stub components. Although several other prying formulations have been developed, including those developed by Chen et al. (6) and Jaspart and Maquoi (7), they will not be addressed in this work.

In the discussion of the existing models, the notations used by the original authors will be converted to that used in this work so that a clearer comparison can be made. The notation that will be used is illustrated Figure 1. The analysis of an angle flange is made easier by considering the width of the angle that is tributary to one bolt. This tributary width will be called p and can be calculated as

$$p = \frac{W_{\text{Angle}}}{n_{\text{tb}}} \quad \text{EQ 1}$$

where

W_{Angle} = the width of the angle perpendicular to the beam axis
 n_{tb} = the number of tension bolts

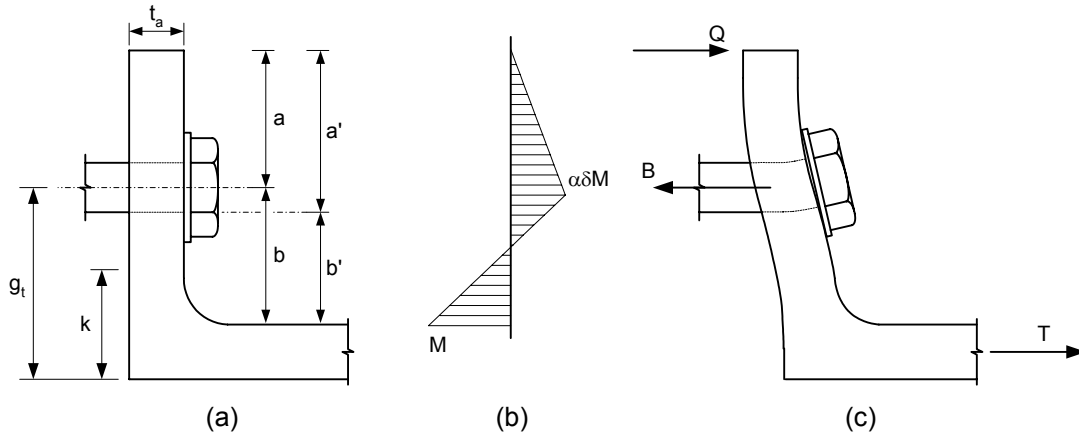


Figure 1: Clip Angle Geometry Notation

Other parameters that appear in the discussion of clip-angle components are:

- T = the applied angle force per tension bolt
- B = the force present in a tension bolt at any given time
- B_n = the tensile capacity of a bolt
- B_o = the initial pretension of a bolt.
- Q = the prying force per bolt.
- g_t = the distance between the heel of the angle and the center line of the tension bolts
- a = the distance measured from the bolt centerline to the edge of the upstanding angle leg
- b = the distance measured from the bolt centerline to the face of the angle leg that is bolted to the beam flange
- a' = the distance measured from the inside edge of the bolt to the edge of the upstanding angle leg
- b' = the distance measured from the inside edge of the bolt to the face of the angle leg that is bolted to the beam flange

Additional parameters that are specific to particular models will be introduced as needed. It is crucial to understand that T is the applied load per tension bolt. Therefore, the total applied load is equal to $T \cdot n_{tb}$.

In both of the models considered in this work, a prying force is assumed to develop as the flange deforms. This prying force is added to the conventional force present in the tension bolts and effectively reduces the load that can be safely applied to the angle. The basic mechanism is shown in Figure 1c and fundamental equilibrium shows that the bolt tension, B, is the sum of the prying force, Q, and applied load, T. The prying forces can generally be minimized by reducing the tension bolt gage, g_t , or by increasing the flange thickness. The assumption that the prying force acts at the tip of the flange is generally accepted and is considered accurate until the length of the flange exterior to the bolt becomes large or until the flange thickness becomes small (5). Figure 2 shows an angle specimen just prior to a tension bolt fracture.

AISC-LRFD

The prying model use in the AISC-LRFD specification for the ultimate strength determination of clip-angle components is based on the model developed by Kulak et al (5). Although the model was originally developed to predict prying forces in T-stub components, the model can be applied to clip angles with minor modification. In this model, the bolt force is assumed to act at the inside edge of the bolt shank as opposed to acting at the centerline of the bolt. This premise is based on the assumption that as the flange deforms, more of the bolt force is transmitted to the angle flange under the inside of the bolt head than under the outside. This is a result of the stiffness of the bolt head and the degree of bending present in the flange and bolt. To accommodate this idea in the model, equilibrium is based on the dimensions a' and b' instead of a and b . The parameters a' and b' are defined in Equations 2 and 3. The magnitude of the length a is limited to $1.25b$ in this model in recognition of the prying force, Q , may not act as a concentrated force for wider flanges.

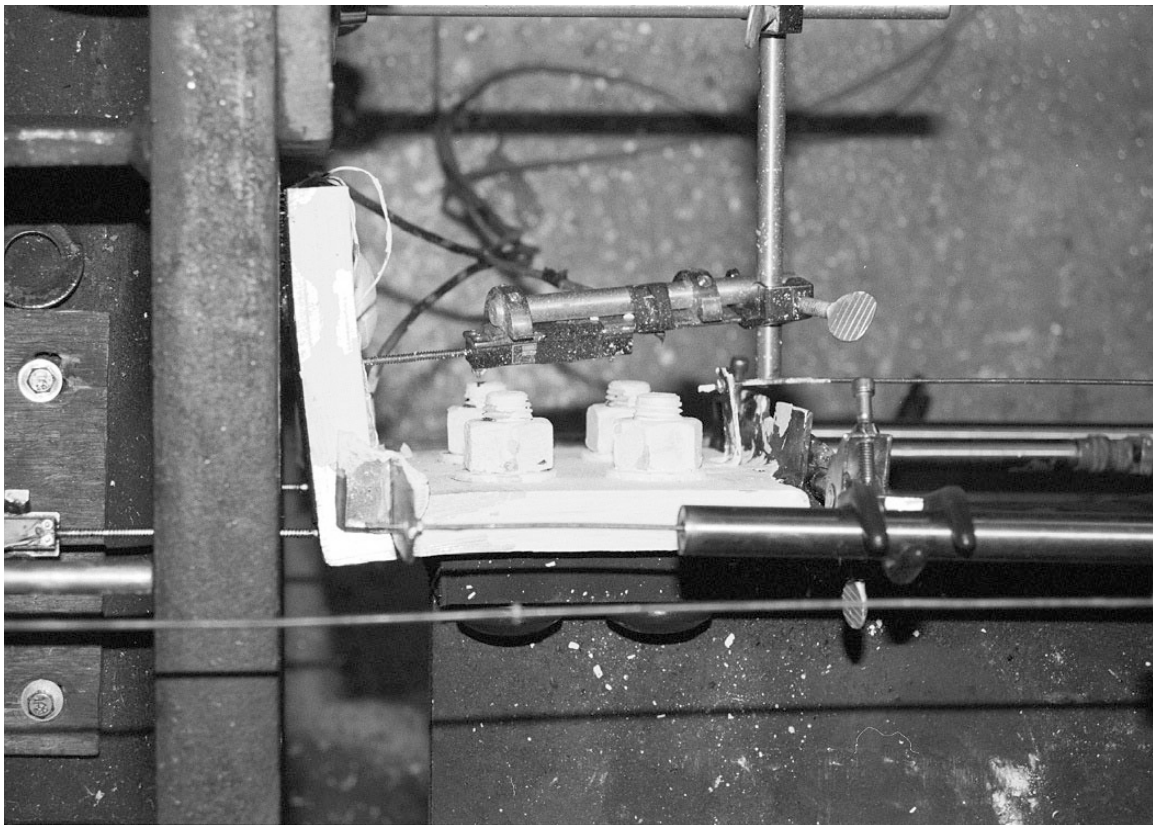


Figure 2: Angle Component During Testing Prior to Tension Bolt Fracture

$$a' = a + \frac{d_b}{2} \quad \text{EQ 2}$$

$$b' = b - \frac{d_b}{2} \quad \text{EQ 3}$$

The parameter α (Figure 1b) is defined by Kulak et al. as the ratio of the moment at the bolt line to the moment at the face of the angle leg that is bolted to the beam flange (hereafter referred to as the angle stem), and is an indicator of the level of prying present. Physically, α is limited to values between 0 and 1. A value of 1 is achieved if the bolt is stiff enough to cause the flange to act as a fixed-fixed beam and a value of 0 results when the flange separates completely from the column. In calculating the prying capacity, however, α is not limited. If $\alpha \leq 0$ then the flange is in single curvature, the prying forces are zero, and the bolts are subjected to conventional tension only. If $\alpha \geq 1$ then the flange is in double curvature and the prying forces are maximized. When $0 \leq \alpha \leq 1$, a combination of flange yielding and bolt prying will occur (8). M is the moment at the face of the stem and δ is the ratio of the net section of the flange at the bolt line to the gross section at the face of the stem, excluding the fillet. δ can be written as

$$\delta = 1 - \frac{d_h}{p} \quad \text{EQ 4}$$

Moment equilibrium of the flange between the face of the stem and the bolt line, using b' , results in Equation 5, moment equilibrium of the flange to the exterior of the bolt line, using a' , results in Equation 6, and force equilibrium of the entire flange results in Equation 7.

$$T \cdot b' = (1 + \alpha \cdot \delta)M \quad \text{EQ 5}$$

$$Q \cdot a' = \alpha \cdot \delta \cdot M \quad \text{EQ 6}$$

$$B = T + Q \quad \text{EQ 7}$$

Equation 5 can be solved for α as shown in Equation 8.

$$\alpha = \left(\frac{1}{\delta} \right) \left(\frac{T \cdot b'}{M} - 1 \right) \quad \text{EQ 8}$$

At failure, M will be the plastic moment capacity of the flange and can be written as

$$M_p = \left(\frac{p \cdot t_a^2}{4} \right) F_y \quad \text{EQ 9}$$

Substitution of M_p into Equation 8 yields α as a function of the applied load, T , as shown in Equation 10.

$$\alpha = \left(\frac{1}{\delta} \right) \left(\frac{4T \cdot b'}{p \cdot t_a^2 \cdot F_y} - 1 \right) \quad \text{EQ 10}$$

Manipulation of the equilibrium equations provides the prying force, Q , as

$$Q = T \left(\frac{\alpha \cdot \delta}{1 + \alpha \cdot \delta} \right) \left(\frac{b'}{a'} \right) \quad \text{EQ 11}$$

The capacity of an existing angle is then calculated based on the minimum value resulting from Equations 12, 13, and 14 which correspond to a flange mechanism, mixed mode failure, and a tension fracture, respectively. These three equations represent the possible failure modes of the flange and tension bolts. As was previously mentioned, a flange mechanism will develop if $\alpha \geq 1$, bolt prying combined with flange yielding will govern if $0 \leq \alpha \leq 1$, and conventional bolt strength with no prying governs if $\alpha \leq 0$. Note, however, that the capacity of an existing angle can be computed without calculating α . This is convenient because α is a function of the applied load per bolt, T , and the solution would otherwise be iterative.

$$T = \frac{(1 + \delta)}{4b'} \rho \cdot F_y \cdot t_a^2 \quad \text{EQ 12}$$

$$T = \frac{B_n \cdot a'}{a' + b'} + \frac{\rho \cdot F_y \cdot t_a^2}{4(a' + b')} \quad \text{EQ 13}$$

$$T = B_n \quad \text{EQ 14}$$

A solution space for a typical angle is shown in Figure 3. The solution space is the result of plotting an angle's flange capacity as a function of the angle thickness. The bold line OABC defines the capacity of the flange and tension bolts and the region below this line, OABCD, represents an adequate design. Segment OA defines the flange mechanism strength and is calculated using Equation 12 which assumes that $\alpha = 1$, segment AB is defined by the bolt capacity including the effects of prying and is computed using Equation 13, and segment BC represents the conventional strength of the bolts without prying and is computed as shown in Equation 14.

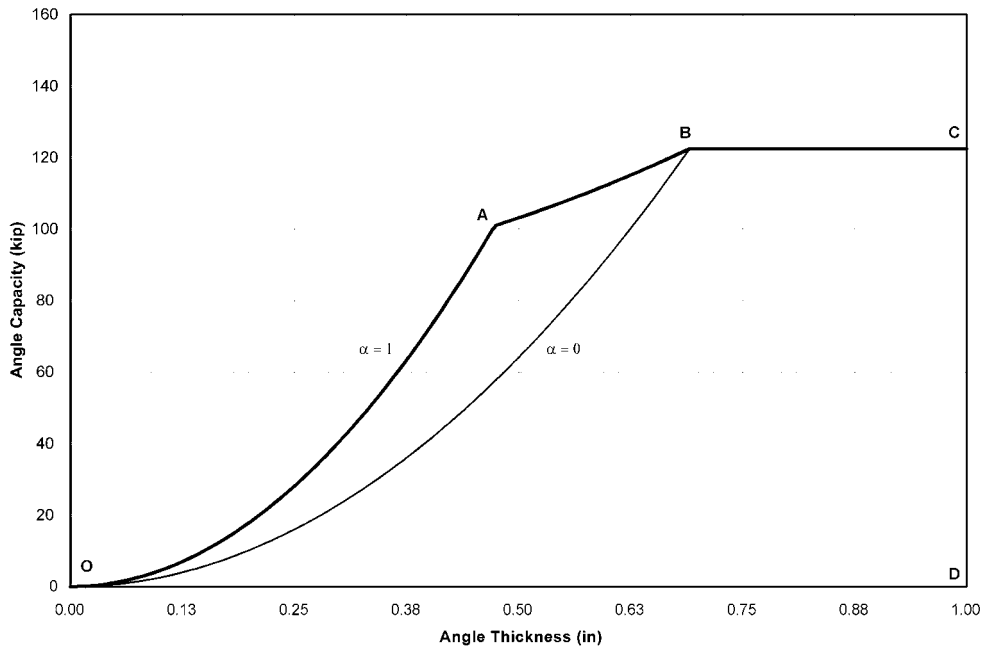


Figure 3: General Solution for Angle Capacity

The line segment OB represents the case of $\alpha = 0$. The region OBCD represents a design with negligible prying effects, as would be desired when considering fatigue. The angle thickness associated with the point B is often referred to as the critical thickness, t_c , because an angle with a thickness greater than t_c will have negligible prying and will develop the full tensile strength of the bolts. The point A is generally considered to represent a balanced failure because the full strength of the flange is exhausted at the same time that the bolt forces, including prying, become critical (9). The critical thickness and balanced load are written as

$$t_c = \sqrt{\frac{4B_n \cdot b'}{p \cdot F_y}} \quad \text{EQ 15}$$

$$T_o = \frac{B_n}{1 + \left(\frac{\delta}{1 + \delta}\right)\left(\frac{b'}{a'}\right)} \quad \text{EQ 16}$$

Table 1 shows a comparison of the experimental angle capacities of the ten specimens from the SAC investigation with the model predictions. The column labeled “Experimental Capacity” contains the maximum loads recorded during the testing of each T-stub, and the percent difference was calculated using Equation 17. As a result, a positive percent difference represents a conservative prediction of the angle capacity. All capacity predictions listed in the table were computed using the actual material properties and are based on either the combined flange mechanism and bolt capacity ($0 \leq \alpha \leq 1$) determined by Equation 13 or the conventional bolt strength without prying ($\alpha \leq 0$) determined by Equation 14. No attempt was made to identify the load at which a flange mechanism formed ($\alpha \geq 1$).

$$\% \text{ Difference} = \frac{\text{Experimental Capacity} - \text{Predicted Capacity}}{\text{Experimental Capacity}} \quad \text{EQ 17}$$

Table 1: Comparison of Experimental and Predicted Angle Capacities

Test ID	Exp.	AISC - LRFD		Eurocode		Proposed Model	
	Capacity	Capacity	% Diff	Capacity	% Diff	Capacity	% Diff
	Kip	Kip		Kip		Kip	
CA-01	108.3	131.1	-21.0%	93.7	13.4%	112.4	-3.8%
CA-02	125.3	133.1	-6.2%	106.0	15.4%	120.5	3.8%
CA-04	84.3	93.6	-11.0%	73.2	13.2%	85.1	-0.9%
CA-17	120.9	132.8	-9.8%	94.9	21.5%	113.8	5.9%
CA-18	119.2	133.4	-11.9%	95.3	20.1%	114.4	4.1%
CA-09	125.2	167.7	-33.9%	115.3	7.9%	143.7	-14.8%
CA-10	159.3	171.2	-7.5%	133.9	15.9%	156.0	2.0%
CA-12	109.2	120.5	-10.4%	91.5	16.3%	109.6	-0.3%
CA-14	136.8	149.1	-9.0%	116.5	14.9%	135.1	1.2%
CA-16	95.2	104.8	-10.1%	80.0	15.9%	95.3	-0.1%
		Ave:	-13.1%	Ave:	15.5%	Ave:	-0.3%
		Var:	0.7%	Var:	0.1%	Var:	0.3%

The capacities predicted by AISC-LRFD model were all higher than the observed experimental capacities. The average percent difference was -13.1% with a coefficient of variation of 0.7%[†]. The over prediction of strength is likely related to the location of the plastic hinge near the angle stem. The AISC-LRFD model assumes that a plastic hinge forms at the face of the stem. Yield lines and deformation of the test specimens (Figure 2), however, indicated that the hinge formed in the stem of the angle and not in the upstanding leg. By calculating the angle capacity under the assumption that the hinge is located in the upstanding leg when it is actually in the stem, the moment arm, b' is underestimated which leads to a lower moment in flange and lower prying forces in the tension bolts.

Eurocode Model

Annex J of the Eurocode 3 (4) addresses the design of beam-to-column connections. The model used by the Eurocode for clip-angle strength closely resembles the theory developed by Kulak et al. The code recognizes the same three failure modes documented by Kulak, et al., shown as Equations 18, 19, and 20, which predict a flange mechanism, mixed mode failure, and simple tension bolt fracture, respectively. The primary differences between the Eurocode and the AISC-LRFD model are the way that the dimensions are defined and the fact that the Eurocode makes no strength reduction for flange material lost to the drilling of the bolt holes. The geometric definitions for the Eurocode model are illustrated in Figure 4. Like the dimension a in the AISC-LRFD model, n is limited to a value no greater 1.25 m . The length m is defined as the distance from the centerline of the bolt to the face of the stem, minus 80% of the radius of the fillet in the K-zone. No modification is made to the location of the concentrated bolt forces as is done in AISC-LRFD model.

$$T = \frac{p \cdot F_y \cdot t_a^2}{2m} \quad \text{EQ 18}$$

$$T = \frac{n \cdot B_n}{m+n} + \frac{p \cdot F_y \cdot t_a^2}{4(m+n)} \quad \text{EQ 19}$$

$$T = B_n \quad \text{EQ 20}$$

The most significant difference between the Eurocode model and the AISC-LRFD model is that the Eurocode recognizes that a plastic hinge is likely to form in the angle stem instead of the upstanding leg when the gap between the end of the beam and the column face, the beam set-back, is sufficiently large. When the beam set-back is less than or equal to 40% of the angle thickness, the length m is measured from the bolt centerline to the face of the stem minus 80% of the fillet radius (Figure 4a). When the beam set-back is greater than 40% of the angle thickness, however, m is measured from the bolt centerline to the center of the angle stem (Figure 4b). This difference in the definition of m leads to an increased capacity prediction when the beam set-back is less than $0.40t_a$ and to reduced capacity predictions when the set-back is greater than $0.40t_a$ when compared to the AISC-LRFD model.

[†] The experimental capacity of angle CA-09 is consistently lower than the calculated values for all models examined. No explanation for this, besides random variability of material properties is suggested.

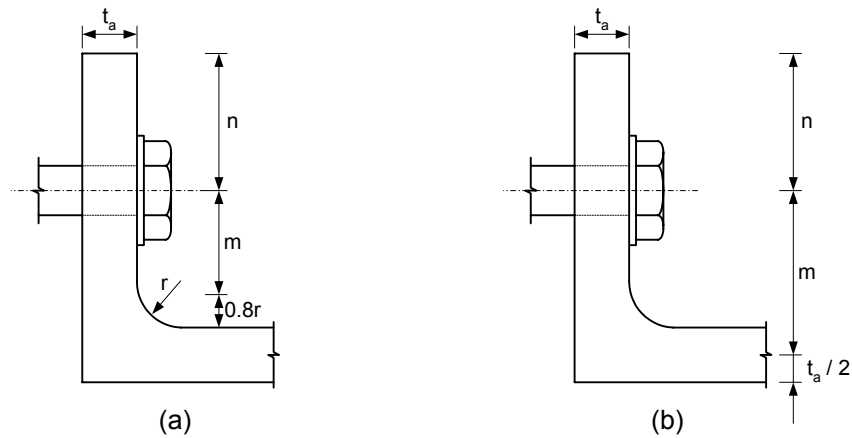


Figure 4: Eurocode Geometry

Flange capacities predicted using the Eurocode model are compared to the experimental capacities and AISC-LRFD predictions in Table 1. The average percent difference of the predictions is 15.5% with a coefficient of variation of 0.1%. No resistance factors were used for the Eurocode capacity predictions.

Proposed Model

A combination of the AISC-LRFD and Eurocode models was considered next. The values shown in the columns labeled "Proposed Model" in Table 1 were obtained by using the dimension definitions shown in Figure 5. The parameters a and b are identical to m and n of the Eurocode. These dimensions were then used in the AISC-LRFD equations (Equations 1-14). The resulting model provided better results than either of the other two models alone. An average percent difference of -0.3% with a coefficient of variation of 0.3% was obtained.

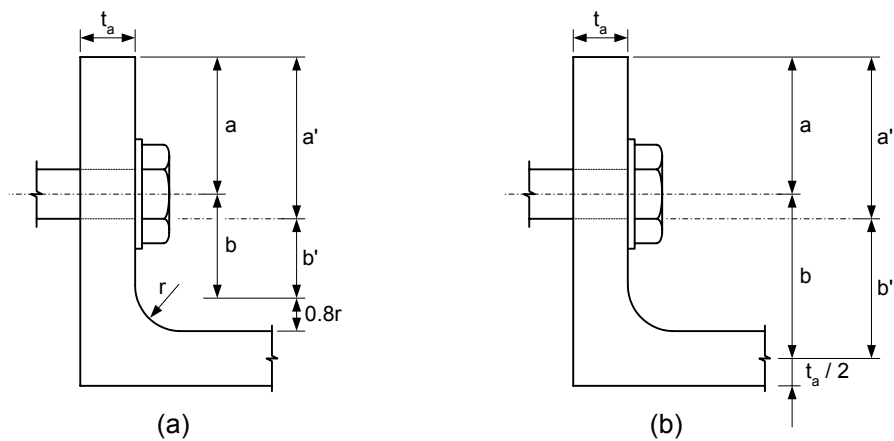


Figure 5: Proposed Model Geometry

DISCUSSION AND CONCLUSIONS

Both the AISC-LRFD model and the Eurocode model provided consistent results when their predictions were compared to the experimental results. The coefficients of variation of the models were 0.7% and 0.3%, respectively. The strength predictions obtained using the AISC-LRFD model were unconservative by an average of approximately 13% while predictions obtained using Eurocode were conservative by an average of approximately 15%. The proposed model, which was developed by combining ideas from the first two models, yielded results that were both consistent and accurate when compared with the experimental results.

It should be restated that the experimental data used for this evaluation was taken from tests of angle components with thicknesses significantly greater than those used in typical angle connections. Furthermore, all of the specimens used for comparison in this work had beam setbacks greater than 40% of the angle thickness. As a result, the geometries in Figures 4a and 5a were not used in any calculations. An evaluation using results from a broader, more typical base of data would lead to stronger conclusions.

ACKNOWLEDGEMENTS

The experimental data used for this research was generated as part of a SAC research project (SAC Task 7.03) that was conducted at the Georgia Institute of Technology under the sponsorship of FEMA. Portions of the analytical work associated with this project were funded by the Mid-America Earthquake (MAE) Center as part of the work under Task ST7.

REFERENCES

- 1 Swanson, J. A. 1999. "Characterization of the Strength, Stiffness and Ductility Behavior of T-stub Connections," Ph.D. Dissertation, Georgia Institute of Technology, Atlanta, GA.
- 2 Swanson, J. A. and Leon, R. T., 2000. "Bolted Steel Connections: Tests on T-stub Components," *J. Struc. Engrg.*, ASCE, Vol. 126, No. 1, pp. 50-56.
- 3 AISC, 1994. Load and Resistance Factor Design, 2nd Ed., American Institute of Steel Construction, Chicago, IL
- 4 Eurocode 3, 1993. "Design Procedures to C-EC3 - Concise Eurocode 3 for the Design of Steel Buildings in the United Kingdom," The Steel Construction Institute, Ascot, UK.
- 5 Kulak, G. L., Fisher, J. W., and Struik, J. H. A., 1987. Guide to Design Criteria for Bolted and Riveted Joints, 2nd Ed., John Wiley & Sons, New York.
- 6 Chen, W. F., Goto, Y., and Richard Liew, J. Y., 1996, Stability Design of Semi-Rigid Frames, John Wiley & Sons, Inc.
- 7 Jaspart, J. P., and Maquoi, R., 1991, "Plastic Capacity of End-Plate and Flange Cleated Connections - Predictions and Design Rules" Proceedings of the 2nd Intl Workshop on Connections in Steel Structures: Behavior, Strength and Design, Pittsburgh, USA, April
- 8 Thornton, W. A., 1985, "Prying Action - A General Treatment," Engineering Journal, American Institute of Steel Construction, Vol. 22, No. 2
- 9 Astaneh, A., 1985 "Procedure for Design and Analysis of Hanger-type Connections," Engineering Journal, American Institute of Steel Construction, Vol. 22, No. 2

SEISMIC BEHAVIOUR OF WELDED BEAM-TO-COLUMN JOINTS: EXPERIMENTAL AND NUMERICAL ANALYSIS

Luis CALADO¹, Carlo A. CASTIGLIONI², Claudio BERNUZZI²

¹ Dept. of Civil Engineering and Architecture, Instituto Superior Tecnico, Lisbon - P.

² Dept. of Structural Engineering, Politecnico di Milano, Milan - I.

ABSTRACT

A study on welded beam-to-column joints in moment-resisting steel frames is presented, comprising both an experimental and a numerical analysis. Main features of two series of joint specimens, which have been tested to identify key parameters influencing joint response as well as low-cycle fatigue endurance are summarised. A criterion to predict the type of failure and an approach to appraise the fatigue endurance are presented. The results of a finite element study on the stress distribution in the nodal zone are discussed.

INTRODUCTION

Moment-resisting (MR) steel frames are traditionally designed assuming that the structural system has to provide sufficient strength, ductility and energy dissipation capabilities to resist severe earthquake, although severely damaged (1). As pointed out by Zandonini et al. (2), several researches carried out in the last decades on joints in moment-resisting (MR) frames permitted to develop a satisfactory knowledge on joint cyclic behaviour (3), (4), (5). As a consequence, modern seismic provisions require that dissipation occurs at the beam ends and, eventually, at the base section of the columns. Nodal zones should hence embody sufficient strength and rotational stiffness so as to allow yielding as well as strain hardening in the dissipative zones, without any brittle fracture of the key structural components. Therefore, during Northridge (1994) and Kobe (1995) earthquakes, a lot of MR frames suffered local damages in several beam-to-column joints (6 - 8). Unprecedented combined phenomena (i.e., notch effect due to backing bars, lack of preheating for thick flange plates and inadequate workmanship and inspection) appear as key factors responsible of the severe failure modes of joints. Moreover, high strain rate effects, which are associated with ground motion, generated material overstrength and, as a consequence, joint ductility resulted remarkably reduced, in comparison with the one expected on the basis of previous experimental studies. Several studies (2) were hence carried out to explain both fracture locations and failure modes, which were observed during the aforementioned earthquakes.

A research project is currently in progress between some European Universities (Athens, Lisbon and Milan), with the aim of defining suitable criteria for the seismic design of steel frames with rigid and semi-rigid joints. This paper is focused on the behaviour of welded beam-to-column joints in MR steel frames. The experimental phase of the study, which comprised cyclic tests performed in Lisbon (BCC5 and BCC6) and in Milan (C1, C2 and C4), is summarised and key features of joint response are presented. A suitable definition of a threshold value of displacement is proposed to predict the type of failure (i.e., brittle, ductile or mixed failure). Moreover, an approach to assess fatigue endurance is discussed, which depends on the threshold value, too.

Finally, the results of a finite element study on the nodal zones are outlined, mainly with reference to the local strains in the vicinity of the weld toes, where unexpected brittle fractures could occur, as observed during tests as well as recent earthquakes.

EXPERIMENTAL PROGRAMME

A multi-specimen testing programme (9 – 14) on several types of rigid joints, carried out at the Universities of Lisbon and Milan, is herein shortly presented. Table 1 shows the general layout of all the considered tests on rigid joints (fig. 1). In particular, details are reported about the loading history, the total number of cycles performed during the tests, N_{tot} , and the number of cycles to conventional failure, N , which has been evaluated in accordance with the approach presented in the following. Moreover, the type of failure is reported, too. As a general remark, it should be mentioned that the spread of plasticity was observed only in the nodal zone, while beam and column remained in the elastic range in the other parts of the specimen. As a consequence, joint behaviour is herein presented with reference to the global response of the specimen, i.e., by considering the relationship between the force applied at the beam free end, F , and the associated displacement, v .

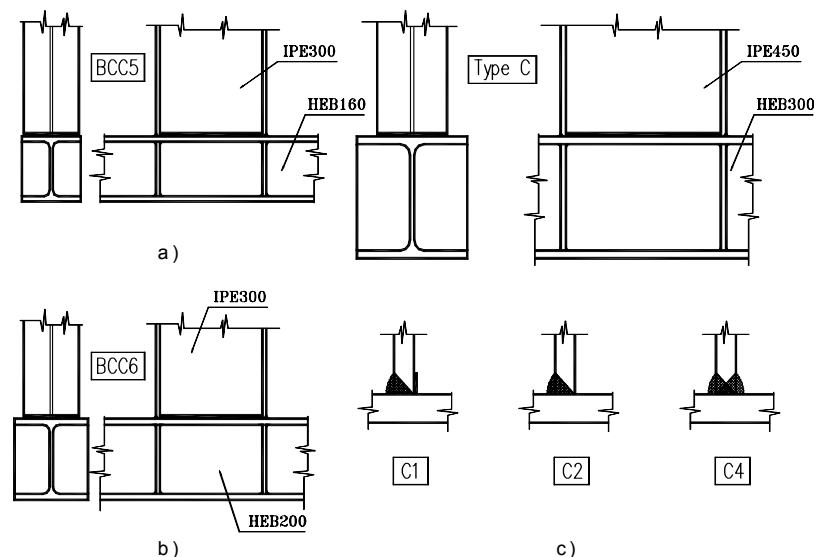


Figure 1: Test specimen details

Among the large number of tests carried out by the authors, a series of 29 tests executed on 5 different types of beam-to-column connections is considered in this paper with the aim of evidencing the main parameters affecting the cyclic response of rigid joints (10, 15). The tested specimens were representative of a node to external columns (i.e., a stub beam attached to a column by means of the connection details). For each typology of joint, several specimens were realised and tested, under constant amplitude loading histories.

The Lisbon Tests

Two different series of welded joint specimens were tested: BCC5 and BCC6 (fig. 1a) and 1b), differing in the type of profile (i.e., HEB160 and HEB200) used for the columns. For each typology of connection, the specimen is identified by means of a letter (A, B, D or E), each one associated to a different loading history. Rigid joint with the weaker column (BCC5) exhibited a

very stable behaviour, in terms of F-v hysteresis loops (fig. 2), with a very limited deterioration of stiffness, strength and energy absorption capabilities. Collapse was due to the fracture of the (IPE300) beam flange in the vicinity of the welded connections. Also in case of joint with stronger column (BCC6), the behaviour resulted very stable.

The column profile influenced remarkably the failure mode. In the case of a stronger column (BCC6) a well defined plastic hinge always formed in the zone of the beam flanges interested by local buckling. Failure was associated with cracking in these zones due to large plastic deformations. However, in the case of small amplitude cycles, brittle failure was observed with cracking in the welds. On the contrary, in the case of a weaker column (BCC5), the plastic hinge was not so evident, the plastic deformation of beam flanges was smaller with respect to BCC6 specimens, and the failure occurred due to cracking at the welds.

TABLE 1
LISBON AND MILAN JOINT TEST CHARACTERISTICS

JOINT	SPECIMEN	LOADING HISTORY	N _{tot}	N	FAILURE MODE
BCC5	A	S with $\Delta v = 100$ mm	20	15	B1
	B	S with $\Delta v = 150$ mm	8	4	B1
	D	S with $\Delta v = 76$ mm	27	21	B1
	E	M			
BCC6	A	S with $\Delta v = 100$ mm	19	14	D
	B	S with $\Delta v = 150$ mm	15	10	D
	D	S with $\Delta v = 76$ mm	22	16	B1
	E	M			
C1	A30	S with $\Delta v = 60$ mm	16	8	B2
	C30	S with $\Delta v = 60$ mm	16	12	B2
	B50	S with $\Delta v = 100$ mm	19	17	B2
	C50A	S with $\Delta v = 100$ mm	2	2	B3
	C50B	S with $\Delta v = 100$ mm	51	48	D
	D50	S with $\Delta v = 100$ mm	1	1	B1
	B75	S with $\Delta v = 150$ mm	20	18	M
	B100	S with $\Delta v = 200$ mm	14	12	D
C2	B30	S with $\Delta v = 60$ mm	82	75	B2
	B50	S with $\Delta v = 100$ mm	36	36	B1
	B75	S with $\Delta v = 150$ mm	4	3	B1
	C75	S with $\Delta v = 150$ mm	33	32	M
	B100	S with $\Delta v = 200$ mm	15	14	D
	B125	S with $\Delta v = 250$ mm	8	7	D
C4	B30	S with $\Delta v = 60$ mm	52	48	B1
	B50A	S with $\Delta v = 100$ mm	8	6	B1
	B50B	S with $\Delta v = 100$ mm	10	8	B1
	B75	S with $\Delta v = 150$ mm	28	26	M
	B100	S with $\Delta v = 200$ mm	15	13	D
	B125	S with $\Delta v = 250$ mm	12	8	D
	C125	S with $\Delta v = 250$ mm	7	7	D

LOADING HISTORY:

S =symmetrical constant amplitude

M=monotonic

FAILURE MODE:

D =ductile

B1=brittle with crack formed at the centre of the weld, between beam and column flanges

B2=brittle with crack formed at the edges of the weld, between beam and column flanges

B3=lamellar tearing

M =mixed

A comparison between the responses of the two types of specimens shows no remarkable differences in terms of hysteretic behaviour, as it can clearly be seen from fig. 3, which presents two cycles selected at different level of displacement, while the column type affects moderately the peak values of the force.

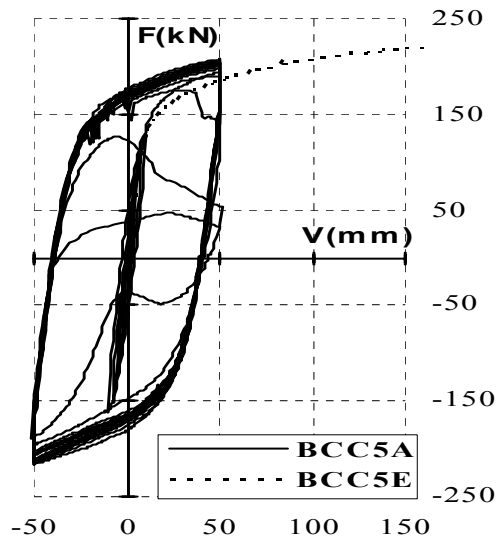


Figure 2 : Hysteresis loops for BCC5A
BCC5
and BCC5E joint specimens

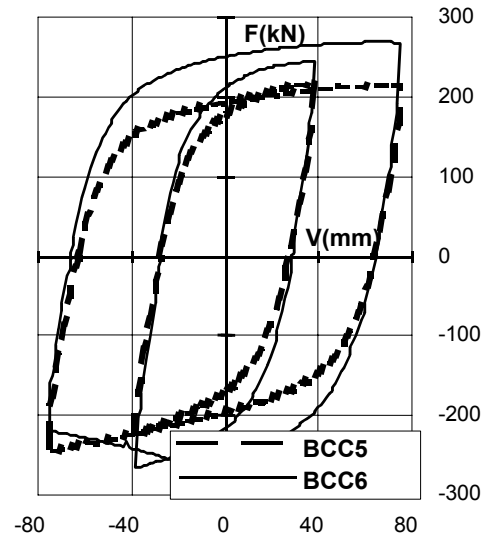


Figure 3: Hysteresis loops for
BCC5
and BCC6 joint specimens

The Milan Tests

In the past, several experimental studies were carried out at Politecnico di Milano on the cyclic behaviour of both beams and beam-columns in order to identify key parameters affecting member response (11). Recently, attention has been paid also to beam-to-column joints for steel and steel-concrete composite frames. As far as joint tests in MR frames are concerned, the tested specimens, very similar to the ones tested in Lisbon, consisted in a beam (IPE450A profile) attached to a column (HE300B) by means of rigid welded connections, with butt welds connecting beam flanges to the column flange.

Three different welding procedures (14) which represent solutions commonly used to weld beam-to-column joints in accordance with European and North American steel construction practice, were considered. In particular, the following types of connections were tested (fig. 1c):

- connection C1, typically adopted in the US practice. All welds are executed in a flat position with single bevel V groove with a steel backing bar underneath, usually not removed after welding;
- connection C2, similar to the C1 one but with a copper backing bar easily removable after welding. One additional weld pass is executed from underneath to melt down eventual defects and flows and to remove the eventual presence of weld slag almost unavoidable in the C1 specimens;
- connection C4, realised by means of butt welds, with K grooves. It normally corresponds to shop welding, and is typical for the Italian (and in general European) steel constructional practice.

It has been decided to analyse the behaviour of some specimens with column stiffeners, in order to investigate the influence of the stiffness of the panel zone on both resistance and ductility of the connection.

Moreover, some specimens were modified to assess also the influence of the web access hole in the beam web in order to have a continuous weld along the whole (lower) flange and to allow continuous backing bar to be positioned also on the upper flange. With reference to table 1, the label of each specimen (of the series C1, C2 and C4) is composed by an index (first letter A, B, C or D) indicating the geometry of the welded node, as explained later, by the value of half displacement range ΔV under which constant amplitude test has been executed and, eventually, by a letter (A or B) related to the number of test replications (under the same displacement amplitude). The index (first letter) A and B are related to specimens with the web access holes and with or without column stiffeners, respectively. Specimens without the web access holes are labelled as C, if with column stiffeners, and D, if without column stiffeners.

Five constant amplitude loading histories, each of them characterised by a different value of the imposed displacement (Tab. 1), have been selected and considered for the experimental analysis. As a general remark, it can be said that the behaviour of these types of welded joints is generally characterised by stable hysteresis loops and by a satisfactory energy dissipation capabilities. Moreover, independently on the welding procedure, three types of collapse were observed.

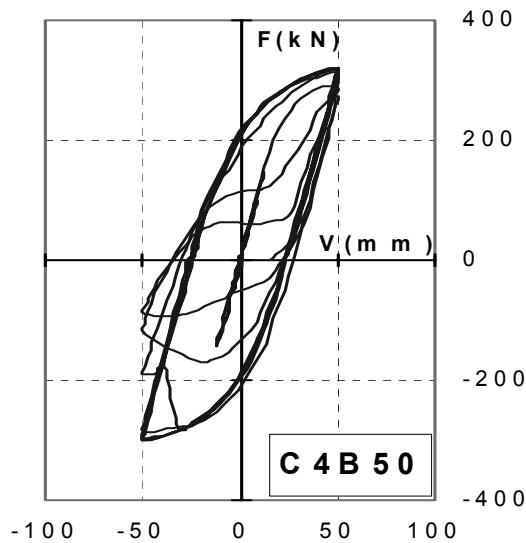


Figure 4: Hysteresis loops for C4B50 joint specimen

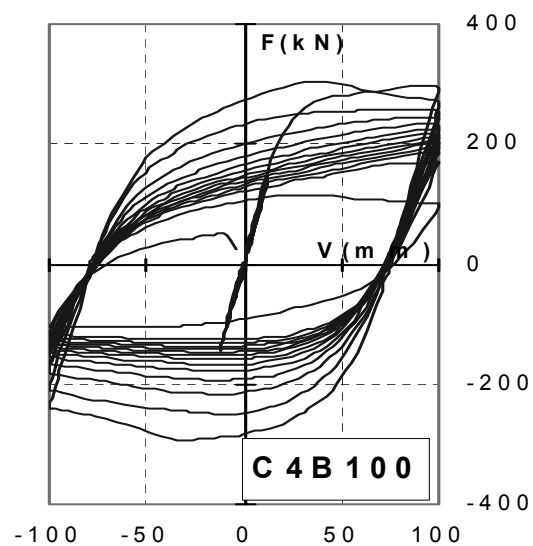


Figure 5: Hysteresis loops for C4B100 joint specimen

RE-ANALYSIS OF TEST RESULTS

A re-analysis of test results shows that the collapse modes occurred for different values of the ductility range $\Delta v/v_y$, defined as the ratio between the imposed displacement range (Δv) and the conventional yield displacement (v_y), evaluated in accordance to the ECCS procedure (16). In particular, the observed collapse modes are:

- brittle failure mode, which was usually achieved under cycles corresponding to small values of $\Delta v/v_y$. Specimen response (see, as an example, fig. 4) was not affected by remarkable deterioration of strength, stiffness and for energy absorption capability. Collapse was sudden, without warning signs, owing to a crack either at the weld toes or in the base material;
- ductile failure mode, generally associated with a large ductility range $\Delta v/v_y$. Joint performance was significantly affected (fig. 5 can be considered an example) by a remarkable and progressive deterioration of the key behavioural parameters, with the formation of a plastic hinge associated with local buckling of the beam flanges. Collapse was caused by the gradual propagation of a crack initiating at surface striations forming, due to attainment of the maximum tensile strain of the material, at the buckles at the plastic hinge location.
- mixed failure mode, which appears as a combination of the two previously described failure modes. It is characterised by a progressive deterioration of the key behavioural parameters, such as stiffness, strength and dissipated energy. This failure mode was usually associated with both plastic hinge formation and local buckling phenomena in the beam flange. However, collapse was generally due to a crack at the weld toes.

Furthermore, in case of brittle collapse, two different failure modes were observed, conventionally identified as B1 and B2. The first one, which was due to a crack formed in the centre of the weld between the beam flange and the column and propagated toward the edges, was observed in all the types of considered rigid joints. Otherwise, failure mode B2, observed only in some C1 and C2 specimens, was caused by through cracks starting at the beam flange edges and propagating toward flange centre.

It must be noticed that the previous definitions of “brittle” or “ductile” failure modes are not correct, in terms of fracture mechanics or metallurgy. However, it is intention of the authors to give an “engineering” definition associated with the “global” behaviour of the joints, and not with “local” parameters, such as those usually adopted in the metallurgic and/or fracture mechanics approach. As far as these ones are considered, all the observed fracture modes should be considered as ductile, as large “local” plastic deformations of the material microstructure occurred.

The Threshold Value of the Displacement Range

Re-analysis of the constant amplitude test data confirms that the previously mentioned types of failure mode depend on the imposed displacement. For each set of similar specimens, joint responses were compared also in terms of F-v envelopes, in order to single out differences related to the observed failure modes (17). As a result, a suitable threshold displacement range, Δv_{Th} , was identified. It has been defined as the displacement associated with the maximum strength obtained from a monotonic test, suitably amplified in order to take into account the cycling loading history. Moreover, a criterion to predict the type of failure and an approach to assess fatigue endurance of the tested components have been developed, both strictly depending on the value of Δv_{Th} .

In absence of experimental data, an approach to estimate the value of Δv_{Th} by means of a simple equation has been developed and validated, with reference to the aforementioned joint tests as well as to other components tested under cyclic loading. In particular, it has been assumed that Δv_{Th} depends on the following parameters:

- the conventional elastic displacement, v_y , which in the following has been identified in accordance with the ECCS procedure (16);

- the beam web slenderness ratio, $\lambda_w = d/t_w$, defined as the ratio between the depth of the profile, d , and the web thickness, t_w ;
- the beam flange slenderness ratio, $\lambda_f = c/t_f$, where c represents half width of the flange and t_f is its thickness;
- the weld quality and/or the severity of the detail, globally accounted for by the introduction of the numerical coefficient η . This term ranges from $\eta=0.5$ for poor quality welds, to $\eta=1.0$ for good quality (or no) welds.

The threshold value, Δv_{Th} , has been hence defined as:

$$\Delta v_{Th} = \frac{\gamma v_y}{\eta \lambda_f \lambda_w} \quad (1)$$

As to the non-dimensional coefficient γ , on the basis of the available experimental data, a value of $2000 \pm 15\%$ (i.e., in the range 1700 - 2300) was suggested, independently on the considered component.

The value of Δv_{Th} related to each tested specimen has been directly obtained also from the envelopes of the cyclic response. The scatter between these values for each set of similar specimens and the ones obtained via eq. (1) is quite limited, confirming the validity of the proposed approach.

In this paper, the threshold value is presented with reference to the displacement, which represents the parameter governing the considered tests. However, it should be noted that the threshold value can be proposed in term of generalised displacement, i.e., if the control parameter is the rotation, the associated value of the threshold rotation can be obtained from eq. (1) by substituting v_y with the conventional yielding rotation Φ_y .

Prediction of the Type of Collapse

As previously mentioned, the value of the threshold displacement, Δv_{Th} , can be used to identify the type of failure mode. In case of constant amplitude loading history, on the basis of the considered displacement range Δv , the following collapse modes are expected:

- brittle failure mode, if Δv is lower than Δv_{Th}^B , defined as $0.85 \Delta v_{Th}$;
- ductile failure mode, if Δv is greater than Δv_{Th}^D , defined as $1.15 \Delta v_{Th}$;
- mixed failure mode, if Δv falls in the range $[\Delta v_{Th}^B, \Delta v_{Th}^D]$.

It should be noted that the approach has been proposed with reference to constant amplitude tests. However, some preliminary results indicate its validity also in case of variable amplitude tests for which term Δv has been considered as an equivalent displacement range (13).

Failure Prediction

Calado and Castiglioni proposed a criterion to assess the fatigue endurance of steel components (15, 18) under cyclic loading. In case of constant amplitude tests, failure is achieved in correspondence of the first cycle that satisfies the following condition:

$$W_f \leq \alpha_f W_0 \quad (2)$$

where W_f is the absorbed energy at the considered cycle (i.e., the cycle during which failure occurs), W_0 represents the absorbed energy at the first cycle in the plastic range, and α_f is a

constant value, for which the value of 0.5 was recommended. Ballio et al. (9) already proposed for the term α_f the value of 0.5, which was conservative only for ductile fracture phenomena; hence a new value of α_f was defined on the basis of the cycle displacement amplitude Δv by the same authors.

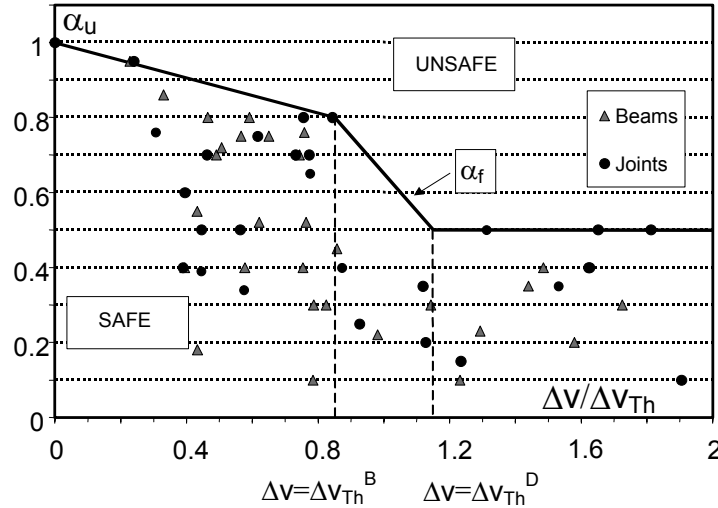


Figure 6: Criterion to predict the type of failure

In the present study, a more refined criterion is proposed (19), which takes into account the failure mode by considering the dependency of α_f from $\Delta v / \Delta v_{Th}$. Figure 6 shows the value of α_u (i.e. the value of the ratio W_u / W_0 , with reference to W_u , the dissipated energy experimentally evaluated at complete failure of the specimen) plotted versus, $\Delta v / \Delta v_{Th}$. An appraisal of the fatigue life can be obtained in the region where the experimental values of α_u are non contained. For the sake of simplicity, the value of α_f governing eq. (2) which bounds this “safe” domain can be defined by the following simplified multi-linear relationship:

$$\begin{aligned}
 \alpha_f &= 1 - 0.235 * (\Delta v / \Delta v_{Th}) & \text{if} & \quad \Delta v / \Delta v_{Th} < 0.85 \\
 \alpha_f &= 1.65 - (\Delta v / \Delta v_{Th}) & \text{if} & \quad 0.85 < \Delta v / \Delta v_{Th} < 1.15 \\
 \alpha_f &= 0.5 & \text{if} & \quad \Delta v / \Delta v_{Th} > 1.15
 \end{aligned} \quad (3)$$

It can be noted that for values of $\Delta v / \Delta v_{Th}$ greater than 1.15 (i.e. for $\Delta v > \Delta v_{Th}^D$) a ductile failure mode is expected, and a constant value of $\alpha_f = 0.5$ is recommended, in accordance with the original Calado and Castiglioni (15, 18) proposal. If $\Delta v / \Delta v_{Th}$ falls in the range [0.85-1.15], i.e., $\Delta v \in [\Delta v_{Th}^B, \Delta v_{Th}^D]$, where a mixed failure mode is expected, a strong dependence of α_f on the cycle amplitude Δv is accounted for by means of a slope equal to unity. For $\Delta v / \Delta v_{Th}$ lower than 0.85, i.e. $\Delta v < \Delta v_{Th}^B$, a brittle failure mode is expected and α_f is assumed moderately decreasing when increasing Δv .

NUMERICAL ANALYSIS

The influence of the key joint components can be singled out from experimental analyses, which result nevertheless a costly approach and are however essential to establish the fundamental background for the validation of all theoretical approaches, but have, by their very nature, a limited

scope. Hence, the necessary parametric investigations appear possible only by means of finite element (FE) simulations, which enable for an exhaustive understanding of both global joint behaviour and local transfer force mechanisms between frame members through joints, over a sufficiently extensive range of both mechanical and geometrical parameters.

In the framework of the current study, an extensive numerical FE analysis has been carried out on the tested joints. The main scope is to analyse local strains near the weld toes, where unexpected brittle fractures were observed after recent earthquakes as well as during the tests previously described. The first results of some numerical simulations, which were executed using the FE non-linear code ABAQUS, (20) are in the following briefly outlined. A three-dimensional (3D) model of the complete specimen (specimen model) was at first developed, which encompassed of 1465 nodes and of 1554 shell elements (fig. 7a). In the nodal zone, i.e., in the part of beam and column in the vicinity of the joint, the mesh was refined to allow a more accurate appraisal of the transfer force mechanisms. In order to simulate local buckling effects, an initial out of straightness was considered by means of geometrical imperfections, which were taken into account via a linear combination of the first two buckling modes with a sinusoidal shape characterised by an amplitude of 0.02mm (i.e, approximately $L/10000$, where L is the beam length in the model). The FE model simulated the complete tested specimens. As a consequence, the load was applied normally to the beam at its free edge; only the transversal displacements at the top of the beam were restrained, consistently with the actual testing conditions.

Moreover, to obtain more accurate information about the local behaviour in the nodal zone, reference was made to the substructuring technique, and a second 3D model (fig. 7b) was considered to simulate the response of a part of the nodal zone (node model), by means of 1200 nodal points and 1150 shell elements. Two models of the node were considered, respectively with and without the web access hole.

As to the constitutive law of the materials, on the basis of the tensile coupon tests, both a bilinear model with strain hardening and a Ramberg-Osgood model (21), which was approximated by means of a multi-linear relationship, were considered. These uni-axial stress-strain relationships, for which a kinematic hardening was considered, have been correlated to the more complex and representative state of loading via the von Mises yielding criterion with associated plastic flow.

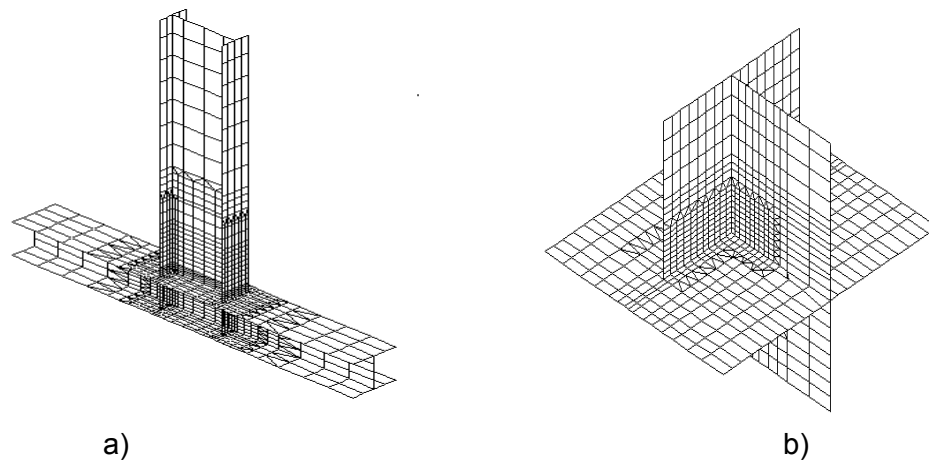


Figure 7: Specimen (a) and node (b) F.E. model

The accuracy of the specimen models was evaluated on the basis of the experimental data, by comparing not only the shape of the hysteresis loops, but also the absorbed energy (both per cycle and cumulated) and the peak values of the force in each cycle as well as the stiffness and strength degradation. An agreement more than satisfactory between numerical and experimental data was observed for all the considered numerical cases. Moreover, an accurate analysis of the local behaviour in term of stresses and strains has been carried out on the models of the node (fig.7b). Five different cyclic loading conditions were considered, four constant amplitude and one variable amplitude loading history. Numerical simulation of nodal zone pointed out a strong dependency of the trend of the principal strains on the loading history. The part of the beam in the vicinity of the welds results subjected to a severe state of stress, when small displacement cycles (i.e., with $\Delta v < \Delta v_{Th}$) are imposed to the specimen. In these cases, the amplitude of the strains near the welds increases remarkably during the loading phase with a moderate decreasing during the unloading phase. The final results is that the strains however increase «in mean» with the number of the cycle. As an example, in case of a cycle amplitude $\Delta v = \pm 50\text{mm}$, the strains assume approximately a value up to 0.3 in the first cycles, independently on the constitutive law adopted for the material and, in correspondence of the 5th-6th cycle reach the maximum tensile strain of the material. It should be noticed that the strains in the beam flange, at the expected plastic hinge location, are negligible. No local buckling effects are evident and there is a shakedown phenomenon (the stresses in the beam flanges are in the elastic range) (Fig. 8).

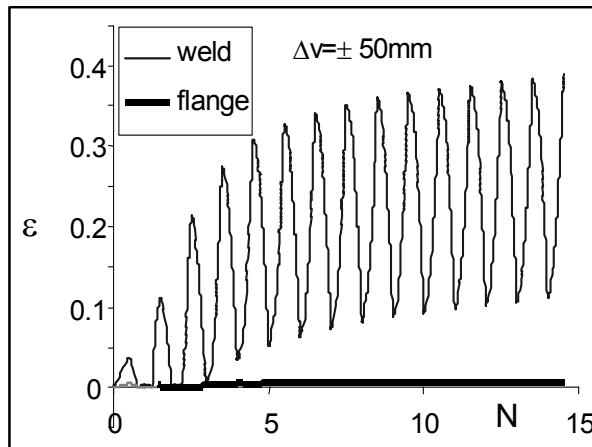


Figure 8: Strain trend vs cycle number for a cycle amplitude $\Delta v = \pm 50\text{ mm}$

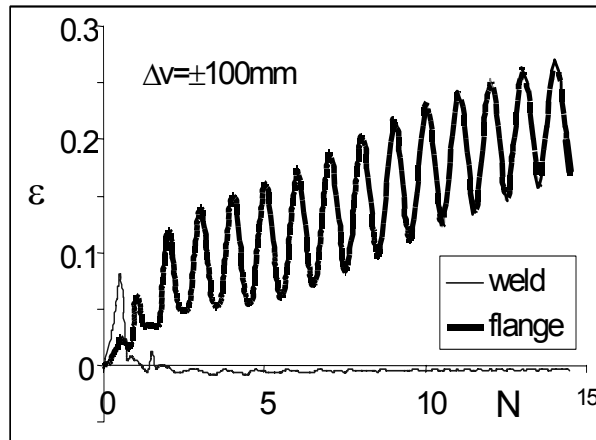


Figure 9: Strain trend vs cycle number for a cycle amplitude $\Delta v = \pm 100\text{ mm}$

On the contrary, when the imposed displacements are greater than the value of Δv_{Th} , the principal strains near the weld decrease after the first cycles and the associate stresses are contained in elastic range, so that the weld zone seems not to be interested by the phenomenon of crack propagation. At the same time, however, the strains in the beam flange increase with the cycle number (fig. 9) and cause the formation of a plastic hinge in the beam, accompanied by evident local buckling of both the web and the flanges (fig. 10) up to the complete failure of the joint, in accordance with experimental features. In case of small amplitude cycles, the presence of the web access hole affected remarkably the values of the local strains in the weld area, which result greater than those associated with the model without access holes. Strain values indicate an earlier collapse due to weld failure or cracking of the base material in the weld area. On the contrary, if large amplitude cycles are considered, when collapse is achieved

at the plastic hinge location, the presence of the web access hole does not influence the failure conditions.

These results show a very good qualitative agreement with the experimental study. In particular, it can be noted that failure modes observed in tests can be associated with different limit conditions of material. If $\Delta V > \Delta V_{Th}^D$, numerical results seem to indicate a local state of strain causing collapse for low-cycle fatigue. In case of $\Delta V < \Delta V_{Th}^B$ brittle failure mode is due to the ratcheting of material.

CONCLUDING REMARKS

A study on the behaviour on joints in moment-resisting steel frames, which comprises both experimental and numerical phases, is briefly presented in the paper.

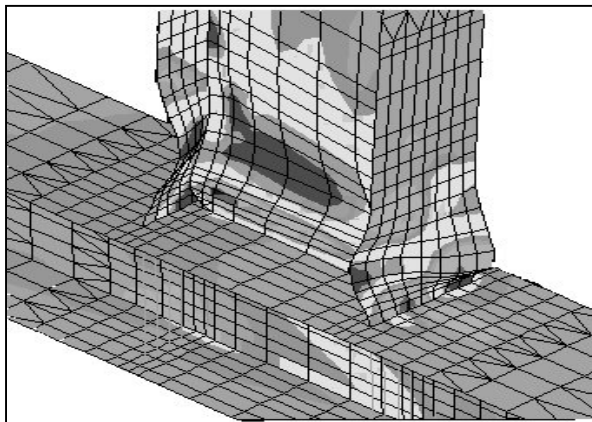


Figure 10: Deformed shape of the joint at collapse

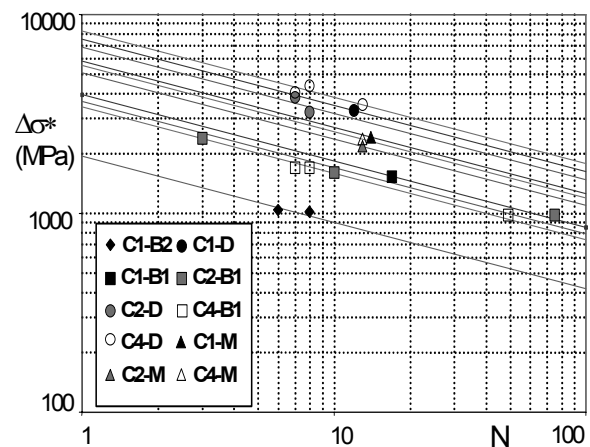


Figure 11: Fatigue resistance lines for tested joints

As to the experimental part of the research, which was carried out on 5 different types of rigid joints for a total of 29 tests, it has been pointed out that different failure modes can occur on the basis on the applied loading history. With reference to constant amplitude loading history, failure modes have been correlated to the cycle amplitude Δv by a suitable threshold value of the displacement range Δv_{Th} . As a consequence, ductile, brittle or mixed failure mode can be predicted with a satisfactory degree of accuracy. It should be noted that, by using the unified approach proposed by Ballio and Castiglioni (22) to assess low-cycle fatigue resistance of steel components, different resistance lines are associated with the identified failure modes. It can also be noted that the connection detail has a limited influence on the fatigue life. As an example, figure 11 plots in the $\log \Delta \sigma^* - \log N$ scale the experimental points related to failure and the fatigue resistance lines defined on the basis of the experimental data. It should be noted that the limit lines related to the ductile failure mode (C1-D, C2-D and C4-D) are the highest, while the ones associated with brittle failure (C1-B1, C1-B2, C2-B1 and C4-B1) are the lowest.

The numerical phase of the study, which encompasses numerical finite element analysis of the nodal zone, is currently in progress. First results indicate that the local strains in the vicinity of the node strictly depend on the loading history and, as a consequence, different failure modes can be expected. Moreover, numerical results indicate that, owing to low-cycle fatigue or ratcheting of the base material, the presence of the web access hole leads to earlier collapse in the weld area in the case of small amplitude cycles while, in the case of large amplitude cycles,

it doesn't influence the failure conditions.

As part of the same research, some full-scale tests on steel frames are presently being carried out at the shaking table facility of the Laboratory for Earthquake Engineering of the National technical University of Athens (Greece). The preliminary results seem to be in good agreement with the conclusions of this paper.

ACKNOWLEDGEMENTS

The research was supported by grants from the Italian Ministry of University and Scientific and Technological Research (M.U.R.S.T.), Co-financed Research Program 1997, from CNR and ICCTI Joint Research Program and from E.C., Environment & Climate Program STEELQUAKE, Contract n. ENV4-CT96-0278, Prop. N. PL950671

NOTATION

c = half width of the flange of an I steel profile

d = depth an I steel profile

E = Young's modulus

F = applied force

f_y = yield strength of the material

N = number of cycles to conventional failure

N_{tot} = total number of cycles experimentally imposed to a specimen

t_f = thickness of the flange of an I steel profile

t_w = thickness of the web of an I steel profile

v = displacement

v_y = yield displacement

W_f = energy absorbed in the cycle at which conventional failure occurs

W_u = energy absorbed in the cycle at which testing was terminated due to complete failure of the specimen

W_0 = energy absorbed in the first complete cycle in the plastic range

$\alpha_f = W_f / W_0$

$\alpha_u = W_u / W_0$

$\gamma = 2000 \pm 15\%$ non-dimensional coefficient in eq. (1)

Δv = displacement range (i.e. amplitude of the imposed displacement cycle)

Δv_{TH} = Threshold value of the displacement range

$\Delta v_{TH}^B = 0.85 \Delta v_{TH}$

$\Delta v_{TH}^D = 1.15 \Delta v_{TH}$

$\Delta \varepsilon$ = strain range

η = numerical coefficient accounting for weld quality and/or severity of the detail in eq. (1)

$\lambda_f = c / t_f$

$\lambda_w = d / t_w$

ϕ_y = yield rotation

$\Delta \sigma^*$ = $E \Delta \varepsilon$ effective value of the stress range, corresponding to the real strain range ($\Delta \varepsilon$) in an ideal indefinitely linear elastic material

REFERENCES

1. Mazzolani F.M., Piluso V., 1996, *Theory and Design of Seismic Resistant Steel Frames*, Chapman and Hall, E&FN Spon.
2. Zandonini R., Bernuzzi C., Bursi O., 1997, *Steel and Steel-Concrete Composite Joints Subjected to Seismic Actions*, **General report of the STESSA'97 Conference, Kyoto-Japan.**

3. Enghelard M.D., Husain A.S., 1993, *Cyclic-Loading Performance of Welded Flange-Bolted Web Connections*, **J. of Struct. Eng. ASCE**, **119:12**, 3537-3549.
4. Tsai K.C., Shun W., Popov E., 1995, *Experimental Performance of Seismic Steel Beam-Column Moment Joints*, **J. of Struct. Eng. ASCE**, **121:6**, 925-931.
5. Plumier A., 1994 *Behaviour of Connections*, **Journal of Constructional Steel Research**, **29**, 95-119.
6. Bertero V., Anderson J.C., Krawinkler H., 1997, *Performance of Steel Building Structures during the Northridge Earthquake*, EERC, University of California, Berkeley.
7. Tremblay R., Timler P., Bruneau M., Filiatrault A., 1995, *Performance of Steel Structures during the Northridge Earthquake*, **Canadian Journal of Civil Engineering**, **22:4**.
8. Kuwamura H., Yamamoto K., 1997, *Ductile Crack as Trigger of Brittle Fracture in Steel*, **J. of Struct. Eng. ASCE**, **123:6**, 729-735.
9. Ballio G., Calado L., Castiglioni C. A., 1997, *Low cycle fatigue behaviour of structural steel members and connections*, **Fatigue & Fracture of Engineering Materials & Structures**, **20: 8**, 1129-1146
10. Bernuzzi C., Calado L. Castiglioni C.A., 1998, *Behaviour of steel beam-to-column joints under cyclic reversal loading: an experimental*, **Stability and Ductility of Steel Structures**, Edited by T.Usami & Y. Itoh, Elsevier Science Ltd, , pp. 279-292.
11. Ballio G., Castiglioni C.A., 1994, *Seismic Behaviour of Steel Sections*, **Journal of Constructional Steel Research**, **29**, 21-54.
12. Calado, L., Castiglioni, C. A., Barbaglia, P., Bernuzzi, C., 1998, *Seismic design criteria based on cumulative damage concepts*, **Proc. of 11th European Conf. on Earthquake Engineering, Paris**.
13. Calado, L., Castiglioni, C. A., Barbaglia, P., Bernuzzi, C., 1998, *Procedure for the assessment of low-cycle fatigue resistance for steel connections*, **Liege Conf. on Control of the Semi-Rigid Behaviour of Civil Engineering Structural Connections, Liège**.
14. Plumier, A., Agatino, M. R., Castellani, A., Castiglioni, C. A., Chesi, C., 1998, *Resistance of steel connections to low-cycle fatigue*, **Proc. of 11th European Conf. on Earthquake Engineering, Paris**.
15. Castiglioni C. A., Calado L., 1996, *Seismic damage assessment and failure criteria for steel members and connections*, **Int. Conf. on Advances in Steel Structures, Hong Kong** vol. II, pp.1021-1026.
16. European Convention for Constructional Steelworks (ECCS) 1986, *Recommended testing procedure for assessing the behaviour of structural elements under cyclic loads*, **Technical Committee 1, TWG 1.3 - Seismic Design, ECCS Publication No. 45**.
17. Castiglioni C.A., Bernuzzi C. Calado L., Agatino M.R., 1997, *Experimental study on steel beam-to-columns joints under cyclic reversal loading* , **Proc. Of the Northridge Earthquake Research Conference, Los Angeles**, pag. 526-533.
18. Calado L., Castiglioni C.A., 1996, *Steel Beam-to-Column Connections Under Low-Cycle Fatigue Experimental and Numerical Research*, **Proc. of the XI World Conf. on Earthquake Engineering, Acapulco**
19. C.A. Castiglioni, 1999, *Failure criteria and cumulative damage models for steel components under low-cycle fatigue*”, **Proc. XVII C.T.A. Conference, Napoli**
20. Hibbitt, Karlsson & Sorensen Inc., 1996, “*ABAQUS User's Manual*” Version 5.5
21. Ramberg W., Osgood, W., 1943 *Description of stress-strain curves by three parameters*, **Technical Note n° 902, NACA**
22. Ballio G., Castiglioni C.A., 1995, *A unified approach for the design of steel structures under low and high cycle fatigue*, **J. of Constructional Steel Research**, **34**, 75-101

Performance of Jumbo Beam-to-Column Connections with High Strength Steel

Sheng-Jin Chen, National Taiwan University of Science and Technology,
P.O. Box 90-130, Taipei, TAIWAN

ABSTRACT

This paper describes the experimental studies of the seismic moment connections with jumbo sections and high strength steel. The steel selected is the ASTM A572 Gr. 60 steel and the flange thickness of steel beams is 50 mm. The flange plate of beam in the pre-selected zone is tapered to let the provided moment strength equal to the seismic moment demand. The plastic rotational angle can be more than 0.03 radians. It is also suggested that the end tabs should be removed.

INTRODUCTION

The fractures of beam-to-column connections of steel buildings in the Northridge and Kobe earthquake generated concern about the reliability of conventional steel moment connections. Due to the nature of seismic force, the strain is concentrated toward the complete joint penetration (CJP) weld between beam flange and column flange of beam-to-column connections, leading to the inadequate ductility of the traditional connection. Prior to the Northridge and Kobe events, the author has suggested to trim part of the beam flanges to significantly enhance the ductility of the connection by still meeting the moment demand. By this simple arrangement, an enlarged plastic zone can be obtained in the area away from the weld, thereby fully utilizing large deformation capacity of the steel plate. Series of studies have been conducted on this type connection. These experimental studies cover the beam sizes and steel grades that are commonly used in practice. However, occasionally it is necessary to design steel frames adopt jumbo sections and/or high strength steel, especially in the high-rise buildings. Although the weldability of high strength steel and thick plate is questionable in the seismic design of beam-to-column connection, however, the ductile connection method proposed by the author is aimed at depending the energy dissipation capacity on the steel plate itself and rely on the higher strength of the weld. Since the proposed connection method is able to provides an enlarged plastic zone on the steel plate that is away from the field weld, the energy dissipation capacity can be assured even with high strength steel and thick plate welding. This paper described the experimental studies of the seismic moment connections with jumbo sections and high strength steel. A series of experimental studies of using high strength steel and jumbo section are performed. The steel selected is the ASTM A572 Gr. 60 steel and the flange thickness of steel beams is 50 mm (2 inches). The deformation capacities of the beam-column assemblages were examined. The effects of end tabs and backing bars on the ductility of the connection were also discussed. The following is a brief description of this

connection method.

DUCTILE BEAM-TO-COLUMN CONNECTION

Although the reliability of field welding has always been questionable and is generally blamed for the fracturing of the connection, a lack of deformation capacity has also been reported from large-size experimental studies in the laboratory (1). Brittle fractures of moment connection also indicate that ductile materials do not ensure ductile structure, but the geometry, type of loading and material properties may affect the structural behavior. The stress (strain) concentration from the seismic moment gradient may severely interfere with the spread of the plastic area around the connection and this may account for the brittle fracture of the connection (2). This can be explained by Fig. 1 in which the moment diagram along the beam of a moment frame under seismic lateral force is shown in Fig. 1a, and this can be modeled by the equivalent cantilever beam shown in Fig. 1b. For a typical wide flange steel beam, the flexural strength comes primarily from the flange plates; the bending moment of Fig. 1b would result in the normal stress of the flange plate along the beam length as shown in Fig. 1c. The stress state of Fig. 1c can be represented by the equivalent steel plate shown in Fig. 1d that has a varying width and is subjected to a uniform tensile load at its far end. However, based on the theory of strength of material, a high stress (strain) concentration will result on the fixed end of the equivalent plate and very limited deformation capacity is obtained. This phenomenon can be further explored by examining the tension coupons in Fig. 2. Fig. 2a shows tension coupons under uniform forces at their ends. When the loads are gradually increased, the reduced sectional area of Fig. 2a yields uniformly; however, the tension coupon of Fig. 2b with a varying width along its length yields about the section of minimum width only. As the plastic deformation concentrate on a limited area as shown in Fig. 2b, only limited capacity for energy dissipation is expected and its deformation characteristics are classified as brittle. Although the tension coupon shown in Fig. 2c has the same sectional properties as Fig. 2a except greater length of constant stress area, Fig. 2c possesses a larger plastic volume and dissipates more energy than Fig. 2a. Comparing Fig. 1d and Fig. 2b, one can easily found that brittle fracture will occurred. The stress gradient markedly affects the capacity of the spread of the plasticity around the connection. Moreover, with the effect of large thermal input during welding and stress concentration due to abrupt geometry variation, the capacity of steel beam to deform is severely inhibited. This phenomenon provides another explanation why steel beam-to-column connection may possess only limited ductility. For the same reasons ductile materials fail to ensure a structure to be invariably ductile unless a proper design is made.

Figure 1 indicates that the stress state around the connection markedly interferes with the formation of a plastic hinge. Increasing the deformation capacity of the connection must be solved according to the fundamental mechanism of deformation about the connections. It is of interest to examine Fig. 2c in which a large area of constant stresses is produced; if the load is increased, the yielding stress is attained simultaneously in the middle part of the coupon. On the basis of this concept, the author proposed a beam-to-column moment connection method that can create a finite area of plastic zone by means of the concept of constant stresses. This objective is attained by shaving the beam flanges near the connection according to the moment demand so as to produce an enlarged area of a plastic hinge (2). Using this arrangement, the beam in the pre-selected area can be plastified simultaneously and an enlarged plastic zone can be obtained as shown in Fig. 3. Series of experimental and analytical studies showed that the proposed connection method can achieve an enlarged plastic zone and the deformation capacity can be improved. These included experimental studies of large size beam-to-column subassemblage with and without floor slabs, and reduced scale shaking table test of steel frames (2~5). The following described the study of jumbo size beam-to-

column connection that applying this connection method.

EXPERIMENTAL STUDIES

The beam selected for experimental studies is H700X300X25X50. The length of beam from loading point to the column surface is 3725mm. The column is H600X600X25X50 with the length of 2945 mm. ASTM A572 Gr. 60 steel is used for both beam and column. Both beam and column are of built-up sections. The design of the specimen is shown in Fig. 4. The CJP weld between column flange and beam flange is done by SMAW with electrode of E8016- ϕ 5mm. In order to create the most severe condition around the CJP weld, the thickness of beam flange, column flange, and continuity plates are all of 50 mm.

All the design follows the current AISC-LFRD and the Taiwanese seismic code. The backing bars of Specimen No. 1 and No. 2 were removed and back gouged to sound weld, then an supplemental weld in over-head position was added. The backing bars of Specimen No. 3 and No. 4 were left in place in order to compare with Specimen No. 1 and No. 2.

The specimen were loaded with two elastic cycles of $0.3\delta_y$ and $0.6\delta_y$. Then the specimen were loaded to δ_y and follows with the increment of $1\delta_y$ in the inelastic ranges. However, due to the limitation of the stroke of the actuator, in larger displacement amplitudes, it was necessary to unload and re-center the position of the actuator. Depend on the required amplitude, it might need to unload and reload couple times before the designated displacement amplitude is reached.

DISCUSSION OF EXPERIMENTAL RESULTS

Failure Modes

All the specimen tested exhibited yielding at the pre-selected zone. Before final fracture occurred, cracks were found at both edges of the beam flange plate and center of flange plate that was near the weld access hole. The cracks were first observed at $2\sigma_y$. Fracture occurred at $3\sigma_y$ for Specimen 1 due to the propagation of cracks at the junction between end tabs and flange plates (Fig. 5). The end tabs of Specimen 2~4 were then removed and after the tiny initial crack at $2\sigma_y$, yielding in the pre-selected zone caused the joint continues deformed and the crack gradually propagated in the subsequent loading cycles (Fig. 6, Fig.7). Finally, the fracture occurred at $6\sigma_y$. Different from the failure modes of most connecting tests done before, no local buckling was observed in these jumbo specimen. This was because these tests use thick plate that preventing local buckling. The final failure mode was the fracture of the connection (Fig. 8). Since the average strength of the specimens is 1.08 Mp which is larger than the required strength 0.8 Mp ($\underline{6}$), it seems that the strength in the object zone can be further reduced. For example, if the strength in the object zone is 20% less than the nominal required value (10% reduction is adopted for these specimen), the stress at the joint can be reduced and it is believed that the deformation capacity can be further increased.

Effect of End Tabs and Backing Bars

The role of end tab is to facilitate sound weld for the full length of the joint. Cracking and porosity are easily developed at the start and termination point of the weld. By using end tabs, these defects can be kept out of the length of the joint. However, if these end tabs are left in place, the possible defect are still exist in the weld and the stress will be transmitted to the real full length of the weld (including the end tabs). As the applied load gradually increased, crack may initiated from this area. Specimen 1 was the only specimen that the end tabs were left in

place and the crack was initiated from the junction of the end tabs and the flange plate as shown in Fig. 5. This also reflected on the plastic rotational angle of the connection. The average plastic rotational angle of Specimen No. 1 was only 0.016 radians, while the average plastic rotational angle of Specimen 2~4 was 0.039 radians. It is suggested to remove the end tabs to ensure good welding quality in the whole length of the weld.

Steel backing bars were used at the CJP weld between beam flange and column flange plate. Although backing bars are used to support the weld during welding process and is not considered to the strength of the joint. However, after the welding, the backing bars become part of the permanent structure and do participate in the stress transfer between the joint members. The gape between the backing bar and the beam flange and/or column flange become a natural crack and may lead to the premature fracture of the joint. After Northridge earthquake, some specifications suggest to remove the backing bars, at least the backing bar of bottom flange connection (Z). However, to remove the backing bar and add supplemental weld in overhead position in the field is very difficult. In this study, the backing bars of Specimen 1 and 2 were removed while the backing bars of Specimen 3 and 4 were left in place. The end tabs of Specimen 1 were left in place while the end tabs of all other specimens were removed. The welding details of Specimen 2~4 were the same except the backing bars of specimen 2 were removed. From the experimental results of specimen 2~4, there was no clear evidence of the benefit of removing backing bars. The strengths and plastic rotational angle of these specimens were about the same.

Ultimate Strength

The ultimate strengths of the specimen are listed in Table 1. In current design practice, the required strength of reduced beam section method is 0.8 Mp (6). Although the specimens tested were designed to achieve the strength 10 % less than the nominal value, the average true strength to that of nominal strength is 1.08, which is considered adequate for the strength requirement.

Ductility

Fig. 9 shows the hysteresis behavior of the connections tested. The plastic hysteresis behavior of the connections shown in Fig. 9 were obtained by deducting the elastic deformation from the total deformation. The maximum plastic rotational angle attained was listed in Table 1. Compared to previous test results (3), tests in this series also demonstrate the stable and reliable features of the hysteresis behavior that is not difficult to understand as the plasticity is mainly from the yield of a steel plate and the effect of welding has been minimized. Although jumbo section and high strength steel is used in this study, it seems that by designing a pre-selected zone to let uniform yielding can occurred in this region, the sensitivity of welding due to thick plate can be relaxed and good energy dissipation behavior can be obtained.

SUMMARY AND SUGGESTIONS

The brittle fractures of the welded moment connections from recent earthquakes indicated that the conventional method is not able to ensure ductile behavior of steel frames under seismic load. By trimming the flanges of the beam around the connection to let the provided moment capacity be equal to that of the demand value, an enlarged plastic zone can be achieved and the deformation capacity can be improved. By forcing yielding to occur in the pre-selected area which is away from the CJP weld of the connection, the sensitivity of welding is relaxed and the energy dissipation becomes much more reliable. Experimental studies of jumbo section which was made from high strength steel also demonstrated good energy dissipation capacity. From experimental studies, it was found that in or around the end tabs, there might be some welding

defects and the end tabs was suggested to be removed. However, no clear evidence on the benefit of removing the backing bars and re-weld at the overhead position. It was also found that the amount of the tapering could be increased to reduce the stress level at the junction of beam and column so that the crack initiation could be deferred.

ACKNOWLEDGMENTS

The work presented in this paper was sponsored by China Steel Company. Specimens were fabricated by China Steel Structure Company.

REFERENCES

1. Chen, S.J. and Chen, G.K. (1990). Fracture of steel beam to box column Connections, Chinese Inst. Engrg., 16(3), 381-394
2. Chen, S.J. (1993). Failure modes of beam-to-column connections in steel high-rise buildings and development of ductile beam-to-column connections", The 14th ROC-Japan Engineering workshop (in Chinese)
3. Chen, S. J. and Yeh, C.H. (1994). Enhancement of ductility of steel beam-to-column connections for seismic resistance. SSRC 1994 Tech. Session, Lehigh University, Pa.
4. Chen, S.J., Yeh, C.H. and Chu, J.M. (1996). Ductile steel beam-to-column connections for seismic resistance. J. Struct. Engrg., ASCE, 122 (11)1292-1299.
5. Chen, S.J., Chu, J.M. and Chou, Z.L. (1997). Dynamic behavior of steel frames with beam flanges shaved around connection. J. Constructional Steel Research, 42 (1) 49-69.
6. SAC Joint Venture (SAC). (1999). Interim Guidelines Advisory No. 2, Supplement to FEMA-267, FEMA-267B, Sacramento, Ca.
7. AISC, (1997), Seismic Provisions for Structural Steel Buildings.

Table 1 Test Results of Large Scale Specimens

Specimen	$M_u / M_{p,n}$	$M_u / M_{p,m}$	θ_p (radian)
No. 1	+0.993	0.88	+0.0116
	-1.069	-1.009	-0.0204
No. 2	+1.063	+1.003	+0.0333
	-1.081	-1.019	-0.0285
No. 3	+1.115	+1.052	+0.0425
	-1.085	-1.023	-0.0276
No. 4	+1.145	+1.080	+0.0355
	-1.115	-1.052	-0.0361
Average	+1.083	+1.015	+0.0294

- Note: 1. Positive loading: top flange of beam is under compression.
 Negative loading: top flange of beam is under tension.
2. $M_{p,n}$: nominal maximum strength of steel beam
3. $M_{p,m}$: maximum strength of steel beam based on true material strength

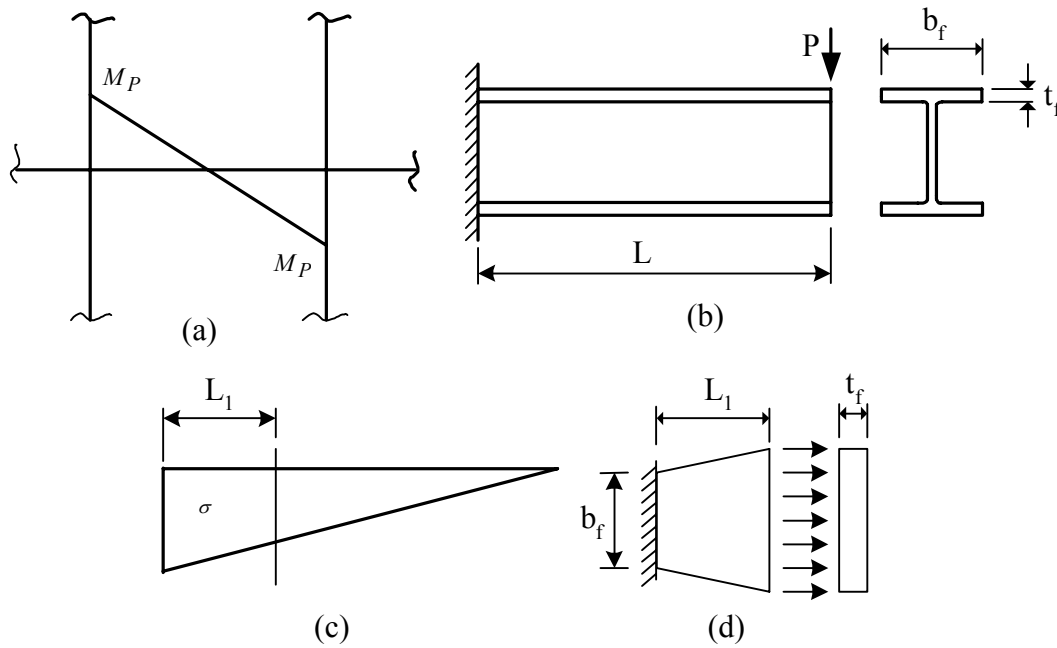


Fig. 1 Stress states of a frame under earthquake loading

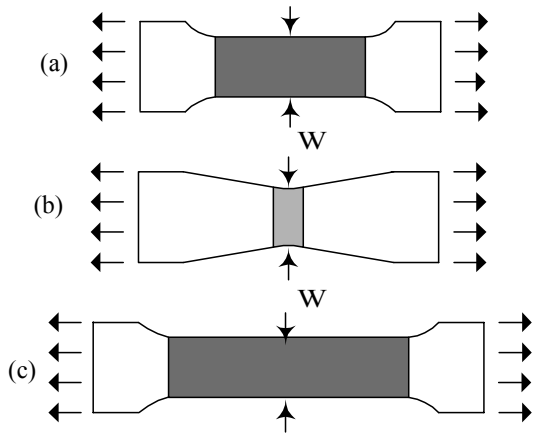


Fig. 2 Tension coupons under uniform forces

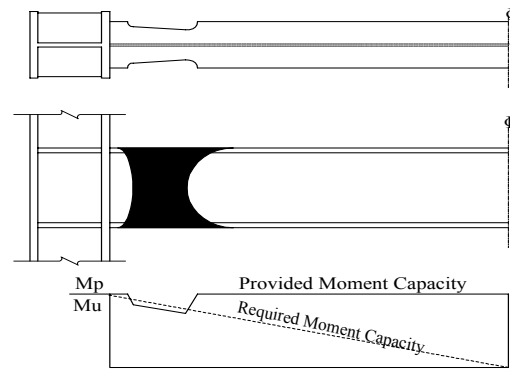


Fig. 3 Enlarged plastic zone of proposed connection method

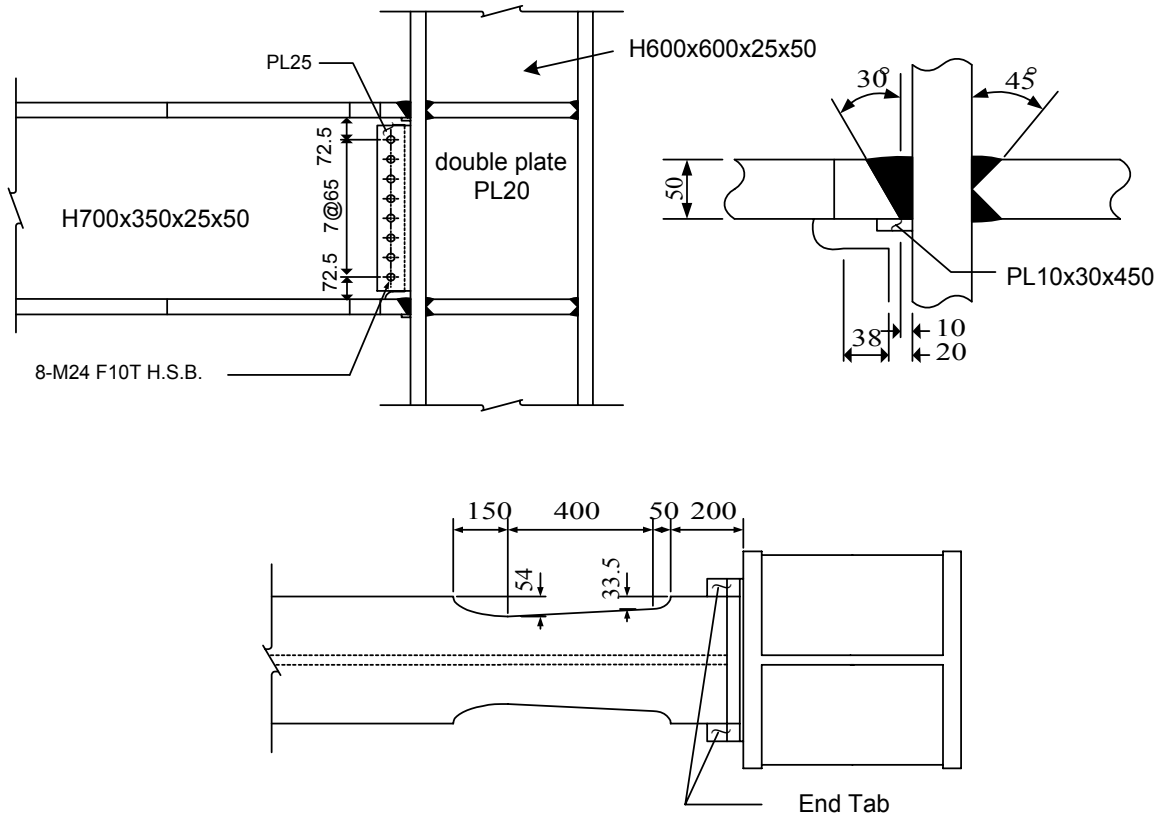


Fig. 4 Design of specimens



Fig. 5 Fracture of Specimen No. 1



Fig. 6 Typical yielding zone on web

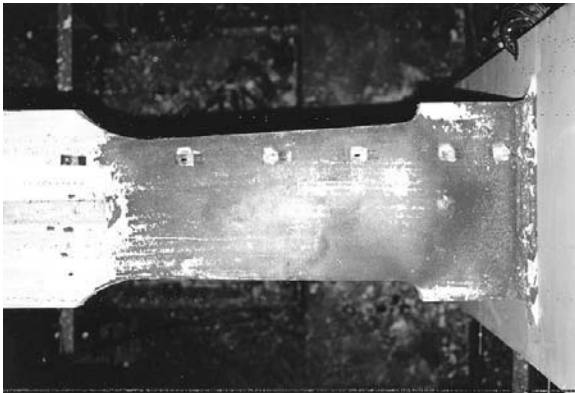


Fig. 7 Typical yielding zone on flange



Fig. 8 Fracture of Specimen No. 2

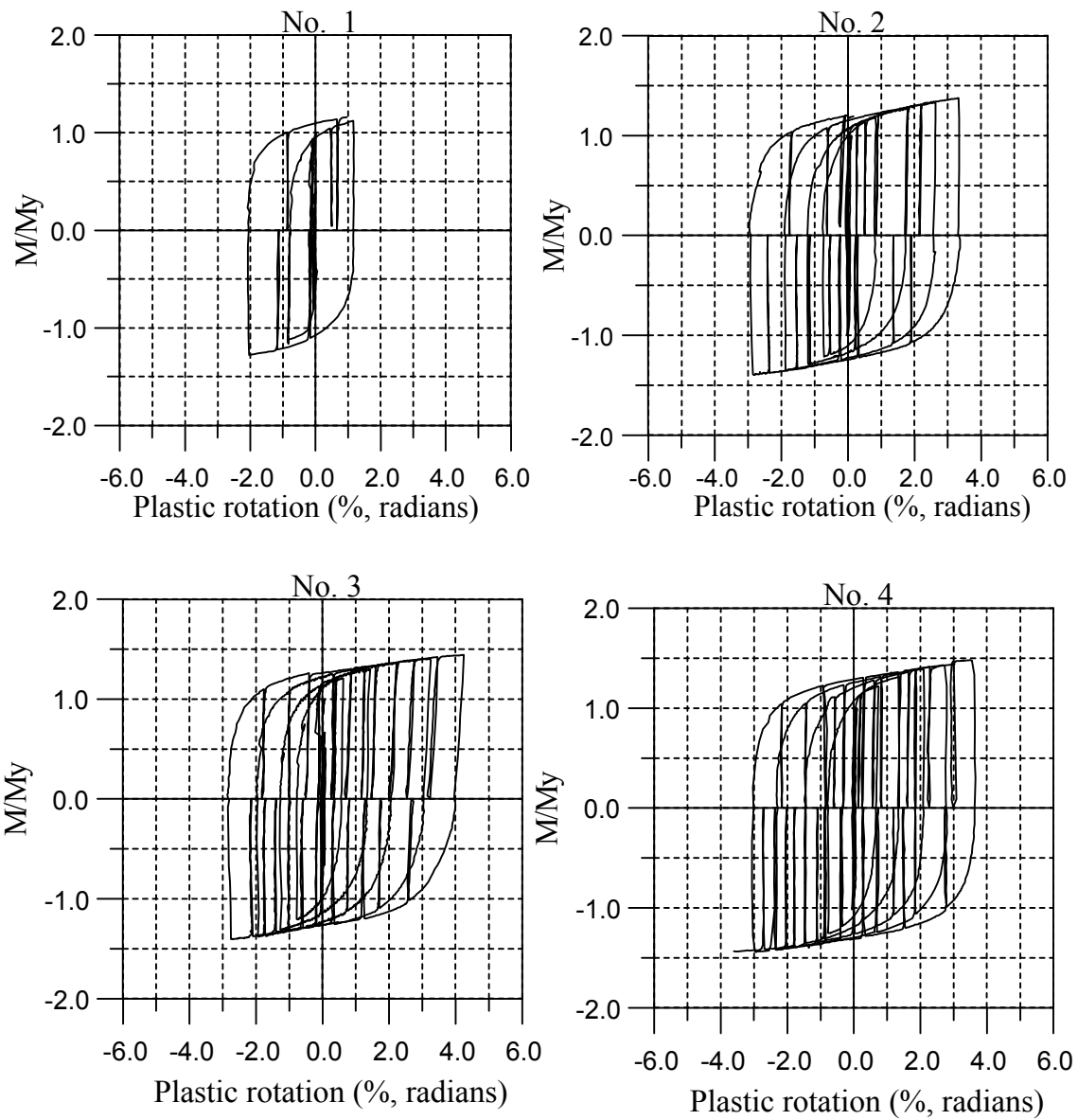


Fig. 9 Hysteresis behavior of specimens

Experimental Testing of Retrofit Steel Moment Connections

Scott A. Civjan, University of Massachusetts, Amherst
Michael D. Engelhardt, University of Texas, Austin

ABSTRACT

An experimental program is described which investigated two methods of retrofitting existing pre-Northridge steel moment resisting frame connections. Typical pre-Northridge connections were retrofit either by the addition of a bottom flange reduced beam section (dogbone) or by the addition of a welded bottom flange haunch. Tests included matched pairs of specimens, one bare steel and one including a composite slab. This paper provides a summary of the experimental program and effects of the composite slab.

INTRODUCTION

In response to steel moment resisting frame connection failures in the 1994 Northridge Earthquake, major testing programs were initiated to establish safe connection detail standards. The purpose of this project was to evaluate two promising new construction details for use in the retrofit of existing structures. These two techniques were i) the addition of a welded haunch at the beam bottom flange, and ii) the addition of a reduced beam section (RBS), also known as a dogbone, cut at the beam bottom flange. These techniques were believed to be among the most promising for retrofit based on past experimental data. The welded haunch had shown good performance in a limited number of tests for repair and retrofit of existing connections (Shuey and Engelhardt (1), Uang and Bondad (2)) but had not been previously tested with a slab. The RBS connection had shown good performance in new construction applications (Chen and Yeh (3), Engelhardt et al (4), Iwankiw and Carter (5), Tremblay et al (6)), but had not been tested for retrofit applications. Both the RBS and haunch retrofits investigated in this program were chosen to require little or no modification to the beam top flange, thereby minimizing the need to remove or alter the floor slab. This would make them well suited to retrofit applications. An acceptance criterion of 0.02 radian of plastic rotation was chosen in accordance with Gross et al (7), although comparisons to the current new construction standard of 0.03 radian were also made.

TEST SETUP

Tests were performed on full sized interior joint subassemblages. Points of inflection were assumed at column story mid-heights and at beam mid-spans. A typical story height and beam

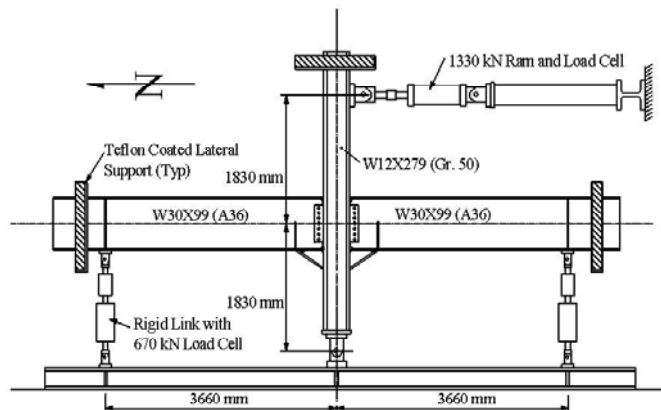


Figure 1 : Test Setup

span were assumed. The overall test frame schematics can be seen in Fig 1. The test specimens were chosen to be representative of building construction details in common use prior to the Northridge Earthquake, and to not duplicate specimens investigated elsewhere. Beams were W30X99 sections of A36 steel. Columns were W12X279 sections of A572 Grade 50 steel to provide strong column, weak beam action and to provide for a strong panel zone. Three pairs of specimens were tested. Each pair consisted of a bare steel specimen and a similar specimen with a composite slab attached. In the first pair the RBS retrofit was investigated. In the second and third sets a haunch retrofit with slightly differing weld procedures was investigated.

In keeping with the actual construction sequence the specimens were assembled as an “original connection”, and then retrofitted. Specimens of pre-Northridge design with W30X99 beams were tested previously as part of the SAC program (“Connection” (8)). These previous results were referenced as a benchmark for the performance of the retrofit specimens. Overall specimen details are compiled in Table 1. Additional information can be found in Civjan et al (9). Beam materials came from four separate heats of steel with average measured stresses of: static yield of 329 MPa (47.7 ksi), dynamic yield of 345 MPa (50.0 ksi) and dynamic ultimate of 452 MPa (65.6 ksi). The “original” connection was designed, detailed, and constructed in a manner typical of mid 1970’s pre-Northridge building construction.

Table 1: Specimen Details

Specimen	Type of Retrofit	Modification to Beam Flange Welds		Composite or Bare Steel
		Top Flange	Bottom Flange	
DB1	Bottom Flange Dogbone	None	Backing Bar and Weld Tabs Removed	Bare Steel
DB2	Bottom Flange Dogbone	E70T-4 Completely Removed Reweld with E71T-8 Weld Tabs Removed, Backing Bar Left in Place with Seal Weld to Column	E70T-4 Completely Removed Reweld with E71T-8 Backing Bar and Weld Tabs Removed	Composite
HCH1	Bottom Haunch	None, Flaws Left in Place in North & South beams	None, Flaws Left in Place in South beam	Bare Steel
HCH2	Bottom Haunch	None, Flaws Left in Place in North & South beams	None, Flaws Left in Place in South beam	Composite
HCH3	Bottom Haunch	None	None, Flaws Left in Place in North and South beams	Bare Steel
HCH4	Bottom Haunch	Weld Tabs Inadvertently Removed	None, Flaws Left in Place in North beam	Composite

The RBS retrofit method required some special considerations. First, discussions with fabricators indicated that cutting an RBS in the beam top flange in the presence of a floor slab would likely be difficult and costly. Consequently, an RBS cutout was provided in the bottom flange only. Second, the flange area reduction was limited to a maximum of 50 percent of the total flange area due to concerns over the stability of the beam should larger reductions be provided. RBS specimens (DB1 and DB2) were therefore reduced with a radius cut contour with a 50 percent flange reduction at the bottom flange only. This differs from new construction designs where both the top and bottom flanges would commonly be reduced. The haunch retrofit (HCH1, HCH2, HCH3 and HCH4) consisted of welding a wide flange section into the area of intersection of the bottom beam flange and column flange. Sizing of the haunch was chosen to replicate details tested by Uang and Bondad (2).

One of each pair of similar specimens included a 2440 mm (8 ft) wide composite slab. The goal was to observe the effects of a typical building slab on composite connection performance. Detailing was representative of past construction practice in California and was recommended by practicing engineers. Metal decking was oriented perpendicular to the beams and lightweight concrete was used. The number and location of shear studs was chosen to be representative of existing buildings. These shear studs did not provide fully composite action, but were chosen to provide the capacity of the expected maximum compressive force in the concrete slab. This force was estimated to be $1.3f_c$ times the effective slab area in contact with the column flange, per Du Plessis and Daniels (10). Specimens DB1, HCH1, and HCH3 were bare steel specimens, while DB2, HCH2, and HCH4 were composite. Concrete compressive strengths on the day of testing were 33.7, 42.3, and 22.2 MPa (4883, 6132, and 3220 psi) for specimens DB2, HCH2, and HCH4 respectively.

Welds in the “original” connection were made using the self shielded flux core arc welding (SS-FCAW) process with a 3 mm (0.120 in.) diameter E70T-4 electrode. Backing bars and weld tabs were left in place for the “original” connection. All “retrofit” welds were made using SS-FCAW with a 1.8 mm (0.072 in.) E71T-8 electrode.

RESULTS

Overall hysteretic response for several specimens, plotted as the load versus column tip deflection as well as story drift, can be seen in Fig. 2. Specimens HCH1 and HCH2 results were very similar to HCH3 and HCH4 respectively. A summary of the test results is presented in Table 2. Noted observations on composite behavior included the failure of many shear studs during testing, reduced top flange strains, unchanged bottom flange strains, and an improvement in resistance to observed instabilities. Photographs of selected specimens after testing are shown in Fig. 3.

Overall Performance:

The bare steel bottom flange RBS (DB1) exhibited the poorest performance of all specimens tested. Bottom flange groove welds for both beams failed within the existing low toughness weld metal, near the weld-beam interface, at low levels of total plastic rotation (0.006 and 0.009 radian). This specimen did not provide any increase in performance over a non-retrofitted connection. The composite bottom flange RBS (DB2) exhibited a marked improvement over specimen DB1, achieving beam plastic rotations of 0.020 radian. Both connections, however, still failed by fracture of the bottom flange groove welds. Bottom flange fractures in DB1 and DB2 appeared to initiate at the center of the beam flanges, near the beam web cope. Inspection of the weld fracture surfaces revealed some rather large slag inclusions in DB2 not detected by ultrasonic testing which may have contributed to the weld failures. Specimen DB2 still sustained much higher levels of plastic rotation than DB1, likely due to a substantial benefit from the higher toughness weld metal (composite slab effects were also involved.) Once the bottom flange welds failed, the behavior was extremely poor and degraded substantially during later load cycles. Although specimen DB2 obtained beam plastic rotations meeting or exceeding the 0.020 radian of plastic rotation acceptance criteria, the weld fractures occurred at levels very close to this acceptance criteria. Variations in slab details, such as stronger concrete, more reinforcing steel, or steel decking oriented in the other direction, may cause earlier fractures. Therefore, the connection detail tested must be viewed with caution. It is felt that additional flange reduction, either to top and bottom flanges or greater than 50%, could be a potential solution to preventing the early weld fractures. The latter possibility has not been tested and may be susceptible to stability problems.

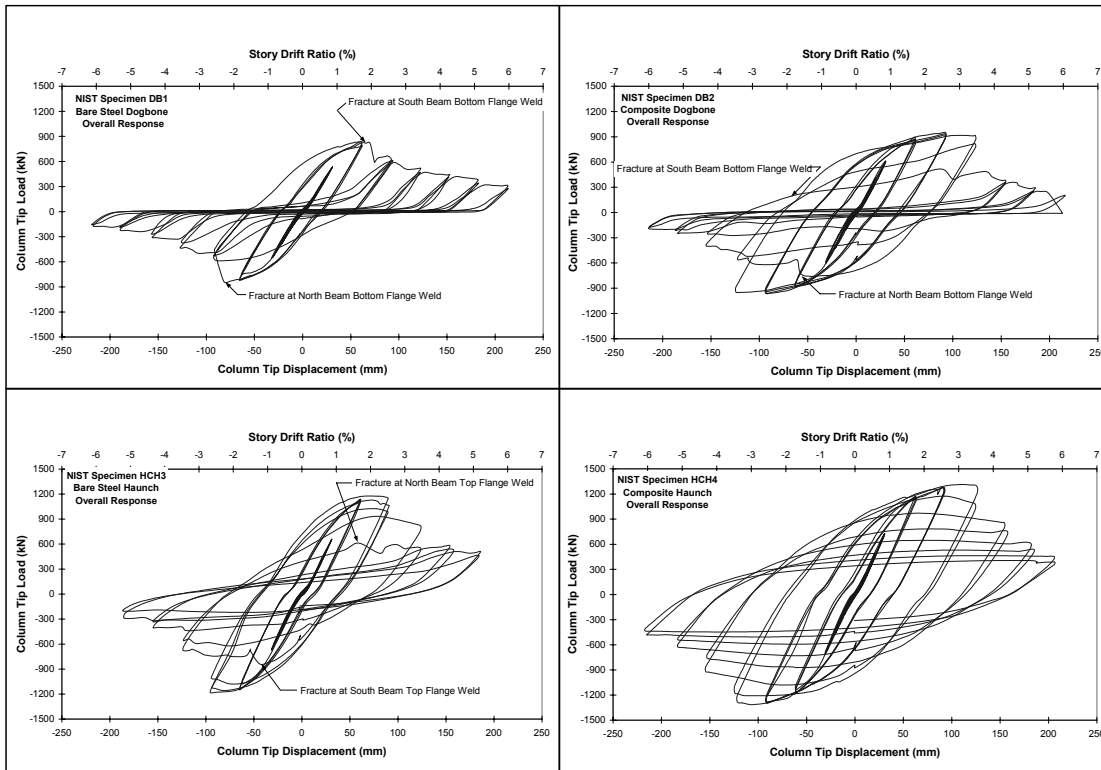
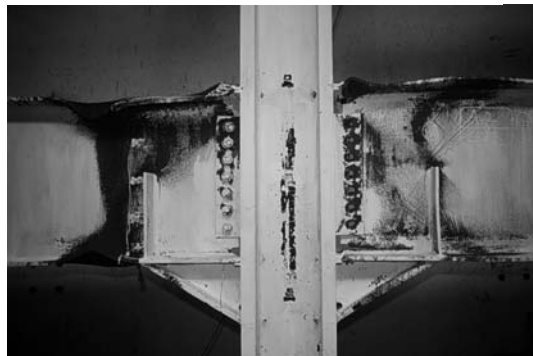


Figure 2 – Specimen Load vs. Story Drift/Tip Deflection



a) DB1



b) HCH3



c) DB2



d) HCH4

Figure 3: Specimens After Testing

Table 2: Test Results

Specimen	Brief Description of Failure		Total Plastic Rotation*	
	North Beam	South Beam	North Beam	South Beam
DB1	Fracture of Bottom Flange Weld	Fracture of Bottom Flange Weld	0.009 radian	0.006 radian
DB2	Fracture of Bottom Flange Weld	Fracture of Bottom Flange Weld	0.020 radian	0.020 radian
HCH1	Fracture of Top Flange Weld	Gradual Deterioration in Strength Due to Local and Lateral Buckling	0.012 radian	0.044 radian
HCH2	Gradual Deterioration in Strength Due to Local and Lateral Buckling	Gradual Deterioration in Strength Due to Local and Lateral Buckling	0.030 radian	0.030 radian
HCH3	Fracture of Top Flange Weld	Fracture of Top Flange Weld	0.023 radian	0.013 radian
HCH4	Gradual Deterioration in Strength Due to Local and Lateral Buckling	Gradual Deterioration in Strength Due to Local and Lateral Buckling	0.050 radian	0.050 radian

*Note: 1) Total plastic rotation is computed with respect to the centerline of the column.

Three of the four bare steel bottom haunch connections (specimens HCH1 and HCH3) failed by fracture of the existing E70T-4 top flange welds at total plastic rotations in the range of 0.012 to 0.023 radian. The similar behavior of specimen HCH3 confirmed that that the haunch retrofit is vulnerable to fracture at the existing low toughness top flange weld, even when precautions are taken to ensure that the existing weld contains no rejectable defects. The fractures appeared to initiate at the edge of the beam flanges. Little deterioration in the overall strength of the specimen was observed until the fracture propagated across the full flange width. Significant local buckling and lateral torsional buckling of the beams as well as some twisting of the column were observed in the latter cycles of the test. With the addition of a composite floor slab (specimens HCH2 and HCH4) the connection behavior was greatly improved. All four composite connection beam flexural capacities deteriorated gradually due to local and lateral buckling of the beams. The top weld fractures of specimens HCH1 and HCH3 were prevented. Testing of both composite specimens was stopped due to testing limitations, with total plastic rotations of 0.030 to 0.055 radians. These peak rotations were associated with substantial loss of load carrying capacity. All connections which achieved 0.020 radian of total plastic rotation, (with the exception of the north beam of HCH3), sustained in excess of 80 percent of the peak attained moment when reaching this critical rotation.

Slab Effects:

The addition of a composite slab significantly reduced the top flange strains at the center of the RBS and end of haunch sections. This was most pronounced in specimen HCH2, which had the highest concrete compressive strength. Peak tensile strains were similar for all specimens, indicating that the slab had little influence when in tension. Strains at the bottom beam flanges were not significantly affected by the presence of the slab.

As testing proceeded to larger deformation levels, the beams of all specimens experienced varying degrees of local flange, local web, and lateral torsional buckling. This buckling results in a shortening of the beams in the test specimens. Beam shortening was measured as the

change in distance between the south column flange and beam stiffener above the south beam reaction. Measurements were taken at approximately 230 mm (9 in.) east and west of the beam centerline.

A comparative measure of instability between bare steel and composite specimens could be inferred from the beam shortening plots of Fig. 4. In comparing the beam shortening effects through the 90 mm (3.6 in.) load cycles it was seen that all of the bare steel specimens had divergent values for the east and west sides of the beam. These differences in values from the east to west sides of the beam indicated that there was significant twist and distortions of the beam. Such behavior was still evident, but at a much smaller scale in the composite specimens. This disparity became even more extreme at later loading cycles.

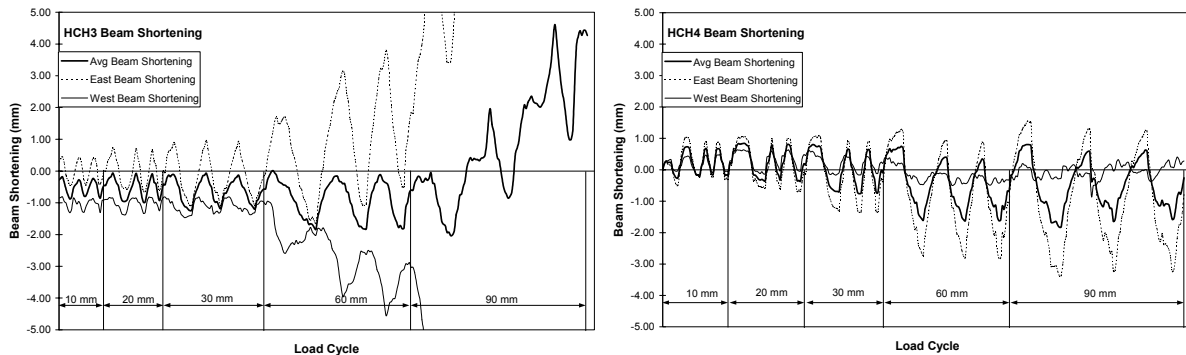


Figure 4: Measured Beam Shortening

Another significant effect on local instabilities can be seen in Fig 5. It appeared that top flange buckling was somewhat controlled by the slab. Weld failures in both bare steel haunch specimens appeared to initiate at the edge of the beam flange in contrast to the dogbone weld fractures, which appeared to initiate at the center of the welds. It is possible that beyond the brittle fractures that occurred in Northridge and in specimen DB1, the next weld failure mode may be due to low cycle fatigue from high amplitude distortions associated with local buckling of the flange. The presence of a slab appeared to control this behavior at the top flange.

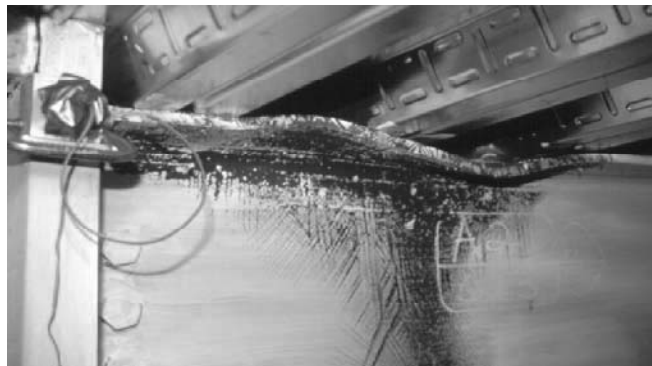


Figure 5: HCH4 Buckled Shape of Top Flange (120mm Load Cycle)

Maximum moments attained in the beams of each test specimen are compared to the computed plastic flexural strength (M_{ecr}) for each beam of each specimen in Table 3. Estimated strengths

were determined from simple plastic analysis of the cross section and actual material properties. These values are located at the critical section of each specimen, which was taken at the center of the RBS or at the end of the haunch. Ratios greater than 1.0 likely reflect the influence of strain hardening.

The composite haunch specimens (HCH2 and HCH4) developed larger moments than their bare steel counterparts, for both positive and negative moments. For negative moment, the composite specimens developed moments that ranged from 1 to 17 percent larger than the corresponding bare steel specimens. One possible source of this additional strength may be some tensile capacity contributed by the slab. However, at the point when peak negative moments were attained in the composite haunch specimens, the slab was generally extensively cracked in a direction transverse to the beam. The ability of the slab to contribute significant tensile capacity under these circumstances is questionable. Another possible explanation for the larger negative moments in the composite haunch specimens is the stabilizing effect of the slab on the beam. Since beam buckling generally results in strength degradation, the delayed buckling in the composite specimens may have permitted the development of larger moments.

The maximum attained positive moments in the composite haunch specimens were in the range of 10 to 25 percent larger than in the bare steel specimens. This likely reflects both the effects of composite action, as well as the stabilizing effect of the slab. The data in Table 3 shows that the ratio of attained positive moments to the estimated plastic capacity of the composite haunch specimens are generally close to 1.0. The plastic capacity of the sections was computed assuming an effective concrete stress of $1.3f_c$ (per Du Plessis and Daniels, (10)). However, since these specimens appear to have substantially strain hardened, ratios would be expected to be in the range of 1.05 to 1.10 (similar to the bare steel specimens). Thus, the data in Table 3 suggests that the assumed effective concrete stress of $1.3f_c$ may not have been achieved in the composite haunch specimens. Additional data in Table 3 shows that an effective concrete stress assumption of $0.85f_c$ results in attained to estimated strength ratios similar to those attained in the bare steel specimens. It appears that effective concrete stresses realized in the specimens were at or below this value.

Table 3: Attained Versus Estimated Plastic Moment Capacities (At Critical Sections)

Specimen	Estimated Capacity M_{cr} (kN-m)		North Beam Attained Ratio		South Beam Attained Ratio	
	M-	M+	M-	M+	M-	M+
DB1	1400	1400	1.026	0.978	0.897	0.970
DB2	1400	1820	0.970	0.931	1.026	0.925
HCH1	1670	1670	1.096	1.103	1.035	1.076
HCH2	1670	2290 (2100)	1.150	0.938 (1.022)	1.218	0.997 (1.086)
HCH3	1730	1730	1.047	1.047	1.047	1.054
HCH4	1710	2060 (1940)	1.192	1.080 (1.145)	1.066	0.970 (1.029)

- Notes: 1) Composite values based on $1.3f_c$ slab compressive stress over the column face. Numbers in parenthesis correspond to a value of $0.85f_c$ slab compressive stress acting over the column face.
2) Critical section is the center of the dogbone or end of haunch location

Shear Stud Failures:

During the testing of the composite specimens, failure of the shear studs at their welds often occurred. Typically, shear stud welds severed, although at least one shear stud sheared completely through the stud itself. These failures indicated that the shear stud/weld interface (which coincides with the point of slip of the slab with respect to the beam) was the weakest link during cyclic behavior. The assumed effective slab compressive force of $1.3f_c$ (per Du Plessis and Daniels (10)) was not generally attained prior to the shear stud failures.

Shear stud failures may have been due to shear stud capacities being less than design values, other forces acting on the studs, or inadequate shear stud to beam flange weld quality. It was not possible to conclusively identify the cause of shear stud failures in the specimens. Shear stud failures similar to these do not appear to be cited in the literature on previous testing of composite sections, however most testing to date has used fully composite specimens. Results from more recent cyclic testing of composite specimens also reported failure of shear studs (Engelhardt and Venti (11) Fry (12)). Recent push-pull specimen research has showed the strength of shear studs to be significantly reduced by low cycle fatigue when subjected to reversed loadings (Taplin and Grundy (13) Bursi and Gramola (14) Bursi and Caldara (15)).

CONCLUSIONS

A large inventory of buildings exist which contain connection detailing similar to those found to be inadequate in the Northridge Earthquake. To provide an adequate level of safety, many of these structures would need to be retrofit to some degree. This study was undertaken to evaluate two potential retrofit methods.

The use of the bottom flange RBS, by itself, did not provide an improvement in connection performance. In order to achieve an improvement in plastic rotation capacity, it was necessary to remove the existing low toughness E70T-4 weld metal at the top and bottom beam flange groove welds, and re-weld the beam with a higher toughness electrode. When replacement of the weld metal was combined with the bottom flange RBS in a composite specimen, plastic rotations of about 0.020 radian were achieved. These connections, however, still failed by fracture of the beam flange groove welds. RBS connections for new construction differ significantly from the RBS retrofit details tested here. The tested RBS cutout permitted substantially less moment reduction at the face of the column and less extensive detailing compared to typical RBS connections tested for new construction applications. These results do not indicate inadequacy of the details or methods for new construction.

The welded bottom haunch specimens tested generally showed better performance than the RBS specimens. In the welded haunch specimens, no modifications were made to the existing beam flange groove welds. Three of the four bare steel haunch specimens failed by fracture at the existing E70T-4 top flange welds at plastic rotations ranging from 0.012 to 0.023 radian. With the addition of a composite slab, the haunch specimens showed outstanding performance. Of the four composite haunch connections tested in this program, none experienced a fracture at the existing beam flange groove welds. Rather, the strength of these specimens deteriorated gradually due to local and lateral buckling of the beams without failure of the connection. These connections all developed in excess of 0.030 radian of plastic rotation without connection failure. At total plastic rotations of 0.020 radian, beam moments exceeded 80 percent of the peak values achieved in the tests. The composite specimens retrofitted with a bottom haunch therefore showed performance comparable to new construction standards, even though the

existing low toughness E70T-4 beam flange groove welds were left in place. Similar performance was observed in bottom haunch retrofit tests by Uang et al (17).

Composite specimens achieved greater plastic rotations than similar bare steel specimens. Composite specimens also exhibited a slight increase in initial elastic stiffness, and strength increases on the order of 10 to 25 percent over similar bare steel specimens. Top flange strains were significantly reduced from the bare steel specimens, while bottom flange strains were similar between bare steel and composite specimens. Resistance to local and lateral instabilities of the beam sections was improved in specimens which included a slab. Several shear studs failed during specimen testing. Almost all of these failures occurred at the shear stud weld. The cause of these failures is unclear but is likely due to low cycle fatigue. Composite capacities were lower than predicted based on previous research estimates of the compressive force in the slab at the column face.

Acknowledgements

Primary sponsorship of this research was provided by a grant from the National Institute of Standards and Technology. The research was co-sponsored by the Northridge Steel Industry Research Fund. In addition, the Structural Shape Producers Council donated the structural steel used for the construction of test specimens. The writers gratefully acknowledge the support of these organizations.

References

- 1) Shuey, B. and Engelhardt, M. D. *Testing of Repair Concepts for Damaged Steel Moment Connections*. SAC Report. 1996.
- 2) Uang, C. M., and Bondad, D. *Static Cyclic Testing of Pre-Northridge and Haunch Repaired Steel Moment Connections*. SAC Report. 1996.
- 3) Chen, S. J. and Yeh, C. H. "Enhancement of Ductility of Steel Beam-to-Column Connections for Seismic Resistance." Paper presented at SSRC Task Group Meeting & Technical Session. Lehigh University. Pennsylvania. 1994.
- 4) Engelhardt, M. D., Winneberger, T., Zekany, A. J. and Potyraj, T. J. "The Dogbone Connection: Part II." *Modern Steel Construction*. August 1996. pp. 46-55.
- 5) Iwankiw, N. R. and Carter, C. J. "The Dogbone: A New Idea to Chew On." *Modern Steel Construction*. April 1996. pp. 18-23.
- 6) Tremblay, R., Tchegotarev, N. and Filiatrault, A. "Seismic Performance of RBS Connections for Steel Moment Resisting Frames: Influence of Loading Rate and Floor Slab." *Proceedings - STESSA 1997*, Kyoto, Japan. August, 1997. pp. 4-7.
- 7) Gross, J.L., Engelhardt, M.D., Uang, C.M., Kasai, K. and Iwankiw, N. R. "Modification of Existing Welded Steel Moment Frame Connections for Seismic Resistance." *Steel Design Guide Series No. 12*. American Institute of Steel Construction. 1999.
- 8) *Connection Test Summaries*. FEMA-289. Federal Emergency Management Agency. Washington D. C. June 1997.
- 9) Civjan, S. A, Engelhardt, M. D., and Gross, J. L. "Retrofit of Pre-Northridge Moment Resisting Connections." *ASCE Journal of Structural Engineering*. April 2000. pp. 445-452.
- 10) Du Plessis, D. P. and Daniels, J. H. *Strength of Composite Beam to Column Connections*. Report No. 374.3. Fritz Engineering Laboratory. Lehigh University. Bethlehem. PA, 1972.
- 11) Engelhardt, M. D. and Venti, M. *Unpublished Preliminary Test Reports for SAC Phase 2 Tests*. University of Texas at Austin. 1999.

- 12) Fry, G. *Unpublished Preliminary Test Reports for SAC Phase 2 Tests*. Texas A&M University. 1999.
- 13) Taplin, G. and Grundy, P. "Incremental Slip of Stud Shear Connectors Under Repeated Loading." *Composite Construction – Conventional and Innovative – Conference Report*. September 16-18, 1997. pp. 145-150. Innsbruck, Austria.
- 14) Bursi, O. S. and Gramola, G. "Behavior of Headed Stud Shear Connectors Under Low-Cycle High Amplitude Displacements." *Materials and Structures*. Vol. 32, No. 218. 1999. pp. 290-297.
- 15) Bursi, O. S. and Caldara, R., "Composite Substructures with Partial Shear Connection: Low Cycle Fatigue Behaviour and Analysis Issues." *12 World Conference on Earthquake Engineering – Conference Proceeding*. February, 2000. Auckland, New Zealand. Paper #0498.
- 16) Plumier, A. "European Research and Code Developments on Seismic Design of Composite Steel Concrete Structures." *12 World Conference on Earthquake Engineering – Conference Proceeding*. February, 2000. Auckland, New Zealand. Paper #1147.
- 17) Uang, C.M., Yu, Q.S. and Noel, S., "Rehabilitating Pre-Northridge Steel Moment Frame Connections: RBS and Haunch Approaches Considering Slab Effects," *Proceedings; 6th US National Conference on Earthquake Engineering*. Earthquake Engineering Research Institute 1998.

SHEAR FORCE AND WELDED STEEL MOMENT CONNECTIONS

Subhash C. Goel, Prof. of Civil Engin., The University of Michigan, Ann Arbor, MI
Božidar Stojadinović, Asst. Prof. of Civil Engin., University of California, Berkeley, CA
Jaehyung Choi, Ph. D., Dept. of Civil Engin., The University of Michigan, Ann Arbor, MI
Kyoung-Hyeog Lee, Ph. D., CALTRANS, Oakland, CA

ABSTRACT

Following extensive damage to welded steel beam-to-column moment connections during the 1994 Northridge and the 1995 Kobe earthquakes, analytical studies showed that the flow of shear stresses at the connection is concentrated near the beam flanges. This concentration overloads the beam flanges in that critical region and can be a major cause for their failures. This observation led to the development of truss analogy for the connection designs in contrast to the commonly used beam theory.

Introduction

Beam-to-column moment connections in steel frames have been traditionally designed by using classical Euler-Bernoulli beam theory, which leads to the assumption that flanges transfer moment while the web connection primarily resists the shear force. The results of a recent finite element study at The University of Michigan show that stress distribution in the vicinity of moment connections fundamentally differs from the pattern assumed in the classical beam theory. This is in agreement with the boundary effect postulated in the famous Saint Venant's Principle. The finite element study showed that the magnitude and direction of the principal stresses in the connection region are better approximated by using truss analogy rather than the classical beam theory. Thus, both the bending moment and the shear force are transferred across the connection near the beam flanges through diagonal strut action. As a result, the beam flange region of a traditionally designed moment connection is overloaded. This conclusion mainly explains the recent observed steel moment connection failures during the 1994 Northridge earthquake and 1995 Kobe earthquake.

Based on realistic stress conditions in the connection region, two types of beam-to-column connections have been developed at The University of Michigan. The first connection type, called the Michigan connection, utilizes the truss analogy in order to resist beam flange overload and stress concentration by using reinforced connection elements to the beam flanges. The second connection type, called the Free Flange connection, is designed to create constraint-free region in the beam flange of sufficient length from the column face to the weld access hole. In this paper, the design concepts of these two connections are introduced and test results of full size connection specimens are summarized.

STRESS DISTRIBUTION AND FORCE FLOW IN THE CONNECTION REGION

Following the 1994 Northridge earthquake, considerable research has been carried out in the U. S. through the SAC/FEMA Joint Venture Program to find the reasons of premature failures of welded beam-to-column moment connections and to improve their behavior [FEMA/SAC, (1)]. Since most connection fractures occurred in or near the beam and column welding region, poor welding practice and use of low toughness weld metals were initially considered as the main reasons. Thus, widely used weld metals, whose notch-toughness was not specified or controlled, were replaced by notch-tough weld metals with a specified minimum Charpy V-notch toughness of 20 kips-ft at -20°F and backing bar and run-off tabs of the beam bottom flange were removed after beam flange groove welding. However, experimental results have shown that those improvements alone were not sufficient to achieve adequate ductility in the connections. Realistic stress distributions and force transfer mechanisms also need to be considered.

To examine the actual stress distributions and force flow in the conventional connections, finite element analyses were carried out. Exterior beam-to-column connection sub-assemblages were taken from the exterior frame of the building at points of inflection under lateral loading. The finite element models were prepared using a multi-layered shell element (S4R) with reduced integration points [Hibbit *et al* (2)]. The results of elastic analysis were obtained using ABAQUS finite element analysis program. Figure 1 shows the principal stress vectors in a pre-Northridge connection.

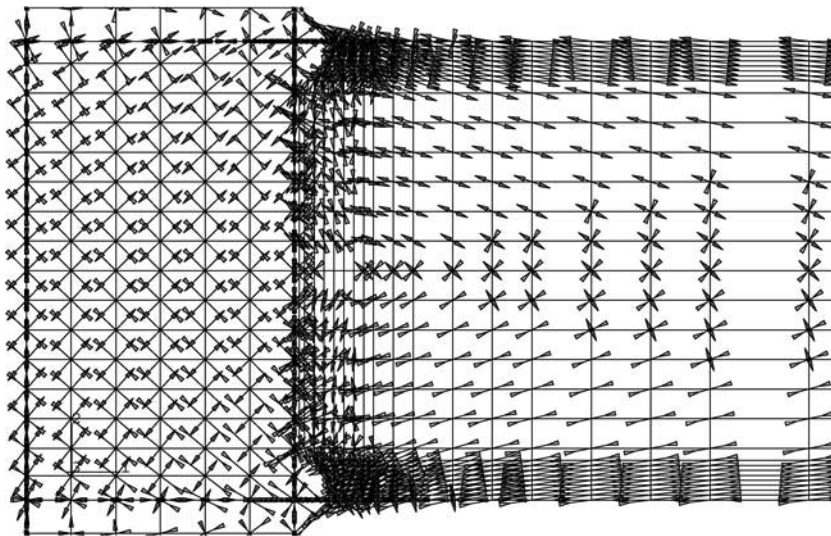


Figure 1 Principal stress vectors in pre-Northridge connection

As can be seen in Figure 1, the principal stresses near the column face are directed toward the top and bottom corners of the beam web. Stress-free region is observed in the middle of the beam web at the column face.

The normal stress distribution along the beam flange width at the connection interface and the shear stress distribution along the shear tab are shown in Figure 2. The results obtained using ABAQUS are compared with the results of the classical beam theory. Figure 2 shows that the actual stress distributions in the connection region are fundamentally different from the results

obtained from the conventional beam theory. Normal stress distribution along the beam flange width at the column face is supposed to be uniform. In reality, the stresses are largest in the central part of the beam flange and decrease toward the edges. The actual shear stress distribution in the beam web is reversed compared to the parabolic distribution given by the classical beam theory. In addition to stress concentrations along the beam flange width, local flange bending produces a large difference of normal stresses through the beam flange thickness and can cause yielding in a very localized region of the beam flange. These results imply that the possibility of brittle fracture in the beam flange is much higher than elsewhere in the connection.

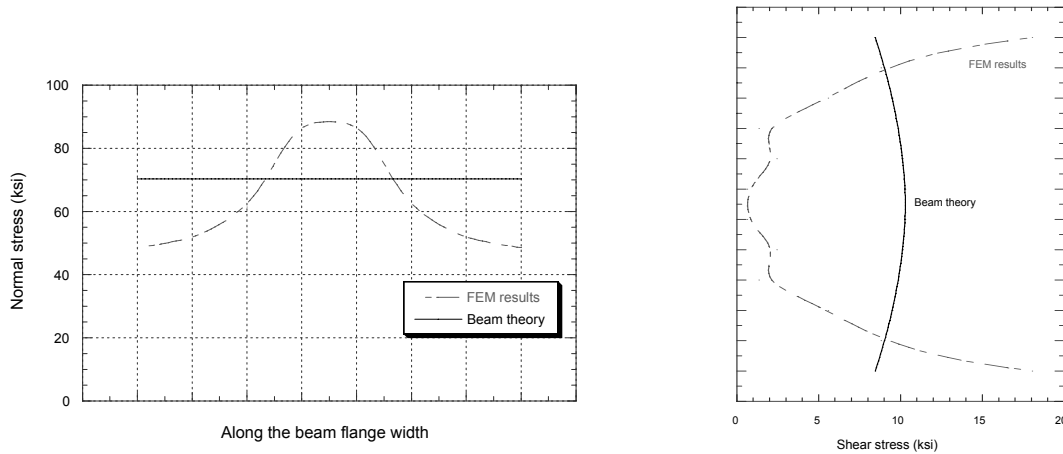


Figure 2 Normal and shear stress comparison between FEM and beam theory at column face

The stress distribution phenomenon due to local curvature was studied in a recent report [Lee *et al* (3)]. As discussed in that report, the column face is significantly stiffer than beam flange. Such difference in stiffness restrains shear deformation of the beam flange and causes further redistribution of shear stresses in the beam web. This redistribution is such that the shear stresses concentrate at the corners of the beam web where the restraint of shear deformation is largest. This additional shear force causes local bending of the beam flange. Moreover, column flange prying action, induced by column bending, produces additional flange curvature and further increases the stress concentration at the center of the top layer of the beam flange. A typical stress gradient through the thickness of the beam top flange is shown in Figure 3. Pronounced local flange curvature causes concentrated yielding in a very restricted area, the center of the top layer of the beam flange. This volume of yielded material is surrounded by still elastic and stiff material, which prevents spread of yielding out to the beam web and further into the flange. Such restrained stress state is main reason for beam flange brittle fracture instead of ductile yielding.

Based on the above observations, it can be concluded that the pre-Northridge connection configuration cannot achieve ductile response by change of weld metal or improvements in welding detail alone. Thus, improved connection configurations and design procedures need to be devised in order to achieve adequate ductility.

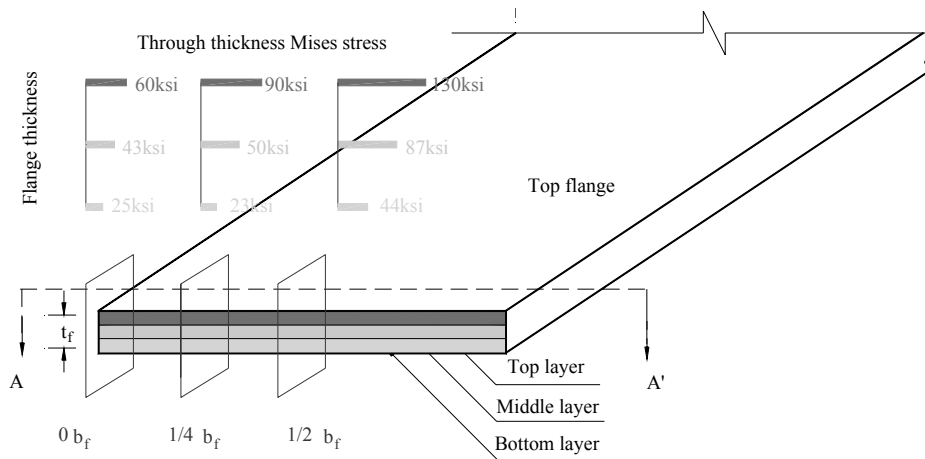


Figure 3 Different stress level in top and bottom layers of the top flange

DESIGN CONCEPTS OF NEWLY DEVELOPED CONNECTIONS

The analytical study of conventional connection shows that the connection should not be designed by methods based on classical beam theory. To reflect actual stress distributions and shear transfer mechanism in connection design, two types of beam-to-column connections were developed at The University of Michigan by using truss analogy and parallel-shear spring model. In this paper, design concepts of the two connections are briefly discussed and optimal connection configurations are presented.

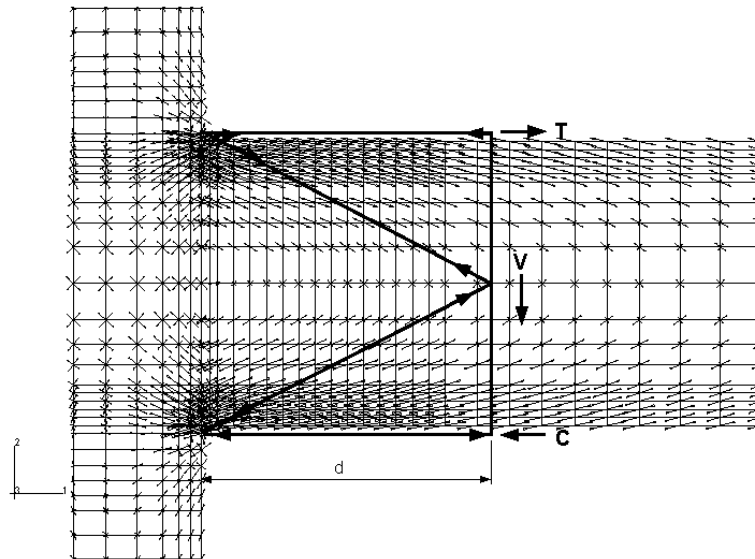


Figure 4 Principal stress vectors and force transmission in the truss model

Michigan Connection

As illustrated through the principal stress vectors, most stresses and shear force in the connection region are concentrated at the corners of beam web and flanges, leaving a practically stress-free region in the middle of the beam web. The Michigan connection was developed to account for this stress flow. Figure 4 shows the principal stress vectors and force transmission along with the truss model for practical design purposes.

According to the truss model, the combined shear and normal forces are reacted at the top and bottom corners of the connection, which is in good agreement with the principal stress flow. Therefore, the connection is designed to resist these concentrated forces at the top and bottom corners near the beam flanges. The connection is made with several elements, such as flange plate and vertical rib plates in order to resist normal and shear forces at the top and bottom corners of the connection. A suggested configuration of these connecting elements is shown in Figure 5. The top and bottom beam flanges are indirectly connected to the column face through the connecting elements in order to eliminate the constraining boundary effects at the junction of the web. The normal force due to beam moment is shared by the flange plate and vertical rib plates, whereas the shear force is assumed to be resisted by the rib plates only. Thus, the rib plates are designed for their share of normal force and full vertical force. For practical reason, the inner vertical rib plates at the top and bottom can be combined into one C-shape web plate, allowing the erection bolts to be used near mid-depth of the beam web. The sizes of the vertical rib plates and horizontal flange plates and the connecting welds are determined by using the reaction forces as calculated from the truss model and Von Mises yield criteria. By means of the connecting plate elements, the stress concentrations in the beam flanges are sufficiently reduced and the location of the plastic hinge can be moved away from the vulnerable connection region. The detailed design procedure for the Michigan connection is presented elsewhere [Goel *et al* (4)].

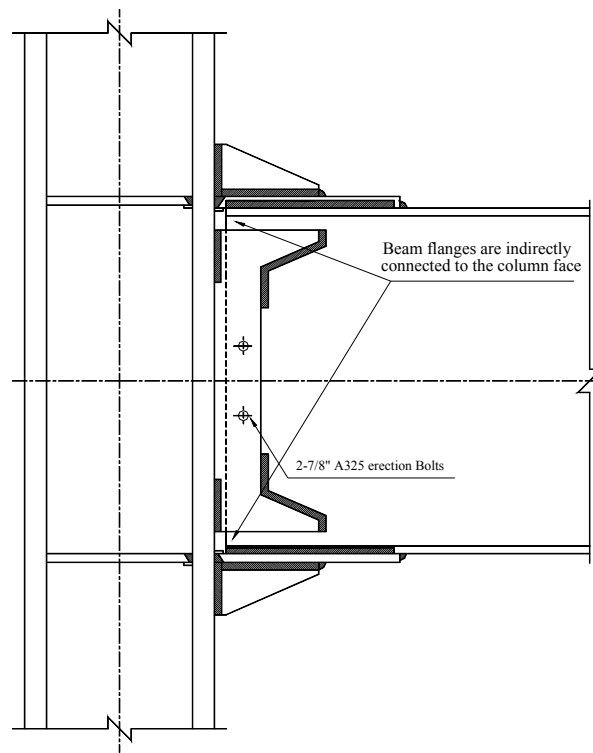


Figure 5 Optimal configuration of Michigan connection

Free Flange Connection

The design of Michigan connection was based on direct stress flow as governed by the boundary effects. The Free Flange connection, on the other hand, is based on altering the beam flange stress concentrations and shear force flow by providing enough free length of the beam flange to deform so that constraining effects in the connection region are sufficiently reduced. The Free Flange connection is a new connection configuration designed to alleviate both local flange deformation and flange overload problems. Both objectives are achieved by cutting the web of the beam back and away from the column, thus creating portions of the beam flanges where they are not constrained by the web. The length of the web cutback, i.e., the distance between the column face and the beginning of the tapered web cut, is called the free flange length. Figure 6 shows the location of the free flange length. The free flange is essential for ductile behavior of the connection. Ductility of the connection is achieved not only by using ductile materials but also by providing constraint-free conditions in the connection region. The free flange length serves two main purposes. First, it reduces the shear stiffness of the flanges, thus, redirecting most of the shear force (the force that causes local flange bending) back into the beam web. Second, the free flange lowers the strains and allows yielding to occur over larger length. Larger web cutout also provides easier access for field welding.

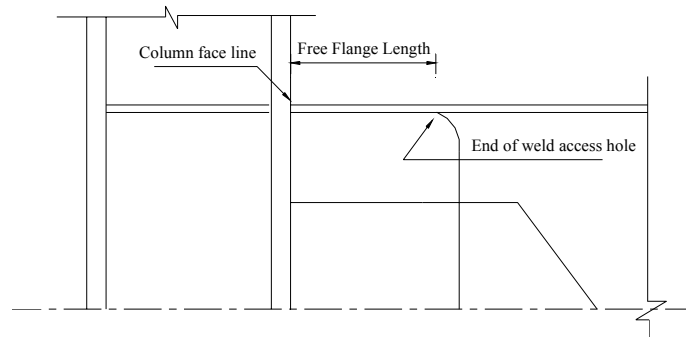


Figure 6 The free flange length

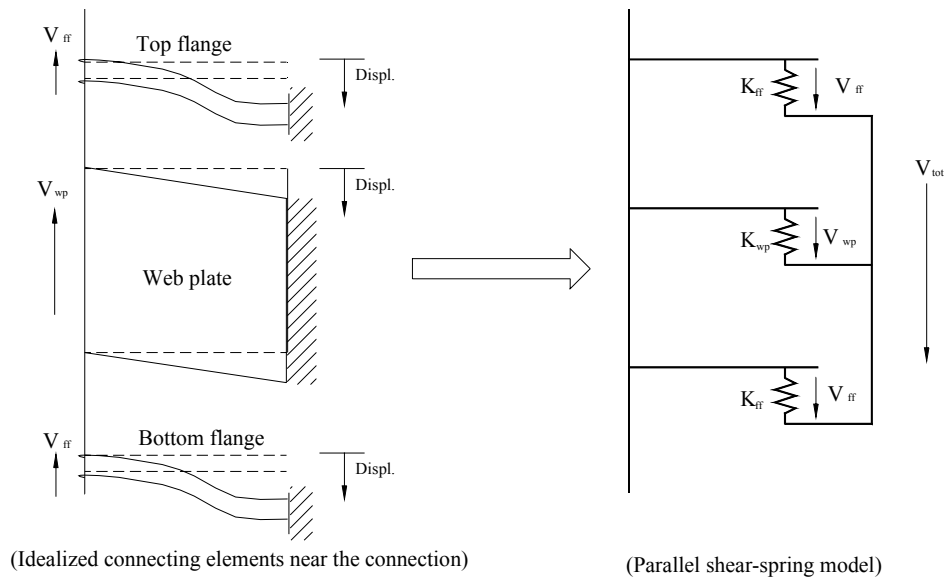


Figure 7 Parallel shear-spring system

The shear transfer mechanism in the Free Flange connection can be effectively presented by employing a parallel shear-spring model as shown in Figure 7. The Free Flange connection consists of three elements: the top flange, the beam web and web plate, and the bottom flange. These three elements have the same vertical displacement when the beam undergoes shear deformation. Thus, the shear stiffness of the Free Flange connection can be modeled as a parallel spring system shown in Figure 7. In this figure, V_{tot} is the total tip load applied at the beam end, V_{wp} is the shear force acting on the web plate and V_{ff} denotes the shear forces acting on the top or bottom flanges, assumed to be equal in magnitude. The beam flanges and the web plate are assumed to have a fixed boundary at the column face and at the end of the free flange length. Thus, the portion of resultant shear force in the beam flange and web plate can be calculated as follows:

$$\frac{V_{ff}}{V_{tot}} = \frac{K_{ff}}{2K_{ff} + K_{wp}} = \frac{E \left(\frac{b_{ff} t_{ff}^3}{L_{ff}^3} \right)}{E \left[\frac{(6L_{wp} b_{ff} t_{ff}^3) + (L_{ff}^3 h_{wp} t_{wp})}{(3L_{wp} L_{ff}^3)} \right]} = \frac{1}{2 + \left(\frac{1}{3} \right) \left(\frac{h_{wp} t_{wp}}{L_{wp} b_{ff}} \right) \alpha^3}$$

where K_{ff} is flexural stiffness of the free flange, K_{wp} is stiffness of the web plate, L_{ff} is length of the free flange, and b_{ff} and t_{ff} are width and thickness of the free flange. L_{wp} is length of the web plate, and h_{wp} and t_{wp} are height and thickness of the web plate, respectively. The factor α is free flange length to thickness aspect ratio. Using the above equation, the portions of the shear force in the flange and in the web plate can be calculated. As shown in this equation, the portion of the resultant shear force in the beam flange decreases hyperbolically as the free flange length increases. Extensive analytical study on the free flange connection showed that local beam flange bending is sufficiently reduced and resultant shear force in the beam flanges is reduced from more than 50% of total shear force for the conventional connection to about 15% by using free flange connection. As presented in the parallel shear-spring model, use of stiff web plate with adequate free flange length is essential to redirecting shear force in the flanges back into the web connection. Figure 8 shows optimal configuration and connection design forces of the free flange connection based on the analytical results [Choi *et al* (5)].

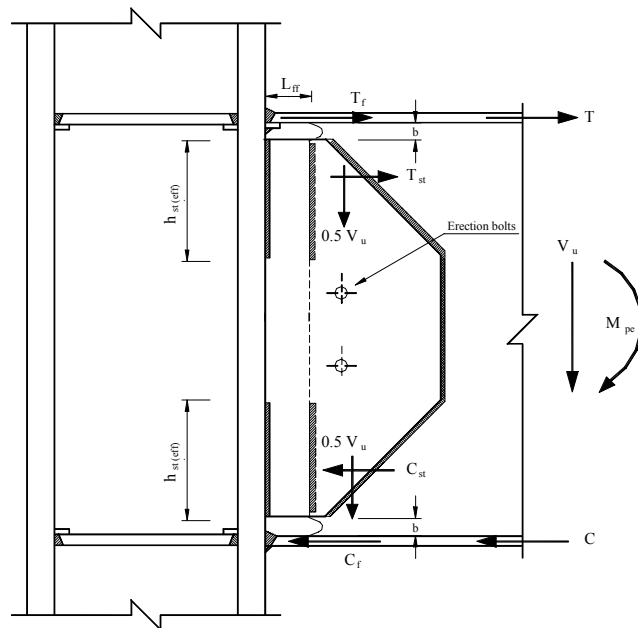


Figure 8 Optimal connection detail and force transfer mechanism

The length of beam free flange, L_{ff} , the distance from the column face to the toe of the access hole, is computed as $L_{ff} = \alpha t_{ff}$; where t_{ff} is thickness of the beam flange, and α is free flange aspect ratio with a value between 5.0 and 6.0, which represents a balance point between reduction of shear in the beam flange and increasing potential for buckling of the free flange. A stiff and properly sized web plate is used to divert more shear force from the beam flanges and to cover vulnerable weld access hole. Detailed design procedure is presented in the original report by the authors [Choi *et al* (5)].

RESULTS OF CONNECTION TESTS

Full size beam-to-column connection specimens were tested in order to evaluate their ductility and to validate the design procedures. Two identical Michigan connection specimens with a W30×99 beam and W14×257 column section, and five Free Flange connection specimens with pairs of beam and column as W24×68 and W14×120, W30×99 and W14×176, and W30×124 and W14×257, were tested. All tests followed the SAC Joint Venture Phase 2 connection testing protocol. General test setup for both connection specimens is shown in Figure 9.

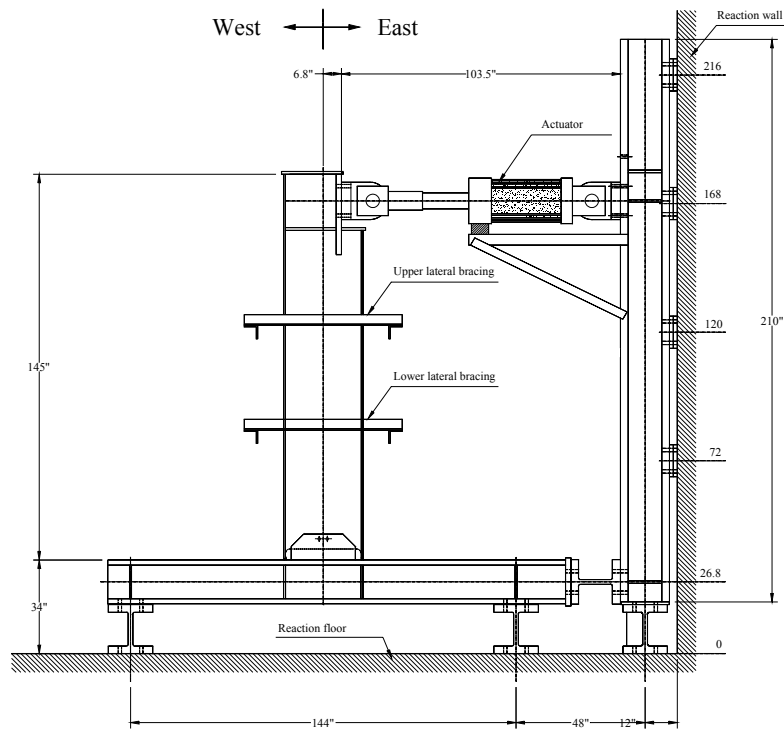


Figure 9 General test setup

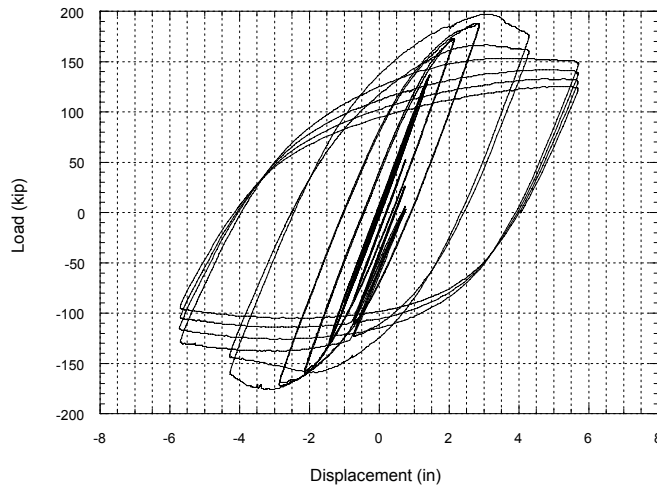


Figure 10 Load-displacement response of Michigan connection (MI-1)

Figure 10 shows typical load-displacement hysteretic response at the center of the column for the Michigan connection specimens. Significant beam flange yielding was observed outside of the connection region. This flange yielding spread into the beam web as plastic hinging progressed. At 3% drift level, localized flange and web buckling occurred due to complete yielding of that region and some drop in strength and stiffness was observed. Due to limited actuator capacity, maximum 4% drift cycles were repeated several times and testing was stopped. The connection behavior was very ductile and stable without any major connection damage or cracks.

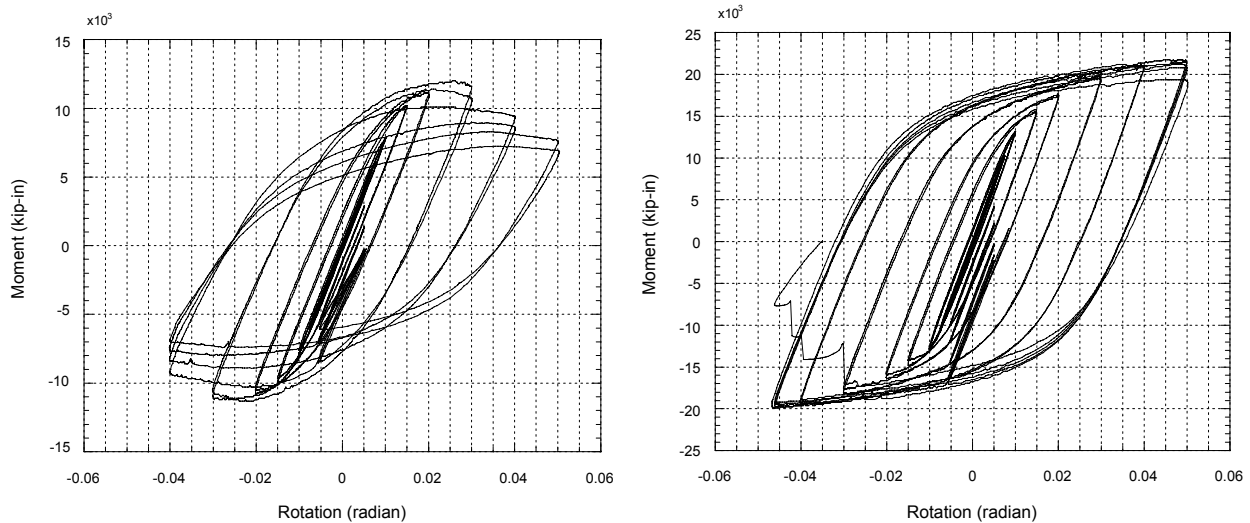


Figure 11 Moment-rotation response of Free Flange connection (Left: strong panel zone specimen, Right: Weak panel zone specimen)

Figures 11 and 12 show typical moment-connection rotation responses at the center of the column for the Free Flange connection specimens with weak and strong panel zone strengths, respectively. As can be seen in these figures, Free Flange connection specimens reached 4% drift

without any significant cracking or fracture. Slight local buckling of the free flanges was observed at the 2% or 3% drift level, but the strength or stiffness of the specimen was not affected

Although the Free Flange connection specimens showed excellent ductile behavior, some differences in seismic responses were observed depending on the panel zone strength. In the strong panel zone specimens, complete beam flange yielding spread into the beam web, forming typical “hourglass” pattern plastic hinge approximately at one-half of the beam depth away from the column face. However, most connection rotation occurred in the beam, which caused lateral-stability problem and increased need for better lateral support. In the weak panel zone specimens, excellent ductile connection behavior was observed in terms of rotation capacity. It sustained more than 4% drift without any significant degradation of the connection strength or cracking in the beam flanges. However, excessive panel zone yielding causes column flange kinking, leading to beam flange fracture at large drift levels. Another undesirable effect of excessive deformation in a weak panel zone is “incomplete” formation of the beam plastic hinge. Thus, the contribution of the beam to total plastic rotation of the specimen is limited. Therefore, inelastic rotation of the panel zone should be limited within an acceptable range, where the panel zone undergoes some yielding but still has sufficient post-elastic stiffness.

Figure 12 shows the maximum drift angle and total plastic rotation of Michigan and Free Flange connection specimens. All specimens achieved a total drift of 4% or more with good connection plastic rotation capacity. Complete design procedure for the Free Flange connection and more details of the experimental program are presented in the original report [Choi *et al* (5)].

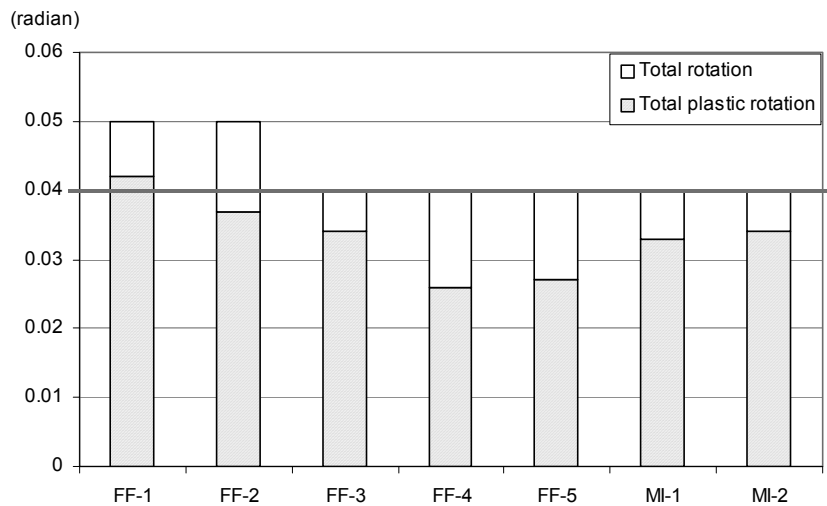


Figure 12 Maximum drift angle and plastic rotation

CONCLUSION

Recent analytical and experimental research shows that welded beam-to-column moment connections should be designed by using models that reflect actual stress distributions and force flow in the connection region. Truss analogy and parallel-shear spring models, as discussed in this paper, can be used for practical design work. Newly developed Michigan connection and Free Flange connection showed excellent ductile behavior achieving more than 4% total connection rotation.

REFERENCES

1. Federal Emergency Management Agency. Interim Guidelines advisory No. 1, Report No. SAC-96-03, Supplement to FEMA-267, 1997.
2. ABAQUS, User's Manual – Version 5.7, Hibbit, Karlsson, and Sorenson, Inc, 1080 Main Street, Pawtucket, RI 02860, 1997.
3. Lee, K. H., Goel, S. C., and Stojadinovic, B., "Boundary effects in Welded Steel Moment Connections." Technical Report UMCEE 97-20, Dep. of Civil and Environmental Eng., The University of Michigan, 1997.
4. Goel, S. C., Lee, K. H. and Stojadinovic, B., "Design of Welded Steel Moment Connections Using Truss Analogy." AISC Engineering Journal, 1st Qtr., pp 31 – 40, 2000.
5. Choi, Jaehyung, Goel, S. C., and Stojadinovic, B., "Development of Free Flange Moment Connection." Technical Report UMCEE 00-15, Dep. of Civil and Environmental Eng., The University of Michigan, 2000.

Cyclic Response and Design Recommendations of RBS Moment Connections with Deep Column

Chia-Ming Uang, University of California, San Diego
Brandon Chi, Forell/Elsesser Engineers, Inc., San Francisco

ABSTRACT

Design engineers frequently use deep columns in a steel special moment resisting frame to control drift. As the Reduced Beam Section (RBS) moment connection is becoming popular after the Northridge earthquake, recent tests showed that the deep column is prone to twisting, causing premature strength degradation. The twisting was caused by the eccentric beam flange force due to significant lateral-torsional buckling of the beam. In this paper, cycle tests results of three full-scale RBS moment connections with deep columns are presented. An analytical study shows that the warping stress is highly dependent on the h/t_{cf}^3 ratio. A design procedure is proposed that can be used to evaluate if column twisting is a concern.

INTRODUCTION

A significant amount of research on Reduced Beam Section (RBS) steel moment connections has been conducted in the United States since the 1994 Northridge earthquake. This type of connection is gaining wide acceptance by the design engineers in high seismic regions due to its robust performance of delivering large plastic rotations. In the seismic design of steel moment-resisting frames, design engineers often use deep columns to control drift. Nevertheless, the majority of the testing was conducted using shallow wide flange sections (e.g., W14 shapes).

OBJECTIVES

The first objective of the study was to investigate experimentally the cyclic behavior of RBS moment connections with deep wide-flange sections. The second objective was to develop design procedures for this type of connection.

TEST SPECIMENS

A total of three full-scale specimens were tested. Overall dimensions of the specimens and test setup are shown in Figure 1. Member sizes of the specimens are shown in Table 1. A992 steel was specified for all beams and columns. The design of the RBS moment connections was based on the procedure recommended by Engelhardt (4) and the AISC Seismic Provisions (2). Table 2 provides a brief summary of the design data.

The test specimens were constructed by a commercial fabricator. All filler metals were specified

to have a minimum Charpy V-Notch impact value of 27 N-m at -29°C. To simulate field conditions, the beam was installed and the moment connection of each specimen welded with the column in an upright position. Self-shielded flux-cored arc welding (FCAW) was used for all specimens. The E70T-6 filler metal was used for making beam flange groove welds, while the E71T-8 filler metal was used for other field welding.

TEST RESULTS

The standard SAC loading protocol (Clark et al. 3) was used for testing. Figure 2 summarizes the global response and failure mode of each specimen. Yielding was observed in the panel zone first. Web local buckling in the RBS region then occurred, which was followed by lateral-torsional buckling (LTB) and flange local buckling. Response that was not commonly observed in shallow-column RBS moment connections includes the following. Columns of all three specimens experienced twisting and out-of-plane bending (see Figure 2). Specimen DC-3 experienced fracture along the k line in the column web.

ANALYSIS OF COLUMN TWISTING PHENOMENON

The twisting of a deep column is caused by two factors. First, RBS beams tend to buckle more laterally, creating higher torsion in the column. Second, the torsional characteristics of the deep section tend to produce high warping stress. Figure 3(a) shows the deformed beam of Specimen DC-2. Figure 3(b) shows that the inclined beam flange force due to LTB imposed not only weak-axis bending but also torsion to the column. The beam flange force, F , can be estimated by multiplying the reduced beam flange area by the expected yield strength at section A–A. The force has a transverse component $F\sin\theta$. This transverse component produces a torsion $e_y F\sin\theta$ in the column. The longitudinal component of the force ($F\cos\theta$) is also offset from the column centerline by a distance e_x . Therefore, Figure 3(c) shows that the total torsion imposed to the column is $F(e_x\cos\theta + e_y\sin\theta)$. Assuming that the column is simply supported for flexure and torsion at the mid-height of the story (i.e., the assumed inflection point), components of flexural stresses due to strong-axis bending, weak-axis bending, and torsion can be computed using elastic theory.

Based on the measurements of LTB amplitude of six RBS moment connection specimens, the LTB amplitude (e_x) at 4% drift was estimated to be $0.2b_f$, where b_f is the unreduced beam flange width (Gilton et al. 5).

The torsional resistance provided by a wide flange member is the sum of the components due to pure torsion and warping:

$$T = T_p + T_w = GJ\phi' - EC_w\phi''' \quad (1)$$

where G , J , E , and C_w are the shear modulus of elasticity, torsional constant, modulus of elasticity, and warping constant, respectively. ϕ' and ϕ''' are the first and third derivatives of the angle of twist with respect to the longitudinal (z) axis of the member. The warping torsion,

causing one flange to bend in its own plane in one direction while the other flange bends in the opposite direction, produces stress (f_{ws}) in the flanges. The relationship between f_{ws} and T (Seaburg and Carter [7]) is:

$$f_{ws} = \frac{EW_{no}\beta}{GJ a_c} T \quad (2)$$

where W_{no} ($= hb_{cf}/4$) is the normalized warping function at a point at the flange edge, $h = d_c - t_{cf}$, β is equal to $\phi''Ga_cJ/T$, and $a_c = \sqrt{EC_w/GJ}$. For example, when the torsion is applied at $z = 0.4l$, where l is the length of the column, β is computed from ϕ as follows:

(i) for $0 \leq z \leq \alpha l$:

$$\phi(z) = \frac{Tl}{GJ} \left[(1 - \alpha) \frac{z}{l} + \left(\frac{\sinh\left(\alpha \frac{l}{a_c}\right)}{\tanh\left(\frac{l}{a_c}\right)} - \cosh\left(\alpha \frac{l}{a_c}\right) \right) \frac{a_c}{l} \sinh \frac{z}{a_c} \right] \quad (3)$$

$$\beta = \frac{\phi''Ga_cJ}{T} = \sinh\left(\frac{z}{a_c}\right) \left[\frac{\sinh\left(0.4 \frac{l}{a_c}\right)}{\tanh\left(\frac{l}{a_c}\right)} - \cosh\left(0.4 \frac{l}{a_c}\right) \right] \quad (4)$$

(ii) for $\alpha l \leq z \leq l$:

$$\phi(z) = \frac{Tl}{GJ} \left[(l - a_c) \frac{\alpha}{l} + \frac{a_c}{l} \left(\frac{\sinh\left(\alpha \frac{l}{a_c}\right)}{\tanh\left(\frac{l}{a_c}\right)} \sinh \frac{z}{a_c} - \sinh\left(\alpha \frac{l}{a_c}\right) \cosh \frac{z}{a_c} \right) \right] \quad (5)$$

$$\beta = \frac{\phi''GJa_c}{T} = \frac{\sinh\left(0.4 \frac{l}{a_c}\right)}{\tanh\left(\frac{l}{a_c}\right)} \sinh\left(\frac{z}{l} \frac{l}{a_c}\right) - \sinh\left(0.4 \frac{l}{a_c}\right) \cosh\left(\frac{z}{a_c}\right) \quad (6)$$

Charts are also available to determine the β values (Seaburg and Carter [7]).

To gain insight into the warping stress, the torsional constant J is approximated as:

$$J \approx 2J_f + J_w = (2 + C_1)J_f \quad (7)$$

where $J_f = (b_{cf}t_{cf}^3/3)$ is the torsional constant of one flange, and $J_w [= (d_c - 2t_{cf})t_{cw}^3/3]$ is the torsional constant of the web. In Eq. (7), C_1 is defined as the ratio between J_w and J_f . Substituting $G = E/2.6$ into Eq. 2, the warping stress produced by a unit torsion becomes:

$$\frac{f_{ws}}{T} = 2.6 \left(\frac{W_{no}}{J} \right) \left(\frac{\beta}{a_c} \right) \quad (8)$$

where

$$\frac{W_{no}}{J} = \frac{hb_{cf}/4}{(2+C_1)b_{cf}t_{cf}^3/3} = \frac{3}{4(2+C_1)} \left(\frac{h}{t_{cf}^3} \right) \quad (9)$$

Therefore, Eq. 8 can be re-written as:

$$\frac{f_{ws}}{T} = \frac{1.95}{2+C_1} \left(\frac{h}{t_{cf}^3} \right) \left(\frac{\beta}{a_c} \right) \quad (10)$$

The variations of h/t_{cf}^3 for some shapes are shown in **Figure 4**. The h/t_{cf}^3 ratio is lower for shallow (i.e., W12 and W14) sections than it is for the heavier sections, which implies that the induced warping stress will also be lower. For example, the h/t_{cf}^3 ratio is equal to 0.104/cm² (0.671/in²) for a W14×398 section [$I_x = 2497 \times 10^6$ mm⁴ (6000 in⁴)]. If the designer chooses a deep section W27×161 for a comparable moment of inertial [$I_x = 2619 \times 10^6$ cm⁴ (6280 in⁴)] to control drift, the h/t_{cf}^3 ratio is drastically increased to [3.3/cm² (21.04/in²)]. Table 3 lists the components on the right-hand side of Eq.10 for both column sections mentioned above. The unit warping stress of the deep section is 4.2 times that of the shallow section. Because the h/t_{cf}^3 ratio of the deep column is 32 times that for the shallow section, it is obvious from Table 3 that the factor h/t_{cf}^3 is mainly responsible for the much higher warping stress in the column.

DESIGN VERIFICATION PROCEDURE FOR DEEP-COLUMN RBS CONNECTIONS

The combined stress (f_{un}) in the column flange at the beam flange level comprises the in-plane bending stress (f_{bx}), out-of-plane bending stress (f_{by}), and warping stress due to torsion (f_{ws}).

The verification procedure presented herein aims to limit the combined stress to the design yield strength (ϕF_{yn}) of the column (AISC 1994):

$$f_{un} = f_{bx} + f_{by} + f_{ws} \leq \phi F_{yn} \quad (\phi = 0.9) \quad (11)$$

1. Referring to Figure 3(b), assume that LTB produces an eccentricity $e_x = 0.2 b_{bf}$.
2. Figure 5 shows a typical one-sided moment connection. The inclined angle of beam flange force due to LTB of the beam is:

$$\theta = \tan^{-1} \left(\frac{e_x}{\frac{L}{2} - a - \frac{b}{2}} \right) \quad (12)$$

3. The beam flange force can be estimated as:

$$F = b'_{bf} t_{bf} F_{ye} \quad (13)$$

where b'_{bf} is the reduced beam flange width at the narrowest location, and $F_{ye} (= R_y F_{yn})$ is the expected yield strength. Strength degradation usually occurs at 4% story drift. Therefore, no strain hardening factor is included in Eq. 13.

4. The torsion produced by F in the column of a one-sided moment connection is [Figure 3(c)]:

$$T = F(e_x \cos \theta + e_y \sin \theta) \quad (14)$$

where $e_y = \frac{d_c}{2} + a + \frac{b}{2}$. For a two-sided moment connection without a concrete slab, the torsion in Eq. 14 is contributed by both beams; that is, T computed from Eq. 14 for each beam is assumed additive. Nevertheless, when a concrete slab is present and can be counted on to provide lateral bracing for the beam in positive bending, the torsion in Eq. 14 does not have to be doubled because it is only contributed by the beam under negative bending.

5. The warping stress, f_{ws} , is computed from Eq. 2. For a one-sided moment connection, the torsion is applied at the bottom flange level, and the warping stress is computed at the same location. This is also applicable to a two-sided moment connection with a concrete slab. For a two-sided moment connection without the benefit of concrete slab for lateral bracing, the column torsion contributed by both beams is applied at the mid-depth of the beams, but the warping stress is still computed at the bottom flange level, where the f_{bx} value is the highest, in order to combine with f_{bx} and f_{by} in Eq. 11.
6. The in-plane bending moment produces the maximum column moment (M_c) at the beam flange level. This moment can be computed as the product of the column shear and the distance from the column inflection point to the beam flange level. (The M_c value is higher for two-sided moment connections). The strong-axis bending stress, f_{bx} , due to this moment is:

$$f_{bx} = \frac{M_c}{S_{xc}} \quad (15)$$

where S_{xc} is the elastic section modulus of the column.

7. The out-of-plane bending moment in the column is caused by the transverse component of the beam flange force (i.e., $F \sin \theta$). Applying $F \sin \theta$ at the compression flange level of the beam, and treating the column as simply supported at two inflection points, the out-of-plane bending stress, f_{by} , can be computed by beam theory. This stress can be ignored for two-sided moment connections without slab because the force components tend to cancel each other out.
8. Check Eq. 11 to see if the combined stress is less than the design stress per Formula (H2-1) in the LRFD Specifications (AISC 1). If the combined stress is too high, the designer may consider changing the column size to obtain improved torsional properties. It was shown in Eq. 10 that h/t_{cf}^3 plays the most important role for the value

of warping stress. The selection should be guided to lower the h/t_{cf}^3 value. The most effective way to minimize the torsional problem is to add extra lateral bracing a short distance outside the RBS region to minimize the amplitude of LTB (e_x). Experimental results showed that the maximum bracing force could reach 7% of the compressive force in the beam flange (Yu et al. 8). For design purposes, it is suggested that extra bracing be designed for 6% of the expected nominal strength of the beam flange. The third option to prevent column twisting is to brace the column flange instead of the beam flange.

SUMMARY AND CONCLUSIONS

Based on both experimental results and analytical studies, the following conclusions can be made regarding the deep-column RBS moment connections:

1. Specimens DC-1 and DC-2 achieved 0.03 radian of plastic rotation. For both specimens, the column flange connected to the beam experienced severe out-of-plane bending or column twisting. Specimen DC-3 experienced brittle fracture along the k-line of the column just before reaching 0.03 radian of plastic rotation.
2. Twisting in the deep column is caused by two factors: 1) RBS beams tend to buckle more laterally, introducing torsion in the column, and 2) the torsional property of deep sections tends to produce higher warping stress in the column. It was found that the high h/t_{cf}^3 ratio of the deep section was mainly responsible for the higher warping stress.
3. A verification procedure is developed for deep column RBS moment connections. In case twisting of the column is significant, providing extra lateral bracing near the RBS region is effective to minimize the torsional problem.

ACKNOWLEDGEMENTS

Funding for this research was provided by the Federal Emergency Management Agency through the SAC Joint Venture. SAC is a partnership of the Structural Engineers Association of California, the Applied Technology Council, and California Universities for Research in Earthquake Engineering. This research was conducted as part of Task 7.11 in Phase II of the SAC Joint Venture. Mr. J.O. Malley was the Project Director of Topical Investigation. Mr. D. Long of PDM/Strocal donated the fabrication service.

REFERENCES

- [1] AISC (1993), Load and Resistance Factor Design Specification for Structural Steel Buildings, Second Edition, Chicago, IL.
- [2] AISC (1997), *Seismic Provisions for Structural Steel Buildings*, Second Edition, Chicago, IL, with Supplement No. 1 (1999).
- [3] Clark, P., Frank, K., Krawinkler, H., and Shaw, R., (1997) "Protocol for Fabrication, Inspection, Testing, and Documentation of Beam-Column Connection Tests and Other Experimental Specimens," *Report No. SAC/BD-97/02*, SAC Joint Venture, Sacramento, CA.
- [4] Englehardt, M.D., (1998) "Design of Reduced Beam Section Moment Connections," *Proceedings*, 1999 North American steel Construction Conference, AISC, pp.1-3 to 1-29.
- [5] Gilton, C., Chi, B., and Uang, C.-M. (2000), "Cyclic Response of RBS Moment Connections: Weak-Axis and Deep Column Effects," *Report No. SSRP-2000/03*, Department of Structural Engineering, University of California, San Diego, CA.
- [6] SAC (1997), *Interim Guidelines Advisory No. 1.*, FEMA-267A, SAC Joint Venture, Sacramento, Ca.

- [7] Seaburg, P.A. and Carter, C.J. (1997), "Torsional Analysis of Structural Steel Members," *Steel Design Guide Series 9*, AISC, Chicago, IL.
- [8] Yu, Q.S., Gilton, C., and Uang, C.-M. (2000), "Cyclic Response of RBS Moment Connections: Loading Sequence and Lateral Bracing Effects," *Report No. SSRP-99/13*, Department of Structural Engineering, University of California, San Diego, CA.

Table 1 Specimen Member Sizes

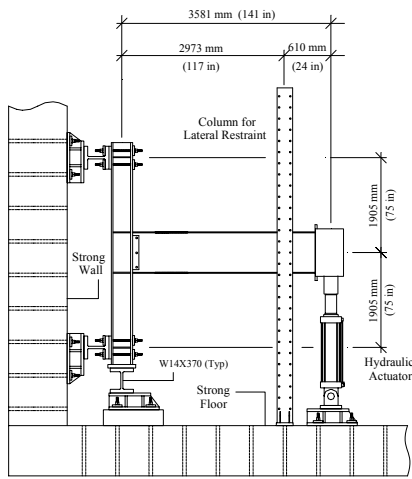
Specimen	Beam Size	Column Size	Doubler Plate
DC-1	W36×150	W27×146	9.53 mm (3/8 in.)
DC-2	W36×150	W27×194	N/A
DC-3	W27×194	W27×194	15.9 mm (5/8 in.)

Table 2 Summary of Design Data

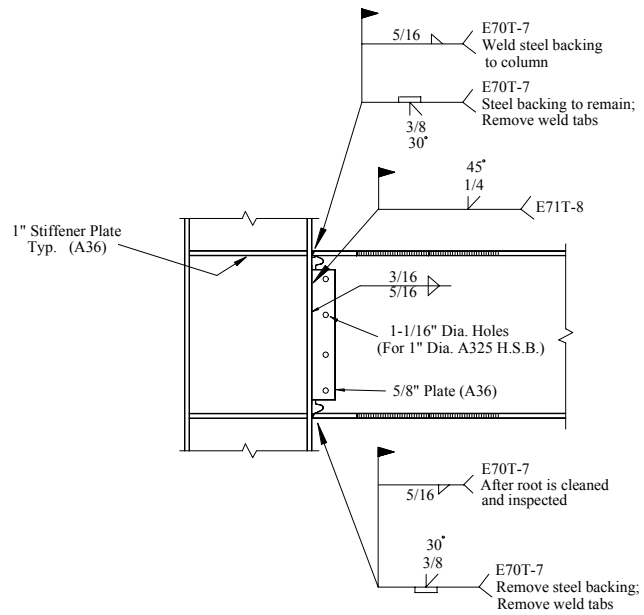
Specimen	Flange Reduction (%)	M_{pd} (kN-m)	V_{pd} (kN)	$\frac{M_f}{(Z_b F_{ye})}$	V (kN)	V_{pz} (kN)	$\frac{\sum M_{pc}^*}{\sum M_{pb}^*}$
DC-1	50	2626	1001	0.90	2359	2780	1.45
DC-2	50	2626	1006	0.90	3097	2804	1.97
DC-3	43	2945	1113	0.92	3173	4236	1.78

Table 3 Comparison of Warping Stress Components

Section Type	$\frac{1.95}{2 + C_1}$	$\frac{h}{t_{cf}^3} \left(\frac{1}{cm^2} \right)$	a_c (cm)	β	$\frac{f_{ws}}{T} \left(\frac{\times 10^{-4}}{cm^3} \right)$
W14×398	0.893	0.104	89.2	0.48	5.00
W27×146	0.808	3.3	315	0.25	21.2

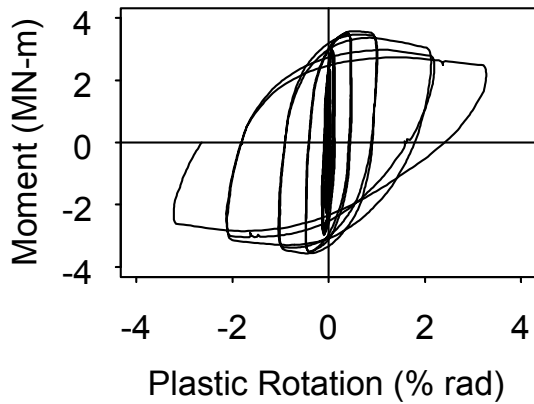


(a) Test Setup

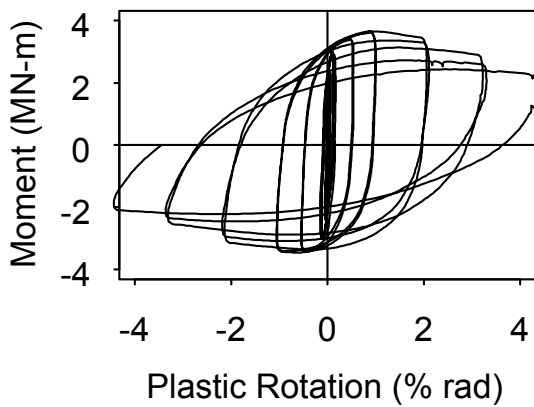
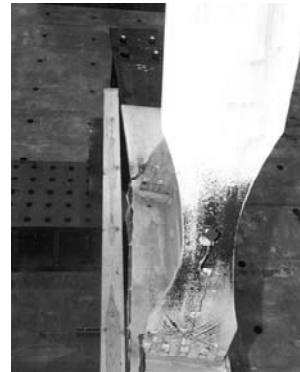


(b) Typical Connection Details

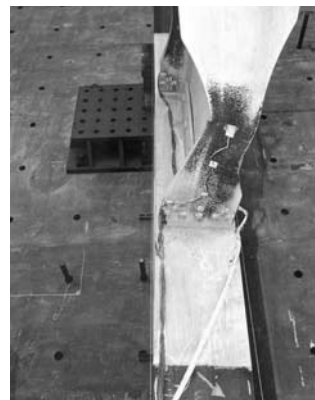
Figure 1 Test Setup and Moment Connection Details

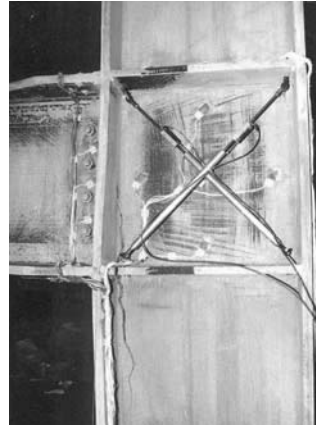
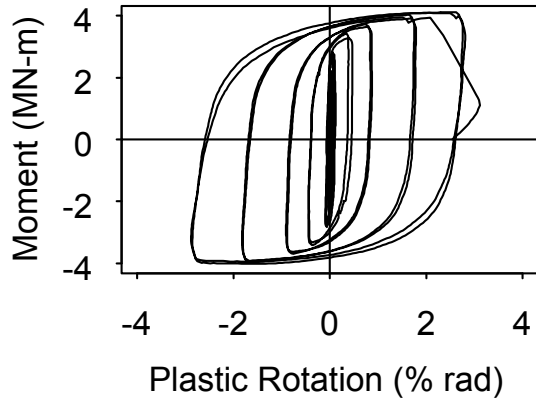


(a) Specimen DC-1

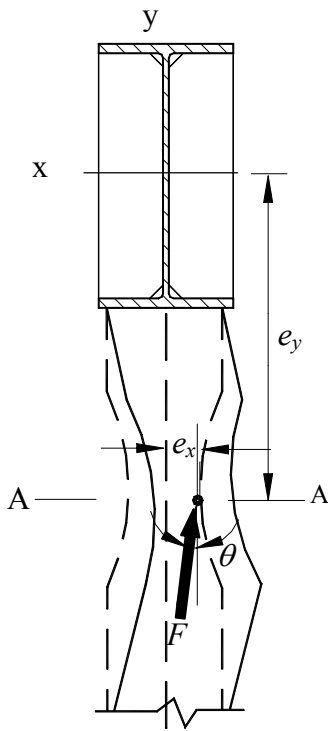


(b) Specimen DC-2

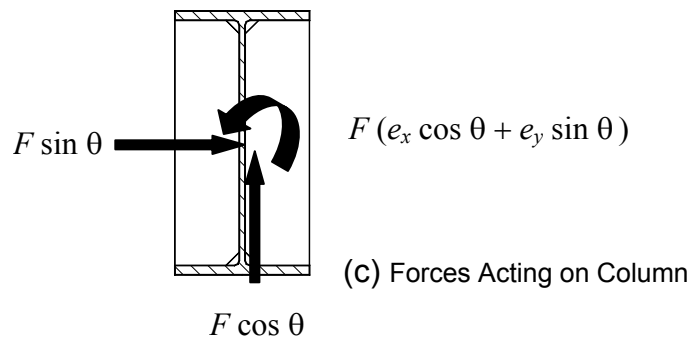




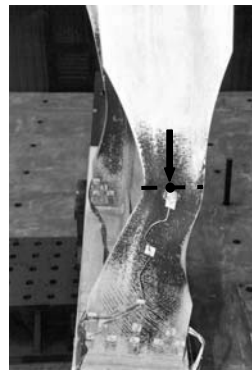
(c) Specimen DC-3
Figure 2 Global Response and Failure Mode



(b) Inclined Beam Flange Force



(c) Forces Acting on Column



(a) Deformed Beam at 4% Drift

Figure 3 Eccentric Beam Flange Force to Column

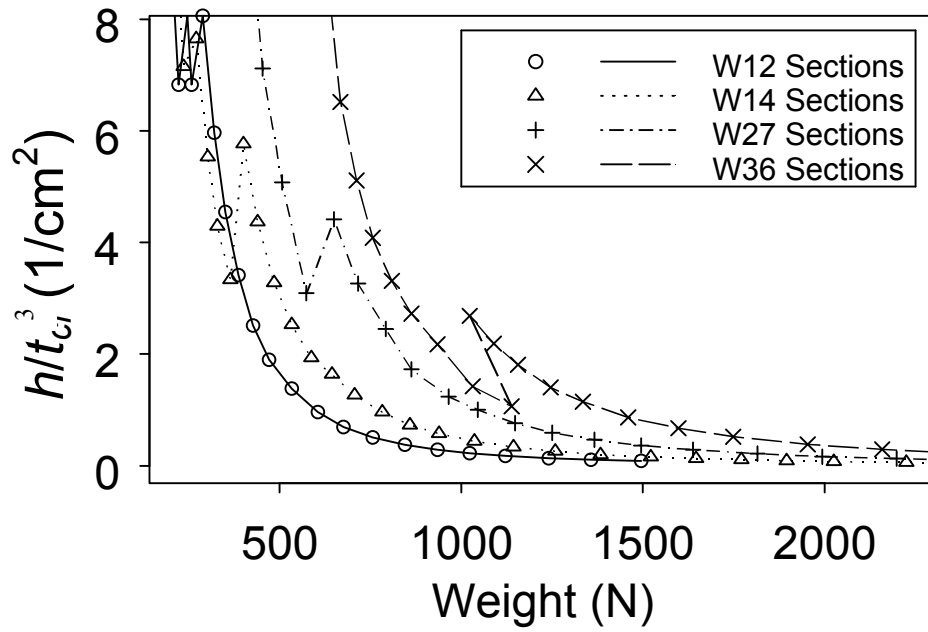


Figure 4 Variations of h/t_{c1}^3 with Respect to Weight

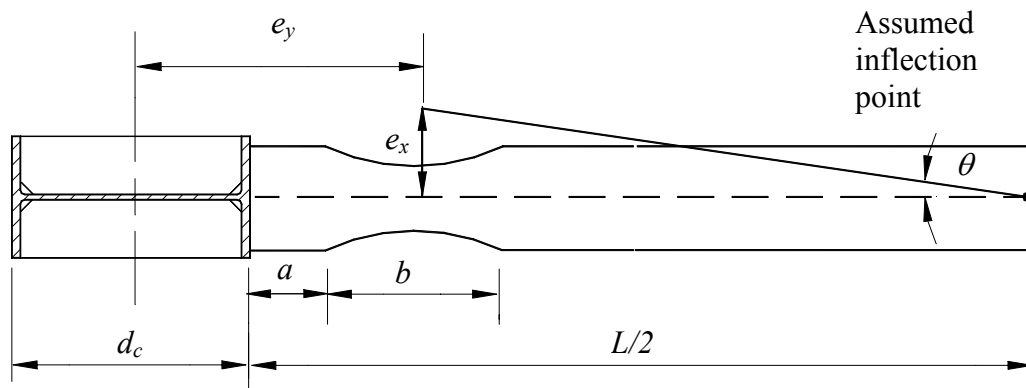


Figure 5 Evaluation of Angle θ

A MEMBRANE METHOD FOR TRANSVERSELY LOADED COLUMN WEBS

William A. Thornton
President, Cives Engineering Corporation, Roswell, Georgia, USA

ABSTRACT

Existing methods for estimating the nominal strength of column webs subjected to loads delivered by plates parallel to the column flanges and centered on the web are based on either elastic beam or plate theory, or on plastic plate (yield line) theory. These methods have been shown by physical testing to greatly underestimate the nominal strength. A method based on non-linear membrane action has been developed and compared with the results of physical tests. Excellent correlation between the actual and predicted nominal strengths has been achieved. The development of the method, comparison to physical tests, and application to a design example will be presented.

INTRODUCTION

The basic problem is shown in Fig. 1. The plate is welded to the center of the column web as shown, and is loaded transverse to the column web. This problem occurs with knee braces and other bracing situations.

There are two solutions available in the literature. Blodgett (1) gives an elastic solution based on beam theory. Anand and Bertz (2) present a yield line solution, although they have access to a series of physical tests which show that the yield line solution is very conservative and that membrane action is necessary to predict the actual behavior.

If the recommended elastic method (1) or the yield line method (2) are used, the capacity of this connection will be very small and stiffeners such as those shown in Fig. 2 will almost always be necessary. Because this is an expensive solution, it is the purpose of this paper to develop a membrane method which more accurately predicts the load carrying capability of this connection.

THEORY

The membrane model is shown in Fig. 3. The central portion of length l , will pull up under a tension load as a 2-link mechanism. Following Timoshenko and Young (3), the tensile force P_u will be given by

$$P_u = 2\sqrt{2}t_w l \sqrt{\frac{F_y^3}{E}} \quad (1)$$

when the links reach their ultimate strength of $F_y t_w$ per unit length, where F_y is the yield stress and t_w is the column web thickness. Eq. 1 is the basic membrane formula. The web displacement at the load P_u is

$$\delta = \frac{1}{\sqrt{2}} \sqrt{\frac{F_y}{E}} h \quad (2)$$

One advantage of the membrane method over a yield line method is the capability to calculate a displacement as in eq. 2. This equation will assist in arriving at a reasonable failure criterion for this connection.

Returning to eq. 1, which represents only the central portion of the displacement pattern shown in Fig. 3, consider that the circular end portions of the pattern will also add some capacity. Taking the average length of the radial links as their mid length, the l in eq. 1 is replaced by

$$l_T = l + \frac{a\pi}{2} = l + \frac{h\pi}{4}$$

Thus eq. 1 becomes

$$P_u = 2\sqrt{2} t_w l_T \sqrt{\frac{F_y^3}{E}} \quad (3)$$

A radial fan yield line can exist perpendicular to the link lengths, and from Park and Gamble (4), the extra capacity is

$$2\pi m_p = 2\pi \frac{1}{4} F_y t_w^2 = \frac{\pi}{2} F_y t_w^2$$

So eq. 3 becomes

$$P_u = t_w F_y \left[2\sqrt{2} \sqrt{\frac{F_y}{E}} l_T + \frac{\pi}{2} t_w \right] \quad (4)$$

Referring again to Fig. 3, if l is too long, the column flanges will not be able to sustain the pull of the links of $t_w F_y$ per unit length and will tend to become closer together. To prevent this happening at the load P_u , consider the length of flange noted by v in Fig. 3. Considering Fig. 4, the flange will be able to sustain the pull $t_w F_y$ as long as

$$t_w F_y v \frac{v}{2} \leq 2 \frac{1}{4} F_y b_f t_f^2 \quad (5)$$

where b_f and t_f are the column flange width and thickness, respectively. Then, from eq. 5, if

$$\nu = t_f \sqrt{\frac{b_f}{t_w}} \text{ and } l \leq 2\nu, \text{ the original model can be sustained. Setting } l_T \text{ of eq. 4. equal to } l_{eff} + \frac{\pi}{4}h \text{ where } l_{eff} = \min\{l, 2\nu\} \quad (6)$$

and recognizing that if l_{eff} is less than l , the portion of the pattern in the middle, i.e., $l - l_{eff}$ is no longer sustaining membrane action but can still develop yield line strength $(l - l_{eff}) \frac{1}{4} F_y t_w^2$ (4), eq. 4. is finally completed as

$$P_u = t_w F_y \left[2\sqrt{2} \sqrt{\frac{F_y}{E}} \left(l_{eff} + \frac{\pi}{4}h \right) + \frac{t_w}{h} \left(\frac{\pi}{2}h + l - l_{eff} \right) \right] \quad (7)$$

This is the proposed membrane method equation for transversely loaded webs.

EXPERIMENTAL VERIFICATION

A large number of laboratory tests were performed by Csernak (5) on this connection. His data are presented in Table 1. All material used was A36, but only one coupon test was reported in (5), although several were reported to have been done. The material was definitely established as A36. The reported properties of F_y and E were 36.5 ksi and 31,600 ksi, respectively. Because of the lack of data, Table 2 was produced with $F_y = 36$ ksi and $E = 29,000$ ksi. The (P_u) test in Table 2 was determined from the load-deflection curves of (5). The value of deflection was calculated from eq. 2. At this value of δ , the value of (P_u) test was determined from the load-deflection curve and listed in Table 2. The value of (P_u) theory was calculated from eq. 7. The last column of Table 2 shows a fairly good agreement of the “test” and “theory” values of (P_u) . The statistical error in any one observation in the last column of Table 2 is 11.9%, which gives some confidence that the predicted load capacity (nominal strength) of this connection can be determined to within $\pm 12\%$, which is satisfactory for engineering calculations. From Table 2, it can be seen that the deflection at the nominal strength δ is generally smaller than the column web thickness. Since this a reasonable displacement for most structures, the nominal strength (or ultimate load) (P_u) predicted by eq. 7 is a reasonable strength prediction.

AN EXAMPLE (From 6)

Consider a W16x50 column of A572-50 steel with a plate $\frac{1}{2} \times 24 \times 18$ of A36 steel welded to the center of its web. What design load can this configuration carry? See Fig. 1.

For the column, $d = 16.26$, $t_f = .630$, $h = 16.26 - 2 \times .630 = 15.0$, $b_f = 7.070$, $t_w = .380$;

For the plate, $l = 24$. Then

$$v = t_f \sqrt{\frac{b_f}{t_w}} = .630 \sqrt{\frac{7.070}{.380}} = 2.717$$

$$l_{eff} = \min\{2x2.717, 24\} = 5.44$$

$$P_u = .380x50 \left[2\sqrt{2} \sqrt{\frac{50}{29,000}} \left(5.44 + \frac{\pi}{4} x 15.0 \right) + \frac{.380}{15.0} \left(\frac{\pi}{2} x 15.0 + 24 - 5.44 \right) \right] = 58.7 \text{ kips}$$

and the design strength is $\phi P_u = .9x58.7 = 52.8^k$

For comparison, a yield line solution (2) is $P_u = 2t_w^2 F_y \left(\sqrt{2} + \frac{1}{2} \frac{l}{h} \right)$ which will yield

$P_u = 2x.380^2 x 50 \left(\sqrt{2} + \frac{1}{2} x \frac{24}{15} \right) = 31.9$ kips and $\phi P_u = .9x31.9 = 28.8$ kips, which is about half of the membrane solution for this case.

CONCLUSIONS

A membrane theory method for transversely loaded column webs has been developed and shown to be validated by physical tests. The method generally gives greater capacities than the usual yield line method with displacements which are on the order of the column web thickness.

REFERENCES

1. Blodgett, Omer W., *Design of Welded Structures*, The James F. Lincoln Arc Welding Foundation, Cleveland, Ohio, page 6.6-6, 1966.
2. Anand, S.C., and R.F. Bertz, *Analysis and Design of a Web Connection In Direct Tension*, AISC Engineering Journal, 2nd Quarter, 1981, pp. 48-52.
3. Timoshenko, S., and D.H. Young, *Theory of Structures*, McGraw Hill Book Company, 1945, p. 223.
4. Park, R., and W.L. Gamble, *Reinforced Concrete Slabs*, Wiley Interscience, New York, 1980, p. 306.
5. Csernak, S.F., *Evaluation of the Strength of Column Web Connections*, MS Thesis, Clemson University, Feb. 1976.
6. Celentano, A., V.A. Mouras, and J.T. Young, *Strength of a Tension Loaded Web Plate*, Report Submitted to T.M. Murray, Virginia Polytechnic Institute and State University, Dec. 1996.

Table 1 Test Specimens (from Csernak 6)

Test No.	Column Type	Plate Size
1	W6 x 8.5	4 x 3/8
2	W6 x 15.5	8 x 3/8
3	W6 x 16	4 x 3/8
4	W6 x 16	8 x 3/8
5	W6 x 25	4 x 3/8
6	W8 x 10	8 x 3/8
7	W8 x 24	4 x 3/8
8	W8 x 24	6 x 3/8
9	W8 x 24	8 x 3/8
10	W8 x 31	2 x 3/8
11	W8 x 31	4 x 3/8
12	W8 x 31	6 x 3/8
13	W8 x 31	8 x 3/8
14	W8 x 31	8 x 3/8
15	W10 x 11.5	8 x 3/8
16	W10 x 21	4 x 3/8
17	W10 x 21	4 x 3/8
18	W10 x 21	4 x 3/8
19	W10 x 21	8 x 3/8
20	W10 x 33	8 x 3/8

Table 2 Comparison of Physical Test Data With the Theory

Test no.	l in.	2ν in.	h in.	l_{eff} in.	t_w in.	$(P_u)_{test}$ kips	δ in. Eq. 2	$(P_u)_{theory}$ kips Eq. 7	$\frac{(P_u)_{test}}{(P_u)_{theory}}$
1	4	1.78	5.54	1.78	.175	6.02	.138	5.2	1.16
2	8	2.69	5.56	2.69	.240	11.3	.138	15.5	.73
3	4	3.15	5.44	3.15	.265	11.4	.136	13.0	.88
4	8	3.15	5.44	3.15	.265	13.3	.136	16.0	.83
5	4	3.98	5.42	3.98	.325	16.6	.136	19.3	.86
6	8	1.97	7.46	1.97	.180	7.83	.186	7.0	1.12
7	4	3.89	7.20	3.89	.275	13.7	.179	15.5	.88
8	6	3.89	7.20	3.89	.275	14.5	.179	18.2	.80
9	8	3.89	7.20	3.89	.275	15.2	.179	17.1	.89
10	2	4.35	7.28	2	.305	13.7	.181	15.2	.90
11	4	4.35	7.28	4	.305	15.9	.179	18.8	.85
12	6	4.35	7.28	4.35	.305	18.0	.181	21.5	.84
13	8	4.35	7.28	4.35	.305	18.0	.181	26.0	.69
14	8	4.35	7.13	4.35	.295	17.1	.178	22.5	.76
15	8	1.89	9.60	1.89	.180	8.66	.239	6.5	1.33
16	4	3.36	9.31	3.36	.245	12.9	.232	10.3	1.25
17	4	3.36	9.31	3.36	.245	12.9	.232	10.3	1.25
18	4	3.36	9.31	3.36	.245	12.9	.232	10.3	1.25
19	8	3.36	9.31	3.36	.245	12.9	.232	14.4	.90
20	8	4.63	8.99	4.63	.295	18.5	.224	20.0	.93

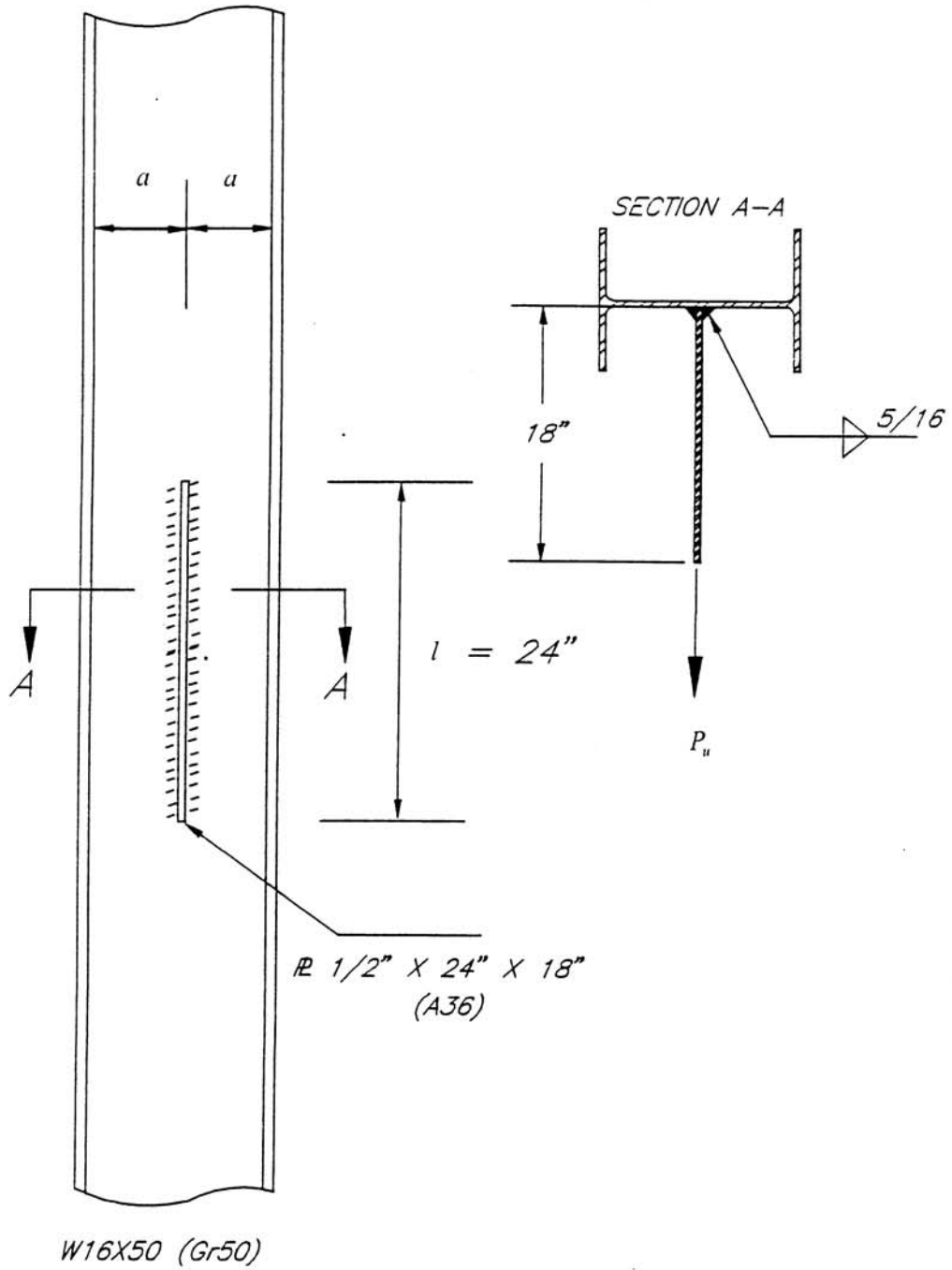


FIG. 1 TRANSVERSELY LOADED COLUMN WEB (FROM 6)

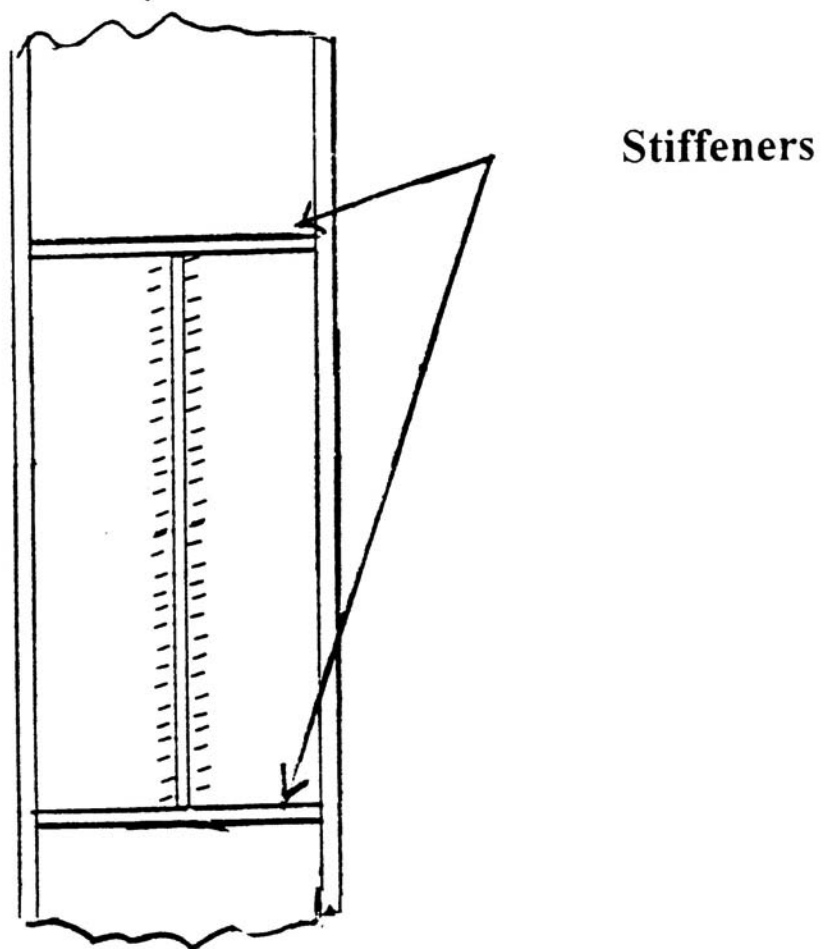


FIG 2. STIFFENERS MAY BE REQUIRED TO CARRY LOAD TO COLUMN FLANGES

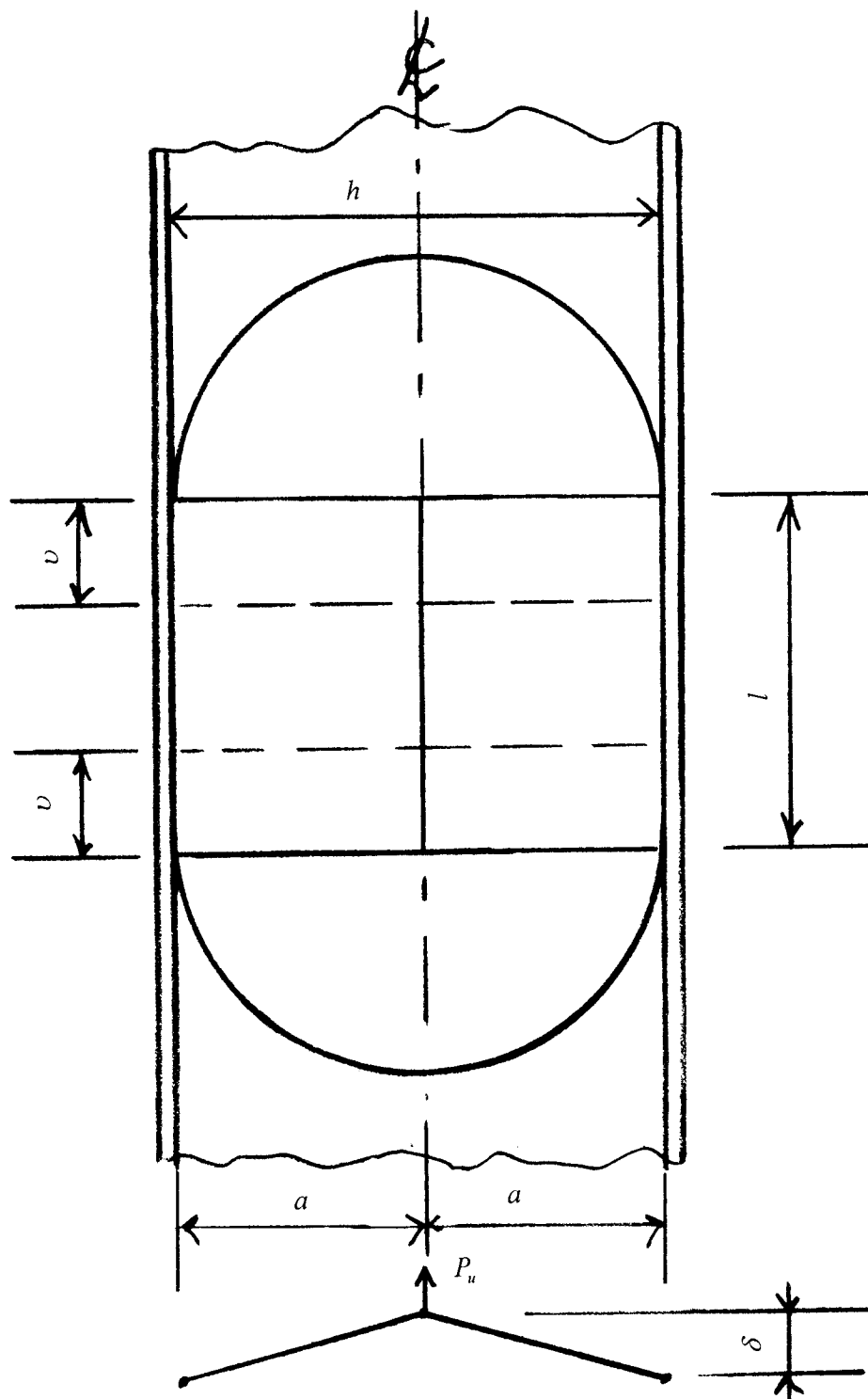


FIG. 3 MEMBRANE MODEL

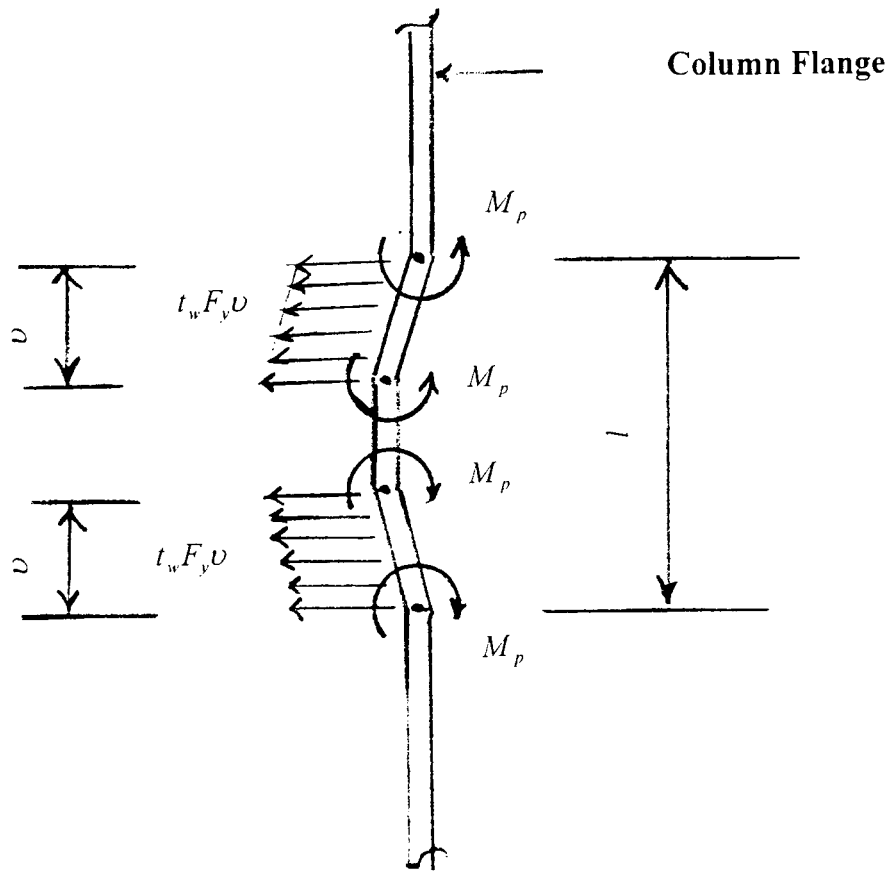


FIG. 4 FLANGE MECHANISM INDUCED BY WEB MEMBRANE FORCES

DESIGN AND BEHAVIOR OF GUSSET PLATE CONNECTIONS

J.J. Roger Cheng and Gilbert Y. Grondin
Dept. of Civil and Environmental Engineering
University of Alberta
Education
Edmonton, Alberta, Canada T6G 2G7

Michael C.H. Yam
Department of Construction
Hong Kong Inst. of Vocational
Education
Hong Kong

ABSTRACT

The behavior and design of gusset plate connections are reviewed and summarized. The paper first reviews the existing design methods for proportioning gusset plates under monotonic loading as well as under seismic loading. A summary of recent research at the University of Alberta on the monotonic and cyclic behavior of gusset plate connection is then presented. Based on the monotonic test series, a modified design method is proposed for proportioning the gusset plate to support compressive forces from brace members. The cyclic behavior of gusset plate connections is described using the results of experimental and analytical studies. The interaction between the gusset plate and the brace member is considered in the study. Current research programs are presented regarding the effect of various parameters on the cyclic behavior of gusset plate connections and the potential of a bracing system where the bracing member is designed as the strong element and the gusset plate is designed as the weak element.

INTRODUCTION

Because of the complex behavior of the gusset plate in concentrically braced frames (CBF's), the design of gusset plate connections has traditionally involved highly simplified methods (1-3). Although these methods have proven to be adequate, it is believed that the factor of safety associated with their usage is highly variable (4). Up until recently, the majority of the research on gusset plates has focused on elastic stress distributions or the inelastic behavior of gusset plates loaded monotonically in tension. Relatively little attention has been given to compressive or cyclic behavior. Typically, concentrically braced frames are designed to dissipate energy through yielding or buckling of the brace members. The remaining members and connections are designed to carry the forces that are present in the structure at the load level that causes the brace member to yield or buckle. This design approach embodies the philosophy of capacity design (5).

A series of tests and analytical studies were conducted recently at the University of Alberta (6-10) to investigate the compressive and cyclic behavior of gusset plate connections. In the compression test series (6-7), it was found that when a gusset plate is loaded in monotonic compression, normally significant yielding of the plate takes place before plate buckling. However, if a thin plate is used, the gusset plate can buckle at a

load much lower than the yield load. As for the cyclic test series (8), it showed that the tensile capacity of the gusset plate remains stable under cyclic loading. The study also showed that the post-buckling capacity of the gusset plate, although less than the load required to buckle the gusset plate initially, tends to be stabilized after a few cycles. Based on these observations, a design approach that would take advantage of the energy dissipation potential of the gusset plate was proposed (8). This approach consists of designing the gusset plate as the weak element rather than the brace member. The behavior of gusset plate connections under cyclic loading was further verified and studied by a numerical investigation (9) using the finite element program ABAQUS (11) and full-scale tests (10). The analysis considered the effect of gusset plate support condition (rigid support versus flexible support provided by a beam and column assembly), initial imperfections in the plate, material yielding, slip of the bolted connection, bracing member – gusset plate interaction, and load history. The testing program included interaction between bracing member and gusset plate, and effect of edge stiffeners on the cyclic behavior of gusset plates.

The following presents a summary of the behavior of gusset plate connections, in both monotonic and cyclic behavior. The design method for gusset plate connection is reviewed and presented. The weak gusset plate – strong brace member concept is also examined as an alternative for concentrically braced frames (CFB's) under cyclic loading.

BEHAVIOR UNDER MONOTONIC LOADING

An experimental program by Whitmore in the early 1950's (1) studied the stress distribution in a gusset plate connection, a detail commonly found in Warren truss type bridges. The main objective of Whitmore's investigation was to determine the location and magnitude of the peak stress in the gusset plate. Based on the results of his investigation,

Whitmore proposed a method for predicting the peak stress in a gusset plate for a given brace load. It was proposed that the peak stress could be estimated by taking the brace load and dividing it by an area equal to the plate thickness times what later became known as the "Whitmore effective width". The Whitmore effective width is defined as the distance between two lines radiating outward at 30° angles from the first row of bolts in the gusset-to-brace connection along a line running through the last row of bolts as shown in Fig. 1.

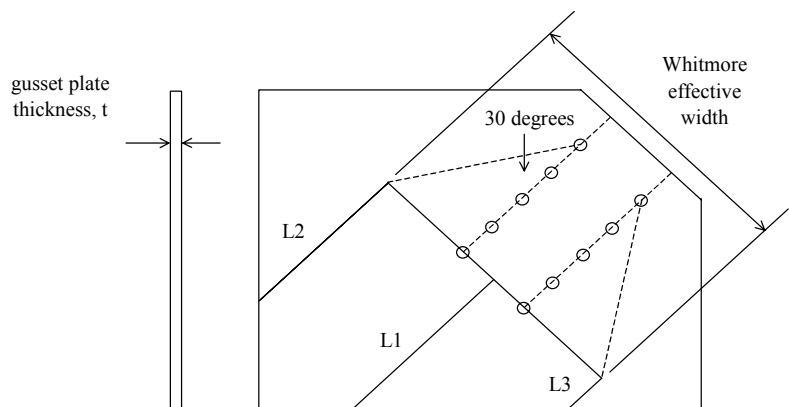


Figure 1 – Whitmore Effective Width

In 1957 Irvan (12) carried out a similar investigation with a model of a double gusset plate Pratt truss connection detail. Irvan's investigation showed that stress distributions computed with the beam method did not match well with test results. Irvan proposed a method of determining the peak stress that was similar to the Whitmore method. Hardin (13), Davis (14), and Varsarelyi (15) investigated the stresses in gusset plates loaded in

the elastic range. Hardin's experimental investigation confirmed Irvan's conclusions regarding the beam method and supported Irvan's method for determining the magnitude of the peak stress in the gusset plate. Davis and Varsarelyi carried out finite element investigations of the elastic stresses in gusset plates. In general, these investigations confirmed the findings of the Whitmore's experimental investigations regarding the stresses in gusset plates loaded in the elastic range.

The behavior of gusset plate connections in the inelastic range also received some attention. Chakrabarti and Bjorhovde (16) and Hardash and Bjorhovde (2) looked at the inelastic behavior of gusset plate connections in tension. From their tests and those of other investigators, a block shear model was proposed to predict the ultimate capacity of gusset plate connections in tension. They proposed that the ultimate strength of the gusset plate is the sum of the tensile strength of the net area between the last row of bolts and the shear strength along the connection length.

Thornton (3), investigating the compressive strength of steel gusset plates, proposed an intuitive and lower bound approach whereby the compressive force in the steel gusset plate is carried by an equivalent column between the end of the bracing member and the beam to column joint. The method proposed by Thornton for calculating the elastic buckling load was expanded to include inelastic effect (17). The technique proposed by Thornton is based on the buckling capacity of unit strips of length L_1 , L_2 , and L_3 (see Fig. 1) below the Whitmore effective width. The critical length of the column strip is taken as the maximum of L_1 , L_2 , or L_3 . Once the length of the column strip has been established, the compressive resistance of the column strip can be evaluated according to the column formulas in the design standards. The effective length factor was recommended to be 0.65. The gusset plate will not buckle if the buckling stress of the critical unit strip is greater than the normal stress on the Whitmore effective area.

Hu and Cheng (6) conducted an experimental and analytical investigation of the buckling behavior of gusset plate connections loaded monotonically in compression. Their test program focused on the effects of plate thickness, geometry, boundary conditions, eccentricity and reinforcement. The work of Hu and Cheng showed that thin gusset plates tend to buckle at a load much lower than the yield load predicted using the Whitmore effective width. In general, either sway or local buckling modes were observed depending on the out-of-plane brace restraint conditions. Further analytical work (18) showed that an increase in the stiffness of the gusset-to-brace splice plate of two to four times the gusset plate thickness should result in an increase in the buckling strength of the gusset plate. It was recommended that the distance between the end of the splice plate and the gusset-to-frame boundaries be kept to a minimum.

To investigate the compressive behavior of gusset plate connections, a total of thirteen full-scale tests were conducted by Yam and Cheng (7). One of the test setups is shown schematically in Fig. 2. The test parameters included gusset plate thickness, size, brace angle, out-of-plane brace restraint conditions, and moments in the framing members. The specimen dimensions and designations are shown in Table 1. The test specimens used in this investigation were stockier than those of Hu and Cheng (6), and, as a consequence, displayed more inelastic behavior. The compressive capacity of the gusset plate specimens was almost directly proportional to their thickness. The effects of beam and column moments and brace angle on the capacity of the test specimens in compression were found to be small.

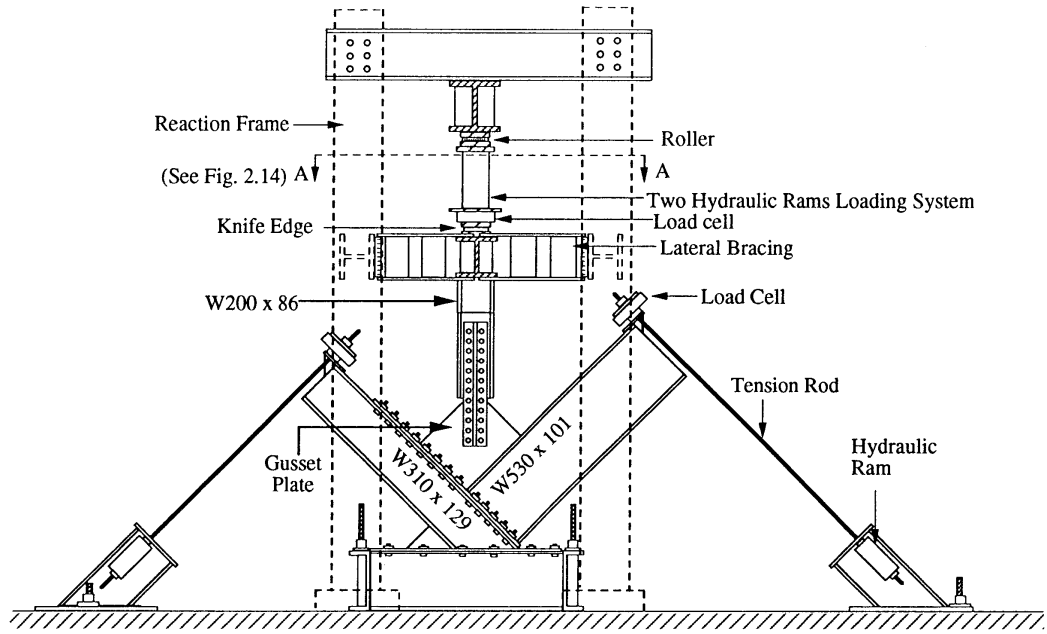


Figure 2 – Typical Test Setup

Table 1 Compressive Specimens Description and Summary of Test Results

Specimen Designation	Plate Size (mm x mm)	Plate Thickness (mm)	Brace Angle	Beam Moment (kN·m)	Column Moment (kN·m)	Ultimate Load (kN)
GP1	500 x 400	13.3	45°	–	–	1956
GP2	500 x 400	9.8	45°	–	–	1356
GP3	500 x 400	6.5	45°	–	–	742
SP1	850 x 700	13.3	45°	–	–	1606
SP2	850 x 700	9.8	45°	–	–	1010
AP1	500 x 400	13.3	30°	–	–	1720
AP2	500 x 400	9.8	30°	–	–	1210
AP3	500 x 400	6.5	30°	–	–	728
MP1	500 x 400	13.3	45°	250	125	1933
MP2	500 x 400	9.8	45°	250	125	1316
MP3	500 x 400	6.5	45°	250	125	721
MP3A	500 x 400	6.5	45°	375	187.5	819
MP3B	500 x 400	6.5	45°	0	0	821

A numerical analysis of the test specimens was subsequently performed (19) by using the finite element program ABAQUS (11). A three dimensional mesh was used to model the connection with the splice member placed on both sides of the gusset plate. The beam and column boundaries were fully restrained to simulate a rigidly welded connection. At the junction between the bracing member and the gusset plate, infinite rotational restraint was imposed on the top of the splice member. Point loads were applied on the splice member to simulate the load transferred from the bracing member. The bolted connection was simulated by rigid beam elements at the bolt locations. To account for the influence of bolt clamping force on the gusset plate, it was assumed that a 30 mm square surface was rigidly connected at the bolt locations by the rigid beam elements. For the MP type specimens, the beam and column were included in the model and allowed the application of beam and column moments. The analytical ultimate loads of the specimens based on the load-deflection analysis are shown together with the test results in Table 2. The analytical predictions are in good agreement with the test results.

To evaluate the validity of current design methods, the Whitmore load (P_W) based on the material static yield strength and the Thornton load (P_T) based on the effective length factor of 0.65 are included in Table 2.

Table 2 Comparison of Test Loads with Analytical and Design Loads

Specimen Designation	Ultimate Load, P_u (kN)	P_{ABAQUS} (kN)	$\frac{P_u}{P_{ABAQUS}}$	Whitmore Load, P_W (kN)	Thornton Load, P_T (kN)	Modified Thornton, P_T' (kN)	$\frac{P_u}{P_W}$	$\frac{P_u}{P_T}$	$\frac{P_u}{P_T'}$
GP1	1956	1987	0.98	1216	1142	1792	1.61	1.71	1.09
GP2	1356	1301	1.04	930	828	1300	1.46	1.64	1.04
GP3	742	710	1.04	555	439	689	1.37	1.69	1.08
SP1	1606	1608	1.00	1852	1072	1744	0.87	1.50	0.92
SP2	1010	993	1.02	1416	592	963	0.71	1.70	1.05
AP1	1720	1680	1.02	1216	1119	1757	1.56	1.54	0.98
AP2	1210	1177	1.03	930	801	1257	1.55	1.51	0.96
AP3	728	732	0.99	555	404	634	1.31	1.80	1.15
MP1	1933	1901	1.02	1216	1142	1792	1.59	1.69	1.08
MP2	1316	1348	0.98	930	828	1300	1.42	1.59	1.01
MP3	721	700	1.03	555	439	689	1.30	1.64	1.05
MP3A	819	805	1.02	555	439	689	1.48	1.87	1.19
MP3B	821	725	1.13	555	439	689	1.48	1.87	1.19

As can be seen from the table, the Whitmore method provides a conservative estimate of the design load for the specimens, except for the SP type specimens since the SP type specimens are more susceptible to the stability failure. The Thornton method, however, provides conservative estimates for all the specimens. The test to predicted

ratios varied from 0.71 to 1.61 for the Whitmore method and from 1.31 to 1.87 for Thornton's method. The reason for the conservatism observed with Thornton's method is due to the extensive yielding in most of the specimens. Yielding allowed load redistribution in the specimens. In order to account for this load redistribution, it is proposed that a 45° dispersion angle be used to evaluate the effective width, instead of 30°. This modification of Thornton's method is then used to calculate the buckling strength (P_T') of the specimens using extended effective width and the appropriate column curves. The values of P_T' are listed in Table 2. The ratio of test loads to the modified Thornton loads varies from 0.92 to 1.19.

BEHAVIOR UNDER CYCLIC LOADING

Compared to the information available on the cyclic behavior of bracing members, the amount of information on the cyclic behavior of gusset plates is quite small. Jain et al. (20) studied the effect of gusset plate bending stiffness and bracing member length on the cyclic behavior of bracing members. Although the bracing member was the main subject of the investigation, three different gusset plates were used and the length of the brace member was varied. From a test program comprising 18 test specimens, none were designed to have the yield strength of the gusset plate lower than the bracing member. It was concluded that there is no advantage in making the flexural stiffness of the gusset plate greater than the flexural stiffness of the bracing member. An increase in flexural stiffness of the gusset plate was found to result in a decrease in the effective length of the bracing member. This, in turn, improves the cyclic behavior of the bracing member.

Astaneh-Asl et al. (21) studied the cyclic behavior of brace members composed of back-to-back double angles connected to gusset plates. The focus of their investigation was also the behavior of the bracing member. Both in-plane and out-of-plane buckling of the brace member was investigated. Single gusset plates connected only to a beam element were used in the investigation. Current code design procedures were found to be deficient. For brace members that buckle out-of-plane, Astaneh-Asl et al. stressed the importance of designing the gusset plates so that they can accommodate the formation of a plastic hinge, allowing brace buckling to take place without tearing of the connection.

Rabinovitch and Cheng (8) tested five full-scale specimens to study the behavior of gusset plate connections under cyclic loading. The effects of plate thickness, geometry, edge stiffness, and bolt slip were studied. With the exception of one test specimen, all the test specimens were rectangular and similar to the specimens tested in the compression series by Yam and Cheng (7). One test specimen, however, was designed to allow the free formation of a plastic hinge under compressive buckling deformation as per the recommendation of Astaneh-Asl et al. (21). The behavior of this latter test specimen was significantly different from that of the other specimens, it failed more rapidly than other more compact specimens and fracture was observed at the plastic hinge closed to beam and column. It also required much larger plate to accommodate the plastic hinge requirement. All other four specimens were governed by tensile fracture between last row of bolts in the gusset plate as was observed in the earlier tests by Chakrabarti and Bjorhovde (16). The tensile capacity of gusset plates under cyclic loading remained stable and the post-buckling compressive capacity tends to be stabilized after buckling. The addition of edge stiffeners was found to significantly

improve the post buckling compressive strength and the energy dissipation characteristics of the gusset plate tested.

Based on the stable post-buckling strength of gusset plates under compression, a design approach that would take advantage of the energy dissipation potential of the gusset plate was proposed (8). This approach, referred to as the “weak gusset plate – strong brace member” concept, consists of designing the gusset plate as the weak element rather than the brace member. Nast et al. (10) tested four gusset plate – bracing member subassemblies, as shown in Table 3, to further investigate this concept. The first two test specimens were designed with the gusset plate as the weak element in compression; one with free edge stiffeners, and the second one without. The other two were designed with the brace member as the load-limiting element in compression; again one included free edge stiffeners, and the other did not.

Table 3 Summary of Test Specimens under Cyclic Loading

Specimen	Gusset Plate (mm x mm x mm)	Free Edge Stiffener Width x Thickness (mm x mm)	Bracing Member (mm)	Ultimate Tensile Load (kN)	Ultimate Compressive Load (kN)
T-1	450 x 550 x 9.5	50.7 x 9.5	1100	N/A	1951
T-2	450 x 550 x 9.6	N/A	1100	1819	1690
T-3	450 x 550 x 9.5	50.5 x 9.5	5250	1837	1350
T-4	550 x 450 x 9.5	N/A	5250	1841	1322

The axial load vs. axial deformation hysteresis plots for these four specimens are presented in Fig. 3. The ultimate tensile and compressive loads, based on the envelopes of the hysteresis curves, are listed in Table 3. Both tensile and compressive strengths were predicted accurately by the block shear model and modified Thornton’s method, respectively. The presence of free edge stiffeners does not have a significant effect on the gusset plate buckling strength, but increases the energy absorbed by the gusset plate – brace member assembly in the compression cycle. Little effect in the tension cycle by the stiffeners was observed.

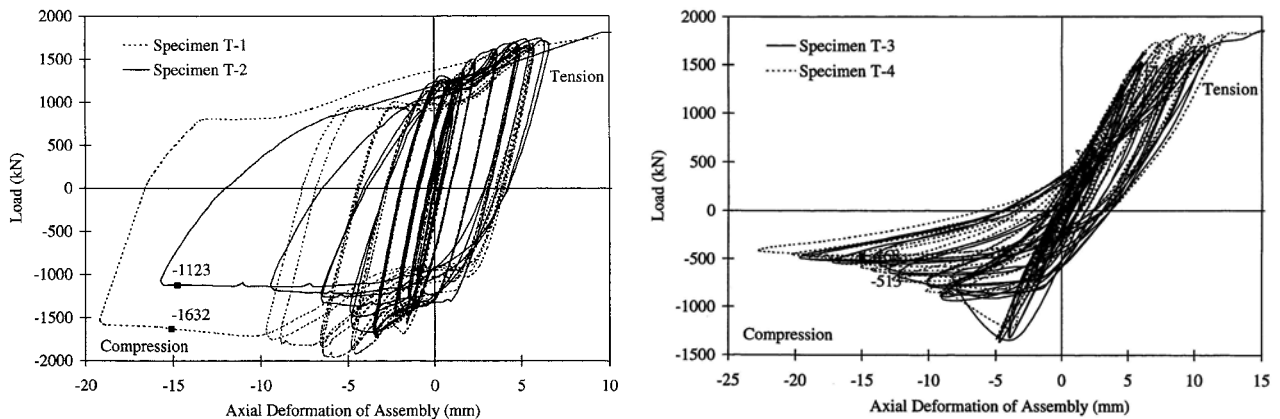


Figure 3 – Behaviour of Gusset Plate Assembly Under Cyclic Loads

As shown in Fig. 3, the energy dissipated by Specimens T-1 and T-2 was much higher than Specimens T-3 and T-4. Yielding of the gusset plate in compression in the first two tests helped the connection to dissipate significantly more energy than buckling of the bracing member in the other two tests. However, all the connections failed in tension in the gusset plate with a relatively small deformation. This may limit the use of the “weak gusset plate – strong brace member” concept in seismic applications.

Walbridge et al. (9) investigated analytically the behavior of gusset plate – brace member assemblies for a number of parameters that were not investigated experimentally. A parametric study was conducted to study the effects of gusset plate – brace member interaction and load sequence on the behavior of steel gusset plate connections under cyclic loading. The various factors affecting the behavior and energy dissipation characteristics of gusset plate connections under cyclic loading conditions were considered.

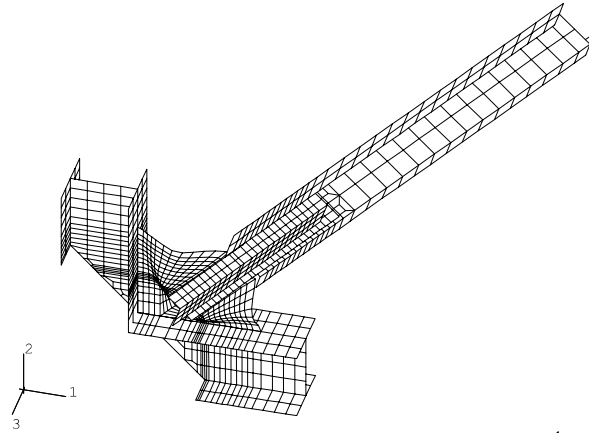
Four types of behavior were studied for the gusset plate – brace member assemblies:

- 1) Effect of the bracing member yielding in tension before yielding of the gusset plate;
- 2) Effect of the gusset plate yielding in tension before yielding of the brace member;
- 3) Effect of buckling of the brace member before buckling of the gusset plate;
- 4) Effect of buckling of the gusset plate before buckling of the bracing member.

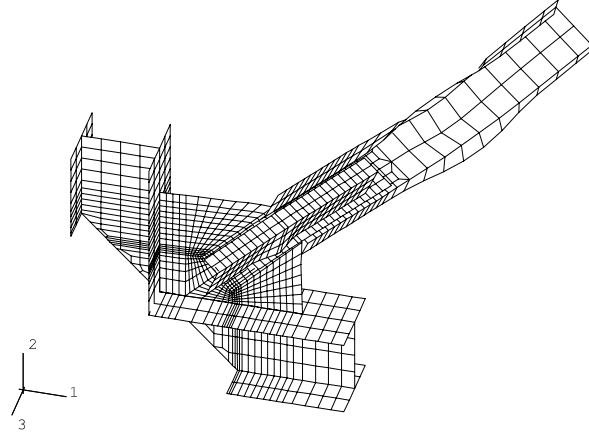
The models investigated were designed to investigate the above four cases for a 450 x 550 mm gusset plate of three different plate thicknesses, 6, 9, and 12 mm. The capacity in the tension cycle was either limited by yielding of the brace member or yielding of the gusset plate, depending on the design adopted for the specimen. In the compression cycle, the load carrying capacity was limited by either buckling of the gusset plate as shown in Fig. 4(a), or by buckling of the brace member about its weak axis, i.e. out of the plane of the gusset plate, as shown in Fig. 4(b). The specimens used in the analysis were designed so that each combination of tension and compression load limitation mechanisms would be exhibited.

The results of this investigation showed that there is very little effect on the behavior the assembly by different load sequences. As for the plate thickness, the analyses showed that the thicker gusset plate gave fuller hysteresis loop for the assemblies having a tension capacity limited by yielding of the gusset plate and a compression capacity limited by buckling of the gusset plate.

Fig. 5 shows the difference in behavior of the gusset plate – brace member assembly for different load limitation mechanisms for a 6 mm gusset plate (GP1). Fig. 5(a) represents the behavior when the load in tension is limited by yielding of the gusset plate and the load in compression is limited by buckling of the gusset plate. Fig. 5(b) represents the behavior when the limiting condition in tension is yielding of the gusset plate and the limiting condition in compression is buckling of the brace member. A comparison of Fig. 5(a) with Fig. 5(b) shows that buckling of the brace member as a limiting condition in the compression range results in a more significant reduction in compression capacity under cyclic loading and a deterioration of the load carrying capacity in tension. This reduction in tension stiffness at zero load can be quite significant when the compression capacity is limited by buckling of the bracing member, as shown in Fig. 5(b). This reduction in tension stiffness was not observed when buckling of the gusset plate limited the compression capacity. The same observation as Fig. 5(a) was made when the limiting condition in tension is yielding of the brace member and the limiting condition in compression is buckling of the gusset plate.

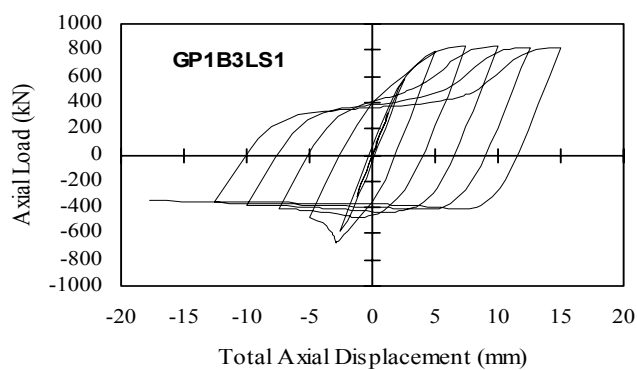


(a) Buckling of Gusset Plate

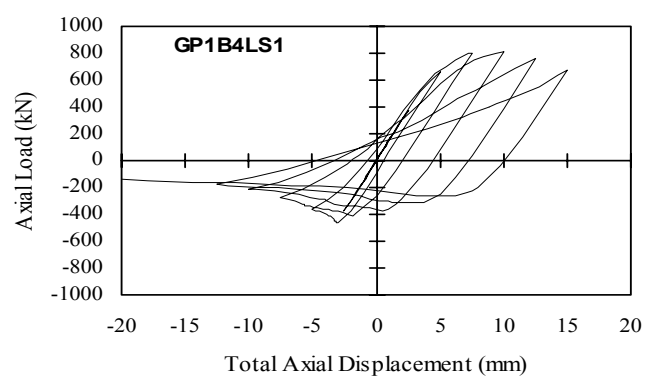


(b) Buckling of Brace Member

Figure 4 – Failure Modes of Gusset Plate – Brace Member Assembly



(a) Gusset plate yielding – gusset plate buckling



(b) Gusset plate yielding – brace buckling

Figure 5 – Effect of Load Limitation

SUMMARY AND CONCLUSIONS

Recent developments in the behavior of gusset plate connections, both monotonic and cyclic behavior, were reviewed and summarized in the paper. Full-scale tests were conducted under both monotonic compression and cyclic loading. Numerical investigations were carried out using the finite element method, incorporating the effect of material and geometry non-linearity and initial imperfections.

The tensile strength of gusset plates can be predicted accurately by the block shear failure proposed by Chakrabarti and Bjorhovde (16). Based on the monotonic compression test results, a modified Thornton method has been proposed for proportioning the gusset plate to support compressive forces from brace members. In the modified Thornton method, a 45° dispersion angle is proposed to evaluate the effective width, instead of 30°, to account the load redistribution in the gusset plate. Good agreement is obtained with the test results by using the proposed method.

From the cyclic tests, the tensile capacity of gusset plates under cyclic loading remained stable and the post-buckling compressive capacity tends to be stabilized after buckling. The addition of edge stiffeners was found to have little effect on the gusset plate buckling strength but significantly improve the post buckling compressive performance and hence increase the energy absorbed by the gusset plate – brace member assembly in the compression cycle. This observation might prove the validity of the “weak gusset plate – strong brace member” concept, consists of designing the gusset plate as the weak element rather than the brace member. Further tests and analyses on the interaction between gusset plate and brace member also showed that yielding and stable post-buckling strength of the gusset plate in compression helped the connection to dissipate significantly more energy than buckling of the bracing member. In general, hysteresis plots for the weak gusset – strong brace member models exhibited less pinching and sustained higher post-buckling compressive loads than conventionally designed subassemblies. However, all the connections failed in tension in the gusset plate with a relatively small deformation. This may limit the use of the “weak gusset plate – strong brace member” concept in seismic applications.

Currently, a research effort is in progress to enhance the tensile performance of a gusset plate. Two approaches are used. One is to utilize the post-fracture behavior of the gusset plate. Leon and Swanson (22) showed that a well designed gusset plate could possess significant post-fracture capacity. The other approach is to provide an active fracture control mechanism in the gusset plate. The ultimate goal of the project is to assess the effectiveness of using gusset plates as the energy dissipators in seismically loaded braced structures.

REFERENCES

1. Whitmore, R.E. 1952. Experimental Investigation of Stresses in Gusset Plates. Bulletin No. 16, Engineering Experiment Station, University of Tennessee.
2. Hardash, S.G. and Bjorhovde, R. 1985. “New Design Criteria for Gusset Plates in Tension.” Engineering Journal, AISC, Vol. 22, No.2, pp. 77-94.
3. Thornton, W.A. 1984. Bracing Connections for Heavy Construction. Engineering Journal, AISC, Vol. 21, No. 3, pp. 139-148.
4. Kulak, G.L., Fisher, J.W. and Struik, J.H.A. 1987. Guide to Design Criteria for Bolted and Riveted Joints. John Wiley and Sons, Second Edition, New York.

5. Redwood, R.G. and Jain, A.K. 1992. Code Provisions for Seismic Design for Concentrically Braced Steel Frames. Canadian Journal of Civil Engineering, April, pp. 1025-1031.
6. Hu, S.Z. and Cheng, J.J.R. 1987. Compressive Behavior of Gusset Plate Connections. Structural Engineering Report No. 153, Department of Civil Engineering, University of Alberta, Edmonton, Alberta.
7. Yam, M.C.H. and Cheng, J.J.R. 1993. "Experimental Investigation of the Compressive Behaviour of Gusset Plate Connections." Structural Engineering Report No. 194, University of Alberta.
8. Rabinovitch, J.S. and Cheng, J.J.R. 1993. "Cyclic Behaviour of Steel Gusset Plate Connections." Structural Engineering Report No. 191, Department of Civil Engineering, University of Alberta.
9. Walbridge, S.S., Grondin, G.Y., and Cheng, J.J.R. 1998. An Analysis of the Cyclic Behaviour of Steel Gusset Plate Connections, Structural Engineering Report No. 225, Department of Civil & Environmental Engineering, University of Alberta, Edmonton, Alberta.
10. Nast, T.E., Grondin, G.Y., and Cheng, J.J.R. 1998. Cyclic Behavior of Stiffened Gusset Plate-Brace Member Assemblies. Structural Engineering Report No. 229, Department of Civil & Environmental Engineering, University of Alberta, Edmonton, Alberta.
11. ABAQUS/Standard User's Manual Volume I and II, Version 5.5, Hibbitt, Karlsson & Sorensen Inc., 1995.
12. Irvan, W.G. 1957. Experimental Study of Primary Stresses in Gusset Plates of a Double Plane Pratt Truss. Bulletin No. 49, University of Kentucky, Engineering Experiment Station.
13. Hardin, B.O. 1958. Experimental Investigation of the Primary Stress Distribution in the Gusset Plates of a Double Plane Pratt Truss Joint with Chord Splice at the Joint. Bulletin No. 49, University of Kentucky, Engineering Experiment Station.
14. Davis, C.S. 1967. Computer Analysis of the Stresses in a Gusset Plate. M.Sc. Thesis, University of Washington, Seattle.
15. Varsarelyi, D.D. 1971. Tests of Gusset Plate Models. Journal of the Structural Division, ASCE, February, pp. 665-678.
16. Chakrabarti, S.K. and Bjorhovde, R. 1983. Tests of Full Size Gusset Plate Connections. Research Report, Department of Civil Engineering, The University of Arizona, Tucson, Arizona.
17. Williams, G.C. and Richard, R.M. 1986. Steel Connection Design Based on Inelastic Finite Element Analysis. Research Report, Department of Civil Engineering and Engineering Mechanics, The University of Arizona, Tucson, Arizona.
18. Cheng, J.J.R., Yam, M.C.H., and Hu, S.Z. 1994. "Elastic Buckling Strength of Gusset Plate Connections." Journal of Structural Engineering, ASCE, Vol. 120, No. 2, pp. 538-559.
19. Yam, M.C.H., Sheng, N., lu, V.P., and Cheng, J.J.R. 1998. Analytical Study of the Compressive Behaviour and Strength of Steel Gusset Plate Connections. Proceedings of the CSCE 1998 Annual Conference, Halifax, Nova Scotia.
20. Jain, A.K., Goel, S.C., and Hanson, R.D. 1978. Inelastic Response of Restrained Steel Tubes. Journal of the Structural Division, ASCE, Vol. 104, ST6, pp. 897-910.
21. Astaneh-Asl, A., Goel, S.C., and Hanson, R.D., 1981. "Behaviour of Steel Diagonal Bracing." ASCE Conference, October 26-31, St. Louis, Missouri.
22. Leon, R.T. and Swanson, J.A., 1998. T-Stub Connection Component Tests. http://www.ce.gatech.edu/~sac/documents/progress_reports/sept-98/presentation/index.htm

LOCAL FLANGE BENDING AND LOCAL WEB YIELDING LIMIT STATES IN STEEL MOMENT-RESISTING CONNECTIONS

Sara D. PROCHNOW¹, Yanqun YE¹, Robert J. DEXTER¹,
Jerome F. HAJJAR¹, and Sean C. COTTON¹,

ABSTRACT

Nine pull-plate experiments were conducted to examine the effect of column stiffening on the limit states of local flange bending and local web yielding. The results show that AISC provisions for these limit states are reasonable and slightly conservative. Weld fractures did not occur despite the fact that some of the specimens were significantly under-stiffened. The use of half-thickness continuity plates fillet welded to the column web and flanges was shown to be sufficient in comparison to full-thickness continuity plates with CJP welds.

INTRODUCTION

Beam-to-column flange welds fractured in some girder-to-column connections in steel moment frames during the 1994 Northridge earthquake. These welds fractured primarily because of low fracture toughness of weld metal combined with a backing bar forming a notch at the weld root and weld root defects, Fisher, et al. (1). Subsequently, there has been a tendency to be overly conservative in the design and detailing of these connections. For example, there has been a tendency to over-specify column stiffeners even though there is no definitive evidence that inadequate column stiffeners contributed to the Northridge weld fractures. Continuity plates and web doubler plates have been specified when they are unnecessary and, when they are necessary, thicker stiffeners have often been specified than would be required and complete joint penetration (CJP) welds of the continuity plates have been specified when more economical fillet welds may have sufficed.

The tendency to be overly conservative with column stiffeners is understandable since they do have a significant effect on the stress and strain distribution in the connection and on connection performance. For example, Roeder (3) observed that girder-to-column joints with modest continuity plates and/or doubler plates performed better in cyclic loading tests than joints without such reinforcement. Also, it has been observed from finite element analyses of these joints that there is a decrease in stress concentration at the middle of the girder flange-to-column flange weld when continuity plates are used, e.g., Roeder (3), El-Tawil et al. (4).

The limit states of local web yielding (LWY), local flange bending (LFB), local web crippling (LWC), and panel zone (PZ) shear yielding are mitigated by the use of column stiffening. The design criteria for these limit states are provided in Section K1 of Chapter K of the AISC LRFD Specification for Structural Steel Buildings (5). There were additional, more stringent provisions in the requirements for Special Moment Frames

¹ Department of Civil Engineering, 500 Pillsbury Drive SE, University of Minnesota, Minneapolis, Minnesota 55455-0116, E-mail: dexter@tc.umn.edu.

(SMF) in the 1992 AISC Seismic Provisions for Structural Steel Buildings. However, the 1997 AISC Seismic Provisions (6) removed all design procedures related to continuity plates, requiring instead that they be proportioned to match those provided in the tests used to qualify the connection. As part of the SAC Joint Venture, interim guidelines and an advisory were published, FEMA (7), (8), that pertained to these column reinforcements in seismic zones. For example, the guidelines call for continuity plates at least as thick as the beam flange that must be joined to the column flange in a way that fully develops the strength of the continuity plate, i.e., this encourages the use of CJP welds. However, the SAC 100% draft document, FEMA (9), has reestablished design equations to determine whether continuity plates are required and, if so, what thickness they need to be. The present provisions for local web yielding, local flange bending, and panel zone shear are largely based on limit-load analyses that were developed in conjunction with girder-to-column joint subassembly test data, Graham et al. (10), Krawinkler et al. (11), Bertero et al. (12). The criteria for panel zone shear strength have been refined by numerous tests and analyses of girder-to-column subassemblies for seismic moment frames, e.g., Krawinkler (13) and Popov et al. (14).

Recent research has revealed that excessively thick continuity plates are unnecessary. El-Tawil et al. (4) performed parametric finite element analyses of girder-to-column joints. They found that continuity plates are increasingly effective as the thickness increases to about 60% of the girder flange. However, continuity plates more than 60% of the girder flange thickness brought diminishing returns.

Furthermore, over-specification of column reinforcement may actually be detrimental to the performance of connections. As continuity plates are made thicker and attached with highly restrained CJP welds, they are sometimes causing cracking during fabrication. CJP welds have also been specified for the attachment of continuity plates to the web, where fillet welds have traditionally been adequate. Yee et al. (15) performed finite element analyses comparing fillet welded and CJP welded continuity plates. Based on principal stresses extracted at the weld terminations, it was concluded that fillet welded continuity plates may be less susceptible to cracking during fabrication than if CJP welds are used.

The research described in this paper is part of an ongoing project sponsored by AISC to reassess the design provisions for column stiffeners for non-seismic and seismic conditions, and to investigate new alternative column stiffener details. The project includes three components: monotonically-loaded pull-plate experiments to investigate the need for and behavior of transverse stiffeners, cyclically-loaded cruciform girder-to-column joint experiments to investigate panel zone behavior and local flange bending as well as innovative doubler plate and continuity plate details, and parametric finite element analyses to corroborate the experiments and assess the performance of various transverse stiffener and doubler plate details.

The test matrices for this project were designed by examining all practical combinations of girder and column sizes to identify which girder-to-column joints satisfy the limit states of LFB, LWY, web crippling, and panel zone yielding, as well as which combinations satisfy the strong-column/weak-beam (SCWB) provisions according to AISC (5,6). A parametric study was then conducted using three-dimensional nonlinear continuum finite element analysis (FEM) to model the behavior of these connections and the performance of various transverse stiffener and doubler plate details. These analyses permitted the behavior of these connections to be characterized in detail. Criteria were

established to identify the limit states of LWY, LFB and panel zone yielding flange for stiffened and unstiffened specimens. The results of the parametric study showed that web crippling did not control the need for column stiffening in any of the practical combinations of girder and column sizes, and therefore was not further investigated in the research program. The results of the finite element analyses and the comprehensive investigation of the limit states for all beam and column combinations were then coupled with the results of past experiments to establish the test matrices for the present project. Nine laboratory experiments were conducted with pull-plates (simulating a girder flange) attached to column sections for the study of localized flange bending and web yielding, investigating both common and new alternatives for detailing. These monotonic tests focus on the non-seismic behavior, with some consideration given to seismic design as well. Additional experiments are then being conducted on five full-scale cyclic girder-to-column joint subassemblies. These tests will focus on seismic behavior, although they will provide useful information for non-seismic design as well.

This paper outlines the results of the nine pull-plate experiments and corresponding finite-element analyses. The complete literature review, including extensive background information on the various limit states investigated, description of the details of the nine pull-plate and five cruciform experiments and testing procedure, and further detail of the background of this research and justification for specific specimen selection were presented in Dexter et al. (16).

TESTING PROCEDURE

Figure 1 shows the basic schematic drawings of the pull-plate specimens. The pull-plate specimens consisted of three-foot-long sections of A992 columns between pull plates that represent the flanges of the girders in the actual connections.

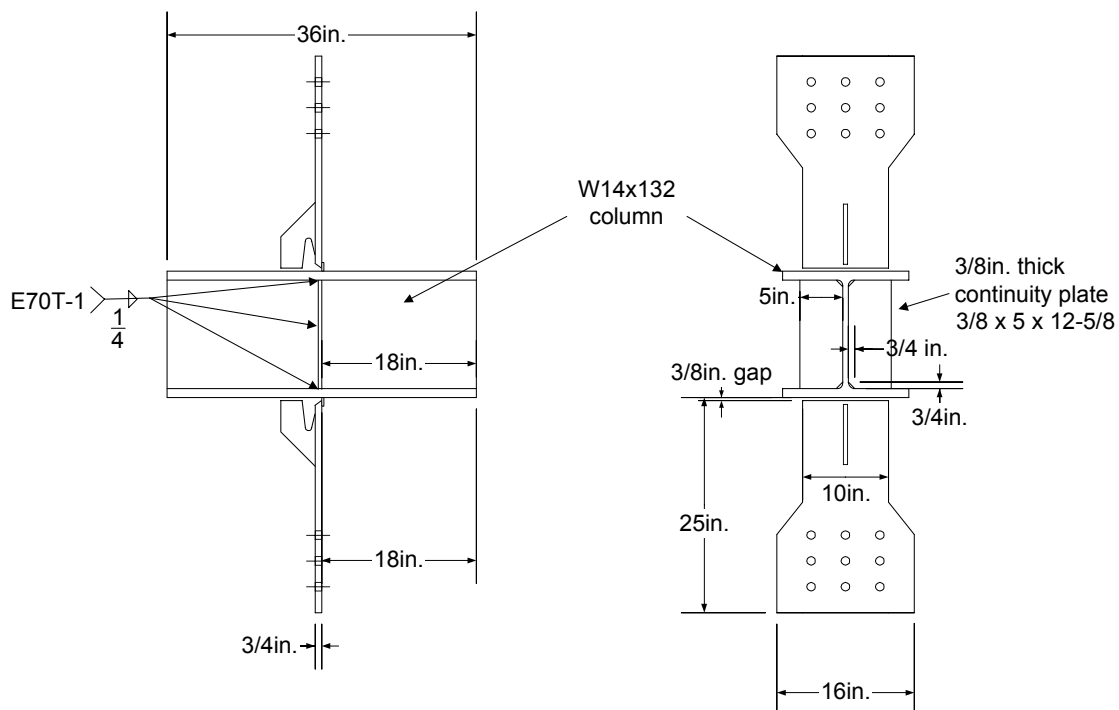


Figure 1 Typical pull-plate specimen with a half-thickness continuity plate, fillet welded to the column flange and web

The CJP welds joining the pull plates to the column sections were made using the self-shielded FCAW process and E70T-6 filler metal with a minimum Charpy V-Notch (CVN) energy of 20 ft-lb at 0° F. The E70T-6 wire had a diameter of 0.068 in. Figure 2 shows the detail of the girder tension flange-to-column flange connection, including the weld type and access hole dimensions. Continuity plates and web doubler plates were fillet welded using the 100% carbon dioxide gas-shielded FCAW process and E70T-1 filler metal with a 0.063 in. diameter. In one case, CJP welds were used to join the continuity plate to the column flanges and in another case CJP welds were used to join the web doubler plate to the column flanges. These CJP welds were also made with the gas-shielded FCAW process and E70T-1 filler metal.

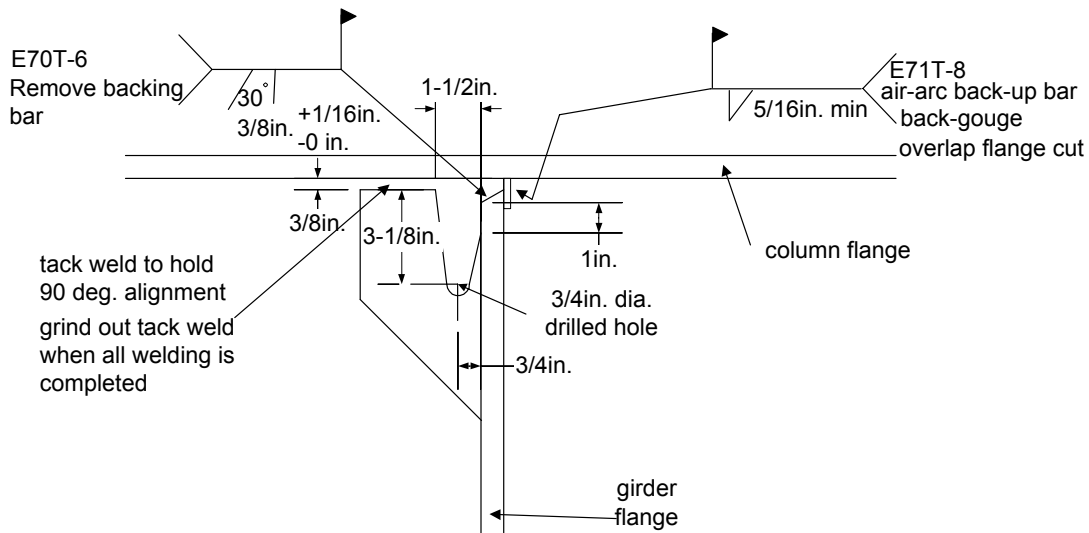


Figure 2 Girder to column weld detail

Table 1 is a comparison of the coupon test results and the mill reports. The reported coupon yield strength was defined by the 0.2% offset. All values given in Table 1 are averaged values and are in units of ksi.

The pull-plates for all specimens were based on the size of a girder flange from a W27x94 section. The variations of the specimens were the type and size of stiffeners and the column size. Three different column sections were tested, W14x132, W14x145, and W14x159. The stiffener details varied between half thickness and full thickness (relative to the pull-plate thickness) continuity plates and a doubler plate box detail. The nine specimens could be grouped into three categories - specimens used to evaluate local web yielding, specimens focused on local flange bending, and specimens aimed at investigated the effects of stiffening details on the connections.

Table 1 Material properties

	W14x132	W14x145	W14x159	Pull-plate	HCP*	FCP*	DP Box*	DP*
Coupon Yield	49.2–54.4	58.2–59.4	51.1– 2.2	48.2	50.0	46.0	46.5	56.2
Mill Yield	53.0	57.0	53.5	51.2	61.3	61.3	61.3	57.0
Coupon Tensile	69.4–70.3	74.1–75.1	71.5-71.8	72.5	72.2	72.5	72.5	73.8
Mill Tensile	70.5	73.5	72	72.1	80.4	80.4	80.4	71.0

HCP = half-thickness continuity plate, FCP = full-thickness continuity plates, DP Box = doubler plate box detail, DP = doubler plate

The nine pull-plate specimens were as follows:

1. Specimen 1-LFB: W14x132 without continuity plates, with doubler plates, examined LFB
2. Specimen 2-LFB: W14x145 without continuity plates, with doubler plates, examined LFB
3. Specimen 1-LWY: W14x132 without any stiffeners, examined LWY and LFB
4. Specimen 2-LWY: W14x145 without any stiffeners, examined LWY and LFB
5. Specimen 3-UNST: W14x159, without any stiffeners, examined LWY and LFB
6. Specimen 1-FCP: W14x132, with full-thickness continuity plates and CJP welds
7. Specimen 1-HCP: W14x132, with half-thickness continuity plates and fillet welds
8. Specimen 1B-HCP: repeat of 1-HCP to verify results
9. Specimen 1-DP: W14x132, with doubler plate box detail

Specimens 1 and 2 had beveled doubler plates fillet welded to the column flange to avoid welding in the column k-line. The doubler plates stiffened the web of the two specimens in order to isolate local flange bending as the governing limit state. Specimens 3 through 5 were unstiffened connections that looked at the interaction between local web yielding and local flange bending.

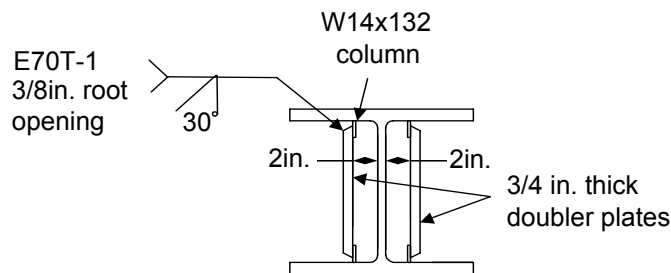


Figure 3 Box detail with doubler plates welded to column flange away from web with CJP welds

Specimens 6 through 8 tested connections either with full-thickness continuity plates and CJP welds, replicating details often seen in present practice, or half-thickness continuity plates with fillet welds. Specimen 9 included no continuity plate, but rather two doubler plates placed out towards the column flange tips, as shown in Figure 3. These plates thus act both as continuity and doubler plates. This detail, first investigated by Bertero et al. (12), is included in AISC (6) and provides an economical alternative to connections that require two-sided doubler plates plus four continuity plates.

Testing of the pull-plate specimens followed the SAC protocol, SAC (17), where it was applicable. Since, the SAC protocol does not specify a strain rate for monotonic tensile tests, a high strain rate of 0.004 sec^{-1} was used, which approximates the strain rate from seismic loading at about a 2 second period. The high strain rate increases the yield strength of the materials and increases the probability for brittle fracture, thereby testing the specimens under the most severe conditions. There were three basic instrumentation plans, one for each of the three categories of specimens. All nine specimens had high-elongation strain gages on the pull-plates and LVDTs that measured the overall specimen elongation and the separation of the column flange tips. The data acquisition system collected 56 channels of data at 100 Hz.

RESULTS AND ANALYSIS

Before testing began, connection failure criteria were developed for the LWY and LFB limit states. The primary indicator of failure was whether the weld fractured prematurely. Brittle fracture was potentially still a possibility, because the fracture toughness of the E70T-6 weld metal is only marginally better than the E70T-4 weld metal that was used in the pre-Northridge connections, FEMA (18). If brittle fracture occurred in some cases but not in others, the influence of column stiffener details on the occurrence of brittle fracture could be investigated clearly. However, there may be other undesirable behavior besides premature fracture, such as excessive deformation. In these experiments, none of the welds fractured prior to the pull plate fracturing, so secondary failure criteria were established based on excessive deformation to identify problematic limit states.

The criteria were based on FEM analyses, AISC provisions for LWY and LFB, and previous research, e.g. Sherbourne and Jensen (19), Graham et al. (10). For each specimen, the column section was examined for failure at non-seismic and seismic girder demand load levels, R_u , calculated as: $R_u = F_{yg} A_{gf}$ (non-seismic) and $R_u = 1.1R_y F_{yg} A_{gf}$ (seismic) where $R_y = 1.1$ for grade 50 or 65 rolled shapes (see AISC (5,6) for variable definitions). The calculation of the seismic girder demand takes into account strain hardening of the girder and includes an overstrength factor, R_y , of the shapes. Using the yield strength and non-seismic and seismic girder flange (pull-plate) dimensions, the girder flange demands were approximately 385 and 450 kips, respectively.

For each limit state, a two-part failure criterion was developed. The connection was classified as failing by LWY if at 450 kips the strain in the column k-line directly under the pull-plate was greater than 3.0%, or the strain in the column k-line was greater than the yield strain for the entire $5k+N$ area. The connection was defined as failing by LFB if at 450 kips the column flange tip separation was greater than $\frac{1}{4}$ in. The continuity plates were characterized as failed if the entire full-width region of the continuity plates was above the yield strain.

Justification for the LWY failure criterion can be seen in Figure 4, which plots the FEM results for the three unstiffened column sections. Using similar failure criterion of Graham et al. (10), which based LWY failure on yielding of the $5k+N$ region of the column k-line, the W14x132 specimen would fail by LWY. Figure 4 shows that the strain in the W14x132 (1-LWY) k-line is greater than yield for the entire $5k+N$ region, while the W14x145 (2-LWY) and W14x159 (3-UNST) are not. Therefore, if it is assumed that the W14x132 (1-LWY) fails and the W14x145 (2-LWY) does not, then another failure guideline could be a strain greater than 3% directly below the pull-plate.

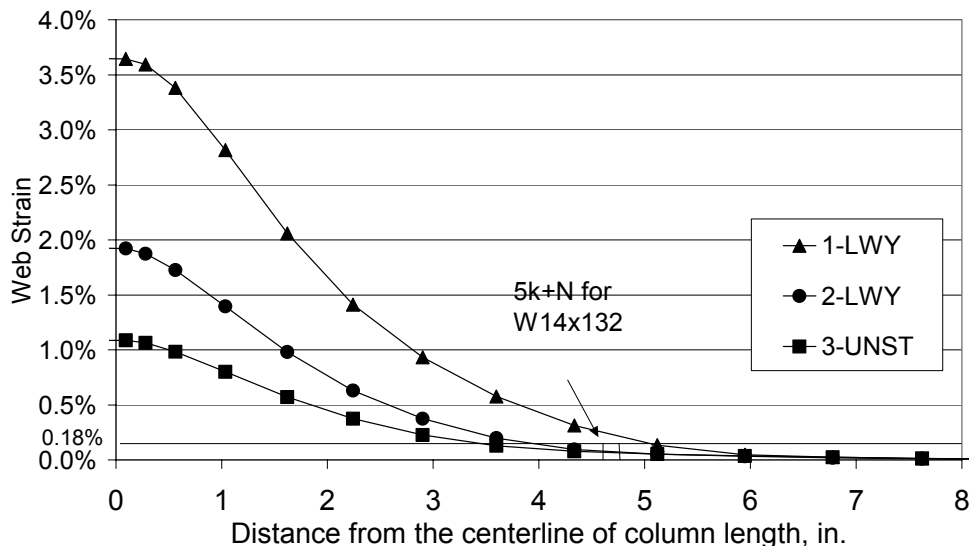


Figure 4 FEM strain distribution along the column k-line at 450 kips

Figure 5 shows the experimental strain distribution in the k-line of the column web for all seven specimens that were gaged to evaluate LWY. As shown in Figure 5, none of the specimens had strain levels exceeding 3% directly under the pull-plate and only the unstiffened W14x145 specimen (2-LWY) had strain values greater than yield for the entire $5k+N$ region. Initially these results seemed implausible, since a W14x145 nominally has a thicker web than a W14x132 section. However, measurements showed that the specific W14x145 section used in the test actually had a thinner web than the specific W14x132 section, which justifies the difference in the strain distribution between these specimens. There is no tolerance on web thickness in ASTM A6; the tolerance is only on the weight per foot, ASTM (20). The strain distribution also shows a much steeper gradient for the W14x132 (1-LWY) than the other two unstiffened sections. This gradient is also likely due to its thinner column flange. The thicker column flanges of the W14x145 and W14x159 act to distribute the load more evenly into the column web.

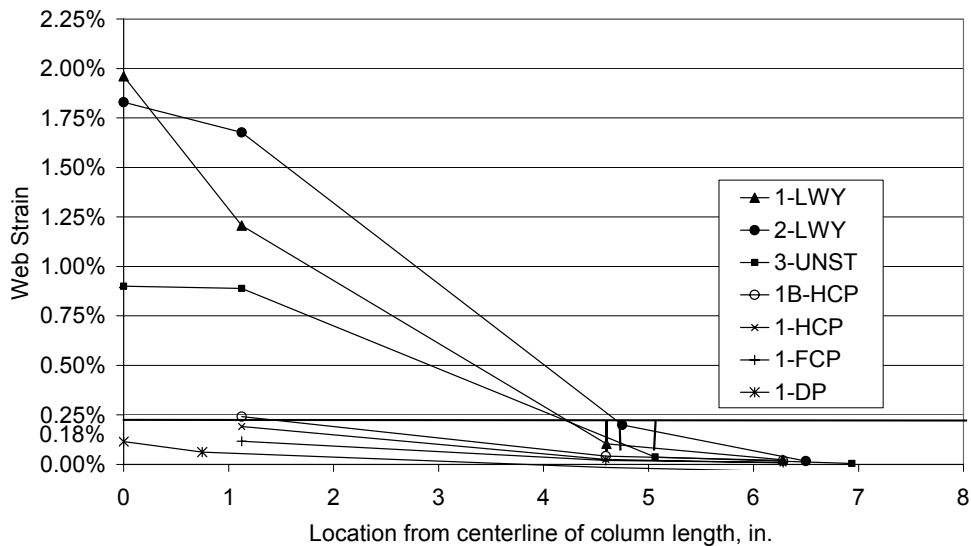


Figure 5 Strain distribution in the column k-line at 450 kips

The LFB failure criterion was based on the permissible variations in cross section sizes, ASTM (20). The provisions allow the flanges of a W section to be $\frac{1}{4}$ in. out of square. Presumably, this amount of flange out-of-flatness is tolerable and still has sufficient resistance to local flange buckling. Therefore, it was assumed that it would also be acceptable to have this much out-of-flatness caused by deforming of the girder flanges. The probability of an initially out-of-square flange combining with additional deformation due to the girder was deemed to be insignificant.

Figure 6 shows the separation of the flanges near the tips of the flanges along the column length for all nine specimens. The W14x132 unstiffened and the W14x132 with doubler plates on the web (1-LFB) both failed this LFB criterion. By comparing the specimens without continuity plates but with web-doubler plates (1-LFB and 2-LFB) to those with no stiffeners at all (1-LWY and 2-LWY), it can be seen that a significant portion of the flange separation is due to web deformation. In the case of the W14x145 (2-LWY and 2-LFB), which has a stiffer flange and, as it turns out, a thinner web, half of the flange separation is due to web deformation.

The results of the stiffened specimens (1-HCP, 1B-HCP, 1-FCP, and 1-DP) showed that, at least for monotonically loaded connections, a half-thickness continuity plate was adequate to avoid web yielding and flange bending. Figures 5 and 6 show a significant difference between the unstiffened and stiffened specimens and that the half-thickness continuity plates (1-HCP and 1B-HCP) are well below the LWY and LFB failure criterion.

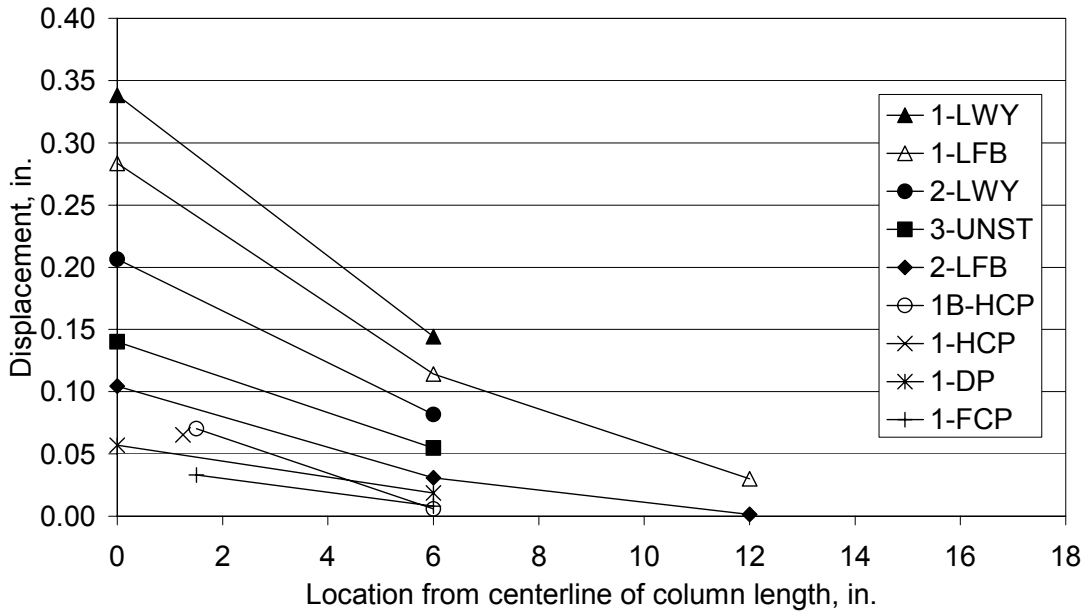


Figure 6 Column flange separation at 450 kips

The failure criterion for the continuity plates was complete yielding across the full-width section of the plates at 450 kips. The full width portion of the continuity plates, as shown in Figure 7, was defined as the area just outside of the 3/4 in. clips. Figure 8 shows a comparison of the results of the strain distribution in the continuity plates of the 1-HCP and 1-FCP specimens. Neither of the specimens fully yielded across the width of the continuity plates, and therefore both were still capable of resisting load and had not failed. The half-thickness continuity plates fillet welds also did not fracture. The CJP welds of the full-thickness continuity plates did not cause any problems during fabrication or testing.

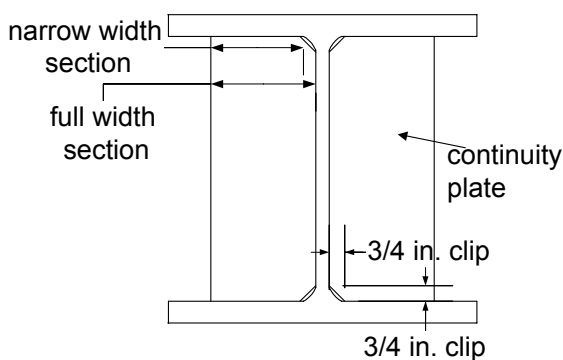


Figure 7 Narrow and full-width sections of continuity plates

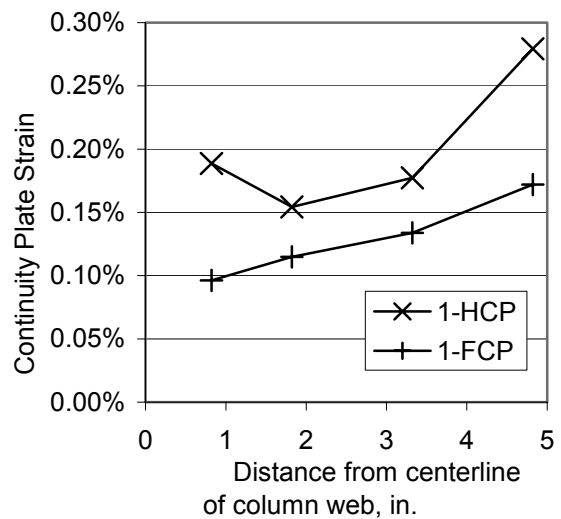


Figure 8 Continuity plate distribution along full-width of plate at 450 kips

CONCLUSIONS

This paper has summarized the results of nine pull-plate tests and corresponding finite-element analyses studying column-stiffening details. The preliminary conclusions from these tests are focused on monotonic loading applications and will be synthesized with future cyclic loading experiments.

- The AISC provisions for LWY and LFB are reasonable and slightly conservative in calculating the need for column stiffening.
- None of the E70T-6 CJP welds fractured despite plastic deformation, even when the flange tip separation was over $\frac{1}{4}$ in, indicating that column stiffener details may have little influence on the potential for brittle weld fracture provided the weld is specified with minimum CVN requirements and backing bars are removed.
- The use of half-thickness continuity plates fillet welded to both the column web and flanges is sufficient in comparison to the traditional full-thickness continuity plates with CJP welds.
- The new stiffener details, i.e. the box detail and beveled doubler plates fillet welded to the column flanges, performed satisfactorily and provided sufficient stiffness to avoid LWY and LFB.

The research project continues as five cruciform tests are underway. Results of the cyclically tested cruciform specimens will be combined with the pull-plate test results to evaluate the local web yielding and local flange bending criteria and new stiffener details in seismic applications.

ACKNOWLEDGMENTS

The American Institute of Steel Construction provided the primary funding for this research. In addition, the University of Minnesota provided student support and the Minnesota Supercomputing Institute provided supercomputing resources. LeJeune Steel Company, Minneapolis; Braun Intertec, Minneapolis; and Lincoln Electric Company, Cleveland; provided in-kind funding and materials. The authors gratefully acknowledge this support. The authors would especially like to thank Lawrence A. Kloiber of LeJeune Steel Company for his assistance in designing, detailing, and fabricating the test specimens and Paul M. Bergson of the University of Minnesota for his assistance in conducting the experiments.

REFERENCES

1. Fisher, J.W., R.J. Dexter, and E.J. Kaufmann, "Fracture Mechanics of Welded Structural Steel Connections", Report No. SAC 95-09, FEMA-288, March 1997
2. FEMA (2000a). "State-of-the-Art Report on Connection Performance," Report No. FEMA 335D, SAC Joint Venture, Sacramento, California.
3. Roeder, C. W. (1997). "An Evaluation of Cracking Observed in Steel Moment Frames," Proceedings of the ASCE Structures Congress, Kempner, L., Brown, C. (eds.), Portland, Oregon, April 13-16, 1997, ASCE, New York, pp. 767-771.
4. El-Tawil, S., Mikesell, T., Vidarsson, E., and Kunnath, S. (1998). "Strength and Ductility of FR Welded-Bolted Connections," Report No. SAC/BD-98/01, SAC Joint Venture, Sacramento, California.

5. AISC (1993). *Load and Resistance Factor Design Specification for Structural Steel Buildings*, Second ed., AISC, Chicago, Illinois.
6. AISC (1997). "Seismic Provisions for Structural Steel Buildings," AISC, Chicago, Illinois.
7. FEMA (1997a). "Interim Guidelines Advisory No. 1," Report No. FEMA 267A (SAC-96-03), SAC Joint Venture, Sacramento, California.
8. FEMA (1997b). "Connection Test Summaries," Report No. FEMA 289 (SAC-96-02), SAC Joint Venture, Sacramento, California.
9. FEMA (2000b). "Recommended Seismic Design Criteria for New Moment-Resisting Steel Frame Structures," Report No. FEMA 350, SAC Joint Venture, Sacramento, California.
10. Graham, J. D., Sherbourne, A. N., Khabbaz, R. N., and Jensen, C. D. (1960). "Welded Interior Beam-to-Column Connections," Welding Research Council, Bulletin No. 63, pp.1-28.
11. Krawinkler, H., Bertero, V. V., and Popov, E. P. (1971). "Inelastic Behavior of Steel Beam-to-Column Subassemblages," Report No. EERC-71/7, Earthquake Engineering Research Center, University of California, Berkeley, California.
12. Bertero, V. V., Krawinkler, H., and Popov, E. P. (1973). "Further Studies on Seismic Behavior of Steel Beam-Column Subassemblages," Report No. EERC-73/27, Earthquake Engineering Research Center, University of California, Berkeley, California.
13. Krawinkler, H. (1978). "Shear in Beam-Column Joints in Seismic Design of Steel Frames," *Engineering Journal*, AISC, Vol. 15, No. 3, pp. 82-91.
14. Popov, E. P., Amin, N. R., Louie, J. J., and Stephen, R. M. (1986). "Cyclic Behavior of Large Beam-column Assemblies," *Engineering Journal*, AISC, Vol. 23, No. 1, pp. 9-23.
15. Yee, R. K., Paterson, S. R., and Egan, G. R. (1998). "Engineering Evaluations of Column Continuity Plate Detail Design and Welding Issues in Welded Steel Moment Frame Connections," *Welding for Seismic Zones in New Zealand*, Aptech Engineering Services, Inc., Sunnyvale, California.
16. Dexter, R. J., Hajjar, J. F., Cotton, S. C., Prochnow, S. D, and Ye, Y. (1999). "Reassessment of Design Criteria and New Alternatives for Column Transverse Stiffeners (Continuity Plates) And Web Doubler Plates: Interim Report," Structural Engineering Report No. ST-99-3, Dept of Civil Engineering, University of Minnesota, Minneapolis, Minnesota.
17. SAC Joint Venture (SAC) (1997). "Protocol for Fabrication, Inspection, Testing, and Documentation of Beam-Column Connection Tests and Other Experimental Specimens," Report No. SAC/BD-97/02, SAC Joint Venture, Sacramento, California.
18. FEMA (2000c). "State of the Art Report on Joining and Inspection," Report No. FEMA 355B, SAC Joint Venture, Sacramento, California.
19. Sherbourne, A. N., and Jensen, C. D. (1957). "Direct Welded Beam Column Connections," Report. No. 233.12, Fritz Laboratory, Lehigh University, Bethlehem, Pennsylvania.
20. ASTM (1998). "ASTM A6/A6M: Standard Specification for General Requirements for Rolled Structural Steel Bars, Plates, Shapes, and Sheet Piling," ASTM, Conshohocken, Pennsylvania.

Block Shear Failure in Steel Members — A Review of Design Practice

Geoffrey L. Kulak and Gilbert Y. Grondin
Department of Civil & Environmental Engineering, University of Alberta
Edmonton, Alberta, CANADA

Abstract

Specifications for the design of steel structures contain provisions for what is customarily termed *block shear*. Test results are available for block shear failures in gusset plates, webs of coped beams, angles, and tees. The design rules for block shear according to specifications from North America (US and Canada), Europe (Eurocode), and Japan are evaluated. For gusset plates, Eurocode rules provide a good prediction, but the other standards are significantly conservative. The North American standards generally give a good prediction for angles, the Japanese standard is conservative, and Eurocode is marginally non-conservative. Results for block shear in the webs of coped beams are mixed, and they include some significantly non-conservative predictions for all but Eurocode. Equally important to these comparisons, in many cases the rule provided by the standards is not reflective of the failure mode observed in the tests. A proposal for a block shear model that is consistent with observed failure modes and which provides a satisfactory comparison with test results is presented.

Introduction

Block shear failure commonly refers to the tearing of a block of material, and it presumes a combination of tension rupture and shear yield or a combination of shear rupture and tension yield. Although the first failure mode is quite common, the latter failure mode is uncommon because of the small ductility in tension as compared with shear. Block shear failure is usually associated with bolted details because a reduced area is present in that case, but in principle it can also be present in welded details. This paper deals only with bolted connections, however.

An example of what is frequently used to illustrate block shear is the gusset plate connection shown in Figure 1(a). The type of failure implied in this sketch does not necessarily correspond to conditions at the time the ultimate load is reached, however. Because of different ductility on the tension and shear surfaces of the failure plane, the ultimate tensile stress is likely to occur on the tension face before the ultimate shear

stress is attained on the shear surfaces. This is illustrated for the two gusset plates (with and without free edge stiffeners) in Figure 2. Other important cases of block shear are those of the web in a coped beam, as shown in Figure 1(b), and the connected leg of an angle tension member, as shown in Figure 1(c). The type of failure conventionally associated with these cases will also be discussed.

Design rules in various codes base block shear failure calculation on a combination of yield and rupture strength of the net or gross areas in shear and tension on the potential failure plane. In the following, an examination is made of various design code provisions for the calculation of block shear capacity. Comparisons between the block shear capacity predicted by design codes and capacities obtained from tests on gusset plates, coped beams, and angle section of various sources are presented.

Code Provisions

A review of available test results indicates that the failure modes seen in two important categories, gusset plate connections and the web of coped beams, are significantly different. With the exception of Eurocode, however, all design codes treat the block shear problem in coped beams in the same manner as block shear failure in gusset plates or other tension members. A comparison of test results with the code provisions is therefore desirable.

AISC 1993

The AISC LRFD rules (1) assume that shear yield and shear ultimate stress can be represented using the von Mises criterion, i.e., $\tau_y \approx 0.6\sigma_y$ and $\tau_u \approx 0.6\sigma_u$. The design rules are as follows:

$$\text{if } \sigma_u A_{nt} \geq (0.6\sigma_u) A_{nv} \quad \text{then } P_u = \sigma_u A_{nt} + (0.6\sigma_y) A_{gv} \quad (1)$$

$$\text{and if } (0.6\sigma_u) A_{nv} > \sigma_u A_{nt} \quad \text{then } P_u = (0.6\sigma_u) A_{nv} + \sigma_y A_{gt} \quad (2)$$

Equation 1 says that if the ultimate tensile resistance is greater than the ultimate shear resistance, then the block shear resistance is the sum of the tensile resistance (on the net section) and the shear yield resistance (on the gross shear area). Conversely, if the ultimate shear resistance is greater than the ultimate tensile resistance (Equation 2), then the block shear resistance is the sum of the ultimate shear resistance (net shear area) and the tension yield force (gross cross-section).

In themselves, the strength statements presented by Equations 1 and 2 are plausible. It is reasonable to think that the block shear capacity could be the ultimate tensile strength in combination with the shear yield strength (Equation 1). However, the possibility of attaining the shear ultimate strength in combination with the tensile yield strength seems unlikely. This requires that the ductility of the material in tension be sufficient to allow shear fracture to be reached. Examination of the test results in the case of gusset plates shows that this is in fact the situation—there is not sufficient tensile ductility to permit shear fracture to occur.

The Commentary to the Specification says that the larger of Equations 1 and 2 is to be taken as the governing value and it provides a rationale for this rule. However, the

comment seems to belong to the block shear rules of the previous edition of the specification (2). At that time, the same equations as given here as Equations 1 and 2 were presented (in the Commentary), and the user was advised to use the larger of the two results. In the 1993 LRFD rules, the qualifying statements that precede Equations 1 and 2 means that the "larger" choice is no longer appropriate.

Draft AISC 1999

A draft LRFD specification is presently under review (3). Insofar as the calculation of block shear is concerned, the new rules are similar to the current LRFD rules except that provisions have been added to limit the capacity of both the shear and tension planes to rupture of the respective net areas. It is expected that in most cases the result will be the same as that obtained using the current LRFD (2) specification.

CSA S16.1-94

The Canadian design standard for steel structures (4) makes the assumption that the tension face of the fracture surface possesses sufficient ductility to enable the stress on the net shear surface to reach its ultimate value before rupture on the net tension face. Thus, the load at which block shear failure occurs is taken as the ultimate tensile strength times the net area in tension plus 0.60 times the ultimate tensile strength (i.e., approximately shear ultimate) times the net area in shear. This is expressed as:

$$P_u = \sigma_u A_{nt} + (0.6 \sigma_u) A_{nv} \quad (3)$$

The condition that the maximum strength in shear and tension can be reached at the same time is usually not satisfied in practice. The Canadian design standard is currently under revision and it is anticipated that the block shear rule will be changed.

Eurocode

The rules presented in Eurocode (5) are based on the fundamental assumption that this mode of failure "consists of tensile rupture along the line of fastener holes on the tension face of the hole group, accompanied by gross section yielding in shear at the row of fastener holes along the shear face of the hole group". Eurocode uses a shear yield stress equal to $\sigma_y / \sqrt{3}$, and thus the block shear capacity of a gusset plate or tension member can be expressed as follows:

$$P_u = \sigma_u A_{nt} + (\sigma_y / \sqrt{3}) A_{gv} \quad (4)$$

Equation (4) is not specifically given in Eurocode, but it can be deduced easily from the description of the mode of failure. A more elaborate procedure is presented for block shear rupture in beam webs. For the common case illustrated in Figure 1(b), the procedure is as follows:

$$P_u = \frac{\sigma_y}{\sqrt{3}} A_{v,eff} \quad (5)$$

where $A_{v,eff}$ is the effective shear area, taken as the product of the web thickness, t , and the effective length in shear, $L_{v,eff}$. The effective shear area accounts for both yielding along the gross shear area and tension rupture along the net tension area. For the coped beam illustrated in Figure 1(b)

$$L_{v,eff} = L_v + L_1 + (a_2 - k d_{o,t}) \frac{\sigma_u}{\sigma_y} \quad (6)$$

where the first two terms on the right hand side of the equation represent the gross shear length, as shown in Figure 1 (b), and the third term represents the net tension area. The dimension a_2 is also illustrated in Figure 1(b), $d_{o,t}$ is the bolt hole diameter and the constant k is taken as 0.5 for one line of bolts and 2.5 for two lines of bolts. When the area obtained using Equation 6 is substituted into Equation 5, it can be seen that the assumed stress on the net tension area is $\sigma_u/\sqrt{3}$. The origin of the stress reduction factor ($1/\sqrt{3}$) on the tension stress is not known.

Architectural Institute of Japan

The procedure adopted by the Architectural Institute of Japan (6) is the most conservative of the provisions reviewed. It uses the net areas on both the shear and tension planes. The block shear capacity is taken as least of: 1) shear yield on net shear area plus tensile ultimate on net tension area or 2) shear ultimate on net shear area plus tensile yield on net tension area. The shear yield is taken as $\sigma_y/\sqrt{3}$ and the shear ultimate as $\sigma_u/\sqrt{3}$. This can be written as:

$$P_u = \sigma_u A_{nt} + (\sigma_y/\sqrt{3}) A_{nv} < \sigma_y A_{nt} + (\sigma_u/\sqrt{3}) A_{nv} \quad (7)$$

Gusset Plate Tests

There are a large number of gusset plate tests reported in the literature for which block shear is the failure mode. A representative sample is shown in Table 1. The results are shown for 36 gusset plate tests from four different sources. In addition, in their paper Hardash and Bjorhovde (7) reported on a total of 14 more tests, from three other sources, which are not included here: the data pool is sufficiently large without these additional tests.

All gusset plate tests show that the ultimate load is reached when the tensile ductility of the gusset plate material at the first (i.e., inner) transverse line of bolts is exhausted. (This mode of failure was also observed in the 14 additional tests cited in the Hardash and Bjorhovde study.) This was true even in cases where oversize holes were used and in cases where the connection was short (i.e., not much shear area available). The tests show that fracture at the net tension section is reached before shear fracture can take place on the other surfaces, i.e., tensile fracture (net section) plus some shear yielding takes place. (The displacement of a block of material is seen only when the test is continued until the parts separate, and this occurs after the ultimate load of the

connection has been reached.) Figure 2 shows typical specimens at the time of ultimate load (8).

An examination of Table 1 for the gusset plate results indicates that the Japanese standard is the most conservative; the test-to-predicted ratio varies from 1.35 to 1.59. This reflects the fact that the net section area is used both for yield and rupture strength calculations. The change proposed in the AISC LRFD draft document (3) is seen to affect some of the strength predictions, which indicates that in some cases the current AISC LRFD standard would predict a capacity greater than the rupture capacity on one or more of the failure planes. CSA-S16.1 provides predictions similar to those in the AISC LRFD draft document. The most accurate code predictions are obtained using Eurocode approach of adding the tension rupture capacity to the shear yield capacity. All the design codes can predict the block shear capacity of gusset plates with similar degree of variability, as indicated by their standard deviation.

Coped Beam Tests

In contrast to the number of gusset plate tests available, there are not many tests of coped beams. Table 1 shows that there is a total of 13 tests. Seven of these involved connections with two lines of bolts and the other six had a single line of bolts. Two tests were for beams that had slotted holes.

The ratio of test ultimate load to the predictions of AISC LRFD (1, 3) and CSA-S16.1 indicates that the code predictions are non-conservative for each of the three series. In the test series that used two lines of bolts (11), the predictions were significantly non-conservative (test-to-predicted ratio of 0.70 for AISC LRFD and 0.65 for CSA-S16.1). The results for the tests in which a single line of bolts was present gave a test-to-predicted ratio that was close to unity, but the standard deviation in the major series (12) is unacceptably large. The more elaborate procedure proposed by Eurocode for block shear failure of beams results in predicted capacities that are conservative. The large standard deviation, however, indicates a large variation in test-to-predicted ratio. Although the Japanese standard gives conservative predictions for two of three test programs, it is significantly non-conservative for the case where two lines of bolts were used (11). It is clear that some of the current rules for block shear are not acceptable for the important case of coped beams. The large variation in test-to-predicted ratios indicates that the predictions for all the codes fail to explain an important aspect of the coped beam behaviour.

Angle Tests

Figure 1 (c) shows a single angle connected to a gusset plate. Experience and test results show that block shear is potentially a failure mode for angles, particularly when the connection is short.

Epstein (13) reported the results of a large number of tension tests for pairs of angles connected by bolts to a gusset plate passing between the angles. A total of 144 tests were conducted on 38 different configurations. The number of variables was large—size of outstanding leg as compared with connected leg, connection geometry (including bolt stagger and pitch), angle size, eccentricity of load, and so on—and this led to different modes of failure. The failure modes included block shear, net section rupture, bolt shear, and various combinations of these. In only 15 individual tests (three tests each of five series) was it considered that block shear was the sole failure mode. It is the opinion of

the writers that, except for three of the 144 test specimens (one of the five series that failed by block shear), these data are not sufficiently coherent to be able to include them in the examination presented herein. The three test specimens singled out had two lines of bolts with no stagger. All other specimens that failed solely by block shear had staggered bolt holes, which introduces another parameter in the strength calculations.

Other test programs have also investigated block shear in single angle connections and in structural tees (14, 15, 16) with one line of bolts. Tests on structural tees have been used to assess the effect of out-of-plane eccentricity inherent with bolted angles (15). Block shear failure of angle sections can be affected by out-of-plane and in-plane eccentricity. Although Orbison et al. (15) found that out-of-plane eccentricity was not a significant factor, Epstein (13) concluded that the factor had to be considered in block shear calculations: in-plane eccentricity was found to be a significant factor. Tests at Bucknell University (14, 15) have shown that the block shear capacity decreases with an increase in eccentricity.

With the exception of the test results presented by Epstein (13), the block shear capacity is satisfactorily predicted by the equations used in the North American standards. The equations overestimate Epstein's test results by 20%. Eurocode yields predictions that are less conservative than the other codes. Again, the Japanese standard is the most conservative and gives test-to-predicted ratios greater than or equal to 1.0 for all cases. It is not clear why the test results by Epstein are overestimated by as much as 20% by most standards. Epstein has suggested that a correction for shear lag effect should be applied to block shear failure. The writers believe that the use of the shear lag correction factor is not appropriate for block shear calculations.

Improved Design Equations

Gusset Plates—A good predictor of the ultimate strength of a gusset plate connection is obtained by adding the ultimate tensile strength (net tensile area) and the shear yield strength (gross shear area). This brings the predicted capacity much more closely into line with the test values. The resulting test-to-predicted ratios are presented in Table 1 under the heading "Test/Proposed". For the 36 gusset plate tests reported in Table 1, the ratio Test/Proposed is 1.13, and the standard deviation is 0.08.

For a better estimate of strength, the proposal made in Hardash and Bjorhovde (7) can be used. The model proposed by these researchers uses net section tensile strength plus a shear strength component that reflects connection length. In the limit, short connections, the contribution from shear is nearly the same as that suggested here, i.e., shear yield acting on the gross shear area. It is clear that the existing AISC LRFD rule, Equations 1 and 2, and the CSA-S16.1 rule, Equation 3, are not satisfactory models of the tests.

Angles—As is the case for the coped beam connection, the shear resistance for an angle is present only on one surface of the potential block of sheared material. There are a number of complicating factors present in the angle connection as compared with the coped beam, however. It is found that the failure model suggested for gusset plates, i.e., tensile fracture of the tension surface followed by shear failure along the shear surface gives reasonably good results. This is also consistent with what is observed in the majority of tests. For the 41 test results on angles and structural tees presented in Table

1, the average test-to-predicted ratio using the rule suggested for gusset plates is 0.93, with a standard deviation of 0.10.

As seen in Table 1, the existing North American rules (Equations 1, 2 and 3) are in better agreement with the angle tests than the model recommended here. However, the writers consider that these equations do not provide a rational explanation for how the block shear phenomenon actually takes place. The approach proposed here is consistent with the Eurocode approach. The small differences observed between the proposed approach and Eurocode lies in the difference in shear strength calculation (0.6 times the tensile strength is proposed compared to $1/\sqrt{3}$ times the tensile stress used in Eurocode).

Coped Beams—The mode of failure in coped beam webs is different than that of gusset plates. Because the shear resistance is present only on one surface, there must be some rotation of the block of material that is providing the total resistance. Although tensile failure is observed through the net section on the horizontal plane in the tests, as expected, the distribution of tensile stress is not uniform. Rather, higher tensile stresses are present toward the end of the web. The prediction of capacity given by the American codes is significantly non-conservative when there are two lines of bolts present. If only one line is present, then the prediction is non-conservative for at least some cases. The predictions given by Eurocode are conservative, but the standard deviation of the test-to-predicted ratio is large. Although the Japanese approach is very conservative for six of the 13 test results, it is significantly unconservative for some of the results.

As already noted, there are relatively few test results for block shear failure in coped beams. However, for these tests a satisfactory simple model is obtained by taking a capacity equal to one-half the tensile fracture load (net section on the horizontal plane) plus the shear yield load (gross section on the vertical plane). This was first suggested by Ricles and Yura (11). In addition, care should be taken to use generous end distances, particularly when slotted or oversize holes are present or when the bolts are distributed more-or-less from the top of the web to the bottom. If the latter detail is used, the bolt arrangement can carry appreciable moment and bolt forces may produce splitting between the bolts and the end of the beam web.

Summary, Conclusions, and Recommendations

This examination has identified that use of current design rules in North America, Europe, and Japan leads to conservative designs for gusset plates, non-conservative designs for coped beams, and satisfactory results for angles. The Japanese rules are very conservative for most cases. All design rules, however, give an inconsistent degree of conservatism. Also, in most cases the North American rules do not reflect the mode of failure observed in the tests.

The writers recommend that the following equations for calculation of block shear resistance be used:

Gusset plates, angles:
$$P_u = A_{nt} \sigma_u + 0.6 \sigma_y A_{gv} \quad (8)$$

Coped beam webs:
$$P_u = 0.5 A_{nt} \sigma_u + 0.6 \sigma_y A_{gv} \quad (9)$$

A resistance factor must be applied to Equations 8 and 9. The value $\phi = 0.75$ is used in the current AISC-LRFD formulation, $0.85 \times 0.9 = 0.76$ in CSA-S16.1, $1/1.11 = 0.91$ in Eurocode, and it seems to be 0.9 in the Japanese standard (0.9 is specified for yield strength but no value is specified for maximum strength calculation). Although these values are likely conservative, further work must be done to establish a more appropriate value.

This review has identified the need for further studies of block shear. Work currently underway at the University of Alberta includes numerical modeling of the block shear resistance of gusset plate and angle connections and physical testing and numerical modeling of block shear in coped beams.

Notation

σ_y	=	tensile yield strength
σ_u	=	tensile ultimate strength
τ_y	=	shear yield strength
τ_u	=	ultimate shear strength
A_{nt}	=	net area subjected to tension
A_{nv}	=	net area subjected to shear
A_{gt}	=	gross area subjected to tension
A_{gv}	=	gross area subjected to shear
$A_{v,eff}$	=	effective shear area

References

1. American Institute of Steel Construction. *Load and Resistance Factor Design Specification for Structural Steel Buildings*. Chicago, IL, 1993.
2. American Institute of Steel Construction. *Load and Resistance Factor Design Specification for Structural Steel Buildings*. Chicago, IL, 1986.
3. American Institute of Steel Construction. *Load and Resistance Factor Design Specification for Structural Steel Buildings*. Draft document, Chicago, IL, 1999.
4. Canadian Standards Association. *Limit States Design of Steel Structures, CAN/CSA-S16.1-M94*, Rexdale, Ontario, 1994.
5. European Committee for Standardisation. *Eurocode 3 : Design of Steel Structures, ENV 1993-1-1*, Brussels, 1992.
6. Architectural Institute of Japan. *Standard for Limit State Design of Steel Structures*, 1990.
7. Hardash, Steve and Bjorhovde, Reidar, "New Design Criteria for Gusset Plates in Tension," *Engineering Journal, AISC*, Vol. 22, No. 2, Second Quarter, 1985.
8. Nast, Trina E., Grondin, Gilbert Y., and Cheng, J.J. Roger, "Cyclic Behavior of Stiffened Gusset Plate-Brace Member Assemblies," *Structural Engineering Report*

- No. 229, Department of Civil & Environmental Engineering, University of Alberta, 1999.
9. Swanson, James A. and Leon, Roberto T., "Bolted Steel Connections: Tests on T-Stub Components," J. of Structural Engineering, ASCE, Vol. 126, No. 1, Jan., 2000.
 10. Rabinovitch, Jeffrey S., and Cheng, J.J. Roger, "Cyclic Behavior of Steel Gusset Plate Connections," Structural Engineering Report No. 191, Department of Civil & Environmental Engineering, University of Alberta, 1999.
 11. Ricles, J. M. and Yura, J.A., "Strength of Double-Row Bolted-Web Connections," J. of the Structural Division, ASCE, Vol. 109, No. 1, January, 1983.
 12. Yura, J.A., Birkemoe, P.C. and Ricles, J.M., "Beam Web Shear Connections: An Experimental Study," J. of the Structural Division, ASCE, Vol. 108, No. ST2, February, 1982.
 13. Epstein, Howard I., "An Experimental Study of Block Shear Failure of Angles in Tension," Engineering Journal, AISC, Vol. 29, No. 2, Second Quarter, 1992.
 14. Gross, Jeremy M., Orbison, James G., and Ziemian, Ronald D., "Block Shear Tests in High-Strength Steel Angles," Engineering Journal, AISC, Vol. 32, No. 3, Third Quarter, 1995.
 15. Orbison, James G., Wagner, Mark E., and Fritz, William P., "Tension Plane Behavior in Single-Row Bolted Connections Subject to Block Shear," Journal of Constructional Steel Research, Vol. 49, 1995.
 16. Barthel, R.J., Peabody, M.T., and Cash, U.M., "Structural Steel Transmission Tower Angle and Rectangular Coupon Tension Testing," Western Area Power Administration Report, Department of Energy, 1987.
 17. Birkemoe, P.C. and Gilmor, M.I., "Behavior of Bearing Critical Double-Angle Beam Connections," Engineering Journal, AISC, Vol. 15, No. 4, Fourth Quarter, 1978.

Table 1 – Block Shear Examination for Selected Cases

Source	Type	No. of Tests	Ratio Test value / code value*								Comments
			Test AISC '93	Test AISC '99	Test S16.1	Test Eurocode	Test AIJ '90	Test Proposed			
Hardash and Bjorhovde (7)	Gusset Plate	28	1.22 (0.08)	1.22 (0.08)	1.19 (0.08)	1.19 (0.06)	1.19 (0.06)	1.35 (0.10)	1.16 (0.06)	(Number in parentheses is standard deviation, shown this way throughout.)	
Swanson and Leon (9)	Gusset Plate	1	1.16	1.18	1.18	1.00	1.48	0.97			
Rabinovitch and Cheng (10)	Gusset Plate	4	1.18 (0.06)	1.22 (0.07)	1.22 (0.07)	1.05 (0.06)	1.45 (0.08)	1.01 (0.06)			
Nast et al. (8)	Gusset Plate	3	1.28 (0.02)	1.35 (0.02)	1.35 (0.02)	1.07 (0.01)	1.59 (0.02)	1.04 (0.01)			
Ricles and Yura (11)	Coped Beam	7	0.70 (0.09)	0.70 (0.09)	0.65 (0.09)	1.08 (0.14)	0.83 (0.11)	1.00 (0.13)		Two lines of bolts, no. of bolts per line not necessarily equal, one test used slotted holes.	
Yura et al. (12)	Coped Beam	5	0.99 (0.19)	0.99 (0.19)	0.96 (0.20)	1.24 (0.17)	1.43 (0.28)	1.19 (0.19)		One line of bolts, one test used slotted holes, bolts spread over most of the beam web depth. Note large std. dev. associated with mean values.	
Birkemoe and Gilmor (17)	Coped Beam	1	0.95	0.95	0.92	1.18	1.25	1.17		One line of three bolts. Connected depth relatively small portion of beam depth.	
Orbison et al. (15)	Single Angles and Tees	12	1.12 (0.07)	1.12 (0.07)	1.09 (0.05)	1.09 (0.05)	1.33 (0.05)	1.06 (0.05)		Block shear in tees was in the stem only.	
Gross et al. (14)	Single Angles	13	0.94 (0.05)	0.96 (0.05)	0.96 (0.04)	0.92 (0.07)	1.19 (0.07)	0.90 (0.07)		One line of bolts.	
Barthel et al. (16)	Single Angles	13	0.99 (0.06)	1.01 (0.01)	1.00 (0.04)	0.89 (0.04)	1.25 (0.05)	0.87 (0.04)		One line of bolts.	
Epstein (13)	Double Angles	3	0.80	0.80	0.80	0.81	1.00	0.80		Two lines of bolts. The average of three tests was presented without the standard deviation.	

Note: Values of the ratio Test/Code Prediction greater than unity are conservative. All predicted values are calculated for a resistance factor of 1.0.

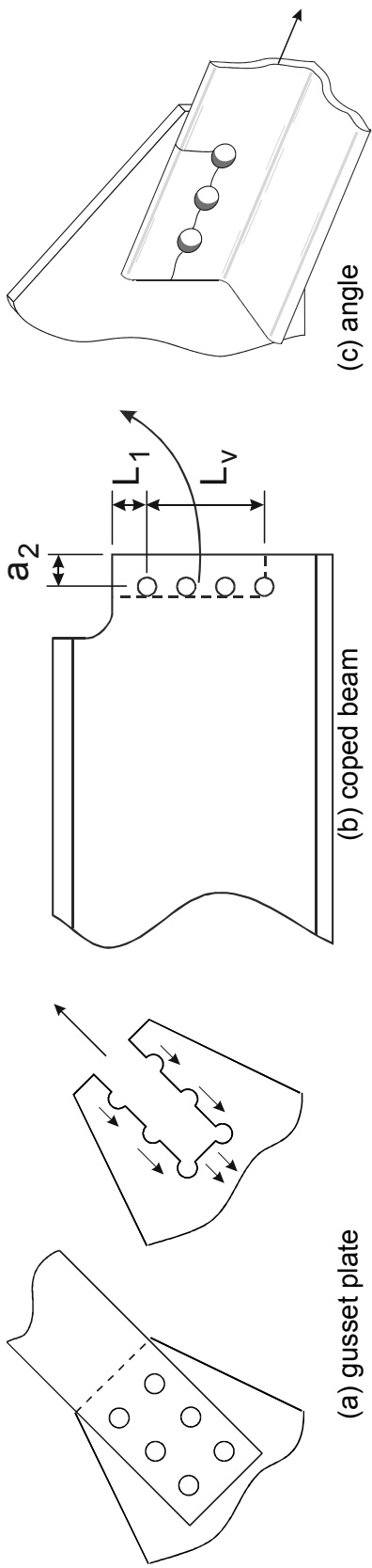


Figure 1 – Examples of Block Shear

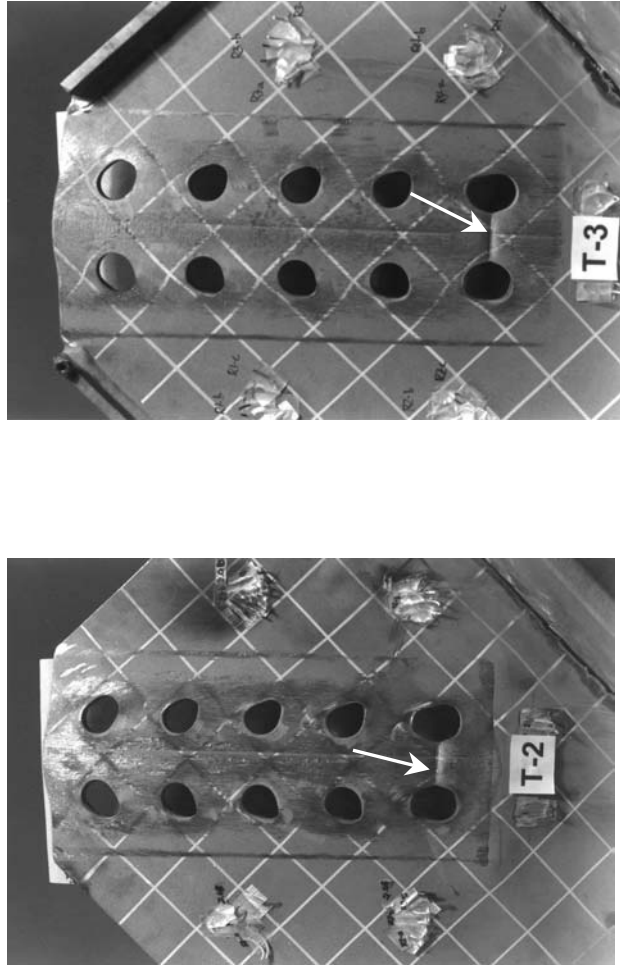


Figure 2 – Rupture on Net Tension Area

BLIND BOLTED MOMENT RESISTING CONNECTIONS TO STRUCTURAL HOLLOW SECTIONS

T. Barnett, School of Civil Engineering, University of Nottingham, UK
W. Tizani, School of Civil Engineering, University of Nottingham, UK
D. A. Nethercot, Department of Civil and Environmental Engineering, Imperial College,
UK

ABSTRACT

Tests using a new blind bolt in an arrangement designed to represent the tensile region of a moment transmitting endplate connection between a hollow section column and an open section beam are reported. The results demonstrate that this bolt possesses the strength and stiffness necessary to achieve a satisfactory connection. Calculations based on the component approach of EC3 predict that because the flexibility of the SHS face will, for most joint arrangements, limit the connection's moment capacity, the strength of the blind bolt will normally be more than is required to match the strength of the equivalent joint configured with ordinary dowel bolts.

INTRODUCTION

The use of structural hollow sections (SHS) as columns in multi-storey construction is attractive due to aesthetics and a high strength to weight ratio. However, their use in this capacity is inhibited by problems in making connections to other members. Early developments in overcoming the connection problem included fully welding the connection, which, in the UK context, is not an attractive site option. The use of standard dowel bolts is often impossible as there is rarely access to the inside of the tube to allow for tightening. The use of components such as gusset plates and brackets overcomes this problem, but is not generally considered aesthetically pleasing. To allow for convenient and efficient connection, several techniques have been devised which permit bolt installation and tightening from one side of the connection only, i.e. blind bolts. Commercially available examples include Flowdrill (1), the Huck High Strength Blind Bolt (2), and the Lindapter Hollobolt (3).

It is the purpose of an ongoing research project to modify the original Hollobolt so as to extend its use to moment resisting connections in steel framed buildings. An important feature of this research is to develop a fundamental understanding of the behaviour of the SHS face when subjected to moments from a connection. To date, tests performed elsewhere (4) have proven that it is possible to design nominally pinned connections (intended primarily to transfer vertical shear) to SHS columns using the Hollobolt and Flowdrill fasteners. The capacities of the bolts and the SHS face are sufficient to withstand a predominantly shear load and the limited tensile loads arising from structural integrity requirements. A guide for the design of connections of this sort is available (5).

BOLT DEVELOPMENT

An important design consideration for connections involving SHS is that high local forces do not induce unduly large deformations in the relatively thin walls of the tubular member(s). A particular example of this is the EC3 (6) limitation on the face out of plane deflection of an RHS to 1% of the chord face.

In order to maximise the performance of bolted endplate moment resisting beam to SHS column connections, it was therefore necessary to ensure that sufficient clamping force could be generated between the plies for separation between the endplate and the RHS column face to be minimised. At an early stage of the research project, the original Hollobolt was altered so that the expanding sleeve clamped directly to the underside of the joint [Figure 1]. This arrangement, hereinafter referred to as the Reverse Mechanism Hollobolt (RMH), has been shown through a series of tests to significantly improve the clamping force between the connected plies as compared with the original arrangement. Details of the clamping force assessment are reported elsewhere (7).



Figure 1: The Reverse Mechanism Hollobolt (RMH).

CONNECTION TESTS

Annex J of EC3 (6) covers moment connection design between open sections by use of the ‘component method’. This is a technique that considers the connection as a series of components, each of which has a specified design check performed upon it. These, in turn, are based upon identification and representation of all possible failure modes and load transfer paths. In the tension region of the connection, the bolts and connected plies may be modelled as a pair of equivalent tee stubs, which represent the flange and web of the column, and the web and end plate of the beam. Failure of an equivalent tee stub is due to either (a) flange bending (i.e. mode i) failure, (b) flange bending and bolt tension (i.e. mode ii) failure, or (c) bolt tension (i.e. mode iii) as illustrated in Fig 2, with the particular form of failure depending upon the thickness of the connected elements and their material properties.

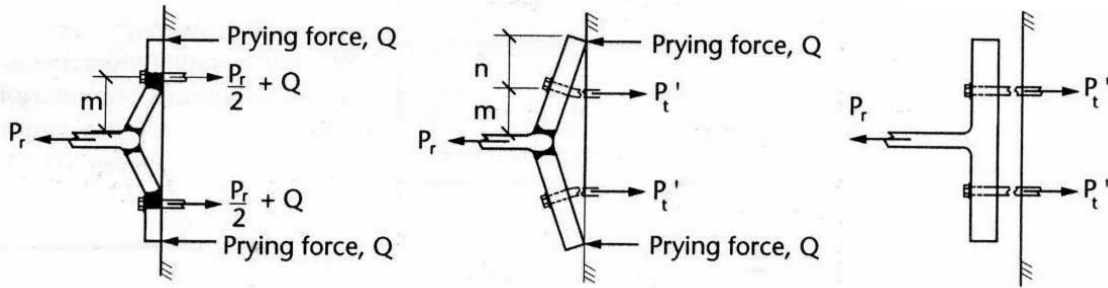


Figure 2: Mode i (left), ii (centre), and iii (right) failure mechanisms (6)

In order to place maximum demand on the bolts during testing, and to effectively model the tension region of a moment resisting connection to an open section, it was decided to place the bolts in back to back tee stubs. The arrangement shown in figure 3 was devised, thereby allowing for convenient testing in a standard tensile machine. Large sections were used to encourage a bolt failure, with failure loads of 333kN, 264kN, and 283kN for modes i, ii, and iii failure respectively. The latter two failure loads were calculated assuming that a standard M16 bolt was present between the plies, and provide a load which was expected to be greater than that for a corresponding blind bolt. In order to evaluate the possible presence of prying force in the bolts arising from double curvature of the plates in a mode ii failure, plate deflections were monitored in the first few tests by placing linear transducers at the plate edges and the bolt lines. In later tests, once it had become evident that prying action was not occurring, the transducers at the plate edges were removed.

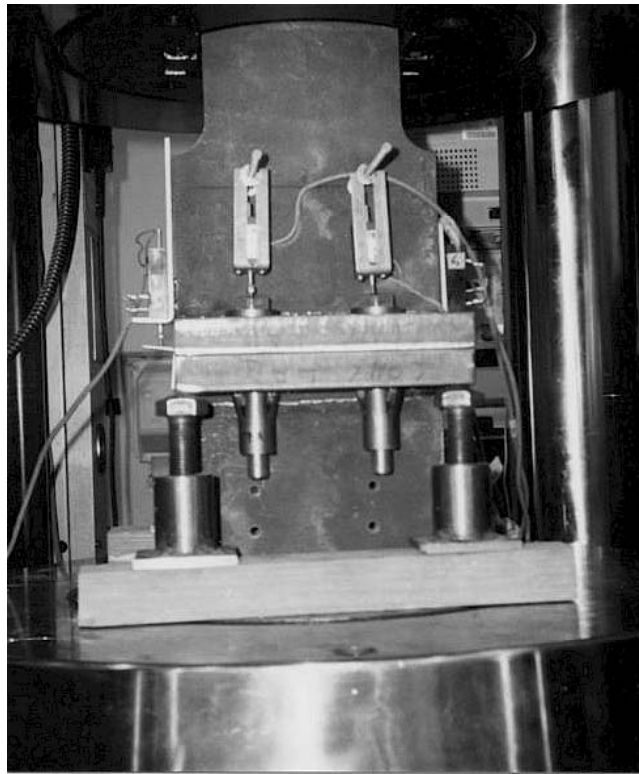


Figure 3: Tee stub test arrangement with RMH

The purpose of these back to back tee stub tests was to determine the suitability of the RMH for use in moment resisting connections by measuring its strength and stiffness. In order to provide a comparison with the performance of the RMH, a series of five tests were performed using the same arrangement, but with the Lindapter Hollobolt as the fastener. In all tests, M16 bolts were used as preliminary calculations had suggested that the inherent flexibility of a SHS face would limit any potential advantage from using a larger bolt size.

Results of the first series of eight RMH tests, expressed as a load / plate separation relationship, are shown in figure 4. From this, it is evident that the initial clamping force exerted on the plates from the expansion mechanism was exceeded at a tension of approximately 230kN. Loading continued until a bolt failure occurred at a load of between 350-450kN, with a plate separation of approximately 2mm. Bolt failure was due to a sudden expansion of the flared legs against the underside of the joint [Figure 5]. Almost immediately after failure of the first bolt in the assembly, a second bolt failed in exactly the same manner.

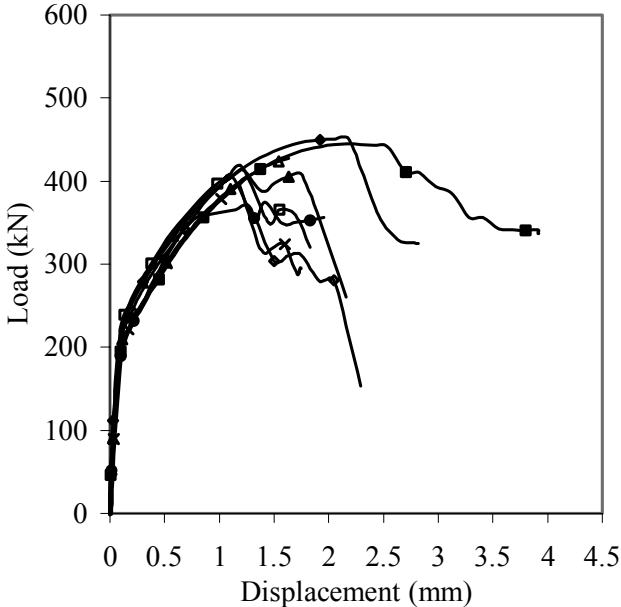


Figure 4: Load v. plate separation for the RMH tee stub tests.

The load v. plate separation relationships for the five tests performed using the Lindapter Hollobolt are presented in figure 6. These indicate that, although the ultimate failure of the assembly was typically in the region of 450kN, the initial clamping force of the bolts was exceeded at a tension of approximately 90kN with excessive plate separation following immediately. Ultimate failure occurred with a plate separation of between 6 and 8mm by a ductile shearing of the legs of the Hollobolt against the inside face of the assembly.

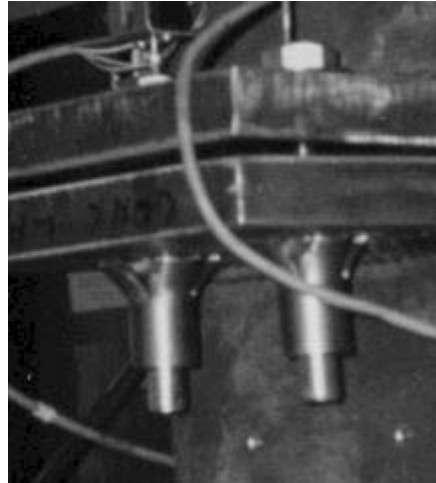


Figure 5: Failure of the RMH.

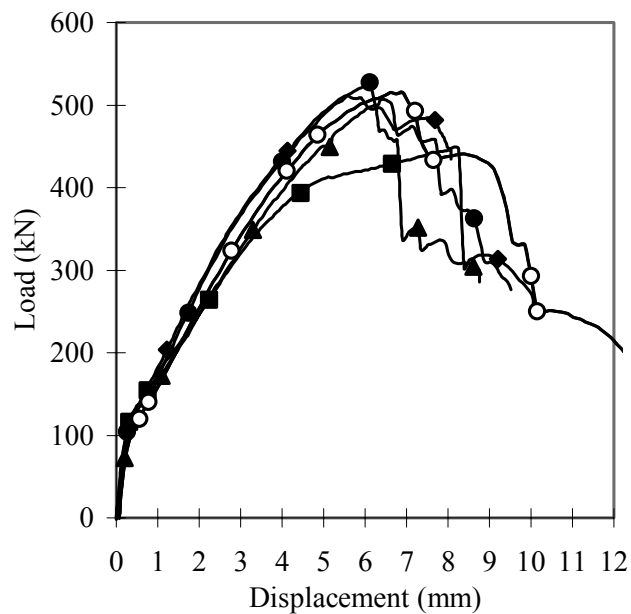


Figure 6: Load v. plate separation for the Lindapter Hollobolt tee stub tests.

Comparing the tee stub test results with the EC3 annex J (6) component method predictions, it is apparent that the behaviour of the RMH exhibited a mode ii / mode iii failure mechanism. This was due to ultimate failure being bolt tension, but with minimal plate separation. The Hollobolt, however, demonstrated purely mode iii failure, as there were large plate separations at the bolt failure load.

Although the behaviour of the tee stubs connected with the Hollobolt demonstrated that development of moment resistance in a connection is compromised by the very large deformations, the use of this fastener in nominally pinned connections is adequate, as any tensile load requirements arising from structural integrity criteria are below the initial

clamping force [British Steel Tubes and Pipes (5)]. The behaviour of the tee stubs joined with the RMH, however, indicated that its use in a moment resisting connection is feasible, with the ultimate capacity of the bolt actually being greater than that of a corresponding standard bolt. The failure mechanism, though, might, at first sight, be considered undesirable as it occurs suddenly with very little deformation.

However, in an application such as a moment resisting connection to SHS, the sudden failure mechanism is unlikely to be an issue, due to the thin wall limiting the level of load that may be resisted by the connection. It may therefore be anticipated that the wall dimensions will restrict the connection to a mode i plate failure or mode ii combined bolt and plate failure. This point is explored further in the next section.

INFLUENCE OF THE SHS FACE FLEXIBILITY

British Steel Tubes and Pipes (8) have provided theoretically derived equations for the determination of the face plastification capacity of a SHS, using yield line analysis [Equation 1], and for the SHS punching shear capacity [Equation 2]. Assuming a nominal yield stress of 275 N/mm² for the SHS material, and a geometrical bolt arrangement as used in the standard tee stub tests, calculations using this equation demonstrate that, unless a relatively thick section such as a 200x200x12.5 SHS is used, the flexibility of the SHS face is likely to be the limiting factor.

$$F_c = \frac{2p_{yc}t_c^2}{1-\beta_1} \left[\eta_1 + 1.5(1-\beta_1)^{0.5}(1-\gamma_1)^{0.5} \right]$$

Equation 1

$$F_{ps} = 4(\pi \cdot d^2 \cdot t_c)0.6 \cdot p_{yc}$$

Equation 2

The use of these equations has shown that a 200x200x8 SHS possesses a theoretical face yielding and punching shear capacity of 123kN and 431kN respectively. Compared with the strength and stiffness of the RMH this means that failure of the SHS face is critical. A larger tube size of 200x200x10 provides enhanced theoretical face yielding and punching shear capacities of kN and kN respectively, again less than the capacity of the RMH.

The largest tube size that was investigated, i.e. 200x200x12.5, demonstrated that the RMH and Hollobolt possess capacities larger than the theoretical capacity of the SHS wall. At the yield capacity of the wall (316kN), there is approximately 0.5mm plate separation with the RMH, which is unlikely to exceed serviceability criteria.

It should be noted, however, that subtle changes in the bolt layout may significantly affect the capacity of the SHS face. Recalculation of the SHS face yield load for a range of bolt pitches and gauges indicate that the smaller bending moment in the hollow section face resulting from a large bolt gauge provides a greater face capacity, as would be expected.

Furthermore, interaction between the rows of bolts is also of significance. The greater the bolt pitch, the less the interaction, hence, a greater face capacity results. When the bolt pitch and gauge are 75mm, the theoretical yield load of a 200x200x12.5 SHS becomes 252kN, which is less than the capacity of an arrangement with four RMH. However, an increase in gauge and pitch to 120mm (the largest practical gauge) results in a capacity of 430kN, which is likely to cause a sudden flaring of the legs of the RMH. The effects of change in bolt gauge and pitch are demonstrated for 200x200x8 and 200x200x12.5 SHS in figures 7 and 8 respectively.

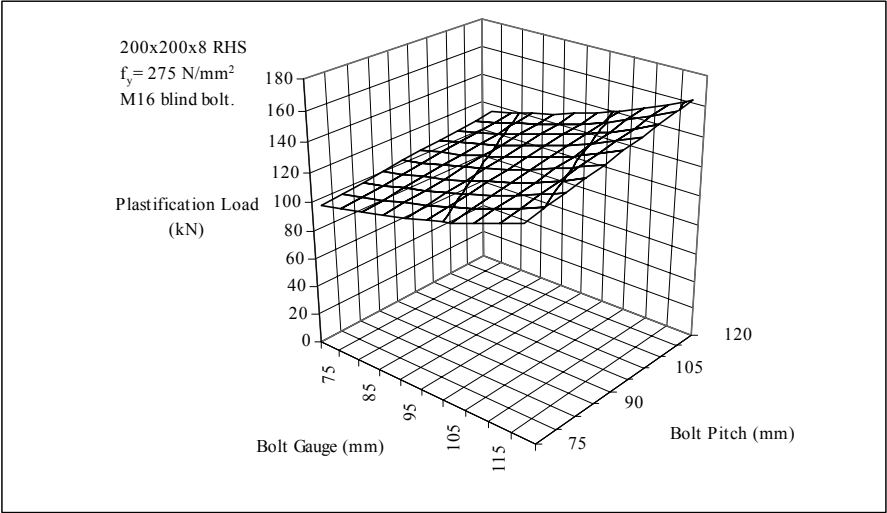


Figure 7: Effect of change in gauge and pitch for 200x200x8 SHS

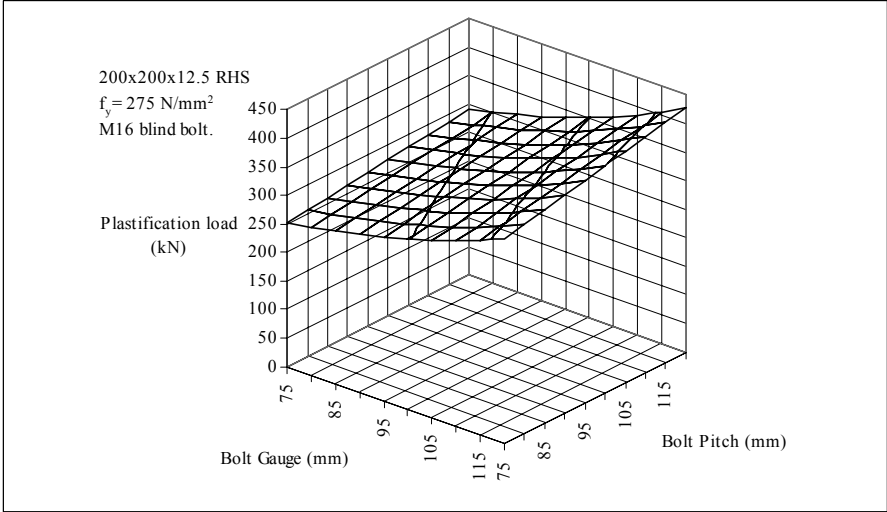


Figure 8: Effect of change in gauge and pitch for 200x200x12.5 SHS

A series of ‘modified’ tee stub tests has been prepared in order to ascertain the efficacy of the yield line theory presented above. It is felt that these tests, where a length of hollow section tube is placed between the tees, will provide details of the yield line shape on the face of the tube, and the load required to cause yield, thereby validating

the theory. Further aims of this series are to determine the potentially complex interaction between the RMH and the SHS, and to evaluate the applicability of the EC3 component method to the tensile region of a moment connection to SHS.

In order to facilitate the understanding of the bolt / SHS interaction, an intermediate series of tests has been arranged where standard dowel bolts are the connector. It is hoped that this series will provide details of the tubes yielding mechanism without interference from the blind bolt.

CONCLUSIONS

The standard tee stub tests have shown that the RMH possesses sufficient strength and stiffness for use in a moment resisting connection. It has been demonstrated theoretically, however, that the flexibility of the SHS face may limit the moment capacity of the connection when thin walls and narrow bolt gauges are employed. Therefore, further series of tests are suggested using a modified tee stub arrangement to determine whether the full capacity of the RMH may be employed. Also, it is hoped that these tests will validate previously a published theoretical model of the tube face failure mechanism.

ACKNOWLEDGMENT

The work described in this paper was carried out at the University of Nottingham with support from Lindapter International and British Steel (Corus) Tubes and Pipes. The assistance of Mr. Simon Klippel and Mr. Neil Gill of Lindapter and Mr. Noel Yeomans and Mr. Eddy Hole of British Steel is gratefully acknowledged.

NOTATION

$$\eta_1 = \frac{(n-1)p - \frac{n}{2}d}{(B - 3t_c)}$$

$$\beta_1 = \frac{g}{(B - 3t_c)}$$

$$\gamma_1 = \frac{d}{(B - 3t_c)}$$

B = The width of the hollow section wall

t_c = wall thickness

n = number of rows of bolts

p_{yc} = hollow section design strength

g = bolt gauge

d = hole diameter

REFERENCES

- (1). FLOWDRILL, Flowdrill B.V., Holland, (1993).
- (2). HIGH STRENGTH BLIND BOLT, Huck International, Japan (1990).
- (3). HOLLOBOLT, Lindapter International, U.K (1995).
- (4). BANKS, G., "Hollobolt Joint Shear Tests", Memos 129 & 146, British Steel Plc, Rotherham (1997).
- (5). BRITISH STEEL TUBES AND PIPES "SHS Jointing: Flowdrill & Hollobolt" (1997).
- (6). EUROCODE 3, "Design of Steel Structures. Part 1.1 General Rules and Rules for Buildings" DD ENV 1993-1-1 (1992).
- (7). BARNETT, T., TIZANI, W., and NETHERCOT, D., "Report on the Clamping Behaviour of the Lindapter Hollobolt and a Blind Bolt Prototype" *Internal Interim Report, the University of Nottingham* (1999).
- (8). BRITISH STEEL TUBES AND PIPES "Hollofast and Hollobolt System for Hollow Section Connections" CIDECT Report No. 6G-14(A)/96 (1996).

INJECTION BOLTS TO REPAIR OLD BRIDGES

A.M. Gresnigt, Delft University of Technology, The Netherlands
G. Sedlacek, RWTH Aachen, Germany
M. Paschen, RWTH Aachen, Germany

ABSTRACT

In 1996 an old riveted steel bridge in Oranienburg near Berlin had to be repaired because of severe corrosion in the web of the main girders. For several reasons it was decided to apply injection bolts to connect new plates at the corroded areas of these webs. German authorities requested the verification of the long duration creep resistance. To that aim, test specimens were made at the construction site and creep tests were started at Delft University at room temperature and at elevated temperature (70 degrees Celsius). These tests are still running. The paper describes the first application of injection bolts in Germany to repair steel bridges. Results of the long duration creep tests are given. These tests indicate that the design bearing resistance of the resin could be increased from the present 130 N/mm^2 , e.g. till 200 N/mm^2 .

INTRODUCTION

In the preparation of the rehabilitation of an old (1934) riveted bridge crossing the river Havel in Oranienburg near Berlin, it appeared that in the web of the main girder serious corrosion had occurred. The extent of the corrosion damage became clearly visible when the concrete bridge deck near the web was removed. Rain and dirt pouring into the gap between the steel and the concrete for many years had caused the corrosion.

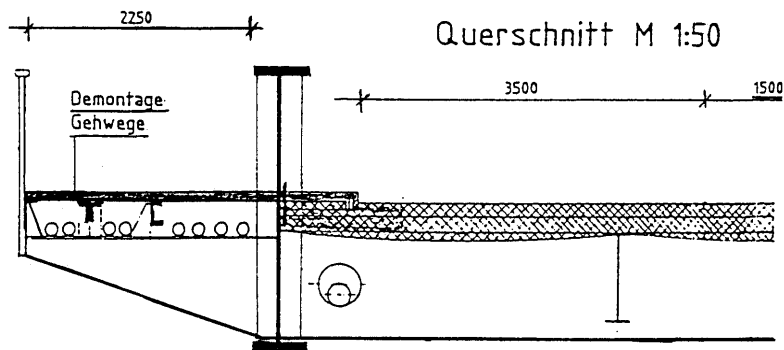


Figure 1. Cross-section of the main girder with concrete bridge deck.

The original thickness of the plate was 14 mm and due to corrosion the remaining thickness was between 0 (at a few places) and 10 mm with an average of about 9 mm. Figure 2 gives an impression of the corrosion pattern.



Figure 2. Corrosion at the bridge deck level.

Repair by welding strengthening plates to the corroded parts was considered to be difficult because of the poor weldability properties of the old steel. Riveting was not attractive either, because of the difficulties to find good equipment and skilled riveters.

Other possibilities are fitted bolts (expensive) and injection bolts. High strength friction grip bolts were not considered a good possibility, because of the very uneven surface of the corroded web and the presence of the paint layers, leading to low friction coefficients.

In The Netherlands, injection bolts (figure 3) were first used in 1970 for the repair of old riveted railway bridges. From the first application it has become standard practice to apply injection bolts for the repair of old bridges, but also for new railway bridges and other structures. Much research has been carried out in the Stevin Laboratory of the Delft University of Technology.

In 1994, "European recommendations for bolted connections with injection bolts" were published by the ECCS (1). These recommendations were also translated into German (2). Further rules are to be found in the Eurocode 3, the part on bridges (4) and in the new part on connections (6). Rules for execution of injection bolts are to be found in (5).

In view of the good results of the application of injection bolts in The Netherlands, the ministry of traffic of the county Brandenburg in Germany decided to apply injection bolts for the repair of the bridge in Oranienburg. TU Delft and RWTH Aachen assisted in the design and application of the injection bolts. In this paper more details are given.

In order to verify and demonstrate the correct structural behaviour of the injection bolts, test specimens were made during the execution of the injection on June 27, 1996. These test specimens were subjected to long duration creep tests in the Stevin Laboratory of TU-Delft. Next sections give more information on injection bolts, their applications and the design bearing stress. Then, the test set-up and the test results of the long duration creep tests are given.

INJECTION BOLTS

Injection bolts are bolts in which the cavity produced by the clearance between the bolt and the wall of the hole is completely filled up with a two component resin. Filling of the clearance of an injection bolt is carried out through a small hole in the head of the bolt. After injection and full curing of the resin, the connection is slip resistant. Shear load is transferred through bearing and shear of the bolt.

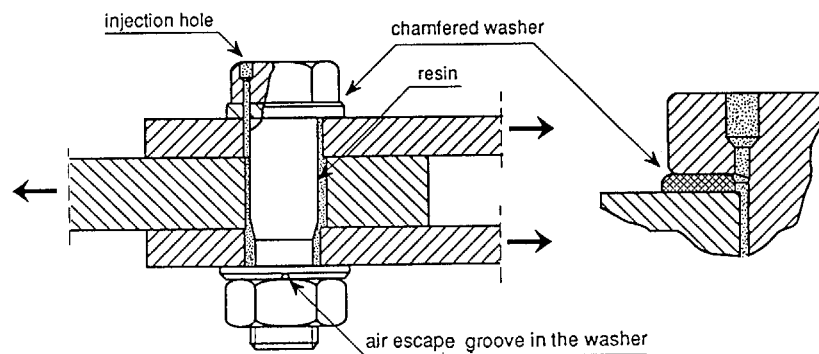


Figure 3. Injection bolt in a double lap joint.

Injection bolts can be manufactured from normal standard structural bolts. The bolts and washers are adapted to enable the injection of the resin.

As compared to other mechanical fasteners, injection bolts have several advantages. A distinction is made between the application in existing structures and in new structures. In many cases the advantages apply both for repair and strengthening of existing structures, as well as for new structures.

Repair and strengthening of existing structures

- *Solution for connections with a low slip factor.* The slip factor for riveted plates is usually very low. The application of new rivets is virtually impossible because of the lack of equipment and skilled labour. Injection bolts have proven to be a good solution for the repair of riveted structures (e.g. old railway bridges).
- Another possibility are fitted bolts. However, as indicated before, fitted bolts are expensive compared to injection bolts. Injection bolts may be installed in standard holes: 2 to 3 mm bigger than the nominal bolt diameter.

- *Good design resistance in bearing.* Assuming a reasonable ratio between the thickness of the plates and the diameter of the bolts, the design resistance in bearing is usually quite sufficient to replace faulty rivets.
- *No internal corrosion.* Since the resin completely fills the cavity, internal corrosion is avoided (also important for new structures).

Application in new structures

- *No slip in case of overload.* In connections with high strength friction grip bolts (HSFG bolts), slip due to overload is possible. With injection bolts, sudden slip is not possible.
- *Good design resistance in bearing.* Assuming a reasonable ratio between the thickness of the plates and the diameter of the bolts, the design resistance in bearing is of the same magnitude as the slip resistance of HSFG bolts.
- *Compact connections.* If the desired load transfer per bolt is very high (e.g. because the available space for bolts in the connection is small), preloaded injection bolts may offer the solution. As the design resistance of a preloaded injection bolt is the sum of its slip resistance and the bearing resistance of the resin, the number of bolts in a connection will be lower.
- *No special requirements for the contact surfaces and no controlled tightening.* For high strength friction grip bolts special requirements are necessary for the contact surfaces to achieve a satisfactory slip factor. If corrosion prevention is necessary, the paint to be used has to guarantee the desired slip factor. With non-preloaded injection bolts, slip can be avoided without any special preparation of the contact surfaces. Also the possibility to avoid the necessary calibration and tightening procedures for HSFG bolts may be an incentive to apply non-preloaded injection bolts.

Costs

Because of the costs, injection bolts should only be applied where the advantages justify doing so. The costs of injection bolts consist of:

- a. The purchase of the bolts themselves (standard 10.9 or 8.8 bolts);
- b. The preparation of the bolts and washers (drilling a hole in the bolt heads and preparing the special washers);
- c. The resin, the preparation of the resin and the injection.

In The Netherlands injection bolts and washers are available from stock (bolt suppliers), ready for use. However, adapting standard bolts and washers can also easily be carried out in the workshop. Because the injection equipment is cheap and the amount of resin per bolt is limited, the material costs for injection are low. The labour costs for injection per bolt depend on:

- a. The total number of bolts to be injected;
- b. The number of bolts per connection;
- c. The accessibility of the bolts;
- d. The size and length of the bolts;
- e. Possible delay because the holes must be dry during injection (weather conditions, shelter from rain).

Roughly, the labour time for injection varies between 1 and 2 minutes per bolt. When injection bolts are used, the number of bolts in a connection will be less, thereby reducing the costs for holes and

bolts. Further, the possibility of larger hole clearances may facilitate erection and consequently also reduce costs. Finally it is noted that dismantling is not easy, unless special arrangements are made in advance, e.g. the application of a special separation liquid to prevent bonding of the resin to the bolt and the walls of the hole.

DESIGN BEARING STRESS

Since resins are susceptible to creep deformation if the bearing stress is too high, the bearing stress has to be kept within certain limits. In the research at the Stevin Laboratory, several resins were tested. The best resin appeared to be the 2-component resin "Araldit", manufactured by Ciba-Geigy (SW 404 with hardener HY 404). About 10 years ago, Ciba-Geigy changed the recipe of the hardener, because the HY 404 hardener appeared toxic. The new hardener is called: HY 2404.

On the basis of the producers' specified material properties of the resin, and on a limited number of tests with the modified resin/hardener in injection bolts in the Stevin Laboratory, it was recommended in the European Recommendations to limit the design bearing stress to 130 N/mm². Tests carried out in 1994 and 1995 indicated that this value is too conservative.

In the design of injection bolts for the Oranienburg bridge in 1996, it was decided to increase the design bearing stress to 150 N/mm². This means that in case of bolts with standard nominal hole clearances (for bolts M24: 2 mm), the maximum displacement at a bearing stress of 150 N/mm² shall be less than 0,3 mm. This is the same limit as is used for riveted and HSFG connections.

The design calculations (8) were carried out according to the rules in the "European recommendations for bolted connections with injection bolts" (1).

INSTALLATION IN THE SCHLOSSBRÜCKE ORANIENBURG

Figure 4 gives a view of the installation of the 700 M24 injection bolts in the bridge. For a description of the procedure of the preparation of the resin and the equipment to be used, reference is made to the ECCS recommendation (1) and the proceedings of the Third International Workshop in Trento (7).

It is noted that because of the hollow spaces between the corroded web and the reinforcing plates, much more resin was used than for the filling of the clearance of the bolts alone. The advantage is that by filling all hollow spaces any further corrosion was completely ruled out.

A crew of two persons carried out the injection. One person for the injection and the other for checking the nut side on the appearance of the resin from the groove in the washer. Including the preparation of the resin, the injection of a group of 20 bolts took about 30 minutes. In this case, a hand driven equipment is used (figure 4). Particularly for longer bolts or where large quantities of bolts are to be injected, air driven equipment is recommended for better progress.

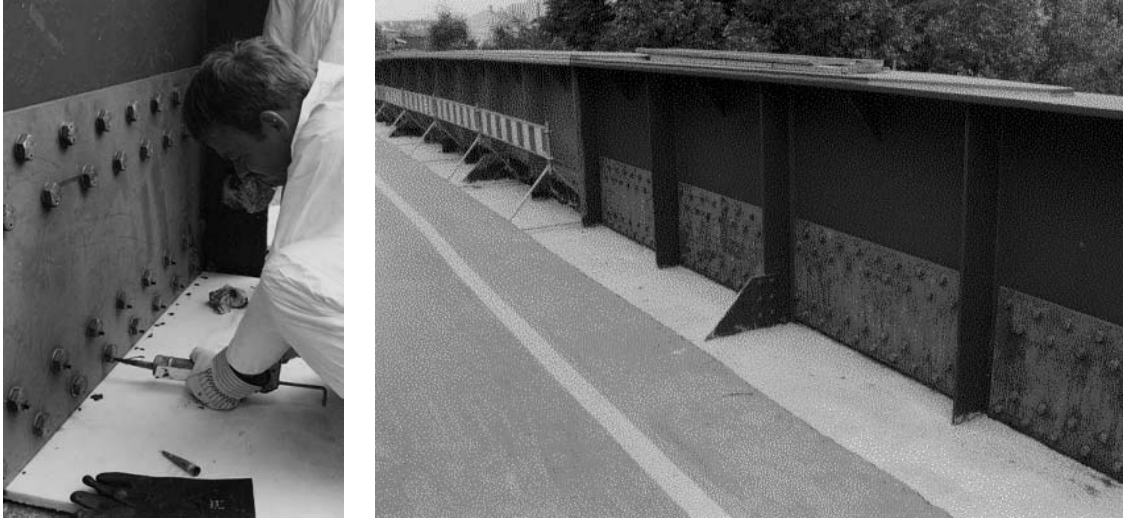


Figure 4. Injection bolts in the Schlossbrücke Oranienburg. Injection in progress and a view of the reinforcement of the web in the main girder.

TEST SPECIMENS, TEST RIG AND MEASUREMENTS

In order to verify and demonstrate the correct structural behaviour of the injection bolts, test specimens were made during the execution of the injection on June 27, 1996 (figure 5). Four test specimens were subjected to long duration creep tests in the Stevin Laboratory of TU-Delft. Another two test specimens were left at the bridge site for later testing.

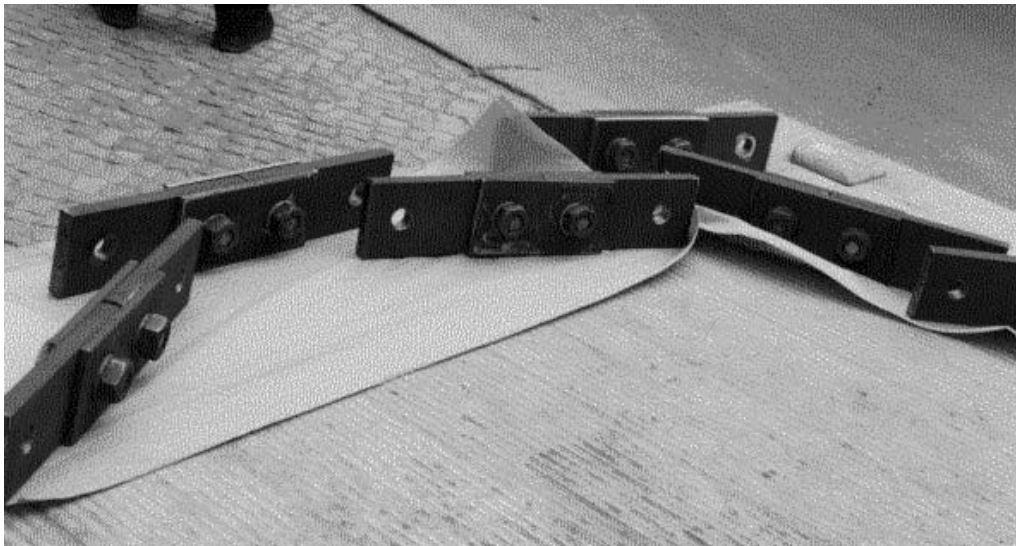


Figure 5. Test specimens at the construction site on June 27, 1996.

In accordance with ENV 1090-1 (5), the position of the bolts in the test specimens was chosen in such a way that at the side of the bearing stress the thickness of the resin would be maximum. This position is the most unfavourable with regard to the deformation due to the elastic

compressibility of the resin and due to creep. In real construction, the position of bolts will be "at random", leading to less deformation.

Test rig and measurements

The test specimens were tested at the Stevin Laboratory of TU-Delft in a standard test rig. Three specimens were tested at ambient temperature (about 20 °C) and one at 70 °C. The temperature of 70 °C is considered to be about the maximum temperature that can occur in real bridge structures (heating by sunshine).

Figure 6 shows the test specimens in the test rig at ambient temperature and the equipment for the test at 70 °C, where the test specimen is mounted in a thermally isolated box. Air at a temperature of a little more than 70 °C is guided through a tube to the box with the test specimen. The regulation of the heating equipment is such that the temperature variations of the air in the box are less than 1 °C.

The load is applied by turning a nut at the top of the test rig. The load is measured with a load cell. Due to creep, the load will decrease, but because of the fact that the elastic deformations in the test rig are large compared with the creep deformation, the decrease of the load will be small. At regular time intervals the load is checked and, if necessary, adjusted.

The displacements in the test specimens at ambient temperature are measured with dial gauges (0,001 mm) as indicated in figure 7. The displacements are measured on both sides of each bolted connection. Small eccentricities will cause some differences between these two measurements. The deformation of each bolted connection is taken as the average of the two measurements. The displacements of the specimen at 70 °C are measured in the same way.

Test procedure

As explained earlier in this paper, the design bearing stress for the injection bolts in the Oranienburg bridge is set at 150 N/mm². The requirement for the deformations is that they are less than 0,3 mm. This is the same value as in HSFGB bolt creep testing.

The load is increased in steps: 24 kN, 48 kN, 62,4 kN, 72 kN, 84 kN, 96 kN, 108 kN and 120 kN. The applied bearing stress σ_b follows from $\sigma_b = F/(d_b \cdot t_{plate})$ where d_b is the applied bolt diameter ($d_b = 24$ mm) and t_{plate} is the plate thickness of the main plate ($t_{plate} = 20$ mm). The thickness of the cover plates equals $2 \times 10 = 20$ mm. Therefore, the bearing stress is the same in the main plate and the cover plates. The resulting bearing stresses are 50, 100, 130, 150, 175, 200, 225 and 250 N/mm² respectively.

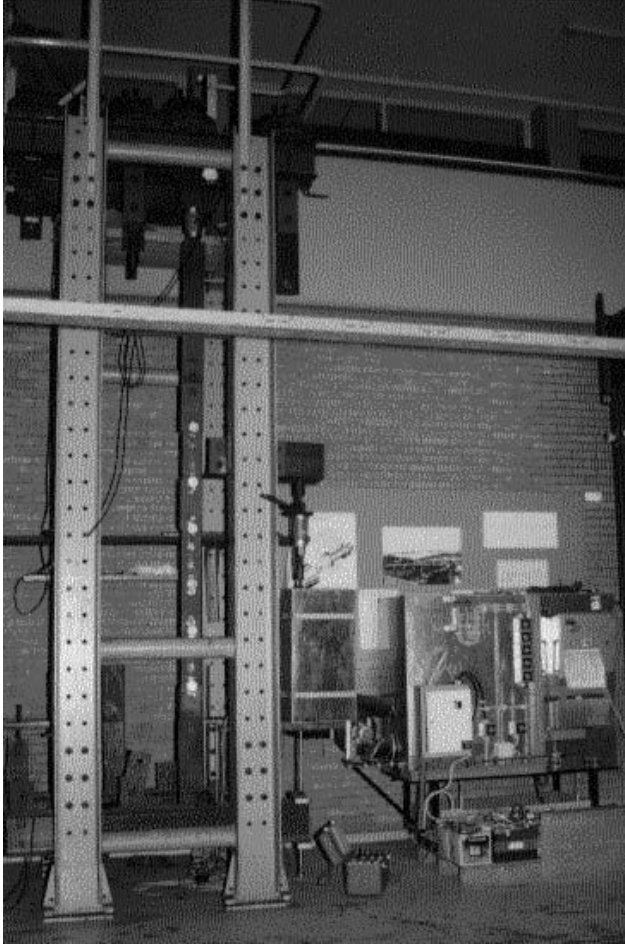


Figure 6. Test rig for creep tests on HSFG bolted or injection bolted connections with the 3 test specimens at ambient temperature and the equipment for the test at 70 °C.

The measured displacements consist of two parts (see figure 7):

- a. Deformation of the plates (elastic);
- b. Deformation of the injection bolt assembly (bolt deformation plus deformation of the resin). The deformation of the resin is partly elastic and partly due to creep.



Figure 7. Measurement of displacements. Each test specimen contains two bolts, so that a total of 8 bolted connections were tested. The displacements at each bolt are measured at the head and at the nut side.

At each load increase, the displacements were measured. Then the load was kept constant and at regular time intervals the displacements were measured. When after some time the displacements showed hardly any further increase, indicating that at the applied stress level no significant further creep was to be expected, the next load step was carried out.

This applied load - time relation is in accordance with the tests as they were carried out during many years in the Stevin Laboratory. In the European Recommendations, however, a different sequence is recommended, i.e. to demonstrate that a resin is suitable for a certain bearing stress, it is recommended to apply that bearing stress from the very start of the test. The difference in the test procedure, however, will not influence the conclusions.

The relation between the applied load (bearing stress) and the time is indicated in the figures 8, 9, 10 and 11. The tests for the ambient temperature started on September 17, 1996. The test at 70

°C started on January 20, 1997. The last measurements were done on October 6, 2000. This means that so far, the tests are running already for 4 years.

TEST RESULTS

The measured displacements are given in the figures 8, 9, 10 and 11. For every test specimen the average is given of the displacements measured with dial gauges k1 (head side of one of the two bolts) and k2 (nut side of the same bolt) and the average of dial gauges k3 and k4 (the other bolt in the same test specimen). In the figures also the applied bearing stress σ_b is given.

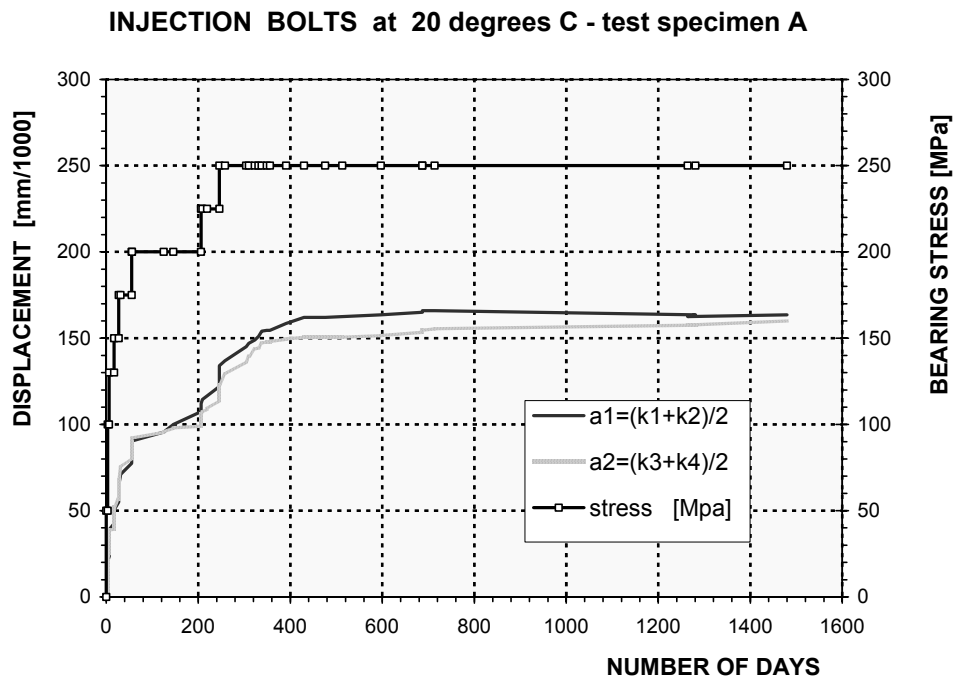


Figure 8. Applied bearing stress and displacements of test specimen A.

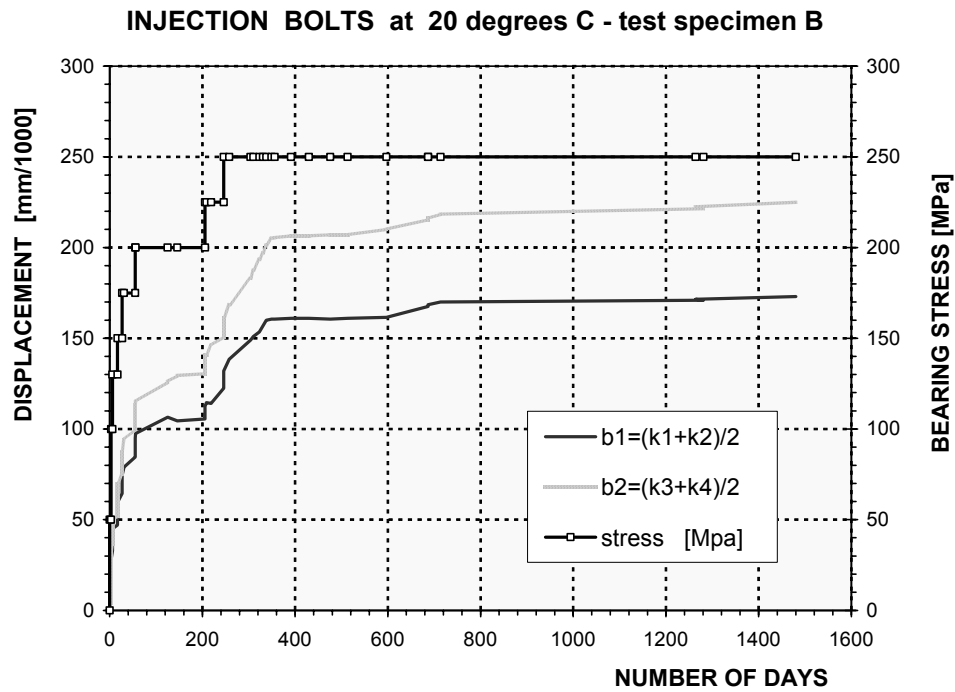


Figure 9. Applied bearing stress and displacements of test specimen B.

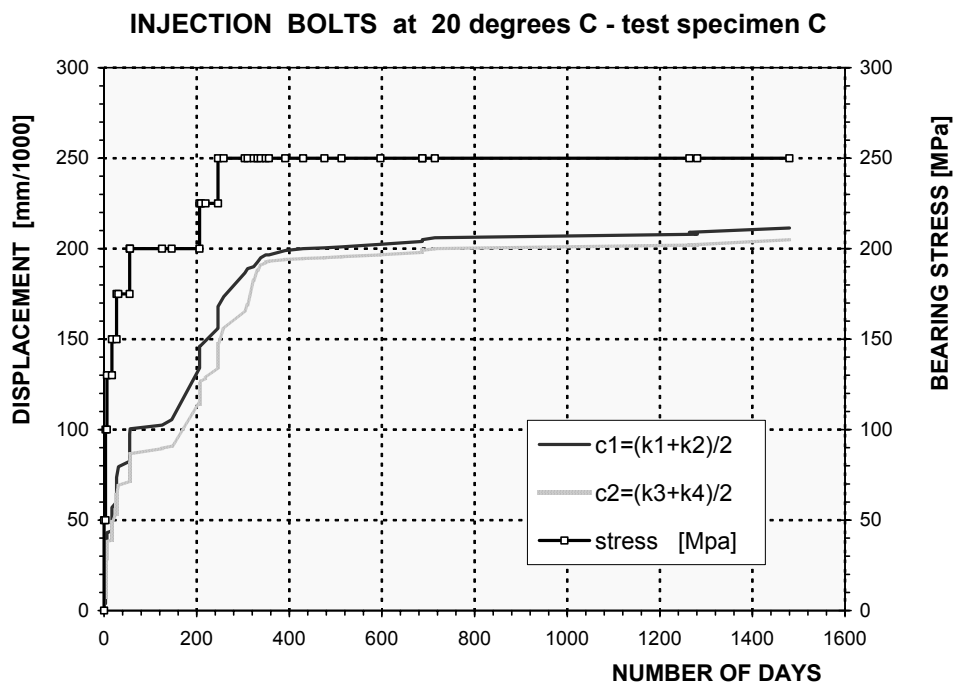


Figure 10. Applied bearing stress and displacements of test specimen C.

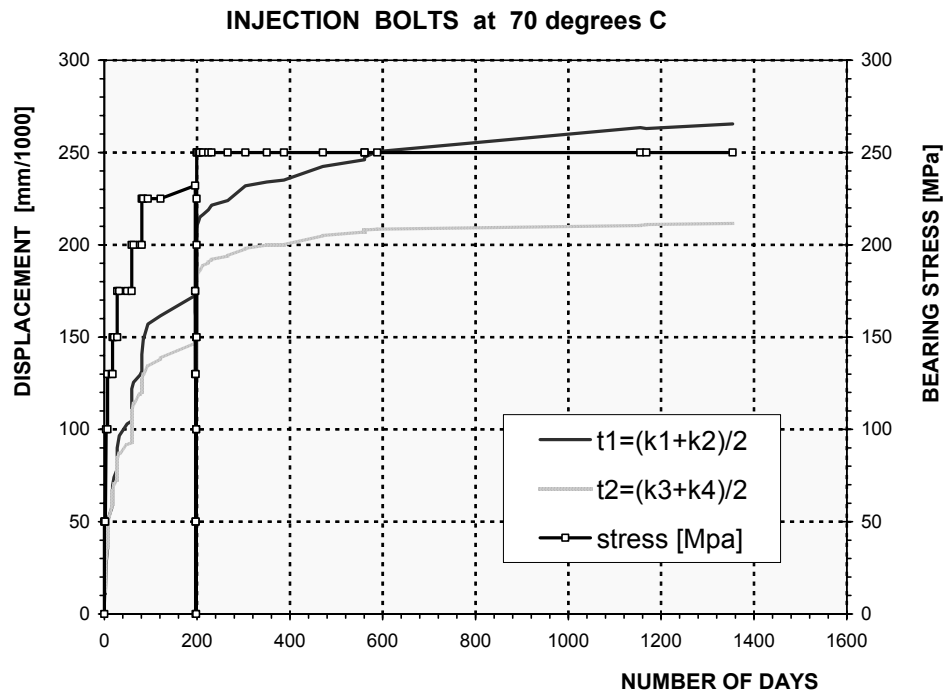


Figure 11. Applied bearing stress and displacements of the test specimen at 70 °C.

It appears that the average of the displacements for specimen T at 70 °C are about 20 % higher than those for the average of the specimens A, B and C at 20 °C.

CONCLUSIONS

In order to verify and demonstrate the correct structural behaviour of injection bolts, applied in the rehabilitation of an old riveted bridge crossing the river Havel in Oranienburg near Berlin, four test specimens, each containing two bolts, were subjected to long duration creep tests in the Stevin Laboratory of the TU-Delft. The specimens were made during the execution of the injection of the bolts at the bridge on June 27, 1996.

The main conclusions are:

- Injection bolts are an excellent alternative for replacing faulty rivets in (old) riveted structures.
- Injection bolts can successfully be used for strengthening of corroded plates, especially where welding or HSFG bolting is difficult to apply.
- Long duration creep tests are still going on at a bearing stress of 250 N/mm².
- The high temperature of 70 °C has only a moderate influence on the deformations. The average creep for ambient temperature (20 °C) is 0,190 mm and for 70 °C 0,240 mm (at a bearing stress of 250 N/mm²)

- e. The test results demonstrate the safety of the applied design value for the bearing stress in the bridge in Oranienburg, namely 150 N/mm^2 .
- f. It is noted that the circumstances in practice usually are much more favourable than in the tests:
 - The applied constant high bearing stress and constant high temperature will not appear in practice.
 - In practice there will be at least some pre-loading, giving some friction.
 - In practice the position of the bolts in the holes will be "at random", leading to a more favourable average thickness of the resin layer in the holes.
- g. The allowable bearing stress may be raised from 130 N/mm^2 up to 175 or 200 N/mm^2 , to be discussed in CEN.

ACKNOWLEDGEMENT

The fruitful co-operation with the ministry of traffic of the county Brandenburg (Ministerium für Stadtentwicklung, Wohnen und Verkehr des Landes Brandenburg) in the performance of the above mentioned project is gratefully acknowledged.

REFERENCES

- (1) ECCS, (1994). *European recommendations for bolted connections with injection bolts*. ECCS publication No. 79, Brussels.
- (2) RWTH Aachen, (1994). *Europäische Empfehlungen für Schraubverbindungen mit Injektionsschrauben*. Lehrstuhl für Stahlbau der RWTH Aachen.
- (3) ENV 1993-1-1, (1992). *Eurocode 3, Design of Steel structures. Part 1.1 - General Rules and Rules for Buildings*. CEN, Brussels.
- (4) ENV 1993-2, (1997). *Eurocode 3, Design of Steel structures. Part 2 – Steel bridges*. CEN, Brussels.
- (5) ENV 1090-1, (1996). *Execution of steel structures, Part 1. General rules and rules for building*. CEN, Brussels.
- (6) prEN 1993-1-8, (2000). *Eurocode 3 Design of Steel Structures, Part 1-8: Design of joints*. (Draft September 2000).
- (7) Gresnigt A.M., Stark J.W.B. *Design of Bolted Connections with Injection Bolts*. Connections in Steel Structures III, Behaviour, Strength & Design, Proceedings of the Third International Workshop, Trento, Italy, 29-31 May 1995, Pergamon, pp 77-87.
- (8) Sedlacek G., Paschen M., Gresnigt A.M. (1997). Bericht zur Erstanwendung der Injektionsschrauben bei der Hauptträgerstegverstärkung an der Schlossbrücke Oranienburg, Berlin, Rheinisch-Westfälische Technische Hochschule, Lehrstuhl für Stahlbau, Aachen, Germany.

Welded Connections in High Strength Cold-Formed Steels

by

Gregory Hancock¹, Tim Wilkinson², Lip Teh³
Centre for Advanced Structural Engineering
University of Sydney
NSW, Australia

ABSTRACT

Cold-formed steel is being used more widely for routine structural steel design including portal frames composed of open and/or closed sections. In Australia, cold-formed channel and Z-sections made of G450 (zinc coated 450 MPa yield) sheet steel are used to construct frames by welding. The cold-formed steel structures are normally designed to the Australian/ New Zealand Cold-Formed Steel Structures Standard AS/NZS 4600:1996 which is based on the 1996 Edition of the AISI Specification. The design rules for welded connections in the AISI Specification and AS/NZS 4600 are based mainly on testing of mild steel (300 MPa) connections at Cornell University in the 1970s and so may not be applicable to high strength steels.

Cold-formed tubular sections made of C450 steel (In-line galvanised 450 MPa yield) are also used to construct portal frames with welded and sleeved knee connections. They are designed to the Australian Steel Structures Standard AS 4100-1998 which is similar to the AISC LRFD Specification. Recent research by Wilkinson and Hancock reported in the Journal of Structural Engineering of the ASCE (March 2000) has shown that fracture may occur in the heat affected zone of connections of this type.

The paper describes the results of two ongoing research programs investigating welded connections in high strength cold-formed steel sections. The results of butt welds and fillet welds are described at this stage. The nature and stress of fracture in the heat affected zone are described in detail. The effect of heat input has also been investigated and is described.

¹BHP Steel Professor of Steel Structures, Centre for Advanced Structural Engineering, University of Sydney, Australia, 2006

²Lecturer, Centre for Advanced Structural Engineering, University of Sydney, Australia, 2006

³Senior Researcher, Centre for Advanced Structural Engineering, University of Sydney, Australia, 2006

1. INTRODUCTION

This paper describes research on the effects of welding on the strengths of G450 Sheet Steel manufactured to the Australian Standard AS 1397-1993 “Steel Sheet and Strip – Hot Dipped or Aluminium/Zinc Coated” (1) and C450 Steel to the Australian Standard AS 1163-1991 “Structural Steel Hollow Sections” (2). The steels are quite different in their methods of manufacture and so need to be studied independently for the effect of welding. However, both steels suffer degradation in the tensile strength in the Heat Affected Zone (HAZ) of the welds and so their structural behaviour is quite similar when tested for a welded connection in tension and/or shear. Consequently, although the paper describes similar phenomena, it is based on two separate research studies. The full study for the “Strength of Fillet Welded Connections in G450 Sheet Steel” can be found in Teh and Hancock (3) and the full study of the “Effect of GMAW on the Mechanical properties of In-Line Galvanised Cold-Formed Steel” can be found in Wilkinson and Hancock (4). This paper separates the descriptions from the two studies, and concentrates on material properties in the HAZ.

During the welding process, the grains of the cold-worked steel recrystallise, and the heat affected zone will soften compared to the cold-formed hardness. Consequently, the ultimate tensile strength (f_u) in the heated affected zone (HAZ) may be less than the yield stress of the parent material. There are several instances in which a steel structure has to demonstrate ductile behaviour. In plastic design, the plastic hinges must rotate sufficiently for moment redistribution to take place in the structure, in order to obtain the strength increase afforded by plastic design. For seismic design, deformation capacity is essential to dissipate the energy caused by the earthquake motion. In such cases, the joints of a steel structure are required to show ductile behaviour. However, if there is a small HAZ in a welded joint, where the ultimate tensile strength is less than the yield stress in the adjacent unaffected steel, the HAZ will fracture before significant plastic deformations occur near the joint. This renders the structure unsuited for plastic design or seismic applications. A previous investigation examining the suitability of portal frame knee joints for use in a plastically designed structure constructed from cold-formed rectangular hollow sections (RHS), found that under opening bending moment, the connection fractured in the HAZ before large plastic deformation occurred. It should be noted that the connection displayed adequate strength, as opposed to ductility, which means that it was still suitable for use in elastic design.

1.1 G450 Cold-Reduced Zinc-Coated Steel to AS 1397

In Australia and New Zealand, the design rules for cold-formed steel members including connections are specified in AS/NZS 4600 (5) which is similar to the AISI Specification (6). The design equations for welded connections in thin sheet steels less than 3.0 mm (2.5 mm for fillet welds) specified in the standard are adapted from the AWS D1.3 Structural Welding Code (7), which is based on the testing results of Pekoz & McGuire (8) on double-lap welded connections in mainly mild sheet steels. Since the welds in thin sheet steels are generally as thick as or thicker than the sheets, and the weld metal must be at least as strong as the weaker of the sheets being joined, these equations use the sheet material strength and the sheet thickness (rather than the weld metal strength and the weld throat size) in determining the nominal capacity of the connections. Unfortunately, it is not clear how applicable the equations are to welded connections in high-strength sheet steels manufactured to AS 1397. In Clause 1.5.1.4 of AS/NZS 4600, it is stated that “The effect of welding on the mechanical properties of a member shall be determined on the basis of test on the full section containing the weld within the gauge length. Any necessary allowance for such effect shall be made in the structural use of the

member.” However, no significant research has been conducted on welded connections in cold-reduced high-strength sheet steels such as G450, G500 and G550 steels, which are manufactured to AS 1397. Zhao and Hancock (9) have pointed out that as the tensile strength of the steel is increased by cold working, the heat-affected-zone (HAZ) may play a more important role in the strength of welded connections.

It is noteworthy that with regard to milder steels including cold-formed tubular sections, it has previously been concluded that welding does not affect the steel properties significantly (Wardenier & Koning (10)). This conclusion supports the existing design equation for the nominal capacity of a transverse fillet welded connection in sheet steel, as specified in Clause 5.2.3.3 of AS/NZS 4600. It is also consistent with the statement of Pekoz & McGuire that a butt or transverse fillet welded connection can be expected to develop the full strength of the sheet. However, recent research by Chen et al. (12) shows that the tensile strength of the heat-affected-zone (HAZ) of G550 sheet steel drops substantially from a nominal value of 550 MPa to about 450 MPa. This considerable decrease in tensile strength due to welding puts into question the applicability of current design equations to welded connections in cold-reduced high-strength sheet steels such as G450, G500 and G550 sheet steels. Additionally, there is a concern about the effect of reduced ductility especially of G550 steel on the ability of a (long) welded connection to redistribute the stresses prior to fracture in the stress concentration area. It may be noted that with regard to the tensile strength assumed in the design of bolted connections in G550 sheet steel, liberalisation of the design rule which requires that the yield and ultimate strengths be reduced to 75% was recently proposed by Rogers and Hancock (13).

This paper describes the laboratory tests conducted on full width transverse fillet welded connections in 1.5-mm and 3.0-mm G450 sheet steels, which are cold-reduced high-strength steels having a design yield strength of 450 MPa and a design tensile strength of 480 MPa. These thicknesses represent the minimum and the maximum thicknesses commonly available, respectively, for G450 sheet steel. The use of these thicknesses ensures that any proposed design rules are applicable to the whole range of thicknesses available to the designer. The G450 sheet steel materials used in the laboratory tests, which have a trade name GALVSPAN, were manufactured and supplied by BHP Coated Products, Port Kembla. The coating class designation is Z350, which indicates zinc coating of a nominal mass density of 185 g/m² on each side of the sheet steel. Tensile testing of the specimens was performed using a 2000-kN capacity Dartec servo-controlled testing machine manufactured in Stourbridge, England, and an MTS Teststar digital controller. Tensile loading of all specimens was in the rolling direction of the G450 sheet steel. The main objective of the tests was to determine the tensile strength in the HAZ of the G450 steel.

1.2 C450 In-line Galvanised ‘DuraGal’ Section Steel

A recent innovation in steel products in Australia is the DuraGal range of cold-formed in-line galvanised hollow and open sections produced by BHP Structural and Pipeline Products (formerly known as Tubemakers) (14). The typical steel strip used in the manufacturing process has a nominal yield stress (f_y) of 300 MPa. After cold-forming and in-line galvanising, the final product has a nominal yield stress in the range 350 - 450 MPa, depending on the exact process and the shape of the product.

If the sections are tubular, they can be designed to the Australian Steel Structures Standard AS 4100-1998 (15) where the weld strength is usually based on weld metal strength. If the sections are open sections, they can be designed to AS/NZS 4600:1996 where the weld strength is

based on parent metal strength as described in 1.1 above. C450 tubular sections are specified to the Australian Standard AS 1163 Structural Steel Hollow Sections (2).

This paper summarises the initial portion of a research project on C450 steel examining the strength in the HAZ of butt welded connections.

2. TENSILE STRENGTHS IN THE HAZ

2.1 G450 Cold-Reduced Zinc Coated Steel to AS 1397

Each specimen was a double-lap transverse fillet welded connection consisting of two $350 \times 130 \times 10$ mm hot-rolled plates of Grade 450, manufactured to AS/NZS 3678 (16), abutted together and joined by two 100×100 mm G450 sheets as illustrated in Fig. 1. The weld length is the same as the sheet width so that the tensile stresses are assumed to be uniform in the cover sheets. As mentioned previously, the tensile load, which was transverse to the welds, was in the rolling direction of the cover sheets. Each specimen was gripped at the hot-rolled plates on both ends, and the distance between the two grips was approximately 400 mm. Such a set-up was also used for subsequent double-lap connection specimens used to verify the reliability of existing design equations and described fully in Teh and Hancock (3).

Although it is not the purpose of the present work to find the optimum welding procedure for G450 sheet steel, two different electrodes and two different shielding gases were used for the specimens. The two electrodes are 0.8-mm ES6-GC/M-W503AH wire and 0.9-mm ES4-GC/M-W503AH wire, both of which are manufactured to AS/NZS 2717.1 (17) and are pre-qualified welding consumables for gas metal-arc welding (GMAW) of G450 sheet steel according to Clause 4.5.1 of AS/NZS 1554.1 (18). Both shielding gases are argon and carbon-dioxide based, with one containing helium. The settings of the GMAW machine were varied from specimen to specimen while ensuring that acceptable welds were produced. The welding voltage, current and time were recorded using a WeldPrint monitoring machine (19).

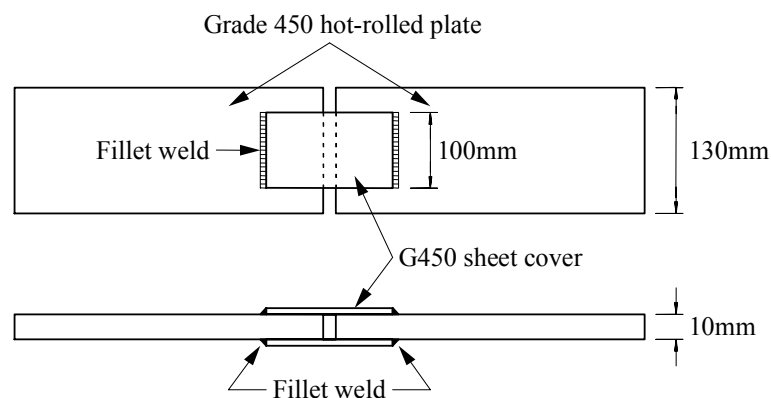


Figure 1: Diagram of a HAZ Specimen

The welding procedure for each HAZ specimen is given in Appendix 1 of Teh and Hancock (3). All the specimens failed in the HAZs of the cover sheets rather than in the welds, as illustrated in Fig. 2, so it can be inferred that the weld fusion and penetration of each specimen were

satisfactory. Hydrogen cracking was not a concern as G450 sheet steel does not have a sensitive microstructure and the double-lap joints were not highly constrained. It may also be noted that both the electrodes used in the welding are hydrogen controlled as denoted by the letter “H” at the end of the classifications.

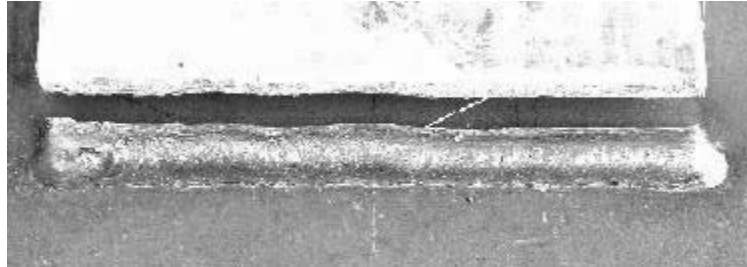


Figure 2: HAZ Failure in 3.0-mm G450 Sheet Steel

The HAZ tensile strength f_{uh} of each specimen is computed from the ultimate test load P_t and the actual dimensions of the cover sheets. The actual dimensions are the average sheet width and the average base metal thickness (with the zinc coating removed). The ultimate test loads listed in Tables 1 and 2 were obtained using a stroke rate of 0.2 mm/minute, which translates to strain rates of the order of 10^{-5} per second for the cover sheets. The average tensile strength of the HAZs in the 1.5-mm sheet steel was found to be 488 MPa, and that in the 3.0-mm sheet steel was found to be 495 MPa.

Table 1. Strength of HAZs in 1.5-mm G450 Sheet Steel

	Arc energy (kJ/mm)	1.1 1.2 Dimensions (mm ²)	P_t (kN)	f_{uh} (MPa)	f_{uh}/f_{un}
1.2.1.1 HAZ15.1	0.24	101×1.53	152.0	492	1.03
HAZ15.2	0.29	101×1.53	149.0	482	1.00
HAZ15.3	0.28	101×1.53	149.0	482	1.00
1.3 HAZ15.4	0.27	101×1.53	150.0	485	1.01
1.4 HAZ15.5	0.25	101×1.53	150.5	487	1.01
1.5 HAZ15.6	0.29	100×1.48	144.5	488	1.02
1.6 HAZ15.7	0.27	100×1.48	144.0	486	1.01
1.7 HAZ15.8	0.43	100×1.48	143.0	483	1.01
1.8 HAZ15.9	0.43	100×1.48	145.5	491	1.02
1.9 HAZ15.10	0.30	100×1.48	150.0	507	1.06

The last columns of Tables 1 and 2 show the ratios of the measured HAZ tensile strengths f_{uh} to the nominal design tensile strength f_{un} of 480 MPa specified in AS/NZS 4600 for G450 sheet steel. It is evident that irrespective of the arc energy and the welding procedures, the tensile strengths of the HAZs do not differ significantly from the nominal tensile strength, although they are significantly lower than the actual tensile strengths of the corresponding coupons cut from the same sheets. The average tensile strength of the 1.5-mm G450 sheet steel in the rolling direction was found to be 596 MPa, and that of the 3.0-mm G450 sheet steel was found to be 529 MPa. Thus the close agreement between the tensile strengths of the HAZs and the nominal tensile strength of 480 MPa used in the design of fillet welded connections is fortuitous.

Table 2. Strength of HAZs in 3.0-mm G450 Sheet Steel

	Arc energy (kJ/mm)	Dimensions (mm ²)	P _t (kN)	f _{uh} (MPa)	f _{uh} /f _{un}
1.9.1.1 HAZ30.1	0.46	101×2.97	302.0	503	1.05
HAZ30.2	0.53	101×2.97	284.0	472	0.98
HAZ30.3	0.55	101×2.97	280.5	466	0.97
1.10 HAZ30.4	0.52	101×2.97	298.0	496	1.03
1.11 HAZ30.5	0.48	100×2.97	298.5	502	1.05
HAZ30.6	0.48	100×2.97	296.0	498	1.04
HAZ30.7	0.63	100×2.97	294.5	496	1.03
HAZ30.8	0.63	100×2.97	305.5	514	1.07
1.12 HAZ30.9	0.65	100×2.97	302.0	508	1.06

More research is required to correlate the tensile strengths of HAZs in G450 sheet steel to the virgin strength and the welding procedures used to produce the fillet welds. It is also noted that while the average virgin strength of the 1.5-mm sheet steel is higher than that of the 3.0-mm sheet steel, the reverse is true with regard to their average HAZ strengths.

2.2 C450/C400/C350 In-line Galvanised ‘DuraGal’ Section

Full strength butt welds were used to test the C400 and C350 steel.

2.2.1 Steel Properties

Rather than testing an entire butt welded connection between two RHS, it is more convenient to perform a tension test on the flat faces of the RHS that have been welded together in the same manner. To further simplify the production of test specimens and to avoid having to cut the flat faces from the RHS, two flat bars of cold-formed DuraGal steel were connected. Currently, there is no Australian Standard applicable to the manufacture of cold-formed open profiles, and hence the sections are manufactured to an internal BHPSPS Specification, TS100. In most respects, the properties of the cold-formed open profile sections are the same as those for the cold-formed hollow sections manufactured to AS 1163.

2.2.2 Weld Metal Properties

Two types of welding wire were used in the GMAW process. Autocraft LW1 ($f_{yn} = 390$ MPa, $f_{un} = 500$ MPa) and Autocraft Mn-Mo ($f_{yn} = 530$ MPa, $f_{un} = 630$ MPa), to AS/NZS 2717.1 were used. More details on the wire properties can be found in CIGWELD (20).

2.2.3 Typical Welding Parameters

Two methods of GMAW were employed, the “dip-transfer” and “spray-transfer” modes. Generally, the spray transfer method requires a higher wire speed and higher current, and consequently a higher heat input. It is not possible to include the full details of all welding procedures in this paper, due to length requirements, however full details are given in Wilkinson and Hancock (4).

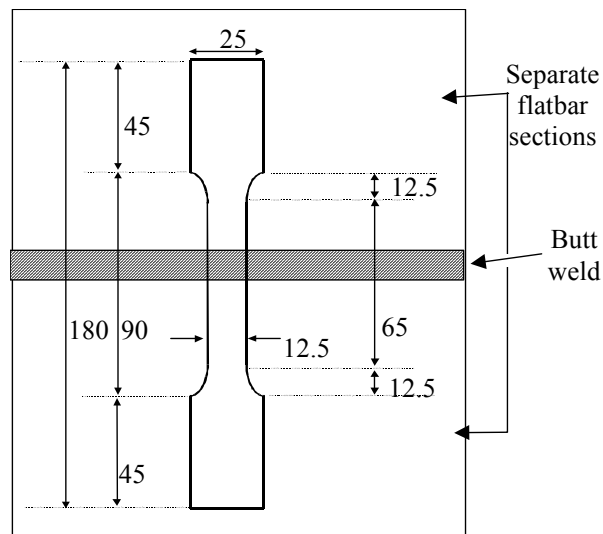


Figure 3: Dimensions and Location of Tensile Coupon within Welded Plate (all dimensions in millimetres)

2.2.4 Test Procedure

Two 150 mm long plates were butt welded together. The sections were either 100 mm wide (3.8 mm thick specimens) or 150 mm wide (8 mm thick sections). Different tests were performed in accordance with AS 2205 (21).

A tensile coupon was cut longitudinally from the plate in accordance with AS 2205.2.1 (22) as shown in Figure 3. The butt weld was located transversely at the middle of the coupon. The tensile coupons were prepared and tested to AS 1391 (23). An extensometer was used to measure strain. The coupons were tested in a 300 kN capacity SINTECH Testing Machine with friction grips to apply the loading. A constant strain rate of approximately $1.0 \times 10^{-3} \text{ s}^{-1}$ was used. In some cases the weld reinforcement was removed so that a completely flat coupon was tested. In the remaining cases the weld reinforcement remained.

The properties of the weld metal itself were obtained by performing an all-weld-metal tensile test to AS 2205.2.2 (24). Properties of the unwelded steel were determined to AS 1391. Macro specimens were also cut from the specimens. However the results of the macro section examination and Vickers Hardness tests are not presented in this paper

2.2.5 Test Results

The values of yield stress and ultimate stress can also be seen in Figures 4 to 7. Since the steel is cold-formed there is no well-defined yield stress, and the yield stress quoted is the dynamic 0.2% proof stress. The term dynamic is used since the stress was determined while the testing machine was loading at a constant rate of stroke.

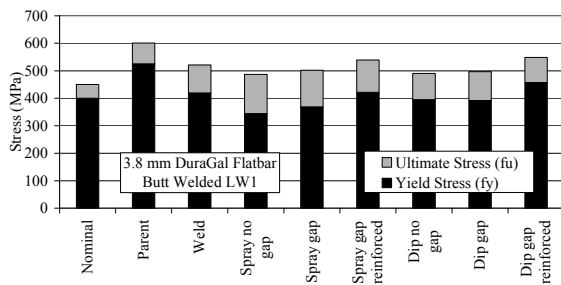


Figure 4: Results - 3.8 mm steel, LW1

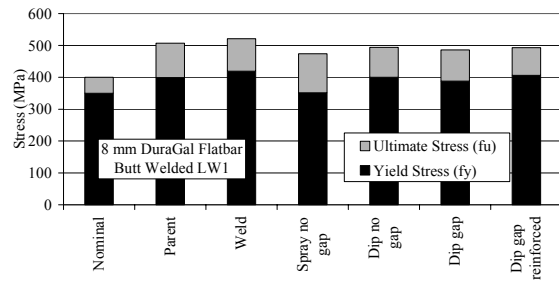


Figure 5: Results - 8 mm steel, LW1

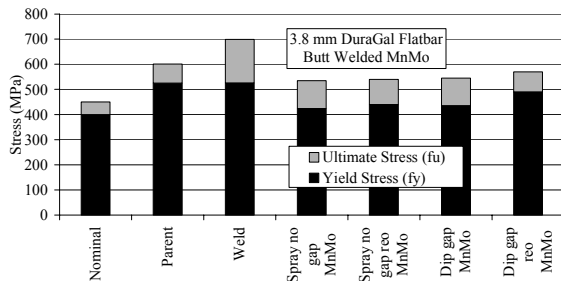


Figure 6: Results - 3.8 mm steel, Mn-Mo

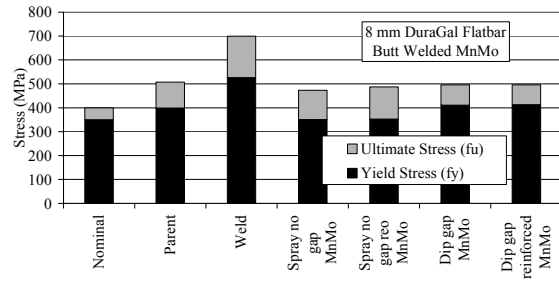


Figure 7: Results - 8 mm steel, Mn-Mo

2.2.6 Discussion

Several observations can be made from the test results.

There is considerably more variation in the results of the 3.8 mm steel compared to the 8.0 mm steel. There is a statistically significant drop in yield and ultimate stresses in the welded 3.8 mm steel, compared to the unwelded material. The change in properties for the 8 mm steel is small.

The measured properties of the unwelded 3.8 mm steel are significantly higher than the nominal properties. This is very common, but as a result, the strength of the 3.8 mm steel is higher than that of the commonly used welding wire, Autocraft LW1. It is usual practice to match the strength of the welding consumable to that of the parent metal. In two instances (3.8 mm, dip

method, LW1), fracture occurred in the weld rather than in the parent metal. For the corresponding case using the spray method (higher heat input), failure occurred in the HAZ, indicating that the higher heat input had reduced the strength of the HAZ by a greater amount compared to the dip method.

Welding produces a greater percentage reduction in strength for the 3.8 mm steel, compared to the 8 mm steel. The 3.8 mm steel is more heavily cold-worked to produce its higher nominal strength compared to the 8 mm steel. Consequently, there is greater scope for strength reduction in the HAZ. This is similar to the G450 steel described in Section 2.1.

The higher strength electrode (Mn-Mo) produced greater capacity in the 3.8 mm sections compared to the LW1 electrode despite a similar heat input. The Mn-Mo electrode had an almost negligible effect on the 8 mm steel, compared to the results of the LW1 electrode.

The higher heat input method of spray transfer compared to dip transfer produces a larger reduction in yield and ultimate stresses.

There are several instances in which the ultimate strength of the welded 3.8 mm specimens drops below the yield stress of the parent material. Consequently, a welded connection of this type would not be able to provide the amount of ductility required for seismic or plastic design applications. The ultimate strength of the welded 8 mm samples did not fall below the yield stress of the parent material.

It should be noted that to utilise the available feedstock most efficiently, BHPSP use virgin strip with yield stress $f_{yn} = 360$ MPa for the 3.8 mm flat bar, and a different strip with yield stress $f_{yn} = 300$ MPa for the 8.0 mm flat bar. This is the most likely cause of the 3.8 mm steel exhibiting strength considerably higher than the nominal properties. It is possible that BHPSP may change the feedstock, so that all DuraGal flatbars are produced from the 300 MPa strip. It is possible that flat bar made from this material will not experience as significant changes in the strength of the HAZ, compared to the product tested.

This paper has considered the preliminary results of the initial stage of this project. Future examinations will consider microhardness determination, macro cross section examination, and fillet welded specimens.

3. CONCLUSIONS

Based on the following test results of the specimens, the following conclusions can be made.

- For sections of G450 sheet steel which were transverse fillet welded to a Grade 450 plate.

The tensile strength of the HAZ in G450 steel is significantly lower than that of the virgin G450 steel for 1.5 mm and 3.0 mm sheets but is generally higher than the nominal tensile strength of 480 MPa. Hence they may still produce reliable designs as discussed by Teh and Hancock (3).

- For sections of cold-formed flats in C450 steel which were butt-welded together using either the dip transfer method or the spray transfer method using either LW1 or Mn-Mo electrode.

There was a small reduction in the yield and ultimate stresses in the welded 8.0 mm steel compared to the unwelded steel. The 3.8 mm samples displayed a more significant drop in yield and ultimate stresses when welded, and the drop in strength was greater when the higher

heat input spray method was used. The 3.8 mm steel had a higher nominal strength than the 8.0 mm steel due to more cold working in the manufacturing process, so it is not unexpected that this steel experienced a greater drop in strength when welded. Significantly, there were some occasions in which the ultimate strength of the welded 3.8 mm specimens dropped below the yield stress of the parent material.

4. REFERENCES

- (1) Standards Australia, 1993, *Sheet Steel and Strip-Hot-Dipped or Aluminium/Zinc-Coated*, AS 1397-1993, Standards Australia, Sydney, Australia.
- (2) Standards Australia, 1991, *Structural Steel Hollow Sections*, AS 1163-1991, Standards Australia, Sydney, Australia.
- (3) Teh, LH and Hancock, 2000, "Strength of Fillet Welded Connections in G450 Sheet Steels," *Research Report* No R802, Department of Civil Engineering, University of Sydney, Sydney, Australia.
- (4) Wilkinson T and Hancock GJ, 2000, "Effect of GMAW on the Mechanical Properties of In-line Galvanised Cold-Formed Steel", IIW Asia Pacific International Congress, Melbourne, November.
- (5) Standards Australia/New Zealand Standards, 1996, *Cold-Formed Steel Structures*, AS/NZS 4600:1996, Standards Australia, Sydney, Australia.
- (6) American Iron and Steel Institute, 1996, *Specification for the Design of Cold-Formed Steel Structural Members*, Washington DC.
- (7) American Welding Society, 1989, *Structural Welding Code: Sheet Steel*, AWS D1.3.
- (8) Pekoz, T and McGuire, W, 1980, "Welding of Sheet Steel", *Proceedings, Fifth International Specialty Conference on Cold-Formed Steel Structures*, St Louis, Missouri, pp 637-662.
- (9) Zhao, X-L and Hancock, GJ, 1996, "Welded Connections in Thin Cold-Formed Rectangular Hollow Sections", *Connections in Steel Structures III*, editors R Bjorhovde, A Colson and R Zandonini, Pergamon, Oxford, pp 89-98.
- (10) Wardenier, J and Koning, CHM, 1975a, "Static Tensile Tests on T-Joints in Structural Hollow Sections", *Research Report*, IBBC-TNO and TH-Delft.
- (11) Wardenier, J and Koning, CHM, 1975b, "Ultimate Static Strength of Welded Lattice Girder Joints in Rectangular Hollow Sections", *Research Report*, IBBC-TNO and TH-Delft.
- (12) Chen, YW, Dunne, D, Norrish, J and Szalla, J, 1990, "Effect of GMA Welding on Microstructure and Mechanical Properties of G550 Sheet Steel", *Research Report*, Department of Materials Engineering, University of Wollongong.
- (13) Rogers, CA and Hancock, GJ, 1997, "Ductility of G550 Sheet Steels in Tension", *Journal of Structural Engineering*, Vol 123, pp1586-1594.
- (14) BHP Structural Pipeline Products, 1999, "Structural Cold Formed Hollow Sections and Profiles", *Technical Information*, BHP Structural and Pipeline Products, Mayfield, Newcastle, Australia.
- (15) Standards Australia, *Steel Structures*, AS 4100-1998, Standards Australia, Sydney, Australia.
- (16) Standards Australia/Standards New Zealand, *Structural Plates – Hot-rolled Plates and Slabs*, AS/NZS 3678:1996, Standards Australia, Sydney, Australia.
- (17) Standards Australia/Standards New Zealand, 1996, *Welding – Electrodes – Gas Metal Arc – Ferritic Steel Electrodes*, AS/NZS 2717:1996, Standards Australia, Sydney, Australia.

- (18) Standards Australia/Standards New Zealand, 1995, *Structural Steel Welding – Welding of Steel Structures*, Amendment No 1 to AS/NZS 1554.1:1995, Standards Australia, Sydney, Australia.
- (19) Welding Technology Institute, 2000, *WeldPrint, Build 2.70EN*, University of Sydney, Australia.
- (20) CIGWELD, (1993), *Welding Consumable Guide*, Part No. WCGUIDE, Preston, Victoria, Australia.
- (21) Standards Australia, 1997, *Methods for Destructive Testing of Welds in Metal; Method 1: General Requirements for Tests*, AS 2205.1, Standards Australia, Sydney, Australia.
- (22) Standards Australia, 1997, *Methods for Destructive Testing of Welds in Metal; Method 2.1: Transverse Butt Tensile Test*, AS 2205.2.1, Standards Australia, Sydney, Australia.
- (23) Standards Australia, 1991, *Methods for Tensile Testing of Metals*, AS 1391, Standards Australia, Sydney, Australia.
- (24) Standards Australia, 1997, *Methods for Destructive Testing of Welds in Metal; Method 2.2: All-weld-metal Tensile Test*, AS 2205.2.2 Standards Australia, Sydney, Australia.

BRACING CONNECTIONS TO RECTANGULAR HSS COLUMNS

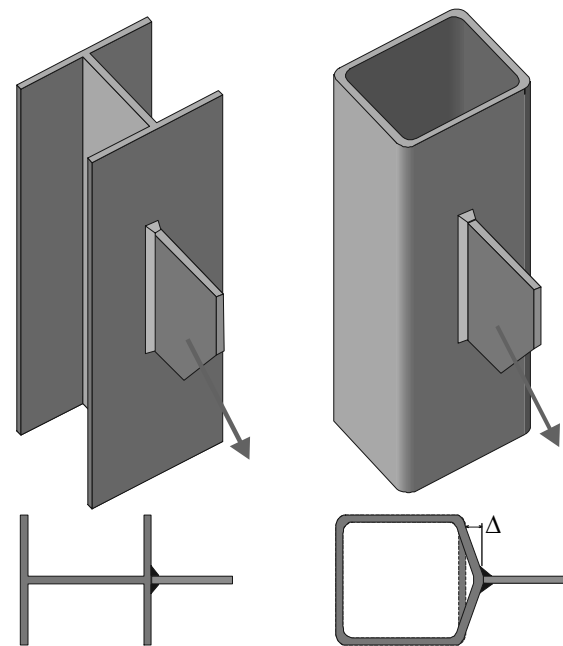
N. KOSTESKI¹ AND J.A. PACKER²

ABSTRACT: Bracing members are frequently site-bolted to a plate welded longitudinally to a column member. For Hollow Structural Section (HSS) columns, and particularly for square or rectangular HSS members, this mode of application produces a very flexible connection with the resistance typically governed by a deformation limit. Many structural designers are unfamiliar with this type of connection behavior and corresponding design models. This paper presents an overview of recent research at the University of Toronto on this connection type and related stiffened connections.

INTRODUCTION

In recent years, the use of Rectangular Hollow Sections (RHS) as columns has become increasingly popular. In many instances, RHS column members are replacing customary I-section members due to their superior column performance. In turn, welded longitudinal plates have been a traditional and convenient method for the connection of brace members and other attachments to I-section, and now RHS, columns. Figure 1 shows these two cases of longitudinal plate connections. For the case of the I-section column, the plate is welded along the center of the column flange so the load from the plate is transferred to the web of the column directly. The situation is different for the case of the RHS column because the load from the brace plate must be carried indirectly through the flexible column face into the adjacent column webs. A conventional longitudinal plate-to-RHS member connection tends to result in excessive distortion or plastification of the RHS connecting face. Such a connection results in a low design resistance that is governed by the formation of a yield line mechanism and this design resistance ought to satisfy an ultimate deformation limit and a serviceability deformation limit for the RHS connecting face. An extensive experimental and analytical study on longitudinal plate-to-RHS connections by Cao et al. (1) has resulted in published limit states design procedures for these types of connections.

In an effort to reduce the inherent flexibility of longitudinal plate connections, stiffening plates or structural tees are sometimes welded to the RHS connecting face. Also, a "through-plate" connection can be used to potentially double the strength of a standard longitudinal plate connection. Another method of reducing the out-of-plane deformation of the RHS connecting face involves simply welding the connecting plate transversely to the RHS member axis. Figure 2 shows these "alternative" plate connections.



(a) Plate to I-section

(b) Plate-to-RHS

Figure 1: Longitudinal brace plate connections

¹Doctoral Candidate, Dept. of Civil Engineering, Univ. of Toronto.

²Prof., Dept. of Civ. Engrg., Univ. of Toronto, 35 St. George St., Toronto, ON, M5S 1A4 Canada, E-mail: packer@civ.utoronto.ca

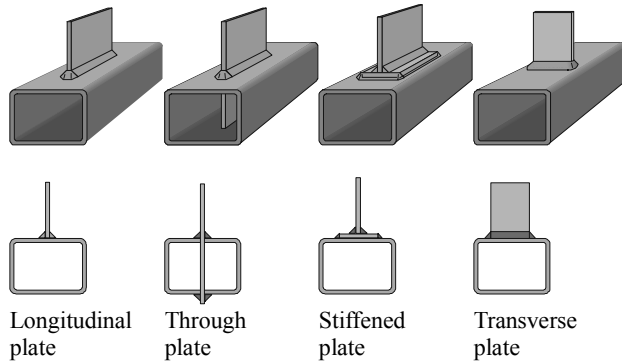


Figure 2: Branch plate to RHS member connection types

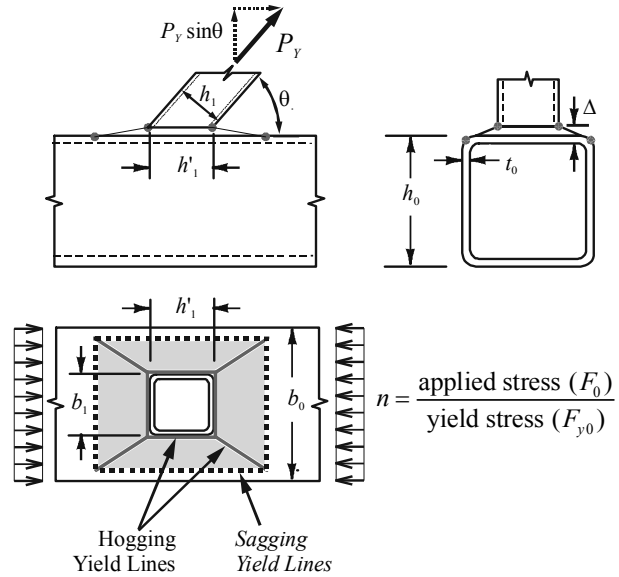


Fig. 3: Yield Line Pattern for an RHS X-Connection

ANALYTICAL MODELS

The three principal failure modes for a welded branch plate connection are failure of the branch plate, failure of the weld, and failure of the RHS face. Relatively simple criteria for the branch plate thickness and the weld size can be applied to the design of these two components. Failure of the RHS face is usually the weakest link among these three failure modes. The focus of the experimental program was the strength and behavior of the critical third failure mode: failure of the RHS connecting face.

General Yielding of the RHS Connecting Face

The yield line method of analysis has been used successfully for estimating the strength of different RHS connections due to development of yield line mechanisms (or plastification) of the connecting face of the main member. Figure 3 shows a general case of an RHS connection. The yield load of a 90° connection without any axial load present in the chord was first derived by Jubb and Redwood (2). This calculated yield load has been incorporated in the design formulae of the International Institute of Welding (3) and the design guide of Packer and Henderson (4) for T, Y and X connections between RHS members and connections between RHS members and plates. A recent analysis by Cao et al. (5) has accounted for non-90° connections as well as the influence of an axial load present in the chord member resulting in Equation (1). The RHS wall thickness and weld size are considered to determine the "effective" connection dimensions, as recommended by Davies and Packer (6).

$$P_Y \sin \theta = \frac{F_{y0} t_0^2}{(1 - \beta')} \left(2 \frac{h'_1}{b'_0} + 4 \sqrt{1 - \beta'} \sqrt{1 - n^2} \right) \quad (1)$$

Ultimate Deformation and Serviceability Deformation Limit States

The notion of a limit on deformation has been proposed numerous times for structures that do not show a pronounced peak load. In conjunction with hollow section connections, which are known to be generally very flexible, ultimate deformation limits, at which the connection is deemed to have "failed", have been suggested by Yura et al. (7), Korol and Mirza (8) and Lu et al. (9). In the latter an ultimate deformation for

the RHS face of 3% of the member width ($0.03b_0$) was proposed. The load corresponding to this deflection compared reasonably well with the connection peak load in many RHS connections which did exhibit a pronounced peak load. Furthermore, for transverse plate-to-RHS connections the $0.03b_0$ deformation level was close to the points where the load-displacement curves crossed each other, for various RHS wall slenderness values. The suitability of this ultimate deformation limit for a variety of RHS connections was investigated by Lu et al. (9) and Zhao (10) and it was subsequently adopted by the International Institute of Welding Subcommittee XV-E.

For RHS connections a connecting face deflection of 1% of the main member width ($0.01b_0$) has generally been used as a serviceability deformation limit, as given the International Institute of Welding (3). For this connecting face deformation of $0.01b_0$, one can obtain a corresponding load in a plate branch member ($P_{s,1\%}$). Similarly, a branch plate load can also be obtained for the "ultimate" load level ($P_{u,3\%}$) corresponding to a connecting face deformation of $0.03b_0$. Figure 4 shows the load-displacement curves for a series of 12 experimental test specimens from Kostasiki and Packer (11). The ultimate deformation limit and the serviceability deformation limit have been used to define the "strength" of these connections. Kostasiki and Packer (11) documents that the predicted yield load (P_Y) by Equation (1) corresponds well (avg. $P_Y/P_{u,3\%} = 0.91$) with the notional 3% b_0 ultimate deformation limit ($P_{u,3\%}$) load level. Thus, the calculable connection yield load (P_Y) can be used in lieu of the 3% b_0 ultimate deformation limit ($P_{u,3\%}$) load level.

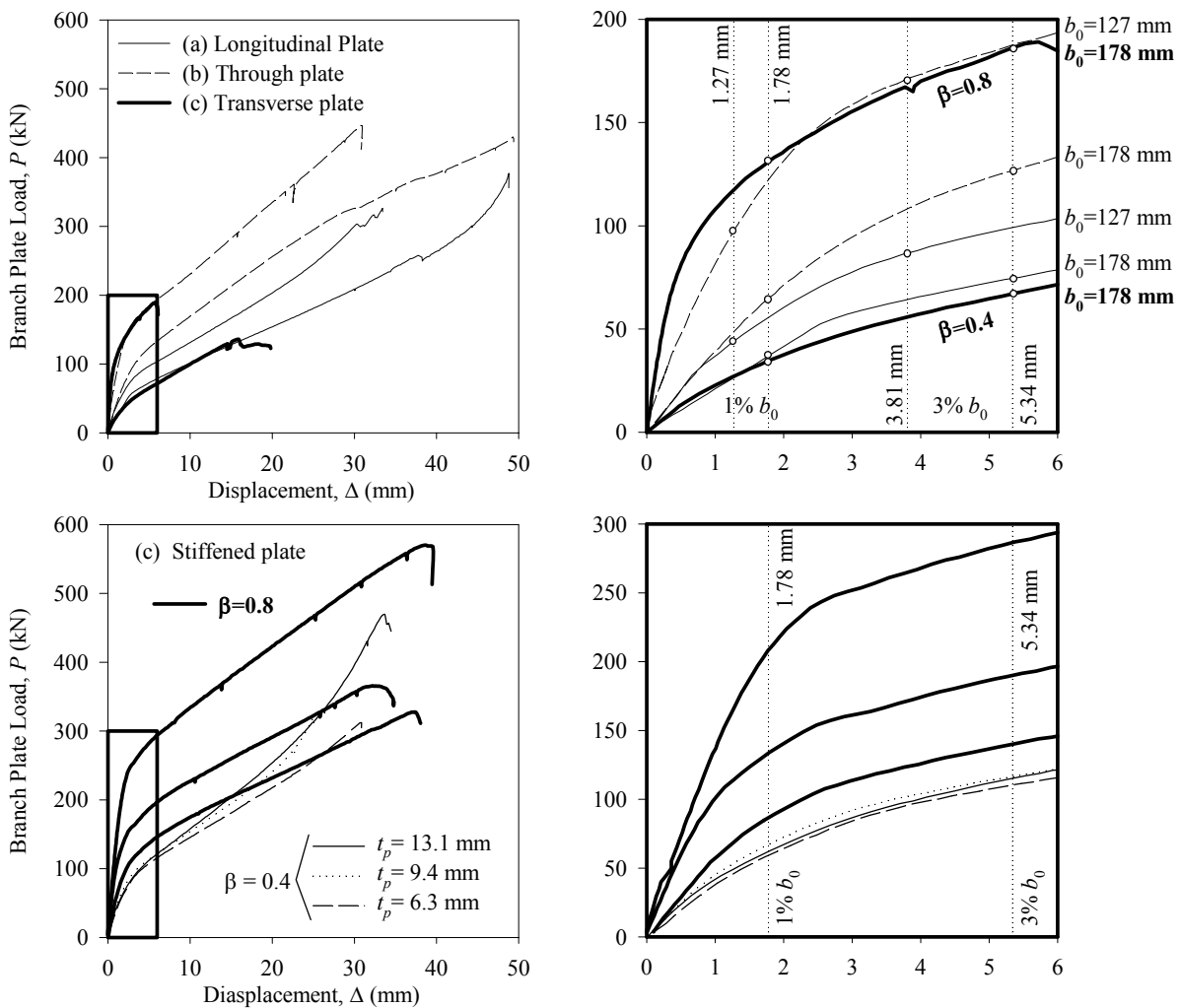


Figure 4: Load-Displacement Curves

Governing Strength or Serviceability Condition

Based on a ratio of factored to unfactored loads of 1.5, Lu et al. (9) suggested using the ratio $P_{u,3\%} \div P_{s,1\%}$ to decide whether the ultimate deformation limit state or the serviceability deformation limit state governs as demonstrated by Equation (2).

$$\text{for, } \frac{P_{u,3\%}}{P_{s,1\%}} > 1.5, \text{ serviceability limit governs} \quad (2a)$$

$$\text{for, } \frac{P_{u,3\%}}{P_{s,1\%}} \leq 1.5, \text{ ultimate limit governs} \quad (2b)$$

In our case, we have replaced the notional ($P_{u,3\%}$) ultimate deformation limit state with an actual connection yield load limit state (P_Y) calculated using Equation (1).

Zhao (10) proposed that the governing deformation limit states expressed in Equation (2) could be predicted by the geometric properties of the connection using Equation (3).

$$\beta < 0.6 \text{ and } \frac{b_0}{t_0} > 15, \text{ serviceability governs} \quad (3a)$$

$$\beta \geq 0.6 \text{ or } \frac{b_0}{t_0} \leq 15, \text{ strength governs} \quad (3b)$$

FEM RESULTS

EXPERIMENTAL RESULTS

from Koteski and Packer (11)

Longitudinal plate		Longitudinal plate	
Cao et. al. (1)		● $b_0/t_0=37.1$	
■ $b_0/t_0=23.4$		○ $b_0/t_0=26.5$	
□ $b_0/t_0=15.6$			
Stiffened plate		Through plate	
Koteski and Packer (15)		▼ $b_0/t_0=37.1$	
● $b_0/t_0=48.0$		▽ $b_0/t_0=26.5$	
○ $b_0/t_0=40.0$			
▼ $b_0/t_0=32.0$			
▽ $b_0/t_0=28.0$			
■ $b_0/t_0=20.0$			
□ $b_0/t_0=16.1$			
◆ $b_0/t_0=14.0$			
◇ $b_0/t_0=12.0$			
		Stiffened plate	
		◆ $b_0/t_0=37.1$	
		Transverse Plate	
		+ $b_0/t_0=37.1$	

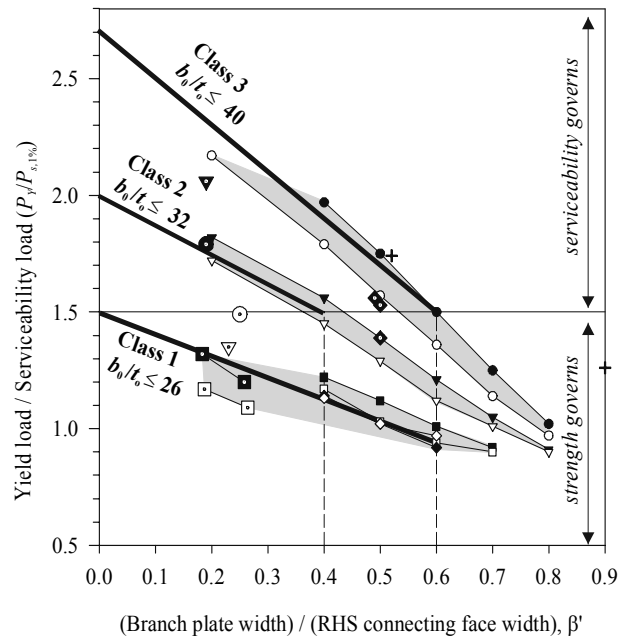


Fig. 5: Governing strength versus serviceability

Figure 5 is a comprehensive plot of experimental test results and FEM-generated numerical data showing the governing strength or serviceability limit state for various connection types. In Figure 5 the calculable connection yield load (P_Y) is used to replace the notional 3% b_0 ultimate deformation limit ($P_{u,3\%}$) load level. The actual governing limit states of branch plate to RHS connections can then be compared with the recommended limit state partitions set forth by Lu et al. (9) and Zhao (10). The ratio of factored to unfactored loads of 1.5 recommended by Lu et al. (9) was plotted as a horizontal reference line using the (yield load /serviceability load) axis in Figure 5. The region above this reference line represents a governing serviceability condition ($P_{s,1\%}$). Likewise, the region below this line represents a governing strength condition (P_Y).

The governing strength or serviceability condition depends on the connection parameters $\beta(=b_1/b_0)$ [or more accurately $\beta'(=b'_1/b'_0)$] and $2\gamma_0(=b_0/t_0)$ [or more accurately $2\gamma'_0(=b'_0/t_0)$]. In general, at high β values the connection can be expected to be stiff and the serviceability limit will not be expected to govern. Conversely, at high b_0/t_0 values, the RHS chord face is very flexible and the serviceability limit will tend to govern. A range of conditions between these two extremes must now be categorized in a rational fashion. Figure 5 shows that for $\beta' \geq 0.6$ the strength limit governs. The $\beta' \geq 0.6$ governing limit state generally agrees with that proposed by Zhao (10) in Equation (3b) but the $b_0/t_0 \leq 15$ limit proposed by Zhao is too conservative. An alternative method of categorising the b_0/t_0 limit would be to base it on the "class of section". For example, the Canadian CAN/CSA-S16.1-94 limits (12) for Class 1, 2, and 3 RHS sections are listed in Table 1.

Table 1: CAN/CSA-S16.1-94 RHS Classes

Class 1	$\frac{b_{flat}}{t_0} \leq \frac{420}{\sqrt{F_y}}$	$\frac{b_0}{t_0} \leq 26$
Class 2	$\frac{b_{flat}}{t_0} \leq \frac{525}{\sqrt{F_y}}$	$\frac{b_0}{t_0} \leq 32$
Class 3	$\frac{b_{flat}}{t_0} \leq \frac{670}{\sqrt{F_y}}$	$\frac{b_0}{t_0} \leq 40$
note: using $b_{flat}=b_0-4t_0$ and $F_y=350$ MPa		

When the strength limit state governs, the connection capacity (P_Y) can be calculated using Equation (1). However, if the serviceability limit state governs, the connection yield load (P_Y) must be reduced to obtain the connection serviceability load ($P_{s,1\%}$). $P_{s,1\%}$ can now be related to P_Y by using the recommended Class 1, Class 2, and Class 3 design lines shown in Figure 5. Recognize that the serviceability limit ($P_{s,1\%}$) governs the deformation of the connection and not the strength (safety). Therefore, the recommended serviceability load design lines shown in Figure 5 are plotted through the existing data without any undue conservatism. The relationship between the connection yield load (P_Y) and the connection serviceability load ($P_{s,1\%}$) for Class 1, 2, and 3 sections takes the form:

$$\text{Class 1} \left(\frac{b_0}{t_0} \leq 26 \right) \quad P_{s,1\%} = \frac{P_Y}{1.5 - 0.9\beta'} \quad (4a)$$

$$\text{Class 2} \left(\frac{b_0}{t_0} \leq 32 \right) \quad P_{s,1\%} = \frac{P_Y}{2.0 - 1.25\beta'} \quad (4b)$$

$$\text{Class 3} \left(\frac{b_0}{t_0} \leq 40 \right) \quad P_{s,1\%} = \frac{P_Y}{2.7 - 2\beta'} \quad (4c)$$

Now, both the connection yield load (P_Y calculated using Equation 1) and the serviceability load ($P_{s,1\%}$ using Equation 4) of a branch plate to RHS member connection can be calculated. The governing strength or serviceability limit condition is determined using Limit States Design (LSD) or Load and Resistance Factored Design (LRFD) principles. The calculated yield load of the connection (P_Y) is compared with the total applied factored load (P_f). The calculated serviceability load of the connection ($P_{s,1\%}$) is compared with the total specified unfactored load (P). Thus, the governing strength or serviceability condition is no longer based on a recommended ratio of 1.5 for the factored to the

unfactored load level. Instead, the strength or serviceability governing condition is determined using the actual factored and unfactored loads. The ratio of P_Y to P_f (Eq. 5a) determines the extent to which the yield load condition has been met. The ratio of $P_{s,1\%}$ to P (Eq. 5b) determines the extent to which the serviceability condition has been met.

$$\text{Ultimate Load Ratio} = \frac{P_Y}{P_f} \quad (5a) \qquad \text{Serviceability Load Ratio} = \frac{P_{s,1\%}}{P} \quad (5b)$$

The lower of the two load ratios determines whether the strength or serviceability condition governs. For design purposes, both ratios must be ≥ 1.0 to satisfy both the strength and serviceability conditions (limit states). The "design loop" would consist of initially designing the connection for the strength condition (P_Y) and then checking to see if the serviceability condition ($P_{s,1\%}$) is met, as is customary with a Limit States Design (LSD) procedure.

OVERALL DESIGN OF BRANCH PLATE TO RHS MEMBER CONNECTIONS

The design and fabrication of connections for RHS members has often been perceived as complicated and expensive. Rational design methods are needed to encompass, and wherever possible to consolidate, the multitude of connections available to the designer. The yield line method has been incorporated in the design formulae of the International Institute of Welding (3), the design guide of Packer and Henderson (5), and the AISC HSS Connections Manual (13), for T, Y and X connections between RHS members and connections between RHS members and plates.

A recent analysis by Cao et al. (5) has accounted for the influence of an axial load present in the main (column) member resulting in Equation (1) and is recommended to be adopted. The results of the experimental program by Kostasiki and Packer (11) indicate that the "alternative" longitudinal through plate, stiffened longitudinal plate, and transverse plate-to-RHS member connections can be grouped under the general case of an RHS T-connection and designed using Equation (1).

Longitudinal and Through Plate Connections

The calculated yield load (P_Y using Equation 1) of a general RHS T-connection is based on an idealized yield line pattern forming around the footprint of the connecting branch plate causing plastification of the connecting RHS chord face. This represents a simplified but effective isolation and approximation of the actual plastification mechanism. Within these limits of idealisation, a through plate connection can be expected to have approximately double the strength of a single plate connection by causing plastification of two RHS chord (column) faces rather than one. Experimental results from Kostasiki and Packer (11) confirm that a through plate connection can be reasonably approximated as having double the strength of a corresponding single plate connection for design purposes.

Transverse Plate Connections

A transverse branch plate to RHS member connection is significantly stiffer (due to a higher β ratio) and hence has a higher design resistance than a longitudinally-oriented branch plate. However, aside from the behavior of the RHS connecting face, the design strength of transverse plate connections may also be governed by an "effective width" criterion applied to the branch plate, which accommodates the highly non-uniform stress distribution in the plate. Moreover, it has been shown by de Koning and Wardenier (14) that the branch plate effective width criterion is the governing limit state for transverse plate connections up to $\beta \leq 0.85$.

Stiffened Longitudinal Plate Connections

A stiffened longitudinal branch plate connection can ultimately achieve a much higher design resistance equivalent to the enlarged "footprint" of the stiffening plate as opposed to the modest footprint of the branch plate itself. In order to achieve this load, the stiffening plate must be "effectively-rigid" with respect to the RHS connecting face such that a plastification mechanism does not occur in the stiffening plate itself. In summary, the branch plate connection strength increases with an increasing stiffening plate thickness until an upper bound plate thickness is reached. Beyond this thickness, the stiffening plate is essentially "rigid" (i.e. achieving a 100% connection efficiency). For design purposes, a more practical "effectively-rigid" stiffening plate thickness was chosen by Kostas and Packer (15) to be a 95% connection efficiency threshold.

Figure 6 presents the results of a comprehensive FEM study by Kostas and Packer (15) related to the minimum required "effectively-rigid" stiffening plate thickness to achieve a 95% connection efficiency threshold. The "best-fit" exponential curve in Figure 6 is an empirical equation used to determine the minimum required "effectively-rigid" stiffening plate thickness $t_{p(\min)}$ to satisfy both the (P_Y) strength condition and the ($P_{s,1\%}$) serviceability condition. The ratio of the stiffening plate thickness $t_{p(\min)}$ to the RHS connecting face wall thickness (t_0) is a function of the "unrestrained" stiffening plate width (b_1^*) to the RHS width (b'_0) ratio (β^*). The "unrestrained" stiffening plate width (b_1^*) is equal to the nominal stiffening plate width (b_1) minus the branch plate width (t_b) and both branch plate welds ($2w$).

Practical Limits of Applicability

Design equations for HSS connections are often governed by limits of applicability related to the two dimensionless parameters $2\gamma_0 (= b_0/t_0)$ and $\beta (= b_1/b_0)$. Yield line mechanism-based formulas are usually valid from low to moderately high β ratios. Different modes of failure such as punching shear or local failure of the HSS side walls tend to govern at higher β ratios approaching unity. Likewise the governing strength or serviceability limit state condition is also generally related to the dimensionless parameters $2\gamma_0$ and β .

Practical limits of applicability also arise from a fabrication standpoint. In general, it is preferred to connect to the "flat width" ($b_{flat\ width}$) of an RHS member. Welding in the corner region of an RHS member is more difficult than welding along a preferred flat surface and therefore introduces additional fabrication costs. Also, the corners of a cold-formed RHS member represent regions of lower ductility. Notwithstanding an increased cost of fabrication, welding in this region of lower ductility may undermine

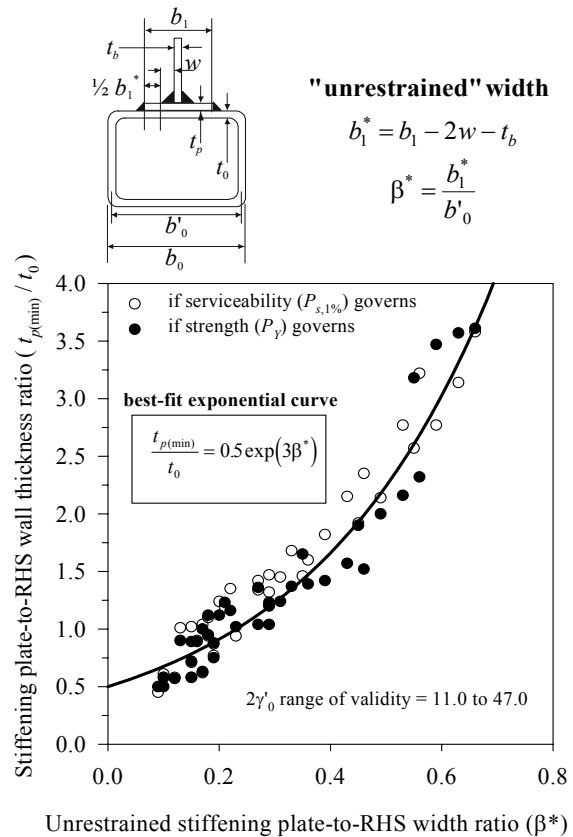


Figure 6: Required stiffening plate thickness

the integrity of the welded joint and may lead to premature weld/base metal fractures. Figure 7 shows the practical limits of applicability for branch plate to RHS member connections.

Referring to Figure 7, longitudinal and through plate connections are characterized by low β' ratios (≈ 0.1 to 0.25). Next, stiffened plate connections may be used to increase the β' ratio up until $\beta'=0.8$. From Equation (1) it can be seen that the strength of the connection increases as β' increases. For $\beta' > 0.8$ the strength of the connection increases rapidly and a prohibitively thick and impractical stiffening plate would be required. Also, as β' approaches unity the strength of the RHS connecting face tends towards infinity and punching shear around the branch, or local failure of the RHS side wall becomes the critical failure mode for $\beta \geq 0.85$ [Packer and Henderson (4)]. Hence, in the upper range of $\beta' > 0.8$, a transverse branch plate connection is recommended since it is much stiffer.

Figure 7 also shows the likely governing strength or serviceability regions for a common ratio of a factored to unfactored load level of 1.5. The actual strength or serviceability governing condition is calculated using the actual factored and unfactored loads and is explicitly determined using a Limit States Design (LSD) procedure [Kosteski and Packer (15)]. Other failure modes relating to a general T-type connection must also be checked. Design criteria for punching shear, chord side wall failure, branch plate effective width, etc., can be found in current HSS design manuals and specifications.

Connection Costs

A rational and efficient design of RHS connections must be coupled with economical fabrication. A study of the relative costs of shear connections to RHS members was presented by Sherman (16) and the applicable results are listed in Table 2. The simple "shear tab" is one of the most economical connection types. A shear tab is oriented parallel to the axis of a column in order to frame directly into the web of a connecting beam. However, when a simple shear tab is used as a branch plate for an RHS member, the tab (or plate) may be oriented

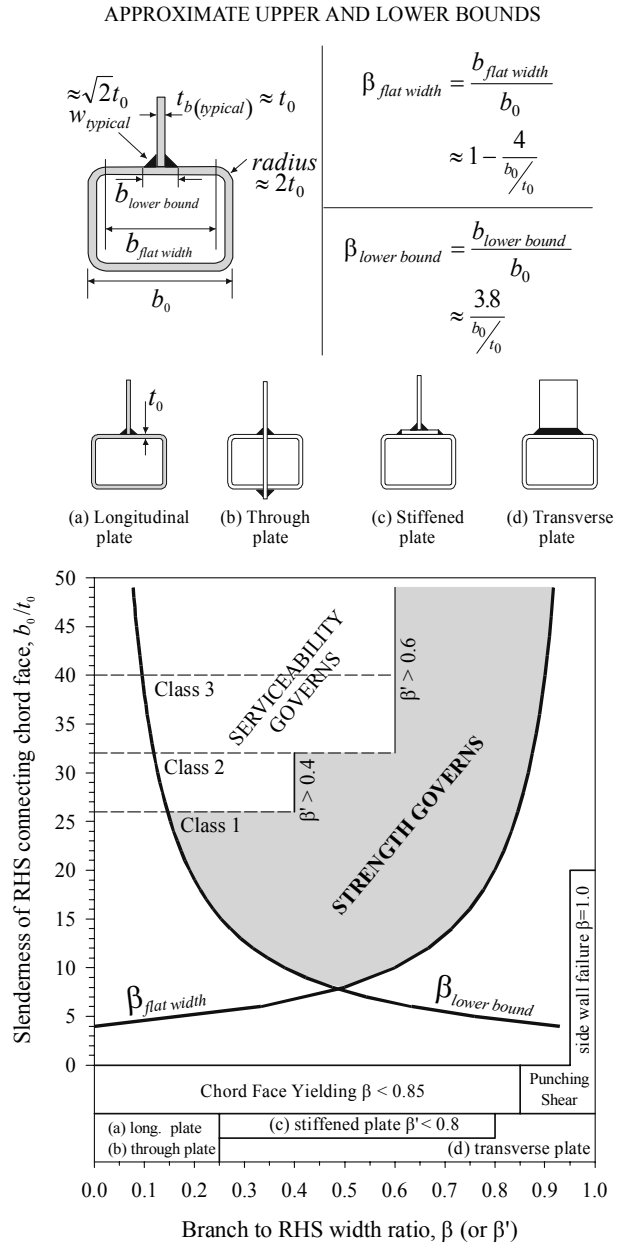


Figure 7: Practical limits of applicability

Table 2: Relative Connection Costs adapted from Sherman (16)

Shear Connection Type	Equivalent Brace Plate Connection Type	Relative Cost
Single Angle, L-shaped Welds	n/a	1.00
Shear Tab	Longitudinal Plate, Transverse Plate	1.05
Tee, Vertical Welds	Stiffened Longitudinal Plate	1.50
Through-Plate	Through-Plate	2.25

either longitudinally or transversely. A single longitudinal plate can accommodate multiple connecting branches (e.g. a KT-type connection) framing along the axis of an RHS member. However, three separate transverse plates would be required to connect each branch of a longitudinally-oriented KT-type connection. Thus, a single longitudinally-oriented branch plate is to be preferred for multiple branches (in one plane) framing along the axis of an RHS member. A transverse branch plate-to-RHS member connection, on the other hand, is significantly stiffer and hence has a much higher design resistance than a longitudinally-oriented branch plate but is more suitable for a single branch framing into an RHS member.

A stiffened longitudinal plate is often necessary to increase the design capacity of a longitudinally-oriented branch plate. A through plate connection will also result in a higher design capacity but is considerably more expensive than a stiffened branch plate. Also, a through plate connection is limited to "doubling" the strength of a longitudinal plate connection. Increasing the effective width of a longitudinal branch plate by using a stiffening plate is a far more effective method of increasing, doubling, or more than doubling the design resistance of a longitudinal plate connection.

CONCLUSIONS

Four different welded connection types, namely longitudinal plate, through plate, transverse plate, and stiffened plate to Rectangular Hollow Section (RHS) members have been studied experimentally, by means of tests on 22 isolated connections. This data was supplemented by yield line analysis plus comprehensive numerical modeling to enable a broader parametric study to be performed. The latter involved non-linear Finite Element Analysis using 20-noded solid elements with realistic modeling of RHS corner radii and weld geometry. The results of the study indicate that these connection types can be grouped under the general case of an RHS T-connection and designed as such. A simplified design approach has been presented to consolidate the various branch plate to RHS member connection types. This design philosophy accounts for a strength and a serviceability limit state.

ACKNOWLEDGEMENTS

Financial support for this project was provided by the Steel Structures Education Foundation, the Steel Tube Institute of North America, the Comité International pour le Développement et l'Étude de la Construction Tubulaire (CIDECT), the Natural Sciences and Engineering Research Council of Canada (NSERC), and the Canadian Institute of Steel Construction (CISC) through a Kellerman Fellowship.

NOTATION

- b_0, b'_0 = outside width of main member, effective width ($= b_0 - t_0$)
- b_1, b'_1, b_1^* = outside width of connecting member, effective width ($= b_1 + 2w$),
unrestrained width ($= b_1 - 2w - t_b$)
- $b_{flat\ width}$ = flat width of RHS member face
- $b_{lower\ bound}$ = approximate minimum practical connection width
- F_0 = main member axial stress
- F_y, F_{y0} = yield stress of material, yield stress of main RHS member
- h_1, h'_1 = outside depth or length of connecting member, effective outside depth or length of
connecting member ($= h_1/\sin\theta + 2w$)
- n = main member "preload" ratio ($= F_0/F_{y0}$)
- P, P_f = specified load, factored load
- P_Y = yield load of connection
- $P_{s,1\%}$ = 1% b_0 serviceability deformation limit connection load level
- $P_{u,3\%}$ = 3% b_0 ultimate deformation limit connection load level

$t_0, t_p, t_{p(\min)}$ = wall thickness of RHS main member, thickness of stiffening plate, minimum required
 "effectively-rigid" stiffening plate thickness
 $t_b, t_{b(\text{typical})}$ = branch plate width, typical branch plate width
 w, w_{typical} = weld size (leg length), typical weld size (leg length)
 β, β', β^* = nominal beta ratio ($= b_1/b_0$), effective beta ratio ($= b'_1/b'_0$), unrestrained beta ratio ($= b_1^*/b'_0$)
 $\beta_{\text{flat width}}$ = flat width beta ratio ($= b_{\text{flat width}}/b_0$)
 $\beta_{\text{lower bound}}$ = approx. min. beta ratio ($= b_{\text{lower bound}}/b_0$)
 $2\gamma_0, 2\gamma'_0$ = width to thickness ratio of main RHS member ($= b_0/t_0, b'_0/t_0$)
 θ = angle of inclination with respect to RHS member axis

REFERENCES

- (1) Cao, J.J., Packer, J.A., Kostaski, N. (1998). "Design guidelines for longitudinal plate to HSS connections," *Journal of Structural Engineering*, ASCE, Vol.124, No.7, pp.784-791.
- (2) Jubb, J. E. M. and Redwood, R. G. (1966). "Design of joints to box sections." *Conference on Industrial Building and the Structural Engineer*, Institution of Structural Engineers, UK.
- (3) International Institute of Welding (IIW). (1989). "Design recommendations for hollow section joints - predominantly statically loaded." *IIW Doc. XV-701-89*, 2nd ed, IIW Subcommittee XV-E, Helsinki, Finland.
- (4) Packer, J. A. and Henderson, J. E. (1997). "*Hollow structural section connections and trusses - A design guide*", 2nd Edition, Canadian Institute of Steel Construction, Toronto, Canada.
- (5) Cao, J. J., Packer, J. A. and Yang, G. J. (1998). "Yield line analysis of RHS connections with axial loads." *J. Constructional Steel Research*, Vol. 48, pp. 1-25.
- (6) Davies, G. and Packer, J. A. (1982). "Predicting the strength of branch plate - RHS connections for punching shear." *Canadian Journal of Civil Engineering*, Vol. 9, pp. 458-467.
- (7) Yura, J. A., Zettlemoyer, N. and Edwards, I. F. (1980). "Ultimate capacity equations for tubular joints." *Proc. Offshore Technology Conference*, Vol. 1, Paper No. 3690.
- (8) Korol, R. M. and Mirza, F. A. (1982). "Finite element analysis of RHS T-joints." *Journal of the Structural Division*, ASCE, Vol. 108, No. 9, pp. 2081-2098.
- (9) Lu, L. H., de Winkel, G. D., Yu, Y. and Wardenier, J. (1994). "Deformation limit for the ultimate strength of hollow section joints." *Proc. Sixth International Symposium on Tubular Structures*, Melbourne, Australia, pp. 341-347.
- (10) Zhao, X. L. (1996). "Verification of the deformation limit for T-joints in cold-formed RHS sections." *Proc. Seventh International Symposium on Tubular Structures*, Miskolc, Hungary, pp. 213-220.
- (11) Kostaski, N. and Packer, J.A. (2001). "Experimental examination of branch plate to RHS member connection types." *Proc. Ninth International Symposium on Tubular Structures*, Düsseldorf, Germany.
- (12) CAN/CSA-S16.1-94 (1994). "Limit states design of steel structures," Canadian Standards Association, Rexdale, Canada.
- (13) AISC (1997). "Hollow structural section connections manual," AISC, Chicago, Illinois.
- (14) de Koning, C. H. M. and Wardenier, J. (1985). "The static strength of welded joints between structural hollow sections or between structural hollow sections and H-sections. Part 2: joints between rectangular hollow sections." *Stevin Report 6-84-19*, Delft University of Technology, Delft, The Netherlands.
- (15) Kostaski, N. and Packer, J.A. (2001). "FEM evaluation of stiffened branch plate to RHS member connections." *Proc. 9th International Symposium on Tubular Structures*, Düsseldorf, Germany.
- (16) Sherman, D. R. (1996). "Designing with structural tubing." *Engineering Journal*, AISC, Vol. 33, No. 3, pp. 101-109.

PERFORMANCE OF JOINTS IN STEEL STORAGE PALLET RACKS

Nadia Baldassino⁽¹⁾, Claudio Bernuzzi⁽²⁾, Riccardo Zandonini⁽¹⁾

⁽¹⁾ Department of Mechanical and Structural Engineering, University of Trento (I)

⁽²⁾ Department of Structural Engineering, Politecnico di Milano (I)

ABSTRACT

Performance of pallet racking systems depends upon the efficiency of beam-end-connectors, which provide, together with column bases, sources of stiffness for down-aisle stability. Knowledge of the actual joint behaviour under static and seismic loading is of fundamental importance for a suitable definition of simplified moment-rotation joint relationships to use into design of semi-continuous frames.

This paper presents the preliminary results of research activities currently in progress in Italy focused on static and seismic behaviour of pallet racking beam-to-column joints.

1. INTRODUCTION

Steel storage pallet racks, which are usually manufactured from cold formed steel members, can be considered typical three-dimensional framed systems (Figure 1). Despite this fact, the design of pallet racks is quite complex, due to the particular geometry of their components. With reference to the European practice, generally beams are realised by means of boxed cross-section members and columns usually contain holes and/or perforations at regular intervals to allow beams and bracings to be attached without bolts or welds (Figure 2).

The behaviour of the perforated columns, which are in many cases thin-walled members, is affected by different buckling modes (local, distortional and global) as well as by their mutual interactions (Hancock, (1); Davies and Jiang, (2)). Furthermore, as shown in figure 1, bracing systems are generally placed only in the cross-aisle direction. The need to organise racking systems in such a way that the product is efficiently stored and sufficiently accessible, hampers in fact the presence of bracing systems in the down-aisle direction.

The model of semi-continuous sway frames (i.e., frames with semi-rigid joints (ECCS (3))), should hence be adopted for structural analysis of pallets racks, taking into account that the response of both beam-to-column and base-plate joints is typically non linear and, in addition, the performance

of base-plate connections depends significantly on the level of the axial load (Godley (4); Markazi et al. (5)).

The performance of pallet racking systems significantly depends upon the efficiency of the beam-end-connectors, which provide support to the beams and are, together with column bases, the sole sources of stiffness for the down-aisle stability.

Knowledge of the actual joint behaviour is hence of fundamental importance for a suitable definition of simplified moment-rotation ($M-\Phi$) joint relationships to use in the design analysis of pallet racks systems.

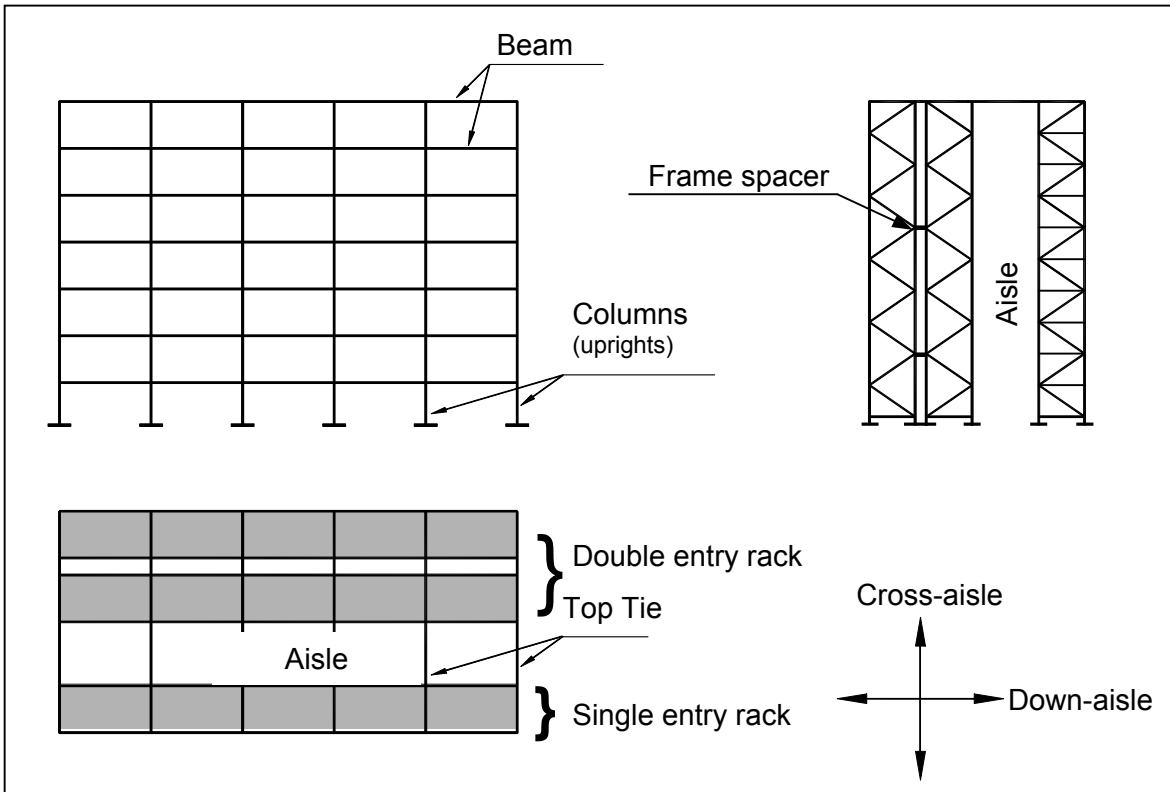


Figure1: Elevation and plan view of steel storage pallet racks.

Due to the great number of types and different geometry of the key rack components, pure theoretical approaches for rack design are not currently available.

Recent design standards for steel storage racks (RAL (6), AS (7), RMI (8), FEM (9)) require, specific tests to evaluate the performance of members as well as of joints in order to understand and to quantify main factors affecting the behaviour of the considered elements and, as a consequence, the response of the whole frame.

The experimental procedures proposed by these design standards, are mainly focused on the knowledge of the static behaviour of pallet racks.

As to racks in seismic zone, only the RMI specification (8) provides practical indications about the seismic design, while the standards for the earthquake resistance of structures don't refer to rack systems.

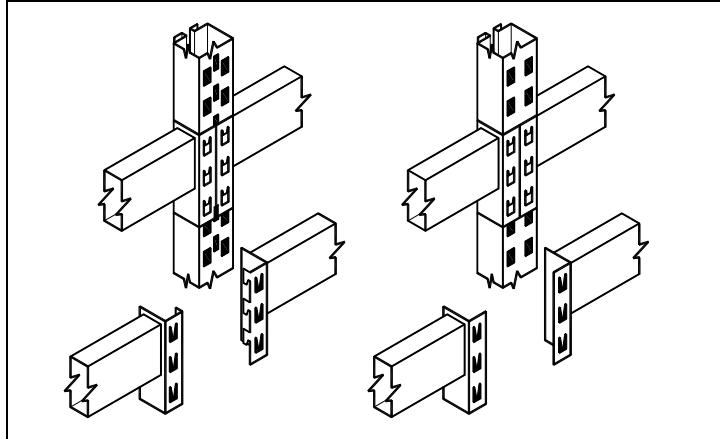


Figure 2: Typical beam-end-connectors of pallet racks.

It should be noted that a suitable design of pallet racks under seismic loading requires the knowledge of the actual cyclic behaviour of the key components, in order to define the performance of possible “dissipative” zones (i.e., the zones in which the energy associated with severe earthquakes could be dissipated). On the authors knowledge, only one research project has been carried out in the past with the aim of investigating the response of racks to dynamic loads (Chen (10)). Nowadays, a direct use of the so-called capacity design approach (Mazzolani and Piluso (11)) is actually prevented, which is based on the concept that the structure possesses sufficient strength, stiffness and absorption capabilities to dissipate the energy associated with severe earthquakes, developing “plastic” mechanisms in dissipative zones. However, the results of a numerical analysis carried out on several planar rack frame configurations in presence of monotonic loading (Baldassino and Bernuzzi (12)) can be considered, in order to have a general indication about the dissipative zones of pallet racks. In particular, it has been shown that frame collapse is generally due to the interaction between instability and plasticity in beam-to-column joints. Columns never achieved their ultimate strength, while, in a very limited number of cases, a plastic hinge occurred approximately at the beam midspan. It seems hence reasonable to assume dissipative zones located at the nodes between beam(s) and column, and the capability to dissipate energy of the racks systems can be considered strictly depending on their hysteretic behaviour (i.e., by their response to cyclic reversal loading). As a consequence, despite the lack of experimental data, a significant influence of beam-to-column joints is expected also on the response of the rack frames in presence of seismic loading.

Research activities on the static and seismic behaviour of pallets racks are in progress in Italy at the University of Trento (Baldassino et al. (13)) and at the Politecnico di Milano (Ballio et al. (14)). One of the main objectives of these studies is to develop simplified design procedures for pallet rack design.

This paper deals with the experimental phase of the researches. In particular, it is focused on the beam-to-column joint behaviour under monotonic and cyclic reversal loading.

The results of 238 monotonic tests on 61 different types of beam-to-column joints performed at the University of Trento are presented and discussed. Moreover, the cyclic behaviour of two different types of beam-to-column joints is presented and discussed on the basis of cyclic tests performed at the Politecnico di Milano.

2. JOINTS IN RACK SYSTEMS

As previously mentioned, the knowledge of the beam-to-column joint behaviour is of fundamental importance for the static and seismic design analysis of pallet racks, owing to the influence of joints on the overall frame performance.

The partial continuity of the rack frame in down-aisle direction is provided by beam-to column and base-plate connections. Moreover the nodal zone between beam(s) and column is expected to be a dissipative zone, influencing remarkably the capability to dissipate energy of the racks systems.

The behaviour of beam-to-column joints under static loading have been extensively investigated, while only few joint tests under cyclic reversal loading have been performed.

In the framework of this research project, the tested specimens consist of a short length column with the ends restrained to the employed counter frame. A cantilever beam is connected to the central zone of the column by the beam-end-connector to test. Specific testing and measuring systems have been designed to analyse the behaviour of the nodal zone (Baldassino et al. (13), Ballio et al. (14)).

Before describing the joint experimental programmes and the main results of the tests, it appears convenient to dwell on the definitions used in the following. In particular, a node is defined as the point at which the axes of two or more interconnected structural elements converge and a nodal zone can be identified where interaction between these members occurs. In this area (Figure 3), one or more joints and connections can be identified. The state of deformation produced by members and by their mutual interactions in the nodal zone is very complex and involves significant local distortions, in rack systems, as well as in multi-storey framed steel buildings (Bernuzzi et al. (15)). Generally, joint response can be described through the sole relationship between the moment in the plane of the down-aisle direction, M , and the associate rotation, Φ , at the beam end section.

In case of rack systems, joint response is mainly influenced by the deformation of beam-end-connectors and of the column nodal zone in shear and bending. As a consequence, these two contributions, indicated in figure 3, as Φ_{bec} e Φ_c , respectively, can be identified in the overall joint rotation Φ .

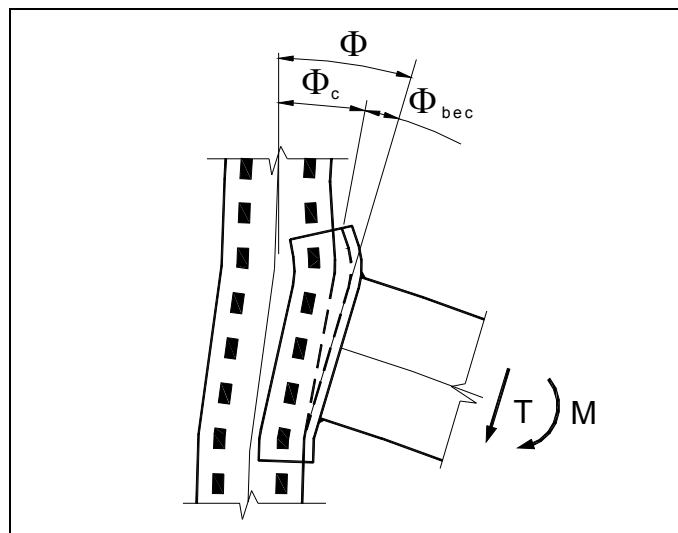


Figure 3: Definition of the main contributions to the overall joint rotation.

3. MONOTONIC TESTS

3.1 Experimental programme

The experimental analysis on beam-to-column connections under monotonic loading comprised of 238 tests on 61 different types of connections.

The tested specimens are characterised by different geometry of the connected members (i.e., beams and columns) as well as of beam-to-column connectors. In particular, it can be noted that:

- beams present close box section. Approximately 80% of the considered beams have regular rectangular sections. The remaining beams are characterised by shapes very similar to the rectangular one;
- columns have in general open perforated section (only 3.3% of the considered columns have close section without perforations). In some cases, columns are simple lipped channels (34.4%). In other cases, additional flanges (called rear flanges) are attached to the lips (37.7%). The remaining column sections have additional lips located at the ends of the rear flanges and normally point outwards (24.6%);
- beam-to-column connections are non symmetrical with reference to the cross- and down-aisle axes (Figure 1). The connection devices are welded to the beams and the connection is physically realised on one side of the column. The typologies of the considered beam-end-connectors are showed in figure 4.

For each type of specimen, four tests were generally executed: three under hogging moments, to appraise the connection behaviour in the usual service conditions, and one under actions generating sagging moments to evaluate the performance in presence of accidental upward action or of frame sway. Generally, tests were interrupted at a high level of connection rotation, out of the range of practical interest for the current usage of beam-end-connectors.

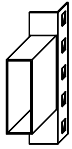
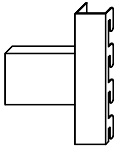
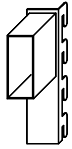
Type of connection		Percentage
C1		52.4
C2		6.5
C3		40.1

Figure 4: Typology of the tested beam-end-connectors.

3.2 Summary of the experimental results

Typical moment-rotation ($M-\Phi$) joint curves obtained from the monotonic tests carried out on one

type of joint are reported in figure 5.

The experimental curves are characterised by an initial slippage due to looseness of the beam-end-connector, and three branches can basically be identified under both hogging and sagging moments:

- elastic, characterised by significant value of the rotational stiffness;
- inelastic, with a progressive deterioration of stiffness;
- plastic, with a significant plateau and, in some cases, also a final softening branch.

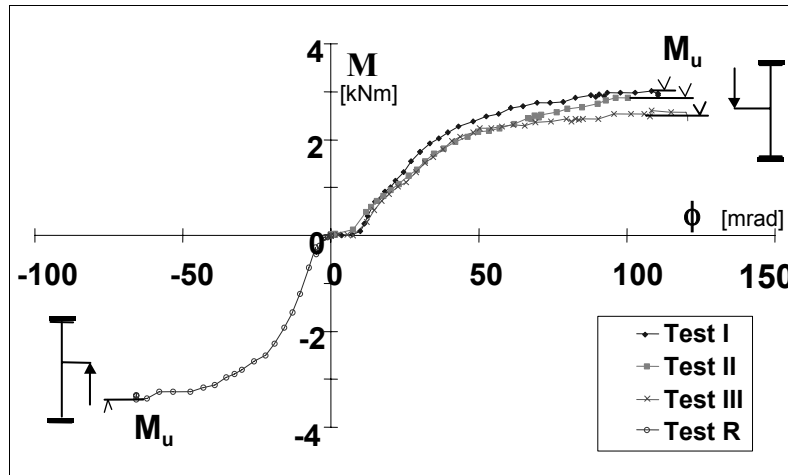


Figure 5. Typical moment-rotation joint curves.

Observed collapses are due to tearing of the column material, yielding of the bracket material or fracture or yielding of the hook itself.

It should be noted that the initial slippage, which can be non negligible, is characterised by a great dispersion. The re-elaboration of the test data showed that under hogging moment, the mean value is 5.91 mrad with an associate standard deviation of 6.16 mrad.

For all the considered types of beam-end-connectors, response under sagging moment was generally characterised by values of rotational stiffness and bending capacity greater than those associated with hogging moment.

3.3 Joint classification

In order to select the frame model (simple, semi-continuous or rigid) to use for the design analysis, the same criteria proposed for joint classification in steel frameworks can be applied to beam-to-column joints for pallet rack systems (Eurocode 3 (16)). Furthermore, in order to have a general idea about the performances of the tested joints, the experimental $M-\Phi$ curves related to the response under hogging moments have been directly compared in non dimensional form, in accordance with the EC3 criteria of for classification of joint in unbraced frames. In particular, from the original $M-\Phi$ curve, a non dimensional $\bar{m}-\bar{\phi}$ relationship has been obtained and considered.

Terms \bar{m} and $\bar{\phi}$ are defined, as:

$$\bar{m} = \frac{M}{M_{p,b}} \quad (1a)$$

$$\bar{\phi} = \Phi \frac{EI_b}{L_b M_{p,b}} \quad (1b)$$

where E is the Young modulus, I_b and L_b are the second moment of area and the length of the beam, respectively, and $M_{p,b}$ represents the beam plastic moment.

With reference to all the $\bar{m} - \bar{\phi}$ joint curves, it should be remarked (13) that:

- for a great number of tests (approximately 31% of the tested specimens) joint response falls in the domain of flexible connection (as curve a in Fig. 6);
- in some cases (in total 14% of the examined joint curves) joints can be considered semi rigid, owing to the value of the rotational stiffness (as curve b in Fig. 6);
- in other cases (in total 9%) joints can be considered semi-rigid, on the basis of the value of the bending strength (as curve c in Fig. 6);
- approximately half (46%) of the tested joints can be considered semi-rigid with reference to both stiffness and strength (as curve d in Fig. 6).

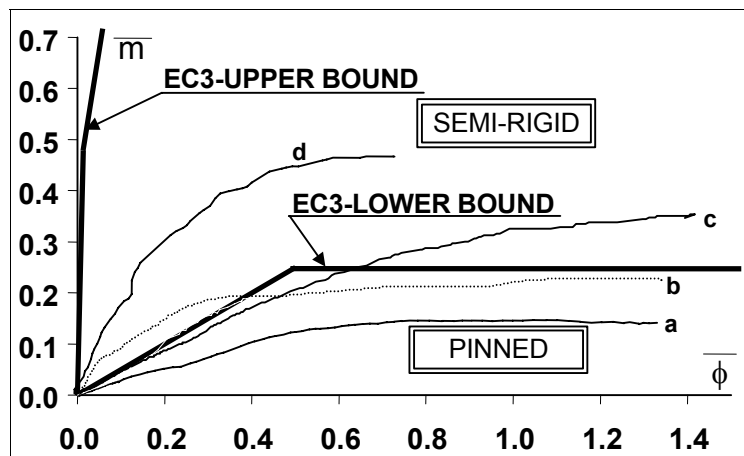


Figure 6: Typical non dimensional moment-rotation joint curves.

From these results related to EC3 joint classification, simple frame model should be used in many cases for the design analysis. However, as it appears from a numerical study on the analysis models for steel buildings (Bernuzzi and Zandonini (17)), joint influence on frame behaviour also in the case of flexible joints is non negligible. Semi-continuous frame design model should hence be always adopted to assess more accurately rack response.

4. CYCLIC TESTS

4.1 Experimental program

The cyclic tests have been performed on two types of beam-to-column connections, which are in the following, named conventionally, A and B and a total of 8 tests have been executed. With reference to the typologies of beam-end connectors showed in figure 4, specimens A are characterised by a connection type C1, while specimens B by a connection type C3.

The tests have been conducted by imposing a constant amplitude loading histories i.e., by performing cycles at the same level of the displacement of the beam end. Several tests have been executed with reference to both symmetrical and unsymmetrical loading histories.

All the tests were interrupted on the basis of the specimen response, directly appraised by the imposed load- beam end displacement relationship, being the scope of the research a general characterisation of the joint behaviour.

No brittle failures due to a sudden collapse of joint components were observed in all the specimens, despite the relevant deformations of the connection devices.

4.2 Summary of the experimental results

With reference to the cyclic tests as a general remark, common for both A and B specimens, it can be said that the form of the hysteresis loops is strictly influenced by the number of executed cycles. In particular, figures 7 and 8 can be considered, related to the tests executed on specimens A and B, respectively, with an imposed displacement of ± 75 mm (tests A150S and B150S). Joint response are here presented with reference to the relationship between the non-dimensional moment \bar{m} (Eq. 1a) versus the joint rotation for some selected cycles. It can be noted that:

- the first cycle is very stable and similar to the ones associated with traditional steel components; reloading branches of the first cycle in plastic range are very close to the monotonic responses;
- after the first cycle, the form of the hysteresis loops changes significantly, owing to the influence of the residual deformations of the connection devices. In particular, increasing the number of the cycles, different forms of hysteresis loops can be noted, depending on the connector types. In case of A joints, the moment-rotation curve is characterised by loops in which the stiffness of the reloading branches decreases progressively with the development of the test. Otherwise, in case of B joints, the effect of subsequent cycles is an initial branch with a very modest slope, the extension of which increases with the number of cycles. The stiffness of the reloading phases is practically constant and equal to the ones of the first cycle and of the monotonic tests. In case of unsymmetrical loading history, these remarks on the forms of the hysteresis loops are confirmed for both A and B joints;
- in correspondence of the zero load level, residual deformation in the tabs were observed, increasing with the number of the executed cycles. Furthermore, cracks appeared also in the tabs and in the column zones in the vicinity of the slots, the amplitude of which increased during the test.

Moreover, it should be noted that for both the types of tested joints, the cyclic response, except than for the first cycle, is significantly different from the ones associated with joints for traditional steel framed buildings, which are generally characterised by a satisfactory stable behaviour. As a consequence, other tests have been planned in order to analyse the relationship between the loading history and the joint response, with the aim of defining a simplified model capable of simulating the joint moment-rotation curve associated with the generic loading history.

5. CONCLUDING REMARKS

Research activities on the static and cyclic behaviour of beam-to-column joints in steel storage pallet racks has been presented, which are currently in progress in Italy. Monotonic tests have been performed on 61 different types of beam-to-column joints (238 tests), while two types of joints (8 tests) have been tested under cyclic loads.

The analysis of the experimental monotonic results shows that the joints are very flexible, if classified in accordance with Eurocode 3 criteria. However, the actual response of beam-end-connectors provides a non negligible degree of lateral stiffness of the frame and, as a consequence, semi-continuous frame model is always suggested for a more refined and “optimal” design analysis.

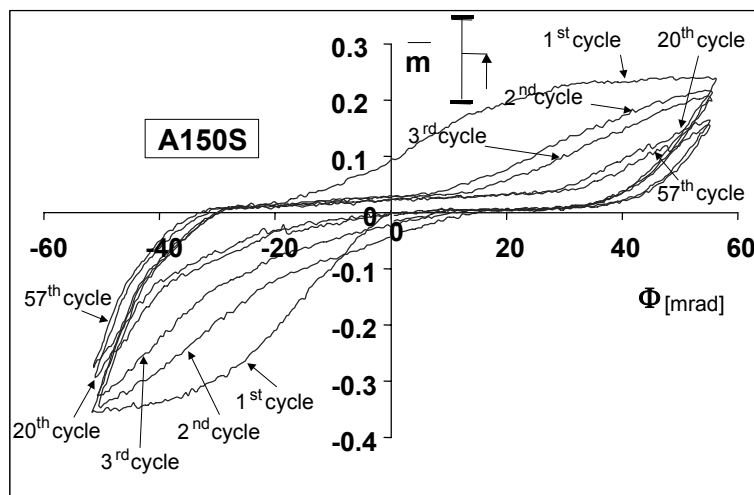


Figure 7: Selected cycles of the \bar{m} - Φ curves for A150S joint test.

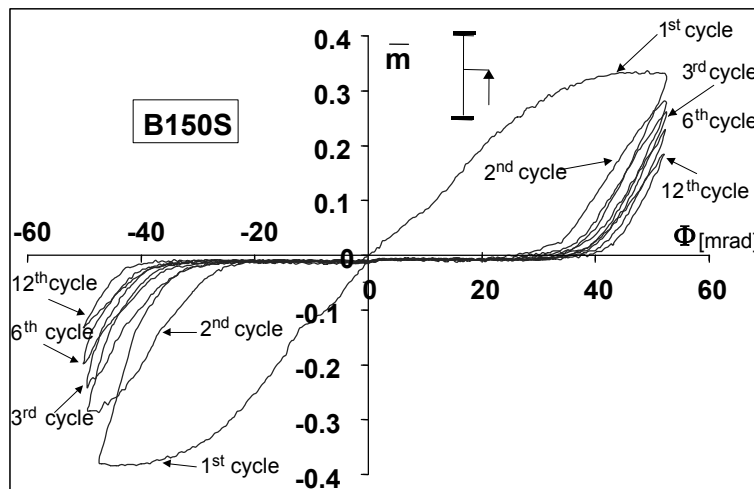


Figure 8: Selected cycles of the \bar{m} - Φ curves for B150S joint test.

As to the cyclic tests, it has been pointed out the relevant differences in the form of the hysteresis loops of rack joints in comparison with the ones associated with traditional steel components and the non-negligible influence of the connection systems on the joint behaviour.

This stresses the importance of the definition of an appropriate design philosophy for pallet racks in seismic zones.

Further tests are however required, which are planned for the next future. These tests will allow to investigate the behaviour of the second important source of stability to lateral load, i.e., base plate joints.

ACKNOWLEDGEMENTS

The data related to the pallets rack frames have been kindly supplied by the Italian Companies involved in the activities of ACAI-CISI (Italian Association of Steel Constructors Rack Manufacturing Companies Group). The authors greatly appreciate the skilful work of the technical staff of the Laboratories of the Department of Mechanical and Structural Engineering of the University of Trento and of the Department of Structural Engineering of the Politecnico di Milano .

REFERENCES

- (1) Hancock, G.J. (1985). "Distortional Buckling of Steel Storage Rack Columns." *Journal of Structural Engineering*, ASCE 111:12, 2770-2783.
- (2) Davies, M. and Jiang, C. (1998). "Design for Distorsional Buckling.", *Journal of Constructional Steel Research* 46:1-3, 174-175.
- (3) ECCS-European Convention for Costructional Steelworks. (1992). *Analysis and Design of Steel Frames with Semi-Rigid Joints*, publication n. 67.
- (4) Godley, M.H.R. (1991). Storage Racking, chapter 1, *Design of Cold Formed Steel Members*, Rhodes ed. Elsevier Applied Science, London, UK, 361-399.
- (5) Markazi, F.D., Beale, R.G. and Godley, M.H.R. (1997). "Experimental Analysis of Semi-Rigid Boltless Connectors.", *Thin-Walled Structures*, **28:1**, 57-87.
- (6) RAL. (1990). *Storage and Associated Equipment*, RAL Deutsches Institut fur Gutersicherung und Kennzeichnung, (German Institute for Quality Assurance and Marketing).
- (7) AS4084. (1993). *Steel Storage Racking*, Standards Australia.
- (8) RMI. (1997). *Specification for the Design, Testing and Utilization of Industrial Steel Storage Racks*, Rack Manufactures Institute.
- (9) FEM. (1997). *Recommendation for the Design of Steel Pallet Racking and Shelving*, Section X of the Federation Europeenne de la Manutention.
- (10) Chen, C.K. (1980). "Seismic study on industrial steel storage racks", prepared for the Antional Science Foundation, URS/ John A. Blume & Associate Engineers, June.
- (11) Mazzolani, F.M. and Piluso, V. (1996). *Theory and Design of Seismic Resistant Steel Frames*, Champmann and Hall, E&FN Spon.
- (12) Baldassino, N. and Bernuzzi, C. (2000). "Analysis and behaviour of steel storage pallet racks.", accepted for publication on *Thin-Walled Structures*.
- (13) Baldassino, N., Bernuzzi, C., Zandonini, R. and Hancock, G. (1998). "Overall, local and distortional buckling in pallet racks.", *Proc. of the Structural Stability Research Concl Conference (S.S.R.C.)*, September, Atlanta U.S.A. (to appear).
- (14) Ballio, G., Bernuzzi, C. and Castiglioni, C.A. (1999). "An approach for the seismic design of steel storage pallet racks.", spec. Ed. of *Stahlbau*, november.
- (15) Bernuzzi, C., Zandonini, R. and Zanon, P. (1991). "Rotational behaviour of extended end plate.", *Costruzioni Metalliche*, n°2, 74-103.
- (16) CEN. (1994). *Eurocode 3: Design of Steel Structures – Part 1.1 General Rules and Rules for Buildings*, European Commitee for Standardization.

- (17) Bernuzzi C. and Zandonini R. (1993). "Serviceability and Analysis Models of Steel Buildings.", *International Colloquium on Structural Serviceability of Buildings*, Goteborg, Sweden, June.

EFFECTIVE LENGTH OF T-STUB OF RHS COLUMN BASE PLATES

František Wald, Valéry Bouguin*, Zdeněk Sokol and Jean-Pierre Muzeau*
Czech Technical University in Prague
*University of Blaise Pascal, Clermont Ferrand

ABSTRACT

The paper presents the application of the component method to column bases of the RHS columns. The decomposition of the connection into the components is described. An analytical model is assembled to determine the moment resistance and the rotational stiffness of the column base under different axial loads. The effective length of T-stub in tension is derived analytically and checked by the FE simulation as a main contribution. The prediction model is verified by comparison with the published test results.

1 INTRODUCTION

The RHS columns are connected to the foundation by base plates and/or by embeddings. In seismic areas are both fixing combined with infilling of bottom part of column by concrete. The base plates are designed thick to transfer primarily compression forces into concrete block and are restrained by stiffener. The anchor bolts are used longer compare to the bolts between plates due to the washer plates, thicker base plate, grout, and embedment in concrete, which allows deformation and separation during the loading. The difference to beam-to-column connection shall be introduced into the prediction of strength, stiffness and rotational capacity of the base plate in tension.

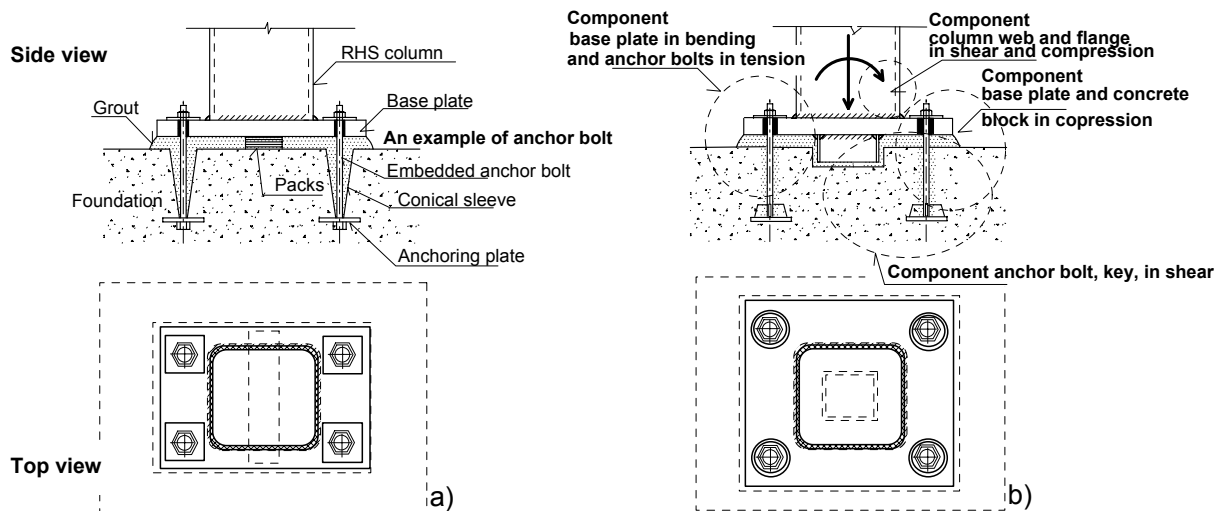


Fig. 1 Example of base plate a) and description main components b)

The compression part of the base plate designed for resistance of the concrete in crushing under the flexible base plate. The model of effective area under the base plates is commonly accepted and applied in design recommendations, see Annex L in (1).

The behaviour of the tension part of the base plate is mostly guiding the column base resistance and stiffness (2) in case of loading by bending moment. The knowledge of behaviour of end plates in beam to column connection were redefined in (1) using models developed in last years by applying the component method. The connection is disintegrated into components, which behaviour is described, and composed back to model connection characteristics.

2 COMPONENT METHOD FOR BASE PLATE

The column base with base plate is in component method divided into components, see at Fig. 1, (2). In the base plate can be recognised the component the base plate in bending and anchor bolt in tension, the component column web and flange in shear and compression, the component the anchor bolt, shear key, in shear and the component column web and flange in shear and in compression. The design procedure is summarised on flow chart on Fig. 2.

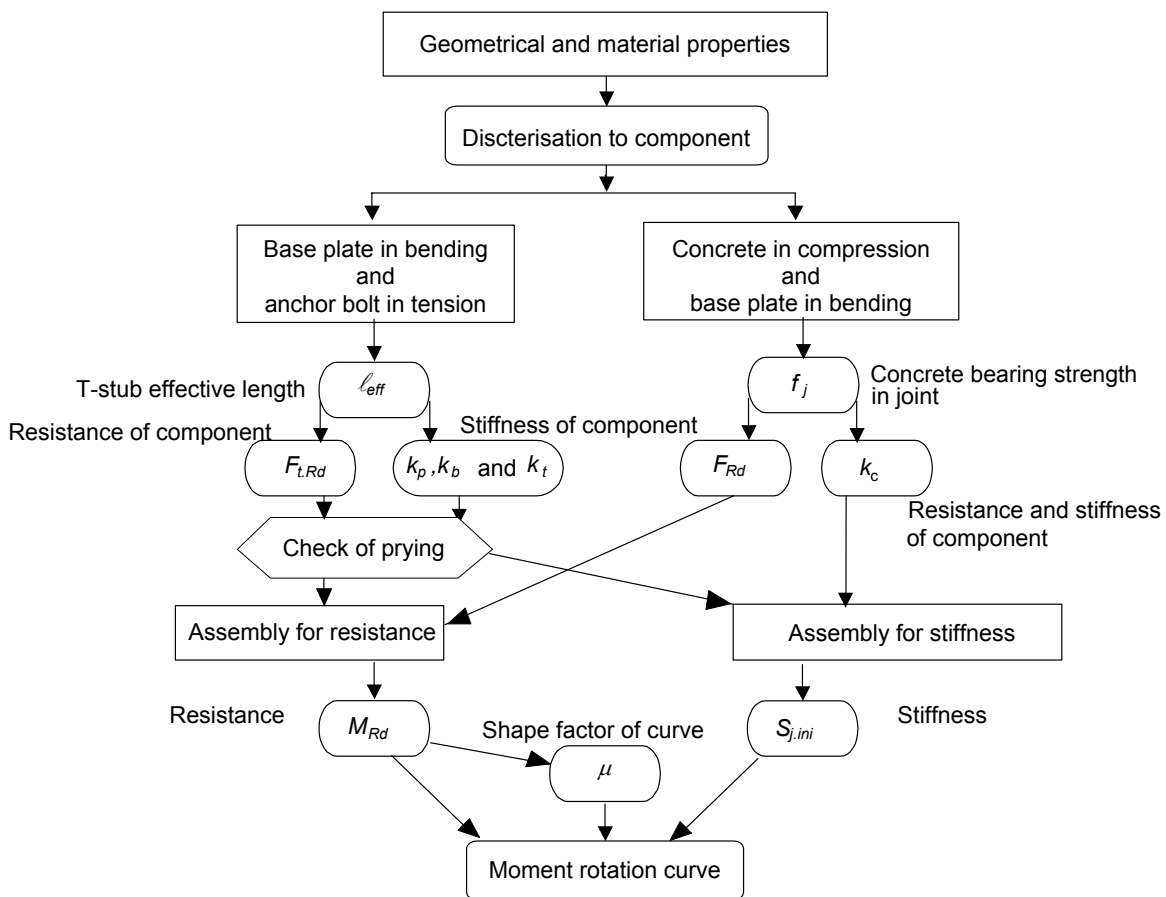


Fig. 2 The design procedure for the base plate of the RHS column

If the anchor bolts are activated in tension, the base plate is subjected to tensile forces and deforms in bending while the anchor bolts elongate. The failure of the tensile zone may

result from the yielding of the plate, from the failure of the anchor bolts, or from a combination of both phenomena. In Eurocode 3 (1) is the design resistance of a T-stub of flange in tension of effective length ℓ_{eff} is derived for three possible plastic collapse mechanisms of T-stub in tension follow for three failure modes. In the particular case of base plates the elongation of the anchor bolts in tension is mostly such, in comparison to the flexural deformability of the base plate, that no prying forces develop at the extremities of the T-stub flange. In this case, the failure results either from that of the anchor bolts in tension (Mode 3) or from the yielding of the plate in bending see Figure 3, where a two hinges mechanism develops in the T-stub flange. This failure is not likely to appear in beam-to-column joints and splices because of the limited elongation of the bolts in tension. This particular failure mode can be named Mode 1*. The corresponding resistance writes

$$F_{1^*.Rd} = \frac{2 \ell_{eff} m_{pl.Rd}}{m} \quad (1)$$

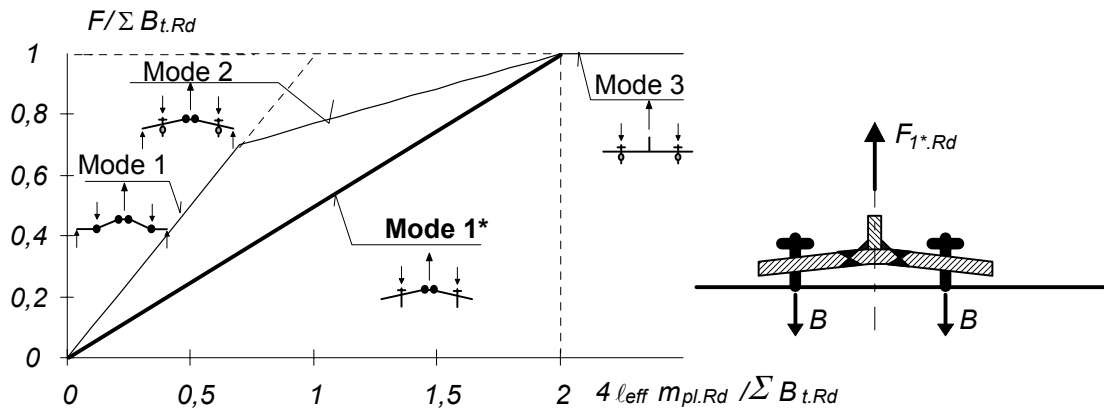


Fig. 3 Failure mode 1*, typical for base plates due to long deformed length of the anchor bolts

When the Mode 1* mechanism forms, large base plate deformations develop; they may result finally in contacts between the concrete block and the extremities of the T-stub plage, i.e. in prying forces. Further loads may therefore be applied to the T-stub until failure is obtained through Mode 1 or Mode 2, see Fig. 3. But to reach this level of resistance, so large deformations of the T-stub are necessary, which are not acceptable in design conditions. The extra-strength which separates Mode 1* from Mode 1 or Mode 2 in this case is therefore disregarded. As a result, in cases where no prying forces develop, the design resistance of the T-stub is taken as equal to

$$F_{Rd} = \min(F_{1^*.Rd}, F_{3.Rd}), \text{ when } F_{3.Rd} = \Sigma B_{t.Rd} \quad (2)$$

The influence on Mode 1* failure under washer plate, cover plate, aimed at strengthening the base plate, which can be considered (1) as

$$F_{1^*.Rd} = \frac{2 \ell_{eff} m_{pl.Rd} + m_{bp.Rd}}{m}, \quad (3)$$

for

$$\ell_{eff} = \frac{c m}{4} \frac{\sqrt{x^2 + y^2}}{x y}, \quad (10)$$

For the resistance can be derived

$$F_{pl} = c m_{pl} \frac{\sqrt{x^2 + y^2}}{x y}, \quad (11)$$

$$\frac{\partial F_{pl}}{\partial c} = m_{pl} \frac{\sqrt{x^2 + y^2}}{x y} = cst \quad (12)$$

Five cases may be observed for the yield lines round by the corner of the column, see Tab. 1 from (4), if are taken into account the modes without the contact of the edge of base plate to the concrete surfaces, e.j. in no prying cases.

Tab. 1 The calculation of the effective length of a T-stub per bolt, Case 1 to 3

Case 1	Case 2	Case 3
$W_{ext} = F_{pl} \delta$	$\delta = \frac{a - a_c - 2 e_a}{a - a_c}$	$\delta = \frac{\sqrt{(b - b_c)^2 + (a - a_c)^2} - 2 \sqrt{e_a^2 + e_b^2}}{\sqrt{(b - b_c)^2 + (a - a_c)^2}}$
$W_{int} = 4 \pi m_{pl} \delta$	$W_{ext} = F_{pl} \delta$	$W_{ext} = F_{pl} \delta$
$F_{pl} = 4 \pi m_{pl}$	$W_{int} = m_{pl} \frac{b}{a - a_c}$	$W_{int} = m_{pl} \left(\frac{e_a}{e_b} + \frac{e_b}{e_a} \right)$
$m = \frac{a - a_c}{2} - e_a$	$F_{pl} = m_{pl} \frac{b}{a - a_c - 2 e_a}$	$F_{pl} = \frac{m_{pl}}{\delta} \left(\frac{e_a}{e_b} + \frac{e_b}{e_a} \right)$
$\ell_{eff.1} = \pi m$	$\ell_{eff.2} = \frac{b}{4}$	$\ell_{eff.3} = \frac{\sqrt{(a - a_c)^2 + (b - b_c)^2}}{8} \left(\frac{e_a}{e_b} + \frac{e_b}{e_a} \right)$

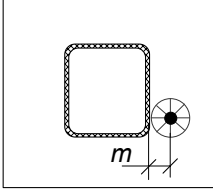
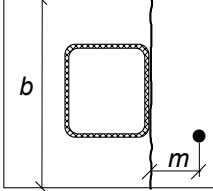
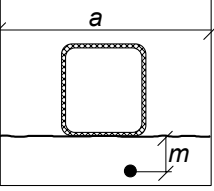
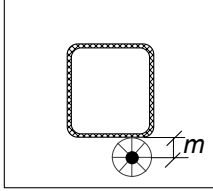
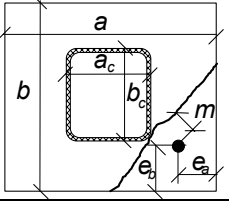
The Case 4 and Case 5 are similar to 2 and 1 respectively. The results of prediction of effective lengths per anchor bolt are summarised in Tab. 2.

The prediction of the base plate stiffness and resistance depends on the prying or no-prying mode. In case of prying the calculation can be based on standard Annex J procedure. The boundaries between modes were developed in (6). The simplified boundaries, for derivation see (2), where prying do not occur are

$$\frac{A_s}{L_b} \leq \frac{\ell_{eff.ini} t^3}{8,82 m^3} \quad (13)$$

The anchor bolts into the concrete is fixed by hooked bars for light anchoring, cast-in-place headed anchors and bounded anchors to drilled holes. Models for the anchoring design resistance compatible with Eurocodes based on the ultimate limit state concept have been prepared (5). The anchor bolt effective free length $L_b = L_{bf} + L_{be}$ consist of physical free length L_{bf} and embedded free length (3). In case of embedded anchor bolts, which can be estimated as $L_{be} = 8 d$. The stiffness of the plate as an independent component of no prying is

Tab. 2 Effective length of a T-stub l_{eff} for base plate of RHS columns for a bolt

			
$l_{eff.1} = \pi m =$ $= \pi \cdot \left(\frac{a - a_c}{2} - e_a \right)$	$l_{eff.2} = b / 4$	$l_{eff.4} = a / 4$	$l_{eff.5} = \pi m =$ $= \pi \cdot \left(\frac{b - b_c}{2} - e_b \right)$
	$l_{eff.3} = \frac{\sqrt{(a - a_c)^2 + (b - b_c)^2}}{8} \left(\frac{e_a}{e_b} + \frac{e_b}{e_a} \right)$		
$l_{eff} = \min (l_{eff.1}; l_{eff.2}; l_{eff.3}; l_{eff.4}; l_{eff.5})$			

$$k_{p,*} = \frac{F_p}{E \delta_p} = \frac{l_{eff.ini} t^3}{2 m^3} = \frac{0,425 l_{eff} t^3}{m^3} \quad (14)$$

and the contribution by the bolt elongation is

$$k_{b,*} = \frac{F_b}{E \delta_b} = 2,0 \frac{A_s}{L_b} \quad (15)$$

The stiffness of the component of base plate in bending and bolts in tension can be summarised from above simplified predictions as

$$1 / k_t = 1 / k_{b,i} + 1 / k_{p,i} \quad (16)$$

The positive influence of washer plate is limited till 5% of deformation and can be for practical design neglected.

The resistance of the component in compression based on effective area under the base plate is described in Eurocode L (1). This component contributes only a bit to the base plate stiffness, but is taken into account for consistency of prediction (2).

The effective area under the flexible base plate is modelled round the column. The position of the neutral axes is calculated from the force equilibrium for resistance. For the stiffness calculation is taken into account the effective area under the flanges only, see Fig. 2 (2). The position of compression force is located at the centre of compression flange. The tensile force is located at the anchor bolts. The force represents the resistances in tension, $F_{t.I.Rd}$ and in compression, $F_{c.I.Rd}$, $F_{c.r.Rd}$. The stiffness is calculated based on component stiffness for the spring in position described at Fig. 8. Two cases are observed, with tension in anchor bolts and without activation of the anchor bolt.

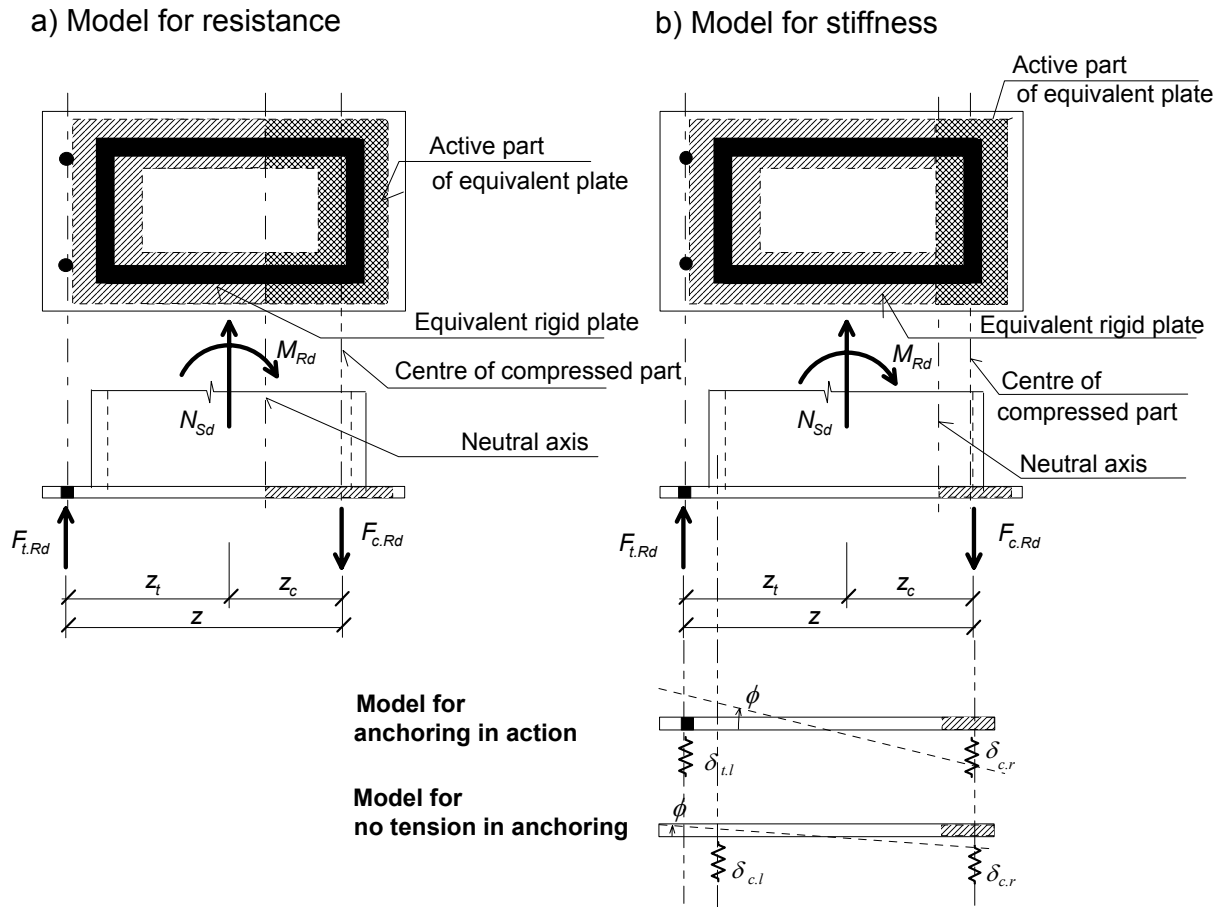


Fig. 5 The force equilibrium of base plate, for the full effective area used for the resistance calculation a), with the effective area under the flanges only applied for the stiffness prediction b), the assembling for large eccentricity and small eccentricity without tension in the anchor bolt

3 EFFECTIVE LENGTH OF T-STUB BY FE SIMULATION*

The boundary between the failure modes were observed using the FE model. Three layers brick model of base plate was applied by code Ansys. The step by step procedure was incorporated with for multi-linear model of material (Z). The position of the bolt was changed round the column corner. The yielding to the base plate, highlights the expected failure mode, see Fig. 6, by reaching the plateau of the material diagram. The size of the bolt nut / washer plate and the relative stiffness of the anchor bolt was studied numerically. For the rigid anchor bolt as a limited case can be observed the prolongation of the yielding in the base plate and column corner on Fig. 7.

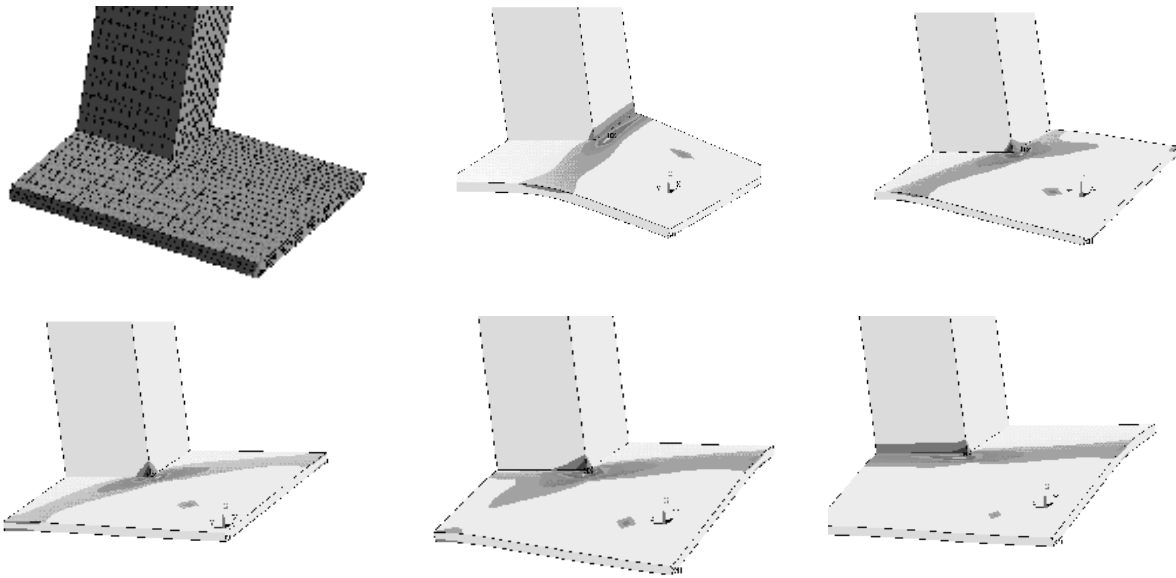


Fig. 6 The FE mesh of simulation, the different yield patterns under the moving of the anchorage round the base plate corner (4)

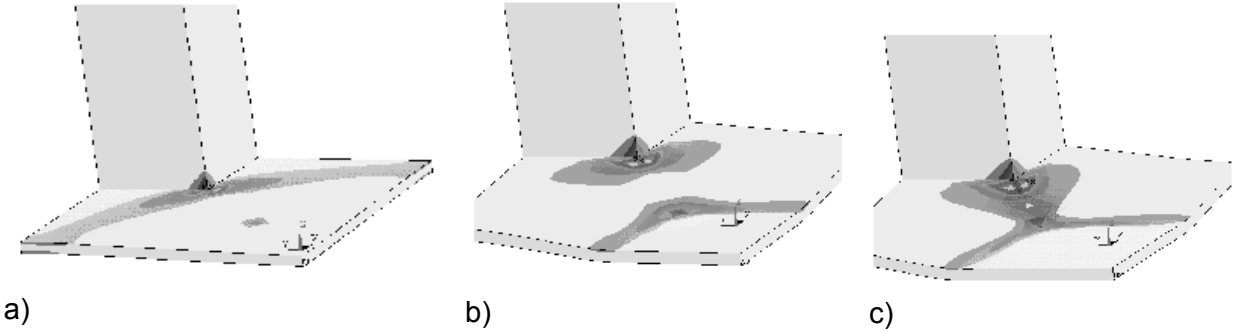


Fig. 7 The influence of the size of the bolt nut, (concentrated load a), nut of diameter 25 mm b), 50 mm, washer plate of 80 mm c)) for the indefinitely stiff bolt

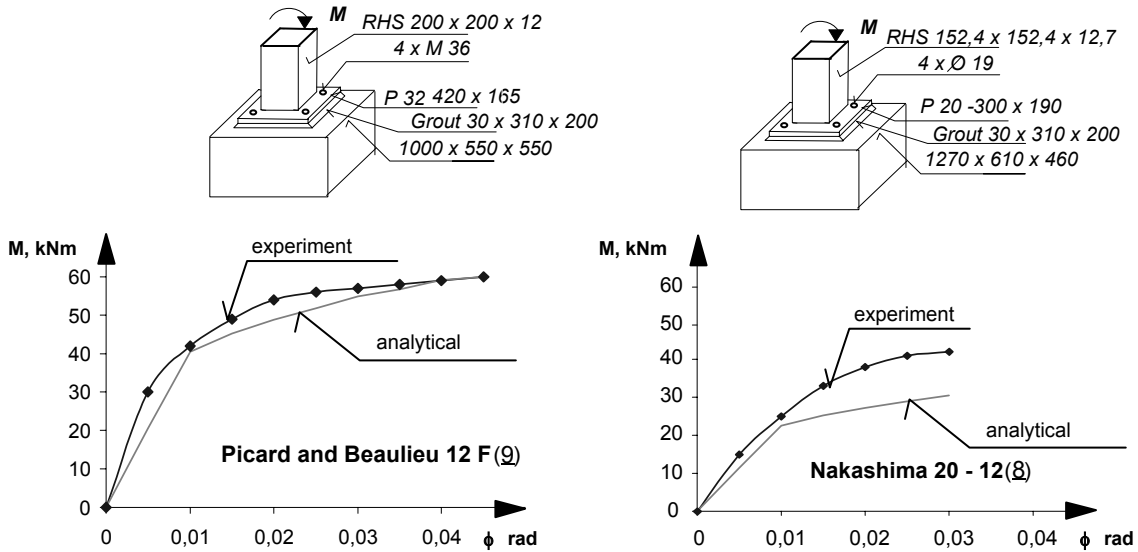


Fig. 8 Comparison of the predicted moment rotation curve to the experimental on of Picard and Beaulieu (9) as well as Nakashima (8)

4 VERIFICATION TO EXPERIMENTS

Two test setups, (8) and (9), with fully described working diagram of the test by $M - \phi$ curve validates the design model (4). The material and geometry is introduced in measured / reported values. The geometrical basic characteristics are shown on the Fig. 8. Both tests were loaded by bending only. For steel the nominal value of material properties was available only. Comparing the initial stiffness, the experimental and analytical results are closed for tests with low influence of axial force. This comes from the steel grade. In the analytical model we did not use measured material property but. The results exhibit a good agreement of proposed prediction model to presented tests. The behavior of base plates loaded by normal forces display the accuracy of prediction of the resistance of the concrete in compression that is more limited.

5 CONCLUSION

The Eurocode 3 procedure based on Annex J and Annex L procedures can determine the resistance and stiffness of base plates of RHS columns. The presented study shows a good prediction of the behavior by the simple engineering model.

ACKNOWLEDGMENT

This work has been supported by the grant of Czech Ministry of Education No. MŠM 21 000 000 1. Within the framework of the activities of the COST C1 European Project (Semi-rigid behaviour of civil engineering structural connections) and the Technical Committee 10 of ECCS (European Steel Fabricator Association) an ad-hoc working group was established to prepare a background document for European standardisation. The authors would like to thanks of all the members for help explicitly to Mr. C. M. Steenhuis, TU Eindhoven and Mr. J. P. Jaspart, University of Liège.

NOTATION

d	diameter of the bolt
f_y	yield stress of steel
k	component stiffness
m	distance from the bolt axes to the weld edge, bending resistance of base plate
t	thickness of the base plate
x, y	axes, coordinates
z	lever arm
B	bolt force
E	Young's modulus of steel
F	force
L_b	free length of the anchor bolt
M	bending moment
N	axial force
S	stiffness
W	work
δ, Δ	component deformation
ϕ	connection rotation
μ	shape factor
γ	partial safety factor
ℓ	length of the T-stub

Subscripts

b	effective free length of bolt
bf	physical free length of bolt
bp	embedded free length of bolt
bp	cover plate
c	compressed
eff	effective
ini	initial
j	joint
l	left
p	plate
r	right
t	tension, T-stub
Rd	design resistance
Sd	acting
pl	plastic
int	internal
ext	external

REFERENCES

- (1) Eurocode 3, ENV - 1993-1-1, *Design of Steel Structures - General rules and roles for buildings*, CEN, Brussels 1992, including Part A2: *Design of Steel Structures - General rules and roles for buildings, Annex J*, European Prenorm, CEN, Brussels 1998.
- (2) *Column Bases in Steel Building Frames*, COST C1, ed. K. Weynand, Brussels, 1999, p.116.
- (3) Wald F.: *Column Bases*, ČVUT, Praha, 1995, p. 137, ISBN 80-01-01337-5.
- (4) Bougin V.: *Column Bases of the Rectangular Hollow Sections Columns*, Diploma theses, Clermont Ferrand, 2000, p. 129.
- (5) *Fastenings to Concrete and Masonry Structures*, State of the Art Report, CEB, Thomas Telford Services Ltd, London 1994, p. 248, ISBN 0 7277 1937 8.
- (6) Wald F., Obata M., Matsuura S., Goto Y.: *Prying of Anchor Bolts*, Nagoya University Report, Nagoya 1993, pp. 241-249.
- (7) Wald F., Baniotopoulos Ch. C.: *Numerical modelling of column base connection*, in COST C1 Conference, Liege, 1998, p. 2-7.
- (8) Nakashima S.: *Experimental Behavior of Encased Steel Square Tubular Column-Base Connections*, in Proceedings of the First Word Conference on Constructional Steel Design, Word Developments, Elsevier Applied Science, ed. Dowling P., Harding J. E., Bjorhovde R., Martinez-Romeo E., Acapulco1992, pp. 240-249.
- (9) Picard A., Beaulieu D.: *Behaviour of a simple column base connection*, Canadian Journal of Civil Engineering, Vol. 12, No. 1, 1985, pp. 126-136.

INFLUENCE OF COLUMN STRAIGHTENING PROTOCOL ON CONNECTION PERFORMANCE

Reidar Bjorhovde
The Bjorhovde Group, Tucson, Arizona, U S A

ABSTRACT

Some of the major findings of a study into the performance of certain types of beam-to-column connections are presented. 17 full-scale specimens used common beam and column sizes as well as welded flanges and cover plates and bolted webs; they were designed in accordance with the AISC Seismic Specification. Some connections had rotary straightened columns, others used gag straightened or unstraightened members. Loading was applied quasi-statically or dynamically. The results show that the form of column straightening has no effect on connection performance.

INTRODUCTION

Steel has been the construction material for a large number of buildings, bridges and other structures for more than 100 years. Its elastic and inelastic responses to loads and load effects make it a material with predictable and reliable behavior under a wide range of service conditions. The ease and speed of fabrication yield significant economies of construction.

The most complex elements of a structure are the connections. For buildings this is especially true for the beam-to-column connections, where details and fabrication processes combine to produce three-dimensional conditions. For reasons of economy and fabrication, over the years certain connection types became common. They were proven through uses in many structures, designers were confident about design methods and details, and fabrication was of high quality. In particular, connections with welded beam to column flange joints and a bolted web were used extensively. Tests and analyses showed that these connections were capable of developing appropriate moment and shear capacities, and the deformation characteristics were very good.

Use of steel structures in high seismicity areas was considered especially advantageous, due to the inherent inelastic deformation capacity of the material, and the structures performed well in a number of minor and major earthquakes. However, the understanding of seismic effects and structural behavior has advanced significantly over the past ten years, and tools such as computers have facilitated increasingly fine-tuned designs. Structural systems have also changed, to satisfy space demands of architects and owners. As a result, structures in some ways have become simpler, with fewer load-carrying elements, but at the cost of reduced redundancy. The effects of earthquakes, for example, therefore have had to be accommodated by fewer members and especially fewer connections.

The 1994 Northridge earthquake had a major influence on state-of-the-art thinking about ductile structural response. Cracks were found in the connections of many steel-framed structures, and it was perceived that the earthquake was the primary reason. It is now clear that many of

the cracks had occurred before the earthquake, and that the same type of cracking had taken place in structures in the absence of seismicity. However, it was also evident that accepted material and structural behavior and design and fabrication approaches needed re-examination.

As an example of a non-seismic cracking incidence, the fabricator for a large California project experienced cracking in the column during the shop fabrication of beam-to-column assemblies. The connections had welded flanges and bolted webs, as well as welded beam flange cover plates and column continuity plates (stiffeners). Figure 1 shows the connection that was used. Although the member sizes shown here are not identical to those of the actual project, they are representative of what was utilized.

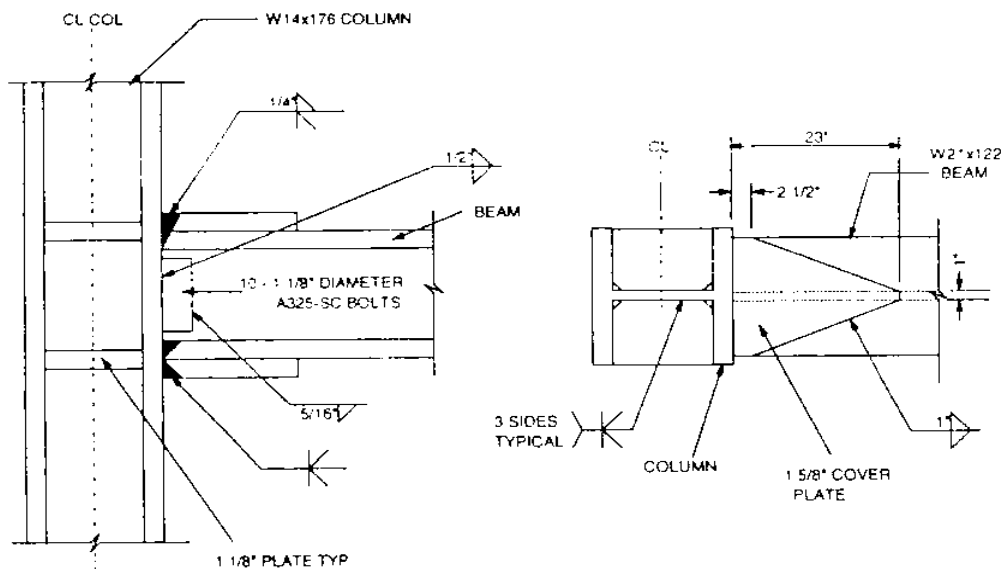


Figure 1 Connection with As-Built Details

The cracks in the as-built connection were found in the web of the column, in the region of the cross section commonly known as the “k-area”. This is a small area of the web surrounding the location where the transition fillet from the flange enters the web. The k-dimension measures the distance from the outside of the flange to the end of the fillet.

Originally the occurrence of the earthquake- as well as the fabrication-related cracks was attributed to inadequate material properties of the steel. Much discussion took place about yield stresses that were significantly higher than the specified minimum values, and some investigators opined that this was a result of faulty steel mill practices. Additional problems evolved as subsequent examinations found that the k-area tended to exhibit high strength and hardness, but low ductility and fracture toughness. These characteristics are related to the fact that many sizes of wide-flange shapes are rotary straightened in the steel mill as a matter of course, to meet the straightness requirements of ASTM (1). Although the straightening is common practice for steel mills all over the world, the properties and response of the k-area material is nevertheless a phenomenon that merited study.

These issues are the background for the study that is presented here. The complete test data are given in the report by Bjorhovde et al. (2).

SCOPE OF TESTING PROGRAM

Table 1 gives the details of the 17 tests. All specimens used W14x176 columns and W21x122 beams; the steel grade was ASTM A572 Grade 50.

Table 1 Major Features of Connection Testing Program

Number Of Tests	Conn. Type	Connection Description*	Straight. Protocol**	Load Prot***
8	As-Built	CJP welds for beam to column and continuity plates to column; 1-5/8" cover plates; 10 1-1/8" A325 bolts for beam web	5R 2G 1U	4Q 4D
6	Revised Type 1	As As-Built, but with 1 inch cover plates and fillet welds for the continuity plates	5R 1U	4Q 2D
1	Revised Type 2	As As-Built, but with a 1/2 inch fillet weld transition from the beam to the column	1R	1D
2	Revised Type 3	As Revised Type 1, plus 1/2" transition fillet weld and repositioned continuity plates	2R	2D

* CJP = complete joint penetration

** Straightening protocols: R = rotary; G = gag; U = unstraightened

*** Loading protocols: Q = slow cyclic (quasi-static); D = dynamic (1 Hz frequency)

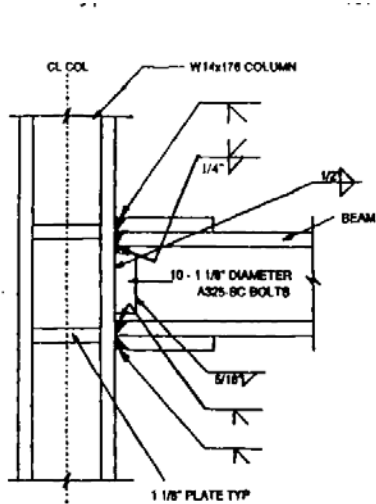


Figure 2 Revised Type 1 Connection

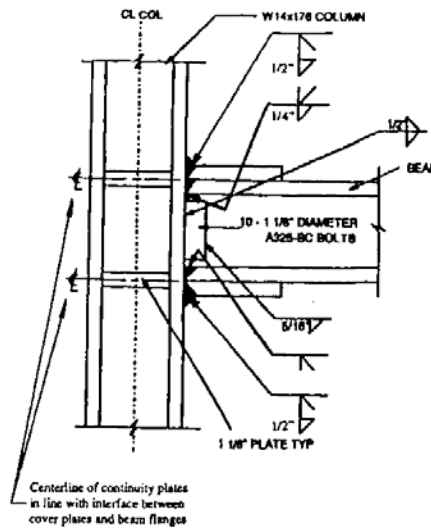


Figure 3 Revised Type 2 Connection

The eight as-built connections reflected current practice. The six Revised Type 1 specimens used thinner cover plates, and in a major departure from current practice it was decided to use the more economical fillet welds for the continuity plates. The single Revised Type 2 specimen had the slight change of the 1/2 inch transition fillet weld

between the beam (cover plate) and the column flange, in an attempt to provide a better force transfer path. Figures 2 and 3 show the Revised Type 1 and 2 Connections.

The Revised Type 3 connections had the same details as the Revised Type 1, plus the ½ inch transition fillet, and, in what turned out to be an important modification, the continuity plates were repositioned to allow for a better load transfer and fracture path for the connection. In traditional usage the continuity plates would be placed with their mid-thickness line at the same level as the interface between the beam flange and the cover plate. For the Type 3 connections it was decided to place the continuity plates with the outside edge in line with the beam flange to cover plate interface. Figure 4 shows the details of the Revised Type 3 connection.

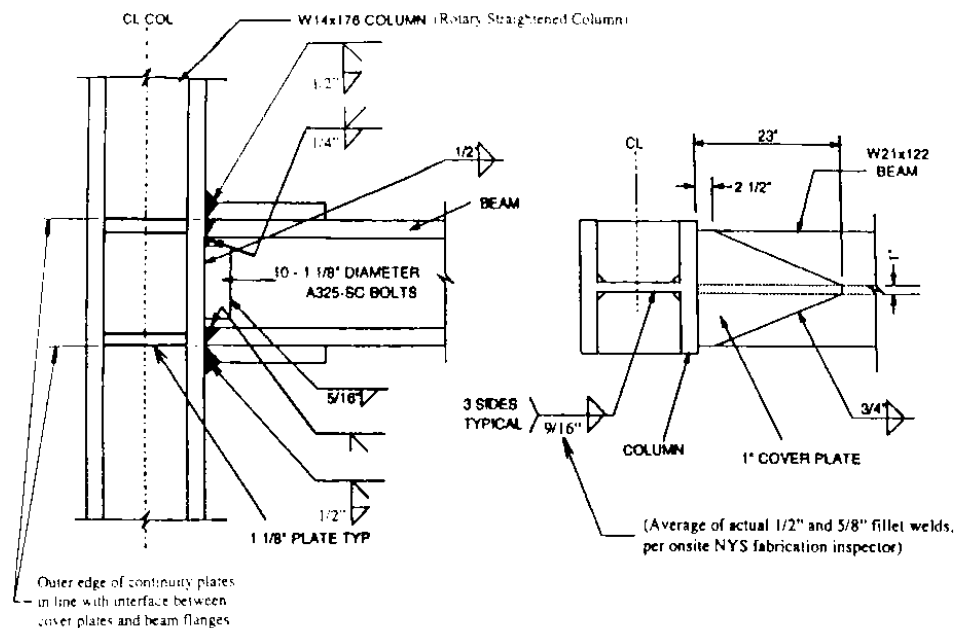


Figure 4 Revised Type 3 Connection

COLUMN STRAIGHTENING PROTOCOLS

One of the issues that prompted the decision to perform the series of tests was the performance of the steel itself in the web of the column. Specifically, the steel was called into question because of the cracks that had developed in the k-area of some columns during welding, and because of the cracks that were found in some structures after the Northridge earthquake. It was also noted that the k-area is deformed heavily because of the nature of the rotary straightening that is used by steel mills to meet the straightness requirements of the materials delivery standard (1). Since this form of straightening is applied continuously, the localized areas of changed material characteristics appear along the full length of a member.

Another factor in the rotary straightening process is the initial out-of-straightness of the shape as it comes from the cooling bed in the steel mill. It is possible to have shapes that are very straight after rolling; these require less straightening effort to meet the delivery criteria. On the other hand, some shape lengths may be fairly out-of-straight; these require larger straightening loads. For ease of production, current US steel mill practice dictates that all shapes be straightened.

Heavier shapes are straightened by the application of concentrated loads at discrete points; this process is termed gag straightening. This procedure does not introduce continuous k-areas of high strength and low ductility in the manner of the rotary straightening because of the way the load is applied.

Unstraightened shapes are not commercially available. However, for the purposes of the testing program it was possible to obtain two unstraightened members, to establish the response of a connection assembly in the absence of the straightening effect.

Overall, as Table 1 shows, of the total of 17 tests, 13 specimens had rotary straightened columns, 2 used gag straightened members and 2 utilized unstraightened columns. It was felt that this testing array would establish conclusively the influence, if any, of the straightening protocol for the columns.

LOADING PROTOCOLS

A number of beam-to-column connections have been tested in past research projects. Many of these used slowly increasing or effectively static loads. Recognizing the importance of dynamic and especially seismic response characteristics, the US Applied Technology Council (ATC) has developed criteria that are based on slow cyclic loads (3). These are often referred to as quasi-static loads, since it is not attempted to model actual earthquake loading. Rather, using a displacement control approach, the load is applied in alternate directions, with increasing amplitudes of the load application point. This is the loading protocol that was used for eight of the connection tests; they are identified by the letter Q in Table 1.

More recent studies have emphasized the need to have the test loading simulate seismic conditions as closely as possible. This led to the development of criteria that focused on loads being applied at certain loading or strain rates, to mimic the earthquake response of the structure. Although the discussion continues as to whether it is more realistic to use dynamic loads, it is all but certain that these will impose more severe demands on the structure and its connections. It was therefore decided to test the second group of nine specimens dynamically, using a frequency of 1 Hz. These tests are identified by the letter D in the Loading Protocol column in Table 1. Three complete cycles were used for each beam tip deflection, with a maximum displacement of ± 10 inches.

CONNECTION DESIGN

The connections were designed in accordance with the criteria of the AISC LRFD Specification, including the 1997 and 1999 seismic requirements (4, 5). In order to achieve optimal seismic performance of structures and their elements, current US principles utilize the “strong column, weak beam” concept, whereby plastic hinges will form in the beams at the ultimate limit state. This leads to improved redundancy and ductile failure modes for the structure as a whole. However, for the tests of this project it was decided to impose the most demanding conditions possible on the column material, primarily since the cracking that had been observed took place in the columns. It was felt that this would represent a worst case scenario. The test specimens therefore reflect assemblies with strong beams and weak columns, where plastic hinges will form in the column panel zones.

DISPLACEMENTS AND ROTATIONS

Measure of Performance

The primary measure of the performance of a connection is its plastic rotation angle (capacity), identified by the symbol θ_p . This expresses the ability of a connection to sustain plastic deformations prior to failure, and is therefore regarded as a criterion by which the connection can be evaluated for seismic performance and suitability.

Assumptions

If the test frame is infinitely stiff, the true beam tip displacement would be defined as the vertical deflection at the beam end, measured from its original, undeformed position. However, the frame is not rigid, and deformations of some magnitude will take place. Therefore, if the displacements were measured in relation to the test frame, the frame deformations would be added to the true specimen displacements, yielding incorrect data. To account for these effects during the testing, vertical and horizontal displacements were measured at the top and bottom column pin supports, at the center of the pin at the beam end, and at the center of the column panel zone. These data were then used to determine the actual beam tip deflections and to eliminate the influence of the test frame flexibility.

In addition to the vertical translations of the column end supports, horizontal movements will occur at both column ends as well as at the panel zone center. The sense of these displacements will indicate whether the entire test specimen rotates as a rigid body around a point on the column close to the bottom pin. Testing of a separate specimen (not one of the 17 listed in Table 1) showed that the top column pin support moved horizontally, in direct proportion to the beam tip deflection, with magnitudes up to ± 0.3 inches. The lower column pin also moved, but in the opposite direction; these displacements were never larger than ± 0.04 inches. It was decided to treat this deformation as insignificant, concluding that the entire specimen rotated as a rigid body about the bottom column pin support.

Plastic Rotations

The deformation demands of an earthquake are partly accommodated by the elastic displacements of the frame. Additional deformations have to be provided by the structure in the form of plastic hinge rotations in the beams and by plastic deformations in the column panel zones. The FEMA Interim Guidelines (6) that have been developed over the past several years recommend that new steel-framed construction should be able to accommodate plastic rotations of at least 0.030 radians in the connection regions. The requirement is reduced to 0.025 radians for retrofitted structures. Further, these rotations must be sustained for at least one full cycle of loading.

Cumulative Plastic Rotations as a Measure of Energy Absorption

The most common presentation of connection test results has been in the form of plastic rotations, the number of cycles to failure, and whether the specimens met the FEMA criteria. Hysteresis loops and failure modes and details are also given, but no data are provided on the

overall energy absorption capacity of the connection, which is a central measure of suitability for seismic conditions.

For the past several years, Japanese reports have included data on cumulative and normalized cumulative plastic rotations (Z). The former is the sum of the plastic rotations associated with each cycle of loading; the latter is a relative measure of the same. It is evident that the cumulative plastic rotation of a connection reflects its energy absorption capacity, and therefore provides key information on its performance ability. The survival of a connection for one cycle, as specified by FEMA (6), says little about its potential response under sustained seismic activity. It is understood that updated Japanese seismic criteria now utilize a cumulative plastic rotation capacity of 0.3 radians as the measure of acceptable performance for a connection.

The cumulative plastic rotation $\Theta_p = \sum \theta_p$ is defined as the sum of the individual plastic rotations that occur during each complete half cycle of the connection test. The quantity also includes the excursion amount that occurs at failure.

PERFORMANCE OF MATERIALS AND CONNECTIONS

Materials Testing

Detailed and extensive testing was conducted for the material in the columns of the test specimens, since the cracking and eventual connection failure was expected to occur in these members. The tests included the usual uniaxial tension tests, chemical analyses, Charpy V-Notch fracture toughness tests, and Rockwell B hardness tests. In addition to the ASTM-required tension (1) specimen location in the flanges of the wide-flange shapes, tensile tests were also conducted for the material in the k-area, web and core. The fracture toughness samples were taken from the same areas in order to map the variability of the CVN values of the material; similar mapping was used for the hardness tests.

As expected, the tensile properties of the web and flange steel met and reasonably exceeded the minimum requirements of the ASTM A572 (50) standard. The k-areas of the rotary straightened columns had higher yield and tensile strengths and lower ductility, also as anticipated. The gag straightened and unstraightened members exhibited nearly uniform strength and ductility at all locations.

The flange and web locations of the rotary straightened columns had excellent CVN toughness; the core and especially the k-area values were much lower. The gag straightened and unstraightened columns did not display reduced toughness in the k-area, other than as part of the typical pattern of variability. The single lowest CVN value for any of the test specimens was 5.0 ft-lbs; it was found in the k-area of one of the rotary straightened columns.

The hardness tests showed the same tendencies as the CVN values. These results also delineated the extension of the high hardness area, showing that it typically extends approximately $\frac{3}{4}$ inch into the web, beyond the end of the transition fillet.

Connection Tests

Figures 1 through 4 show the connections that were tested, and Table 1 gives the structural and fabrication details. It is emphasized that for all but the Revised Type 3 connections, the continuity plates were located with their mid-thickness line at the same level as the interface

between the beam flange and the beam flange cover plate. The Type 3 connections had the outside edges of the continuity plates in line with the beam flange-to-cover plate interface.

Figure 5 shows the column face moment vs. plastic rotation hysteresis loops for Specimen A4. This was an as-built connection with a rotary straightened column; it was tested dynamically. The somewhat "ragged" nature of the curves is a result of the dynamic testing and the high rate of data recording. Failure was initiated through a crack at the toe of the bottom cover plate to column weld. Full stiffness was maintained through one complete cycle of ± 0.028 radians.

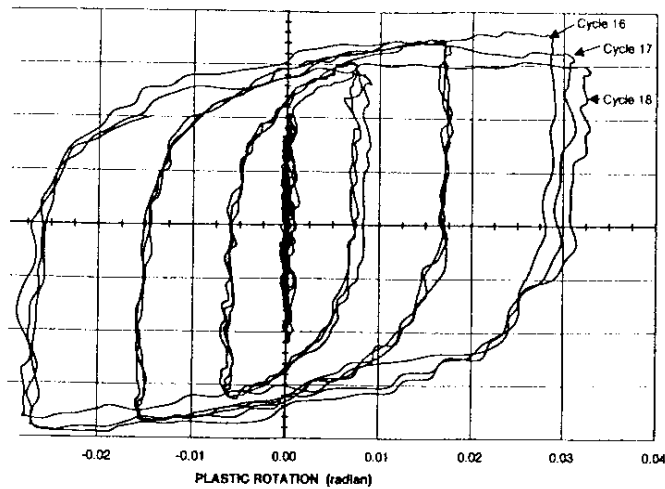


Figure 5 Moment vs. Plastic Rotation Curves for As-Built Connection A4

Figure 6 shows the hysteresis loops for Specimen A7. This was an as-built connection with a gag straightened column; the testing protocol was dynamic. The failure was identical to that of A4, except that the initiating crack took place at the toe of the top cover plate to column weld. The full stiffness was maintained through one complete cycle of ± 0.028 radians.

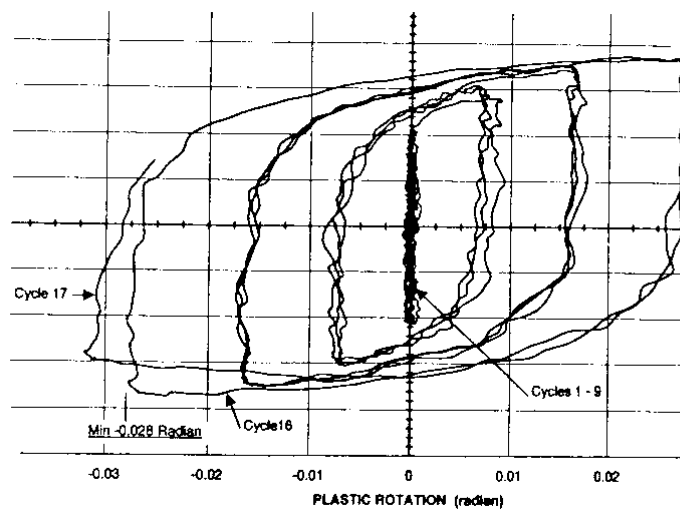


Figure 6 Moment vs. Plastic Rotation Curves for As-Built Connection A7

Figure 7 shows the hysteresis loops for Specimen A8. It had an unstraightened column, and the test was run quasi-statically (this explains the smooth appearance of the curves). As for tests A4 and A7, the failure was initiated by a crack at the toe of one (top) of the cover plate to column welds, although a crack also developed at the edge of the cover plate, close to the edge of the column flange. The full stiffness was maintained through one complete cycle of ± 0.028 radians.

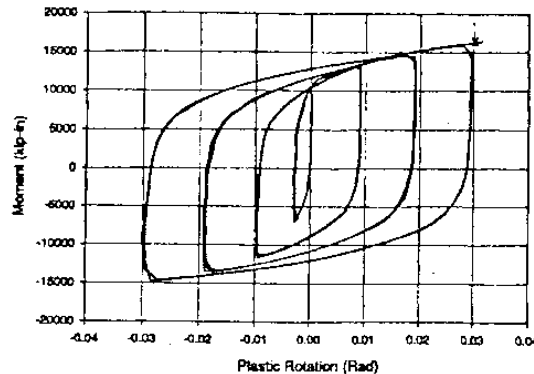


Figure 7 Moment vs. Plastic Rotation Curves for As-Built Connection A8

Influence of Column Straightening Protocol

It is essential to note that the response characteristics, failure modes and rotation capacities for the three specimens A4, A7 and A8 were identical for all practical purposes. The same was observed for the other as-built connections that had rotary straightened or gag straightened columns. Similar behavior in terms of the influence of the straightening protocol was found for the 6 Revised Type 1 connections that were tested, one of which used an unstraightened column and the other five had rotary straightened members. It can therefore be concluded that the column straightening protocol has no influence on the response of beam-to-column connections. These findings have since been further confirmed by research conducted at the University of California at San Diego (8).

Brief Comments on Other Connection Tests in Research Program

The performance of the Revised Type 1 and especially the Revised Type 2 connections was generally very good, and all but three connections met the FEMA single cycle rotation requirement (6). Subsequent fractographic analysis showed that one of these had a significant weld flaw, which contributed to its early failure. The other two non-FEMA acceptable tests would meet the Japanese cumulative plastic rotation requirement of 0.3 radians; this criterion was well satisfied for all of the other connections. The single Revised Type 2 test maintained its full stiffness through two complete cycles of ± 0.038 radians. It is recalled that Type 2 was identical to the as-built connections but for the presence of a $\frac{1}{2}$ inch transition fillet weld between the cover plate and the column.

The two Revised Type 3 connections performed extremely well in all respects. As an example, Figure 8 shows the moment vs. plastic rotation hysteresis loops for Test R3-2; the data for the other Type 3 connection are very similar. The test continued through 26-1/2 cycles, including three at ± 0.038 radians. By the end of the test the cumulative plastic rotation was 1.840

radians; this compares to the values 0.500 to 0.700 radians, which were typically achieved for the as-built, and the Revised Type 1 and Type 2 connections. Clearly the modified placement of the continuity plates had a very major effect on the response of the connections.

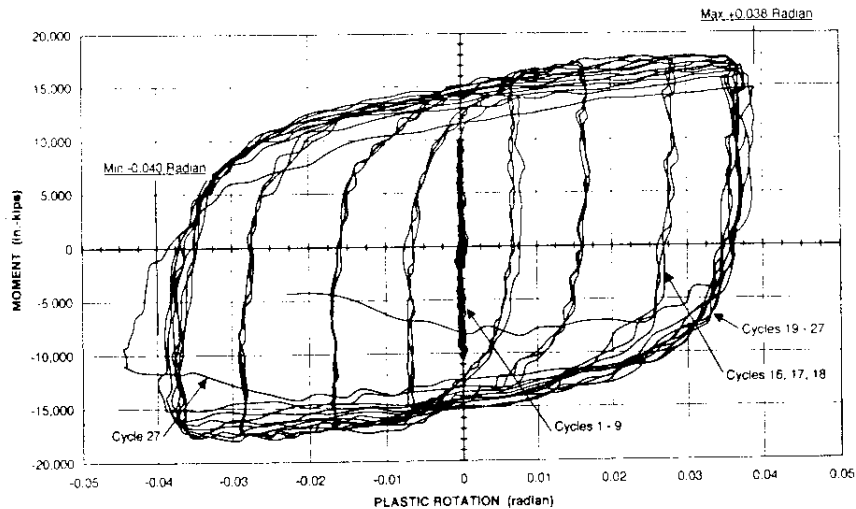


Figure 8 Moment vs. Plastic Rotation Curves for Revised Type 3 Specimen R3-2

CONCLUSIONS AND RECOMMENDATIONS

17 full-scale beam-to-column connections were tested by quasi-static or dynamic loading protocols. The effects of steel mill straightening practices were evaluated through the use of rotary straightened, gag straightened and unstraightened columns. The results show that the straightening protocols have no influence on the performance of the connections.

The results also indicate no significant differences in strength, failure modes and rotation capacities between specimens that were tested quasi-statically and dynamically. The dynamic loading protocol is felt to be more severe, but its complexity and hydraulic testing demands make this approach impractical and very expensive for most testing laboratories. The quasi-static testing remains suitable.

It is recommended that cumulative plastic rotations be used for connection performance assessment rather than the single cycle rotation measurement that is spelled out in current guidelines. The cumulative plastic rotations are more representative of the energy absorption capacity of the connections. Using the updated Japanese criterion of 0.3 radians, all of the connections but one would be satisfactory, and the one that fails the criterion had a significant weld flaw.

The tests of the Type 3 connections demonstrated excellent plastic rotation and energy absorption capacities. It was also found that although cracks developed and eventually propagated through the column material, the propagation was slow and stable, with numerous crack arrests during the testing. Such was also the case for the cracks that propagated into the column k-area, demonstrating that a crack in this region will propagate in stable fashion, given appropriate connection details and fracture paths. Further, these connections used thinner cover plates and fillet welded and repositioned continuity plates. Finally, the cropping of the

continuity plates is important, to the effect that the ends of the welds need to be kept away from the k-area, but this observation applies to all kinds of welds and connections. In brief, fabrication and construction economies will be obtained with the Revised Type 3 connection.

REFERENCES

1. American Society for Testing and Materials (ASTM) (1998), "*Specification for General Requirements for Rolled Structural Steel Bars, Plates, Shapes and Sheet Piling*", ASTM Standard A6. ASTM, Conshohocken, PA.
2. Bjorhovde, Reidar, Goland, L. J., and Benac, D. J. (1999), "*Tests of Full-Scale Beam-to-Column Connections*", Technical Report, Nucor-Yamato Steel Company, Blytheville, AR, August.
3. Applied Technology Council (ATC) (1992), "*Guidelines for Cyclic Seismic Testing of Components for Steel Structures*", ATC Guideline No. ATC-24. ATC, Redwood City, CA.
4. American Institute of Steel Construction (AISC) (1993), "*Specification for the Load and Resistance Factor Design of Steel Building Structures*", 2nd Edition. AISC, Chicago, IL, December 1.
5. American Institute of Steel Construction (AISC), "*Seismic Provisions for Structural Steel Buildings*" (1997) and "*Supplement 1 to the 1997 Seismic Provisions*" (1999), AISC, Chicago, IL.
6. Federal Emergency Management Agency (FEMA) (1995), "*Interim Guidelines: Evaluation, Repair, Modification and Design of Steel Moment Frames*", Report No. FEMA-267, FEMA, Washington, DC.
7. Nakashima, M., Suita, K., Morisako, K., and Maruoka, Y. (1998), "Tests of Welded Beam-Column Assemblies. I: Global Behavior", *Journal of Structural Engineering*, ASCE, Vol. 124, No. 11, November (pp. 1236-1244).
8. Uang, C.-M. (2000), "*Private Communication*", San Diego, CA.

Fatigue life assessment for welded connections repaired under the moving loads

by Günther Valtinat, Technical University of Hamburg-Harburg

ABSTRACT

Repair welds are welded in moving weld seams, the liquid welding material must undergo stretching and forging while cooling down, the amplitude of the opening is decisive for the weld quality, values of about 0,25 mm can be welded by a trained person, larger openings usually have defects in the welds such as pores, welding discontinuities, root defects, hot cracks, the weld quality is evaluated by fatigue tests and the comparison with the fatigue life of welds welded in standstill.

1. INTRODUCTION

Steel constructions in the sea such as offshore-platforms are highly fatigue loaded by oscillating actions due to waves and wind. After many years in action such constructions accumulated damages, especially in constructional details with notches. Welded connections in their different forms are such details. They are the places in constructions, where the damage accumulation is severe and where fatigue cracks can start and propagate.

If inspectors notice such fatigue cracks it is necessary to find out the severity of the damage and the possible consequences. This usually can be done with suitable calculation methods on the basis of fatigue tests, crack propagation rate and fracture mechanics. If it is necessary for safety reasons and for keeping the construction alive to repair such damages it is very often the only way to prepare the crack seams with an edge preparation for repair weld. This edge preparation must be done under moving crack fronts.

Damages of this kind can occur above water and under water.

As the next step after the edge preparation it is necessary to close the prepared crack by a repair weld and this under moving edges and under moving loads. It is of course advisable to wait for the smallest possible movement in a period of calm weather and sea. It will never be possible to have a total standstill of the construction and of the weld edges.

At the crack tip the movement is lower than in other parts of the crack. Therefore it is advisable to start with the welding process at the crack tip and then move along with the welding process into areas with higher movements. The welding process should be adjusted to the amplitude and the frequency of the movement. If the cooling down process of the liquid welding material is quick then we get a temporary connection in the root of the weld and if this connection is strong enough, the moving process comes to a standstill in this area. In this way and with a high skill of the welder it is possible to close the opening by a repair weld step by step. For this it is necessary that with the first layer the weld is capable to resist the oscillating forces.

The second weld layer and the following ones do not to fight against moving weld edges, they can be welded under standstill conditions as usual.

It was our task to really simulate such welding processes in the testing machine under moving loads, to close such welds under moving edges in special test pieces and to undergo afterwards fatigue tests to find out whether the fatigue behaviour, the fatigue stresses and the load cycles with such welds are reduced compared with welds welded under standstill. The number of cycles until rupture gives us an impression and data how much the reduction is.

2. SIMULATION OF THE WELDING IN MOOVING WELD SEAMS IN THE TEST RIG

In a special test rig (figure 1) we produced a displacement controlled loading of a girder with a special joint. The girder consisted of an I-profile with an endplate connection midspan. In this connection only the lower two rows of bolts in the area of the lower flange was placed, on the other flange we fixed two plates with the prepared weld seams on the flange plate by hsfg bolts (see figure 2). The controlled movement of the jack was so, that the weld seams went to and back from each other with an amplitude according to table 1. At the beginning this movement was kinematic and only deformation controlled, no load occurred. For this it

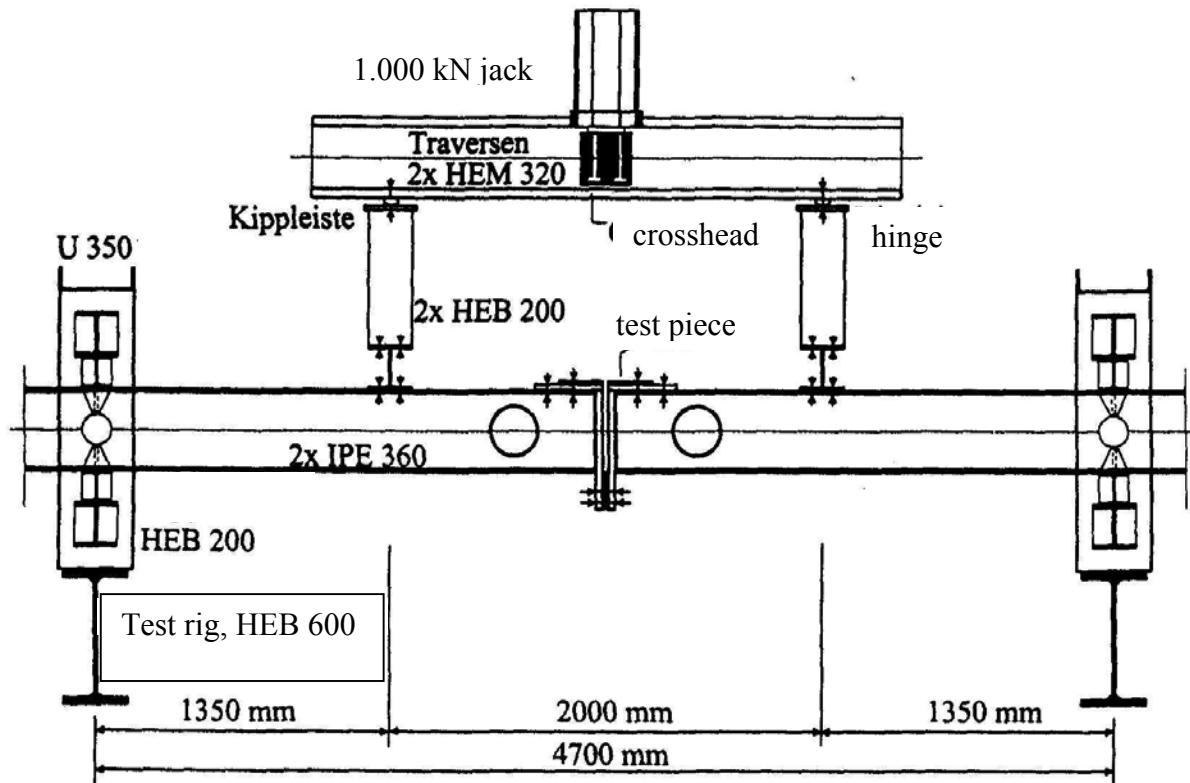


Figure 1: Test rig for welding in moving weld seams

was necessary that the girder deflected to a certain amount. This amount of deflection was kept constant until the end of the welding process. According to the length of the actual weld, the joint became more and more rigid, the bending moment in the joint increased from 0 at the beginning to a proposed maximum value and the load in the jack increased simultaneously. While the girder at the beginning of the process deformed in a kinematic system with a hinge midspan at the end of the welding process the girder had reached a considerable rigidity and deformed in an elastic deformation line with respect to a four point bending girder.

Measurements about the opening displacement of the weld seams and about the deflection of the girder were taken from the beginning up to the end of the welding process. These data give an impression how the amplitude of the displacement of the weld seams decreased and how the rigidity of the girder increased with the continuation of the welding process.

The increase of the load in the jack parallel with the propagation of the closing process showed that the joint developed a certain strength according to the strengthening of the weld due to its temperature.

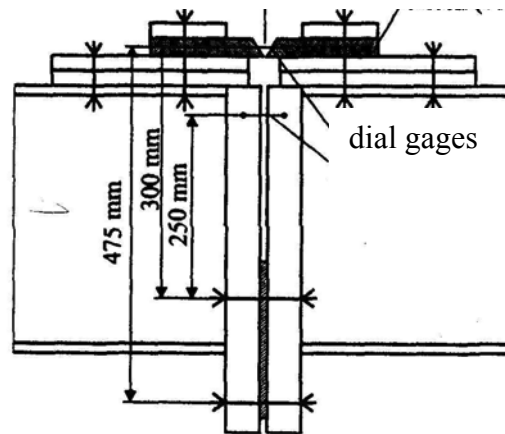


Figure 2: Details of the test set up for the welding in moving weld seams

3. TEST PIECES

Our plate material consisted of S355J2G3. The main test pieces were 8 mm thick, some tests have been done with 15 mm thick plates and some other tests have been done with the steel quality S235. We needed always more than one weld layer.

The data which have been varied while preparing the test pieces are:

- the distance s of the weld seams when moving,
- the frequency f of the movement of the weld seams,
- the plate thickness t and
- the steel quality.

The following table 1 informs about all these data.

Table 1: Number of tests depending on the parameters amplitude s, frequency f and plate thickness t

frequency in Hz	amplitude s of the gap in mm			
	0,125	0,25	0,5	0,75
0,25	18	12 with t= 8 mm 6 with t=15 mm	24	---
0,5	12	18	18 with t= 8 mm 12 with t=15 mm	12

To compare fatigue test results with repair welds under moving with results of fatigue tests with normal welds, welded under standstill we tested

- 18 test pieces with the plate thickness of t = 8 mm and
- 6 test pieces with the plate thickness of t = 15 mm

with usual welds.

4. THE WELDING PROCESS AND MEASUREMENTS

The figures 3 and 4 show the measurement of the displacements while the welding process was going on. Since the weld began asymmetrically on one side the two measurements on both sides of the flange differ from each other. The displacement on the side where the weld started was very soon quite small while on the other side the displacement remained considerably large. Figure 4 shows the gap opening behaviour during the first weld layer after the root weld and during the last weld layer.

Our welder underwent a special training program to achieve the best quality of the intended welds. During this training course we have seen that welding with moving seams is not easy. Depending on the amount of the displacements of the weld edges, especially the first bead can contain pores, welding defects such as hot cracks in the center of the weld, material separation in a certain sequence which is connected with the welding speed and the frequency of the movement. We observed also other defects such as root defects and weld toe discontinuities. The following figures 6 a to c show some of these defects.

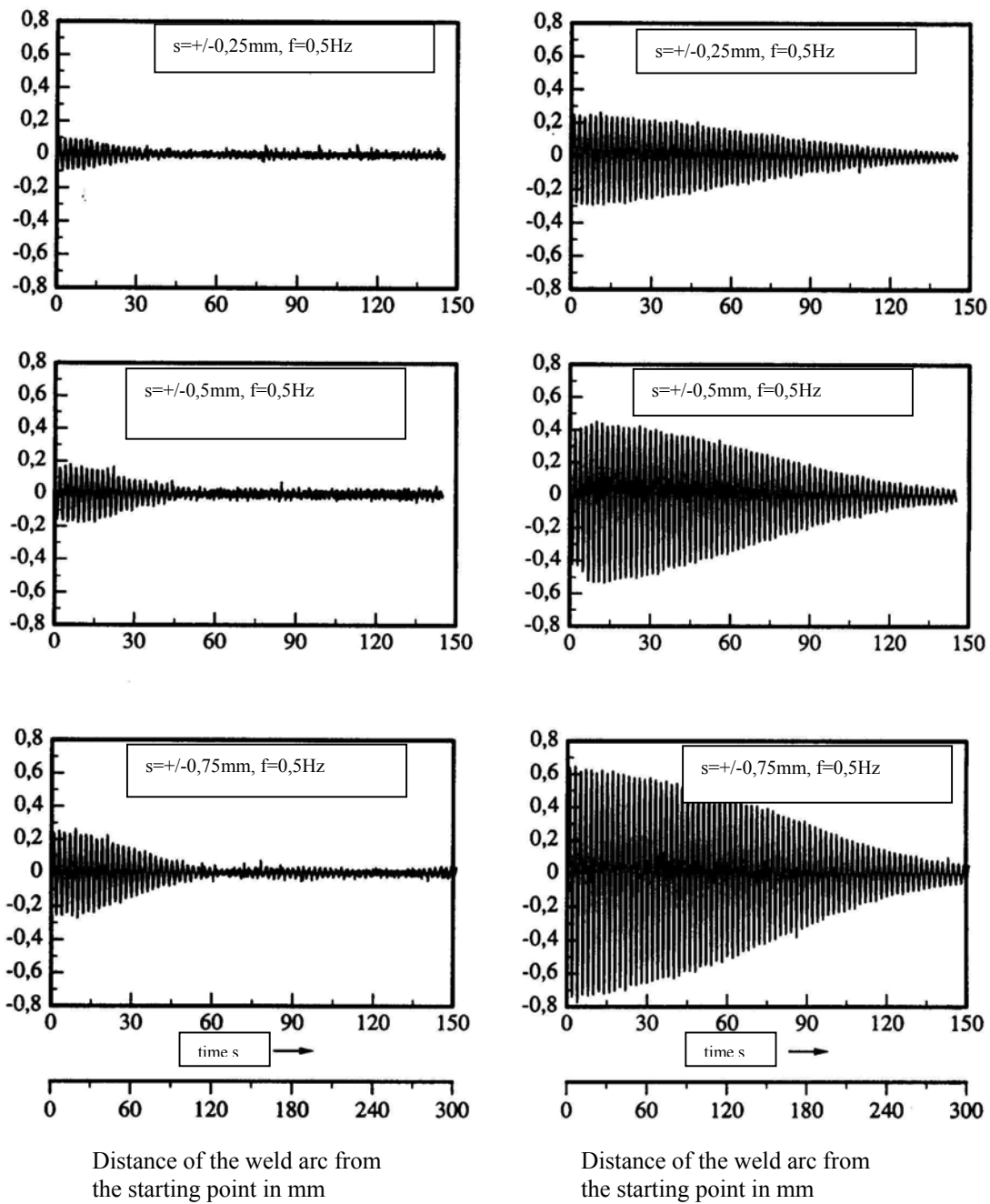


Figure 3: Development of the gap amplitude with the root weld in moving weld seams
 left: gap opening at the weld starting point
 right: gap opening at the weld ending point

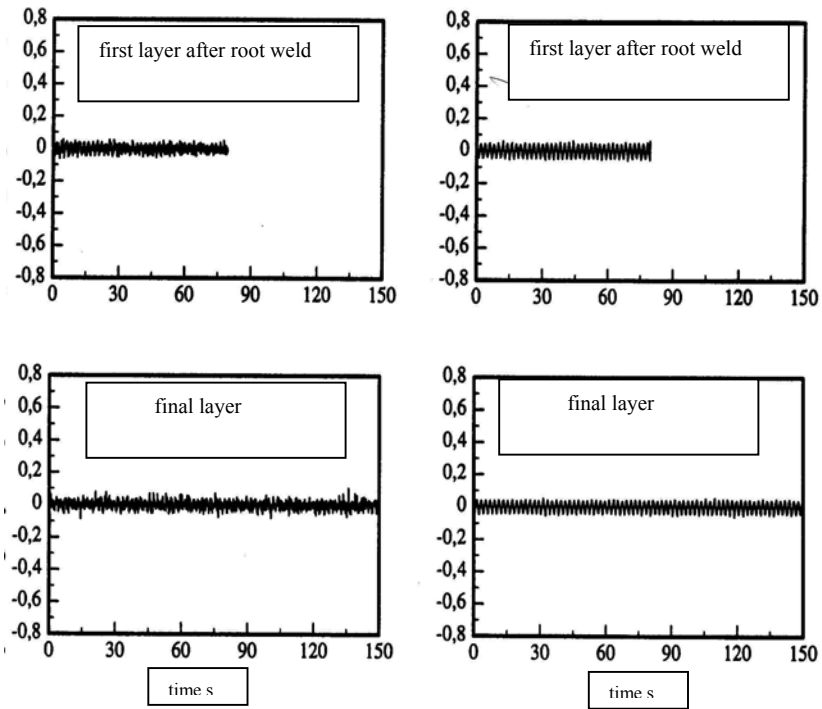


Figure 4: Development of the gap opening amplitude with further weld layers in moving weld seams
 left: gap opening at the weld starting point
 right: gap opening at the weld ending point

The figure 5 represents the increase of the load in the jack while the welding process of the root weld was continued.

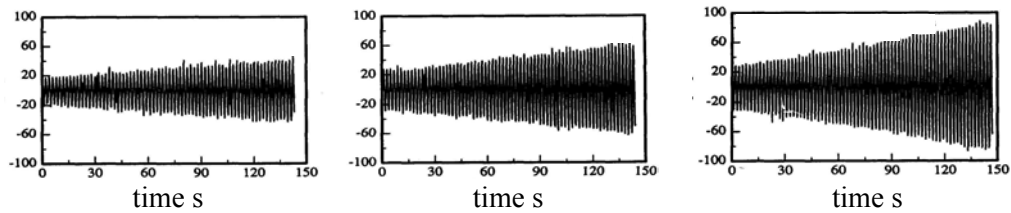


Figure 5: Load increase while closing the gap by root welding
 left: $s = \pm 0,25$ mm, $f = 0,5$ Hz
 center: $s = \pm 0,5$ mm, $f = 0,5$ Hz
 right: $s = \pm 0,75$ mm, $f = 0,5$ Hz

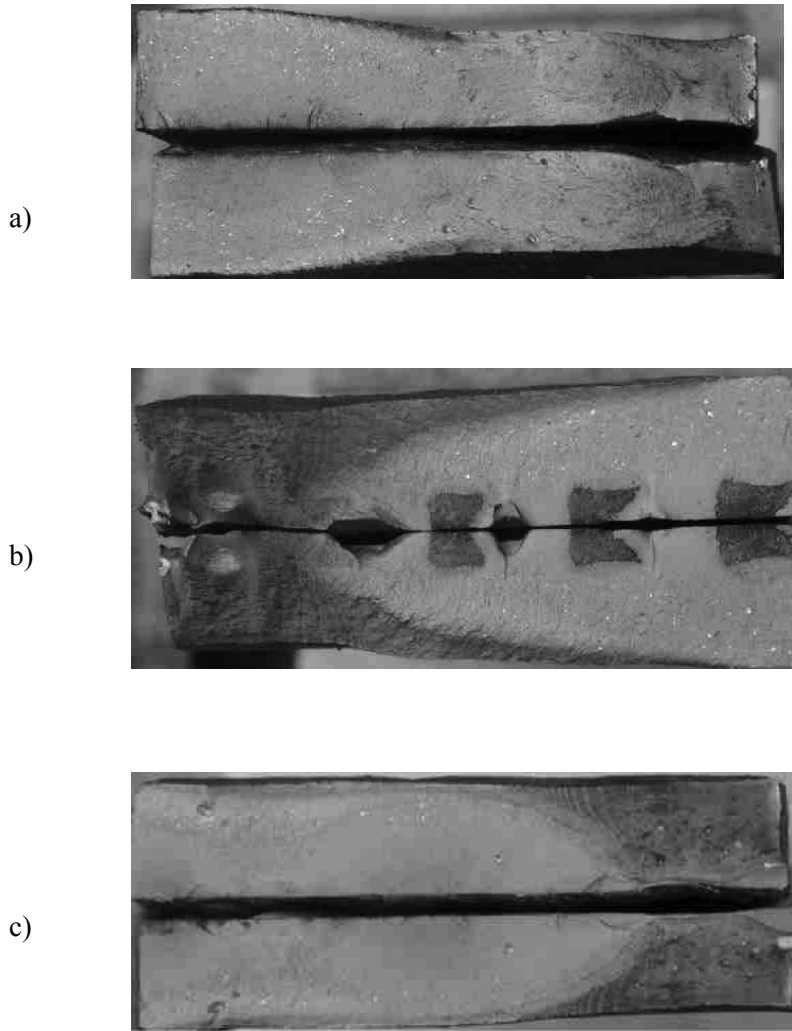


Figure 6: Surfaces of fatigue cracks in welds under moving seams

- a) Test piece A near the starting point of the weld, small opening amplitude 0,25 mm, small frequency $f = 0,25$ Hz, position A
- b) Test piece A near the starting point of the weld, larger opening amplitude 0,5 mm, small frequency $f = 0,25$ Hz, position A, sickle-shaped discontinuities,
- c) Test piece E near the end point of the weld, larger opening amplitude 0,5 mm, small frequency $f = 0,25$ Hz, position E no sickle-shaped discontinuities, root discontinuities as starting point of the fatigue crack

This simulated a repair of a fatigue crack in a tube starting at the crack tip

After the welding process we cut 6 test pieces for the fatigue tests from the hole plate. Little pieces at the starting and the ending point of the weld were taken away. The 6 pieces for the fatigue tests were named A to F, the piece A was that one at the beginning of the weld.

5. FATIGUE TESTS

The fatigue tests were performed with a relation of the lower tension load to the upper tension load of $\kappa = + 0,1$. The final goal was the evaluation of the S-N-curves for various parameters. We suspected that the test results with test pieces A could be worse from those with the test pieces B to F. We suspected furthermore, that the results with test pieces welded with large amplitudes of displacement could be worse than those with small amplitudes. This happened in reality as the photos of the crack surface and the S-N-curves show. The pieces A and sometimes also B had openings, pores and other sickle-shaped defects, while the pieces C to F had no such defects (figure 6).

The details of the fatigue test results are shown in the figures 7 to 10.

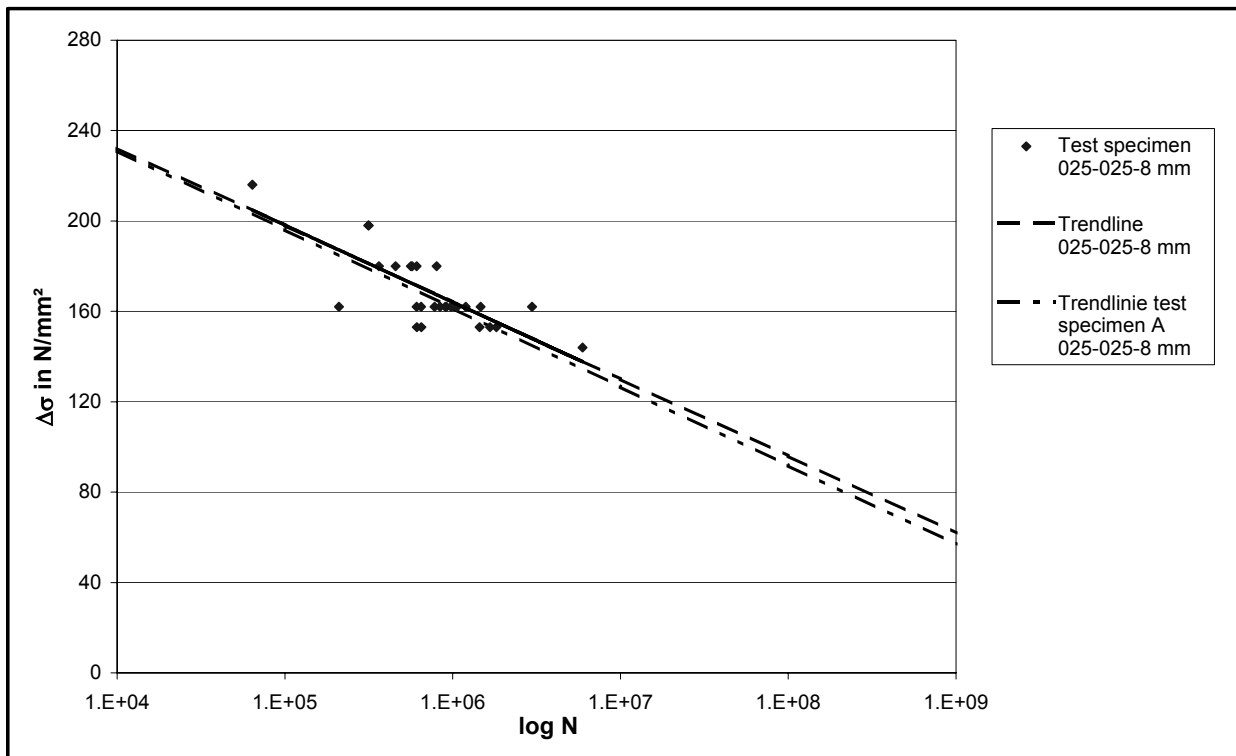


Figure 7: S-N-curves for butt welded connections with welds in moving edges
 Gap opening amplitude $s = 0,25$ mm
 Frequency of the opening $f = 0,25$ Hz
 plate thickness $t = 8$ mm

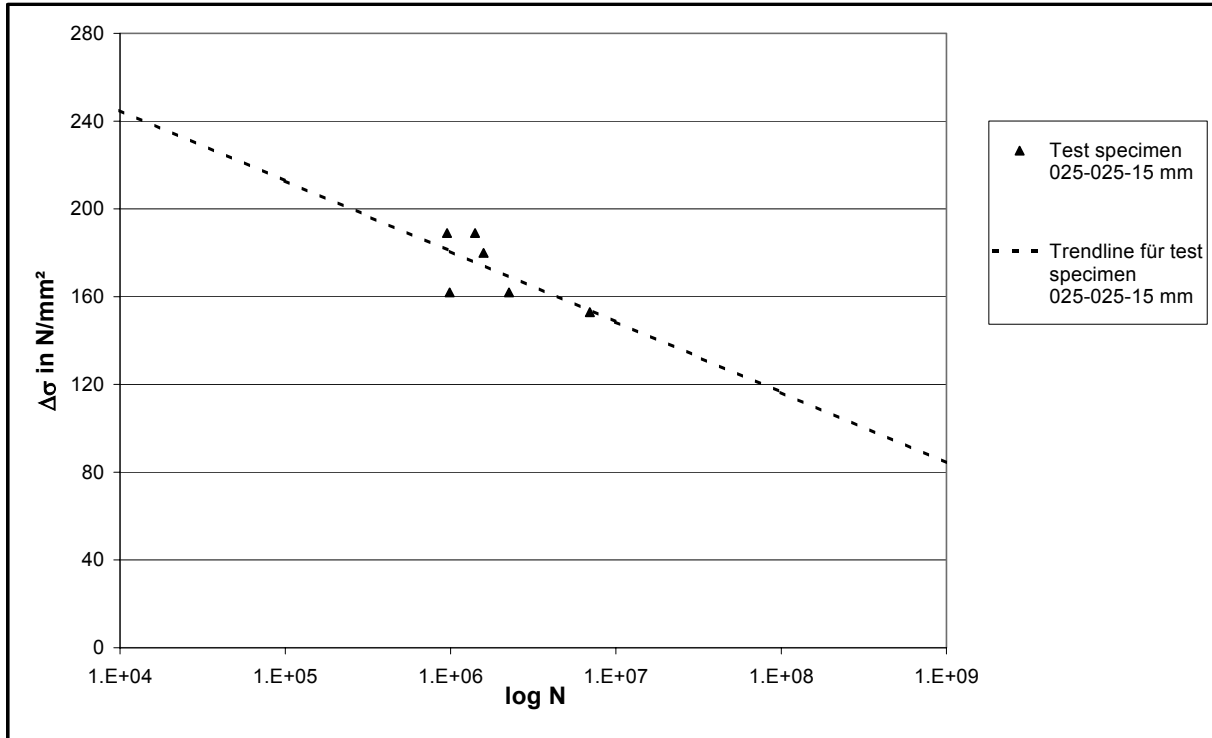


Figure 8: S-N-curves for butt welded connections with welds in moving edges
 Gap opening amplitude $s = 0,25$ mm
 Frequency of the opening $f = 0,25$ Hz
 plate thickness $t = 15$ mm

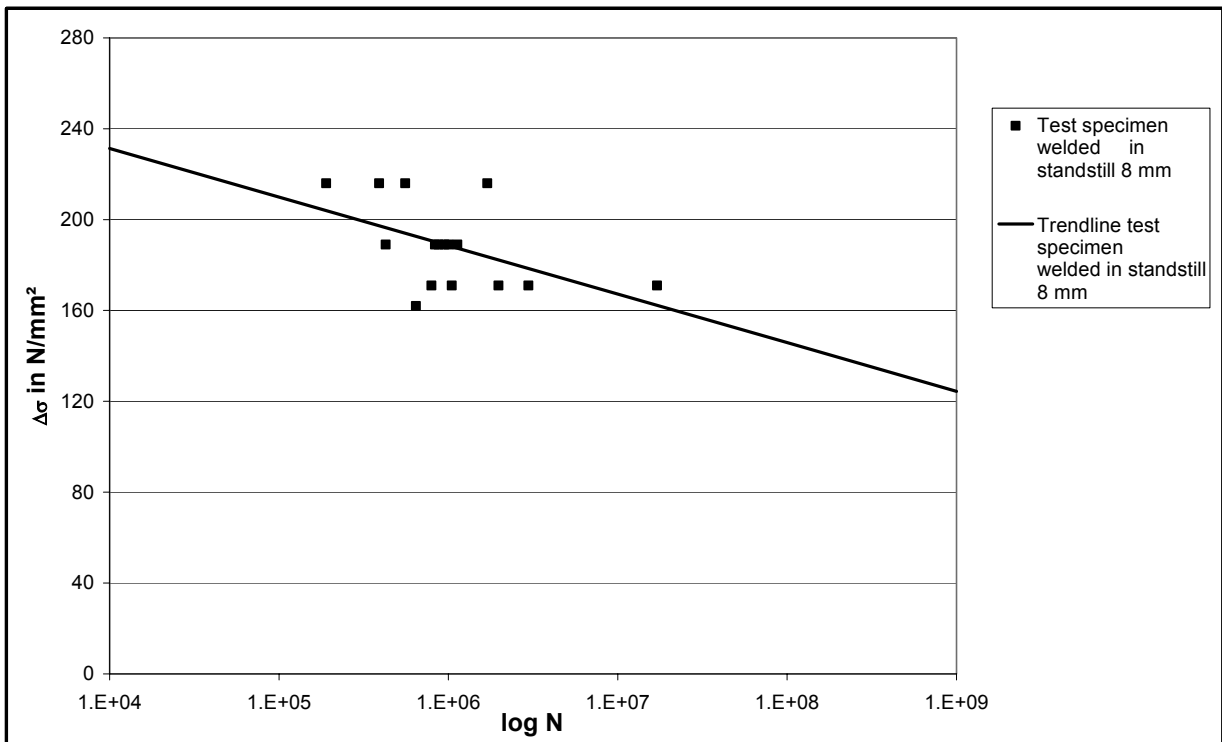


Figure 9: S-N-curves for butt welded connections with welds in standstill

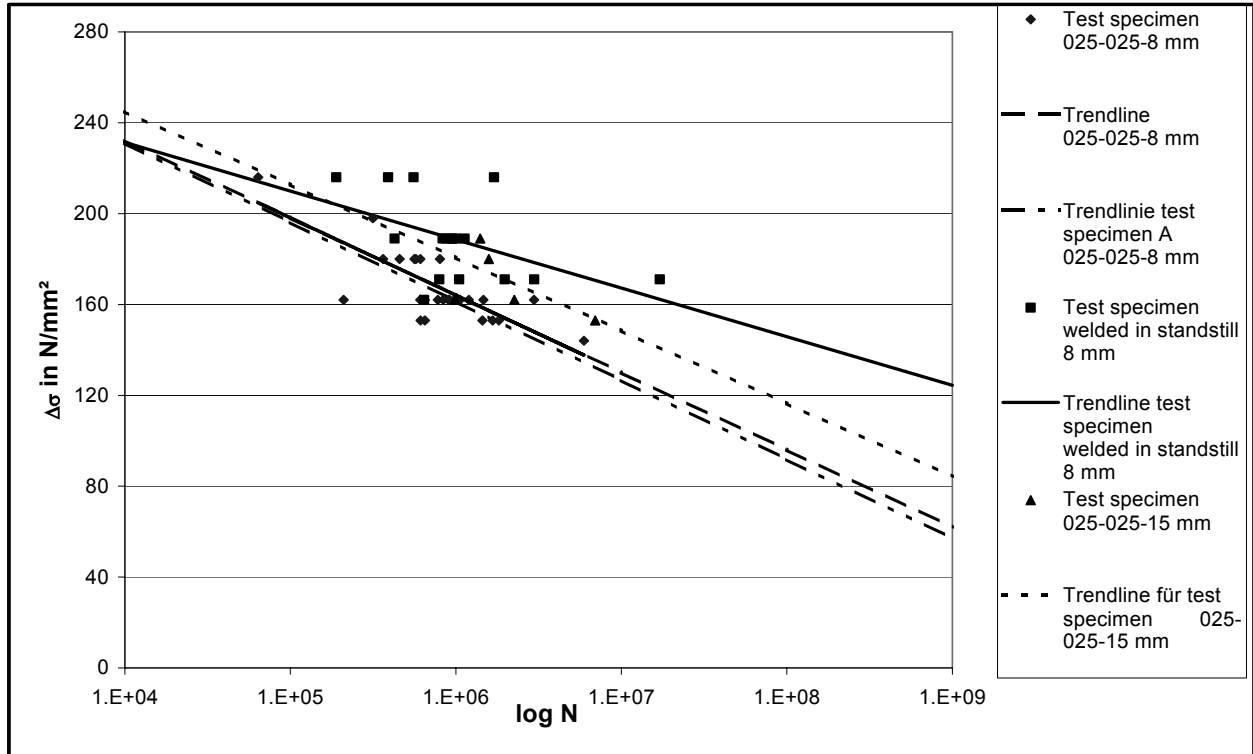


Figure 10: Comparison of S-N-curves for butt welded connections with welds in moving edges and in standstill
 Gap opening amplitude $s = 0,25$ mm
 Frequency of the opening $f = 0,25$ Hz
 different plate thicknesses $t = 8$ and 15 mm

The results have quite a large scatter and it looks like, that the numbers of test results are not yet sufficient enough to make a well based statistical evaluation. It is possible to work out a trendline and to extrapolate into regions where no tests have been performed. It is possible to compare these trendlines for different test parameters to find out in comparison with welds under standstill which results can be achieved under which conditions.

The first conclusion can be drawn as follows:

1. The highest fatigue life in the high cycle range have been achieved with the test pieces welded in standstill.
2. The second best results have those test pieces, which have been welded with an amplitude of $s = 0,125$ mm.
3. The test results where the test pieces welded with an amplitude of $s = 0,25$ mm reach about half the number of cycles compared with number 1.
4. There is no clear tendency in the test results with test pieces which were welded with amplitudes of $s = 0,5$ mm and $s = 0,75$ mm, nevertheless they are the worst ones.

I highly acknowledge that this research project has been supported by the Deutsche Forschungsgemeinschaft over a period of 6 years and within a group of researchers with similar subjects.

DESIGN OF HAUNCHED COMPOSITE CONNECTIONS FOR LONG SPAN BEAM CONSTRUCTION

J Y Richard Liew, Y H Ng and N E Shanmugam

Department of Civil Engineering
National University of Singapore
BLK E1A, 1 Engineering Drive 2, Singapore 117576

ABSTRACT

One of the structural options for beam spans beyond 15m is the haunched beam. By developing continuity at the supports, beam moments and deflections are reduced and this can lead to overall economy by enabling the use of shallower and lighter beam. This paper investigates the behavior of steel-concrete composite haunch connections. Experiments are carried out to study the moment-rotation characteristics of the connections and ultimate moment capacity of the composite sections. Design implications related to composite haunched beams are discussed.

INTRODUCTION

The authors have developed an advanced inelastic analysis model for analyzing the behavior of three-dimensional semi-continuous frames [Liew et al., (1)]. The analysis and design methodology has been verified against test results involving full-scale testing of frames and connections [Liew et al., (2)]. Recent work has been focused mainly on composite frames and their connections [Liew et al., (3)]. Experimental work is currently on going to verify the capability of the analysis model for analyzing building framing systems including the effects of composite beams and connections [Liew et al. (1), (3) & (4)].

In recent times, the demand for long-span and column-free space in buildings has necessitated further research into the behavior of haunched beams since they are considered to be an efficient and economical form for long span construction. Haunched beams are designed by assuming a rigid moment connection between the beams and columns [Lawson and Rackham, (5)]. Depth and length of a haunch may be chosen to enable an economical method of transferring moment into the column and in reduction of beam depth to a practical minimum. Haunched composite beams in which steel beams are designed to act in conjunction with concrete slab of definite width could result in shallow beams, provide a long unobstructed space for services and increase in speed of construction.

Past work on haunched beams focused mainly on steel haunched connections under negative moment. Design methods have been proposed for continuous composite beams, but the hogging beam section and connections are designed as non-composite [Lawson and Rackham, (5); Boswell, (6)]. The object of this paper is to report on the experimental results obtained from sub-assembly tests of composite haunch beams. The experimental program is presented and the results for ultimate moment capacity of the tested haunched connections are given. A design

method consistent with the Eurocode approach for designing continuous composite beam is proposed [Eurocode, (Z)].

SUB-ASSEMBLY TESTS

Five test specimens were chosen to study the effects of haunch length and amount of reinforcement in the slab on the behavior of composite haunched beams. Each specimen consists of two cantilever haunch beams subject to concentrated load applied at the beam ends, as shown in Fig. 1, to simulate an internal joint of a braced frame. The depth of the haunch was chosen equal to the depth of the steel beam. The length was varied from 250 mm to 968 mm, which are equivalent to 3.12%, 5.41%, 8.84% and 12.10% of the beam span. Full depth stiffeners were provided at both sides of the beam web at the haunch tip to prevent lateral-distortional buckling of the beam under negative moment. The details of the test specimens are given in Table 1. Specimen H1 was plain steel specimen whilst the remaining four specimens consist of steel beams act in composite with the floor slab in which sufficient shear studs were provided to develop full composite action.

Table 1 Details of Test Specimens

Specimen	1		2		3		4		5	
Connection	H1	H2	H3	H4	H5	H6	H7	H8	H9	H10
Reinforcement %	0	0	1.34	1.34	2.62	2.62	1.34	1.34	2.62	2.62
Haunch Depth, mm	250	250	250	250	250	250	250	250	250	250
Haunch length, mm	250	433	250	433	250	433	707	968	707	968
Shear Studs per group	Nil	Nil	1	1	2	2	1	1	2	2
Total number of shear studs per beam	Nil	Nil	13	13	26	26	13	13	26	26

Tensile tests were carried out to determine the yield strength and ultimate strength for beams and columns. Similar tests were carried out on the reinforcement bars used in the test specimens and the average values of yield strength and ultimate strength are summarized in Table 2.

Table 2 Properties of steel and reinforcement bars obtained from tensile tests

Item	Diameter (mm)	Yield strength (N/mm ²)	Ultimate Tensile strength (N/mm ²)	Area (mm ²)
Steel Beam	-	309	414	-
Steel Column	-	328	498	-
T20 steel bar	20	565	693	314
T16 steel bar	16	484	584	201
T10 steel bar	10	489	581	79



Figure 1 Typical test Set-up

INSTRUMENTATION AND LOADING PROCEDURE

Inclinometers were placed along the centerline of beam section to measure section rotations. Displacement transducers were used to measure the relative displacements so that the joint rotation can be calculated. Electrical resistance strain gauges were used to measure strain in steel so as to monitor yielding and to determine the failure modes. They were placed at top and bottom of beam flanges near the column flange, at the haunch toe and reinforcement bars. Besides, strain gauges were also placed on some bolts connecting the beams to column flange. This was intended to find out the tensile forces in the bolts at each of the load steps.

The entire load application was performed in three stages. In the first stage, load was applied until the first crack was observed in concrete and, in the second and third stage load was increased up to 60% and 90% of the estimated ultimate load, respectively. This process of loading helps to obtain the initial stiffness of connection and to compare the unloading stiffness at different loading stages. In the final stage, loading was continued until the failure of the specimen.

As mentioned earlier each of the specimens consisted of two haunched connections, one with shorter haunch length and the other with longer haunch length. Therefore, the load application and other measurements were monitored separately. Load was applied in equal increment to each of the haunched beam at the initial stages of loading. Once the weaker beam attained the load close to the failure load, care was taken to balance the load on both beams. When the weaker beam attained its maximum capacity, the load on that beam was maintained at that level whilst the load on the stronger beam was continued until it reached its failure.

PREDICTION OF ULTIMATE MOMENT

Haunch connection without slab reinforcement

Assuming that the bolt will fail in tension and only one tension bolt row is used, the full tension capacity of the bolts is

$$T = R_b < R_{hf}$$

Taking moment about the haunch flange, the moment resistance can be evaluated as

$$M_{hu} = R_b \times (D - D_b + D_h - T/2)$$

Haunch connection with slab reinforcement

It is found that the plastic neutral axis (PNA) lies in the haunch flange when

$$R_r + R_b < R_{hf} + R_{HW}$$

Thus, moment can be determined as follows:

$$y_c = \frac{R_r + R_b - R_{hf}}{1.2 p_y t_{hw}}$$

$$R_{hw} = 1.2 y_c p_y t_{hw}$$

$$M_u = R_r \left(D_r + D + D_h - \frac{T_{hf}}{2} \right) + R_b \left(D - D_b + D_h - \frac{T_{hf}}{2} \right) - R_{hw} \left(y_c + \frac{T_{hf}}{2} \right)$$

where M_u is moment capacity of composite haunch connection, p_y design strength for steel, R_b bolt capacity in tension, R_{hf} haunch flange capacity, R_{hw} haunch web capacity, R_r tensile force in reinforcement, t_{hw} thickness of the haunch web, T_{hf} thickness of haunch flange and y_c distance from the top of haunch flange. In an end-plate composite connection, the first tension bolt row seldom achieves its full tension capacity. In haunched composite connection, the first bolt row always achieve its yielding capacity. This is because the PNA hardly lies above the level of the first bolt row. This has been observed in one of the connections tested (H8) in the current series. The composite beam moment capacity at the tip of the haunch was obtained based on the method given in [Eurocode, (7)] for section under negative bending.

RESULTS AND DISCUSSION

Ultimate moment obtained from the experiments along with those predicted by the present method for all the test specimens are summarized in Table 4. Also, the experimental values are compared with the predicted results, which shows a good prediction within 10% margin.

Effect of Slab Reinforcement Ratio

Figure 2 compares the load-displacement curves obtained from specimens H2, H4 and H6 which have same haunch depth (D_b) and length ($2D_b$), but of different slab reinforcement percentage of 0%, 1.34% and 2.62%, respectively. Higher percentage of reinforcement in the slab shifts the failure from the steel connection to the haunched toe composite section. Failure of H2 connection was triggered by tensile fracture at the bolt thread. Failure of H4 occurred at the haunch toe in which the composite beam section is almost fully yielded, and the compression beam flange at the point of intersection with the haunch toe has buckled inelastically. H6 was the same in all respects as the specimen 2 and 4 except that the concrete slab was reinforced with 10 numbers of T20 deformed bars. Failure occurred at the haunch toe, as shown in Fig. 4, where the composite beam section in negative bending was almost fully yielded in compression. Further increase in reinforcement will not yield significant improvement of load carrying capacity since the limit of resistance for the steel section in compression has been reached with plastic neutral axis shifted to the concrete slab.

Table 4 Summary of Test Results

Specimen	1		2		3		4		5	
Connection	H1	H2	H3	H4	H5	H6	H7	H8*	H9	H10
Ultimate Load (kN)	138	117	162	181	222	241	258	312	306	NA
M_{exp} at haunch toe	214	160	251	248	344	330	282	260	334	NA
M_{exp} at haunch Con	249	211	291	327	399	434	464	562	550	NA
Failure Mode	Con.	Con.	Toe	Toe	Toe	Toe	Toe	Con.	Toe	NA
M_{pred} (kNm)			255	255	319	319	255	533	319	319
M_{exp}/M_{pred}			0.98	0.97	1.08	1.03	1.1	1.05	1.05	NA

*Failure of Specimen H8 occurred at the haunch heel. The values shown in the table are those corresponding to haunch heel.

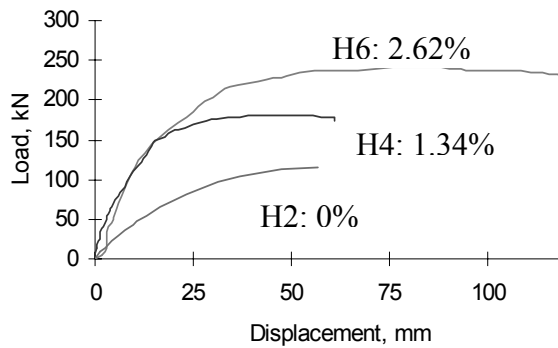


Fig. 2 Effect of reinforcement ratio: haunch depth = D_b ; length = $2D_b$.

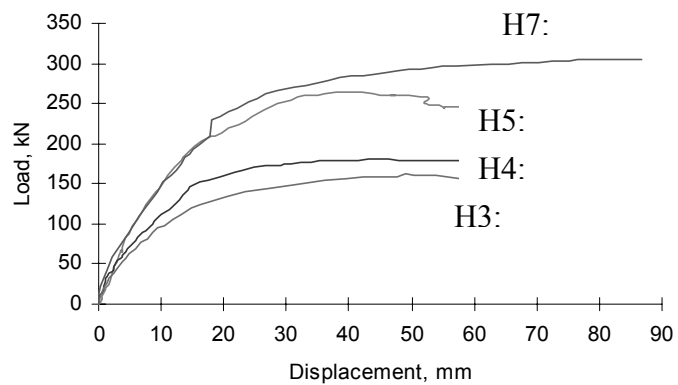


Fig. 3 Effect of haunch length: haunch depth = D_b ; reinforcement ratio = 1.34%

Effect of Haunch Length

Specimens H4, H7 and H8 have been tested as parts of the specimen H3 except the haunch lengths were chosen approximately equal to two times the depth as in H4, three times the depth as in H7 and four times the depth as in H8. The reinforcement in the slab was kept the same as in specimen 2. Figure 3 compares the load-displacement curves obtained from these specimens. For H4 and H7, failure moment for this connection occurred at the haunch toe. For H7, the ultimate capacity of composite section (282 kNm) at haunch toe section was close to the calculated plastic capacity (255 kNm) by Eurocode 4. Connection H8 is the same as H4 except that the haunch length in this case was 968 mm or 12.10 % of an 8-m span beam. Failure occurred at the haunch heel near to the connection as shown in Fig. 5. Failure moment for this connection was found to be 562 kNm, which is close to the predicted value of 533 kNm. The test results show that it is possible to control the failure mode by varying the haunch length and that longer haunch length shifts the failure from haunch toe to haunch heel.



Fig. 4 View after failure of H6

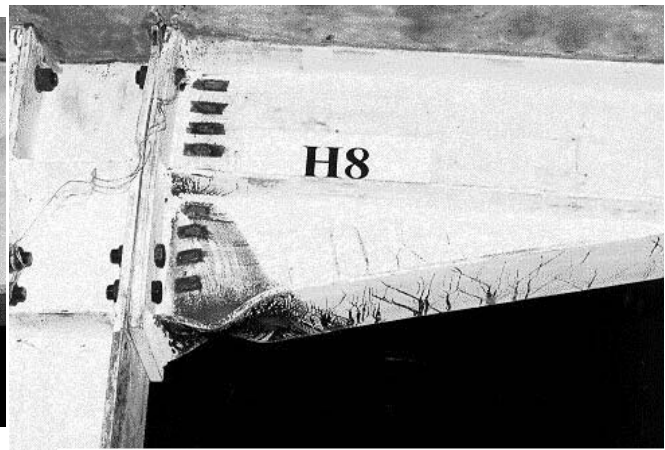


Fig 5 View after failure of H8

TESTING OF COMPOSITE HAUNCHED BEAMS

The purposes of the tests were to model a haunched composite beam within a braced multi-span and multi-story frame, and to investigate the likely redistribution of moments around the frame due to the formation of plastic mechanism in the beam. The load at collapse was compared with that obtained from plastic analysis hence the proposed plastic design method could be established.

The test setup of the composite haunched beam is shown in Figs. 6a&b. The beam is subject to two concentrated loads at the inner span and a point load at the tip of the end spans to simulate the continuous beam action. Four independent actuators were employed, two for the main beam and two for the cantilever beams. Plastic analysis and design methods were adopted. A plastic collapse mechanism was expected in the inner beam, while the columns were designed to remain elastic. This experimental set up is to test the inner span to its ultimate capacity. Thus, care had been taken to prevent failure at the beam-to-column connection at the cantilever beam by providing a stronger haunched connection.

The details of the beam specimens are summarized in Table 5. The beam capacities, based on the total loads applied to the beam at failure, are also reported in Table 5. Comparison of HB1 and HB2 shows that an increase in slab reinforcement from 1.34% to 2.62% leads to 11% increase of beam capacity. Plastic hinges form at the haunch toes follow by inelastic redistribution of forces until a plastic zone occurs at the mid-span. There was no sign of strength degradation even when the beam reached a very large displacement.

Comparison of HB1 and HB3 shows that increasing haunch length from $1.7D_b$ to $3.9D_b$ leads to 25% increase in beam capacity. For HB3, a wide plastic zone was first developed at the mid-span between the two load points followed by failure at the haunched connections. However, the connection failure occurred only when the beam deflected to a very large extent. HB3 was designed to achieve the most optimum load carrying capacity in which the moment resistance of the haunched connections and composite beam could be reached simultaneously.

Table 5 Details and results of beam tests

Beam Specimen	HB1	HB2	HB3
Reinforcement, %	1.34 (8T16)	2.62 (10T20)	1.34 (8T16)
Haunch Depth, mm	250	250	250
Haunch Length, mm	433	433	968
Slab width, mm	1400	1400	1400
Slab thickness, mm	120	120	120
Shear studs per group	1	2	1
Beam Capacity (2P, kN)	540	604	674

B1, B2 and B3: 254 x 146 UB 37 kg/m and C1: 203 x 203 UC 60 kg/m.

DESIGN IMPLICATIONS

Composite haunched beams are designed in a similar manner to continuous beams of uniformed section. The critical sections for design are at the haunch toe, haunch heel or the haunch connection. The depth of the haunch may be selected to develop the required moment in the connection. The length of the haunch is selected to provide an economical design of the beam. The additional of reinforcement in the slab provides higher negative moment resistance to both the haunched connection and the haunch sections. The effect of composite action is to reduce the haunch depth for the same moment. However, large amount of reinforcement will result in an upward shifting of plastic neutral axis (PNA), and the steel section will be subjected to more compression. The result of this is that the available rotation capacity of the composite section is reduced. The test results show that the composite haunched connection is very rigid and the connection rotation is negligible. For all the composite connections (except H8) failure does not occur at the connection because the critical component is in the beam at the haunch toe. By providing a full depth stiffener at both sides of the web at the haunched toe, the haunched section is sufficiently restrained to prevent lateral buckling. There is sufficient rotation capacity at the haunched toe for a plastic mechanism to form in a beam. It should be noted that 'Plastic Analysis' requires only the ultimate moment and rotational capacities. As long as the section is able to resist the limit load and provide sufficient rotations, which allow moment redistribution, connection stiffness is not a requirement in a rigid frame analysis. This is evident from the tests conducted on three continuous haunched beams using the same haunch connections as reported in this paper.

Composite haunched beam can be designed economically for span-to-depth ratio ranging from 25 to 30. For span length beyond $30D$, where D is the depth of steel beam and the slab, deflection and vibration become the main concern. Other innovative structural options needed to be devised to achieve the desired performance.

CONCLUSIONS

Experiments on composite haunch connections are described and results corresponding to ultimate moment capacity, and failure modes are presented. These connections are classified as a full strength rigid connection in accordance with Eurocode 4. It is confirmed by the test results that the measured moment capacity for all connections is larger than the plastic capacity of the beams and rotation in all tests was very small, less than 2 miliradian. Prediction by Eurocode 4 to estimate the ultimate capacity of composite hogging section is sufficiently accurate. Results show that observed moment capacity for the hogging section of the beams falls within 10 % of the predicted value. Haunch toe can be strengthened effectively by means of web stiffener to the full depth of the beam. However, the length of the haunch is limited to 12.10 % of the beam span. Experimental observations show that the failure is localized at the haunch toe section. Haunch length has no significant effect on rotation capacity and it is found that rotation at the ultimate capacity always falls within 30 to 45 miliradian. Increase in reinforcement from 1.34% to 2.62% does not reduce rotation capacity significantly but it increases the ultimate moment capacity of the composite section. Longer haunch length tends to shift the mode of failure to the haunch heel of the connection.

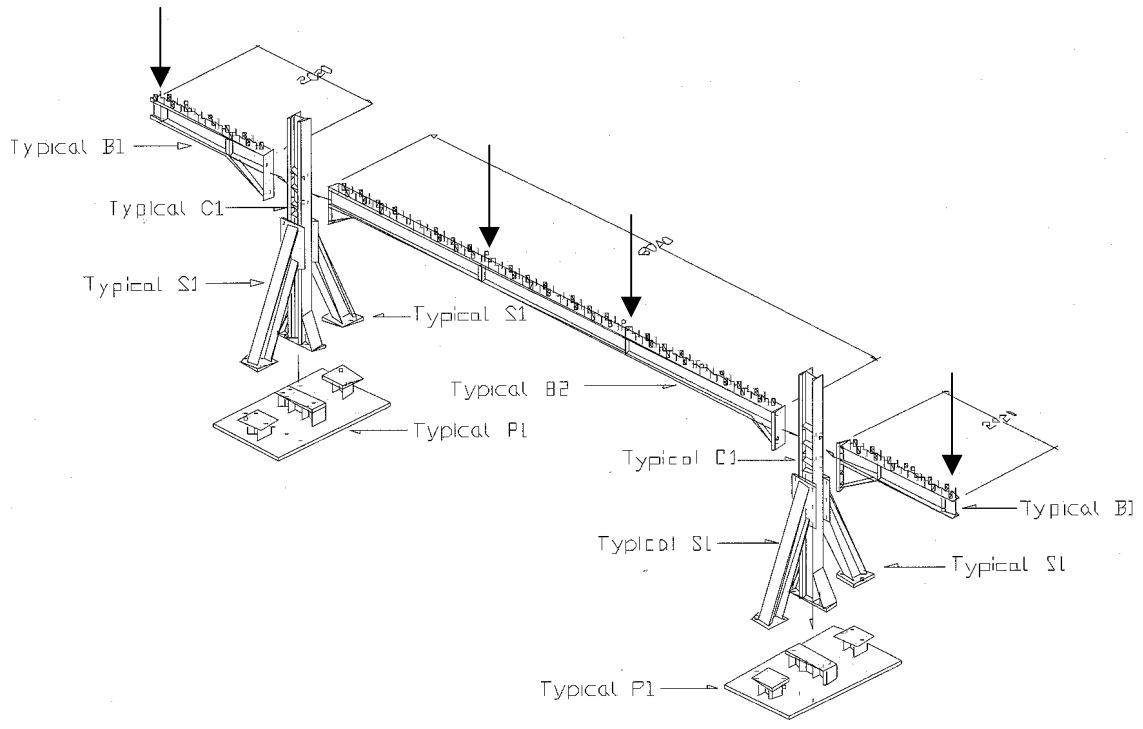


Figure 6a Test set up of composite haunched beam

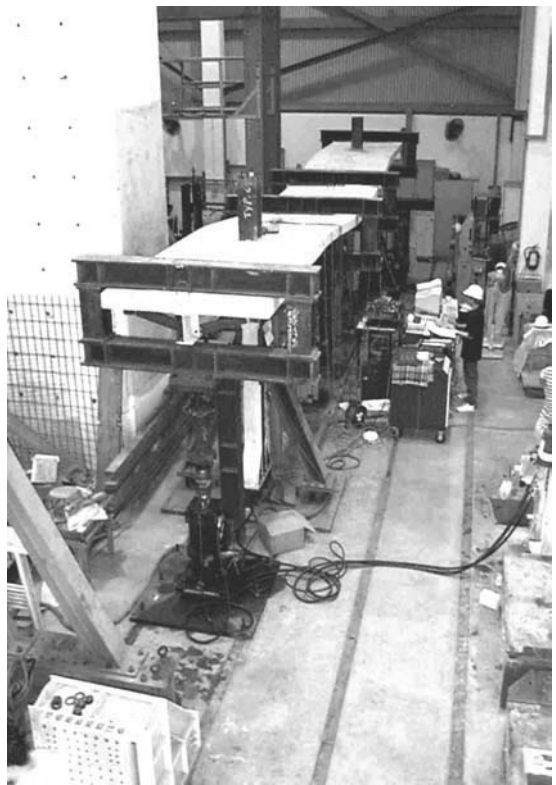


Figure 6b Testing of a typical composite haunched beam

ACKNOWLEDGEMENT

The investigation presented in this paper is part of the research program on Composite Construction for long span structures being carried out in the Department of Civil Engineering at the National University of Singapore. The work is funded by a research grant (RP 3981614) made available by The National University of Singapore. The support from Yongnam Engineering & Construction (Pte) Ltd, Singapore who supplied the test specimens is gratefully acknowledged.

REFERENCES

1. Liew J.Y.R, Chen W.F. and Chen, H., (2000) Advanced inelastic analysis of frame structures, *Journal of Constructional Steel Research*, Elsevier, UK, 55(1-3), 267-288.
2. Liew, J Y R, Yu, C H, Ng, Y H and Shanmugam, N E. (1997) Testing of semi-rigid frames for calibration of second-order inelastic analysis, *Journal of Constructional Steel Research*, Elsevier,UK, 41(2/3), 159-195.
3. Liew, J Y R, Teo, T H, and Shanmugam, N E, and Yu, C H, (2000), Testing of steel-concrete composite connections and appraisal of results, *Journal of Constructional Steel Research*, Elsevier, UK, 56(2), 117-150.
4. Chen H, Liew, J Y R and Shanmugam N E, (2000), Nonlinear inelastic analysis of building frames with thin-walled cores, *Thin-Walled Structures*, Elsevier, UK, 37(3), 189-205.
5. Lawson, R M., Rackham, J W. (1989), *Design of Haunched Composite Beam in Buildings*, Steel Construction Institute, UK, 79pp.
6. Boswell, L F. (1992), *The Structural Behavior of Haunched Composite Beams in Long Span Building Application, Final report to SCI in respect of British Steel Market Development Grant No. MDF P9/90*, City University, London.
7. Eurocode 4, (1994), *DD ENV 1994-1-1: 1992 Design of Composite Steel and Concrete Structures, Part 1.1 General Rules and Rules for Building*, British Standard Institution, London.

Behavior of Bottom Flange Bearing Beam-to-Girder Connections

Angela S. Terry, P.E.

The Charles E. Via, Jr. Department of Civil and Environmental Engineering
Virginia Polytechnic Institute and State University
Blacksburg, Virginia 24061
USA

W. Samuel Easterling, Ph.D., P.E.

Associate Professor and Assistant Department Head
The Charles E. Via, Jr. Department of Civil and Environmental Engineering
Virginia Polytechnic Institute and State University
Blacksburg, Virginia 24061
USA

ABSTRACT

A new type of beam-to-girder connection is the subject of a research project being conducted at Virginia Tech. The connection consists of the beam bearing directly on the bottom flange of the girder. A lateral stabilizing angle and erection bolts through the bottom flanges are required to complete the connection. The connection would be useful with deep deck (> 3 in. (76 mm)) composite slabs to offset the increase in the floor depth caused by the additional slab depth, as well as with commonly used deck (≤ 3 in. (76 mm)) in which floor-to-floor height needs to be minimized. Results from an initial set of tests and yield line analyses are presented. The test results indicate that the connection shows promise as a viable alternative to traditional beam-to-girder connections.

INTRODUCTION

Composite slabs are used in many steel framed buildings. Researchers have conducted studies on many aspects of composite slabs from anchorage to embossment patterns. However, the maximum potential of composite slabs in terms of deck profile depth and span is not fully realized. Research conducted in this area could potentially expand the benefits of composite slabs by taking advantage of large spans and thus eliminating intermediate filler beams. Eliminating filler beams and their connections to supporting girders further reduces building weight, framing costs, and foundation costs. One of the predominant concerns with increasing the depth of the composite slab floor system is the overall effect on floor depth and subsequent structure height. A new type of bottom flange bearing beam-to-girder connection could be used to offset the increase in the overall floor depth caused by the additional slab depth. This connection, illustrated in Fig. 1, is the subject of a research project currently being conducted at Virginia Tech.

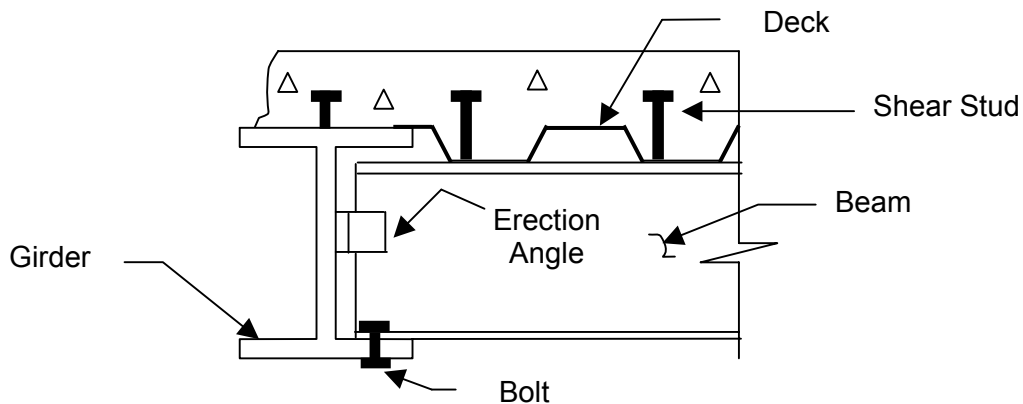


Figure 1. Proposed Beam-to-Girder Connection
(beam shown one side only for illustration purposes)

Maintaining the conventional deck-to-beam arrangement, in which the deck bears directly on the top flange of the beam, takes advantage of the benefits of using continuous span steel deck. These benefits include increased strength, longer allowable span lengths and less deflection. However, the location of the beam relative to the supporting girder may be altered to compensate for the additional structure depth associated with the deep deck profile. To minimize overall structure depth, the beam may bear on the bottom flange of the girder rather than aligning the coped beam top flange with the girder top flange. This variation on conventional framing methods may be more than enough to compensate for the deeper deck. Additionally, the resulting beam-to-girder connection is simpler, requiring less fabrication at both the beam and the girder as well as making for easier erection of the members in composite and non-composite floor systems.

The intent of the current research is to verify the adequacy of the proposed bottom flange bearing connection both analytically and experimentally. The bottom flange bearing arrangement was initially investigated analytically using yield line theory. Five different wide flange girder sections were then experimentally tested to determine the actual yield pattern development and ultimate load when subjected to patch loads on the bottom flange that simulate the beam reaction. Strains and deflections at multiple locations on the girder flange were recorded and analyzed. Refined analyses using the finite element method, confirmatory full-scale tests, and subsequent development of design procedures are planned. This paper describes the progress through the preliminary tests.

EXPERIMENTAL PROGRAM

A loading apparatus was designed and fabricated that allowed a single actuator to simultaneously apply two equal loads to the bottom flange of a wide flange test section, one load on each side of the web as would be the case for an interior girder. Refer to Figs. 2, 3, and 4 for illustration of the loading apparatus and orientation relative to the test section. The center three feet of every test section was whitewashed prior to testing to visually reveal yielding during testing.

The lateral bracing of the top and bottom flange of the test section was located approximately 1 ft. 6 in. (457 mm) to either side of the loading point and is shown in Fig. 4. A frame supported by the columns bolted to the reaction floor laterally braces the loading apparatus. The frame, shown in Fig. 4, does not restrict movement of the loading apparatus in the vertical direction, so

that the entire load from the actuator is delivered to the flanges of the test section. Load transmission was verified by placing redundant load cells at the test section supports.

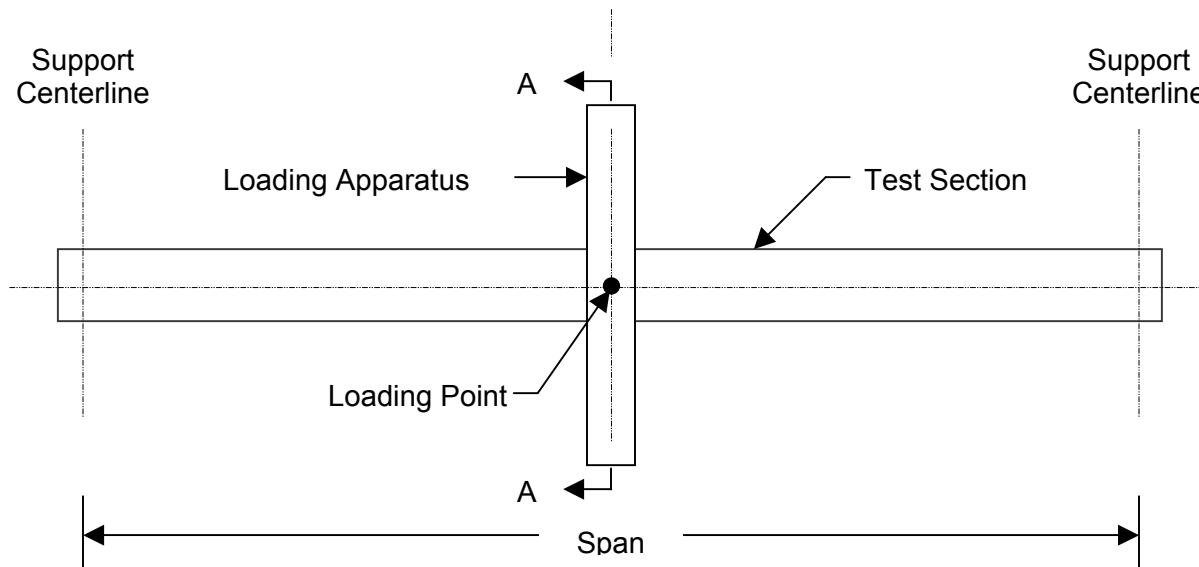


Figure 2. Plan View of Test Setup

The method of load application permitted a simplified simulation of a beam reaction including rotation of the reaction by means of a roller. Two different options were used to actually transmit the load from the loading apparatus to the girder section. One option (Option A) transmits the load through the roller to a bearing plate into the girder bottom flange. The second option (Option B) more realistically represents the load path of a beam-to-girder connection. Option B transmits the load through the roller to a built-up stub beam section with web stiffeners. See Figs. 5 and 6 for illustrations of both options.

Five different wide flange shapes were tested, as noted in Table 1. The maximum load obtained, representative of the sum of two beam reactions at an interior girder, ranged from 79 kips (351 kN) to 280 kips (1245 kN). Table 1 presents a summary of the test results.

Table 1. Test Results					
Section	Fy ksi (MPa)	Span inch (mm)	Load Application Method	Maximum Load kips (kN)	Maximum Flange Edge Deflection inch (mm)
W21x44 (W530x66)	54 (372)	96 (2438)	Option A	79 (351)	0.32 (8.1)
W24x55 (W610x82)	58 (400)	96 (2438)	Option B	145 (645)	0.17 (4.3)
W18x40 (W460x60)	51 (352)	96 (2438)	Option B	169 (752)	0.20 (5.1)
W18x50 (W460x74)	55 (379)	78 (1981)	Option A	214 (952)	1.12 (28.4)
W24x68 (W610x101)	53 (365)	78 (1981)	Option B	280 (1245)	0.79 (20.1)

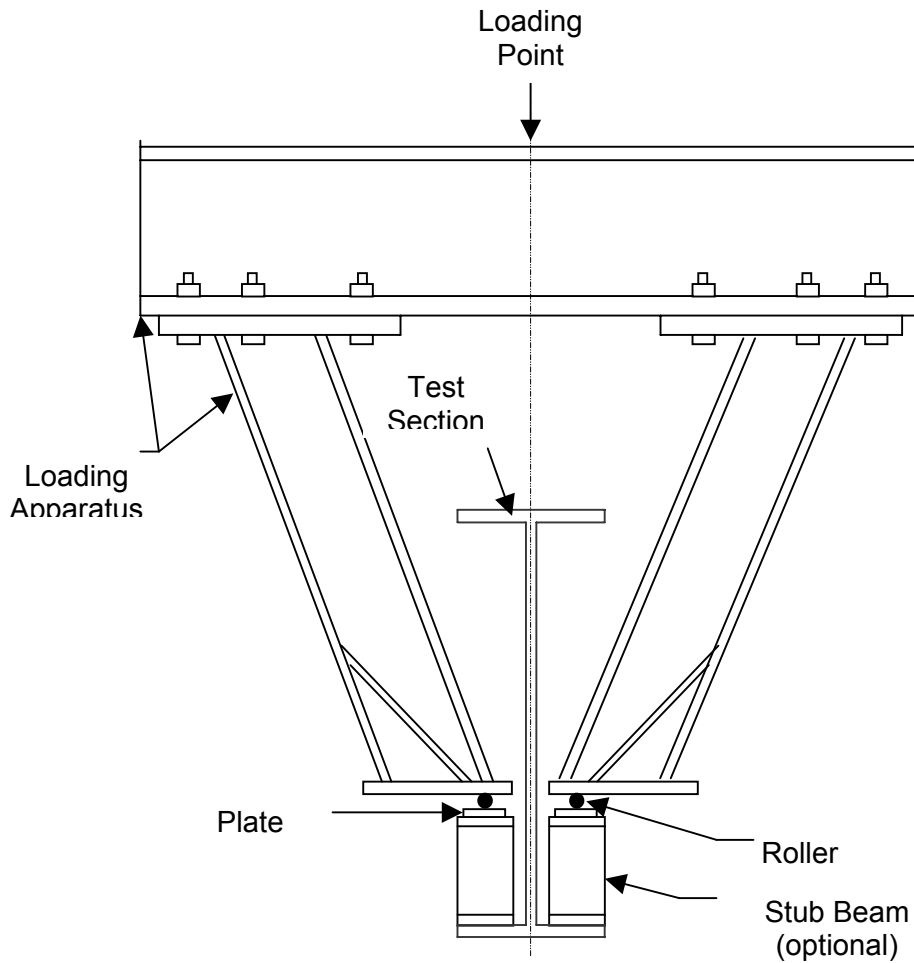


Figure 3. Loading Apparatus Elevation

In addition to the maximum load obtained, deflections and strains were recorded at multiple locations on the girder flange. Displacement transducers were placed along the test section web at one support and at midspan. Two additional transducers were located midspan of the test section at the outer edges of the bottom flange. The average maximum flange deflection, subtracting the web deflection at midspan, is given in Table 1 for each test.

Strains in the girder bottom flange were measured at six locations, three on each side of the web. The locations were isolated based on the results of the yield line analysis. Both sides of the web were instrumented to verify the symmetry of the load application.

Figures 7, 8, and 9, taken during and after testing, show the yield line pattern and deformation of the bottom flange. The same yield line pattern developed in all five tests.

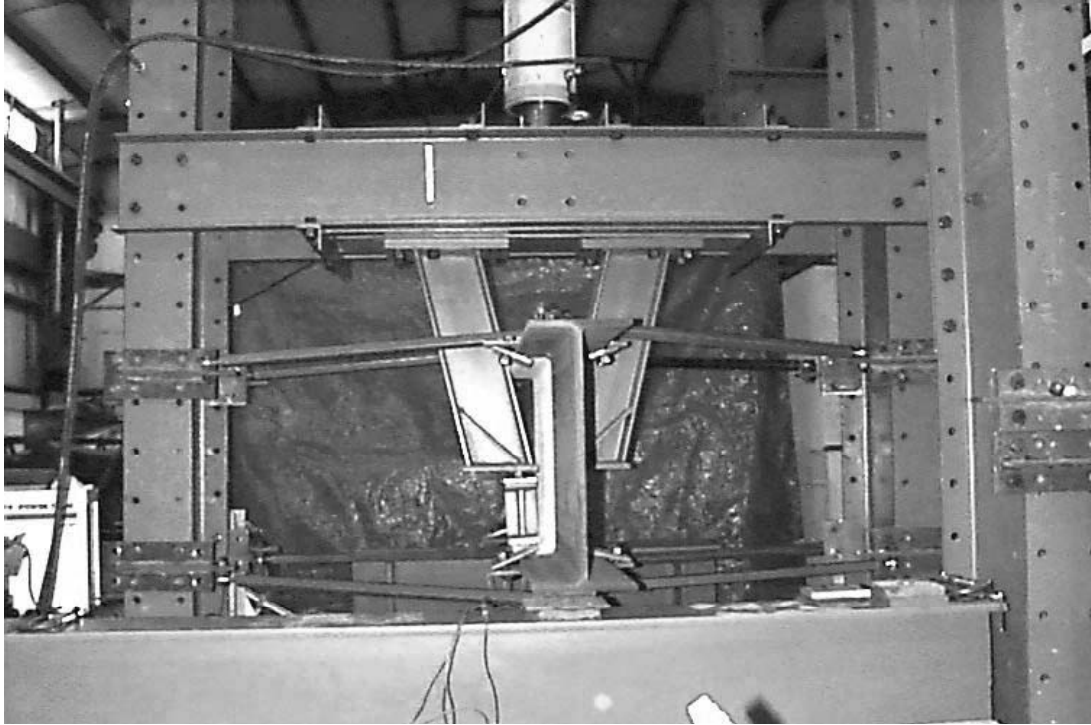


Figure 4. Test Apparatus Elevation

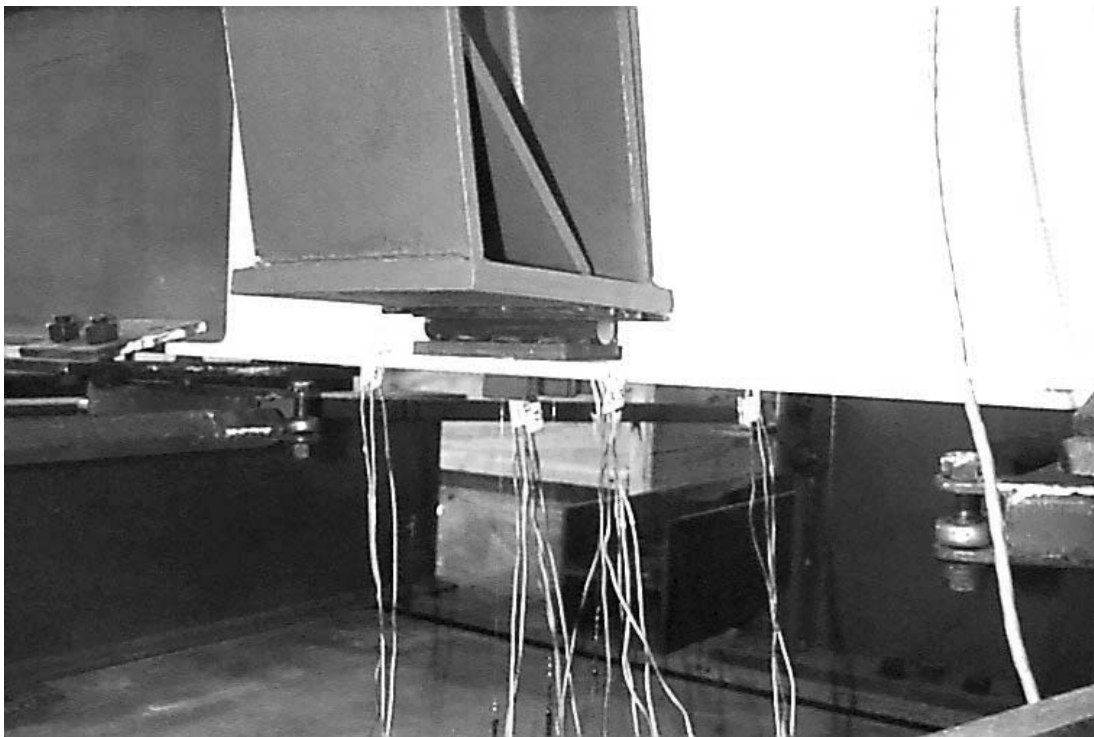


Figure 5. Loading Option A

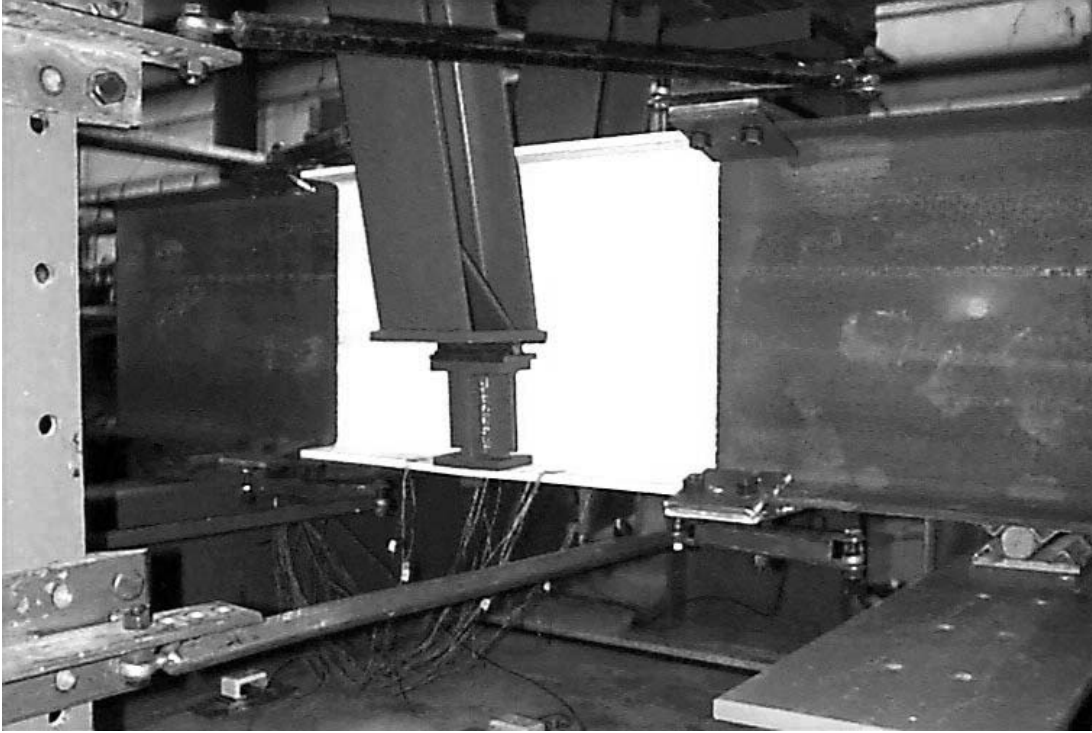


Figure 6. Loading Option B

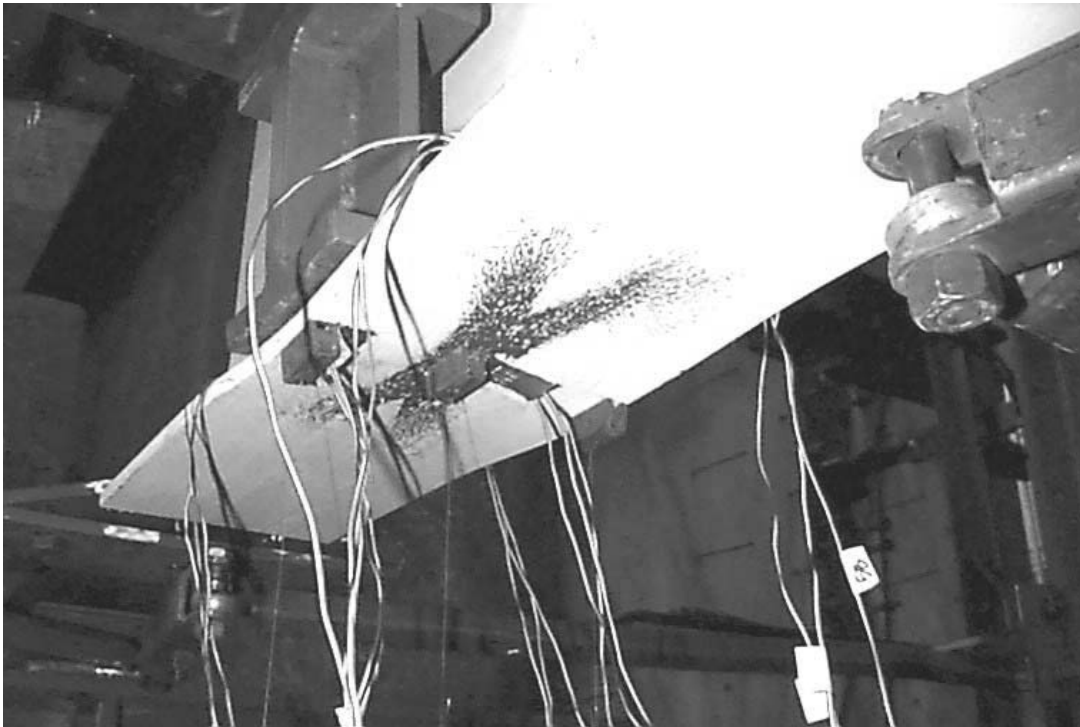


Figure 7. Bottom Flange Yielding During Test

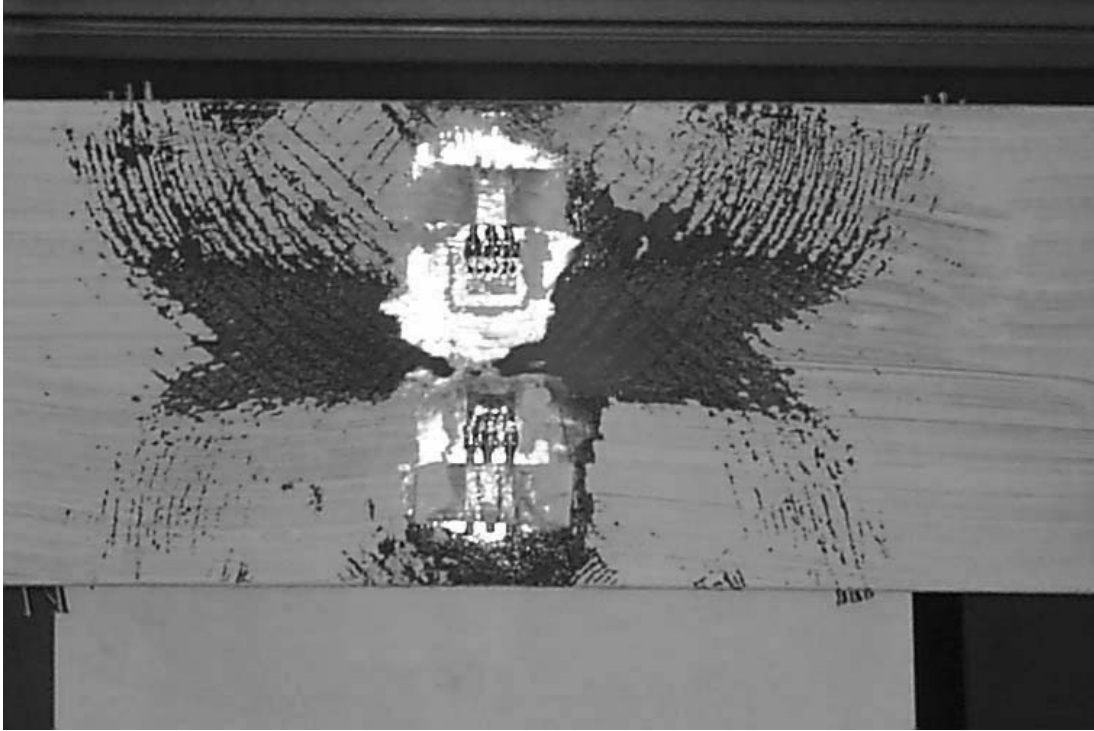


Figure 8. Bottom Flange Yield



Figure 9. Bottom Flange Deformation

YIELD LINE ANALYSIS

The bottom flange bearing arrangement was analytically investigated using yield line theory. The yield line model is illustrated in Fig. 10. The following equation relates the magnitude of the beam reaction at girder flange yield to the geometric and material properties of the beam and girder.

$$R = F_y t_f^2 \left[\frac{\frac{2}{\sqrt{2}} + \frac{b_b}{4b_g}}{1 - \frac{d}{2b_g}} \right]$$

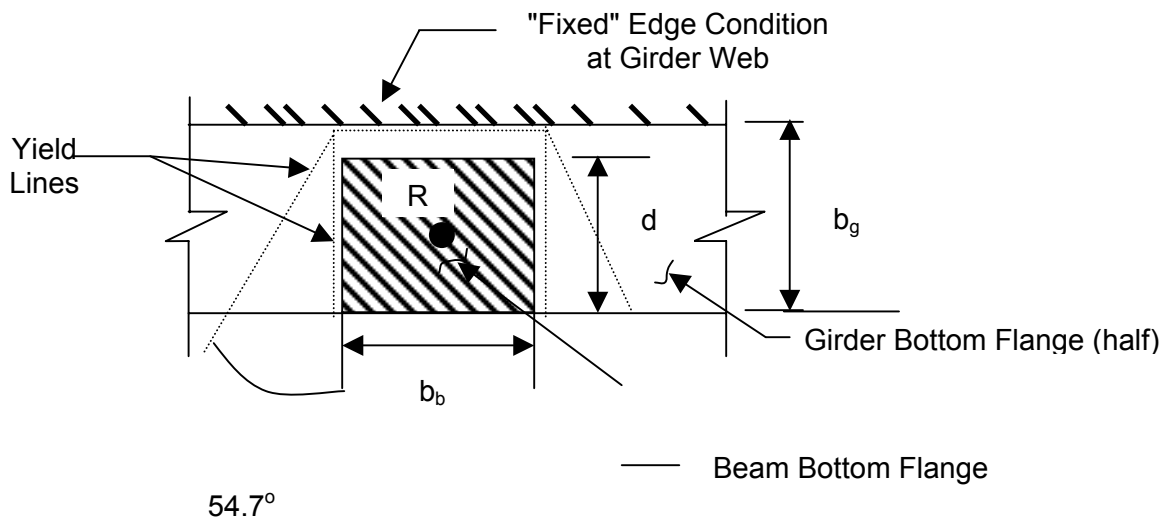


Figure 10. Yield Line Model of Proposed Beam-to-Girder Connection

Results of the yield line analysis for the five shapes tested in the experimental program are tabulated in Table 2.

Table 2. Comparison of Analytical and Experimental Results		
Section	Analytical R kips (kN)	Experimental Load kips (kN)
W21x44 (W530x66)	33 (147)	39.5 (176)
W24x55 (W610x82)	46 (205)	72.5 (322)
W18x40 (W460x60)	44 (196)	84.5 (376)
W18x50 (W460x74)	54 (240)	107 (476)
W24x68 (W610x101)	56 (249)	140 (623)

CORRELATION OF EXPERIMENTAL AND ANALYTICAL RESULTS

The experimental loads were found to be significantly greater than the analytical loads anticipated with greater divergence as the size of the section increases. The actual yield line that developed in the test sections was similar in shape to the one predicted.

Based on the observed displaced configuration of the experimental specimens and the fact that the yield line results did not compare well with the experimental results, it is clear that the yield line model in its present form is not adequate. It is hypothesized that a model that combines the yield line approach with membrane action may be more reflective of the actual behavior. This will be considered in any subsequent analysis.

CONCLUSIONS

Results indicate that the girder flange can adequately support loads greater than typical filler beam end reactions based on preliminary calculations for a typical floor bay, with construction load, live load, superimposed dead load, and partition load. The yield line analysis model resulted in predictive strengths well below those observed in the tests, thus the analytical model needs further development. However, the proposed connection appears to be a promising solution to the issue of increased structural depth of composite slab systems with deep deck profiles as well as simplifying the fabrication and erection of beam-to-girder connections in other floor systems.

FUTURE EXPERIMENTAL RECOMMENDATIONS

In the initial phase, the method of load application through the loading apparatus simulated beam rotation at the connection without the logistics of adding two beam sections to the test setup. Future phases of experimental testing should include one or two large-scale tests. These tests would utilize longer span girder sections and load application through actual beam sections connected to the girder. The subsequent research would verify rotations, strains, displacements, and ultimate loads obtained in the first phase. Second phase tests should also evaluate any effect the stabilizing angle and holes for erection bolts may have on the behavior of the connection.

Further analytical analyses, including combining yield line and membrane action, and finite element studies, will enable a more refined evaluation of the behavior. The refined analyses will hopefully result in a closer prediction of experimental loads, thus leading to an acceptable design procedure for the proposed connection.

NOTATION

R = concentrated beam reaction at girder

F_y = yield strength of girder

t_f = thickness of girder flange

b_b = width of beam flange

b_g = approximately 1/2 width of girder flange

d = length of beam bearing

BEHAVIOUR OF COLD FORMED STEEL TRUSS BOLTED JOINTS

R. ZAHARIA* and D. DUBINA**

* Assist. Prof. Ph.D., The 'Politehnica' University of Timisoara

** Prof. Ph.D., The 'Politehnica' University of Timisoara

ABSTRACT

The paper presents the experimental programme performed at the "Politehnica" University of Timisoara, Romania, in order to study the behaviour of bolted connections in cold formed steel trusses. Tests on T joints provided evidence of the semi-rigid behaviour of such connections. A formula to evaluate the axial and rotational rigidity of connection is calibrated, and a cold-formed steel truss is tested, in order to observe the structural behaviour of joints.

1. INTRODUCTION

Cold-formed steel trusses are frequently used in industrial and residential buildings, mainly as roof structures. The truss members are joined with bolts and screws, or using multiple press joined or "Rosette" type connections. For medium and large span trusses, bolted connections are usually recommended. There are examples of cold-formed steel trusses with built-up back-to-back lipped channel sections in chords and single lipped channels for diagonals, joined by bolts, able to cover spans until 60 meters.

Concerning the joints behaviour of this type of trusses, usually they are with eccentric connections, and this feature must be taken into account in the global analysis. The use of 2, 3 or 4 bolts on each flange of the diagonal members, and accounting for their slenderness, is supposed to modify the assumption of pinned joints, generally accepted in case of trusses. The real behaviour of joints, in this case, is semi-rigid with partial moment resistance, which has as effect a favourable reduction in the buckling length of diagonals, but in the same time, due to the rigidity and eccentricities of connections, it induces supplementary bending moments in members. To evaluate the real characteristics of the joints, the deformability of connection, due to the bearing work of bolts in the thin plates, associated with the hole elongations, bolts tilting and slippage, must be considered. In order to estimate the performance of bolted joints in cold-formed steel trusses, an extensive research programme was developed in the Laboratory of Steel Structures of the "Politehnica" University of Timisoara. The present paper summarises the main results of this research.

2. EXPERIMENTAL EVIDENCE OF JOINT SEMI-RIGIDITY

To evaluate the bending moment – rotation curve, ten T joint specimens were tested (1)-(3). They are shown in Figure 1 with the dimensions from Table 1. The testing arrangement is shown in Figure 2. Two inclinometers, I_1 and I_2 were placed on the diagonal, in order to measure its rotation, one on the axis of the connection, and the second on the face of the chord.

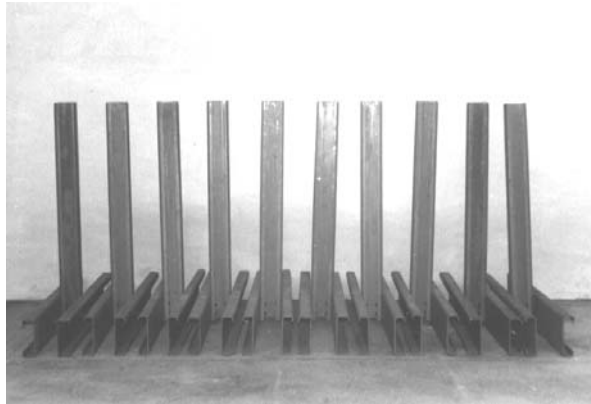


Fig. 1. T joint specimens

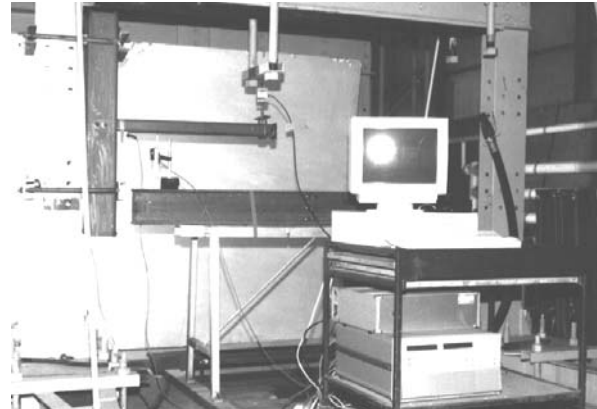


Fig. 2. T specimen in testing machine

Table 1 - Test specimen dimensions [mm]

Node	Chord				Diagonal			
	h	b	c	t	h	b	c	t
1	135	43	19	3	79	51	20	2.05
2	130	45	20	3	81	49	20	3.00
3	135	45	22	3	84	59	20	2.05
4	135	45	20	3	81	56	20	3.00
5	135	40	20	4	81	50	19	2.05
6	140	39	19	4	82	50	20	3.00
7	140	39	20	4	80	46	18	4.05
8	140	38	21	4	84	59	20	2.05
9	138	38	20	4	81	58	20	3.00
10	140	38	22	4	77	55	21	4.05

Table 2 shows the mechanical characteristics corresponding to the different thickness t of the cold-formed sections. Table 3 contains the representative measured values for all tested specimens. Corresponding to inclinometers 1 and 2, subscripts 1 and 2 were used to specify the related values of the resistant moment and initial stiffness of the joint, while M_s is the slippage moment. Figure 3 shows the experimental bending moment - rotation curve, for one of the tested joints, compared with the EC3 boundary for rigid full resistant beam-to-column connection in a braced frame (4).

Table 2 - Mechanical characteristics [N, mm]

t	f_y	f_u	ϵ_u (%)
2.05	341.6	476.6	27
3.00	297	421.2	28
4.05	374	562.4	22

Table 3 - Measured characteristics for tested specimens [daN, m, rad]

Node	M_s	θ_1	M_{Rd1}	K_1	M_{Rd2}	K_2
1	30	0.07	169	1013	151	1005
2	18	0.08	215	1248	200	1184
3	25	0.05	180	1027	170	1018
4	27	0.11	210	1111	205	951
5	23	0.075	168	1056	144	980
6	25	0.095	220	1532	200	1393
7	20	0.11	305	2118	295	1890
8	25	0.02	170	1097	155	960
9	20	0.058	225	1549	210	1130
10	23	0.087	315	2036	310	1810

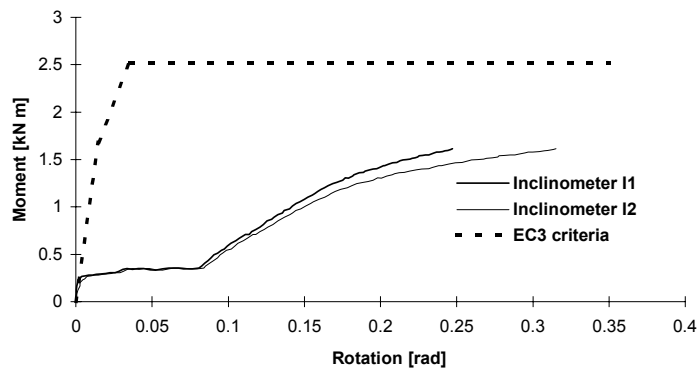


Fig. 3. Experimental bending moment - rotation curves

It can be concluded that, for all tested specimens, the rotational flexibility is mainly due to the bearing work of the bolts, considering both the elastic and plastic deformations of the bolt holes. The differences introduced by the local deformations of connected members (the values corresponding to inclinometer I_2) are generally small. Consequently, the rotational rigidity of the joint can be evaluated if the axial rigidity of the relevant single lap bolted connection in shear is known. If the initial rotational slippage is neglected, then, according to Eurocode 3, all tested joints

can be classified as semi-rigid and partial moment resisting. In fact, the triangulated shape of truss, which is geometrically and kinetically stable, and the presence of the axial forces in connected members prevent, or limit, at least, the initial rotational slippage in joint. In order to provide the evidence of this assumption, a cold-formed steel truss is tested in the third step of this experimental programme.

3. AXIAL RIGIDITY OF SINGLE LAP JOINT

Experimental studies in order to calibrate a formula for the flexibility of single lap bolted connection of two thin plates were systematically performed at the University of Salford (5). This formula gives the axial flexibility of a single lap connection in terms of plate thicknesses and considering the threaded portion of the bolt into connection. The Salford formula was calibrated for a M16 bolt and a 2mm clearance of the bolt hole.

In case of specimens tested at Timisoara, M12 bolts with 1mm clearance of the bolt hole, as used in Romanian practice, were considered. This part of the experimental programme was aimed to calibrate a formula for the axial rigidity of single bolt lap joints, subjected to shear, depending of plate thickness and bolt diameter, considering the practical case of threaded portion of the bolt into connection, and 1mm hole clearance. Three different thicknesses for the plates, between 1.85-3.75mm, and five bolt diameters, between 8-16mm, were considered (6). Table 4 shows the plate thickness/ bolt diameter combinations used for specimens. Mechanical characteristics of steel plates were experimentally established and are given in Table 5.

Table 4 – Plate thickness – bolt diameter combinations

Plate thickness [mm]	Bolt				
	M8	M10	M12	M14	M16
1.85	X	X	x		
3.15		X	x	x	
3.75			x	x	x

Table 5 – Mechanical characteristics [N, mm]

t	f _y	f _u
1.85	279.8	402.1
3.15	276.8	392
3.75	258.5	375.5

The experimental arrangement is shown in Figure 4. The plate dimensions were in accordance with those used in Salford study. The specimens were tested in a ZWICK universal-testing machine, using an angular displacement transducer to record the extension readings. The loading rate was of 1kN/min, as used in Salford experimental programme (5) and specified in the European Recommendations (7). Typical load – extension curves for an identical set of parameters are shown in Figure 5.

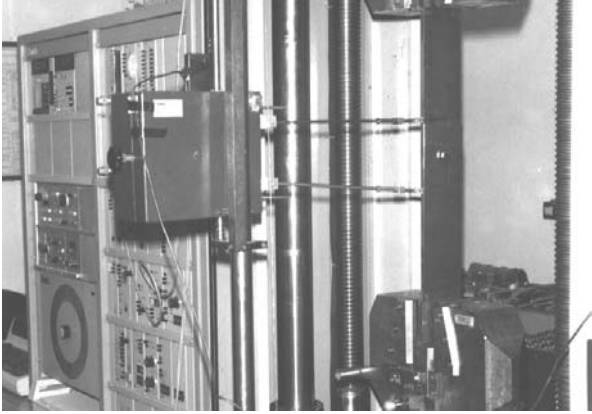


Fig. 4. Experimental arrangement

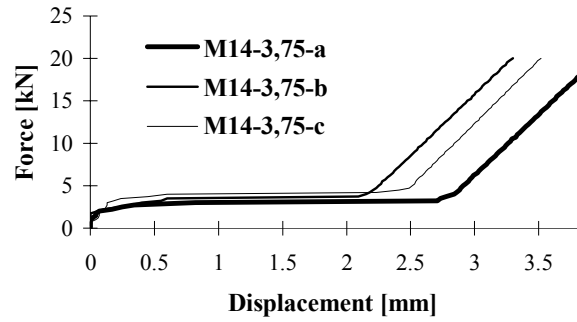


Fig. 5. Typical load – extension curves

The formula of the axial rigidity of single lap bolted joints was calibrated using the Annex Z of EUROCODE 3 (8) and it is (6)

$$K_{\text{axial}} = 6.8 \frac{\sqrt{d}}{\left(\frac{5}{t_1} + \frac{5}{t_2} - 1\right)} \quad [\text{kN/mm}] \quad (1)$$

with a partial safety factor $\gamma_R = 1.25$, in which “d” is the nominal diameter of the bolt and “ $t_{1,2}$ ” are the thicknesses of joined plates.

The ranges of validity of this formula are the bolt diameter between M8-M16 and the thickness of plates between 2-4mm. It can be noticed that the partial safety factor for this formula is identical with the partial safety factor used in EUROCODE 3 Part1.3 (9) for the resistance of bolted connections.

4. COMPUTATION MODELS FOR ROTATIONAL RIGIDITY OF TRUSS JOINTS

The computation scheme for the rotational rigidity of a diagonal-to-chord joint, with two bolts on each flange of the diagonal, is shown in Figure 6.

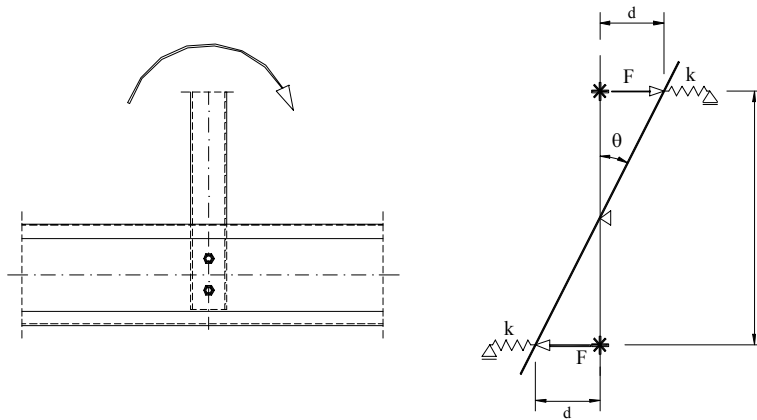


Fig. 7. Computation model for two bolts joint

Using the notations from Figure 6, the rotational rigidity of the joint, $K_{nod,t}$, can be expressed in terms of total bending moment and corresponding rotation, θ , as

$$K_{nod,t} = \frac{M_{tot}}{\theta} = \frac{2kda}{\left(\frac{d}{0.5a}\right)} = ka^2 = \frac{6.8a^2\sqrt{d}}{\left(\frac{5}{t_1} + \frac{5}{t_2} - 1\right)} \quad [\text{kNmm/rad}] \quad (2)$$

in which

$$F = k \times d \quad (3)$$

and

$$\text{tg}\theta = \theta = \frac{d}{0.5a} \quad (4)$$

The partial safety factor to be used is the same as in formula (1) $\gamma_R = 1.25$.

Table 6 shows a comparison between the theoretical and experimental values of rotational rigidities of the T joints, $K_{nod,t}$ and $K_{nod,e}$, respectively.

A good correlation between the experimental results and the characteristic values of the rotational rigidity can be observed. The average report between the theoretical characteristic values and the experimental ones is 1.036 and the correlation coefficient is $\rho = 0.982$.

Considering the design theoretical value of the formula, $K_{nod,d} = K_{nod,t} / \gamma_R$, it can be observed that all theoretical values are in the safe range. Similar models may be established for three and four bolts truss joints (6).

Table 6. Comparison between experimental and theoretical values of joint rigidity

Node	t_1 [mm]	t_2 [mm]	$K_{nod,e}$ [kNmm/rad]	$K_{nod,t}$ [kNmm/rad]	$K_{nod,t} / K_{nod,e}$	$K_{nod,d} / K_{nod,e}$
1	3	2.05	10130	9830	0.971	0.777
3			10270		0.958	0.766
2	3	3	12480	13083	1.047	0.838
4			11110		1.177	0.942
5	4.05	2.05	10560	11418	1.080	0.864
8			10968		1.041	0.833
6	4.05	3	15320	16057	1.048	0.838
9			15490		1.037	0.830
7	4.05	4.05	21189	20779	0.981	0.785
10			20361		1.021	0.817

5. TEST ON TRUSS STRUCTURE

In order to prove that the initial rotational slippage observed in case of tested joints, is not significant when the joint is working in the truss structure, and to validate the theoretical assumptions introduced above, a full-scale test of a truss specimen was performed.

The dimensions of the experimental model are shown in Figure 7. All connections are made with M12, 8.8 grade bolts. The cross section characteristics are presented in Table 7 and the mechanical properties of materials in Table 8.

Figure 8 shows the experimental arrangement. The load was introduced by means of a 500 kN QUIRI actuator. The load introduction was controlled in terms of displacements, with a rate of 2.5mm/min. Two inclinometers measured the global rotation of the diagonals. In order to measure the axial slippage in connections, two LVDT displacement transducers were placed on the axis of each diagonal. Four potentiometric displacement transducers were used to control the displacements in structure.

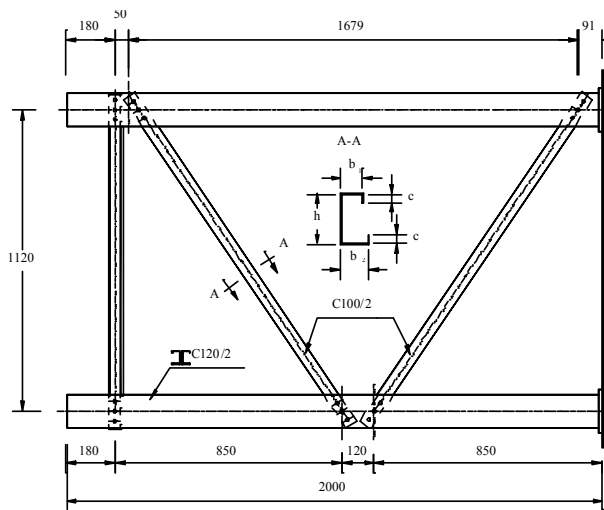


Fig. 7. Experimental model

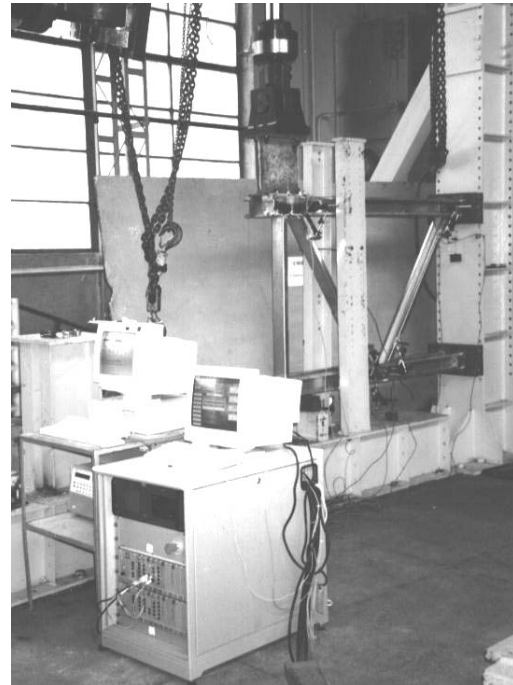


Fig. 8. Experimental arrangement

Table 7. Cross-section characteristics [mm]

Profile	Dimension				
	h	b ₁	b ₂	c	t
C100/2	100	40	45	20	1.91
C120/2	120	40	45	20	1.91

Table 8 Materials characteristics [N, mm]

Profile	f _y	f _u	e _u (%)
C100/2	367.2	542	19
C120/2	354	493.4	14

The load increased until the structure failed due to the flexural instability of the diagonal in compression, in the plane of the truss, as shown in Figure 9. A local buckling in the lower chord, due to the shear of the web panel, located between diagonals was also observed, before the buckling of diagonal was reached. This phenomenon contributes to the deformability of the joint, too.

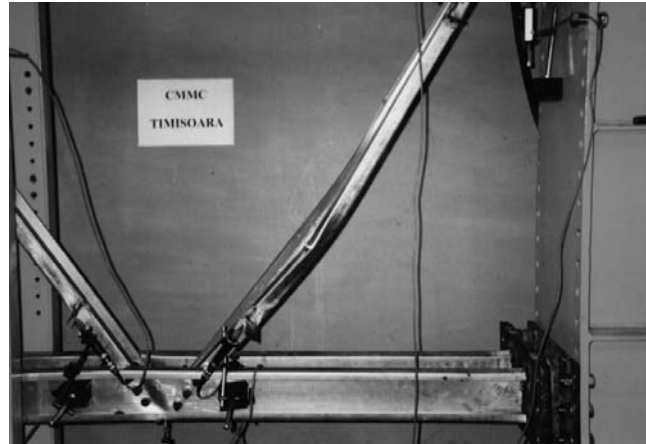


Fig. 9. Failure mechanism

Figure 10 presents the axial displacements reported by the LVDT transducers. It can be observed the typical behaviour of a thin plate bolted connection in shear. After the attainment of load corresponding to the initiation of slippage in connection, this can be developed until the hole clearance is consumed.

Figure 11 shows the evolution of the diagonal rotations. Corresponding to the load range in which the axial slippage occurs, very small rotations are observed only. Until the structure 'shake down', the presence of the axial forces and the triangulation effect prevent the developing of significant rotational slippage in connections.

Practically, the initial rotational slippage, observed during the test of joints, is almost totally restraint into structure. Consequently, the rotational rigidity evaluated without considering the initial slippage, is a real one and can be used in the global analysis, and to evaluate the buckling length of relevant members.

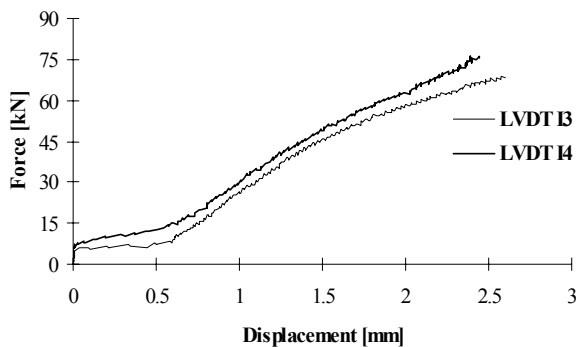


Fig. 10. Axial displacements of the diagonals

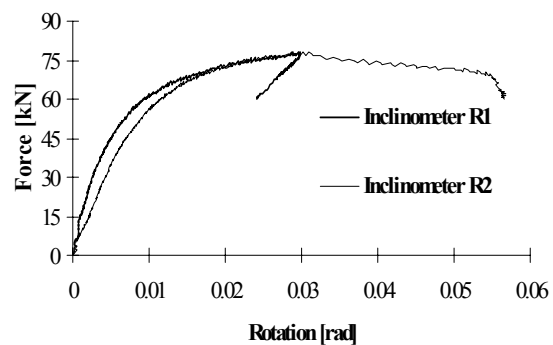


Fig. 11. Diagonal rotations

6. NUMERICAL ANALYSIS OF TRUSS

The tested truss was numerically analysed with PEP-micro programme (10), which is a specialised tool for the non-linear inelastic analysis of steel structures with semi-rigid joints. The static scheme of the structure is shown in Figure 12. The connection eccentricity, e_0 , was taken into account by introducing some rigid links at the ends of diagonals.

On the purpose of the stability checking of a structure, EUROCODE 3 (4) allows for a second order analysis with initial sinusoidal equivalent imperfection of the members. Lipped channels, are classified according to EUROCODE 3 Part 1.3 (9) on the buckling curve B, which corresponds to an initial equivalent imperfection $e_0 = l/380$. The ultimate load of the member is attained when the yield stress is reached in the external fiber of cross section, accounting for the second order effects – the ‘divergence’ model. A step by step second order analysis was performed, with a load increment corresponding to 1% of the ultimate load.

The structure was analysed with and without considering the effect of the axial rigidity of the diagonal connections. The PEP-micro programme is not able to model this axial rigidity of connections, and, on this purpose, an equivalent finite element was used to simulate this behaviour. The equivalent cross section area of this finite element can be find by equalising the expression of the axial rigidity of the member in compression/ tension with the axial rigidity of connection, and it is

$$K_{axial} = \frac{EA_{ech}}{L_{ech}} \quad (5)$$

in which K_{axial} is taken from formula (1).

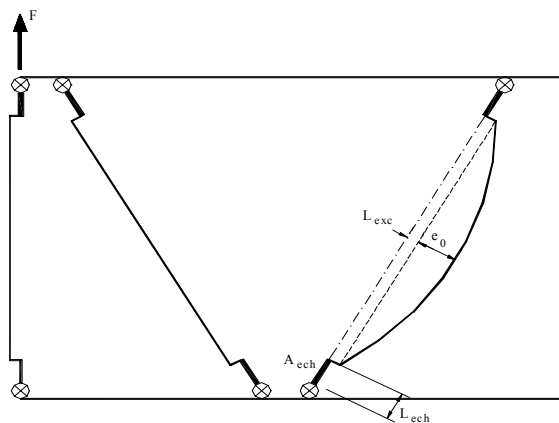


Fig. 12 Static scheme of the experimental model

Figure 13 compares the experimental load-displacement curve of this truss, with the theoretical bi-linear ones. The experimental curve shows an initial “structural” slippage, at the load intensity which corresponds to the axial slippage in diagonal connections (Fig. 10). Neglecting this initial slippage, the structural rigidity obtained accounting for both axial and rotational rigidities of connections, K_{axial} and K_{nod} respectively, is close to the experimental one.

Table 9 presents the results of the numerical analysis, in comparison with the experimental ones. The analysis accounting for both axial and rotational rigidity of connections gives differences of 2% in case of ultimate load and 37% for the corresponding displacement. This

significant difference in displacement values is due to the initial axial slippage in connections, which were not considered in the numerical analysis. The comparison between theoretical and experimental initial rigidities, after consumption of slippage, gives differences of 5% only. Without considering the axial rigidity, the difference in displacement would be significantly greater.

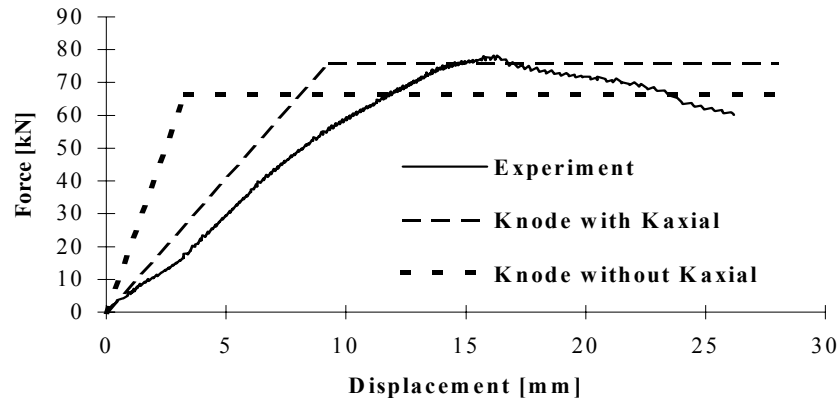


Fig. 13 Comparison between experimental and numerical analysis

Table 9. Results of the numerical and experimental analysis

K_{nod} Without K_{axial} (1)	K_{nod} with K_{axial} (2)	Experiment (3)	(1)/(3)	(2)/(3)
Ultimate load [daN]				
6650	7665	7820	0.85	0.98
Displacement [mm]				
3.3	9.9	15.8	0.21	0.63
Structural rigidity [daN/mm]				
2015	774	734	2.74	1.05

6. CONCLUSIONS

The evidence of the semi-rigid character of cold-formed steel truss bolted joints was provided, by means of tests on T typical joints. The joint deformability is mainly due to the bearing work of the bolts, and consequently, the rotational rigidity of the connection can be determined on the base of the single bolt lap joint behaviour.

In order to evaluate the axial rigidity of a single bolt lap joint, in terms of the thickness of plates and bolt diameter, an experimental programme was carried out. The characteristic and design axial rigidities were calibrated by means of the Annex Z of EUROCODE. Computation models for the rotational rigidity of the truss joints were established, depending of the axial rigidity of single bolt lap joint. The theoretical model for two bolts joint proves a good correlation of results with the ten tests on T joints.

The test on full-scale truss, shown that the initial rotational slippage observed during the T joint tests, do not appear in structure. A local buckling in the web of lower chord liped channel section, due to the shear of the web panel between the connections of diagonals, was observed before the attainment of the ultimate load. This phenomenon increases the deformability of the joint, thus influences its semi-rigid behaviour, and must be considered in further studies. The initial slippage on the direction of the diagonal axial efforts contributes only to the ultimate

displacement state, without effect on the ultimate load value. The axial rigidity of the connections has also an important influence on the displacement of the structure, but is not significant for the value of the ultimate load. It is recommended, for the global analysis of trusses, and also for the analysis of any other structure built by cold-formed sections with bolted joints, to consider both axial and rotational rigidities of the connections. For displacement analysis, and for computation of the buckling length of the members, the design values of the rotational and axial rigidity of the connections, as proposed in this paper, can be used, while for connection design, the characteristic values are recommended.

NOTATIONS

f_y - yield stress

f_u - ultimate tensile stress

ε_u - ultimate strain

h, b, c – cross – sectional dimensions for lipped channel

t - thickness

M_s - slippage moment

M_{Rd} - ultimate bending moment of the connection

θ_1 - initial slippage

K_{axial} – axial rigidity of the joint

$K_{nod,t}, K_{nod,d}, K_{nod,e}$ – characteristic, design and experimental value of rotational rigidity of joint

REFERENCES

1. Dubina D., Zaharia R., The influence of node semi-rigidity of the thin-walled steel trusses bolted joints, Advances in Steel Structures ICASS'96 - Hong Kong, September 1996
2. Dubina D., Zaharia R., Experimental evidence of semi-rigid behaviour of some cold-formed steel truss bolted joints, International Conference on Experimental Model Research and Testing of Thin-Walled Steel Structures, Prague, Czech Republic, October 1997
3. Dubina D., Zaharia R., Cold-Formed Steel Trusses with Semi-Rigid Joints, Thin-Walled Structures Vol. 29, Nos. 1-4, Special Issue on Cold-Formed Steel and Aluminium Structures, Elsevier Science Ltd, 1998
4. EUROCODE 3, Part 1.1, 'General Rules and Rules for Buildings', 1992
5. Zadanfarrokh F., Bryan E. R., Testing and design of bolted connections in cold-formed steel sections, Eleventh International Specialty Conference on Cold-Formed Steel Structures, St. Louis, Missouri, USA, October 20-21, 1992
6. Zaharia R., Contributions to the safety study of the cold-formed steel structures, PhD Thesis (in romanian), The 'Politehnica' University of Timisoara, 2000
7. ECCS - TC7 European Recommendations for Steel Construction: The Design and Testing of Connections in Steel Sheeting and Sections, Publication No. 21, 1983
8. Annex Z - Determination of Design Resistance from Tests - EUROCODE 3 Part 1.1: 1992/prA2: 1994
9. European Convention for Standardisation, EUROCODE 3 Design of steel structures Part 1.3 General rules, Supplementary rules for cold formed thin gauge members and sheeting, Brussels, Belgium, 1996
10. PEP - micro. Analyse plastique au second ordre de structures planes a barres. Galea Y., Bureau A., Centre Technique Industriel de la Construction Metallique, 1992

Non-Destructive and Ultimate Testing of Semi-Rigid Connections

Richard Kohoutek
Faculty of Engineering
University of Wollongong 2522,
Australia

Testing of Semi-rigid Connections using dynamic nondestructive investigation of connection rigidity was carried out and is reported in this paper. Several test specimens were dynamically excited and modal analysis carried out experimentally. The effect of connections rigidity was evaluated using the Dynamic Deformation Method, where the coefficient can be used in static, dynamic and stability analyses of frame structures. The experimental determination of the rigidity in combination with the analytical model provides a possibility to investigate the effects of detailing on the overall performance of a structure. Furthermore, possible modification to the existing structures that are experiencing problems in three related areas of analyses (static, stability and dynamics) is also feasible.

INTRODUCTION

The basic assumption of structural analysis of frames is complete transfer or zero moment transfer at a connection. These assumptions are reflected in structural analyses and codes through the world, however, the situation is changing in both structural analyses and codes.

The fact that this assumption is unrealistic (zero and complete transfers) has been known since the 1930s, but the technological developments did not allow any other treatment of the problem until several years ago. It is the technological advances in computers, computational techniques, and closely related measurements equipment and techniques developed during the last few decades that open a new era.

The advances are essential for our ability to measure full scale structures or their large models, in particular, under dynamic loads. Dynamic measurements, if possible, are inherently more accurate than static measurements. There is a price to be paid for this improvement in more complicated analyses, measurements and processing time and cost. However, a better understanding of behaviour with better utilization of materials is the result - a path we have taken historically in the development of science and engineering.

EXPERIMENTAL MODAL ANALYSIS

Three groups of tested connections are presented; welded I-cross section, tubular cross section and combination of I-cross section with tubular cross section.

The first series of tests were nondestructive; then all connections were strain gauged and tested for ultimate loads. All connections had the overall length dimensions 1,600 mm (chord) and 830 mm (branch) with variations of chord and branch sizes as shown in Table 1.

Project supported by the Transfield Pty Ltd and Tubemakers Pty Ltd.

Table 1a - Dimensions of welded connections, all I-sections (mm)

	Chord			Branch			Connection detail
	Depth	Width	Web	Depth	Width	Web	
W1/3/250	97	99	5	97	99	5	fillet weld (f.w.)
W2/3/250	97	99	5	97	99	5	f.w. and stiffeners
W3/3/250	97	99	5	97	99	5	W2 with cross stiff.
W4/3/250	97	99	5	97	99	5	W2 with two sh. pl.

Note: Variation is in stiffeners only

Table 1b -Dimensions and nondimensional parameters of tubular connections (mm)

	Dimensions		Nondimensional parameters			
	Chord size	Branch size	β	γ	τ	α
T1/3	219.1x8.2	219.1x4.0	1.0	13.36	0.49	13.69
T2/3	219.1x8.2	114.3x6.0	0.52	13.36	0.73	13.69
T3/3	219.1x8.2	114.3x4.8	0.52	13.36	0.59	13.69
T4/3	219.1x8.2	60.3x3.9	0.28	13.36	0.48	13.69

Nomenclature listed on the end of this paper

Table 1c- Dimensions of tubular chords and I-sections branches (mm)

	Chord size	Branch			Connection detail
		Depth	Width	Web	
TC11/1/250	139.7x4.88	97	99	5	weld. channel 100 (ch.)
TC12/1/250	139.7x4.88	97	99	5	ch. with bolts
TC13/1/250	139.7x4.88	97	99	5	ch. with bolts and stiff.

Modal analysis was performed on specimens with the support conditions approximating a hinge, which was verified experimentally. The excitation for modal analysis was generated by using an instrumented hammer and acceleration measured along the chord and branch in a number of points. The signal processing was made using the Tektronix Analyzer 2630 and Modal Analysis using the STAR package. This study concentrated on bending modes in the plane of a chord and a branch, where other modes were eliminated by the direction of the excitation force.

Details of the testing procedure and analytical model are described in Kohoutek (5). In principle, a variation of the first bending natural frequency is influenced by the performance of the connection. A connection is defined as not only a detail of the intersection of two beams but also the intersection's surrounding regions, which will deform under an applied load. The procedure to determine the rigidity index Γ consists of several basic steps:

- design full or scaled down model of a connection, bearing in mind clarity of behaviour of all boundary conditions (supports and tested connection),
- make an analytical model using the Dynamic Deformation Method,
- experimentally test the model using Modal Analysis, which will reveal any large discrepancies in assumptions about boundaries and behaviour of modes,
- from the previous step, measured natural frequencies are used as the criterion to match analytical model performance with the experiment by finding the *correct* rigidity index Γ .

Table 2a - Calculated and measured first and second natural frequencies in bending (Hz) with calculated rigidity index Gamma for the connection

Connection	DDM		Algor		Measured		Γ
W1/3/250	87.2	129.93	90.52	114.96	84.2	103.2	0.72
W2/3/250	87.2	129.93	90.52	114.96	86.8	110.1	0.81
W3/3/250	87.2	129.93	90.52	114.96	83.8	116.7	0.85
W4/3/250	87.2	129.93	90.52	114.96	84.5	119.2	0.89

Table 2b - Calculated and measured first natural frequencies in bending (Hz) with calculated rigidity index Γ for the connections

Connection	DDM ^a	SAP ^b	SAP ^c	Measured	Γ
T1/3	123.3	124.1	127.5	95	0.79
T2/3	69.3	68.8	69.2	55	0.85
T3/3	70.2	69.9	70.2	56.3	0.85
T4/3	37.2	36.7	36.7	33.8	0.95

^a support conditions - hinges

^b support conditions - hinges

^c support conditions - fixed

Table 2c - Calculated and measured first and second natural frequencies in bending (Hz) with calculated rigidity index Γ for the connections

Connection	DDM		Algor		Measured		Γ
TCI1/1/250	87.2	129.93	90.52	114.96	94.3	299.1	0.9
TCI2/1/250	87.2	129.93	90.52	114.96	75.2	266.3	0.45
TCI3/1/250	87.2	129.93	90.52	114.96	88.6	271.1	0.55

Connections made of I-sections were investigated for the effect of stiffeners. The basic geometry of T-sections tested is the same and only stiffeners were added. First, two stiffeners were added on the chord in the extension of the flanges of the branch (W2), then additional diagonal brace in the square created by the stiffeners and the flanges of the chord (W3), and

finally double shear plate in the same square (W4). The results confirm earlier tests on different size of cross sections reported in Kohoutek (4,5).

The results which are shown in the Table 2a demonstrate a considerable increase in the global stiffness of the connection due to additional stiffeners. The highest Γ is a double shear plate, which is also most demanding to fabricate.

The tubular sections were selected based on nondimensional parameters after survey of off shore applications. These are currently becoming a focus of interest in the building industry. Several conclusions can be made from Tables 1b and 2b.

First, the samples T2 and T3 have the same rigidity index ($\Gamma = 0.85$), where variation is only in the thickness of the branch, 6.0 mm and 4.8 mm, respectively. However, all their first frequencies in bending are also similar for all their analytical models. This indicates the sensitivity of the method.

Second, the rigidity factor is inversely proportional to the relative stiffness of the intersecting elements (T1 and T4).

Third, the sample's first natural bending frequency is not very sensitive to supporting conditions - the result is not strongly influenced by a minor variation in supports.

The test samples where the cross section of the chord is tubular and the branch is I-section were tested dynamically with results shown in Table 2c. However, the ultimate load was applied to the first connection only (TC11). The work is in progress on other connections.

ULTIMATE LOAD

The specimens were supported in a strong frame with the chord in the vertical position and the end of branch connected to a hydraulic jack as shown in Figure 1. Each connection was then progressively loaded to its ultimate capacity while readings of deflections and strains were taken from strain gauges installed.

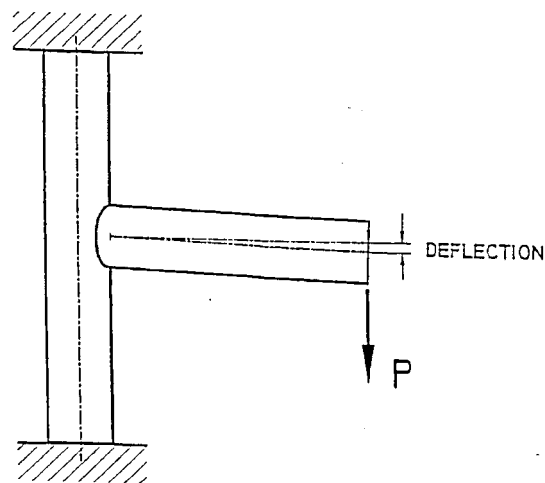


Figure 1 - Ultimate load test-set up (diagrammatic only).

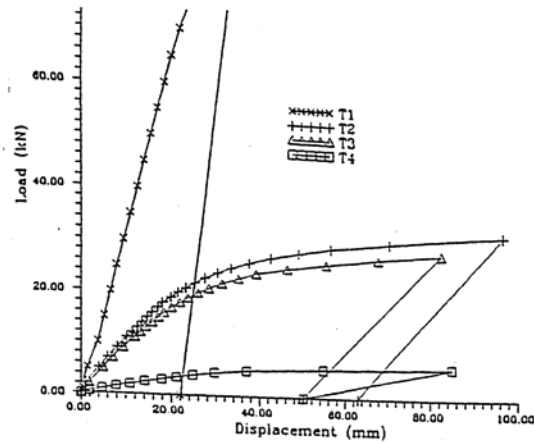


Figure 2 - Force-deflection diagram for tested connections.

This section concentrates on the performance of tubular/tubular and tubular/I-section connections.

The force-deflection diagram for the tested tubular connections shows large differences in the ultimate capacities between T1 and T4, and consequently, large slope differences. The trend appears to contradict rigidity factors measured dynamically earlier and shown in Table 2b. However, the values need to be normalized because there is a large difference in the capacities of connections. The normalization chosen here is based on the ultimate capacity of the smallest connection (T4), where a measure of the capacity is when the section starts to yield. That is σ_{ult} reached at the top and bottom of the cross section, where the rest of the section is still elastic. Since the yield is possibly reached at other regions of the connection, including adjoining areas of contact, this may not be the first point in the connection to yield. The other uncertainty is determining when the plastic deformations are small enough to be included in the total *elastic* deflection. The results of this normalized process are in Table 3.

A number of strain gauge readings were taken in the ultimate loading process, but are not shown here because of space limitations. It is clear from those readings and also from observations of the deformation process of the connections that *hot-spots* not only develop but also *move around* due to redistribution taking place within the connection as the load increases.

Table 3 - Ultimate and Normalized Force – Deflection Values

Connection	I^a	I_T/I_{T4}	Force/deflection ^b	Normalized F/d ^c	Γ^d
T1/3	1.6521-5	49.1994	833.3	16.6	0.79
T2/3	3.5184-6	10.4778	188.4	17.97	0.85
T3/3	2.8147-6	8.3822	158.23	18.88	0.85
T4/3	3.3580-7	1.0000	33.10	33.10	0.95

^a Moment of inertia $I - (\pi d^3 t)/8$

^b Force in N, deflection in mm

^c Base used is T4

^d from Table 2

The only ultimately loaded connection from the last group was TCI1 (work on others is in progress). The load was increased in 1 kN increments until the ultimate capacity was reached (12 kN) with the corresponding deflection of 60.5 mm.

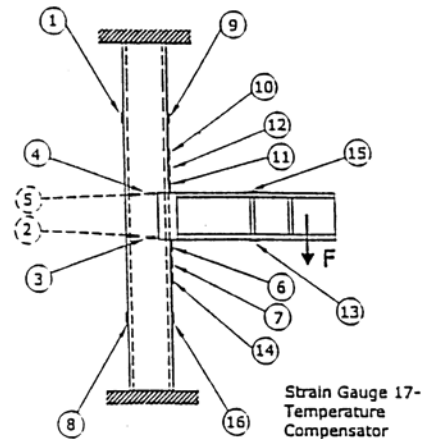
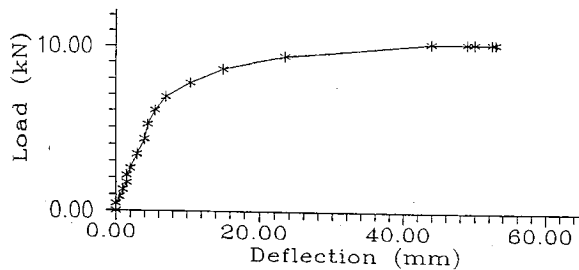


Figure 3 -a) Load/deflection diagram for TCI1.

b) position of the strain gauges on TCI1

The range from 0 to 7 kN is almost linear with the corresponding moment of 5.74 kNm for the upper limit. A failure of the specimen initially occurred in the tubular section just below the welded fillet connection. The final failure was tearing of the two fillet welds at maximum load. The strain gauges positions are shown in Figure x and the results of loading strain gauges are presented in Figure 4.

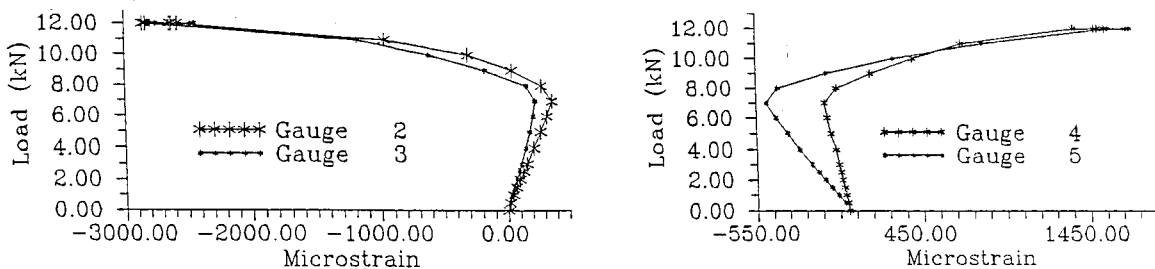


Figure 4 - a) strain gauges #2 #3 over the loading range
b) strain gauges #4 #5 over the loading range

Figure 4 confirms the linear performance in the range 0 to 7 kN, while the strain gauges also indicate local recovery due to redistribution of stresses (hot spots) mentioned for tubular/tubular sections above.

CONCLUSION

A method of dynamic nondestructive loading has been compared with the ultimate capacities of the same connections and some tentative correlations can be made between the two states. Dynamic loads are very small and cannot generate any inelastic strains in connections where the ultimate load produces large concentrations of stresses, which yield material locally. Furthermore, these localized yielding regions *move* due to redistribution that is taking place while the load is increasing. Therefore, it is very difficult to make definite correlations from the relatively small sample of specimens.

However, the elastic analysis of rigidity factor agrees with the ultimate load in the general trends, especially when ultimate results are normalized. It is expected that further work is needed on this normalization process before qualitative results between two states - elastic and inelastic can be finalized. The work on this project is still in progress.

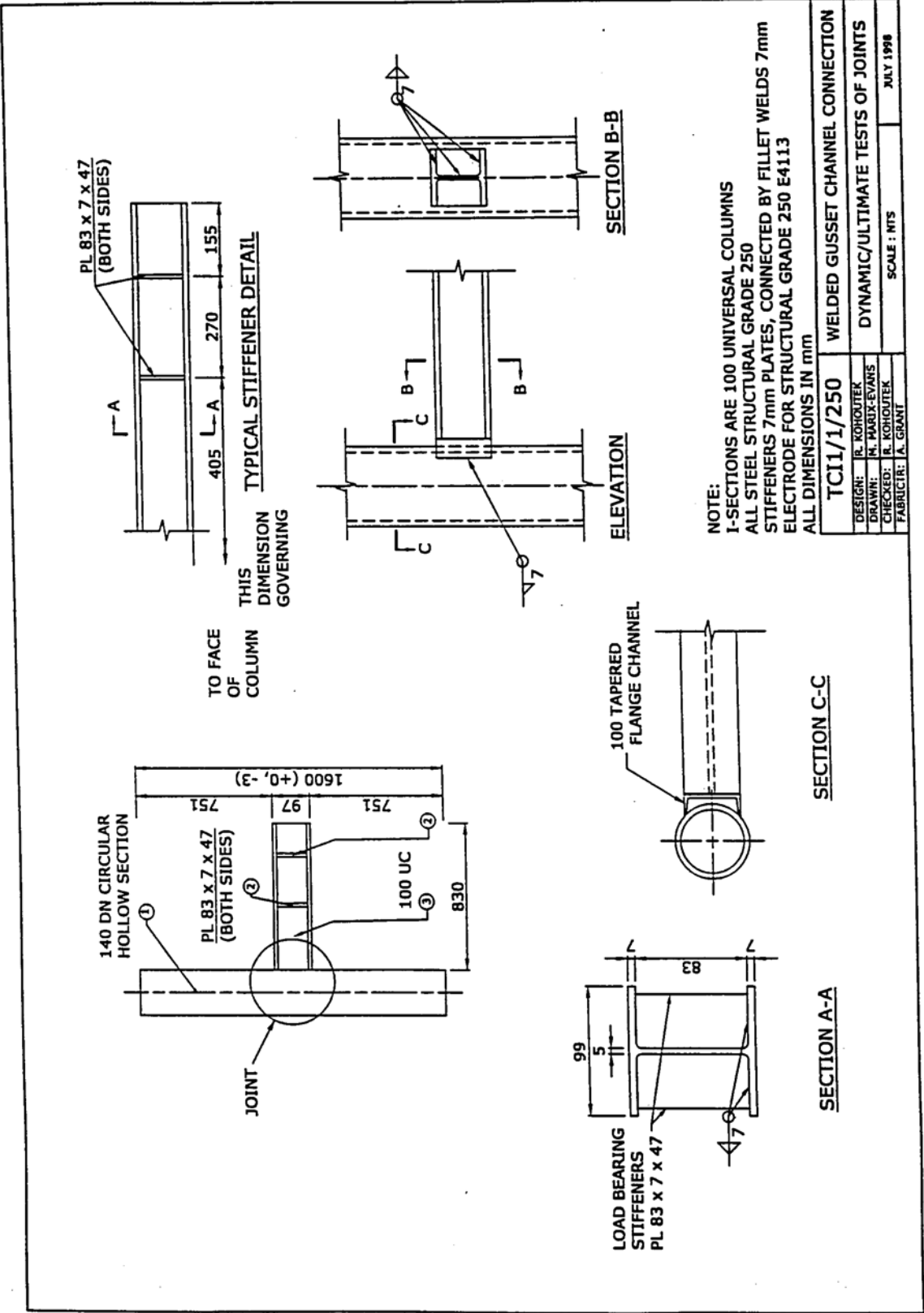
ACKNOWLEDGEMENT

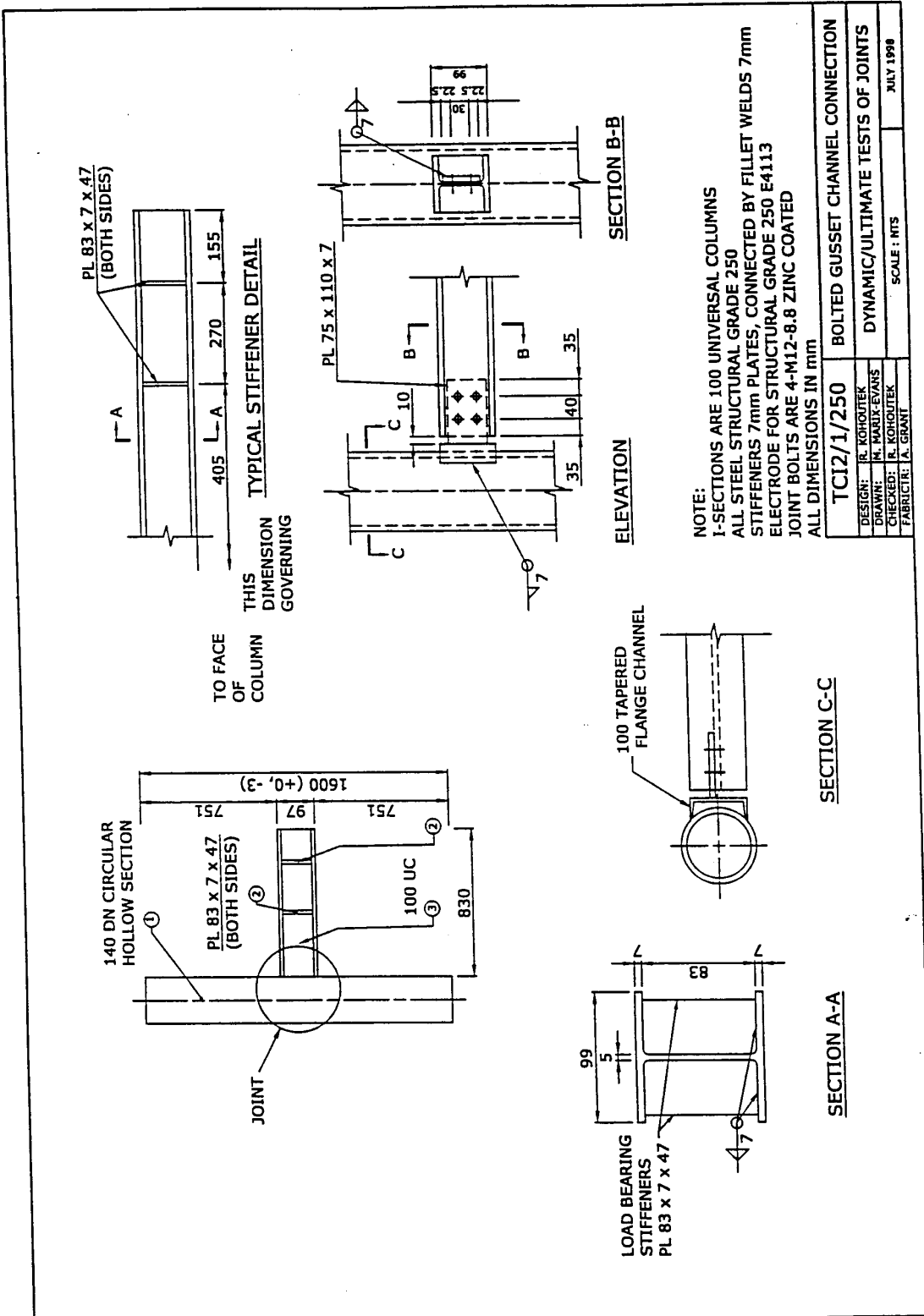
The author would like to acknowledge contribution of Messrs M.Marix-Evans, C.McConville and Dr I.Hoshyari with the experimental part of this project. The project was supported by Transfield Pty Ltd and Tubemakers Pty Ltd.

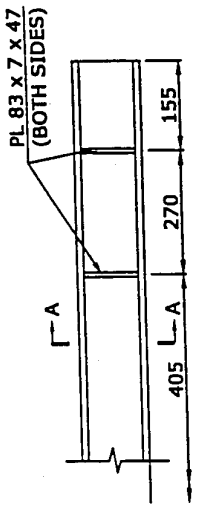
Dchord diameter, d branch diameter, T chord thickness, tbranch thickness, L chord length, l branch length $\alpha = L/2D$, $\beta = d/D$, $\gamma = D/2T$, $\tau = t/T$

REFERENCES

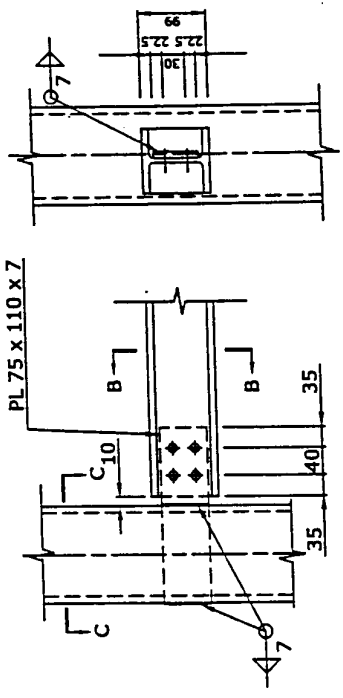
- (1) Kohoutek, R., (1985). *Analysis of Beams and Frames*, Chapter 4 in *Analysis and design of foundations for vibrations*, pp 99-156; P. Moore, ed., 512pp, 1985, published by A.A.Balkema.
- (2) Kohoutek, R. (1990). "Relationship between Static and Dynamic Stabilities for Structures with Semi-Rigid Joints", *P. of The Twelfth Australian Conference on the Mechanics of Structures and Materials*, September 24-26, Queensland University of Technology, Brisbane, pp191-196.
- (3) Kohoutek, R. (1990). "Dynamics of Beam with Semi-Rigid Joints, Part I - Analytical Model," *P. of The Australian Vibration and Noise Conference 1990*, September 18-20, Monash University, Melbourne, pp 339-343.
- (4) Kohoutek, R. and Behrens, M. (1990). "Dynamics of Beam with Semi-Rigid Joints, Part II - Experimental Evaluation," *P. of The Australian Vibration and Noise Conference 1990*, September 18-20, Monash University, Melbourne, pp 344-348.
- (5) Kohoutek, R. (1991). "Dynamic Tests of Semi-Rigid Connections," *P. of The Second International Workshop on Connections*, Invited paper, Pittsburgh, April 10-12, 9pp.
- (6) Kohoutek, R. and Hoshyari, I. (1992). "Parametric Formulae of Rigidity for Semi-Rigid Joints," *P. for Offshore Mechanics and Artic Engineering*, Calgary, Canada, June 7-11.
- (7) Kohoutek, R. (1995). "Stress prediction by Analytical Model verified by Modal Analysis," *P. of The Thirteenth International Conference on Modal Analysis (IMAC)*, February 13-16, Nashville, Tennessee, pp710-717.
- (8) Kohoutek, R. (1993). "Tests on Bridge over Talbragar River at Dubbo," *P. of The International Conference on Modal Analysis (IMAC)*, 1-4 February, Kissimmee (Orlando), Florida, pp1168-1174.
- (9) Rotter, T. Kohoutek, R. and Marusiak, G. (1994). "Modal Analysis of Railway Bridge in Mlada Boleslav," *P. of The Twelfth International Conference on Modal Analysis (IMAC)*, January/February 31-4, Honolulu, Hawaii, pp1316-1320.
- (10) Kohoutek, R. and Marshall, P. (1994). "Use of Modal Analysis of Nattai Bridge: Mittagong bypass," *P. of The Twelfth International Conference on Modal Analysis (IMAC)*, January/February 31-4, Honolulu, Hawaii, pp706-712.





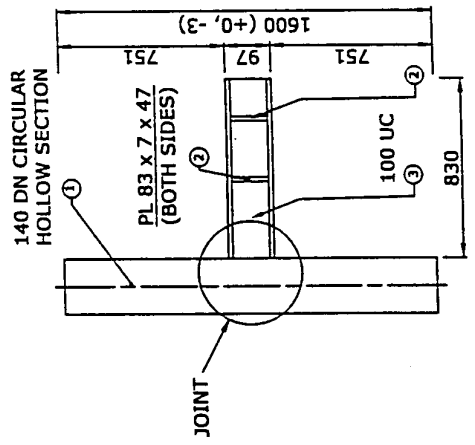


TYPICAL STIFFENER DETAIL
THIS DIMENSION GOVERNING

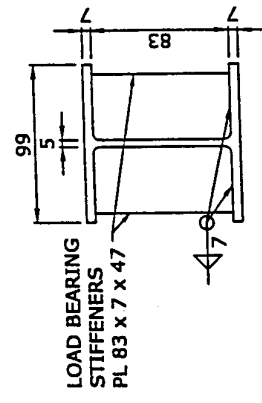


ELEVATION

SECTION B-B

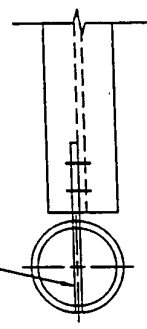


TO FACE OF COLUMN



SECTION A-A

PL 75 x 110 x 7



SECTION C-C

NOTE:
I-SECTIONS ARE 100 UNIVERSAL COLUMNS
ALL STEEL STRUCTURAL GRADE 250
STIFFENERS 7mm PLATES, CONNECTED BY FILLET WELDS 7mm
ELECTRODE FOR STRUCTURAL GRADE 250 E4113
JOINT BOLTS ARE 4-M12-8.8 ZINC COATED
ALL DIMENSIONS IN mm

TC13/1/250		SLOTTED COLUMN WITH SIDE PLATE CONNECTION	
DESIGN:	R. KOHOUTEK	DYNAMIC/ULTIMATE TESTS OF JOINTS	
DRAWN:	M. MORIX-EVANS	SCALE : NTS	
CHECKED:	R. KOHOUTEK	JULY 1998	
FABRICATOR:	A. GRANT		

Strengthening of riveted and bolted steel constructions under fatigue loading by preloaded fasteners - experimental and theoretical investigations

by Günther Valtinat, Ingo Hadrych and Holger Huhn,
Technical University of Hamburg-Harburg/Germany

ABSTRACT

The paper contains results on the problem: How can the fatigue resistance of riveted or bolted steel construction members under repeated loads be improved. The main idea is to develop a preload rectangular to the surface of the members by means of a preloaded bolt to protect the area around the hole. The results can be used for strengthening of old railway bridges and of masts and towers under wind loads constructed from galvanized steel members with punched holes.

1. INTRODUCTION

We have in Germany many old railway bridges sometimes more than 100 years old. A lot of them is still in use and many years ago the problems came up how their today resistance against repeated loads is. These old bridges are mainly riveted. From many tests in the thirties we know, that steel members with holes or with riveted connections have a considerable drop down in fatigue behaviour under repeated loading.

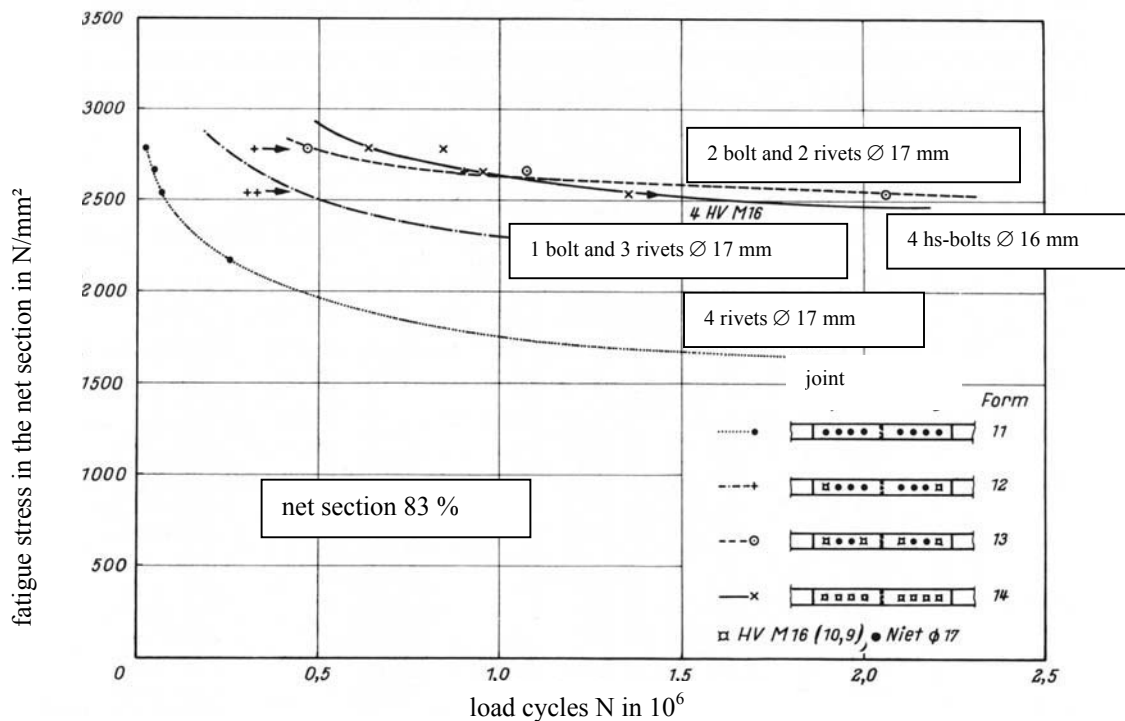


Figure 1: Fatigue resistance of pure and mixed riveted and bolted connections

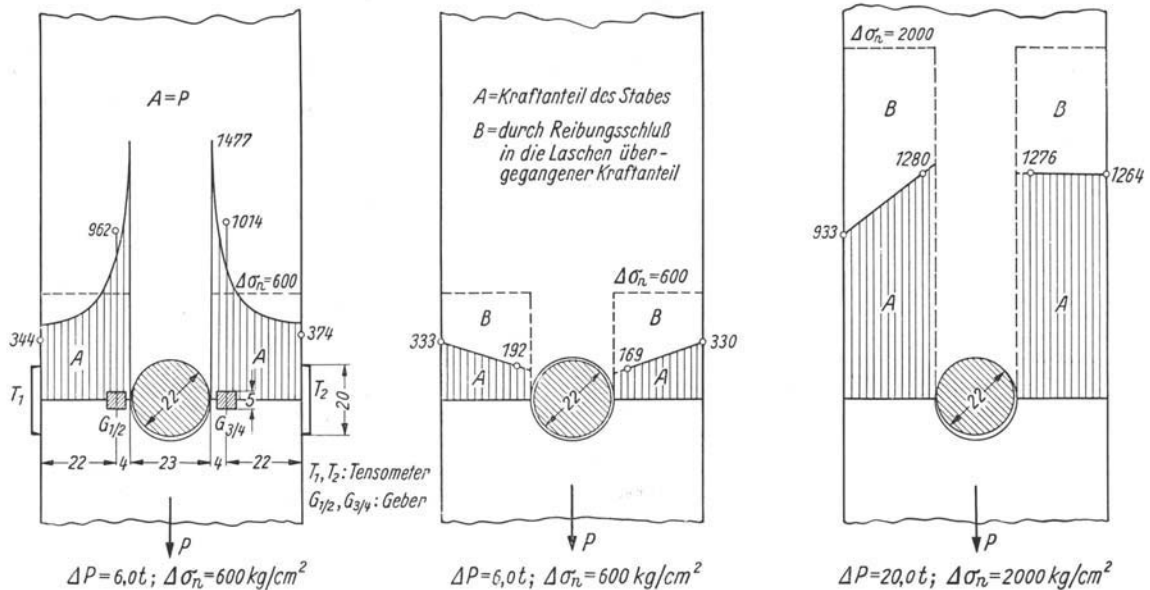


Figure 2: Stress distribution in net sections
left: net section with a rivet
center: net section in a high strength friction grip connection
right: net section in a high strength friction grip connection after slip

In the fifties and sixties the high strength friction grip connections with preloaded bolts have been developed and tests have shown that the fatigue behaviour of members with these connections is very much better than that one with rivets. The increase in capacity which means in stress range $\Delta\sigma$ or load cycles N was so immense that sometimes the fatigue behaviour of plain bars could be reached (figure 1). The reason for that increase was assumed to be the high pressure under the washers of the bolts around the hole. This high pressure gives a certain protection of the hole area, so that the stress distribution in the net section became much more favourable than for example with fitted bolts without preload (figure 2).

From this knowledge we started an investigation what advantage the preload in a hot driven rivet can have because after the rivet is driven it cools down, the material wants to shrink which is not possible and thus produces a preload of a certain amount. When old bridges were taken down for renewing we asked for test pieces with riveted connections to find out which preload such a rivet has. The procedure was to plant a strain gage in a deep hole in the center of the rivet, to machine the rivet head off and to press the rivet out of the hole. By this procedure the rivet under tension could freely shrink and from the measurement of the contraction we could evaluate the preload in the rivet. Test pieces of that old material with old drilled holes got installed high strength bolts which were tightened up to that preload which we measured in the rivets. Hereafter we did fatigue tests. All test pieces had a certain artificial crack starting from the hole wall into the net section (see figure 3). We wanted to know the speed of the crack propagation in connections with non preloaded bolts and in connections with bolts with a preload up to that one of the rivets. We have found that the number of cycles between the two increased up to 4 times to 7 times as much under a certain relatively low preload (see figure 4). From these results we know that connections with hot driven rivets have a much higher fatigue resistance than equivalent test pieces with normal bolts show. The life time of old riveted bridges can be prolonged by this idea up to 2 times or 3 times. That gave the railway authorities enough time for planning a new bridge or for a correction of the railway line with new bridges [1].

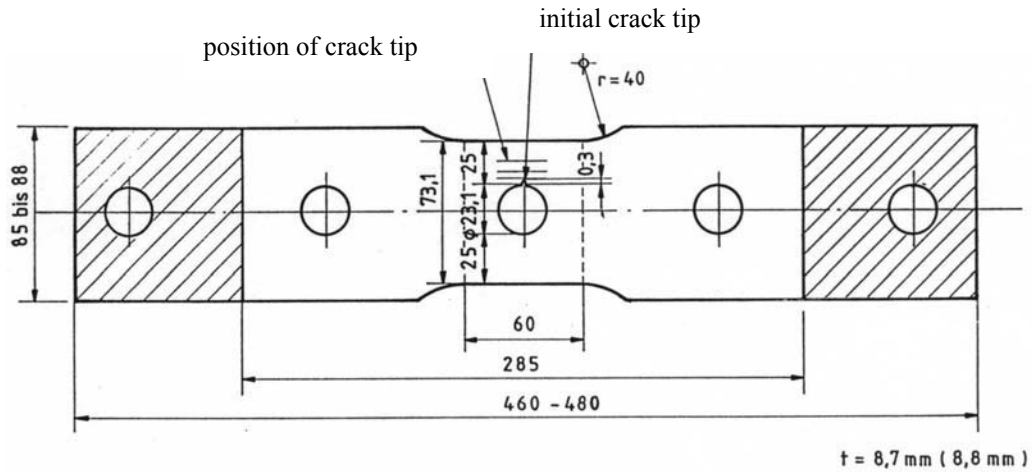


Figure 3: Bar with a hole and an artificial crack tip

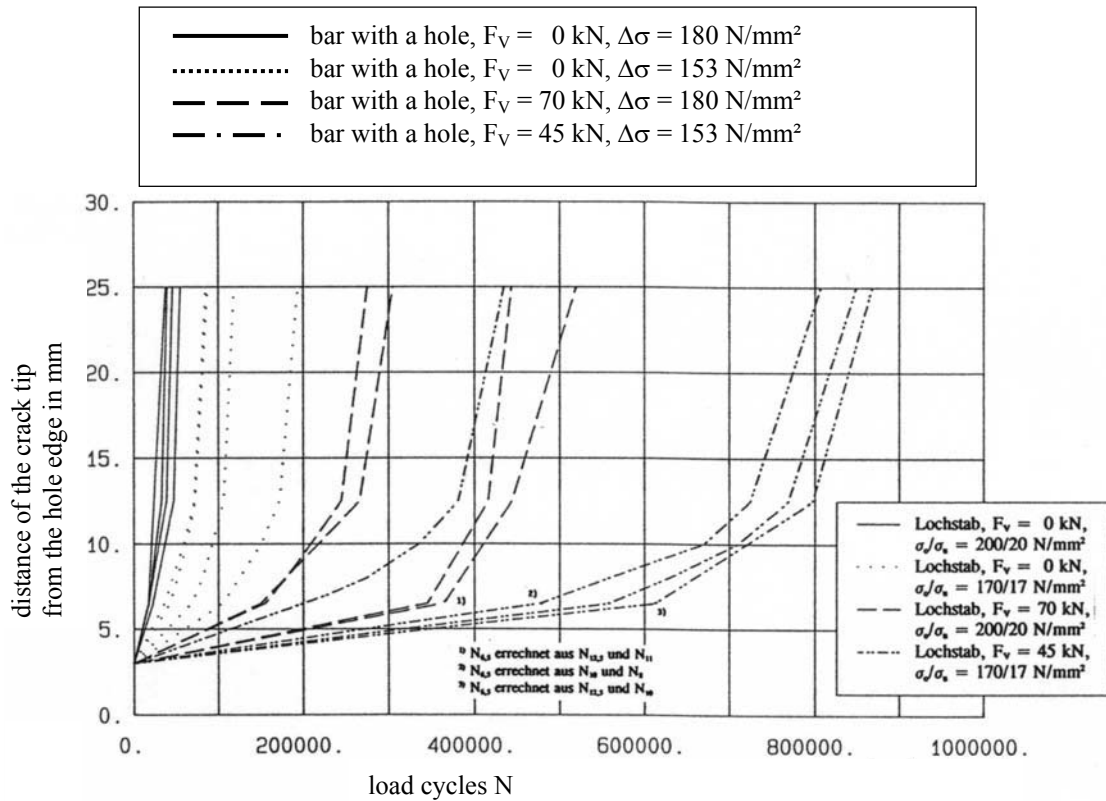


Figure 4: Reduction of the crack propagation speed in the net section of a bar with a hole due to the preload of the high strength bolt

2. TESTS, TEST PROCEDURE AND TEST RESULTS

In figure 5 the test specimen for a steel bar with a hole and an artificial initial crack tip in the direction of the net section is shown. The high strength bolt with the 2 washers and nut were fixed up to certain preload. The washers covered a certain area around the hole and brought a certain pressure due to preload in. These test pieces were tested by fatigue loading and for us it was important to see the crack propagation. The method to make that visible was to bring in stress blocks with high and with low stress ranges. The stress blocks with the low stress ranges produce a marking line on the rupture surface which is shown by the thin dark lines in figure 6. The bright areas represent the stress block with the high stress range and all the same number of cycles. We can see that the stress propagation is nearly equal within a certain length of the crack but it speeds up towards the crack comes through [2].

The literature gives a lot of information about the stress distribution in a net section of a bar with a hole or with a crack. But we did not find a stress distribution in such a member which is influenced by a pressure under the washer across the thickness of the member coming from the preload of a high strength bolt. We did computer simulations for this special stress situation (see figure 7). In order not to do a finite element calculation every time we looked in the literature for papers with a simpler and faster method to find the stress distribution in a crack starting from a hole wall. We found the investigation by Grandt and Kullgren [3] which has the following basis (see figure 8):

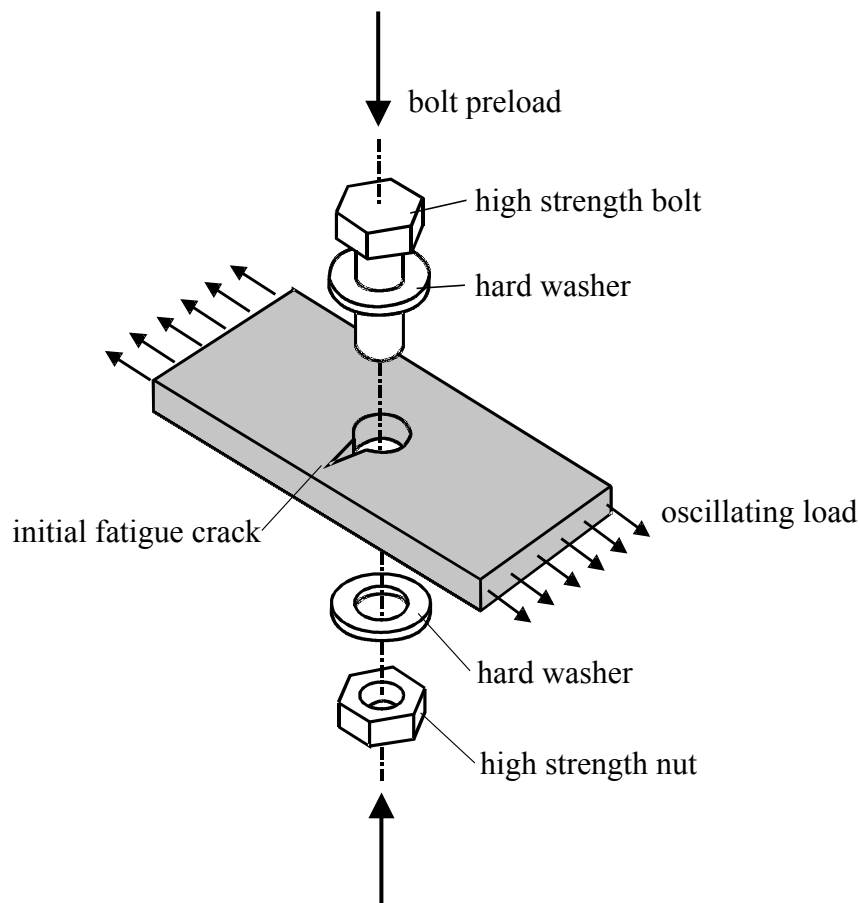


Figure 5: Plate with a hole and an initial fatigue crack

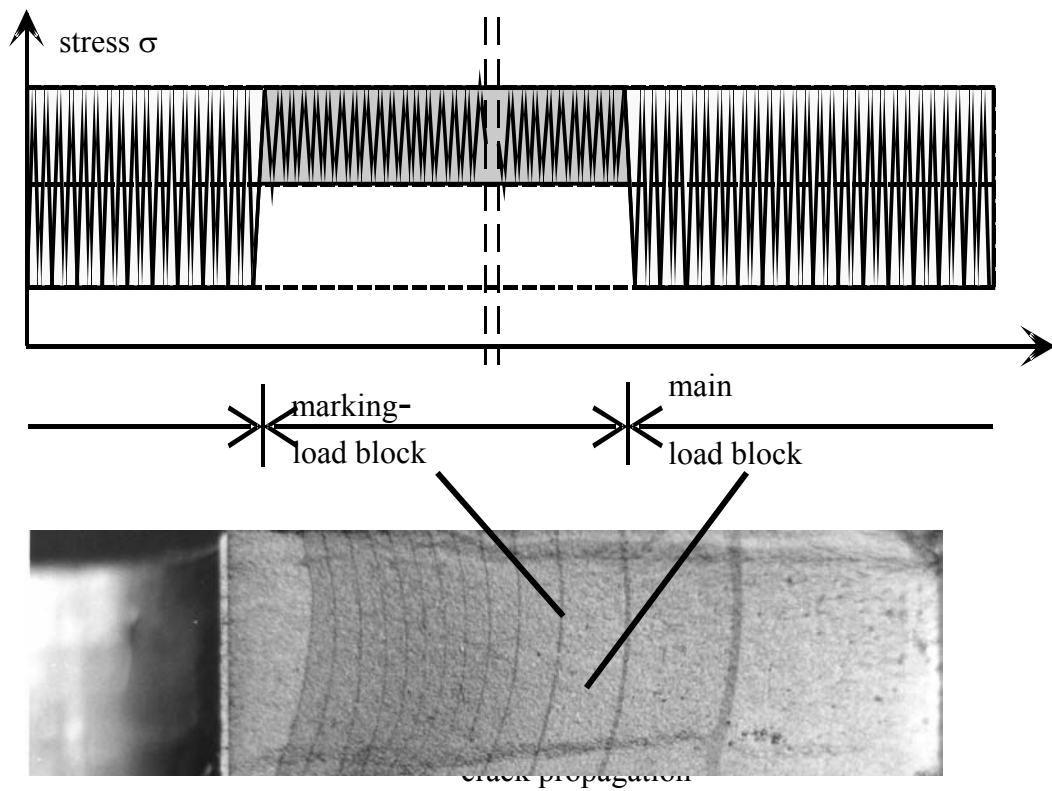


Figure 6: Measurement of the crack propagation

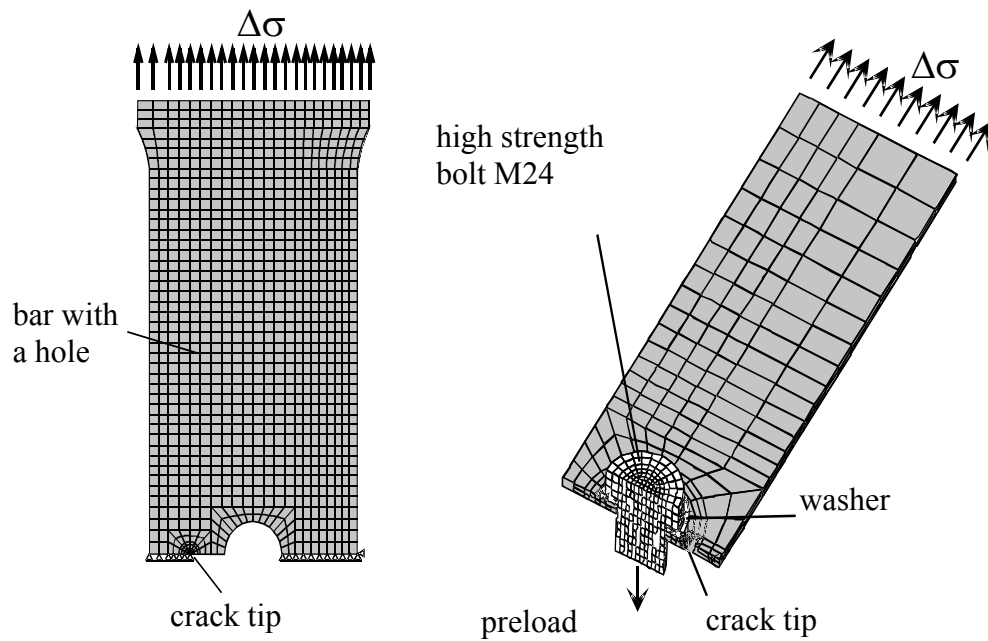
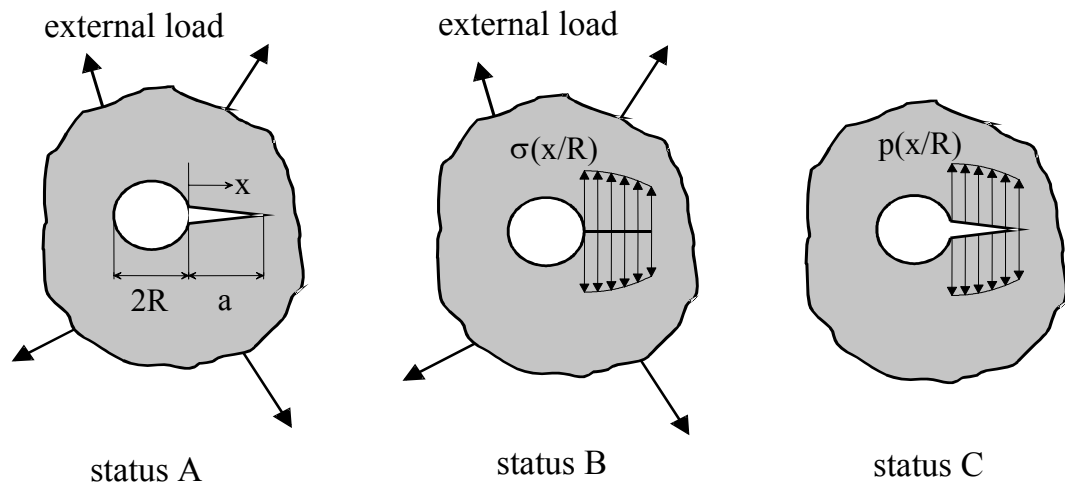


Figure 7: Grid for the finite element simulation

1. An infinite plate with the hole with the diameter of $2R$ with external load has a crack with a crack length of a (status A) started from the edge of the hole. This was assumed to be the reality.
2. The stress distribution in an externally loaded infinite plate with a hole along a fictive crack line could be calculated by finite element method and could be replaced by analytical functions. If now a crack appears this stress must become 0. This zero stress can only be reached if in the status C the stress distribution of the status B is imposed to both sides on the crack surfaces to make the stress 0. The curve of this stress distribution can be replaced by simple analytical formulae built as a polynomial. A reduction to a non infinite plate is possible.



$$K_A = K_C \text{ with } p(x/R) = \sigma(x/R) \text{ status without crack}$$

Figure 8: Model and stress distribution according to Grandt and Kullgren

The stress intensity factor ΔK over the crack length a depends on the preload of a bolt which is placed in this hole. We see in figure 9 that this factor ΔK drops down with an increasing preload and that is equivalent to an increase of number of cycles under fatigue loading.

There is also an influence of the friction μ between the washers and the steel member (see figure 10). If this friction coefficient is high a small part of the load moves out of the member into the washer and back again behind the hole and results also in a decrease of the ΔK -factor [4].

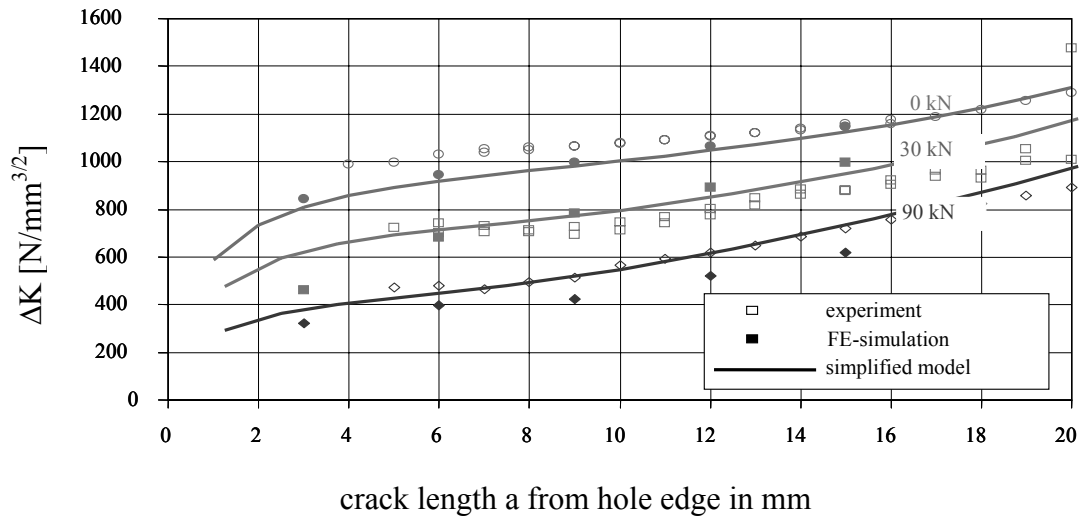


Figure 9: Stress range intensity factor ΔK depending on crack length and preload bar with a hole $d=24$ mm, $\mu=0,4$, $\Delta\sigma_{\text{gross}}=110$ N/mm², $R=0,1$

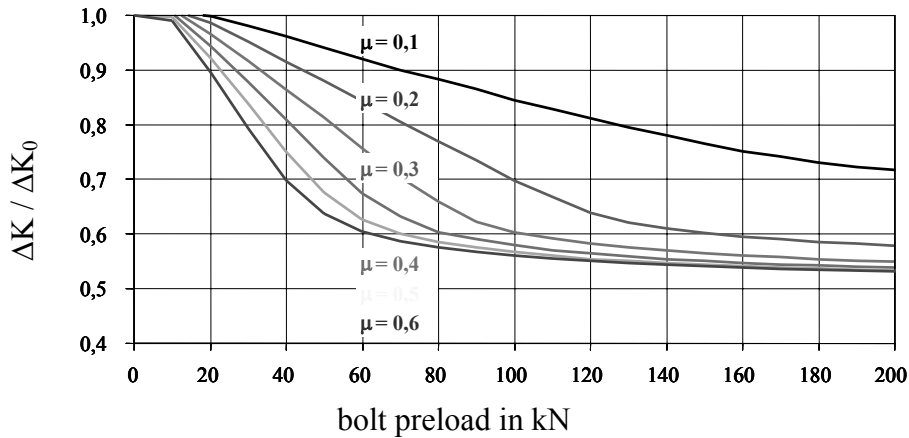


Figure 10: Related stress intensity factor $\Delta K / \Delta K_0$, dependent on bolt preload and friction μ
crack length $a=10$ mm, $d=24$, $\Delta\sigma_{\text{gross}}=110$ N/mm², $R=0,1$

We all know the diagrams with the stress propagation rate da/dN over the stress intensity factor ΔK . From the above demonstrated evaluations whose result the ΔK -factor is we can go into the da/dN -diagrams and give answer how many load cycles a steel member in a riveted or bolted connection with a certain preload can resist until rupture.

3. FATIGUE BEHAVIOUR OF HOT DIP GALVANIZED STEEL MEMBERS WITH PUNCHED HOLES

The idea from above could be transmitted to the problem of the fatigue behaviour of hot dip galvanized steel members with punched holes which are usually taken for mast and tower constructions. Such constructions are loaded by wind which can arrive from different directions. From that and from the vibration of the constructions we have oscillating stresses in the members. If the members have punched holes as usual we know that around the hole there is a certain punch affected zone with an influence on the ductility, on the yield strength and on the ultimate strength. If the member is hot dip galvanized afterwards there may be an additional ageing effect on these material data. Punching may induce very small crack initiations from which obviously an earlier start of a fatigue crack can be expected. The idea to cover this area around the hole by a high strength preloaded bolt and hence induce a certain pressure under the washer has been transferred to this type of connection. The figure 11 shows by microscopic photos how much the material along the hole wall changes its flow pattern when the punch is driven through the material. Additionally to this the distribution of the hardness in three different levels with respect to the thickness of the plate (near the entrance of the punch, in the middle plain of the plate, near the outcome of the punch) has been worked out and we found that the values near to the hole wall increase by about 50 %.

Only a few diagrams hereafter may show which advantage the use of a preloaded bolt in such connection has. Figure 12 show the results of a lot of test pieces with just a hole (no connection). The open circles demonstrate the fatigue behaviour of a member with a hole but without any bolt. The dotted line with the full squares shows the load cycles of equivalent members where a preloaded bolt is installed in the hole. The increase in load cycles is about 700 % [5,6].

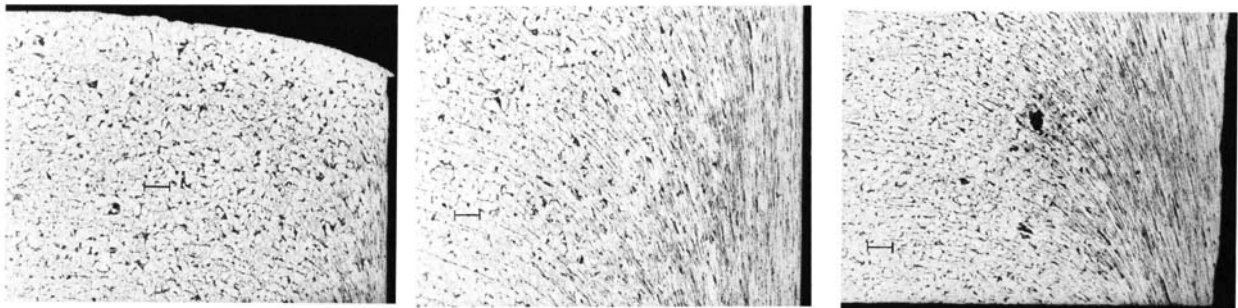


Figure 11: Material flow around a punched hole (calibration line 0,1 mm)
a) Upper part when punch enters the plate (first zone)
b) Cut in middle of the member (second zone)
c) Lower part when punch leaves the plate (third zone)

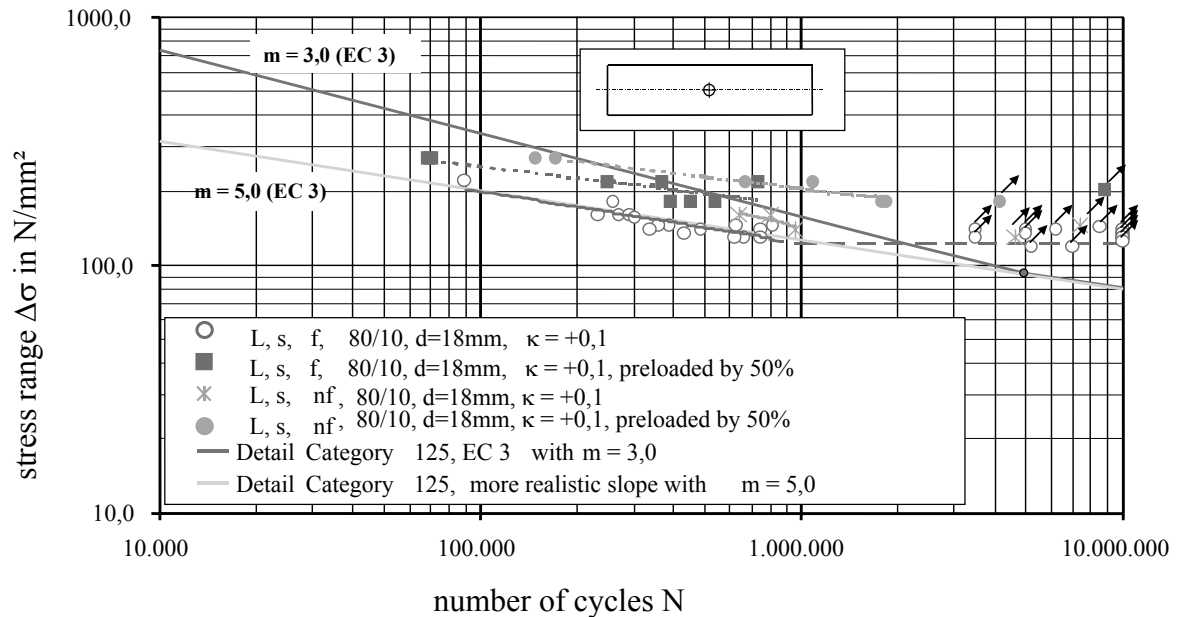


Figure 12: Comparison between experimental S-N curves for hot dip galvanized and non-galvanized members with punched hole without and with 50% preloaded bolts and the S-N curve of EC 3 (detail category 125), (L = member with a hole, s = punched hole, f = hot dip galvanized, nf = black, $\kappa = \min \sigma / \max \sigma$, m = slope of the S-N-curve of EC3).

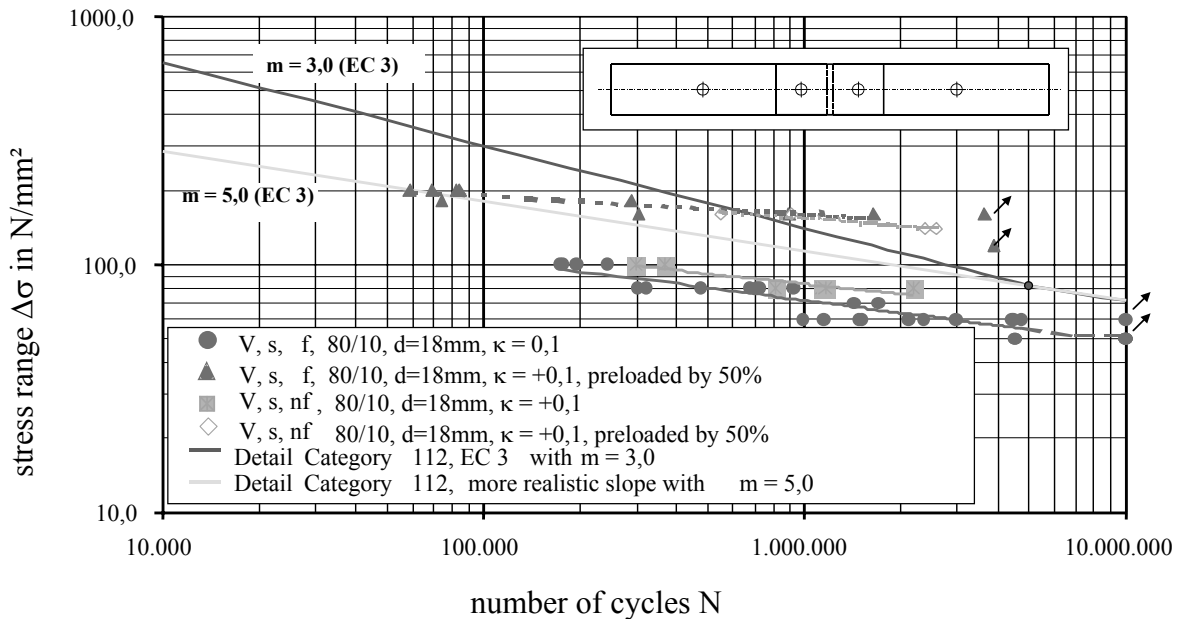


Figure 13: Comparison between experimental S-N curves for hot dip galvanized and non-galvanized shear-bearing connections with punched hole without and with 50% preloaded bolts and the S-N curve of EC 3 (detail category 112), (V = connection, s = punched hole, f = hot dip galvanized, nf = black, $\kappa = \min \sigma / \max \sigma$, m = slope of the S-N-curve of EC3)

Figure 13 shows the equivalent results for connections. The full circles and the lowest line show the load cycles of connections with non preloaded bolts, the full triangles and the dotted line represent the results of equivalent connections with preloaded bolts tightened up to 50 % of the required preload. The increase can much better be expressed by the stress range $\Delta\sigma$ than by the number of cycles. We found a step from 70 N/mm² to about 160 N/mm² at 1 million cycles. And this S-N-curve lies for high numbers of load cycles above the S-N-curve of the detail category 112 of EC 3 with a slope of $m = 3,0$.

4. CONCLUSION

The idea to protect the net section area around a hole with a rivet and a punched hole by installing a preloaded bolt with two washers has shown, that a remarkable influence on the fatigue life can be achieved. As well old riveted bridges can be strengthened by this idea using the preload in the rivet as other fatigue loaded constructions can be improved by installing high strength preloaded bolts.

I highly acknowledge that the institution AiF (Arbeitsgemeinschaft industrieller Forschungsvereinigungen in Bonn, Germany), the minister of economy of the Federal Republic of Germany, Berlin, and the GAV (Gemeinschaftsausschuss Verzinken e.V., Düsseldorf) financially supported this research (Research project AiF no. 11097/N1 and AiF no. 12547/N1).

REFERENCES

- [1] Valtinat, G.: Restnutzungsdauer bestehender Brückenbauwerke. In Berichte aus Entwicklung, Forschung und Normung 18/1992 - Vorträge der Fachsitzung I zum Deutschen Stahlbautag (Berlin 1992), DAST Deutscher Ausschuss für Stahlbau.
- [2] Valtinat, G. and Hadrych, I.: Stahlbau-Schrauben - Internationale Forschung und Entwicklung. Paper presented on the Deutscher Stahlbautag 1998 in Leipzig/Germany.
- [3] Grandt Jr., A. F. and Kullgren, T. E.: Tabulated stress intensity factor solutions for flawed fastener holes. Engineering Fracture Mechanics 18, 2 (1983), S. 435-451.
- [4] Hadrych, I.: Wachstum von Ermüdungsrissen an Niet- und Schraubenlöchern unter Berücksichtigung von Vorspannkräften der Verbindungsmittel. Diss. Technical University of Hamburg-Harburg, Hamburg 2000.
- [5] Valtinat, G. and Huhn, H.: Betriebsfestigkeit von SL-Verbindungen mit zugbeanspruchten, feuerverzinkten Bauteilen und gestanzten Löchern. In Beiträge zum 18. Steinfurter Stahlbau-Seminar (Rheine, 1999), Fachhochschule Münster.
- [6] Valtinat, G. and Huhn, H.: Fatigue assessment of bearing type joints (shear-bearing-connections) of hot dip galvanized steel construction members with punched holes. Edited proceedings of the Nineteenth International Galvanizing Conference, Berlin 2000. Published by European General Galvanizers Association, Caterham Surrey CR3 6RE/UK, and Institut Feuerverzinken GmbH, Düsseldorf/Germany, ISSN 0261 6599.